

THE JOURNAL OF PHYSICAL CHEMISTRY

Registered in U. S. Patent Office © Copyright, 1966, by the American Chemical Society

VOLUME 70, NUMBER 2 FEBRUARY 15, 1966

Cryoscopic and Calorimetric Investigations of Betaine and Betaine Hydrochloride

by J. C. Ahluwalia, Frank J. Millero, Robert N. Goldberg, and Loren G. Hepler

*Department of Chemistry, Carnegie Institute of Technology, Pittsburgh, Pennsylvania 15213
(Received September 27, 1965)*

Results of cryoscopic, calorimetric, and conductometric investigations of betaine and betaine hydrochloride in aqueous solution are presented and used in subsequent thermodynamic calculations. For the ionization of aqueous $[(\text{CH}_3)_3\text{N}^+\text{CH}_2\text{COOH}]$ we find $\Delta G^\circ = 2.50 \text{ kcal mole}^{-1}$, $\Delta H^\circ = -0.08 \text{ kcal mole}^{-1}$, $\Delta S^\circ = -8.7 \text{ cal deg}^{-1} \text{ mole}$, and $\Delta C_p^\circ \cong -7 \text{ cal deg}^{-1} \text{ mole}^{-1}$. A new freezing point apparatus utilizing thermistors is described.

Betaine $[(\text{CH}_3)_3\text{N}^+\text{CH}_2\text{COO}^-]$, betaine hydrate $[(\text{CH}_3)_3\text{N}^+\text{CH}_2\text{COO}^- \cdot \text{H}_2\text{O}]$, and betaine hydrochloride $[(\text{CH}_3)_3\text{N}^+\text{CH}_2\text{COOH}]\text{Cl}^-$, abbreviated in this paper to B, $\text{B} \cdot \text{H}_2\text{O}$, and BHCl , respectively, are of interest for a variety of reasons related to the dipolar character of the betaine species and also because of relevance to biological problems. This paper reports results of calorimetric, cryoscopic, and conductance measurements undertaken to provide information about aqueous solutions of these compounds and the heat of hydration of betaine.

Precise measurements of freezing points of aqueous solutions of betaine have yielded activity coefficients of aqueous betaine at $\sim 0^\circ$. Similar measurements on solutions of betaine hydrochloride have yielded the acid ionization constant of $[(\text{CH}_3)_3\text{N}^+\text{CH}_2\text{COOH}]$ (aq), abbreviated to $\text{BH}^+(\text{aq})$, at $\sim 0^\circ$. Calorimetric measurements have yielded the heat of hydration of B(c) and the heat of ionization of $\text{BH}^+(\text{aq})$, both at 25° . Conductance measurements have been made

to obtain the ionization constant of $\text{BH}^+(\text{aq})$ at 25° . These results have been used in several thermodynamic calculations.

Experimental Section

A common method of determining freezing point depressions of solutions is the Beckmann procedure involving cooling curves. Even with the most sensitive temperature measuring device, it is likely that the uncertainties will be more than 0.001° . The difficulties inherent in the Beckmann method can be largely overcome by proper use of the "equilibrium" method that has been developed and applied by Richards, Adams, Harkins, Scatchard, and others. An accuracy of 10^{-5} deg has been claimed for this method, but accuracy of the order of 10^{-4} deg is more usual and corresponds to what we have attained with the apparatus described below.

Although most precise measurements of freezing point depressions have been made with multijunction

thermocouples and a microvolt (μv) potentiometer with high-sensitivity galvanometer, we have used the thermistor bridge circuit shown in Figure 1 with a Rubicon Type B potentiometer and a Leeds and Northrup 9835A amplifier. A few measurements were made with a Wenner potentiometer.

The apparatus itself consists of two identical 450-ml dewars (Fisher Scientific Co. 10-198A), unevacuated and unsilvered. These dewars were suspended by a wooden cover in a 2-l. silvered dewar flask which contained a slurry of ice and salt for cooling purposes. Both dewars were closed with tapered aluminum stoppers that were covered with rubber sleeves to assure snug fits. Three aluminum glide tubes through the stoppers were used for introducing thermistors, stirrers, and a platinum resistance thermometer. The Fisher Scientific Co. 14-515 stirrers were run by Variac-controlled electric motors.

Closely matched thermistors with resistances of 1000 ohms at 25° and a negative temperature coefficient of about 4% were obtained from the Yellow Spring Instrument Co. Each of these thermistors was immersed in silicone oil contained in a 5-mm Pyrex tube. The leads of these thermistors were connected to the legs of a bridge circuit (see Figure 1) by means of shielded wire. A constant current (8.6×10^{-5} amp) through the circuit was maintained by means of two 6-v batteries connected in series and a variable resistor adjusted so that the potential drop across a 1000-ohm resistor was constant as measured by a Rubicon potentiometer.

In all experiments the water and solution were pre-cooled to 0.8° below their respective freezing points, poured into the dewars, and seeded with ice crystals on a spiraled steel wire. The temperature of the bath in which the dewars were suspended was kept about 0.2° below the freezing point of the solution. The solution and pure water were allowed to stand for about 2 hrs to reach equilibrium with ice.

For determination of the relation between measured potential (V) and difference between equilibrium freezing points (Θ) of the solution and pure water we used either of two platinum resistance thermometers, one of which had been calibrated in the Petroleum Research Laboratory at Carnegie Institute of Technology. Measurements with the platinum resistance thermometers were made with a Leeds and Northrup G-2 Mueller bridge and HS galvanometer. It was found that the results of the calibration experiments could be fitted to an equation of the form

$$\Theta = aV + bV^2 \quad (1)$$

The values of a and b in (1) changed slightly with time,

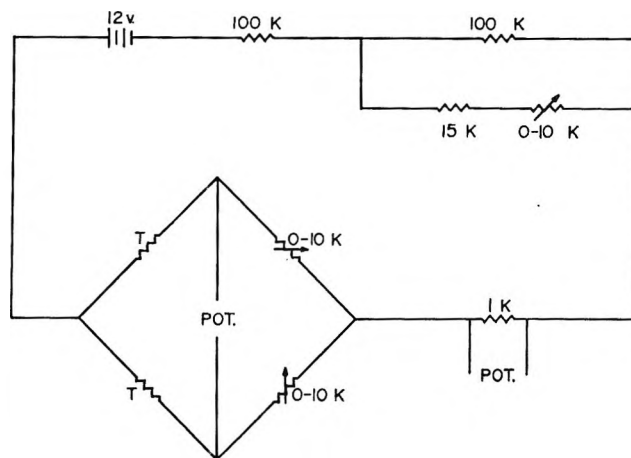


Figure 1. Circuit diagram for apparatus for determination of freezing point depressions. Each T represents a thermistor. One thermistor was immersed in each freezing point cell.

so that the calibration had to be checked periodically. Typical values of a and b were 3.87×10^{-4} and 2.8×10^{-9} , respectively, with V expressed in microvolts. For small temperature changes we thus have a sensitivity of $0.0004^\circ/\mu\text{v}$, compared to the sensitivity of $0.0005^\circ/\mu\text{v}$ obtained by Scatchard and Prentiss¹ with 48 thermocouple junctions.

In application of the equilibrium method of determining freezing point depressions it is necessary to determine the concentration of solute in the solution in equilibrium with ice. Concentrations of KCl and BHCl were determined conductometrically. A Leeds and Northrup Type 4666 Jones bridge with a General Radio Co. Type 1323A tuned amplifier and null detector and Type 1302A oscillator was used for the conductance measurements. A dipping-type conductivity cell was immersed in a bath whose temperature was held constant to within $\pm 0.005^\circ$. The absolute temperature was $298.15 \pm 0.05^\circ\text{K}$.

Because of the slight hydrolysis of betaine, concentrations of reasonably concentrated solutions could be determined conductometrically. Determinations of the same accuracy could be obtained from conventional chemical analysis of equilibrium solutions. For dilute solutions, however, neither conductivities nor chemical analysis for nitrogen yielded adequately determined concentrations. In some of our experiments with dilute solutions we separated the ice from the equilibrium solution immediately after measuring the potential leading to the desired Θ . Since the concentrations and amounts of solutions put into the freezing point dewars were known, determination of

(1) G. Scatchard and S. S. Prentiss, *J. Am. Chem. Soc.*, **55**, 4355 (1933).

the masses of ice formed permitted calculation of the concentrations of the equilibrium solutions. It had also been noted earlier that equilibrium concentrations of all KCl, BHCl, and concentrated betaine solutions were $1.0 \pm 0.3\%$ greater than the concentration of the corresponding initial solution. Concentrations of some of the dilute equilibrium solutions of betaine were obtained from initial concentrations by applying this factor. Concentrations obtained from mass of ice formed as described above were $1.0 \pm 0.2\%$ greater than initial concentrations for dilute solutions of betaine.

In order to test our apparatus, we measured the freezing point depressions (θ) for three solutions about $0.01 m$ and three solutions about $0.10 m$ in KCl and compared our results with those interpolated from the data of Scatchard and Prentiss.¹ For the three $0.01 m$ solutions with $\theta \cong 0.036^\circ$, the largest discrepancy between our results and those of Scatchard and Prentiss was 0.00012° . The average discrepancy amounted to 0.00010° . For the three $0.10 m$ solutions with $\theta \cong 0.348^\circ$, the average discrepancy was 0.0007° . We conclude that uncertainties in our θ values range from 0.0001° for dilute solutions to 0.001° for more concentrated solutions.

The calorimeter used is patterned after one previously described,² except that a Mueller G-2 bridge and HS galvanometer have been used with a nickel wire resistance thermometer for temperature measurements. Also, the resistance thermometer and calibration heater are contained in a glass spiral filled with paraffin oil rather than wound on a silver cylinder. All of the calorimetric work reported here was carried out with 950 ml of water or solution in the calorimetric dewar at $25.0 \pm 0.2^\circ$.

Highest purity betaine hydrate and betaine hydrochloride were obtained from Fisher Scientific Co. Betaine was obtained from K & K Laboratories, Inc. Kjeldahl analysis of the betaine hydrate yielded 99.82% of the theoretical amount of nitrogen. Betaine hydrochloride was analyzed by precipitation of silver chloride and was found to contain 99.84% of the theoretical amount of chloride.

Results and Discussion

The smoothed results of the freezing point depression measurements on solutions of betaine are given in Table I in the form of $j = 1 - \theta/1.860m$, where θ is the freezing point depression, m is the molality, and 1.860 is the value recommended by Pitzer and Brewer.³ The activity coefficients of aqueous betaine have been calculated from the equation

$$-\ln \gamma = j + \int_0^m \frac{j}{m} dm \quad (2)$$

Contributions from higher order terms are negligible for solutions more dilute than $0.5 m$.³ We estimate that uncertainties (mostly due to uncertainties in

Table I: Smoothed j Values and Activity Coefficients for Betaine in Aqueous Solution at 0°

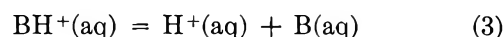
Molality	$-j$	γ
0.005	0.003	1.007
0.010	0.006	1.011
0.025	0.012	1.025
0.050	0.021	1.048
0.075	0.027	1.061
0.100	0.031	1.076
0.200	0.046	1.120
0.300	0.058	1.160
0.400	0.064	1.185

equilibrium concentrations) in our reported γ values range from a maximum of ± 0.03 at $m = 0.4$ to ± 0.01 at $m = 0.1$. The only other activity coefficients for betaine that we know of are those determined isopiastically at 25° by Smith and Smith.⁴

Table II: Freezing Point Depression Data for Betaine Hydrochloride in Water

Moles of BHCl/kg of water	$\theta, ^\circ\text{C}$	$K_2 \times 10^2$
0.0100	0.0486	1.34
0.0200	0.0924	1.51
0.0250	0.1142	1.70
0.0350	0.1544	1.55
0.0500	0.2127	1.39
0.0800	0.3261	1.46

The smoothed freezing point depression data for aqueous solutions of betaine hydrochloride are given in Table II. We interpret these data in terms of the equilibrium constant for the process represented by eq 3



(2) W. F. O'Hara, C. H. Wu, and L. G. Hepler, *J. Chem. Educ.*, **38**, 519 (1961).

(3) G. N. Lewis and M. Randall, "Thermodynamics," 2nd ed, revised by K. S. Pitzer and L. Brewer, McGraw-Hill Book Co., Inc., New York, N. Y., 1961.

(4) P. K. Smith and E. R. B. Smith, *J. Biol. Chem.*, **132**, 57 (1940).

If solutions of betaine hydrochloride were ideal, the freezing point data could be used directly to obtain the degree of dissociation of $\text{BH}^+(\text{aq})$ and thence the desired equilibrium constant. Since total concentrations of $\text{H}^+(\text{aq})$ and $\text{Cl}^-(\text{aq})$ ions in the solutions for which data are given in Table II range from about 0.02 to 0.16 m , we know that the solutions are sufficiently nonideal that the simplest calculation cannot be used.

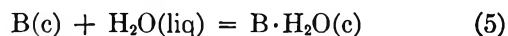
We have calculated values of the equilibrium constant for reaction 3, designated K_3 , from the freezing point depression data in Table II by first assuming that

$$\Theta = 1.860(\text{B}) + \Theta_i \quad (4)$$

The first term on the right of this equation represents the contribution of $\text{B}(\text{aq})$ to the observed freezing point depression (Θ), on the assumption (supported by the results given in Table I) that the behavior of $\text{B}(\text{aq})$ in these very dilute solutions is nearly ideal. Since we know the concentration of $\text{Cl}^-(\text{aq})$ in the solutions, we also know the sum of concentrations of $\text{H}^+(\text{aq})$ and $\text{BH}^+(\text{aq})$. The contribution of all of these ions to the freezing point depression is represented by Θ_i and taken equal to the observed¹ Θ values for $\text{KCl}(\text{aq})$ at the same concentrations. Insertion of appropriate values of Θ and Θ_i in eq 4 permits calculation of the concentration of $\text{B}(\text{aq})$, represented by (B) . We see from (3) that $(\text{B}) = (\text{H}^+)$. Subtraction of (B) values from moles of BHCl/kg gives corresponding (BH^+) values. Now, assuming that the ratio of activity coefficients for H^+ and BH^+ is unity, we calculate K_3 values from the simple relation $(\text{H}^+)(\text{B})/(\text{BH}^+)$ with the results shown in Table II. The average is $K_3 = 1.49$ (av dev = 0.08) $\times 10^{-2}$. We estimate that the total uncertainty in this equilibrium constant is about twice the average deviation and take $K_3 = (1.5 \pm 0.2) \times 10^{-2}$ at 273°K .

Conductivity measurements on solutions of BHCl lead to $K_3 = (1.50 \pm 0.06) \times 10^{-2}$ at 298°K . Earlier work⁵ led to $K_3 = 1.46 \times 10^{-2}$, also at 298°K .

Heats of solution of betaine and betaine hydrate are reported in Tables III and IV. Uncertainties indicated in ΔH° values include estimated contributions from extrapolation to infinite dilution and from possible sample impurities. Combination of these heats yields $\Delta H_5^\circ = -0.58 \pm 0.1$ kcal mole⁻¹ for



Heats of solution of betaine hydrochloride in water are presented in Table V. When crystalline $\text{B} \cdot \text{HCl}$ dissolves in water, processes take place that may be

Table III: Heats of Solution of Betaine Hydrate in Water

Moles of $\text{B} \cdot \text{H}_2\text{O}/950$ ml of H_2O	ΔH , kcal mole ⁻¹
0.00979	1.74
0.01137	1.75
0.01451	1.72
0.01766	1.74
0.02101	1.71
0.02279	1.67
0.03299	1.64
$\Delta H^\circ = 1.76 \pm 0.06$ kcal mole ⁻¹	

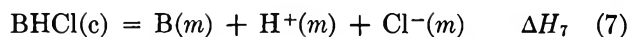
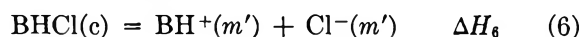
Table IV: Heats of Solution of Betaine in Water

Moles of betaine/950 ml of H_2O	ΔH , kcal mole ⁻¹
0.01819	1.13
0.02504	1.20
0.03159	1.20
$\Delta H^\circ = 1.18 \pm 0.1$ kcal mole ⁻¹	

Table V: Heats of Solution of Betaine Hydrochloride in Water

Moles of $\text{BHCl}/950$ ml of H_2O	ΔH , kcal mole ⁻¹
0.00566	6.23
0.00985	6.23
0.01425	6.22
0.01714	6.23
0.02024	6.21
0.02366	6.20
0.02677	6.20
0.03301	6.19

represented by the following equations in which m and m' indicate concentrations



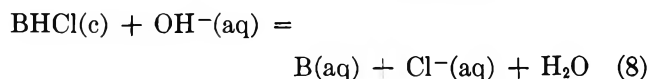
Calculations similar to those carried out earlier⁶ for sulfamic acid permit separation of the total measured ΔH values into ΔH values for reactions 6 and 7. With the assumption that heats of dilution of $(\text{BH}^+ + \text{H}^+) + \text{Cl}^-$ are the same as those⁷ for $\text{H}^+ + \text{Cl}^-$ in dilute solu-

(5) C. A. Grob, E. Renk, and A. Kaiser, *Chem. Ind.* (London), 1222 (1956).

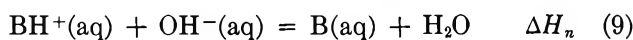
(6) H. P. Hopkins, Jr., C. H. Wu, and L. G. Hepler, *J. Phys. Chem.*, 69, 2244 (1965).

tions (0.005–0.033 *m*), we also obtain standard heats for reactions 6 and 7 for which we report $\Delta H_6^\circ = 6.37$ kcal mole⁻¹ and $\Delta H_7^\circ = 6.28$ kcal mole⁻¹. Subtraction of ΔH_6° from ΔH_7° gives $\Delta H_3^\circ = -0.09$ kcal mole⁻¹ at 298°K for the ionization of BH⁺(aq) shown in (3).

Heats of solution of BHCl(c) into dilute aqueous NaOH are presented in Table VI for the reaction



Combination of the data in Table VI with those in Table V as previously described⁶ leads to the heats of neutralization referring to the process



and reported under ΔH_n in Table VI. In order to obtain a standard heat of neutralization to be represented by ΔH_n° we estimate heats of dilution from known

Table VI: Heats of Solution of Betaine Hydrochloride in 0.0515 *m* NaOH

Moles of BHCl/950 ml of soln	ΔH_s , kcal mole ⁻¹	ΔH_n , kcal mole ⁻¹
0.00892	7.18	-13.38
0.01372	7.24	-13.50
0.01387	7.23	-13.49
0.01432	7.25	-13.53
0.02614	7.20	-13.37

heats for 1:1 electrolytes.⁷ The result is $\Delta H_n^\circ = -13.40$ kcal mole⁻¹. Combination of this value with the heat of ionization of water⁸ gives $\Delta H_3^\circ = -0.06$ kcal mole⁻¹ for the ionization of BH⁺(aq) at 298°K as in (3).

For the heat of ionization of BH⁺(aq) we adopt an average $\Delta H_3^\circ = -0.08$ kcal mole⁻¹ and combine with

$\Delta G_3^\circ = 2.50$ kcal mole⁻¹ from the ionization constant to obtain $\Delta S_3^\circ = -8.7$ cal deg⁻¹ mole⁻¹ for the entropy of ionization of BH⁺(aq) at 298°K according to (3).

Combination of $d\Delta G^\circ/dT = -\Delta S^\circ$ with $d\Delta S^\circ/dT = \Delta C_p^\circ/T$ leads to

$$\Delta C_p^\circ = (\Delta G^\circ_{298} - \Delta G^\circ_{273} + 25\Delta S^\circ_{298}) / (25 + 273 \ln 273/298) \quad (10)$$

Inserting our data for the ionization of BH⁺(aq) as in eq 3 leads to $\Delta C_p^\circ \cong -7$ cal deg⁻¹ mole⁻¹ for this process.

Recent investigations by Ives and Marsden⁹ call renewed attention to the importance of ΔC_p° data for understanding solute–water interactions. These workers and King¹⁰ have pointed out the difficulties and uncertainties associated with calculating ΔC_p° values from equilibrium constants at several temperatures. We suggest that extension of the method employed here to calorimetric determination of heats at several temperatures along with determination of equilibrium constants at several temperatures can reduce the uncertainties in derived ΔC_p° values enough so that it will prove possible to make definite statements about variation of ΔC_p° with temperature.

Acknowledgment. We are grateful to Miss Willis Gelbart for help with the conductivity measurements and to both the National Science Foundation and the National Institutes of Health for financial support of this research.

(7) "Selected Values of Chemical Thermodynamic Properties," National Bureau of Standards Circular 500, U. S. Government Printing Office, Washington, D. C., 1952.

(8) J. Hale, R. M. Izatt, and J. J. Christensen, *J. Phys. Chem.*, **67**, 2605 (1963); C. F. Vanderzee and J. A. Swanson, *ibid.*, **67**, 2608 (1963).

(9) D. J. G. Ives and P. D. Marsden, *J. Chem. Soc.*, 649 (1965).

(10) E. J. King, "Acid-Base Equilibria," Pergamon Press, New York, N. Y., 1965; see especially p 194.

Radiolysis of Binary Mixtures. I. Liquid Phase

Studies with Benzene–Methanol

by A. Ekstrom and J. L. Garnett

*Department of Physical Chemistry, The University of New South Wales, Sydney, Australia
(Received May 18, 1965)*

Addition of small concentrations of benzene to methanol results in a sharp decrease in the radiolysis yields of hydrogen and ethylene glycol. Although this well-known phenomenon is usually interpreted in terms of charge- or energy-transfer mechanisms, the results of this study suggest that free-radical scavenging is of significant importance, scavenging products such as cyclohexadiene, cyclohexadiene–methanol, and anisole being formed as well as a large number of as yet unidentified products of molecular weight as high as 450. The effect of benzene concentration on the yield of the identified scavenging products has been measured. From these data, a reaction scheme has been proposed to account for the formation of the scavenging products.

Introduction

The "protective" effect of benzene on the radiation decomposition of aliphatics has received considerable attention in recent years.^{1–4} As a result of these studies, usually of the cyclohexane–benzene system, it has been customary to attribute the effect to excitation transfer from an excited cyclohexane molecule to benzene, the latter, by virtue of its greater stability, then dissipating the transferred energy without decomposition. Although the role of energy transfer in radiation chemistry appears to be well accepted by some authors,^{5,6} Gaumann⁷ has pointed out that it may still be possible to attribute the drastic effect which benzene has on the radiolysis yield from cyclohexane to radical scavenging rather than energy transfer.

In the benzene–methanol system, the addition of the aromatic to the alcohol results in a decrease in the hydrogen⁸ and glycol⁹ yields similar to the effect of benzene on the hydrogen yield from cyclohexane. Baxendale and Mellows,⁸ who examined the effect of benzene on the hydrogen yield from methanol, attributed the decrease in yields to hydrogen atom scavenging by benzene on the basis that they were able to fit their experimental results to the equation

$$\frac{1}{G_{(0)} - G_{(x)}} = \frac{1}{G(H)} \left[1 + \frac{k_1 (\text{MeOH})}{k_2 (\text{benzene})} \right]$$

which the authors derived from simple scavenging kinetics. ($G_{(0)}$ is the yield of hydrogen from pure methanol and $G_{(x)}$ is yield of hydrogen from methanol–benzene solutions, corrected for the energy absorbed by methanol only, $G(H)$ is the yield of H atoms in pure methanol, k_1 and k_2 are constants.) A similar equation has been used by Hardwick¹⁰ in his work on the reactivity of hydrogen atoms with a variety of compounds. However, an equation of similar form can also be derived from consideration of an energy transfer mechanism,¹¹ hence it is difficult to differentiate between the two mechanisms on this basis alone.

In the present investigation,¹² the radiolysis yields

- (1) J. P. Manion and M. Burton, *J. Phys. Chem.*, **56**, 560 (1952).
- (2) G. R. Freeman, *J. Chem. Phys.*, **33**, 71 (1960).
- (3) B. R. Wakeford and G. R. Freeman, *J. Phys. Chem.*, **68**, 2992 (1964).
- (4) J. F. Merklin and S. Lipsky, *ibid.*, **68**, 3297 (1964).
- (5) M. Burton and S. Lipsky, *ibid.*, **61**, 1461 (1957).
- (6) V. A. Krongauz, *Russ. Chem. Rev.*, **31**, 113 (1962).
- (7) T. Gaumann, *Helv. Chim. Acta*, **44**, 1337 (1961).
- (8) J. H. Baxendale and F. W. Mellows, *J. Am. Chem. Soc.*, **83**, 4720 (1961).
- (9) W. G. Brown and M. K. Eberhardt, "Radiolysis of Liquid Methanol. Inhibitory Effects of Additives," ARL Report 90, Contract No. AF33(616)-3875, The University of Chicago, 1961.
- (10) T. J. Hardwick, *J. Phys. Chem.*, **64**, 1623 (1960).
- (11) J. G. Burr, *Nuclear.ics*, **19**, 49 (1961).

from benzene-methanol solutions have been examined with particular emphasis on the detection and measurement of the yields of scavenging products, in an attempt to evaluate the significance of a radical scavenging mechanism and to compare the results obtained in this study with those reported by Gaumann⁷ for the radiolysis of benzene-cyclohexane mixtures. The methanol system is particularly important since this compound is more polar than cyclohexane which has already been extensively studied, and the results may permit further generalizations with respect to the radiation chemistry of binary mixtures.

Experimental Section

Purification of Materials. BDH methanol was distilled once using a 2-m fractionating column. The middle 80% was dried with sodium metal and again distilled under anhydrous conditions. The middle 80% was then refluxed with 2,4-dinitrophenylhydrazine-sulfuric acid using the above column, methanol being withdrawn from the still head as required.

Analytical reagent grade benzene was purified by three successive recrystallizations, dried with sodium, and distilled prior to use under anhydrous conditions. All other materials were reagent grade and purified by distillation or recrystallization where necessary.

Preparation of Samples. Solutions of benzene and methanol were made up volumetrically and 5-ml samples were transferred to Pyrex irradiation tubes (0.95 cm \times 15 cm). These were attached to a high-vacuum system and outgassed by three successive freeze-thaw cycles. For gaseous product analysis, irradiation ampoules were fitted with break-seals.

Irradiations. Irradiations were carried out in a cobalt-60 source which gave a variety of dose rates. Two Fricke dosimeters were included in each irradiation.

Analysis of Products. Gaseous products were removed from the irradiated samples using the microstill method¹³ and compressed by means of a Toepler pump into a calibrated volume where the pressure and temperature were measured. The composition of the gaseous yield was then determined by mass spectrometry (Metropolitan Vickers, MS-2G) calibrated with standard samples. Ethylene glycol was estimated by reaction with periodic acid according to the method of Jackson.¹⁴ The radiolysis products, anisole, cyclohexadiene-methanol, phenylcyclohexadiene, and biphenyl, were determined by gas chromatography (Perkin-Elmer 800) using a 2-m 1.5% silicone gum SE30 on Chromosorb column, operated at various temperatures. $G(-\text{benzene})$ and the cyclohexadiene isomers were determined on the same

instrument using a 5% β,β' -oxydipropionitrile column operated at 60°.

Results

A great deal of controversy exists as to the correct values of the radiolysis yields from pure methanol.¹⁵ Although some of the variations in yield can probably be traced to impure methanol, preliminary evidence indicates that the total dose affects the radiolysis yield. In the present investigation reproducible results could be obtained under constant conditions of dose, dose rate, and methanol purification.

Figure 1 shows the effect of benzene concentration on the radiolysis yield of hydrogen and ethylene glycol from methanol, the yields showing the characteristic sharp decrease at low benzene concentrations followed by a less pronounced decrease in the region 20-100% by volume benzene. This behavior is similar to the effect of benzene on the hydrogen yield from cyclohexane¹ and agrees well with the effect of benzene on the hydrogen yield from methanol previously reported.⁸

A typical temperature-programmed gas chromatogram of an irradiated solution of benzene in methanol is shown in Figure 2. Peaks 1, 2, 3, 4, 8, 9, and 10 appear also in pure irradiated benzene but not in irradiated methanol and are therefore radiolysis products of benzene. Similarly, peaks 5, 6, and 11 appear only in irradiated solutions of benzene in methanol and are therefore scavenging products. Peaks 1, 2, 3, and 4 have not yet been identified. Peak 5 was identified as anisole, peak 6 occurring just prior to benzyl alcohol (see inset Figure 2) was isolated by preparative gas chromatography and was shown (nmr, ultraviolet, and infrared) to consist of cyclohexadiene-methanol isomers. No benzyl alcohol could be detected. The retention of peak 8 occurring just prior to biphenyl (peak 9) is consistent with that of hydrogenated biphenyl (possibly a mixture of 2,4- and 2,5-phenylcyclohexadiene) also reported by Gaumann.⁷ Peak 10, although not positively identified, may be cyclohexadiene-dimethanol. Two additional products, 1,3- and 1,4-dicyclohexadiene have also been identified using a β,β' -oxydipropionitrile column. These have previously been detected in pure irradiated benzene,¹⁶ but have not been reported in benzene solutions.

Figure 3 shows the effect of benzene concentration

(12) A preliminary communication of this work has been published A. Ekstrom and J. L. Garnett, *J. Am. Chem. Soc.*, **86**, 5028 (1964).

(13) W. van Dusen and W. H. Hamill, *ibid.*, **84**, 3648 (1962).

(14) E. L. Jackson, *Org. Reactions*, **2**, 341 (1944).

(15) M. Imamura, S. U. Choi, and N. N. Lichtin, *J. Am. Chem. Soc.*, **85**, 3565 (1963).

(16) M. K. Eberhardt, *J. Phys. Chem.*, **67**, 2856 (1963).

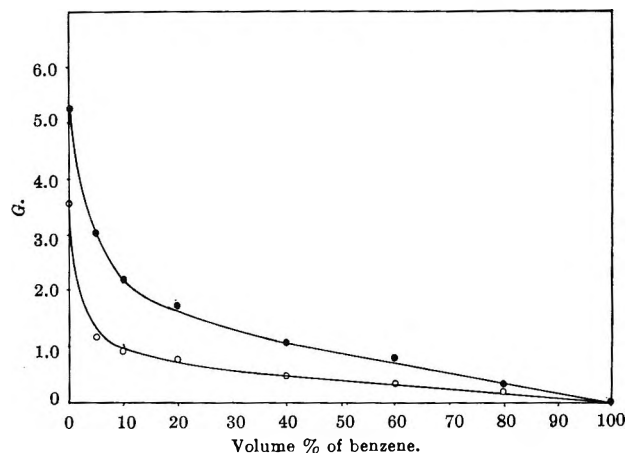


Figure 1. Effect of benzene on the yield of hydrogen and ethylene glycol. Dose, 10^7 rads; dose rate, 2×10^5 rads/hr; O, ethylene glycol; ●, hydrogen.

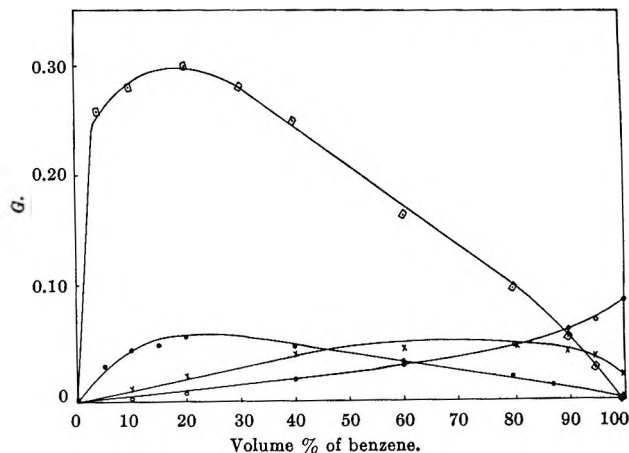


Figure 3. Benzene concentration dependency of some identified scavenging products. Dose, 10^7 rads; dose rate, 2×10^5 rads/hr; □, cyclohexadiene-methanol; ●, anisole; X, phenylcyclohexadiene; O, biphenyl.

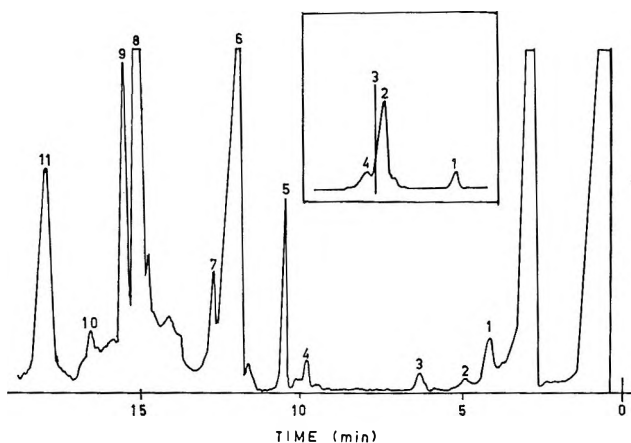


Figure 2. Typical temperature-programmed ($25^\circ/\text{min}$) gas chromatogram of an irradiated solution of benzene in methanol. Inset: constant temperature gas chromatogram showing anisole (1), cyclohexadiene-methanol (2), and the expected retention time of benzyl alcohol (3). Peak 4 has not yet been identified.

on the yield of some of the identified scavenging products. The benzene concentration dependency of cyclohexadiene-methanol and anisole is very similar to that observed by Gaumann⁷ for the yield of phenylcyclohexane from the cyclohexane-benzene system. The yield of the hydrogenated biphenyls is increased by the addition of small concentrations of methanol to benzene, a maximum being reached at approximately 80% by volume of benzene, while the yield of biphenyl is decreased continuously by the addition of methanol, the behavior also being similar to the effect of cyclohexane on the yield of biphenyl from benzene.⁷

Figure 4 shows the effect of benzene concentration on the yield of the 1,4-cyclohexadiene isomer. In agreement with Eberhardt,¹⁶ the 1,4- isomer was found

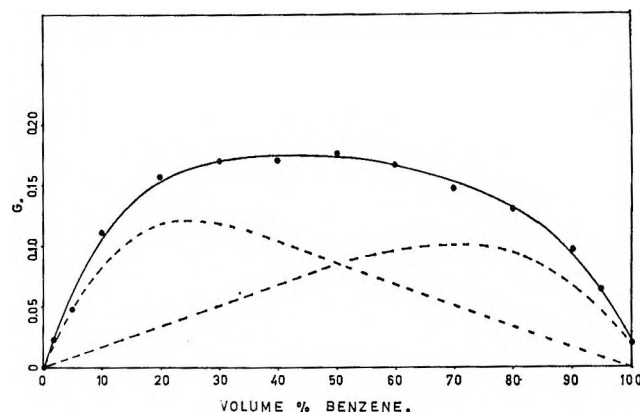


Figure 4. Benzene concentration dependency of 1,4-cyclohexadiene. Dose, 2×10^7 rads; dose rate, 6.5×10^5 rads/hr.

to be preferentially formed in both pure benzene and benzene-methanol solutions. The effect of benzene concentration on the yield of this product is clearly different from that of cyclohexadiene-methanol and phenylcyclohexadiene, a maximum concentration being reached at 50% by volume of benzene. This behavior can probably best be interpreted in terms of two mechanisms operating simultaneously, one resulting in a benzene concentration dependency similar to the cyclohexadiene-methanol, the other resulting in the benzene concentration dependency similar to that observed for phenylcyclohexadiene. These are indicated by the broken lines in Figure 4.

Figure 5 shows the effect of low concentrations of benzene on the hydrogen and glycol yields from methanol, while Figure 6 shows the effect of benzene concentration on the yield of cyclohexadiene-methanol

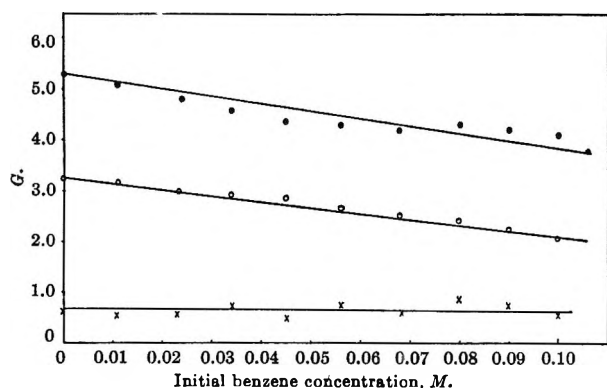


Figure 5. Effect of low concentrations of benzene on the glycol, hydrogen, and methylene glycol yields from methanol. Dose, 10^7 rads; dose rate, 2×10^6 rads/hr; ●, hydrogen; ○, ethylene glycol; ×, methylene glycol.

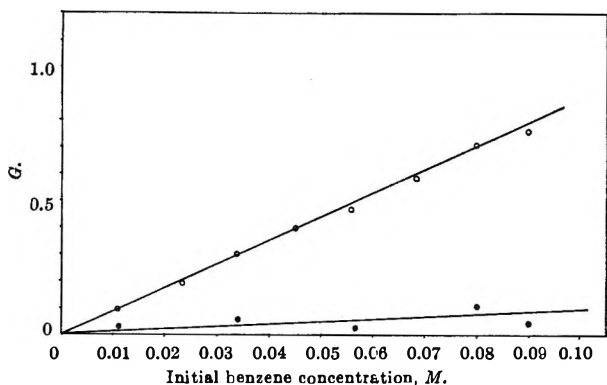


Figure 6. Effect of low benzene concentrations on the yield of cyclohexadiene-methanol and $G(-\text{benzene})$. Dose, 10^7 rads; dose rate, 2×10^6 rads/hr; ○, $G(-\text{benzene})$; ●, cyclohexadiene-methanol.

and $G(-\text{benzene})$ over the same initial benzene concentration range. The corresponding data for the decrease in yield of hydrogen and ethylene glycol per molecule of benzene decomposed are shown in Table I.

The results indicate that for each molecule of benzene decomposed, the total yield of hydrogen and ethylene glycol is decreased by approximately three molecules. Although the cyclohexadiene-methanol was the only scavenging product formed in sufficient concentration for a reliable determination of the yield over the benzene concentration concentration range of up to 10^{-1} M, the results of Figure 6 show that since $G(-\text{benzene})$ is much larger than $G(\text{cyclohexadiene-methanol})$, other scavenging products are also formed. However, as will be discussed in a later section of the manuscript, an unequivocal interpretation in terms of radical scavenging is not possible at this time. In this respect it is significant that a large number of radiolysis products are observed in the mass spectrometric assay of these irradiated solu-

Table I: Effect of Low Concentrations of Benzene on the Yield of Methanol Radiolysis Products

Initial benzene concentration, $M \times 10^2$	$G(\text{glycol})$	$G(\text{H}_2)$	$G(-\text{benzene})$	$[\Delta G(\text{H}_2) + \Delta G(\text{glycol})] / G(-\text{benzene})$
11.2	2.02	3.8	1.0	2.72
10.1	2.08	4.1	0.90	2.62
9.0	2.25	4.2	0.78	2.68
7.9	2.42	4.3	0.70	2.60
6.8	2.52	4.2	0.59	3.08
5.6	2.66	4.3	0.49	3.20
4.5	2.84	4.4	0.40	3.20
3.4	2.90	4.6	0.30	3.12
2.3	2.96	4.8	0.20	3.90
1.1	3.20	5.1	0.10	2.20
0.0	3.24	5.3	0.00	0.00

tions. Thus the mass spectrum of irradiated pure benzene ceases at m/e 310 and shows peaks attributable to bi- (m/e 154), ter- (m/e 230), and quaterphenyls (m/e 306) and their hydrogenated isomers. By contrast, the spectra of irradiated methanol-benzene solutions exhibit a large number of additional peaks extending to m/e 500 even at low concentrations of benzene. Although the complexity of the spectra makes them unsuitable for accurate identification of the products, it is obvious that even if allowance is made for fragmentation patterns, a large number of products of low yield are formed. The data also indicate that, on the average, each benzene molecule is capable of scavenging a number of free radicals. This aspect of the mass spectra interpretation is important and will be referred to again in the Discussion. The present mass spectral results would also explain the lack of material balance observed between $G(-\text{benzene})$ and $G(\text{cyclohexadiene-methanol})$ in solutions containing 1% benzene by volume and demonstrates the difficulty encountered in attempting to fit the experimental results to equations derived from simple scavenging kinetics.¹⁷

Discussion

Although it has not been possible to show conclusively that the decrease in radiolysis yield from methanol in the presence of benzene is due exclusively to radical scavenging (this can only be done by demonstrating a mass balance between the decrease in radiolysis yield and the yield of scavenging products at a given initial benzene concentration), the number and variety of the scavenging products formed strongly suggest

(17) C. E. Klots, Y. Raef, and R. H. Johnson, *J. Phys. Chem.*, **68**, 2040 (1964).

that radical scavenging mechanisms are of significant importance when accounting for the drastic effect of benzene on the radiolysis yield from methanol. In general, there is considerable controversy as to the degree to which the observed decrease in the radiolysis yield from a solvent upon addition of benzene is due to radical, and in particular hydrogen atom scavenging. Thus, while some authors^{2,7,18} have indicated the importance of radical scavenging, the results of Dyne and co-workers¹⁹ and Merklin and Lipsky²⁰ appear to indicate that the yield of H atoms in irradiated cyclohexane is low and that consequently hydrogen atom scavenging by benzene cannot be responsible to any marked degree for the decrease in hydrogen yield.

Despite the obvious similarity between the effect of benzene on the hydrogen yield from methanol (Figure 1) and the effect of benzene on the hydrogen yield from cyclohexane,¹ the nature and the benzene concentration dependency of the scavenging products cyclohexadiene, cyclohexadiene-methanol, and anisole formed during radiolysis of methanol-benzene solutions are difficult to interpret unless free-radical additions to benzene are involved, particularly since a recent electron spin resonance study with irradiated methanol²¹ has indicated the presence of both the CH_2OH and OCH_3 radicals.

The results obtained at low concentrations of benzene ($<0.1 M$) suggest that the total yield $\Delta G(\text{H}_2) + \Delta G(\text{ethylene glycol})$ is reduced by approximately three molecules for each molecule of benzene decomposed. This apparently high value may still be the result of a radical scavenging mechanism if it is postulated that the greater part of the hydrogen and ethylene glycol yields are formed according to reactions 1-3 in pure methanol.

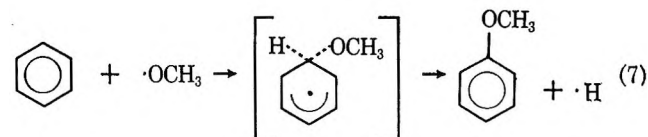
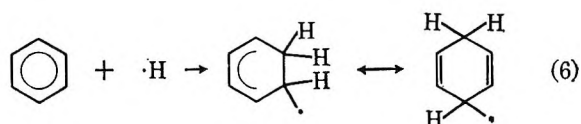
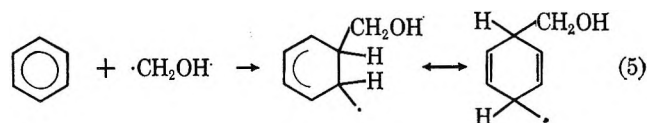
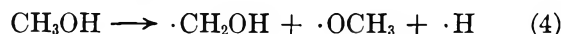


Thus if each benzene molecule on the average scavenges two H atoms formed according to reaction 1, the total yield will be reduced by two hydrogen molecules and one molecule of $(\text{CH}_2\text{OH})_2$. Alternatively, if a benzene molecule scavenges on the average one hydrogen atom and one CH_2OH radical, the total yield of hydrogen and ethylene glycol will be reduced by one molecule of hydrogen and one molecule of $(\text{CH}_2\text{OH})_2$. It would thus appear that if a multiple radical scavenging mechanism by benzene is postulated, the results obtained are consistent with a general radical scavenging mechanism. This interpretation is also supported by the results recently reported by Burr,²²

who showed that in the radiolysis of the cyclohexane-benzene system, two or three hydrogen atoms from the cyclohexane are added to each molecule of benzene or its polymer. The mass spectral data from the present study also confirm the postulate that each benzene molecule scavenges more than one radical.

The benzene concentration dependency of the scavenging yields suggests that two groups of scavenging mechanisms operate. Group I achieves a maximum yield at $\sim 15\%$ by volume of benzene, while group II reaches a maximum at $\sim 80\%$ by volume of benzene. An intermediate case is that of the cyclohexadiene yield; however, it has already been shown that the curve obtained for this product can be the result of the above two mechanisms operating simultaneously. It is suggested that group I is the result of reactions occurring between radicals derived from methanol reacting with benzene molecules, while group II is due to radicals derived from benzene reacting with benzene or with methanol molecules.

The formation of anisole as a scavenging product but the apparent absence of benzyl alcohol implies that a further distinction may be made in the mode of formation of the scavenging products constituting group I, the methoxy radical apparently reacting with benzene by hydrogen atom displacement while the $\cdot\text{CH}_2\text{OH}$ radicals and hydrogen atoms react by addition to a benzene double bond, resulting in a cyclohexadienyl radical intermediate. The following reaction scheme is suggested to account for the formation of the scavenging products comprising group I.



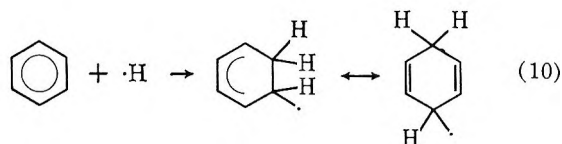
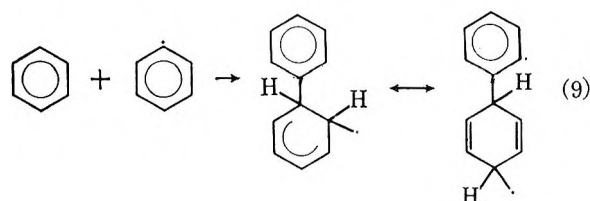
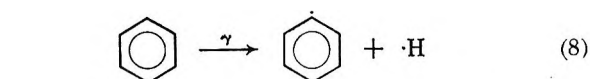
(18) H. A. Dewhurst, *J. Phys. Chem.*, **63**, 812 (1959).

(19) P. J. Dyne and W. M. Jenkinson, *Can. J. Chem.*, **39**, 2163 (1962).

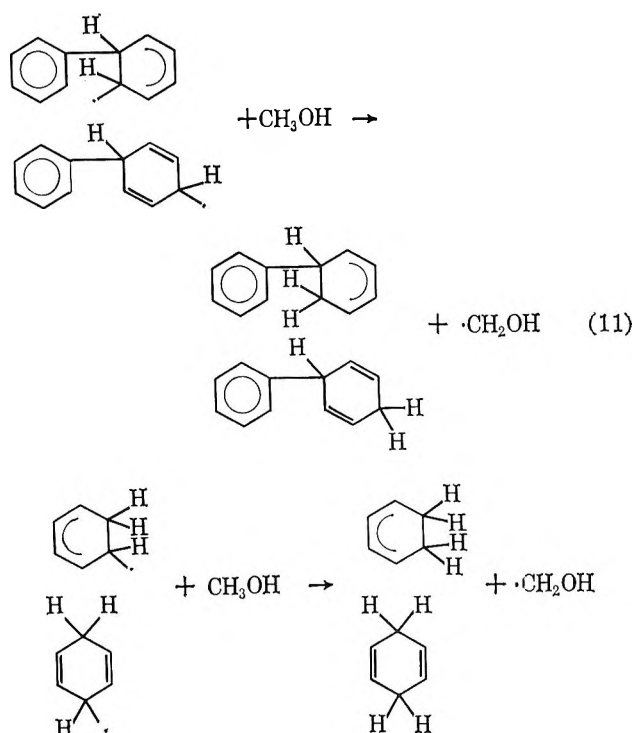
(20) J. F. Merklin and S. Lipsky, "Biological Effects of Ionizing Radiation at the Molecular Level," International Atomic Energy Agency, Vienna, Austria, 1962, p 73.

The formation of the cyclohexadienyl radical intermediate has been suggested on numerous occasions in conventional radical reactions involving benzene²³ and has been proposed by Eterhardt¹⁶ to account for the formation of the cyclohexadiene in the radiolysis of pure benzene. A recent electron spin resonance study of irradiated benzene²⁴ has also been interpreted in terms of this species. Once the cyclohexadienyl or cyclohexadienyl-methanol radicals have been formed, these may (i) react with another H atom or $\cdot\text{CH}_2\text{OH}$ radical to yield cyclohexadiene, cyclohexadiene-methanol, or cyclohexadiene-dimethanol; (ii) abstract a hydrogen atom from methanol to give cyclohexadiene or cyclohexadiene-methanol; or (iii) react with another benzene molecule or cyclohexadienyl radical to give dimeric species. At low percentages of benzene where the concentration of radicals derived from methanol is still relatively high, (i) and (ii) probably predominate. As the concentration of benzene increases reaction iii will become increasingly important.

The second group of scavenging products, *i.e.*, those reaching a maximum at $\sim 80\%$ by volume of benzene, include phenylcyclohexadiene and part of the cyclohexadiene yield, both of which are formed in pure benzene, but are increased by the addition of small amounts of methanol. Radiolysis of benzene containing small concentrations of methanol will result in the preponderance of radicals derived from benzene rather than methanol. In pure benzene these radicals will react with each other or with benzene molecules according to reactions 8-10. These reactions will result in the formation of either the cyclohexadienyl or phenylcyclohexadienyl radicals, both of which can then react with another benzene molecule or with each other to give polymeric species. However, in order to yield cyclohexadiene and phenylcyclohexadiene each of the above two radicals requires another H atom



for which in pure benzene these radicals have to compete with benzene molecules (reaction 10). On the addition of small concentrations of methanol, both the cyclohexadienyl and phenylcyclohexadienyl radicals can obtain the additional hydrogen atom by abstraction from methanol (reaction 11). Hence the addition of small concentrations of methanol to benzene results in an additional mechanism for the formation of the cyclohexadienes and hence yields the observed increase in these products.



It should be mentioned that the above reaction scheme is intended to outline the mechanism of the formation of the simple cyclohexadienyl derivatives only. In order to account satisfactorily for the high molecular weight scavenging products indicated by the mass spectral studies, it is apparent that further radical additions to the cyclohexadienyl and phenylcyclohexadienyl derivatives would be expected to occur.

(21) P. J. Sullivan and W. S. Koski, *J. Am. Chem. Soc.*, **85**, 384 (1963).

(22) J. G. Burr, *Discussions Faraday Soc.*, **27**, 271 (1963); J. Y. Yang, B. Scott, and J. G. Burr, *J. Phys. Chem.*, **68**, 2014 (1964).

(23) C. Walling, "Free Radicals in Solution," John Wiley and Sons, Inc., New York, N. Y., 1957.

(24) S. Ohnishi, T. Tanei, and I. Nitta, *J. Chem. Phys.*, **37**, 2402 (1962).

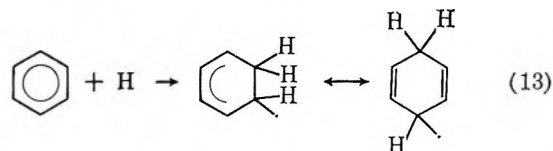
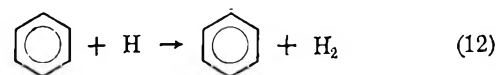
Examination of the effect of benzene concentration on hydrogen and ethylene glycol yields from methanol (Figure 1) shows that the yields of both hydrogen and ethylene glycol are sharply decreased in the region 0–10% by volume of benzene, followed by the region 10–100% by volume of benzene in which the yields of both products are reduced much more slowly. This behavior is commonly interpreted as evidence for two precursors to the yields of both hydrogen and ethylene glycol, one of which is rapidly removed by the addition of small concentrations of benzene, while the other is affected to a much lesser degree by benzene.

This conclusion can be further demonstrated if the present data are plotted according to the scavenging equation proposed by Baxendale and Mellows.¹⁸ The results are in reasonable agreement with those reported by these authors within the limitations imposed by the extrapolation technique.¹⁷

While the yield of hydrogen apparently only slightly affected by benzene has been interpreted in terms of a molecular yield, it is obviously not possible to apply this concept to the yield of glycol which is not affected by benzene. Attempts have been made to attribute this apparently unscavengeable yield to ion-molecule and "hot" atom processes. However the following alternative interpretation of these so-called molecular yields should also be considered.

In the high additive concentration range, the yields of products apparently characteristic of the solvent (*e.g.*, ethylene glycol from methanol) are greater than expected from the extrapolation of the curve for the effect of low concentration of benzene on this product. In the analysis of the scavenging plots no distinction is commonly made between the mechanisms of the radiolysis at high and low concentrations of benzene, although it would be expected that at high concentrations of benzene the radiolysis is dominated by the radiation chemistry of benzene, and that consequently the majority of the reactive species are derived from benzene. Alternatively, radiolysis of dilute solutions of benzene in a solvent will be dominated by the radiation chemistry of the solvent and the majority of the reactive species will be derived from the solvent.

Consider, for example, the fate of a hydrogen atom formed during radiolysis of pure benzene. It is postulated that this hydrogen atom can undergo the possible reactions shown in eq 12 and 13. As the yields of the partially hydrogenated products are greater than the yields of hydrogen,⁷ it would appear that reaction 13 is greatly favored over reaction 12. However, in order to yield H₂, the hydrogen atom



formed during radiolysis of benzene must acquire another hydrogen atom, which in the radiolysis of pure benzene it can obtain according to reaction 12 which must compete with reaction 13. (While it has been postulated that the hydrogen yield from the radiolysis of pure benzene is largely molecular in origin, the data from e.s.r. studies of irradiated benzene all indicate the formation of the cyclohexadienyl radical, which in turn is attributed to the addition of a H atom to a benzene molecule.^{24,25}) On addition of methanol a further mechanism for the formation of hydrogen from a hydrogen atom can occur



with the result that the hydrogen yield will be greater than expected from the direct action of radiation on the individual components of the solution only.

Similarly, reactions 11 and 14 result in the formation of a CH₂OH radical²⁶ for each hydrogen atom abstracted from methanol and consequently the over-all concentration of CH₂OH radicals will be greater than expected from the direct action of radiation on methanol only, leading to a greater probability of CH₂OH radical dimerization.

Alternatively, the radicals formed on radiolysis of methanol containing small concentrations of benzene will be derived from methanol, and consequently abstraction reactions such as (11) will be relatively unimportant as a source of ·CH₂OH radicals.

Acknowledgment. The authors gratefully acknowledge the support of the Australian Atomic Energy Commission which granted study leave and financial assistance to A. E., the Australian Institute of Nuclear Science and Engineering which financed the irradiations, Mr. W. Whithers, J. Mason, and B. O'Leary for technical assistance, and Associated Electrical Industries Ltd. for performing the high resolution mass spectrometry on a Metropolitan Vickers MS9 instrument.

(25) M. Cher, *J. Phys. Chem.*, **67**, 605 (1963).

(26) S. Gordon and M. Burton, *Discussions Faraday Soc.*, **12**, 88 (1952).

Vapor Pressure Measurements and a Structural Interpretation in the Liquid System Rubidium Monoxide-Boron Oxide

by C. E. Adams and J. T. Quan

U. S. Naval Radiological Defense Laboratory, San Francisco, California 94135 (Received April 7, 1965)

By use of the transpiration method, the vapor pressures of the liquid system $\text{Rb}_2\text{O}-\text{B}_2\text{O}_3$ between pure B_2O_3 and $\text{Rb}_2\text{O}\cdot\text{B}_2\text{O}_3$ have been measured. The vapor over the entire composition range was an equimolar mixture of Rb_2O and B_2O_3 . Data from other sources indicate that the vapor molecule should be RbBO_2 . The activity of the RbBO_2 in the melts showed a pronounced discontinuity at about 16 mole % Rb_2O . The activity of the RbBO_2 in the melts could be decreased by the addition to the melts of oxygen-complexing cations.

Introduction

The properties and molecular structures of alkali borates have stimulated much interest since the early theory of Biscoe and Warren¹ regarding the "boron oxide anomaly."

The boron oxide anomaly refers to abrupt changes in many of the physical properties of alkali borate glasses and melts which occur at certain concentrations of alkali oxides. There has been much controversy over the nature of the changes in molecular structure of the glasses or melts which are presumed to cause the boron oxide anomaly.

As part of a continuing program devoted to studying vapor-liquid reactions in oxide systems, a study of the composition and pressure of the vapor over melts of the $\text{Rb}_2\text{O}-\text{B}_2\text{O}_3$ system as a function of temperature and melt composition was undertaken. It was anticipated that the information obtained would help in reconciling the divergent points of view regarding the structure of alkali borates.

Experimental Section

Apparatus. The transpiration method was used for the determination of the vapor pressures. The apparatus consisted essentially of a furnace chamber into which a removable alumina tube containing the sample was inserted (Figure 1). The furnace was heated inductively through power supplied by an Ajax 20-kw. spark-gap converter. A cylindrical graphite crucible packed in powdered graphite insulation was

used as a susceptor. The graphite susceptor was protected from oxidation by being lined on the interior with a dense, high-purity alumina crucible and lid. Two openings into the furnace chamber were provided. One was a fixed alumina tube on whose outer end were a window and an air inlet. The furnace temperature was determined by sighting a Leeds and Northrup optical pyrometer through the window; dry air was introduced through the inlet in order to keep the window clean and to maintain an oxidizing atmosphere in the furnace chamber. The second opening consisted of an open alumina tube through which a dense, gastight alumina sample tube could be inserted into the furnace chamber. The dense alumina parts were obtained from the McDanel Refractory Porcelain Co.

Into that end of the sample tube which entered the furnace chamber was cemented a platinum capsule which contained the sample whose vapor pressure was to be measured. On the outer end of the sample tube was a window for optical pyrometer readings and an inlet where the carrier gas was introduced.

It was necessary that the sample capsule be made of platinum as rubidium vapor can form a thermally stable compound with alumina. The capsule consisted of a platinum cylinder about 1 cm. in diameter and 3.5 cm. long. One end of the cylinder was completely closed except for a hole about 0.5 mm. in diam-

(1) J. Biscoe and B. E. Warren, *J. Am. Ceram. Soc.*, **21**, 287 (1938).

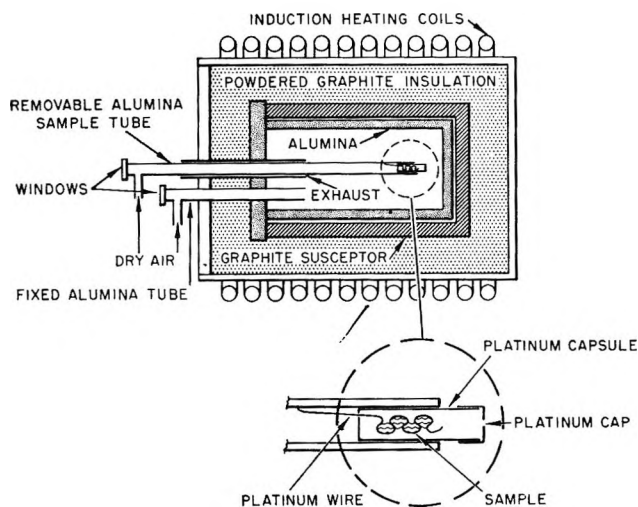


Figure 1. Schematic drawing of high-temperature vapor pressure apparatus.

eter which served as the inlet for the carrier gas. The other end of the cylinder was open. A close-fitting platinum cap in the shape of a cylinder was made to fit over the open end of the capsule. The cap was provided with a 0.5-mm. hole in its end for the outlet of the carrier gas.

The sample itself was fused onto a series of four adjacent loops bent in the end of a platinum wire. The platinum wire sample holder was secured in the capsule by passing the straight end of the wire through the hole behind the capsule for a distance of about 3 cm. so that it rested against the interior top of the alumina sample tube. The loops of wire containing the sample were then balanced in the center of the capsule. The wire was not large enough to block the carrier gas entry hole completely. The platinum cap then could be placed over the end of the capsule, and the whole assembly was inserted into the furnace.

It was found that the sample, about 100 mg. in weight when melted, did not drop off the platinum wire loops. This arrangement was chosen because the rubidium content of the sample was to be determined by radioactive counting, and it was planned to insert the whole sample into a crystal γ counter. Also, a large area of the sample could be exposed, thereby making a saturated vapor pressure easier to maintain during the experimental runs.

During the runs, the temperature of the sample was determined by sighting an optical pyrometer through the window of the alumina sample tube onto the end of the platinum capsule. Previous measurements had shown that the temperature read off the back of the capsule was the same as that read by sighting through the gas inlet hole into the interior of the capsule,

where blackbody conditions prevailed. A correction for absorption in the window was applied. The optical pyrometer was calibrated by comparison with an NBS calibrated ribbon filament lamp at the Navy Standards Laboratory, Pomona, Calif. By manual adjustments of the temperature control, the temperature of the sample was kept constant to within about ± 1 to 2° .

During the runs, a measured amount of constantly flowing dry air had to be supplied through the alumina sample tube to act as the carrier gas. To accomplish this, two 1000-ml. burets were mounted in parallel so that a measured volume of air could be forced from the burets into the sample tube by the injection of a stream of silicone oil into the burets. The oil was introduced into the burets by siphoning from a Mariotte bottle, thus maintaining a steady flow during the run. The volume of air displaced was determined by reading the oil level in the burets before and after each run. The air was dried by passage through anhydrous magnesium perchlorate before it was admitted to the burets and also as it left. The temperature of the air in the burets was determined by means of a mercury thermometer.

Preparation of Samples. The $\text{Rb}_2\text{O}-\text{B}_2\text{O}_3$ samples were prepared by fusing radioactive Rb_2CO_3 and B_2O_3 together in a platinum dish. The Rb_2CO_3 was obtained from A. D. Mackay, Inc., and from K & K Laboratories, Inc. The Rb_2CO_3 was purified by dissolving it in water, filtering it, and recrystallizing it by evaporation. The purity was then checked spectroscopically, and negligible amounts of impurities were found.

Radioactive rubidium in tracer amounts was introduced into the carbonate by the use of radioactive Rb^{86}Cl supplied by Oak Ridge National Laboratory. The radioactive RbCl , in HCl solution, was evaporated to dryness in a platinum dish. The Rb_2CO_3 was dissolved in water and added to the radioactive RbCl in the platinum dish, and the solution was stirred well. The solution was then evaporated to dryness, and the radioactive Rb_2CO_3 was recovered and dried thoroughly. A negligible amount of chloride was introduced into the carbonate by this process.

The B_2O_3 was prepared by the dehydration of reagent grade boric acid obtained from J. T. Baker Chemical Co. The B_2O_3 was dried by heating in a platinum dish in air for several hours at 1000° .

Weighed amounts of boron oxide and radioactive Rb_2CO_3 were fused together in a platinum dish and stirred well. The resulting $\text{Rb}_2\text{O}-\text{B}_2\text{O}_3$ mixture was left in the platinum dish and stored in a desiccator. Samples were removed by remelting the solution and dipping into the melt with a platinum wire. The

liquid sample drops were quickly transferred to the loops on the platinum sample wire. The final composition of two of the $\text{Rb}_2\text{O}-\text{B}_2\text{O}_3$ mixtures were determined by wet chemical analysis and were found to be equal, within experimental error, to the compositions computed using the batch weights of the initial components.

In order to remove completely all interfering traces of water, it was necessary to reheat the B_2O_3 samples on the platinum sample holder before weighing and inserting into the furnace chamber. This was done by mounting the platinum sample wires holding the B_2O_3 onto the end of an alumina rod and inserting the sample through a port into a furnace. There they were further dried for about 2 hr. at 1000° . As the melts became richer in Rb_2O the water was less tenaciously held and a less rigorous dehydration procedure was required. The mixture of 50% $\text{Rb}_2\text{O}-50\%$ B_2O_3 dried easily at 600° for 0.5 hr. Because of the pronounced hygroscopicity of the carbonate and borates, all materials and samples were weighed in a drybox.

Treatment of Experimental Data. The transpiration method of measuring vapor pressure relies on a determination of the moles of sample vapor per unit volume of carrier gas-sample vapor mixture. Assuming that the ideal gas law holds, then

$$P_s = \frac{n_s}{V}RT \quad (1)$$

where P_s is the partial pressure of the sample, V is the total volume of the carrier gas-sample vapor mixture and can be approximated by the volume of the carrier gas when the volume of the sample vapor is small, T is the temperature at which V is measured, and n_s is the number of moles of sample vapor in V .

In using the transpiration method, it is necessary to have the flow of carrier gas fast enough so that diffusion losses of the sample vapor are negligible compared with the amount of vapor entrained by the carrier gas. However, it is also necessary to avoid using such a high flow rate that the carrier gas is undersaturated with sample vapor. If the experimental conditions are properly chosen, the plot of sample vapor mass carried off per unit time against carrier gas flow rate for a series of runs at constant temperature will give a straight line whose extrapolation to zero flow rate will pass through the origin.²

In the method used here, the samples were mounted in the platinum capsule, and the alumina sample tube was inserted into the furnace and allowed to remain a few minutes so that the samples could reach thermal equilibrium with the furnace before the flow of carrier

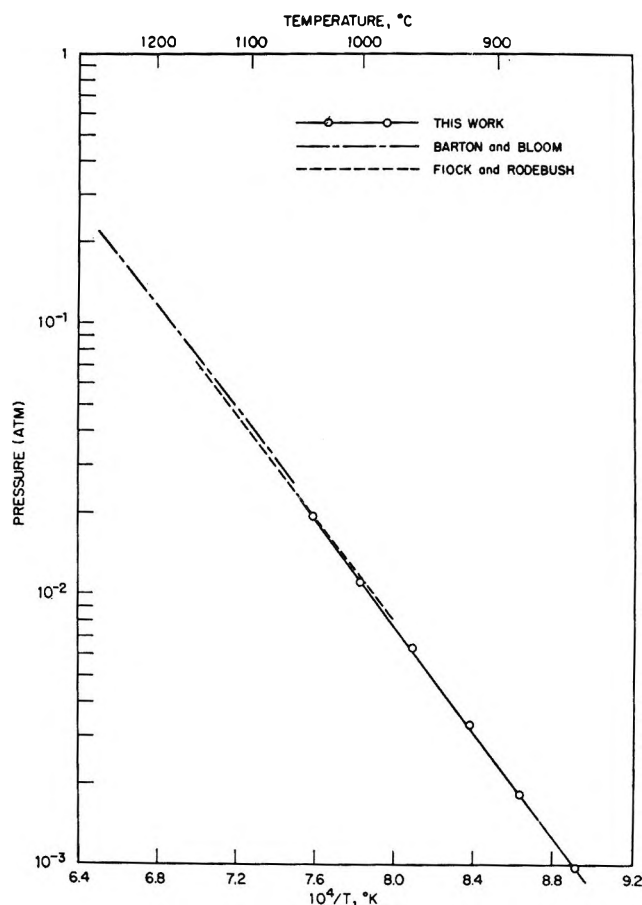


Figure 2. Total vapor pressure (monomer plus dimer) of liquid NaCl .

gas was started. Also, at the conclusion of each run, the carrier gas was shut off, and the sample tube was slowly withdrawn from the furnace and allowed to cool. During both of these periods, sample vapors were lost by diffusion. In order to correct for this diffusion loss, a series of runs at constant temperature was made for each sample. In each series, the time schedule for the warming up and cooling off periods as well as for the time during which the carrier gas was flowing (either 40 or 80 min.) was made the same. The plots of the weight losses of the samples against total volume of carrier gas gave a straight line, whose intercept at zero flow rate gave the diffusion weight loss and whose slope gave the concentration of the sample vapor in grams per milliliter, which could then be converted to moles per liter and substituted into eq. 1.

In using the transpiration method with a two-component liquid where the vapor has a different com-

(2) U. Merten, *J. Phys. Chem.*, **63**, 443 (1959).

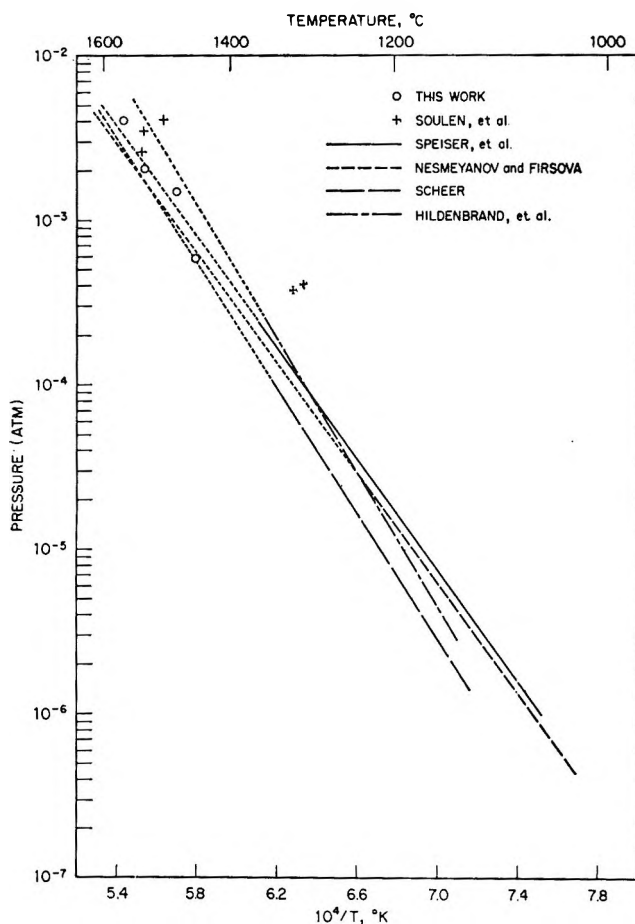


Figure 3. Vapor pressure of liquid B_2O_3 .

position than the liquid, the liquid composition will change during the run. In the $Rb_2O-B_2O_3$ solutions there was only one volatile constituent. During the runs, the samples became somewhat depleted in this constituent so that the actual vapor pressure decreased, giving an erroneously low weight loss. To correct for this effect the apparent vapor pressures of the volatile constituent were determined for a series of different compositions, and a graph showing the change in vapor pressure as a function of composition was made. From this information and from a knowledge of the initial and final compositions of the samples, a curve could be constructed which corrected the observed weight losses for the effect due to the depletion of the volatile constituent. Usually, this correction factor amounted to about 1 to 5% of the observed weight losses, except for the solution containing the least amount of Rb_2O , in which case some of the corrections were as much as 20 to 40%.

The total weight losses were determined by weighing the samples on the platinum wire loops in a drybox

before and after the runs. The weight loss of the Rb_2O was determined by the loss in radioactivity during the run. The B_2O_3 weight loss was measured by the difference between the total weight loss and the Rb_2O weight loss. As a check, the compositions of some of the samples were determined after the runs by wet chemical analysis as well as by the radioactive tracer method. The determinations of the total weight of each component in the samples agreed to within 2 to 3%, and experience indicated that the radioactive tracer method was as accurate as the chemical analysis method.

Test of Experimental Method. To test the experimental procedures and the method of handling the data, the vapor pressures of liquid $NaCl$ and B_2O_3 were measured and compared with the results of other investigators. The $NaCl$ was obtained from J. T. Baker Co., A.R. grade, and further purified by solution, filtration, and recrystallization. The vapor pressure of the $NaCl$ was determined at six temperatures from 846 to 1038°.

Sodium chloride vapor consists predominantly of a mixture of the monomer and dimer. In calculating the vapor pressure from the experimental data it is necessary to know the proportions of these species in order to assign an average molecular weight to the vapor. By use of the monomer-dimer equilibrium data and free energy functions for sodium chloride presented by Brewer and Brackett,³ the corrected total vapor pressure of sodium chloride (monomer plus dimer) was calculated and plotted in the graph of Figure 2. Also plotted are the vapor pressures as determined by Fiock and Rodebush⁴ using a quasi-static manometric method and by Barton and Bloom⁵ using a boiling point method. The measurements of these authors seem to be the most reliable near the temperature range covered by the data of this report, and the agreement is quite good. The slope of the least-squares fit of the data of this report gives a ΔH_{vap} of 44.9 kcal./mole. Barton and Bloom derive an expression from their data which gives the ΔH_{vap} as a function of temperature. Using this relation at the average temperature reported here gives a ΔH_{vap} of 44.1 kcal./mole. Fiock and Rodebush give an average ΔH_{vap} of 43.05 kcal./mole for the temperature range 977 to 1155°.

The enthalpy of sublimation at 298°K. for sodium chloride vaporizing to the monomer was also calcu-

(3) L. Brewer and E. Brackett, *Chem. Rev.*, **61**, 425 (1961).

(4) E. J. Fiock and W. H. Rodebush, *J. Am. Chem. Soc.*, **48**, 2522 (1926).

(5) J. L. Barton and H. Bloom, *J. Phys. Chem.*, **60**, 1413 (1956).

lated (with the aid of data from Brewer and Brackett) for the six vapor pressure measurements reported here. The average value was $\Delta H^{\circ}_{298} = 55.58 \pm 0.13$ kcal./mole. From an evaluation of the various NaCl vapor pressure data reported in the literature, Brewer and Brackett computed the best value of ΔH°_{298} to be 55.5 ± 0.5 kcal./mole. Again the agreement is quite good.

Four determinations of the vapor pressure of B₂O₃ were made between 1440 and 1554°. The vapor pressure was computed on the basis of evaporation to the monomer, and the results were plotted in Figure 3 where they are compared with the vapor pressure data of five other groups of investigators. Speiser, Naiditch, and Johnston⁶ and Nesmeyanov and Firsova⁷ used Knudsen cell methods, and Scheer⁸ and Hildenbrand, Hall, and Potter⁹ used a torsion-effusion method.

The vapor pressure data reported here, although showing considerably more scatter than the NaCl data, are in general agreement with the extrapolated data of these authors. Soulen, Sthapitanonda, and Margrave¹⁰ have also used a transpiration technique. Their data fall into two groups of which the points at the higher temperature agree moderately well with results reported here but their measurements at the lower temperature seem to be too high.

Results

Transpiration measurements were made over six liquids ranging in composition from 4.2 mole % Rb₂O-95.8 mole % B₂O₃ to 50 mole % Rb₂O-50 mole % B₂O₃, and the experimental data are presented in Table I. It is necessary to know the molecular weight of the vapor species before vapor pressures can be calculated from the transpiration data. The fourth column of Table I shows that the vapor composition is close to 50 mole % Rb₂O-50 mole % B₂O₃ over the whole range of liquid compositions. This strongly suggests that the vapor is composed of an equimolar compound of Rb₂O and B₂O₃.

As the transpiration method can give no more indication of the vapor species, further information must be obtained from other sources. The most direct evidence concerning the nature of this vapor species comes from infrared and mass spectrographic studies of the vapors from lithium and sodium metaborates reported by Büchler and Berkowitz-Mattuck.¹¹

These authors report that the vapor in equilibrium with sodium metaborate between 620 and 830° consisted predominantly of monomeric sodium metaborate, NaBO₂. Appreciable amounts of the dimer were observed, as well as minor amounts of several other molecules. The proposed structure of the monomeric molecule is a linear (OBO)⁻ group with the sodium

Table I: Experimental Data

Compn. of melt, mole %	Sample temp., °C.	Cor. sample wt. loss, mg./l.	Mole % Rb ₂ O in vapor
4.2% Rb ₂ O 95.8% B ₂ O ₃	1209	1.4	66
	1243	2.6	41
	1275	5.2	46
	1311	8.6	40
	1353	17.6	39
			Av. 46
11.1% Rb ₂ O 88.9% B ₂ O ₃	1151	2.9	45
	1193	6.8	45
	1218	8.7	51
	1249	14.6	49
	1280	20.8	60
			Av. 50
20.0% Rb ₂ O 80.0% B ₂ O ₃	1033	3.3	51
	1069	7.6	58
	1090	10.8	55
	1115	12.5	47
	1146	23.3	57
			Av. 54
28.0% Rb ₂ O 72.0% B ₂ O ₃	962	5.9	63
	993	12.2	57
	1008	16.8	61
	1054	26.4	54
	1079	46.2	57
			Av. 58
33.3% Rb ₂ O 66.7% B ₂ O ₃	910	5.1	52
	947	10.6	51
	984	21.5	51
	1004	29.6	53
	1028	43.5	50
			Av. 51
50% Rb ₂ O 50% B ₂ O ₃	878	6.2	50
	909	12.6	50
	935	20.5	50
	967	40.2	50
	999	67.6	50
			Av. 50

(6) R. Speiser, S. Naiditch, and H. L. Johnston, *J. Am. Chem. Soc.*, **72**, 2578 (1950).

(7) A. N. Nesmeyanov and L. P. Firsova, *Zh. Fiz. Khim.*, **34**, 1032 (1960).

(8) M. D. Scheer, *J. Phys. Chem.*, **61**, 1184 (1957).

(9) D. L. Hildenbrand, W. F. Hall, and N. D. Potter, *J. Chem. Phys.*, **39**, 296 (1963).

(10) J. R. Soulen, P. Sthapitanonda, and J. L. Margrave, *J. Phys. Chem.*, **59**, 132 (1955).

(11) A. Büchler and J. B. Berkowitz-Mattuck, *J. Chem. Phys.*, **39**, 286, 292 (1963).

ion attached at one end. Analogous to the alkali halides, the metaborate vapor with larger alkali ions should consist of an even higher percentage of the monomer.

Additional evidence of the stability of the monomer is furnished by the infrared spectral studies of Morgan and Staats.¹² These authors, after studying traces of metaborate dissolved in solid solutions of alkali halides, concluded that the metaborate ion occurs in these dilute solutions as the monomer with a linear structure.

The monomer HBO_2 has been reported as the major species in the vapor of metaboric acid by White, *et al.*¹³ The gaseous molecule also consists of a linear O-B-O group with the hydrogen attached at an angle at one end.

Büchler and Berkowitz-Mattuck also reported data on the infrared spectra of gaseous NaBO_2 and CsBO_2 .¹¹ Both of these vapors gave similar spectra with absorption peaks at 5.2 and 17 μ . As a check on the molecular species of vaporized rubidium metaborate, the infrared absorption spectrum of the vapor over the 50% Rb_2O melt was obtained. This was accomplished by heating the melt in a platinum crucible inside an alundum tube furnace closed at each end with NaCl windows. Directed through one end of the tube furnace was a Nernst glower, and at the other end was a Perkin-Elmer infrared spectrometer, Model 12. The furnace was operated at 1000 to 1200°. The background radiation from the furnace was eliminated by use of a rotary beam-chopping wheel between the Nernst glower and the furnace window. This device modified the incoming light signal to 13 c.p.s. so that, with a modification in the analyzer unit of the spectrometer, the direct radiation from the furnace itself could be electronically filtered out.

The spectrum of the rubidium metaborate showed a prominent absorption peak at 5.1 μ . The peak at 17 μ was not sought, as it lay beyond the limits of the spectrometer. This result indicates that the vapor over rubidium metaborate is similar to that over sodium and cesium metaborates and that it consists mainly of the monomer RbBO_2 .

Owing to the small weight losses, occurring during the runs, the experimental error in determining the $\text{Rb}_2\text{O}:\text{B}_2\text{O}_3$ ratio could be fairly large. This is apparent in the most dilute solution, 4.20% Rb_2O , where the total weight losses amounted to only 1 to 10 mg. From Table I it can be seen that the experimentally measured mole per cent of Rb_2O in the vapor over this melt varies considerably from one series to another although the average comes out close to 50%. On the other hand, in the case of the 50.0% Rb_2O melt, where

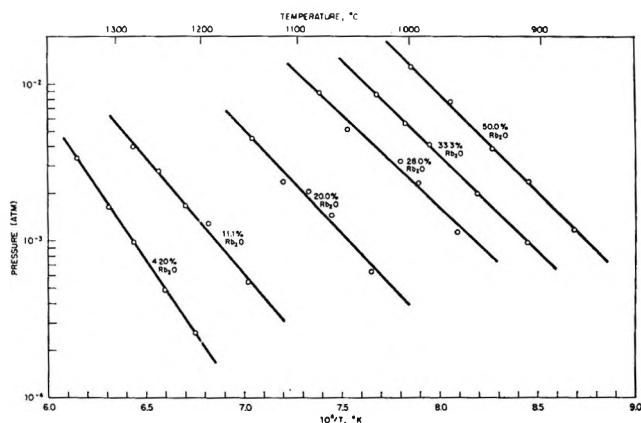


Figure 4. Vapor pressure of RbBO_2 over $\text{Rb}_2\text{O}-\text{B}_2\text{O}_3$ melts.

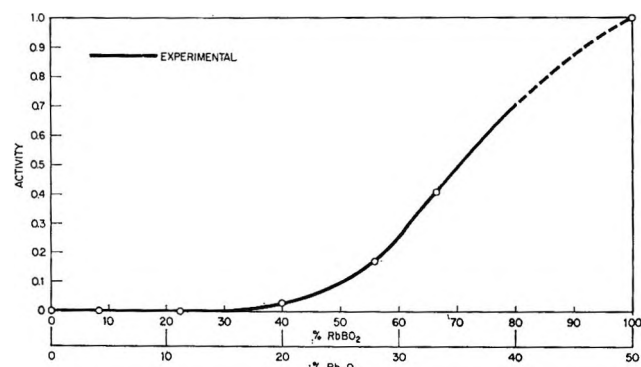


Figure 5. Activity of RbBO_2 in $\text{Rb}_2\text{O}-\text{B}_2\text{O}_3$ melts at 1050°.

it was possible to evaporate much larger amounts without changing the composition of the liquid, the measured Rb_2O concentration in the vapor was equal to 50% for each series of runs.

Of the six melts, the only important deviation from a vapor composition of 50% Rb_2O was in the case of the 28.0% Rb_2O melt. In this case the average vapor concentration was 58% Rb_2O . Whether this represents a significant difference in the vapor composition or whether it is due to experimental variation is not known. In view of the lack of precision in determining the vapor composition and because this variation occurs in only one melt out of six, it will be assumed here that the vapor composition over the 28.0% Rb_2O melt is the same as that over the other melts. Lacking more precise information, it is felt that the assignment of RbBO_2 as the major vapor species over all of the melts is the best possible choice.

(12) H. W. Morgan and P. A. Staats, *J. Appl. Phys. Suppl.*, **33**, 364 (1962).

(13) D. White, D. E. Mann, P. N. Walsh, and A. Sommer, *J. Chem. Phys.*, **32**, 481 (1960).

On this basis the vapor pressures of RbBO₂ for each series of runs was computed by converting the corrected sample weight losses, column 3 of Table I, to moles per liter and substituting these quantities for the term n_s/V in eq. 1. The term T in eq. 1 refers to the temperature of the carrier gas at which its volume was measured and was in the range 24 to 26°.

The values for the computed vapor pressures have been plotted in a $\log P$ vs. $1/T$ graph (Figure 4), and the lines have been drawn according to the least-squares fits. The vapor pressure for each melt can also be expressed by the equation

$$\log P = A - \frac{10^4 B}{T(^{\circ}\text{K.})} \quad (2)$$

The constants A and B and the temperature interval over which the vapor pressure of each melt was measured are listed in Table II.

Table II: Constants for Vapor Pressure Equation for RbBO₂

Liquid compn., mole % Rb ₂ O	$\log P = A - \frac{10^4 B}{T(^{\circ}\text{K.})}$		Temp. range, °C.
	A	B	
4.2	8.919	1.852	1209-1353
11.1	7.167	1.482	1151-1280
20.0	7.034	1.331	1033-1146
28.0	6.683	1.183	962-1079
33.3	7.333	1.223	910-1028
50.0	7.968	1.253	878-999

The heat of vaporization of RbBO₂ from pure liquid rubidium metaborate (50% Rb₂O) has been computed from the slope of the $\log P$ vs. $1/T$ graph and is found to be 57.3 ± 0.8 kcal./mole over the temperature range of the experimental measurements.

Results and Discussion

By means of the experimental vapor pressure data and by assuming ideal behavior of the RbBO₂ at low partial pressures, the activity of the RbBO₂ in the melts at 1050° was computed and plotted as a function of liquid composition (Figure 5).

This graph shows that the activity of the RbBO₂ is essentially zero until a composition of approximately 16 mole % Rb₂O is reached. After this point the activity begins to increase appreciably with increasing Rb₂O content. This behavior suggests the formation of complex structural groups in the melts.

Similar abrupt changes in several of the physical

properties of alkali borates at about this same composition have given rise to the term "boric oxide anomaly." These properties include density, viscosity, expansivity, and heat of solution. A structural explanation of the boric oxide anomaly was first suggested by Biscoe and Warren.¹ According to these authors, boron oxide glass consists of a three-dimensional random network of boron and oxygen ions in which each boron ion is surrounded by three oxygen ions lying in a plane, and each oxygen ion is situated between two boron ions. Biscoe and Warren postulated that, as alkali oxide is added to the trigonally coordinated boron-oxygen network, the additional oxygen enters into the structure, not by breaking a bond of adjacent trigonal BO₃ groups and forming a pair of nonbridging oxygen groups but by coordinating tetrahedrally with boron and forming a bridge between two BO₃ groups. This process does not continue indefinitely but comes to a halt when the composition reaches about 16 mole % alkali oxide. The extra oxygens furnished by the addition of further alkali oxide do not form a continuous tetrahedral network with the boron but rupture the boron-oxygen bonds, forming nonbridging boron-oxygen groups. It is the beginning of this transition from a strong, continuous network to a broken, open structure which causes the abrupt changes in physical properties referred to as the boric oxide anomaly.

Although this theory has been criticized by many investigators and various modifications have been proposed, the concept of the coordination change of boron from three to four as oxygen ions are added seems well established. However, Krogh-Moe and his co-workers, after studying many alkali borate glasses and crystals using X-ray diffraction and nuclear magnetic resonance techniques, have concluded that the formation of tetrahedrally coordinated boron continues as alkali oxide is added to boron oxide until a composition of 33 mole % alkali oxide has been reached and 50% of the borons are in tetrahedral configuration.^{14,15} Krogh-Moe has further postulated, by means of indirect evidence from melting point curves obtained from the phase diagrams of the system Na₂O-B₂O₃, that the formation of tetrahedrally coordinated boron also continues in sodium borate melts (and probably other alkali borate melts) up to the composition of 33 mole % alkali oxide.¹⁶

Bearing in mind the foregoing interpretation of the

(14) S. E. Svanson, E. Forslind, and J. Krogh-Moe, *J. Phys. Chem.*, **66**, 174 (1962).

(15) J. Krogh-Moe, *Phys. Chem. Glasses*, **3**, 1 (1962).

(16) J. Krogh-Moe, *ibid.*, **3**, 101 (1962).

boric oxide anomaly, one should now return to the data on the activity of the RbBO_2 in the $\text{Rb}_2\text{O}-\text{B}_2\text{O}_3$ melts (Figure 5) where the activity-composition curve showed a pronounced break at about 16% Rb_2O . The similarity of this change to the physical changes referred to above leads one to surmise a structural arrangement in the $\text{Rb}_2\text{O}-\text{B}_2\text{O}_3$ melts similar to that postulated by Biscoe and Warren for the alkali borate glasses.

It will be assumed here that, as Rb_2O is added to liquid B_2O_3 , the additional oxygen ions will enter into the boron-oxygen network by forming tetrahedral boron-oxygen groups as in the alkali borate glasses. This process will continue up to a Rb_2O concentration of about 16%. The oxygen ions from further additions of Rb_2O will break the boron-oxygen bonds and form nonbridging oxygen groups until a composition of 50% Rb_2O is reached at which point all of the borons will be trigonally coordinated with one nonbridging and two bridging oxygens.

Physically, this explanation can be justified by observing that, as the RbBO_2 vapor molecule contains the $(\text{OBO})^-$ group, it could vaporize much more readily from a liquid that contains nonbridging $>\text{B}-\text{O}^-$ groups than from one that contains only a continuous network of bridging boron-oxygen groups. On this basis, relatively little evaporation of RbBO_2 would be expected from the melts until nonbridging oxygens began to be formed at a composition of about 16% Rb_2O . At liquid compositions richer in Rb_2O , the vapor pressure of the RbBO_2 should be proportional to the concentration of nonbridging oxygen groups. This would lead to an activity-composition curve similar to that in Figure 5.

From the vapor pressure and activity data, the free energy, enthalpy, and entropy of mixing of liquid B_2O_3 and RbBO_2 as a function of liquid composition were computed. The enthalpies and entropies of mixing are plotted in Figure 6 and are measured relative to the pure liquids B_2O_3 and RbBO_2 as the standard states and represent average values over the temperature range of the experimental data.

The curve of integral enthalpy of mixing is asymmetric and shows a maximum of about -5.8 kcal./mole at a composition of about 17% Rb_2O . This suggests molecular association in the liquid over the region where the formation of the tetrahedral BO_4 groups has been postulated. The integral entropy of mixing curve is generally negative where the enthalpy of mixing curve has the largest negative values and increases to positive values in the Rb_2O -rich region, where it is postulated that the relatively ordered network structure of the melt is broken down by the for-

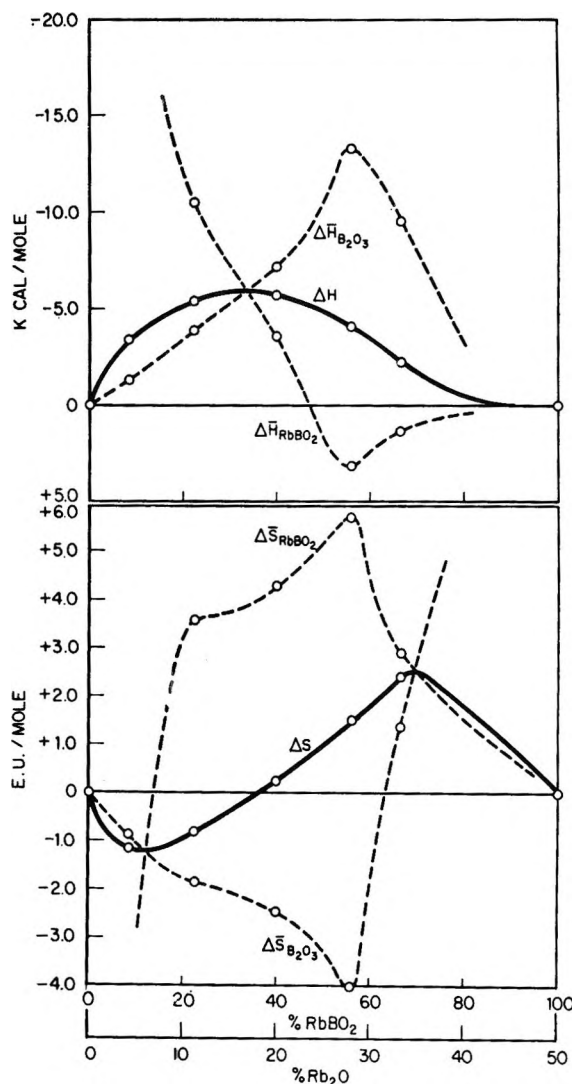


Figure 6. Integral and relative partial enthalpies and entropies of mixing of liquids RbBO_2 and B_2O_3 .

mation of nonbridging oxygen groups. It should be emphasized that the data and the suggested structural model described in this report are applicable only to the $\text{B}_2\text{O}_3-\text{RbBO}_2$ system and that no data were obtained for liquids richer in Rb_2O than RbBO_2 .

The results of this study indicate a significant change in the structure of liquid rubidium borate at about 16% Rb_2O . This change has been correlated with changes in the coordination number of boron and is in agreement with the theory of alkali borate glass structure of Biscoe and Warren. It is not in agreement with the theory of Krogh-Moe, who considers that tetrahedral BO_4 groups should continue to form until a composition of 33% alkali oxide. However, infrared studies of rubidium borate glasses at room temperature by the present authors indicate no abrupt changes

in structure at the 16% Rb_2O composition but rather a continuous formation of tetrahedral BO_4 groups to at least a composition of 38% Rb_2O .¹⁷ These results are in agreement with those of Krogh-Moe and seem to contradict the findings reported here.

The two points of view may be reconciled if it is assumed that an equilibrium exists between trigonal and tetrahedral boron groups which is not only affected by the addition of alkali oxide but is also temperature dependent so that increasing the temperature decreases the concentration of tetrahedral groups. Shartsis originally suggested this temperature dependence in order to explain the anomalous viscosity data of the alkali borates.¹⁸ If it is assumed that the tetrahedral groups are relatively more stable at low temperatures, their existence can be understood in high concentrations in cool glasses and crystals containing up to 33% alkali oxide. At high temperatures the equilibrium shifts in the melts to favor the formation of trigonal groups with nonbridging oxygen.

Variation of the RbBO_2 Vapor Pressure by Complex Formation. A feature of the proposed model for liquid alkali borates is the concept of measuring the concentration of the RbBO_2 in the melt in terms of the nonbridging boron oxygen groups. It follows that any process which decreased the concentration of the $>\text{B}-\text{O}^-$ groups in the melt would also lower the vapor pressure of the RbBO_2 . This might be done by adding a third cation to the melt, which would form a strong complex with the nonbridging oxygen ions. This would not only reduce the concentration of nonbridging oxygen groups but also, depending upon the oxygen complexing ability of the added cation, tend to reconstitute the liquid network.

This concept was tested experimentally. A series of radioactive rubidium metaborate melts was prepared, each with a third oxide whose cation was likely to form a stable complex with oxygen ions in the melt. The cationic composition of each melt was 45 mole % B^{3+} , 45 mole % Rb^+ , and 10 mole % added third cation. The vapor pressure over each melt was measured at 930° , and the results compared with the vapor pressure of pure rubidium metaborate at the same temperature. Any decrease in the vapor pressure of the RbBO_2 beyond that due only to dilution should be due to the complexing of the $>\text{B}-\text{O}^-$ groups in the melt and the corresponding decrease of the activity of the RbBO_2 .

The vapor pressure of the RbBO_2 over the melts was computed on the basis that the only vapor species was RbBO_2 . This assumes that the added oxides did not vaporize from the melts either independently or in combination with the rubidium oxide. All of

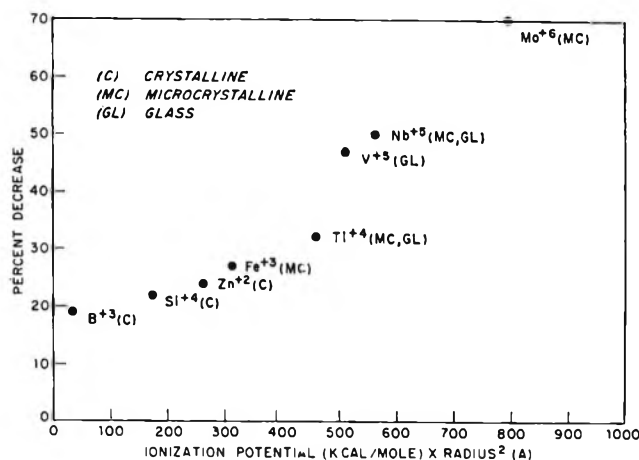


Figure 7. Per cent decrease of RbBO_2 vapor pressure upon the addition of complexing cations to a melt of rubidium metaborate at 930° .

the added oxides are relatively nonvolatile at 930° except MoO_3 which apparently formed a very stable complex in the melt and did not vaporize.

It was found empirically that a plot of the per cent decrease of the RbBO_2 pressure against an artificial factor computed by multiplying the ionization potential (in kilocalories per mole) by the cation radius squared (in Ångström units) gave a roughly linear relationship. This procedure can be justified qualitatively by the fact that the anionic complexing power of the added cation should be proportional to its electric field strength and its surface area. That is, the stronger the electric field of the cation, the greater will be its attraction for oxygen ions; and the larger its surface area, the more easily it can accommodate a greater number of oxygen ions with less geometrical strain. The ionization potential of the cation was taken as a measure of its anionic attracting power, and its radius squared was taken as a relative measure of its surface area. These results are plotted in Figure 7. From the graph it can be seen that Mo^{6+} , Nb^{5+} , V^{5+} , and, to a lesser degree, Ti^{4+} were quite effective in complexing the nonbridging oxygens and decreasing the RbBO_2 vapor pressure. The other ions had little more effect than the boron itself.

It was also noted that several of the added oxides, apparently by virtue of their complexing powers, reconstituted the liquid network so that some of the melts solidified to a glass or mixture of glass and microcrystals. This was determined by observing crushed samples of the solidified melts under a polarizing microscope. In general, those ions which caused the

(17) J. T. Quan and C. E. Adams, *J. Phys. Chem.*, **70**, 340 (1966).

(18) L. Shartsis, W. Capps, and S. Spinner, *J. Am. Ceram. Soc.*, **36**, 319 (1953).

greatest decrease in vapor pressure also tended to convert the crystalline metaborate to a glass. These results are noted in Figure 7.

Acknowledgment. Financial support of this research by the U. S. Atomic Energy Commission is gratefully acknowledged.

The Infrared Spectra of Rubidium Borates of Varying Composition

by J. T. Quan and C. E. Adams

U. S. Naval Radiological Defense Laboratory, San Francisco, California 94135 (Received April 7, 1966)

A series of rubidium borates consisting of varying proportions of rubidium oxide and boron oxide has been studied by infrared spectroscopy in the 2.5–15.5- μ range. The rubidium oxide concentrations varied from 4.2 to 50 mole %. Wave length assignments were made for molecular species present in the borates. It was found that the transition of vitreous boron oxide to crystalline rubidium metaborate occurred in three stages according to the Rb_2O content of the borate: 0–28, 28–33, and 33–50 mole %. At first, several different molecular species are found simultaneously whose concentrations increase uniformly with Rb_2O content. In the next stage, the increases in concentrations are accelerated. Finally, devitrification commences as the end product, rubidium metaborate, is progressively formed. It was also found that devitrification could be inhibited by the addition of certain acidic oxides.

Introduction

This report covers the second part of an investigation of some of the properties and structures of rubidium borates. The first part¹ was concerned with rubidium borate melts at high temperatures, while this report is concerned with the structures of solid rubidium borates at room temperature. Infrared spectroscopy was used to study the borates which varied in composition from pure boron oxide to rubidium metaborate. The spectra were compared with those obtained by previous investigators for other alkali borates. Spectral interpretation was based on empirical relationships which exist between molecular structure and spectral characteristics. Relative intensity measurements were made to compare rates of growth for different molecular groups or species.

Experimental Section

The materials for preparation of the rubidium borates were analytical reagent grade boric acid obtained from

the J. T. Baker Co., and rubidium carbonate which was obtained from the A. D. Mackay Co. and from K & K Laboratories.

The boric acid was heated in a platinum dish over a Meker burner until the expulsion of water was complete. The resulting boric oxide melt was transferred to an electric furnace and heated for several hours at 1000° and then was allowed to cool in a desiccator. The Rb_2CO_3 was purified by dissolving in distilled water, filtering, and recrystallizing. Spectrochemical analysis showed that the purified Rb_2CO_3 contained less than 1% impurities of other alkali metals. It is believed that these impurities did not materially affect the rubidium borate spectra.

Rubidium borates of different compositions were prepared by crushing together known amounts of B_2O_3 glass and Rb_2CO_3 . The mixtures were fused in platinum crucibles until CO_2 was completely expelled from

(1) C. E. Adams and J. T. Quan, *J. Phys. Chem.*, **70**, 331 (1966).

the melts. These were allowed to cool in a desiccator containing magnesium perchlorate as a drying agent. Some of the compositions were checked by titrimetric analysis. Thoroughness of CO_2 expulsion was checked by dissolving the borates in dilute acid solution.

The spectra of B_2O_3 and rubidium borates of low Rb_2O content (4.2, 11, 20, 28, and 33 mole %) were obtained by infrared transmission through thin glass films. The films were formed by collecting molten glass on the tip of a 5-mm. Pyrex tubing and blowing a thin-walled bulb with dry air. A section of the blown film was mounted over a closed wire loop which had been previously dipped in a Canada balsam-xylol solution. The preparation was immediately analyzed to minimize atmospheric hydration effects. The thickness of the films is estimated to be less than 1μ because the film sections selected showed only low-order interference colors.

B_2O_3 films were first tested for freedom from contamination by water. Immediately after their preparation in the laboratory, they were enclosed in cylinders which contained dry air and were capped on the ends with rock salt windows. They were analyzed *in situ*. Traces of moisture in combination with B_2O_3 to form boric acid were always found to be present. This effect on the infrared spectrum of B_2O_3 was small. However, these samples did not differ substantially in water content from others prepared in the same way but analyzed without benefit of the cylinders. For these reasons, it was felt that immediate analysis following sample preparation without additional protection from atmospheric moisture was an adequate analytical procedure, provided the effects of moisture were taken into account in the final results.

The spectra of rubidium borates of higher Rb_2O content (41 and 50 mole %) were not obtainable by the film method because melts of these borates were of lower viscosity and they had a tendency to crystallize upon solidification. Therefore, mulls were formed by crushing and grinding these borates with agate mortar and pestle in the presence of Nujol. A small amount of mull was squeezed between two rock salt plates. The plates were separated and one was arbitrarily selected for analysis after most of the Nujol had been removed by blotting.

Intentional overlap of the two sample preparation techniques at 33 mole % Rb_2O was made in order to compare the spectra of borate samples prepared by the two techniques.

A Perkin-Elmer double-beam infrared spectrometer, Model 21, was used for the analyses. All spectra were obtained in the rock salt prism region of 2.5 to 15.5μ .

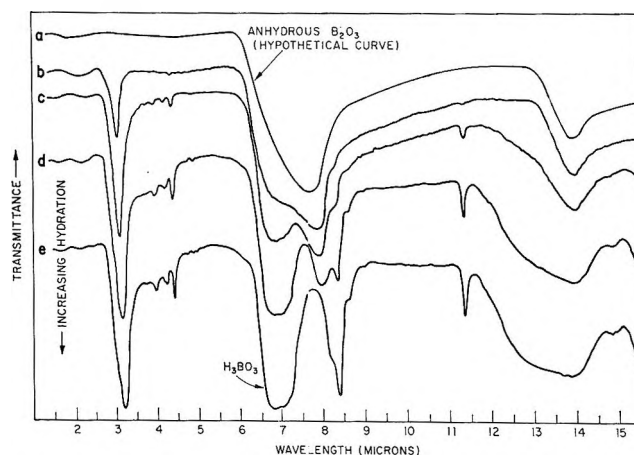


Figure 1. Infrared transmission spectra of progressively hydrated boric oxide.

Results and Discussion

1. The Spectrum of Pure and Hydrated B_2O_3 . Borates of low alkali oxide content tend to be contaminated by moisture.²⁻⁴ The infrared spectra of such borates also contain a superimposed spectrum of boric acid. To resolve this difficulty, the spectra of a thin film of B_2O_3 in progressive stages of hydration were recorded. These are shown in Figure 1 as curves b, c, d, and e (displaced vertically to facilitate comparison). By graphically eliminating from these curves absorption bands due to the effects of water, the hypothetical spectrum of anhydrous B_2O_3 glass was obtained (curve a).

Curve a shows that only the absorption peaks, or bands at approximately 8μ (7.7μ) and 13.9μ are attributable to vibrations of the BO_3 molecular groups which comprise the B_2O_3 glass network. (The designations BO_3 , BO^- , BO_4^- , and boroxol are used for convenience. The proposed atomic arrangements for these molecular groups are given in Table I.) The $8\text{-}\mu$ portion of this spectrum agrees with the work of MacKenzie, *et al.*⁵ They show that upon application of heat to dehydrate moist B_2O_3 , the broad absorption band at 6.25 to 9.1μ is reduced to a better defined peak at 7.9μ . This result compares with the dehydration trend shown in Figure 1.

Curve b represents the spectrum of the vitreous B_2O_3 used as a starting material for preparation of the borates. Hydration effects are evident. Continued

(2) J. Krogh-Moe, *Arkiv Kem.*, **12**, 475 (1958).

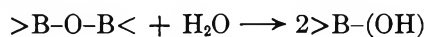
(3) J. L. Parsons and M. E. Milberg, *J. Am. Ceram. Soc.*, **43**, 326 (1960).

(4) N. F. Borrelli, B. D. McSwain, and G.-J. Su, *Phys. Chem. Glasses*, **4**, 11 (1963).

(5) J. D. MacKenzie, R. S. McDonald, and W. K. Murphy, *Rev. Sci. Instr.*, **32**, 118 (1961).

hydration of the same sample yields the spectra shown in curves c, d, and e. Curve e represents the spectrum of the completely hydrated final product, H_3BO_3 , and is similar to boric acid spectra analyzed in detail by other investigators.⁶⁻⁸ From their well-documented absorption characteristics, some are selected for comparison with those of the $\text{Rb}_2\text{O}-\text{B}_2\text{O}_3$ system to ascertain similarities in structural transformations.

These investigators have established that the $6.9\text{-}\mu$ band of boric acid is attributable to the in-plane vibration between the boron atom and the hydroxyl radical. The progressive increase in absorption intensity of this band is due to the continuous formation of this type of grouping. Simultaneous breakdown of the boric oxide glass network is evidenced by the diminishing intensity of the $8\text{-}\mu$ band. Both processes can be represented in



According to the findings of Hornig and Plumb,⁷ the broad $11.5\text{-}14.5\text{-}\mu$ band of H_3BO_3 is assignable to the vibrations normal to the plane of the BO_3 groups. Similarly, the $13.9\text{-}\mu$ band of anhydrous B_2O_3 may be ascribed to the same type of vibrations because the boron-oxygen configuration of both compounds is the same. Their respective BO_3 groups should exhibit only minor variations in vibrational energy.

2. *Spectra of Rubidium Borates and Wave Length Assignments.* The spectra of the rubidium borates are shown in Figure 2. Quotation marks about B_2O_3 denote the slightly hydrated nature of the starting material. The other borates in the figure are also hydrated to lesser degrees, as shown by some absorption at $3.1\text{ }\mu$, but their basic spectra do not appear to be materially affected by moisture. This spectral series resembles that of the sodium borates.^{4,9}

Analogous with spectra of the hydration series shown in Figure 1, successive additions of Rb_2O enhance the absorption intensity of the band at $7\text{ }\mu$ while that at $8\text{ }\mu$ is suppressed. The $7\text{-}\mu$ band migrates to $7.5\text{ }\mu$ at higher Rb_2O concentrations. Its absorption intensity with respect to that of the $8\text{-}\mu$ band increases in a relatively slow, uniform manner between 11 and 28 mole % Rb_2O and very rapidly between 28 and 33 mole % Rb_2O . The emergence of two other absorption bands can be detected: a $9.5\text{-}\mu$ band at 4.2 mole %, and a $10.7\text{-}\mu$ band at 11 mole % Rb_2O .

Formation of the $7\text{-}7.5\text{-}\mu$ band is compared with that of boric acid in which similarity of vibrational energies suggests similar structures. The products in this case, however, are postulated to be terminal BO^- groups formed according to the equation, $>\text{B}-$

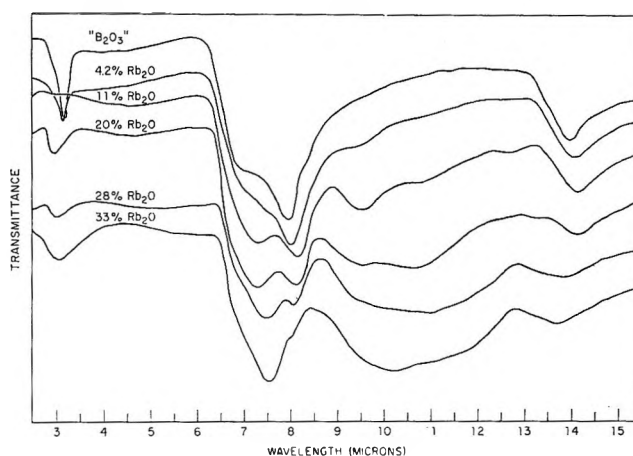
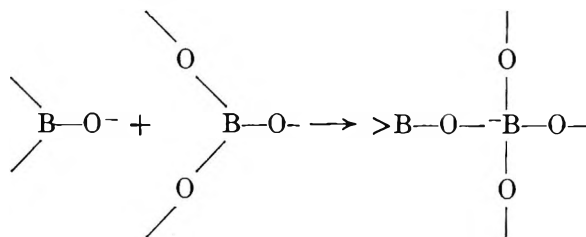


Figure 2. Infrared transmission spectra of thin film B_2O_3 and rubidium borate glasses.

$\text{O}-\text{B}< + \text{O}^{2-} \rightarrow 2>\text{B}-\text{O}^-$. The O^{2-} ion is contributed by Rb_2O . Biscoe and Warren¹⁰ believed that this reaction commences at approximately 17 mole % alkali oxide. The experimental evidence obtained here is contrary to that belief and shows that the BO^- groups exist throughout the entire range of borate compositions studied.

Another effect of adding Rb_2O to B_2O_3 glass is the formation of tetrahedrally coordinated boron. This can be represented by the reaction of $\text{B}-\text{O}^-$ with a trigonally coordinated boron



A new absorption band should be in evidence for the BO_4^- group formed. Its energy is inferred from a finding of Dachille and Roy¹¹ who noted that when the coordination of germanium changes from 4 to 6, the main stretching vibration shifts to a lower frequency. They found that the ratio of the coordination numbers is related by the ratio of the squares of the respective absorption wave lengths. For the

(6) D. E. Bethell and N. Sheppard, *Trans. Faraday Soc.*, **51**, 9 (1955).

(7) D. F. Hornig and R. C. Plumb, *J. Chem. Phys.*, **26**, 637 (1957).

(8) R. R. Servoss and H. M. Clark, *ibid.*, **26**, 1175 (1957).

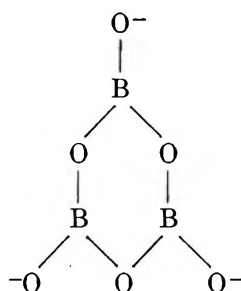
(9) P. E. Jellyman and J. P. Procter, *J. Soc. Glass Tech.*, **39**, 173T (1955).

(10) J. Biscoe and B. E. Warren, *J. Am. Ceram. Soc.*, **21**, 287 (1938).

(11) F. Dachille and R. Roy, *Z. Krist.*, **111**, 432 (1959).

borates, the expected energy of tetrahedrally coordinated boron is found by using 8.1μ as the absorption wave length for trigonally coordinated boron. The calculated wave length of 9.5μ coincides with that of an observed absorption band and therefore a reasonable assignment can be made.

Figure 3 shows the spectra of rubidium borates of high Rb_2O content prepared by the Nujol mull method. No B-O-B network vibration at 8μ is detectable. The spectrum of borate glass of 33 mole % Rb_2O differs from that obtained in Figure 2. Its strong resemblance to that of crystalline $\text{K}_2\text{B}_4\text{O}_7 \cdot 5\text{H}_2\text{O}$ ¹² suggests that the mulled sample is more hydrated and devitrified than its thin film counterpart. When the Rb_2O content of the borate is increased to 50 mole %, some of the bands disappear. The resulting spectrum of crystalline rubidium metaborate is identical with that of sodium metaborate¹² in which strong absorption occurs at 10.7 and 7.6μ . These two metaborate structures, in turn, should be similar to that of potassium metaborate whose negative radical has been described by Zachariassen¹³ as a six-membered boroxol ring comprised of alternate boron and oxygen atoms



Apparently, the alkali ions do not differ in their influence on borate structures. The presence of boroxol groups in borate glasses of low alkali oxide content is inferred from the emergence of a broad absorption band in the glass of 11% Rb_2O , as shown in Figure 2. Krogh-Moe¹⁴ has also postulated the existence of this group in these alkali borates although he has offered no proof of it.

The other prominent peak associated with rubidium metaborate and located at 7.6μ should correspond to the $7.5\text{-}\mu$ peak assigned to terminal BO^- groups. No absorption band attributable to tetrahedrally coordinated boron is present in the metaborate.

The assignments of absorption wave lengths to the various structural groups are given in Table I. Assignments made by two other groups of investigators are compared. There is complete accord in the assignment of the $8\text{-}\mu$ band and the broad $13.9\text{-}14.5\text{-}\mu$ band to the BO_3 vibrations, and the $9.5\text{-}\mu$ band to the BO_4^-

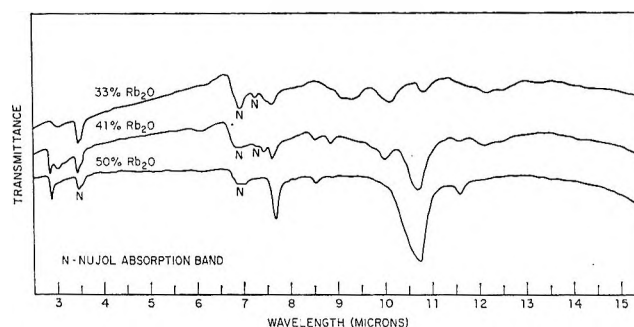


Figure 3. Infrared transmission spectra of rubidium borates of high Rb_2O content prepared by the mulling method.

Table I: Comparison of Wave Length Assignments of the Structural Groups

Structural group	Type of vibration	Wave length, μ		
		This work	Jellyman and Procter ⁹	Moore and McMillan ¹⁵
 (BO_3)	Stretching	8	8	8
	Bending	13.9	14-14.5	13.9 6.9
$>\text{B}-\text{O}^-$	Stretching	7-7.5	10-12	(Not considered)
 (BO_4^-)	Stretching	9.5	7-7.5	7.5
			9.5	9.5
 (boroxol)	(Not specified)	10.7	(Not considered)	(Not considered)

vibration. The $6.9\text{-}\mu$ band obtained by Moore and McMillan¹⁵ is actually due to boric acid.

The $7\text{-}7.5\text{-}\mu$ band in this work was assigned to the BO^- vibration, although this same vibration was assumed by Jellyman and Procter,⁹ without substan-

(12) F. A. Miller and C. H. Wilkins, *Anal. Chem.*, **24**, 1253 (1952).

(13) W. H. Zachariassen, *J. Chem. Phys.*, **5**, 919 (1937).

(14) J. Krogh-Moe, *Arkiv Kemi*, **14**, 553 (1959).

(15) H. Moore and P. W. McMillan, *J. Soc. Glass Tech.*, **40**, 97T (1956).

tiation, to cause the absorption between 10 and 12 μ . On the other hand, Moore and McMillan¹⁵ failed to consider the existence of this molecular group.

In addition to the 9.5- μ band, the other investigators assigned additional bands (7-7.5 and 10.5 μ) to the BO_4^- group on the basis that they appeared together in the same spectra. This does not seem fully justified.

Because of its prominence in the metaborate spectrum, the 10.7- μ band is considered to be a characteristic of the boroxol group. Neither of the other two teams of investigators postulated the presence of this group in the borate glasses.

According to the interpretation of spectra in this work, rubidium borates at each composition should contain two or more of the molecular groups described. A two-dimensional schematic representation of the various structures is shown in Figure 4. Figure 4a illustrates the random network of vitreous B_2O_3 consisting of BO_3 groups. Each group has a trigonally coordinated boron atom joined to oxygen atoms in a planar configuration. As oxide is added, *via* Rb_2O , to the network, B-O-B bonds are cleaved to form B-O⁻ groups. Some of these groups join with trigonally coordinated borons to form tetrahedrally coordinated borons. Boroxol groups are also present, and their presence becomes more apparent at higher rubidium oxide concentrations. The resulting effect on the glass network is depicted in Figure 4b, which represents arbitrary concentrations between 11 and 33 mole % Rb_2O .

It has already been noted that accelerated changes occur in the spectra at Rb_2O concentrations in excess of 28 mole %. Devitrification as shown by diminished BO_3 absorption at 8 μ is accompanied by rapid growth of BO_4^- (9.5 μ), B-O⁻ (7-7.5 μ), and boroxol (10.7 μ) groups. This growth can be illustrated by assuming the existence of some intermediate structure arrangement like that shown in Figure 4c. By rearrangement, the structure shown in Figure 4d can result, which bears resemblance to the crystalline tetraborate structure postulated by Morimoto.¹⁶ Or, as shown in Figure 4e, the addition of more Rb_2O can effect bond cleavage in the vicinity of the tetrahedral boron to yield BO⁻ and boroxol groups. The simultaneous occurrence of these processes will satisfy the conditions for concurrent, rapid growth of the groups. Since the structures in Figures 4d and 4e are composites of existing molecular groups, no new absorption band is expected to appear in the infrared spectrum.

Concentrations of particular molecular groups are usually determined by spectral intensity measurements. However, the impracticability of reproducing thin

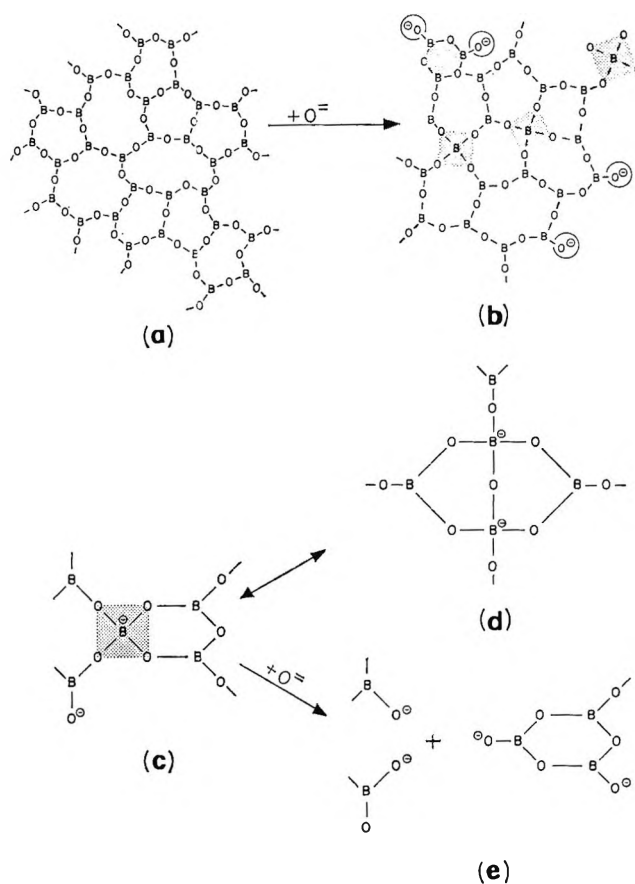


Figure 4. Two-dimensional schematic representation of various borate structures.

borate films to the same thickness precludes making absolute determinations. Moore and McMillan¹⁵ circumvented the difficulty by employing extinction coefficient ratios to determine relative concentrations of molecular groups. They concluded that BO_4^- groups cease to form in an alkali borate which contains alkali oxide in excess of approximately 17 mole %. However, they did not discuss the possibility that the inverse of the ratios which they selected for graphing might lead to a different interpretation. For example, if their graph of the ratio $E_8/E_{9.5}$ vs. Na_2O concentration, which shows two lines intersecting at approximately 15 mole % Na_2O , was plotted with the inverse ratio, $E_{9.5}/E_8$, a single straight line can be reasonably drawn through data points from 0 to 30 mole %. This would cast doubt on the occurrence of an abrupt structural change at the 15-17 mole % composition.

In this study, the possibility that no change occurs at 17 mole % of alkali oxide content is explored. A variation of the method of Moore and McMillan is

(16) N. Morimoto, *Mineral. J.* (Tokyo), 2, 1 (1956).

used to trace the changes in the constitution of rubidium borates. Among the spectral bands of interest (Figure 2) at 7.0–7.5, 8.0–8.2, 9.5, and 10.5–10.7 μ , only the 8.0–8.2- μ band is used as reference because it uniquely diminishes in intensity. By so doing, the computed extinction ratios vary in accordance with observed changes in spectra.

3. *Determination of Extinction Ratios.* Extinction ratios are obtained by first setting the 6- μ position of each trace in Figure 2 on a base line of total transmittance (zero absorption). Then the transmittance, T , of each absorption band is recorded and the extinction value, E , is calculated with the aid of the equation

$$E = \log \frac{1}{T} = kcd$$

where E is the extinction (also called absorbance), T is the transmittance of the sample, k is the specific extinction coefficient (extinction at unit concentration and unit sample thickness), c is the concentration of the absorbing molecular group, and d is the thickness of the sample, or absorption path length.

For a given borate sample, the relative extinction of a given band at a particular wave length, E_λ , and that of a reference band, E_{ref} , has the relationship

$$\frac{E_\lambda}{E_{ref}} = \frac{k_\lambda}{k_{ref}} \frac{c_\lambda}{c_{ref}} = K \frac{c_\lambda}{c_{ref}}$$

where K equals k_λ/k_{ref} . The extinction ratio is therefore proportional to the relative concentrations of the respective molecular groups.

Values of extinction ratios *vs.* rubidium oxide content are plotted as filled circles in Figures 5a, 5b, and 5c. The extinction coefficient data given by Moore and McMillan were used to compute ratios with only the 8- μ band as reference. These are plotted in the same figures for comparison. Their data for lithium borates are indicated by triangles, and for sodium borates by squares. All the plots have similar characteristics. They are linear up to 28–30 mole % with no intervening breaks, while the sharp change which occurs at that concentration conforms to the spectral variations shown in Figure 2. The inference drawn from these plots is that the BO^- , BO_4^- , and boroxol groups increase uniformly in number until the alkali oxide content is 28–30 mole %. At that concentration, the original glassy state undergoes accelerated disintegration which is accompanied by a correspondingly rapid formation of the individual molecular groups. At some rubidium oxide concentration greater than 33 mole %, and in agreement with Krogh-Moe's theory,¹⁷ the tetrahedrally coordinated borons revert

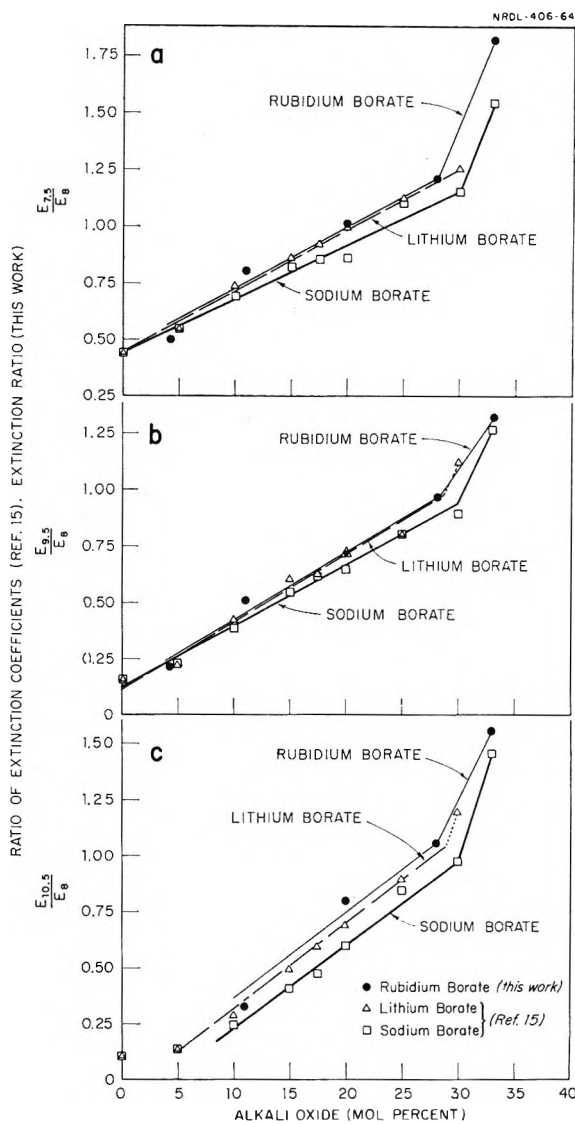


Figure 5. Comparisons of variations in extinction ratios for rubidium borate of this study and in extinction coefficient ratios for lithium and sodium borates.

to trigonal coordination. When conversion to crystalline rubidium metaborate is complete, all boron atoms are trigonally coordinated and incorporated into boroxol structures.

It is realized that the extinction ratio method used here to describe structural changes in the borates has not provided unique answers. However, when the results are considered in conjunction with observed spectral changes, they appear to be at least as plausible as those given by Moore and McMillan.

4. *The Effect of Various Complex-Forming Metals on the $Rb_2O \cdot 2B_2O_3$ Spectrum.* In the report¹ dealing

(17) J. Krogh-Moe, *Phys. Chem. Glasses*, 3, 1 (1962).

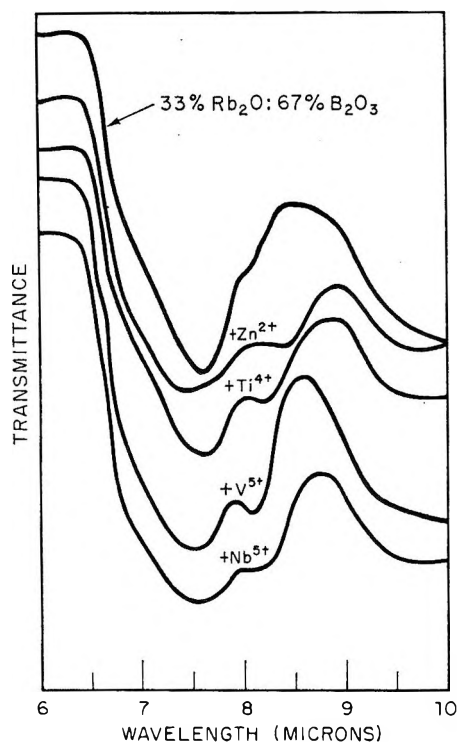


Figure 6. The effect of 5 atom % metal ions on the spectrum of $\text{Rb}_2\text{O}\cdot 2\text{B}_2\text{O}_3$ glass.

with vapor pressures in the liquid $\text{Rb}_2\text{O}-\text{B}_2\text{O}_3$ system, the concept of network reconstitution was introduced to explain lessened chemical activity for liquid borates to which oxides of selected metals are added. The relative complexing power of the metal oxides—a measure of the ability to promote such reconstitution—was determined. The metals are considered to act as electron acceptors, forming dative bonds with the negatively charged oxygens of the BO^- groups. Such bond formation reduces the number of BO^- groups with singly charged oxygens. As a result, the absorption band originally attributed to these groups should exhibit reduced intensity.

The correctness of the original concept was tested by examining the absorption spectra of borate glasses to which ZnO , TiO_2 , V_2O_5 , and Nb_2O_5 were fused separately with $\text{Rb}_2\text{O}\cdot 2\text{B}_2\text{O}_3$. The final cation composition of each glass was 5 atom % complex forming metal, 31.7 atom % rubidium, and 63.3 atom % boron. Thin films of these glasses were prepared in the same manner as before, and their spectra are shown in Figure 6 together with the original $\text{Rb}_2\text{O}\cdot 2\text{B}_2\text{O}_3$ glass. It is noted that the relative intensities of the absorption bands assigned to BO^- groups ($7.5\ \mu$) and BO_3 glass

network ($8\ \mu$) are altered; the former is attenuated while the latter is enhanced. The degree of change is in accordance with the complexing power of the metal oxides. Comparison of these spectra with those in Figure 2 shows a trend which is similar to a reduction in Rb_2O content, *i.e.*, a tendency to return to a glass network structure.

This examination affirms the concept of network reconstitution in the alkali borates, and it reinforces the belief that the assignment of the particular vibrational frequency of the BO^- group was properly made.

Conclusions

The experimental results of this study indicate that vitreous rubidium borate at any given composition is comprised of a mixture of several molecular species. These are the BO_3 groups which constitute the original glass, and BO^- , BO_4^- , and boroxol groups which form as a consequence of the introduction of Rb_2O . Except for BO_3 , all species increase uniformly up to 28 mole % Rb_2O . Between 28 and 33 mole %, the increase is accelerated. Beyond this and up to 50 mole %, tetrahedrally coordinated boron atoms revert to trigonal coordination as complete devitrification yields crystalline rubidium metaborate. However, the absolute quantities of the molecular species are not necessarily equal and their relative proportions have not been determined.

The foregoing concepts are different from those of many other investigators. One in particular is the lack of any discernible discontinuity at 17 mole % Rb_2O . This raises the question of the actual occurrence of an abrupt change in the concentration of any of the molecular species at that composition. Furthermore, the belief that specific molecular groups, such as BO^- groups, begin to form only at a definite composition is untenable, as it has been shown that all species form almost simultaneously at rather low Rb_2O concentrations.

The oxides of rubidium, sodium, and lithium affect the borate glass structure in the same manner, which indicates that the sizes of these alkali metal cations are not important in determining borate glass structure.

Support is found for the view that the borate glass network may be reconstituted by the introduction of certain metal ions which have the ability to enter into complex formation with singly bonded oxygen atoms.

Acknowledgment. Financial support of this research by the United States Atomic Energy Commission is gratefully acknowledged.

Surface Catalysis of the Orthohydrogen-Parahydrogen Conversion on Carbon-Supported Gadolinium and Holmium Sulfates at 77°K Using Ultrahigh-Vacuum Techniques

by Eric Davidson, Tiao-hsu Chang, and Douglas S. Chapin¹

Department of Chemistry, The University of Arizona, Tucson, Arizona (Received June 10, 1966)

The rates of orthohydrogen-parahydrogen conversion have been investigated at 77°K on several concentrations of $Gd_2(SO_4)_3$ and $Ho_2(SO_4)_3$ catalysts using ultrahigh-vacuum techniques. The catalysts were prepared by adsorption of the rare earth ions from dilute aqueous solutions at pH 1 onto Sterling MT 2700 carbon. The number of rare earth sites on the catalyst was determined by neutron activation analysis. It was found that exhaustive baking under vacuum at 450° for 400 to 600 hr led to a plateau in the rate constant *vs.* time-of-heating curves. Rate constants per paramagnetic site were found to be higher at higher site concentrations; a possible explanation postulates adsorption site "cage" structures which depend on surface site concentrations. The ratio of the rate constants of holmium to gadolinium increased from 2.5 to 3.6 as the rare earth site concentration was increased from 0 to 10^{-5} g-ion/g of C. This result is compared to a theoretical ratio of 2.2 calculated on the basis of the Wigner theory.

Introduction

In this paper are reported results of the measurements of the low-temperature orthohydrogen conversion on a known number of rare earth ions supported on highly graphitized carbon exhaustively outgassed in an ultrahigh-vacuum system.

Ever since the discovery²⁻⁵ of the two forms of hydrogen, orthohydrogen with nuclear spins aligned and odd rotational states and parahydrogen with nuclear spins opposed and even rotational states, many investigators⁵⁻¹¹ have attempted to find the factors influencing the rate of interconversion between the two forms of hydrogen. Two mechanisms for the heterogeneous conversion are considered to be valid in two general temperature regions. High-temperature heterogeneous parahydrogen-orthohydrogen conversion is associated with chemisorption in which the atoms of a hydrogen molecule dissociate and recombine in new pairs of atoms to form normal hydrogen which is 25% parahydrogen.⁶ On the other hand, low-temperature heterogeneous orthohydrogen-parahydrogen conversion⁷ is associated with physical

adsorption during which interaction of a hydrogen molecule with a paramagnetic site causes realignment of the nuclear spins to produce hydrogen of equilibrium composition.

Wigner's⁸ theoretical treatment of the homogeneous conversion, which has been experimentally investigated for solutions of paramagnetic gases and ions,⁹⁻¹¹ is the basis for both the two-dimensional gas model¹²

- (1) Correspondence regarding this paper may be sent to this author.
- (2) A. Farkas, "Orthohydrogen, Parahydrogen, and Heavy Hydrogen," Cambridge University Press, London, 1935.
- (3) D. M. Dennison, *Proc. Roy. Soc. (London)*, **A115**, 483 (1927).
- (4) W. F. Giauque and H. L. Johnston, *J. Am. Chem. Soc.*, **50**, 3221 (1928).
- (5) K. F. Bonhoffer and P. Harteck, *Z. Physik. Chem.*, **B4**, 113 (1929).
- (6) H. S. Taylor, *J. Am. Chem. Soc.*, **53**, 578 (1931).
- (7) K. W. Rummel, *Z. Physik. Chem.*, **A167**, 221 (1933).
- (8) E. Wigner, *ibid.*, **B23**, 28 (1933).
- (9) L. Farkas and H. Sachsse, *ibid.*, **B23**, 1, 19 (1933).
- (10) H. S. Taylor and H. Diamond, *J. Am. Chem. Soc.*, **55**, 2613 (1933).
- (11) H. S. Taylor and A. Sherman, *Trans. Faraday Soc.*, **28**, 247 (1932).

and the cage model¹³⁻¹⁶ for the physical adsorption and catalysis of orthohydrogen-parahydrogen. The separation of orthohydrogen-parahydrogen¹⁷⁻¹⁹ and the success of theoretical treatments²⁰⁻²² in accounting for experimental results using the hindered-rotator model¹³ support the cage model. The agreement²³ with the predictions of the two-dimensional gas model should not be taken as evidence against the cage model since the two theories predict the same pressure dependency when examined on comparable bases.

Wakao, Smith, and Selwood²⁴ have investigated the low-temperature orthohydrogen conversion over supported oxides and metals using a flow system in an attempt to find the causes for anomalously low conversion rates on rare earth ions reported by Weitzel, *et al.*²⁵ Relatively short times of outgassing of the samples and surface poisoning²⁶ appear to be factors obscuring the results. Ashmead, Eley, and Rudham^{15,16} have investigated the conversion on a series of rare earth oxides over a wide range of temperatures. They have demonstrated the similarity of the high-temperature mechanism to the hydrogen-deuterium exchange reaction in the region above 400°K and noted a maximum in the conversion rate *vs.* temperature in the intermediate region (140-400°K) for Nd₂O₃, Gd₂O₃, Er₂O₃, but interestingly, no maximum for Dy₂O₃. A beautiful linear correlation of rate constants *vs.* the square of the magnetic moment was obtained for the low-temperature results. Unfortunately, the number of rare earth ions exposed to the gas phase could not be readily known, the results being reported only in terms of unit area.

In the present work the rate constants are related to the number of rare earth sites on the surface of the catalyst. The rate constants were determined after exhaustive outgassing in an ultrahigh-vacuum system; the number of surface sites was determined by neutron activation analysis.

Experimental Section

Catalyst Preparation. A series of carbon-supported rare earth sulfate catalysts was prepared by adsorption from aqueous solution. The support carbon was Sterling MT 2700 which was used without further treatment.²⁷ Samples (2 g) of carbon were impregnated with 25 ml of the appropriate 0-0.2 *M* rare earth²⁸ sulfate solutions whose pH values were adjusted to 1.00 with H₂SO₄. The adsorptions were carried out at approximately 30° in 30-ml glass bottles with shaking over a period varying from 3 to 12 days. The solutions were then decanted, and the catalysts were dried at 120° in air for 2 days.

Total rare earth content was determined by neutron

activation analysis²⁹ of 1-g samples in Lucite vials having polyethylene covers. A series of standards was prepared, each containing 1 g of unimpregnated carbon to which known amounts of rare earth sulfate in solution had been added.

Ultrahigh-Vacuum System. The catalysis was carried out in a bakeable ultrahigh-vacuum system mounted in a furnace. Four Pyrex tubes of approximately 1-cm i.d. and 25-ml volume, each containing 0.100 g of catalyst, were attached in vertical positions through bakeable metal valves³⁰ to a Pyrex manifold. Attached to the manifold, and also in the furnace, were a Vac-ion pump³¹ and a palladium diffusion thimble. Part of the furnace, which was around the Vac-ion pump, could be cooled independently of the main furnace so that after an initial pumpdown and bakeout, the Vac-ion pump could be operated at room temperature for the final outgassing. The Vac-ion pump could be isolated by metal valves. The initial pumpdown was carried out through a liquid nitrogen trap, mercury diffusion pump, and backing pump out-

(12) L. G. Harrison and C. A. McDowell, *Proc. Roy. Soc. (London)*, **A220**, 77 (1953).

(13) Y. L. Sandler, *J. Phys. Chem.*, **58**, 58 (1954).

(14) Y. L. Sandler, *Can. J. Chem.*, **32**, 249 (1954).

(15) D. R. Ashmead, D. D. Eley, and R. Rudham, *Trans. Faraday Soc.*, **59**, 207 (1963).

(16) D. R. Ashmead, D. D. Eley, and R. Rudham, *J. Catalysis*, **3**, 280 (1964).

(17) C. M. Cunningham, D. S. Chapin, and H. L. Johnston, *J. Am. Chem. Soc.*, **80**, 2382 (1958).

(18) W. R. Moore and H. R. Ward, *ibid.*, **80**, 2909 (1958).

(19) L. Bachmann, E. Bechtold, and E. Cremer, *J. Catalysis*, **1**, 113 (1962).

(20) C. M. Cunningham and H. L. Johnston, *J. Am. Chem. Soc.*, **80**, 2377 (1958).

(21) D. White and E. N. Lassettre, *J. Chem. Phys.*, **32**, 72 (1960).

(22) A. A. Evett, *ibid.*, **33**, 789 (1960).

(23) D. S. Chapin and H. L. Johnston, *J. Am. Chem. Soc.*, **79**, 2406 (1957).

(24) N. Wakao, J. M. Smith, and P. W. Selwood, *J. Catalysis*, **1**, 62 (1962).

(25) D. H. Weitzel, W. V. Lobenstein, J. W. Draper, and O. E. Park, *J. Res. Natl. Bur. Std.*, **60**, 221 (1958).

(26) D. S. Chapin, C. D. Park, and M. L. Corrin, *J. Phys. Chem.*, **64**, 1073 (1960).

(27) The carbon was kindly furnished by Dr. W. R. Smith of the Godfrey L. Cabot Corp.

(28) The rare earth oxides were kindly furnished through the courtesy of Dr. F. H. Spedding, Institute for Atomic Research, Ames, Iowa.

(29) The samples were irradiated in the TRIGA reactor in the Department of Nuclear Engineering.

(30) Preliminary back-conversion experiments conducted using ultrahigh-vacuum valves from Granville-Phillips Co., Pullman, Wash., showed that the amount of back conversion under the conditions of the present study were negligible; however, for a different conclusion, see Y. L. Sandler and M. Gazith, *J. Phys. Chem.*, **63**, 1095 (1959).

(31) Varian Associates, Palo Alto, Calif.

NEW SUBSCRIPTION ORDER

*The Journal of
Physical Chemistry*

Please enter my subscription to

THE JOURNAL OF PHYSICAL CHEMISTRY for 1966 (12 issues).

Price for ACS members \$12.00; price for nonmembers \$24.00.

Postage per year: Foreign \$3.00; PUAS and Canada \$2.00

NAME _____

ADDRESS _____

CITY _____ STATE/COUNTRY _____ ZIP _____

SIGNED _____

I AM AN ACS MEMBER.

<input type="checkbox"/> CHECK ENCLOSED <small>(payable to the American Chemical Society)</small>
<input type="checkbox"/> BILL ME LATER

FIRST CLASS

PERMIT No. 1411-R

WASHINGTON, D. C.

B U S I N E S S R E P L Y M A I L

No Postage Stamp Necessary if Mailed in the United States

— POSTAGE WILL BE PAID BY —

AMERICAN CHEMICAL SOCIETY
1155 Sixteenth Street, N.W.
Washington, D.C. 20036

ATTN. R. H. BELKNAP

side the furnace. The temperature of each catalyst tube was controlled during bakeout by means of individual heaters. Since prolonged bakeouts at 450° lead to failure of the metal valves, the main furnace was baked at 300°, and the catalysts were baked at 450°. The catalysts were baked for several periods of approximately 20 hr, near the end of which time the pressure in the system, as estimated by the Vac-ion pump current, was less than 2×10^{-7} torr.

During a kinetic run, the individual catalyst tube furnaces were replaced by dewars of liquid nitrogen which were kept filled very carefully to a constant level.

Normal Hydrogen. Cylinder hydrogen, obtained from the Matheson Chemical Co., was purified by diffusion through hot palladium immediately prior to a kinetic run and just after catalyst bakeout. Normal hydrogen was allowed to accumulate in the manifold until a constant pressure was attained. Pressures were monitored with a Gaertner cathetometer focused on a mercury U-tube manometer located on the upstream side of the Pd thimble. By calibration of the volumes, a predetermined final pressure (55 torr) on the catalyst was obtained.

Orthohydrogen-Parahydrogen Analysis. The analytical system³² was connected to the ultrahigh-vacuum manifold through another metal valve which was baked closed and then opened to admit hydrogen samples to the analytical system at the completion of a kinetic run.

Results and Discussion

Adsorption from Solution. The adsorptions of Gd^{3+} and of Ho^{3+} sulfates from aqueous solutions on Sterling MT 2700 carbon are shown in Figures 1 and 2, respectively. Neutron activation analyses of the prepared catalysts are shown as ordinates plotted against the final concentrations of the rare earth sulfate solutions. Equilibrations were carried out with shaking for 3 days or longer as indicated.

From the data of Figures 1 and 2 it can be noted that holmium and gadolinium adsorptions are very nearly the same at low concentrations. However, at the higher concentrations carbon apparently adsorbs holmium to a greater extent than gadolinium. Excessive scatter in the data at higher concentrations is thought to be due to variations in the amounts of solution left in contact with the catalysts; the data appear to be more consistent at the lower concentrations. Catalysts in the range $0-1.2 \times 10^{-5}$ g-ion/g of carbon were selected for the orthohydrogen-parahydrogen conversion study.

Variation of Rate Constants with Bakeout Time.

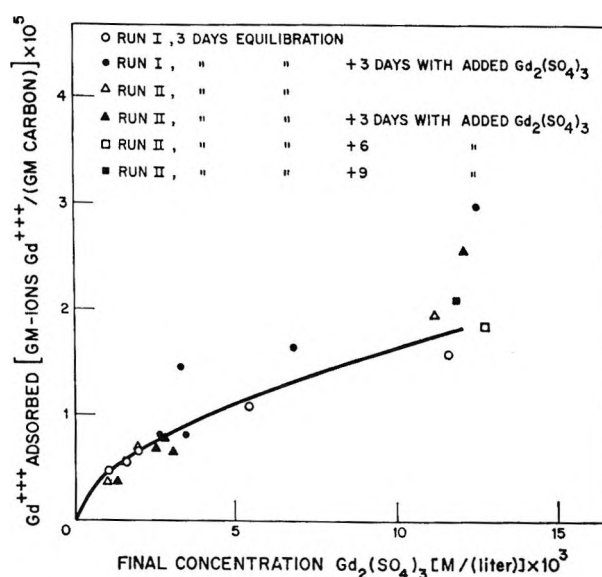


Figure 1. The adsorption of $Gd_2(SO_4)_3$ on carbon from aqueous solution of pH 1.00.

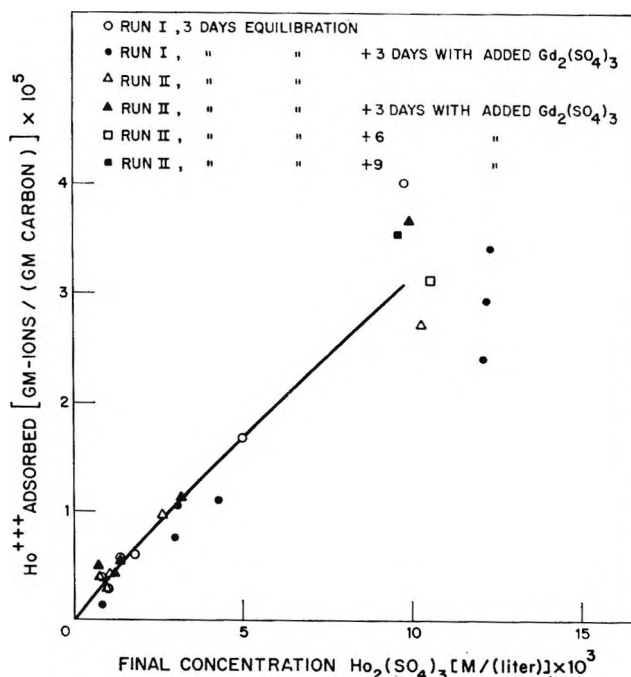


Figure 2. The adsorption of $Ho_2(SO_4)_3$ on carbon from aqueous solution of pH 1.00.

Three concentrations of rare earth sulfate catalysts plus a blank of the support carbon were used in each series of determinations. The total time of bakeout affected the rate constants as is shown in Figures 3 and 4 for Gd^{3+} and Ho^{3+} , respectively. A plateau region

(32) D. S. Chapin and C. D. Park, submitted for publication.

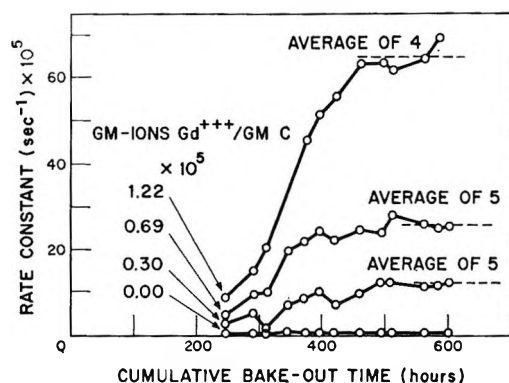


Figure 3. Rate constants vs. bakeout time for the orthohydrogen-parahydrogen conversion.

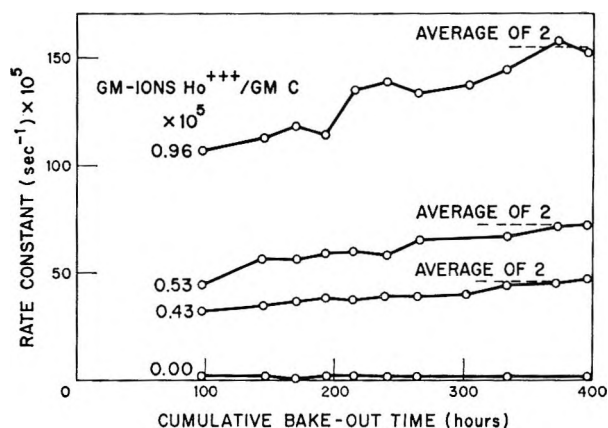


Figure 4. Rate constants vs. bakeout time for the orthohydrogen-parahydrogen conversion.

appears to have been reached at least for the lower paramagnetic ion concentrations. It is supposed that the cleanup of the surface is primarily a process involving the loss of adsorbed water. As the water leaves during bakeout, exposing the rare earth ion on the surface, hydrogen is able to diffuse to and from the site during a rate determination at 77°K causing conversion by the magnetic mechanism.

Variation of Rate Constants with Paramagnetic Ion Concentration. If the last few points of the curves in Figures 3 and 4 are averaged and plotted as functions of the total numbers of paramagnetic ions in gram-ions in the catalyst chamber (on 0.100 g of catalyst), the rate constants vary as shown in Figure 5. Surprisingly, there appears to be a general increase in the effectiveness of catalytic site. Possibly some of the ions adsorbed at the lower concentrations during catalyst preparation are unavailable later to the hydrogen. However, it seems unlikely that a large hydrated ion such as Ho^{3+} , on the one hand, could find a site during

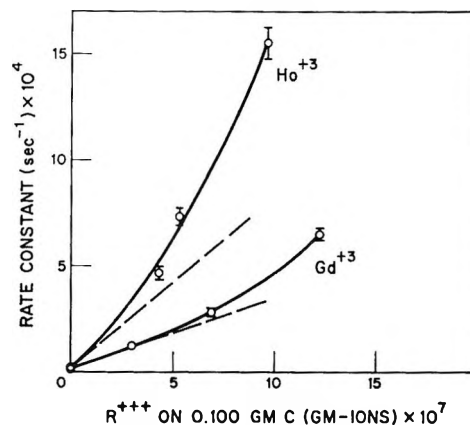


Figure 5. Rate constants vs. total number of paramagnetic ions for the orthohydrogen-parahydrogen conversion.

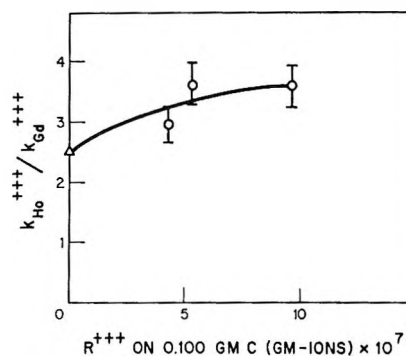


Figure 6. The effect of paramagnetic ion concentration on rate constant ratio.

the adsorption from solution to which the relatively small hydrogen molecule, on the other hand, could not migrate during the orthohydrogen-parahydrogen catalysis. The cause of the upward curvature is not known. If, during the adsorption of the ions on the carbon surface, a piling of cations and anions in the form of crystallites occurred, the opposite curvature would be expected from that observed. It seems reasonable to suppose that ions in close proximity to one another are more effective as catalysts than the same ions would be if separated on the carbon surface by greater distances. A possible explanation, but not a unique one, is as follows.

First, it is assumed that the paramagnetic ions are adsorbed on the surface in patches. Second, it is assumed that the hydrogen molecules are adsorbed on the paramagnetic ions more strongly than they are on the carbon atoms of the surface. Third, it is assumed that the "cage" structure surrounding the paramagnetic ion and, therefore, the rate constant depend on the ion concentration on the surface (and on the degassing time, Figures 3 and 4).

It was of interest to examine further the data by computing the ratios of the rate constants as a function of the catalytic site concentrations from the data presented in Figure 5. The results are shown in Figure 6. The ratio estimated from the zero tangents, $(k_{\text{Ho}^{3+}}/k_{\text{Gd}^{3+}})_0$, is 2.5; as concentration was increased, the ratio increased 3.6. The corresponding ratio of the squares of the magnetic moments $\mu_{\text{Ho}^{3+}}^2/\mu_{\text{Gd}^{3+}}^2 = (10.4)^2/(7.9)^2 = 1.7$ according to data of Cabrera and Duperier³³ which were obtained from measurements on the anhydrous sulfates; the ratio is equal to 1.8 according to theoretical calculations.³⁴ If, however, one calculates¹⁶ the ratio of the quantity $(\mu^2/d^6)_{\text{Ho}^{3+}}$ to $(\mu^2/d^6)_{\text{Gd}^{3+}}$, where d represents the distance of the hydrogen molecule from the magnetic ion, substituting³⁵ for d 1.34 and 1.39 Å, respectively, for Ho^{3+} and Gd^{3+} yields 2.2. This compares very favorably with the ratio of the experimental rates $(k_{\text{Ho}^{3+}}/k_{\text{Gd}^{3+}}) = 2.5$ obtained from the low-concentration data.

Conclusions

A study of the rates of orthohydrogen-parahydrogen conversion measured at 77°K and 55 torr on rare earth sulfates supported at low coverages on graphitized carbon leads to the following conclusions.

(1) The rates of orthohydrogen-parahydrogen conversion increased with time of outgassing at 450° in an ultrahigh-vacuum system; a virtual plateau in rate constant *vs.* time of outgassing was reached in 400 to 600 hr on 0.1 g of catalyst.

(2) The rates of orthohydrogen-parahydrogen conversion increased with total paramagnetic ion content; the rare earth ions adsorbed at low levels on the carbon support were less effective as catalysts than those adsorbed at higher levels. A possible explanation of this effect is made assuming that the "cage" structure around the paramagnetic site depends on the surface concentration of ions on the surface.

(3) The rates of orthohydrogen-parahydrogen conversion increased approximately as the square of magnetic moment due to the 4f electrons in the rare earth ion.

(4) The use of graphitized carbon as a support for catalytic ions which are amenable to neutron activation analysis in conjunction with an ultrahigh-vacuum system has been demonstrated to yield reproducible results in studying the orthohydrogen-parahydrogen conversion mechanism; its use for other catalysts for this and other reactions is recommended.

Acknowledgment. Support under Contract AT(11-1)-367 with the U. S. Atomic Energy Commission is gratefully acknowledged.

(33) J. H. Van Vleck, "Theory of Electric and Magnetic Susceptibilities," Oxford University Press, London, 1932, p 245.

(34) See ref. 33, p 243.

(35) For want of more accurate information the distances used were taken as the sum of the hydrogen covalent radius of 0.37 Å given by L. Pauling in "The Nature of the Chemical Bond," 3rd ed, Cornell University Press, Ithaca, N. Y., 1960, p 226, and the ionic radii of 1.02 and 0.97 Å for Gd^{3+} and Ho^{3+} , respectively, given on p 518.

Structure of Surface Species. Adsorption of Nitrogen Dioxide on Oil- and Silica-Supported Nickel and Iron

by G. Blyholder and Marvin C. Allen

Department of Chemistry, University of Arkansas, Fayetteville, Arkansas (Received June 17, 1965)

The infrared spectrum of surface species formed upon exposure of evaporated-into-oil Fe to 10 mm of NO₂ is interpreted as indicating dissociation to adsorbed NO and adsorbed oxygen. Exposure of a similar sample to 41 cm of NO₂ or exposure of silica-supported Fe to 5 mm of NO₂ gives spectra which are interpreted as indicating formation of two and three oxygen atom-nitrogen oxide complexes in which a bidentate NO₃ complex predominates. Similar results are obtained for evaporated-into-oil Ni and silica-supported Ni. The role of the oil support for the metals and the effect of different surface sites on the spectra of adsorbed species are discussed.

Introduction

In recent years a number of new tools and new uses of old tools have been developed to examine the adsorption of gases on metal surfaces. The presence of many types of adsorbed species formed through the bonding of molecules to metal surfaces have been detected. However, even the recently developed ultrahigh-vacuum methods, which employ such techniques as low-energy electron diffraction, field ion microscopy, and surface potential measurements, do not yield direct information about the structure of polyatomic adsorbed species. Infrared spectroscopy has proven to be one of the most powerful tools for structure determination. Therefore, infrared spectroscopy has been chosen in this work as the most appropriate means of investigating the structure of oxides of nitrogen adsorbed on Ni.

The structure of carbon-oxygen compounds and complexes adsorbed on Fe and Ni has recently been investigated in this and other laboratories by infrared spectroscopy. The spectra have been interpreted in terms of the spectra of known compounds and coordination complexes of transition metals. Carbon dioxide adsorbed on Fe at 20° gives an infrared spectrum indicative of dissociation to form adsorbed CO.¹ Some spectra for CO₂ adsorbed on silica-supported Ni have been interpreted in terms of a carboxylate structure and a (CO₃)⁻ complex structure.² Exposure of CO adsorbed on Fe to O₂ results in the desorption of the CO.¹ For CO adsorbed on Ni, exposure to O₂ results

in the formation of a bidentate CO₃ complex.³ Since nitrogen forms a number of oxides which are analogous to those of carbon, *e.g.*, CO-NO, CO₂-NO₂, and CO₃²⁻-NO₃⁻, the species formed by the adsorption of NO₂ on Fe and Ni were investigated to see if the structure of the stable surface species formed by NO₂ on Fe and Ni would follow the same pattern as CO₂ or if the difference in electronic structure between NO₂ and CO₂ would result in fundamental differences in their behavior.

Relatively little work has been reported in the literature on the adsorption of oxides of nitrogen on metals. Sachtler⁴ has mentioned making surface potential measurements and gas phase composition measurements for NO adsorbed on Ni. Terenin and Roev⁵ have reported the infrared spectrum of NO adsorbed on alumina-supported Ni as well as several other metals. Spectra of NO adsorbed on silica-supported Pt and Pd have also been obtained.⁶ Unfortunately, the alumina support only transmits in the infrared region from about

- (1) G. Blyholder and L. D. Neff, *J. Phys. Chem.*, **66**, 1464 (1962).
- (2) R. P. Eischens and W. A. Pliskin, *Advan. Catalysis*, **9**, 662 (1957).
- (3) G. Blyholder, Proceedings of the Third International Congress on Catalysis, North-Holland Publishing Co., Amsterdam, 1964, Paper I-38.
- (4) W. M. H. Sachtler, *Actes Congr. Intern. Catalyse*, **2^e**, Paris, 1960, 2197 (1961).
- (5) A. Terenin and L. Roev, *ibid.*, 2183 (1961).
- (6) H. Dunkel and H. Hobert, *Z. Chem.*, **3**, 398 (1963).

4000 to 1300 cm⁻¹. Recently, a technique to obtain the spectra of molecules adsorbed on metals over the entire range from 5000 to 250 cm⁻¹ has been developed in this laboratory⁷ and is used in this study. We have found no work on the adsorption of NO₂ on Fe and Ni in the literature. Some results for exposing our metal samples to N₂ and O₂ will also be discussed because of their relevance to the NO₂ work.

Experimental Section

The wide spectral range technique consists of evaporating a metal from an electrically heated 30-mil tungsten filament. The metal to be evaporated is usually wrapped as 5–10-mil wire in short segments around the tungsten filament. The filament is located 3 to 4 cm from the cell windows. The evaporation is carried out in 15 to 20 short bursts of heating lasting 7 sec and spaced about 5 min apart. The filament is usually heated to a temperature just hot enough to melt the evaporating metal. During the evaporation the cell is filled with from 0.25 to 0.5 mm of He. The cell windows are coated with a hydrocarbon oil (Welch Duo-Seal pump oil, infrared spectrum identical with that of Nujol) which has been specially treated to remove all components not of low vapor pressure. The result of the evaporation is essentially a mull of small metal particles on the cell windows. The gas to be studied is then admitted to the cell, and the spectrum of the chemisorbed species is obtained. Spectra are recorded before and after admission of the gas to the cell. Pumping for 5 min has been found sufficient to remove all spectra due to gas phase molecules.

Some spectra were also run of species adsorbed on silica-supported metals. The experimental technique, cells, and sample preparation have previously been described in detail.¹ Essentially, a metal nitrate is dispersed on silica (Cab-O-Sil, donated by Godfrey L. Cabot, Inc., Boston, Mass.) and pressed into a disk, and the disk is placed in a vacuum cell. The metal nitrate is reduced to metal in a stream of H₂ at temperatures up to 400°. This sample transmits infrared radiation over the range from 4000 to 1300 cm⁻¹.

N₂, NO₂, H₂, CO, and O₂ were obtained from the Matheson Co., Inc. All gases were dried by passage through a cold trap. The H₂ was passed over hot copper turnings to remove O₂. The CO was passed through an activated-charcoal trap cooled with liquid air.

The spectra were recorded on either a Perkin-Elmer Model 337 or a Model 21 spectrophotometer. The latter is equipped with NaCl and CsBr prisms.

Results

The results apply to adsorption at 20° on metal evaporated into hydrocarbon oil unless otherwise stated. Relative intensities are indicated by the symbols: s, strong; m, medium; w, weak; v, very; and b, broad. Since our main interest here is in the structure of the stable surface species in all cases, the spectra reported are those obtained after removal of the gas phase by pumping on the cell for over 30 min.

N₂ and O₂. N₂ with Fe and Ni gave no band which could be attributed to adsorbed species with gas pressures up to 500 mm. Adsorption of O₂ at 10 mm over Ni resulted in a very broad band located at 500 ± 30 cm⁻¹. For Ni evaporated into hydrocarbon oil, adsorbed O₂ also produces medium-intensity bands at 1600 and 1300 cm⁻¹. These bands are not produced when the same conditions are used with a fluorocarbon oil. An NiO mull gave a broad band located at about 490 cm⁻¹. Only one very broad band at about 600 ± 30 cm⁻¹ was recorded upon exposure of a freshly evaporated Fe sample to 10 mm of O₂. The great breadth of the bands for oxygen on Fe and Ni is illustrated by Figure 1 which shows the results for O₂ on Fe.

NO₂ Chemisorbed on Fe. A spectrum of surface species formed after exposure of evaporated-into-oil Fe to 10 mm of NO₂ and after removal of the gas phase NO₂ is shown in Figure 2. Bands are recorded at 2005 (vw), 1805 (s), 1720 (m), and about 600 cm⁻¹ (vb). The addition of 20 mm of H₂ is shown in Figure 2 to have no substantial effect on the adsorbed species.

When a much higher NO₂ pressure, 34 cm, is used with a fresh sample, bands are observed at 2010 (w), 1950 (w, sh), 1600 (m), 1560 (s), 1360 (sh), 1270 (sh), 1250 (m), 1030 (sh), 1005 (w), 950 (sh), 830 (vw), 795 (w), 765 (w), and 620 cm⁻¹ (wb).

When silica-supported Fe is used as the adsorbent for NO₂ the spectrum in Figure 3 shows only two strong bands at 1610 and 1525 cm⁻¹.

NO₂ Chemisorbed on Ni. A typical spectrum produced by exposing Ni to 10 mm of NO₂ is shown in Figure 4. Bands are found at 1840 (s), 1555 (m), 1330 (vw), 1090 (vw), and 610 cm⁻¹ (wb). Spectra produced by NO₂ show some variability from sample to sample. Bands are always produced quite close to the same frequencies, but their relative intensities vary. The bands at 1840 and 610 cm⁻¹ maintain the same intensity relative to each other as also do the bands at 1555, 1330, and 1090 cm⁻¹. However, the relative intensities of these two groups show considerable variation; *i.e.*, on a particular sample one group may be down to one-third its intensity on other samples.

(7) G. Blyholder, *J. Chem. Phys.*, **36**, 2036 (1962).

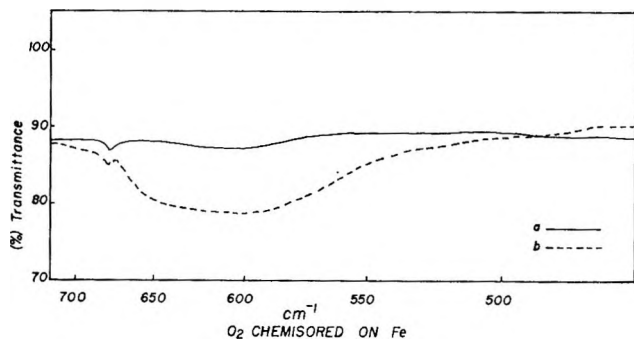


Figure 1. Oxygen chemisorbed on Fe: (a) background; (b) after exposure to 10 mm of O_2 for 1 hr.

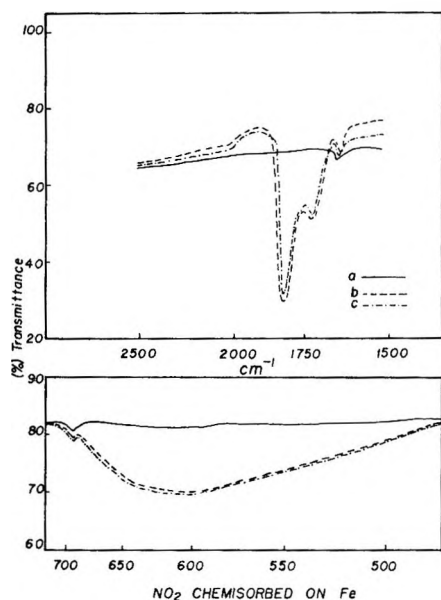


Figure 2. NO_2 chemisorbed on Fe: (a) background; (b) after exposure to 10 mm of NO_2 for 1 hr; (c) after exposure to a further addition of 20 mm of H_2 for 1 hr.

Addition of H_2 to a sample results in a decrease in intensity of the bands produced by the interaction of NO_2 with the surface as is also shown in Figure 4.

The result of using a much higher NO_2 pressure, 41 cm, is shown in Figure 5. Bands are produced at 1745 (w), 1550 (s), 1290 (vs), 1245 (m), 1050 (m), 1020 (m), 840 (vw), 804 (m), 765 (w), and 745 cm^{-1} (w).

In order to check more carefully the $1350\text{--}1550\text{-cm}^{-1}$ region, a sample using a fluorocarbon oil was used. Putting 10 mm of NO_2 in this cell produced the usual bands at 1850 (m), 1580 (m), and about 1330 cm^{-1} , plus apparently some absorption at 1400 cm^{-1} which, as can be seen in Figure 6, is not resolved from the broad 1330-cm^{-1} band.

A check to see if the oil was having a drastic effect on

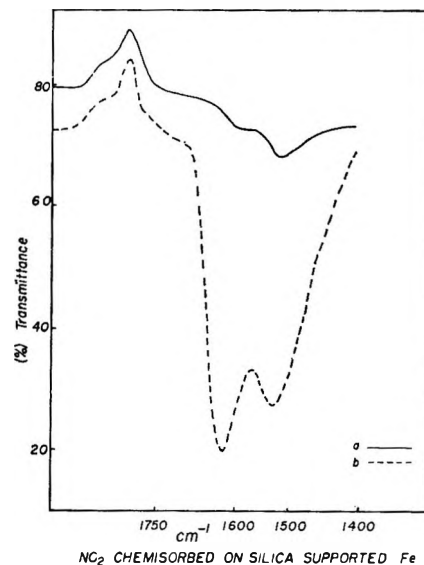


Figure 3. NO_2 chemisorbed on silica-supported Fe: (a) background; (b) after exposure to 5 mm of NO_2 for 1 hr.

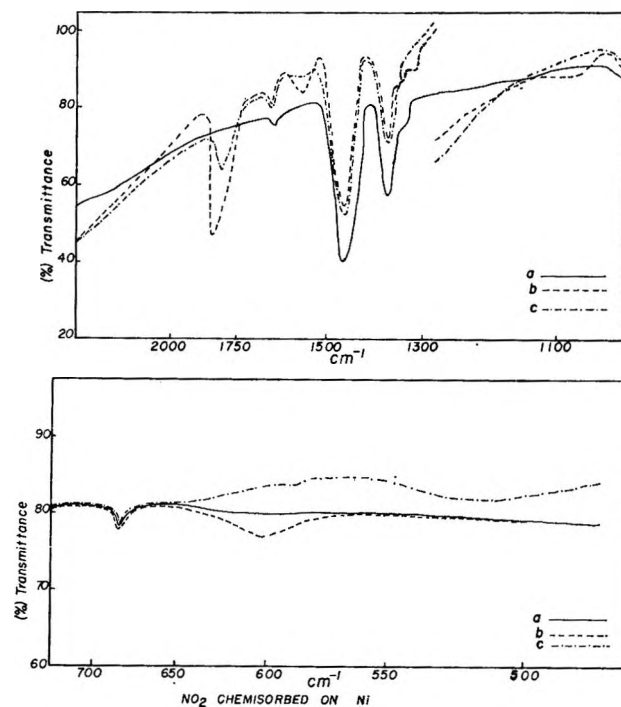


Figure 4. NO_2 chemisorbed on Ni: (a) background; (b) after exposure to 10 mm of NO_2 for 1 hr; (c) after exposure to a further addition of 10 mm of H_2 for 1 hr.

the species formed by NO_2 was made by using a silica-supported Ni sample. Exposure to 10 mm of NO_2 produced bands at 1850 (w), 1555 (vs), and 1440 cm^{-1} (vs). The region below 1350 cm^{-1} is not available for inspection with silica-supported samples.

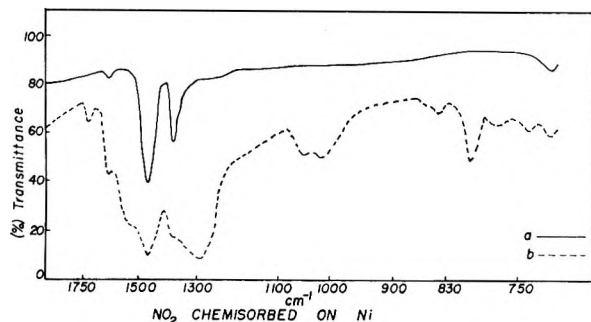


Figure 5. NO₂ chemisorbed on Ni: (a) background; (b) after exposure to 410 mm of NO₂.

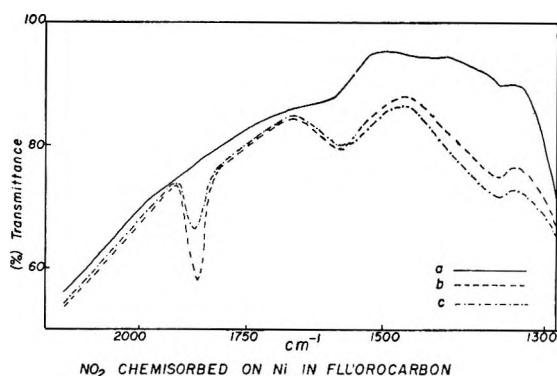


Figure 6. NO₂ chemisorbed on Ni in fluorocarbon: (a) background; (b) after exposure to 11 mm of NO₂ for 1 hr; (c) after exposure to ϵ further addition of 15 mm of O₂ for 16 hr.

As shown in Figure 7 pumping removed the band at 1850 cm⁻¹, but it grew back upon letting the sample set without pumping overnight. This change is notable because continued evacuation or leaving an evacuated cell set for 12 to 24 hr in all other cases of NO₂ adsorption on Fe and Ni in oil- or silica-supported Fe had very little effect on the spectra of the adsorbed species.

Discussion

While it is desirable to obtain adsorption data on "clean" metal surfaces, much interesting and meaningful data can be obtained from metal surfaces which have been contaminated in a known and reproducible way. The evaporated-into-oil metal surfaces belong to this latter class. The relationship between clean and oil-immersed surfaces may be compared to the relationship between gas phase and solution chemistry. Just as the solubility of reactants in the solvent and the interaction of the solvent with the reactants must be considered in solution chemistry so the solubility of adsorbents in the oil and the adsorption of the oil on

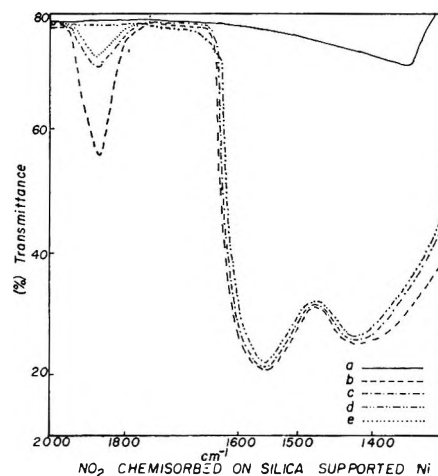


Figure 7. NO₂ chemisorbed on silica-supported Ni: (a) background; (b) exposure to 10 mm of NO₂; (c) after pumping for 30 min; (d) after further pumping for 4 hr; (e) after further sitting overnight without pumping.

the metal surface must be considered for the evaporated-into-oil metals. In the ensuing discussion of the experimental results for silica- and oil-supported metals some of these relations for specific systems will be brought out. Certainly, many catalytic, corrosion, and other surface processes are carried out in solutions.

Besides being an intrinsically interesting medium, the oil allows the obtaining of data that so far have been unobtainable in any other way. When silica or alumina are used as metal-support materials, the infrared spectral range is limited by the support to the region from about 4000 to 1300 cm⁻¹. Evaporation of the metal directly onto the infrared windows either under vacuum or in a small pressure of an inert gas results in a film whose transmission is so low that very little usable data have so far been obtained this way. Light scattering by a powder film is dependent upon the particle size. When clean metal particles come into contact with each other, they readily sinter, thereby increasing the particle size and the light scattering. The oil film serves to keep the metal particles separated and thereby greatly reduces the scattering. Also the scattering of light is dependent on the difference in refractive index between the scattering particle and the surrounding medium. The difference in refractive index between the metal particles and their surroundings is reduced by the presence of the oil with the result that, for a given amount of metal present, the oil increases the transmission. This effect is the basis of the commonly used mull technique for obtaining infrared spectra of solids. The net result of the use of the

oil is that, whereas without it we have not been able to obtain usable spectra of adsorbed species on evaporated metals, with it we have been able to obtain spectra over the entire range from 5000 to 300 cm^{-1} . Although the presence of the oil does introduce some complexity, as noted above, it does allow some unique data to be obtained for the many substances that do adsorb on the metal film in spite of the presence of the oil. For those surface species that are formed, the increased spectral range greatly aids in the attempt to determine their structure.

Eischens and Jacknow⁸ have found that an N_2 pressure near 0.01 mm is required to produce readily observable infrared bands for N_2 chemisorbed on silica-supported Ni at 30°. The adsorbed N_2 has a weak interaction with the surface. It is thus not surprising that no bands were observed for adsorbed N_2 for our samples since the N_2 would have to displace adsorbed hydrocarbons and the concentration of N_2 next to the metal surface is quite low due to the low solubility of N_2 in hydrocarbon oil.

Comparison of the very broad band around 500 cm^{-1} for adsorbed O_2 to the spectrum of NiO which has a broad band near 480 cm^{-1} leads to the assumption that O_2 is dissociatively adsorbed to produce a surface oxide that resembles bulk NiO. No bands were found which could be attributed to an oxygen-oxygen stretching frequency for molecular adsorption. The bands at 1600 and 1300 cm^{-1} produced when O_2 is adsorbed on Ni in oil are presumed to be due to oxidized hydrocarbon oil since these bands are not found when a fluorocarbon oil is used.

Similar to the results with Ni, no bands for adsorbed species were observed upon exposure of the evaporated-into-oil Fe to N_2 while exposure to O_2 produced a very broad band around 600 cm^{-1} . Since a band in this region has been reported for Fe_2O_3 ,⁹ the oxygen is presumed to absorb dissociatively with the formation of a surface oxide layer.

The structures of nitrogen-oxygen complexes will be discussed in terms of structures of known compounds and complexes¹⁰⁻¹⁸ which are summarized in Table I. The assignments and structures for nitro and nitrito complexes seem to be reasonably well established. Even though bands have been found for a bridging NO_2 group, the structure of the group has not been established. Since bands for adsorbed complexes of nitrogen and oxygen do not coincide with the bands for the bridge NO_2 group, the lack of a definite structure need not disturb us here. The situation with respect to nitrate complexes is not so well settled. Many papers have been published giving band assignments for nitrate complexes, but unfortunately most of the com-

plexes have not had their structures definitely established. The band assignments for mononitrate complexes are based on $[\text{Co}(\text{NH}_3)_6\text{NO}_3]^{2+}$ (ref 12) and $\text{Mn}(\text{CO})_5\text{NO}_3$ (ref 13) which, although X-ray structures have not been reported, would seem most likely to be monodentate nitrate because of the usual octahedral structure of Co and Mn complexes. The only bidentate nitrate complex for which we could find an X-ray or electron diffraction structure¹⁴ is anhydrous $\text{Cu}(\text{NO}_3)_2$ so this is used for assignments.¹⁵ Among the many assignments for less well-established structures, no assignments have been proposed for bands much above 1500 cm^{-1} to monodentate nitrate complexes although some assignments for bidentate nitrate complexes have been proposed for bands from 1590 down to 1480 cm^{-1} . Thus, although there might be some question about whether a band around 1500 cm^{-1} was due to a mono- or bidentate group, for a band around 1550 cm^{-1} a monodentate assignment would appear to be most unlikely.

Considering the interaction of NO_2 at 10 mm with evaporated Fe, the bands at 2005, 1805, and 1720 cm^{-1} have been found to be characteristic of NO chemisorbed on Fe^{5,19} although the band around 600 cm^{-1} has been seen here to be characteristic of O_2 on Fe. Although Terenin and Roev⁵ found the relative intensities of the various bands for NO adsorbed on Fe to be a function of the metal support used, for NO adsorbed on evaporated-into-oil Fe an intensity pattern like that in Figure 2 was found.¹⁹ The conclusion seems inescapable that on evaporated-into-oil Fe the main interaction of NO_2 at 10 mm is a dissociative one to produce adsorbed NO plus oxygen. The use of a higher NO_2 pressure or addition of NO_2 to silica-sup-

(8) R. P. Eischens and J. Jacknow, Proceedings of the Third International Congress on Catalysis, North-Holland Publishing Co., Amsterdam, 1964, Paper I-36.

(9) E. A. Richardson, Doctoral Dissertation, University of Arkansas, 1962.

(10) K. Nakamoto, J. Fujita, and H. Murata, *J. Am. Chem. Soc.*, **80**, 4817 (1958).

(11) J. Chatt, L. A. Duncanson, B. M. Gatehouse, J. Lewis, R. S. Nyholm, M. L. Todd, and L. M. Venanzi, *J. Chem. Soc.*, 4073 (1959).

(12) B. M. Gatehouse, S. E. Livingstone, and R. S. Nyholm, *ibid.*, 4222 (1957).

(13) C. C. Addison, M. Kilner, and A. Wojcicki, *ibid.*, 4839 (1961).

(14) R. E. La Vitta and S. H. Bauer, *J. Am. Chem. Soc.*, **85**, 3597 (1963).

(15) C. C. Addison and B. M. Gatehouse, *J. Chem. Soc.*, 613 (1960).

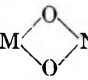
(16) K. Nakonishi, "Infrared Absorption Spectroscopy," Holden-Day, Inc., San Francisco, Calif., 1962.

(17) L. J. Bellamy, "Infrared Spectra of Complex Molecules," Methuen and Co. Ltd., London, 1958.

(18) K. Nakamoto, "Infrared Spectra of Inorganic and Coordination Compounds," John Wiley and Sons, Inc., New York, N. Y., 1963.

(19) G. Blyholder and M. Allen, *J. Phys. Chem.*, **69**, 3998 (1965).

Table I: Frequencies for Nitrogen-Oxygen Complexes

Structure	Obsd frequencies, cm ⁻¹						Ref
NO ₂ gas	1618						18
[ONO] ⁻ free ion			1318			750	18
M-ONO nitrito complex		1465 ± 10	1330	1260	1055 ± 10	830	18
M-NO ₂ nitro complex		1410 ± 30	1340 ± 10			820 ± 10	18
NO ₂ bridge ligand (structure?)		1500 ± 20		1210 ± 20		830	10, 11
CH ₃ NO ₂	1580		1384				647, 18
[NO ₃] ⁻ free ion		1400			1040 ± 20	825	700, 18
M-ONO ₂ nitrate monodentate		1490 ± 10		1280 ± 10	1010	800	12, 13
M  NO nitrate bidentate	1565-1500			1290	1020	790	770, 14, 15
C-ONO ₂ covalent nitrate	1630 ± 10			1280 ± 10		860	760, 16, 17
C-O-N=O covalent nitrite, <i>trans</i>	1665 ± 15					780 ± 30	16, 17
C-O-N=O covalent nitrite, <i>cis</i>	1615 ± 10					780 ± 30	16, 17

ported Fe appears to produce more complex nitrogen-oxygen complexes.

When evaporated-into-oil Fe is exposed to 34 cm of NO₂ pressure, the results indicate the formation of little chemisorbed NO whereas strong bands for oxide complexes are produced. The weak bands at 2010 and 1950 cm⁻¹ are interpreted as indicating a small amount of adsorbed NO. The strong band at 1560 cm⁻¹ is most consistent with a bidentate nitrate structure when compared to the spectra in Table I. This structure is further supported by the appearance of bands at 1270, 1030, 795, and 765 cm⁻¹. The presence of the two bands at 1270 and 1250 cm⁻¹ seems to indicate the existence of two types of NO₃ complex on the surface. The band at 1600 cm⁻¹ upon comparison to Table I could be attributed to either a covalent nitrate or a covalent nitro group as in CH₃NO₂. The band at 1360 cm⁻¹ is consistent with the existence of a covalent nitro group on the surface.

In order to examine the behavior of NO₂ on a surface which has not been covered with oil, the spectrum produced by putting 5 mm of NO₂ in a cell with silica-supported Fe was recorded. The result is different from that where evaporated-into-oil Fe was exposed to 10 mm of NO₂ but is similar to the result with 34 cm of NO₂ in that two intense bands at 1610 and 1525 appeared. By comparison to Table I these bands are tentatively assigned to a structure like a covalent nitrate or nitro group and a bidentate nitrate complex,

respectively. Another covalent structure that the 1610-cm⁻¹ band could possibly be ascribed to is the *cis* covalent nitrite. This was not done because, if the *cis* structure is formed the *trans* structure is also expected. No band in the region expected for the *trans* structure was detected. Also, the *cis* structure places the end oxygen atom in a position where it could readily interact strongly with other surface atoms so that this structure is not expected to be particularly stable.

The behavior of NO₂ at high pressure, 34 cm, on oil-supported Fe is seen to be quite comparable to its behavior at 5 mm on silica-supported Fe in that both adsorbents produce NO₃ complexes and relatively little adsorbed NO. Some differences in adsorbed species are expected since the NO₂ must displace physically adsorbed oil from the oil-supported samples, and the relative proportions of plane face sites and edge or dislocation sites are expected to be different on the evaporated and silica-supported metals. The difference in the nature of the surface species formed, when high and low pressures of NO₂ are used over the oil-supported Fe, is attributed to the difference in concentration of NO₂ at the oil-metal interface. The solubility of NO₂ in oil is low so that the concentration of NO₂ in the oil is much less than the gas phase concentration. Thus, the results with 5 mm of gas pressure over the silica-supported Fe are comparable to those with 34 cm over the oil-supported Fe. When

the low pressure of 10 mm of NO_2 is used over the oil-supported Fe the number of NO_2 molecules reaching the surface is too low to build up NO_3 complexes so the predominant reaction is one of decomposition to adsorbed NO and adsorbed oxygen. The decomposition to NO and the various NO_3 complex building processes are regarded as competitive reactions. These do not seem to be equilibrium processes since the observed spectra do not change appreciably upon evacuating the cells for periods up to 24 hr. We have not followed any samples longer than this.

In order to see why it is at least not unreasonable to propose two rather different types of NO_3 complexes on a silica-supported Fe surface, it is helpful to consider the variation in N-O stretching frequencies of some of the compounds in Table I. It is observed that the asymmetric NO_2 stretching frequency in going from a metal nitro complex to a covalent nitro compound increases by over 100 wavenumbers from 1410 to 1580 cm^{-1} . This change is indicative of an increase in the strength of the N-O bonds which is contributed to by a change in the NO_2 π -electron system. The NO_2 π -electron system in a covalent nitro compound contains four electrons, and this π system does not interact appreciably with the electrons and orbitals of the carbon atom. However, in a metal-nitro complex, the metal has suitably oriented d orbitals to interact with this π system. Simple Hückel molecular orbital calculations indicate that the result of this interaction is the production of a molecular orbital which is above the normally filled two lowest molecular π orbitals of the NO_2 group, is below the isolated metal d orbitals, and is antibonding for the N-O bonds. This orbital will be partially filled depending upon the competition for electrons of other groups around the metal atom. General bonding considerations indicate a metal ligand bond is stabilized by some back donation of charge from the metal to the ligand so this orbital is expected to be partially filled. The result of partially filling this orbital is to weaken the N-O bonds and so reduce the frequency of N-O stretching vibrations. Similar considerations may be used when comparing a monodentate nitrate structure to a covalent nitrate structure where again a 100- cm^{-1} change is observed in the asymmetric stretching frequency. Thus, the ability of the atom to which the nitrogen-oxygen group is attached to put electrons into certain molecular orbitals extending over the ligand affects the observed stretching frequencies. Covalent bonding to a saturated carbon atom merely represents an extreme structure in which no donation of π electrons takes place because no π bond is possible between the ligand group and the atom to which it is bonded.

The above considerations are applied to adsorption complexes on metal surfaces by noting that metal atoms on different sites will have different abilities to back donate electrons into an adsorbate ligand π molecular orbital system. The covalent nitrate structure tentatively ascribed to the 1610- cm^{-1} band observed when a silica-supported Fe sample is used is thus presumed to occupy a site on a metal atom whose interactions with its neighbors are such that it cannot readily donate electrons to the adsorbed species π system. This band at 1610 cm^{-1} has been found to be relatively more intense on the silica-supported sample than the corresponding band at 1600 cm^{-1} for the oil-supported sample. This is consistent with previous interpretations of the difference between silica-supported and evaporated samples in that infrared spectra of adsorbed CO have been interpreted as indicating that evaporated samples have more sites that can donate considerable charge to an adsorbed species π system than silica-supported samples.²⁰

The main features of the spectrum of the adsorbed species produced by exposing Ni evaporated into oil to 10 mm of NO_2 at 25° is the pair of bands at 1840 and 610 cm^{-1} . These bands have been shown to be characteristic of adsorbed NO.^{5,19} The remaining bands at 1555, 1330, and 1090 cm^{-1} are attributed to nitrogen-oxygen complexes containing two or three oxygen atoms. These will henceforth be referred to as oxide complexes, a term which excludes chemisorbed NO. Thus, although one of the main interactions of NO_2 at 10 mm with evaporated-into-oil Ni is decomposition to chemisorbed NO, appreciable amounts of oxide complexes are produced in extents which show variation from sample to sample.

The use of a higher NO_2 pressure, 41 mm, results in the formation of very little chemisorbed NO though very strong bands for oxide complexes are produced. The weak band at 1745 cm^{-1} in Figure 5 is attributed to chemisorbed NO. This band is rather lower in frequency than the usual band for chemisorbed NO but is within the range of the low-frequency tail observed on chemisorbed NO bands. The presence of some specific oxide structures is indicated by a comparison of the bands shown in Figure 5 to the frequencies listed in Table I. The intense band at 1550 cm^{-1} appears to fit best a bidentate nitrate structure. This structure is supported by the appearance in the spectrum of bands at 1290, 1020, 804, and 765 cm^{-1} which also are reported for bidentate nitrate complexes. Though this appears to be the predominant structure, the appearance of

(20) G. Blyholder, *J. Phys. Chem.*, **68**, 2772 (1964).

other bands in the spectrum indicates the presence of lesser quantities of nitro and nitrito type structures.

Since hydrocarbon oil bands interfere with the observation of other bands in the 1350–1500-cm⁻¹ region, a spectrum of the interaction of 10 mm of NO₂ with Ni evaporated into fluorocarbon is shown in Figure 6. This shows essentially the same results as previously except that indeed absorption of radiation around 1400 cm⁻¹ is shown. Absorption in this region is consistent with a nitro complex structure.

The use of a silica-supported Ni sample indicates that, even with 10 mm of NO₂, the amount of free chemisorbed NO as shown by the size of the 1850-cm⁻¹ band is small whereas the bands for oxide structures are very intense. The two intense bands at 1555 and 1440 cm⁻¹ seem to fit best bidentate nitrato and nitro complex structures, respectively. This sample showed interesting phenomena in that several hours of pumping removed the chemisorbed NO, but, upon standing overnight without pumping, the chemisorbed NO reappeared, presumably owing to decomposition of some of the oxide complexes.

The over-all behavior of NO₂ on Ni is much like that on Fe. At low pressures over the oil-supported sample, decomposition to chemisorbed NO was the main reaction. At higher pressures over oil-supported Ni and for the silica-supported Ni the predominant process

was one of forming two and three oxygen–nitrogen oxide complexes. Although the relative amounts of different oxide complexes varied on the silica-supported and high-pressure, oil-supported Ni runs, the general behavior in these two cases is quite similar. The reasons for expecting some variation have already been stated in the discussion of adsorption on Fe.

Comparing the behavior of CO₂ and NO₂ in adsorption on Fe and Ni, one finds NO₂ to be more reactive as one would expect since it is an odd-electron molecule. On Fe the CO₂ merely dissociates to give chemisorbed CO and oxygen whereas NO₂ dissociates, and, if a sufficient gas phase concentration is present as with silica-supported samples, further reaction to produce two and three oxygen complexes occurs. On Ni the CO₂ does not dissociate in adsorption whereas NO₂ dissociates and proceeds to form two and three oxygen atom complexes. It is also interesting to note that, under conditions that can produce three oxygen atom complexes, a bidentate attachment to the surface has been found to be most prevalent for nitrogen surface complexes in this work and for carbon surface complexes in previous work.³

Acknowledgment. Acknowledgment is made to the donors of the Petroleum Research Fund, administered by the American Chemical Society, for partial support of this research.

Electrical Properties of Some Porphyrins under High Pressure

by D. W. Wood,¹ T. N. Andersen, and H. Eyring

Institute for the Study of Rate Processes, University of Utah, Salt Lake City, Utah (Received June 17, 1965)

The electrical conductivities of protoporphyrin, hematoporphyrin free base, hematoporphyrin dihydrochloride, copper protoporphyrin, hemin, hematin, etioporphyrin, and vanadyl etioporphyrin have been measured at the static pressures of 1–90 kbars and at temperatures of 25 to 100°. The study was made in a Bridgman anvil press. A resistivity reduction of as great as five orders of magnitude was observed for the bridged compounds (hemin, hematin, and vanadyl etioporphyrin) over the pressure range, and a corresponding activation energy decrease by more than half was observed in the same pressure range. The resistivity *vs.* pressure curves for these compounds showed a change in slope, and the activation energy *vs.* pressure curves showed a discontinuity near 25 kbars. The resistivities and activation energies of the nonbridged compounds were essentially pressure independent. A hole-conduction mechanism independent of pressure for the nonbridged porphyrins accounts for the observed results. A conduction mechanism for the bridged compounds is proposed which involves passage of the electron from one chelated cation to the next through the bridging anion. Two rate-determining processes in series are required to explain the electron mobility.

Introduction

The electrical conductivity of many organic molecules such as large polyaromatics and polycyclics lies in the semiconducting range,^{2,3} and several of these compounds show a decrease in resistivity of several powers of ten under increased pressure.^{4–9}

Conduction through porphyrins, such as phthalocyanine and hemin, is often explained by π -electron overlap in the conjugated systems of neighboring molecules^{7,10,11} although excitons have also been considered.⁶

In the case of iron porphyrins containing imidazoles in the fifth and sixth coordinating positions, a group-transfer mechanism through the iron–imidazole chain has been suggested.¹²

The porphyrins studied may be divided into three different classifications: those consisting of the parent organic skeleton, those containing a bivalent chelate, and those containing a polyvalent chelated ion with a bridging anion. The molecular structures of the planar or nearly planar molecules^{13–17} are schematically shown in Figure 1. Structural determination of all porphyrins which have been studied show that molecules stack parallel to one another.^{15–17} Unfortunately,

no structural determinations have been made of the bridged-type molecules to determine the shape of the anion–chelated cation–anion chain.

(1) This paper is part of the work carried out in partial fulfillment of a Ph.D. degree.

(2) C. G. B. Garret, "Semiconductors," N. B. Hannay, Ed., Reinhold Publishing Corp., New York, N. Y., 1959, p. 634.

(3) H. Inokuchi and H. Akamoto, "Solid State Physics," Vol. 12, F. Seitz and D. Turnbull, Ed., Academic Press Inc., New York, N. Y., 1961, p. 93.

(4) R. E. Harris, R. J. Vaisnys, H. Stromberg, and G. Jura, "Progress in Very High Pressure Research," John Wiley and Sons, Inc., New York, N. Y., 1962, p. 165.

(5) G. A. Samara and H. G. Drickamer, *J. Chem. Phys.*, **17**, 471, 474 (1962).

(6) R. S. Bradley, J. D. Grace, and D. C. Munro, "The Physics and Chemistry of High Pressure," London Symposium, 1962, Gordon and Breach, Science Publishers, Inc., New York, N. Y., 1963, p. 143.

(7) M. A. Cook, R. T. Keyes, A. G. Funk, and F. A. Olson, Naval Ordnance Test Station Final Technical Report, Dec. 31, 1963, Contract N 123 (60530) 25906A.

(8) H. A. Pohl, A. Rembaun, and A. Henry, *J. Am. Chem. Soc.*, **84**, 2699 (1962).

(9) R. B. Aust, W. H. Bentley, and H. G. Drickamer, *J. Chem. Phys.*, **41**, 1856 (1964).

(10) D. D. Eley, G. D. Parfitt, M. J. Perry, and D. H. Faysum, *Trans. Faraday Soc.*, **49**, 79 (1953).

(11) M. H. Cardew and D. D. Eley, *Discussions Faraday Soc.*, **27**, 115 (1959).

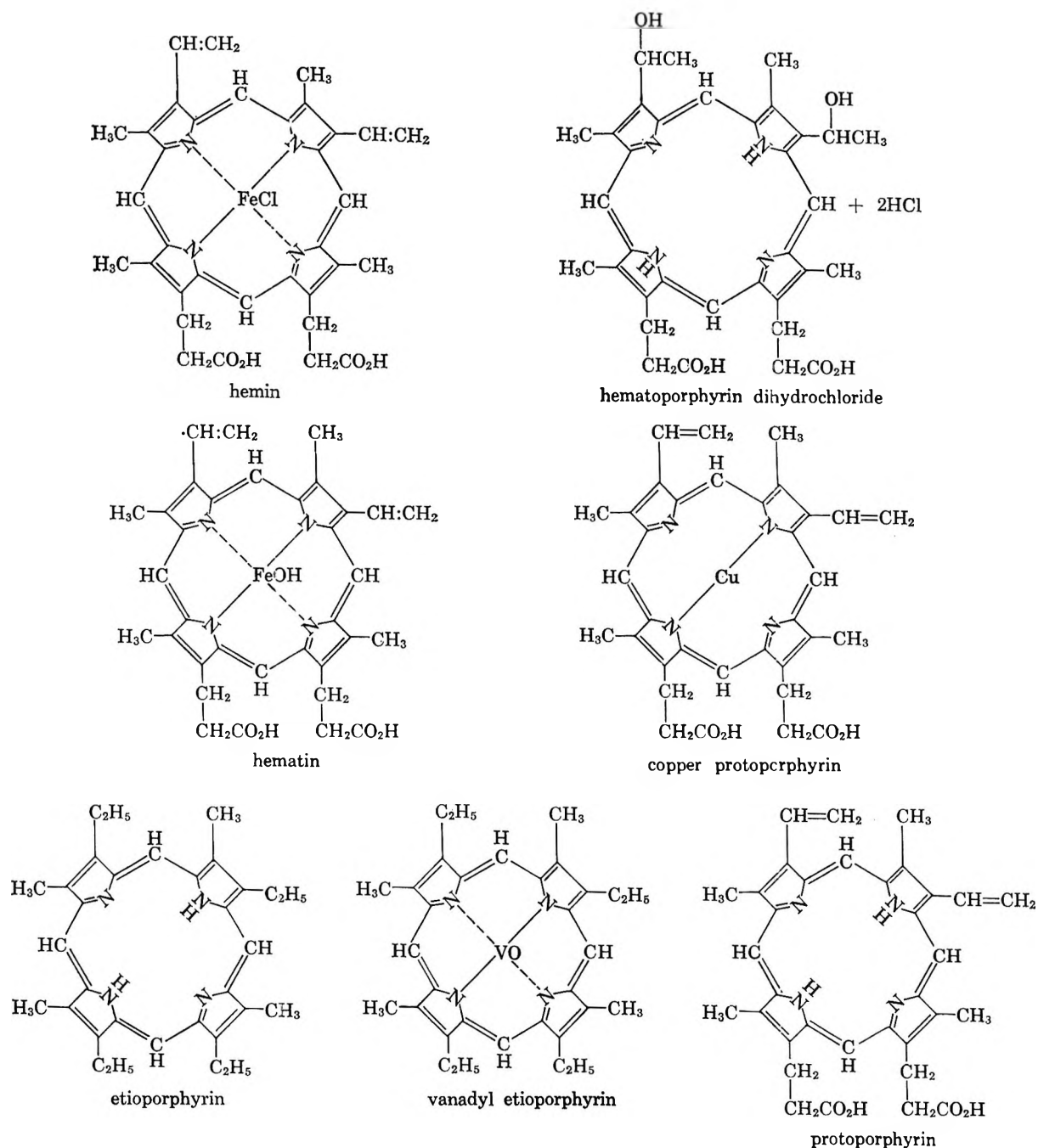


Figure 1. Structural formulas of compounds studied.

Since these materials decompose rather than melt or sublime at elevated temperatures, purification is effected by chromatography and recrystallization. The source and grade of each material studied is given in Table I.

From the Table I it can be seen that minor amounts of impurities are probably present in all samples. The possible effect of these will be discussed later.

(12) D. Urry and H. Eyring, *J. Theoret. Biol.*, **8**, 198 (1965).

(13) A. E. Martell and M. Calvin, "Chemistry of the Metal Chelate Compounds," Prentice-Hall, Inc., New York, N. Y., 1959, pp. 26, 176.

(14) D. F. Koenig, *Acta Cryst.*, **18**, 663 (1965).

(15) J. M. Robertson, *J. Chem. Soc.*, 615 (1935); 1195 (1936).

(16) L. E. Webb and E. B. Fleischer, *J. Am. Chem. Soc.*, **87**, 667 (1965).

(17) M. B. Crute, *Acta Cryst.*, **12**, 24 (1959).

Table I: Source and Grade of Compounds Studied

Porphyrin	Source	Grade
1. Hemin	Sigma Chemical Co.	Recrystallized three times
2. Hematoporphyrin dihydrochloride	Mann Research Laboratories	98% (Spectrograde)
3. Hematoporphyrin (free base)	Mann Research Laboratories	Unspecified
4. Protoporphyrin (Lipostain)	Calbiochem	C grade
5. Hematin	Calbiochem	C grade
6. Copper protoporphyrin	Prepared and donated by Dr. G. Cartwright, Department of Medicine, University of Utah	Multiple recrystallization
7. Etioporphyrin	Prepared and donated by Mr. A. Sonntag, Department of Chemistry, University of Utah	Recrystallized three times and chromatographed
8. Vanadyl etioporphyrin	Prepared and donated by Mr. R. Garvey, Department of Chemistry, University of Utah	Recrystallized and chromatographically homogeneous

Although all of these porphyrins show approximately the same room pressure resistivity after compaction, there is a marked difference observed at high pressures which would indicate that the conduction mechanism in these different molecules is not the same.

Experimental Procedure

A Bridgman opposed-anvil high-pressure apparatus has been used to subject the organic compounds to pressures in excess of 75 kbars. The samples consisted of thin wafers of 0.64-cm. diameter and a thickness after compaction of about 0.25 cm. These samples were kept in a desiccator for several days before being subjected to pressure.

The samples were first subjected to the maximum pressure of the experiment in order that compaction be obtained. The pressure was then released, and all electrical measurements were made as the pressure was again increasing. Constant current values were obtained within 10 min. after the potential was applied. After the initial compaction, repetitive experiments on a sample yielded essentially identical results. The sample resistivity, ρ , was calculated by using the equation $\rho = RA/d$ where R is the measured resistance, A is the cross-sectional area, and d is the final thickness of the sample.¹⁸

Although it is known that pressure gradients exist across flat anvil faces,^{4,19,20} it has been shown for anvils of about the present diameter that the gradient is small if samples of diameter to thickness of approximately 25:1 are used.¹⁹ This was further substantiated experimentally by measuring the resistances of small strips of bismuth embedded in some of the

samples. Quite sharp resistance changes occurred at the expected transition pressures. Although some error undoubtedly exists because of the pressure gradients, it is relatively unimportant for the semi-quantitative purposes of the present experimental data. Therefore, pressures on the sample were calculated assuming uniform distribution of pressure across the anvil faces.

The d.c. resistances of the samples were measured by applying a constant voltage and recording the current through the anvils and sample on a Keithley Model 610A electrometer. Voltage *vs.* resistance calibration showed that the value of the resistance was independent of the applied voltage in the range 1–90 v. Substituting various metal contacts between the sample and anvils gave identical results. These experiments indicate that space charge is negligible and that any contact potential junction must be ohmic. Since the resistances of the samples were much larger than that of the anvils, the resistance of the latter could be neglected. Considering the large resistance changes with pressure, the change in the sample thickness with pressure could also be neglected. It appears certain, also, that the resistance measured is that of

(18) We have chosen to report the results as resistivity, rather than resistance since the difference only involves geometrical differences, and resistivity is generally more useful. The results are, of course, subject to small corrections due to pressure gradients across the anvils and to changing thickness of sample with pressure change. Our results are for a compacted powder and may be somewhat different than for a single crystal.

(19) F. Dacheille and R. Roy, "The Physics and Chemistry of High Pressure," London Symposium, 1962, Gordon and Breach, Science Publishers, Inc., New York, N. Y., 1963, p. 77.

(20) E. R. Lippincott and H. C. Duecker, *Science*, **344**, 1119 (1964).

the substance and not that of loose crystallite contacts. The material is soft, and these contact resistances would be eliminated before the first few kilobars, as was shown for several organic materials by Eley and Parfitt.²¹

The sample was heated by means of a small-split Variac controlled furnace with a thermocouple placed as close to the sample as possible. Equilibrium resistance values were obtained after holding the Variac constant for at least 1 hr. beyond the time required to reach a definite temperature.

The compressibility *vs.* pressure curve for hemin was obtained by means of a piston-cylinder T.E.C. kiloton hydropress. Details of this high-pressure apparatus have been published elsewhere.^{22,23}

Results

The plot of the resistivity *vs.* pressure for the porphyrins is shown in Figure 2. The listed experimental results are the average of from two to as many as ten runs (in the case of hemin), and the deviation in ρ was less than half an order of magnitude at a given pressure. $\log R$ *vs.* $1/T$ plots were obtained from 15 to 100° at various pressures and resulted in single straight lines, the slopes of which gave the activation energies. This activation energy, E_{act} , was calculated on the basis of the equation $\sigma = \sigma_0 \exp(-E_{act}/kT)$ where σ is the conductivity. Therefore

$$\rho = \rho_0 e^{E_{act}/kT} \quad (1)$$

where E_{act} is shown as a function of pressure in Figure 3. Repetitive measurements at given pressures produced a precision of activation energies to within ± 0.05 e.v.

Although the anvils were open to the atmosphere, the effect of oxygen on the resultant curves is not significant as shown by Cook and co-workers,⁷ who compared ρ *vs.* P curves at room temperature for several of these materials with and without vacuum applied to the press. Likewise, adsorption of water vapor from the atmosphere during a measurement was shown not to affect the results (although the previously cited authors⁷ obtained an effect at low pressures for protoporphyrin).

Free volumes of activation, ΔV^* , were calculated in the case of hemin and hematin from the equation

$$\Delta V^* = RT \partial \ln \rho / \partial P \quad (2)$$

The average calculated ΔV^* for hemin is -5.6 cm.³/mole for $P < 25$ kbars and -1.66 cm.³/mole for $P > 30$ kbars. For hematin $\Delta V^* = -2.70$ cm.³/mole for $P < 25$ kbars and -1.59 cm.³/mole for $P > 30$ kbars.

Figure 2 shows that the bridged porphyrins give a marked decrease in resistivity, ρ , with an increase in

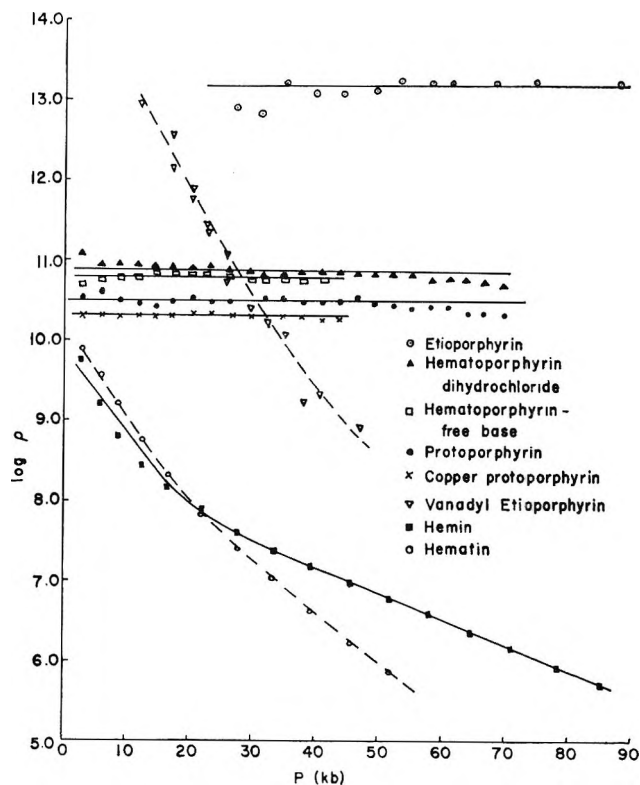


Figure 2. Resistivity, ρ , *vs.* pressure at 25°.

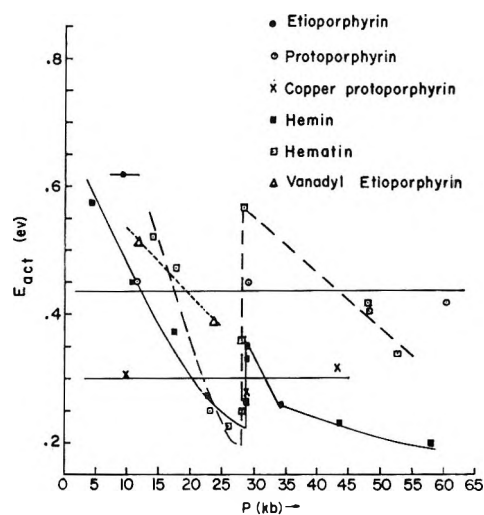


Figure 3. Experimental energy of activation, E_{act} *vs.* pressure.

pressure, showing a change in the slope at 20–30 kbars for hemin and hematin. A break in the activa-

(21) D. D. Eley and G. E. Parfitt, *Trans. Faraday Soc.*, **51**, 1529 (1959).

(22) F. R. Boyd and J. L. England, *J. Geophys. Res.*, **65**, 741 (1960).

(23) G. C. Kennedy and R. C. Newton, "Solids under Pressure," McGraw-Hill Book Co., Inc., New York, N. Y., 1962, p. 163.

tion energy plots also occurs in this region (see Figure 3). For lack of quantity of sample in the case of vanadyl etioporphyrin, the complete curves could not be studied. As a further study of the break in the activation energy in the 20–30-kbar range, a compression study of hemin was made at room temperature with an observed change in slope of the P vs. $\Delta V/V_0$ curve at 25 kbars as shown in Figure 4. The nonbridged porphyrins show no change in resistivity or activation energy with pressure.

Discussion

The mechanism of conduction in the nonbridged porphyrins is insensitive to pressure and also appears to involve the mechanism at least partially operative in the bridged compounds at atmospheric pressure. This conclusion is based on the similarities of zero pressure (extrapolated) resistivities of bridged porphyrins and their respective nonbridged porphyrins, along with the pronounced difference in resistivities of etioporphyrin and the carbonyl-bearing porphyrins. Considering that many polyaromatics and phthalocyanines are p-type semiconductors⁶ and also that hemin is a p-type semiconductor at atmospheric pressure,²⁴ with an activation energy similar to the above compounds, this semiconduction can be understood if it is due to electron trapping by the crystals (principally self-trapping rather than impurity-trapping) followed by hole conduction.^{6,25,26} The fact that the resistances of phthalocyanine, copper phthalocyanine, pentacene, tetracene, pyrolytic graphite, and anthracene decrease with increasing pressure indicates that a bridge is not necessary for semiconduction under pressure if there is enough π -orbital overlapping. One must remember, however, that substituents on the pyrrole ring could prevent appreciable overlap in the case of the porphyrins studied.

The difference between the conductivities of etioporphyrin and the protoporphyrins or hematoporphyrin can be understood as due to the presence of carbonyl groups on the latter compounds (etioporphyrin has only aliphatic groups). The carbonyl groups are in a better geometric position to overlap with neighboring molecules than are the more protected pyrrole rings.

Impurity donors are, of course, a source of charge carriers. Evidence against a major contribution by such extrinsic conduction is the fact that the conductivities of the bridged porphyrins approach that of the respective nonchelated porphyrins at low pressure. Also, if impurities account for semiconduction in both bridged and nonbridged compounds, it is difficult to understand why pressure does not affect the conductivity in both.

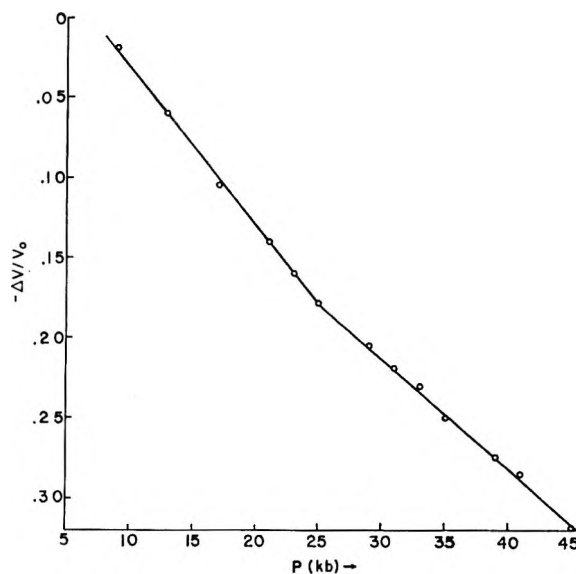


Figure 4. Compression vs. pressure for hemin at 25°.

X-Ray evidence on analogous platelike compounds leads to the expectation that the porphyrins will assume a preferred orientation under pressure with the plane of the porphyrin ring parallel to the anvil faces.²⁷ Since the measurements for Figures 2 and 3 are perpendicular to the anvil faces, the conductivity data reflect changes perpendicular to the molecular planes. This is further substantiated by the fact that the resistance of hemin measured parallel to the anvil faces does not decrease with increased pressure as does the resistance measured perpendicular to the anvils (*cf.* Figure 2).

The following model is accordingly proposed for the n-type conduction in hemin at elevated pressures as well as for the other bridged compounds studied. Some Fe^{3+} ions acquire an electron from the organic conjugated system followed by transport of the electron along the Fe–Cl–Fe chain (the holes left in the organic part of the molecule may also give p-type conduction by migration to neighboring porphyrins). Pressure aids the n-type conduction in two ways: (1) the neighboring Fe–Cl groups are brought more closely together so that the mobility of electrons is increased, and (2) the number of n-type carriers is increased in accord with the general results that semiconductors become more metallike with pressure.

(24) A. Terenin, *Proc. Chem. Soc.*, 321 (1961).

(25) N. Riehl, "Symposium on Electrical Conductivity in Organic Solids," H. Kallmann and M. Silver, Ed., Interscience Publishers, Inc., New York, N. Y., 1961, p. 61.

(26) A. Terenin, *ref. 25*, p. 29.

(27) R. Sehr, M. M. Labes, M. Bose, H. Ur, and F. Wilhelm, *ref. 25*, p. 309.

In this particular case the iron, which at low pressures is out of the porphyrin plane, is forced closer to the conjugated system by pressure thus lowering its energy by delocalization of the extra electrons into the ring system.

Supporting this mechanism are the facts that (a) electron transfer between Fe^{2+} and Fe^{3+} ions, bridged by a third anion such as Cl^- , occurs easily in the case of aqueous solutions²⁸ and (b) the conductivity of solids with a nonintegral number of electrons per atom, such as Fe_3O_4 , is many orders of magnitude higher than the conductivity of solids with an integral number of electrons per atom (cf. Fe_2O_3).²⁹ The criterion for rapid conduction in these systems is that two adjacent metal ions of different valence states are in nearly equivalent potential energy positions. Therefore, when an electron is transferred from one to the other, the final state is at essentially the same energy as the initial state.³⁰

We observe a change in the charge-transport mechanism for hemin and hematin at approximately 25 kbars as evidenced by (a) the change in slope of $\log \rho$ vs. P , (b) the discontinuity in the plot of E_{act} vs. P , and (c) the change in slope of $\Delta V/V$ vs. P . These phenomena show that the resistance to migration is now arising principally from steps which at larger pressures than 25 kbars were relatively inconsequential.

The conductivity, σ , is the product of the number of carriers per milliliter, N , their charge $|e|$, and their mobility μ . Thus³¹

$$\sigma = N|e|\mu = \frac{N|e|}{\sum_i n_i(\tau_i)_{V=1}} \equiv \frac{N|e|^2 F}{\sum_i \left(\frac{n_i R T}{\lambda_i k_i} \right)} \quad (3)$$

Here n_i is the number of barriers of kind, i , that a charge must surmount in moving 1 cm. while $(\tau_i)_{V=1}$ is the time required to surmount each barrier when the applied potential is 1 v./cm. We will designate the jump between neighboring iron atoms as mechanism 1. If λ_1 is the distance between two adjacent iron atoms along the line $\text{Fe}-\text{Cl}-\text{Fe}-\text{Cl}$, then $n_1 = 1/\lambda_1$. The distance spanned by the sum of all other types of λ_i in the electron migration is assumed negligible by comparison. The second type of barrier to migration which experiment reveals as important at pressures above 25 kbars will be described as mechanism 2. There may well be other steps, but they are not significant in our experiments. We can also write³²

$$\frac{1}{(\tau_i)_{V=1}} = k_i = \kappa \frac{kT}{h} e^{-\Delta G_i^*/RT} \quad (4)$$

where, assuming the volume of activation to be pressure independent

$$\Delta G^*_P = \Delta H^*_{P=1} - T\Delta S^*_{P=1} + (P-1)\Delta \bar{V}^* \quad (5)$$

Thus for our case we have for the resistivity

$$\rho = \frac{1}{\sigma} = \frac{n_1(\tau_1)_{V=1} + n_2(\tau_2)_{V=1}}{|e|N} \quad (6)$$

Well below 25 kbars the term $n_2(\tau_2)_{V=1}$ is negligibly small, whereas well above this pressure the term $n_1(\tau_1)_{V=1}$ is negligible.

Equation 6 is for two resistances in series and corresponds to the observed behavior as indicated by the two full lines in Figure 5. Had the two resistances been in parallel, the equation for the resistance would have been

$$\rho = \frac{1}{N|e|} \left(\frac{n_1 \tau_1 n_2 \tau_2}{n_1 \tau_1 + n_2 \tau_2} \right) \quad (7)$$

and would have followed the dotted lines of Figure 5 in disagreement with experiment. n-Type and p-type conduction are for example two parallel mechanisms. Other possible parallel conductors would be impurity acceptors or donors. Such complications are not observed in our experiments.

Barrier one can be considered to be the Cl^- bridge between a Fe^{2+} and Fe^{3+} ion. The second barrier which the mobility exhibits could be understood if there is a misfit in the lattice causing a misalignment in the $\text{Fe}-\text{Cl}-\text{Fe}$ chain at certain places; such a barrier is a modified bridge. Our experiments show that this

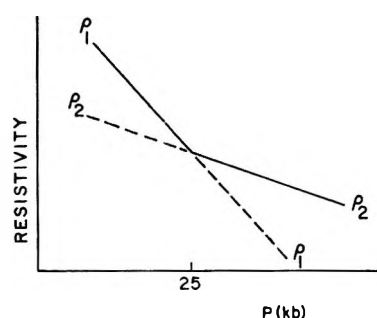


Figure 5. Resistivities ρ_1 and ρ_2 as functions of pressure: solid line, over-all resistivity for ρ_1 and ρ_2 in series; dotted line, over-all resistivity for ρ_1 and ρ_2 in parallel.

(28) H. Taube, *Chemistry*, **38**, 18 (1965).

(29) E. J. Verwey, P. W. Haayman, and F. C. Romeijn, *J. Chem. Phys.*, **15**, 181 (1947).

(30) E. J. Verwey and J. H. deBoer, *Rec. Trav. Chim.*, **55**, 531 (1936).

(31) R. B. Parlin and H. Eyring, "Ion Transport across Membranes," Academic Press Inc., New York, N. Y., 1954, p. 103.

(32) S. Glasstone, K. J. Laidler, and H. Eyring, "The Theory of Rate Processes," McGraw-Hill Book Co., Inc., New York, N. Y., 1941, Chapter IV.

barrier decreases with pressure more slowly than the first. In fact, since experiment only yields the sum of the effects of pressure on ionization and on mobility, we cannot rule out the possibility that the mobility of carriers according to mechanism (2) actually decreases with pressure. This will be evident if one examines eq. 5 and notes how the pressure effect comes into ΔG , the free energy of ionization in carrier production, and into ΔG_i^* , the activation free energy for mobility.

The compression data (Figure 4) indicate that at low pressures the normal lattice undergoes compression resulting in the Cl^- ions being moved into more sym-

metrical positions, thus improving charge mobility. Above 25 kbars the important effect on mobility according to our model is the effect of pressure on misalignment.

Acknowledgment. The authors gratefully wish to acknowledge the Army Research Office (Durham) for financial support of the work under Grant No. DA-ARO-D-31-124-G-618. We also wish to thank contributors of compounds as listed in Table I. The valuable advice of Professors Ivan Cutler and Owen Johnson is gratefully acknowledged.

The Conductance Behavior of the Symmetrical Tetraalkylammonium

Halides in Aqueous Solution at 25 and 10°¹

by D. Fennell Evans and Robert L. Kay

Mellon Institute, Pittsburgh, Pennsylvania 15213 (Received June 28, 1965)

Precise conductance measurements are reported for Me_4NCl , Me_4NBr , Me_4NI , Et_4NBr , Pr_4NCl , Pr_4NBr , Pr_4NI , Bu_4NCl , Bu_4NBr , and Bu_4NI in aqueous solutions at 25 and 10° for the concentration range 5×10^{-4} to 10^{-2} M. Salt purity was verified by the agreement obtained in the limiting ionic conductances. A Fuoss-Onsager analysis gave low ion-size parameters that increased with cation size for the chlorides, remained constant for the bromides, and decreased with increasing cation size for the iodides, indicating increasingly abnormal behavior as the anion size increased. The opposite order and much higher values have been reported for the alkali halides. This effect is attributed to increasing association as both the anion and cation size increases. Only the data for Pr_4NI and Bu_4NI at 25° and Bu_4NI at 10° analyzed directly for any significant amount of association.

Introduction

The symmetrical tetraalkylammonium ions have long been used as good examples of spherical ions having a large variation in size. A number of recent systematic investigations of the properties of these electrolytes in aqueous solution have indicated that the interaction of water with the hydrocarbon portion of the electrolyte is of considerable importance. Linden-

baum and Boyd² have shown that the activity coefficients for the tetraalkylammonium chlorides increase with increasing cation size, whereas the opposite behavior is observed in the case of the bromides and

(1) Presented in part at the 147th National Meeting of the American Chemical Society, Chicago, Ill., Sept 1964.

(2) S. Lindenbaum and G. E. Boyd, *J. Phys. Chem.*, **68**, 911 (1964).

iodides. The order in the chlorides was explained by the enforcement of water structure about the hydrocarbon portions of the cations, while the order in the bromides and iodides was attributed to "water structure-enforced ion pairing," as first proposed by Diamond.³ He suggested that when two large hydrophobic ions are present, the solution can best be stabilized by forming one cavity for an ion pair instead of two separate cavities, one for each ion. Such ion pairs would be stabilized primarily by water-structure considerations, rather than by the coulombic energy of electrostatic ion pairs. Hydration of the chloride ion was assumed to prohibit the formation of ion pairs in the case of the chlorides. Wen and Saito⁴ have discussed the abnormal behavior of the tetraalkylammonium salts in aqueous solution and have measured the partial molar volumes in aqueous solutions of the bromides at concentrations between 0.1 and 10 *m*. They interpreted their results as indicating that overlapping clathrate-like cages of water formed around the hydrocarbon portions of the cations, thereby producing cavities in which both cations and anions could hide. The minima in the partial molal volumes curves were attributed to the decrease in volume due to such occluded ions.

These investigations at best have involved relatively concentrated solutions where theory is least applicable. Owing to the high sensitivity of conductance measurements, we hoped to detect the effects of the interactions of water with the hydrocarbon portion of these electrolytes by noting any deviations from the behavior predicted by existing solvent-continuum theories. For this reason, we have analyzed all the available precise conductance data for the tetraalkylammonium salts in dilute aqueous solution. Kraus and co-workers⁵⁻⁷ have made fairly extensive measurements on many of these salts at 25° but, in most cases, were interested in limiting conductances and, consequently, did not cover the required concentration range. Lange⁸ has measured the chlorides and iodides at 0° and found, in general, that the conductance of the iodides decreased more rapidly with concentration than that of the corresponding chloride. However, his measurements do not have the required precision nor are they extensive enough for an analysis of the concentration dependence by modern theories. In order to make a systematic study, we have made precise conductance measurements on most of the tetraalkylammonium halides at 25 and 10° in the concentration range 5×10^{-4} to 10^{-2} *M*. These measurements for aqueous solutions supplement our previous measurements on acetonitrile,⁹ methanol,^{10a} and D₂O^{10b} solutions of these same salts.

Experimental Section

The electrical equipment, conductance cells, and general techniques were the same as previously described.⁹⁻¹¹ The measurements were carried out with the highest possible precision, using conductance cells of the erlenmeyer type, as described by Daggett, Bair, and Kraus,⁵ which contained 500 ml of solution and had cell constants of about 1.3 cm^{-1} . The cell was fitted with the Hawes-Kay salt-cup dispensing device which permitted the successive addition of salt samples, contained in 11-mm Pyrex cups, to the continuously stirred solution without exposing the cell contents to the atmosphere. Both the cell and the dispensing device contained stopcocks which permitted the cells to be thoroughly swept with argon before addition of solvent, during the addition of solvent, and when the dispensing device containing the salt cups was placed on the cell. Conductivity water was added to the cell directly from an all-glass closed system, and solvents of specific conductance $1-3 \times 10^{-7} \text{ ohm}^{-1} \text{ cm}^{-1}$ were obtained. The solvent underwent almost no detectable conductance change once temperature equilibrium had been attained. Temperature equilibrium was hastened and maintained during a measurement and electrode contamination was minimized by rapid magnetic stirring of the solution using a seamless Teflon-coated magnet. The room temperature was maintained above that of the bath to avoid condensation of the solvent in the salt-cup dispensing device.

The cell constants obtained from a calibration with aqueous KCl¹² were constant over the whole range of resistances encountered in this research. The usual small frequency correction was made on all the resistance measurements. Conductivity water was prepared by passing distilled water through a 1.2-m column of mixed-bed ion-exchange resin that was thoroughly rinsed before each use. The preparation,

(3) R. M. Diamond, *J. Phys. Chem.*, **67**, 2513 (1963).

(4) W. Y. Wen and S. Saito, *ibid.*, **68**, 2639 (1964).

(5) H. M. Daggett, E. J. Bair, and C. A. Kraus, *J. Am. Chem. Soc.*, **73**, 799 (1951).

(6) E. L. Swarts and C. A. Kraus, *Proc. Natl. Acad. Sci.*, **40**, 382 (1954).

(7) R. W. Martel and C. A. Kraus, *ibid.*, **41**, 9 (1955).

(8) J. Lange, *Z. Physik. Chem.*, **A168**, 147 (1934).

(9) D. F. Evans, C. Zawoyski, and R. L. Kay, *J. Phys. Chem.*, **69**, 3878 (1965).

(10) (a) R. L. Kay, C. Zawoyski, and D. F. Evans, *ibid.*, **69**, 4208 (1965); (b) R. L. Kay and D. F. Evans, *ibid.*, **69**, 4215 (1965).

(11) J. L. Hawes and R. L. Kay, *ibid.*, **69**, 2420 (1965).

(12) J. E. Lind, Jr., J. J. Zwolenik, and R. M. Fuoss, *J. Am. Chem. Soc.*, **81**, 1557 (1959).

purification, and drying of all the tetraalkylammonium salts has been described elsewhere.^{9,10}

Results

The density increments, used to calculate volume concentrations at 25 and 10°, are given in Table I.

Table I: Density Increments A and Viscosity B Coefficients for Aqueous Solutions at 25 and 10°

		Cl ⁻		Br ⁻		I ⁻	
		A	B	A	B	A	B
Me ₄ N ⁺	10	0.022	0.09	0.045	0.06	0.078	0.03
	25	0.022	0.11	0.044	0.08	0.078	0.05
Et ₄ N ⁺	10			0.042	0.38		
	25			0.041	0.34		
Pr ₄ N ⁺	10	0.018	1.01	0.038	0.98	0.067	0.93
	25			0.036	0.81	0.065	0.71
Bu ₄ N ⁺	10	0.015	1.49	0.032	1.46	0.060	1.41
	25	0.015	1.27	0.031	1.24	0.060	1.19

They were obtained by density measurements on the most concentrated solution used in the conductance measurements and were assumed to follow the relationship $d = d_0 + A\bar{m}$, where $d_0 = 0.99707$ at 25° and 0.99973^{13} g ml⁻¹ at 10° and where \bar{m} is the concentration in moles per kilogram of solution. The data for the bromides and iodides at 25° were measured directly, whereas the values for the chlorides at 25° were estimated and those for all the salts at 10° were estimated from direct measurements on Me₄NBr and Bu₄NI and the corresponding values at 25°. At worst, the uncertainty in A is estimated to be no more than 0.004 or 0.004% in the density. The viscosity B coefficients, defined by $(\eta - \eta_0)/\eta_0 C^{1/2} = \phi + BC^{1/2}$, are included in Table I and were obtained directly in an independent set of measurements¹⁴ of the viscosity of concentrated solutions of the iodides and bromides at 25 and 10°. The B values for the chlorides were obtained by adding the constant difference of 0.03 to the value for the corresponding bromide.¹⁵

The measured equivalent conductances and the corresponding concentrations in moles per liter are given in Table II for 25° and in Table III for 10°. The data were analyzed by the Fuoss-Onsager conductance theory¹⁶ in the form

$$\Lambda = \Lambda_0 - SC^{1/2} + EC \log C + (J - \theta)C \quad (1)$$

and, in the few cases where association was detected, by

$$\Lambda = \Lambda_0 - S(C\gamma)^{1/2} + EC\gamma \log C\gamma + (J - \theta)C\gamma - K_A C\gamma \Delta f^2 \quad (2)$$

The $\Delta\Lambda$ in Tables II and III are the differences be-

tween the measured Λ and that calculated by eq 1 or by eq 2 in the case of those salts marked with a superscript a .

The computer programs used for the least-squares determination of the conductance parameters given in Tables IV and V have been described in detail elsewhere.^{11,17} These computations used unweighted values of Λ since the measurements were carried out at approximately equal increments in C . The coefficient θ in eq 1 and 2 was set equal to $B\Lambda_0$. The recently determined values¹⁸ of 78.38 and 83.96 were used for the dielectric constant of water at 25 and 10°, respectively. The values of 0.8903 and 1.306 cp were used for the viscosity of water at 25 and 10°, respectively.^{19,20} Included in Tables IV and V are the standard deviations in each parameter and the standard deviations of the individual points σ_A . For convenience of calculation, the values of J have also been included. Runs were repeated if the precision obtained from a single run was felt to be inadequate, but the results for all runs are recorded here. Only the results marked with a superscript a were analyzed by eq 2 since it was found that, if the other salts were treated as associated electrolytes, negative association constants were obtained or the standard deviation in K_A was larger than K_A . In either case, the result is meaningless.

The constants α , β , E_1 , and E_2 have the values 0.2296, 60.62, 0.5307, and 20.52 at 25° and 0.2238, 40.97, 0.5041, and 13.52 at 10°, respectively, where, in eq 1 and 2, $S = \alpha\Lambda_0 + \beta$ and $E = E_1\Lambda_0 - E_2$.

Discussion

Ion Conductances. Limiting conductances for the tetraalkylammonium ions at 25°, obtained from the average values of Λ_0 in Table IV after weighting by their standard deviation, are given in Table VI. These values are the result of subtracting the limiting conductance for the corresponding halide ion as obtained from the self-consistent values for the transference numbers²¹ and the Λ_0 obtained by a Fuoss-

(13) R. A. Robinson and R. H. Stokes, "Electrolyte Solutions," 2nd ed, Butterworth and Co. Ltd., London, 1959, p 457.

(14) R. L. Kay, D. F. Evans, and T. Vituccio, to be published.

(15) H. S. Harned and B. B. Owen, "The Physical Chemistry of Electrolytic Solutions," 3rd ed, Reinhold Publishing Corp., New York, N. Y., 1958, p 241.

(16) R. M. Fuoss and F. Accascina, "Electrolytic Conductance," Interscience Publishers, Inc., New York, N. Y., 1959.

(17) R. L. Kay, *J. Am. Chem. Soc.*, **82**, 2099 (1960).

(18) G. A. Vidulich and R. L. Kay, *J. Phys. Chem.*, **66**, 383 (1962).

(19) J. F. Swindells, J. R. Coe, Jr., and T. B. Godfrey, *J. Res. Natl. Bur. Std.*, **48**, 1 (1952).

(20) J. R. Coe, Jr., and T. B. Godfrey, *J. Appl. Phys.*, **15**, 625 (1944).

(21) See ref 15, p 234.

Table II: Equivalent Conductances in Aqueous Solutions at 25°

10°C	Λ	ΔΛ	10°C	Λ	ΔΛ	10°C	Λ	ΔΛ	10°C	Λ	ΔΛ
Me₄NCl 10 ⁷ κ ₀ = 1.5			Me₄NBr 10 ⁷ κ ₀ = 1.7			Bu₄NBr 10 ⁷ κ ₀ = 2.1			Pr₄NI^a 10 ⁷ κ ₀ = 1.9		
11.274	117.55	0.14	2.911	121.10	-0.04	3.783	95.80	-0.04	4.600	98.35	0.00
23.127	116.020	-0.133	9.203	119.95	0.02	10.347	94.74	0.03	13.479	96.89	0.01
36.821	115.049	-0.032	17.586	118.877	0.001	19.543	93.642	0.010	22.676	95.786	-0.007
54.988	113.951	-0.005	25.399	118.127	0.016	30.306	92.650	0.011	31.193	94.953	0.000
68.468	113.261	0.007	34.359	117.382	0.011	41.452	91.779	0.004	42.969	93.944	-0.003
82.475	112.618	0.013	43.317	116.725	-0.002	52.749	91.018	0.014	56.439	92.943	0.001
98.785	111.934	0.007	55.717	115.938	-0.003	64.481	90.272	-0.007	71.480	91.948	0.005
111.407	111.455	0.006	68.510	115.214	-0.009	76.564	89.581	-0.014	85.132	91.116	-0.003
10⁷κ₀ = 1.3			Et₄NBr 10 ⁷ κ ₀ = 1.6			10⁷κ₀ = 2.1			10⁷κ₀ = 1.4		
25.268	116.087	-0.001	6.083	108.29	0.01	4.291	95.77	0.00	4.457	98.33	-0.01
53.329	114.156	-0.002	19.250	106.559	-0.002	10.049	94.80	0.01	12.209	97.05	0.02
75.887	113.003	0.004	36.992	105.034	-0.011	21.207	93.484	-0.002	21.523	95.905	0.002
116.233	111.351	-0.002	51.933	104.033	-0.006	33.005	92.426	-0.004	30.397	95.022	0.002
148.901	110.232		67.215	103.152	-0.001	45.436	91.485	-0.009	41.049	94.093	-0.007
180.540	109.247		84.336	102.278	0.001	57.811	90.668	-0.005	56.439	92.943	0.001
216.083	108.312		101.550	101.550	0.007	68.174	90.043	-0.003	71.480	91.948	0.005
245.093	107.395					81.356	89.321	0.012	85.132	91.116	-0.003
Bu₄NCl 10 ⁷ κ ₀ = 1.0			Pr₄NBr 10 ⁷ κ ₀ = 1.8			Me₄NI 10 ⁷ κ ₀ = 1.9			Bu₄NI^a 10 ⁷ κ ₀ = 2.4		
9.893	93.01	0.06	2.980	99.91	-0.01	5.835	119.16	-0.05	3.791	94.50	-0.04
18.834	91.931	-0.009	8.268	98.94	0.03	14.116	118.00	0.01	9.454	93.46	0.03
25.586	91.294	-0.037	14.492	98.086	0.004	20.704	117.276	0.023	19.654	92.062	0.031
35.423	90.546	-0.029	20.930	97.387	-0.008	30.057	116.421	0.022	29.893	90.942	0.024
44.128	89.970	-0.021	30.801	96.508	-0.010	42.376	115.470	0.011	40.160	89.927	-0.032
52.540	89.484	0.004	40.251	95.772	-0.028	55.055	114.619	-0.010	52.717	88.896	-0.025
60.919	89.001	-0.012	51.679	95.022	-0.011	84.156	113.029	-0.012	63.272	88.119	-0.010
69.094	88.630	0.044	63.232	94.370	0.031				76.501	87.233	0.020
			75.992	93.648	0.010				86.121	86.597	0.002
			88.346	93.015	0.002				98.506	85.841	0.001
			105.234	92.215	-0.009						
			10⁷κ₀ = 2.0			10⁷κ₀ = 3.1					
			8.261	99.85	-0.03	6.175	94.03	-0.01			
			10.033	98.70	0.03	13.602	92.85	0.01			
			17.615	97.756	0.013	24.765	91.493	0.004			
			26.233	96.919	0.017	34.897	90.479	0.003			
			35.473	96.099	-0.038	48.503	89.288	-0.004			
			45.520	95.399	-0.008	59.808	88.408	-0.005			
			58.799	94.550	0.000	71.519	87.570	-0.002			
			67.132	94.071	0.011	82.875	86.817	0.005			

^a Analyzed as an associated electrolyte using eq 2.

Onsager analysis of existing conductance data.¹⁷ The actual values used here are λ₀ (Cl⁻) = 76.39, λ₀ (Br⁻) = 78.22, and λ₀ (I⁻) = 76.98. As can be seen, there is excellent agreement in our cation conductances from the bromide and iodide salts but somewhat poorer agreement for the hygroscopic chlorides. The agreement with the data of Kraus and co-workers,⁵⁻⁷ Kortüm and co-workers,²² and Levien,²³

after recalculation on the basis of the Fuoss-Onsager equation, is entirely satisfactory. The excellent agreement here for the limiting ionic conductances from different salts with a common cation gives us consider-

(22) G. Kortüm, S. D. Gokhale, and H. Wilski, *Z. Physik. Chem. (Frankfurt)*, **4**, 286 (1955).

(23) B. J. Levien, *Australian J. Chem.*, **18**, 1161 (1965).

Table III: Equivalent Conductances in Aqueous Solutions at 10°

10°C	Λ	$\Delta\Lambda$	10°C	Λ	$\Delta\Lambda$	10°C	Λ	$\Delta\Lambda$	10°C	Λ	$\Delta\Lambda$
Me ₄ NCl 10 ⁷ κ_0 = 0.95			Me ₄ NBr 10 ⁷ κ_0 = 1.4			Pr ₄ NBr 10 ⁷ κ_0 = 1.4			Pr ₄ NI 10 ⁷ κ_0 = 1.6		
17.247	82.50	0.00	11.379	85.00	-0.01	5.556	70.08	-0.02	5.607	69.24	-0.02
35.830	81.419	0.002	18.773	84.400	0.004	12.691	69.36	0.00	12.866	68.47	0.03
52.337	80.688	0.002	32.540	83.524	-0.009	24.133	68.538	0.034	21.214	67.762	0.023
67.557	80.124	0.004	46.633	82.839	0.012	32.339	67.981	-0.025	29.337	67.143	-0.014
81.748	79.651	-0.001	61.223	82.205	0.003	42.150	67.471	-0.010	37.373	66.619	-0.025
96.200	79.218	-0.004	77.464	81.591	-0.003	54.104	66.961	0.048	47.800	66.023	-0.016
108.801	78.869	-0.008	93.102	81.071	0.003	64.582	66.442	-0.019	57.987	65.514	0.018
119.986	78.598	0.009	110.141	80.540	-0.005	74.761	66.040	-0.012	69.866	64.913	0.006
Pr ₄ NCl 10 ⁷ κ_0 = 1.0			Et ₄ NBr 10 ⁷ κ_0 = 1.2			Bu ₄ NBr 10 ⁷ κ_0 = 1.2			10 ⁷ κ_0 = 1.5		
7.590	67.93	-0.02	5.928	76.53	-0.03	4.521	67.51	0.03	4.653	69.38	-0.02
17.305	67.165	0.026	13.813	75.81	0.04	12.097	66.61	-0.03	11.367	68.63	0.03
28.611	66.463	0.011	22.401	75.129	-0.004	22.057	65.846	0.000	17.414	68.056	-0.002
36.771	66.048	0.009	33.023	74.492	-0.001	32.396	65.178	-0.005	25.024	67.479	0.000
44.565	65.665	-0.021	42.940	73.984	0.002	42.583	64.611	-0.005	34.078	66.877	-0.001
53.031	65.330	-0.008	50.573	73.628	0.002	53.070	64.084	-0.005	42.393	66.371	-0.011
62.101	64.996	0.000	61.521	73.167	0.009	63.936	63.595	0.006	52.163	65.849	0.003
70.548	64.705	-0.006	73.172	72.688	-0.013	76.624	63.054	0.006	60.370	65.430	0.003
Bu ₄ NCl 10 ⁷ κ_0 = 1.0			10 ⁷ κ_0 = 2.2			Me ₄ NI 10 ⁷ κ_0 = 1.6			Bu ₄ NI ^a 10 ⁷ κ_0 = 1.5		
9.832	65.16	-0.02	7.550	76.40	0.00	6.407	84.71	-0.02	8.570	66.13	0.01
20.223	64.397	0.010	15.022	75.69	-0.01	15.999	83.81	0.02	19.166	65.032	-0.014
30.873	63.783	0.021	23.375	75.103	0.009	25.978	83.083	0.004	28.316	64.340	0.025
41.091	63.256	0.000	31.946	74.568	-0.006	36.343	82.475	0.005	38.098	63.600	-0.044
52.221	62.770	-0.001	41.408	74.074	0.000	48.656	81.848	0.000	47.619	63.040	-0.017
62.109	62.378	-0.004	51.865	73.587	0.005	60.640	81.305	-0.007	61.300	62.347	0.050
71.671	62.025	-0.009	61.695	73.161	0.000	74.537	80.751	-0.002	71.086	61.847	0.044
80.384	61.739	0.003	72.372	72.735	-0.003	84.394	80.389	0.002	76.660	61.489	-0.055
									10 ⁷ κ_0 = 1.6		
									5.594	66.43	-0.01
									12.414	65.63	0.00
									18.947	65.033	0.016
									25.174	64.514	0.002
									30.015	64.155	0.002
									37.904	63.600	-0.017
									46.439	63.081	-0.004
									61.928	62.217	0.007

^a Equation 2.

able confidence in the purity of our bromides and iodides, and we feel this is as good a criterion of purity as chemical analysis. Included in Table VI are cation conductances obtained from the picrates by Swarts and Kraus⁶ using $\lambda_0(\text{Pic}^-) = 30.6$ as obtained from sodium rather than potassium picrate. This value for the picrate conductance gives cation conductances in much better agreement with our data than those which result from using the conductances of the potassium salt. By combining $\lambda_0(\text{K}^+) = 73.55$ with $\lambda_0(\text{KNO}_3) = 145.12 \pm 0.01^{17}$ to give $\lambda_0(\text{NO}_3^-) = 71.57$, a value

of $\lambda_0(\text{Me}_4\text{N}^+) = 44.38$ results from the $\Lambda_0(\text{Me}_4\text{NO}_3) = 115.95 \pm 0.00$ of Swarts and Kraus⁶ and the agreement with our average value of 44.43 is good. The numbers in the last column of Table VI are our estimates of the best values for the cation-limiting conductances as obtained from the bromide and iodide results.

The limiting conductances for the chloride, bromide, and iodide ions at 10° were obtained from those for 25° by means of the temperature-dependence equation quoted by Harned and Owen²⁴ which is based on precise

Table IV: Conductance Parameters at 25°

Salt	Λ_0	δ	K_A	σ_A	J
Me ₄ NCl	120.39 ± 0.06	2.4 ± 0.1		0.08	129.3
	120.52 ± 0.004	2.37 ± 0.01		0.004	124.9
Bu ₄ NCl	95.59 ± 0.03	3.6 ± 0.1		0.04	165.9
Me ₄ NBr	122.67 ± 0.01	1.77 ± 0.05		0.02	92.5
Et ₄ NBr	110.44 ± 0.006	1.72 ± 0.02		0.008	84.5
Pr ₄ NBr	101.40 ± 0.01	1.86 ± 0.03		0.02	94.1
	101.43 ± 0.02	1.61 ± 0.08		0.02	80.7
Bu ₄ NBr	97.50 ± 0.01	2.21 ± 0.07		0.02	103.3
	97.54 ± 0.006	2.04 ± 0.02		0.008	95.0
Me ₄ NI	121.39 ± 0.02	1.41 ± 0.06		0.03	65.9
Pr ₄ NI	100.20 ± 0.02	0.28 ± 0.02		0.03	-20.4
	100.26 ± 0.008 ^a	2.7 ± 0.4 ^a	2.1 ± 0.3 ^a	0.007	130.4
	100.19 ± 0.008	0.28 ± 0.01		0.01	-21.2
	100.21 ± 0.01 ^a	1.1 ± 0.5 ^a	1.0 ± 0.4 ^a	0.009	46.5
Bu ₄ NI	96.19 ± 0.03	0.11 ± 0.02		0.05	-47.3
	96.28 ± 0.03 ^a	3 ± 1 ^a	3.1 ± 0.9 ^a	0.03	154.0
	96.23 ± 0.02	0.09 ± 0.01		0.02	-52.8
	96.29 ± 0.008 ^a	1.7 ± 0.4 ^a	2.0 ± 0.3 ^a	0.007	79.7

^a Equation 2.

Table V: Conductance Parameters at 10°

Salt	Λ_0	δ	K_A	σ_A	J
Me ₄ NCl	85.02 ± 0.004	2.12 ± 0.01		0.006	74.0
Pr ₄ NCl	69.53 ± 0.01	3.2 ± 0.1		0.02	104.0
Bu ₄ NCl	66.99 ± 0.01	3.66 ± 0.07		0.01	114.0
Me ₄ NBr	87.09 ± 0.005	1.40 ± 0.02		0.007	46.2
Et ₄ NBr	78.03 ± 0.01	1.29 ± 0.08		0.02	39.4
	78.06 ± 0.004	1.21 ± 0.02		0.006	35.9
Pr ₄ NBr	71.50 ± 0.02	1.6 ± 0.1		0.03	48.7
Bu ₄ NBr	68.74 ± 0.01	1.56 ± 0.07		0.02	47.0
Me ₄ NI	86.31 ± 0.008	0.86 ± 0.03		0.01	19.0
Pr ₄ NI	70.70 ± 0.009	0.16 ± 0.02		0.01	-35.4
	70.70 ± 0.02	0.12 ± 0.02		0.02	-27.4
Bu ₄ NI	67.87 ± 0.01	0.023 ± 0.004		0.02	-61.8
	67.91 ± 0.02 ^a	1.9 ± 1.6 ^a	2.5 ± 1.1 ^a	0.01	179.9
	67.91 ± 0.04	0.04 ± 0.02		0.05	-61.8
	68.01 ± 0.08 ^a	5.7 ± 5.7 ^a	5.0 ± 3.4 ^a	0.05	59.9

^a Equation 2.

transference data. The actual values used for 10° are $\lambda_0(\text{Cl}^-) = 54.33$, $\lambda_0(\text{Br}^-) = 56.15$, $\lambda_0(\text{I}^-) = 55.39$. The resulting equivalent conductances for the tetraalkylammonium ions in aqueous solution at 10° are given in Table VII. The best values, given in the last column, were obtained by averaging the results from the bromides and iodides and ignoring the results from the hygroscopic chlorides.

The most interesting feature of the ionic conductances for these large cations is that their variation with size and temperature indicates a very definite dependence

on the three-dimensional structure that is known to be present in liquid water and in aqueous solutions of hydrocarbons.²⁵ A comparison of the conductance-viscosity products for the tetraalkylammonium ions in H₂O at 25° with those for 10° and those for the same ions in nonaqueous solvents indicates that this product

(24) See ref 15, p 233.

(25) G. Némethy and H. A. Scheraga, *J. Chem. Phys.*, **39**, 3401 (1962). The subject of water structure has been reviewed in detail recently by J. C. Kavanau, "Water and Solute-Water Interactions," Holden-Day, Inc., San Francisco, Calif., 1964.

Table VI: Limiting Cation Conductances at 25°

	Cl ⁻	Br ⁻	I ⁻	Pic ⁻	Best value
Me ₄ N ⁺	44.13	44.45	44.41		44.42
	44.23 ^a	44.41 ^e	44.40 ^e	44.5 ^a	
Et ₄ N ⁺		32.22			32.22
	32.62 ^d	32.26 ^d	32.09 ^d		
		31.92 ^a	32.19 ^a		
Pr ₄ N ⁺		23.19	23.26		23.22
		23.19 ^a	23.28 ^b		
Bu ₄ N ⁺	19.20	19.31	19.31		19.31
		19.31 ^c	19.30 ^c		

^a See ref 6. ^b See ref 5. ^c See ref 7. ^d See ref 22. ^e See ref 23.

Table VII: Limiting Cation Conductances at 10°

	Cl ⁻	Br ⁻	I ⁻	Best value
Me ₄ N ⁺	30.69	30.94	30.92	30.93
Et ₄ N ⁺		21.90		21.90
Pr ₄ N ⁺	15.20	15.35	15.31	15.33
Bu ₄ N ⁺	12.66	12.59	12.52	12.56

is too high for the Me₄N⁺ ion and decreases to much too low a value for the Bu₄N⁺ ion. This behavior can best be explained by assuming that, as the hydrocarbon portion of the electrolyte increases in length, water structure enforcement about these chains decreases the ionic mobility. Since the question of ionic effects on solvent structure in both H₂O and D₂O will be the subject of a forthcoming paper, this topic will not be developed in greater detail here.

Concentration Dependence. Although it can be demonstrated that solvent structure plays a large role in determining the magnitude of the limiting conductance, it is not clear that it has much of an effect on the concentration dependence of conductance in the dilute concentration range where present theories are most applicable. In Figure 1 are plotted the ion-size parameters \bar{d} obtained from J in eq 1 for the tetraalkylammonium halides. Included with our results are \bar{d} values for (Me₃Pr)NBr²⁶ and (*i*-Am₃Bu)NBr.²⁷ In contrast to the results obtained for nonaqueous solvents, \bar{d} is not constant and equal to about 3.7,^{9,10} but is much smaller in magnitude and, with increasing cation size at both temperatures, increases for the chlorides, remains about constant for the bromides, and decreases almost to zero for the iodides. This variation in the ion-size parameter is analogous, pos-

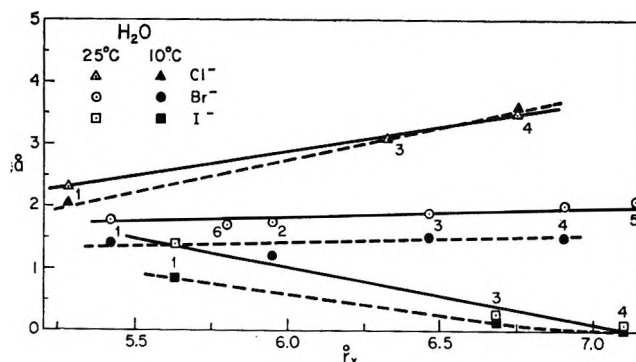


Figure 1. A plot of the ion-size parameters obtained from eq 1 (see Table IV) against the sum of the crystallographic radii for the halides of: 1, Me₄N⁺; 2, Et₄N⁺; 3, Pr₄N⁺; 4, Bu₄N⁺; 5, *i*-Am₃BuN⁺ (ref 27); 6, Me₃PrN⁺ (ref 26).

sibly, to the order found by Lindenbaum and Boyd² for the activity coefficients of these same salts in aqueous solution at 25°.

The obvious explanation for this type of behavior is some type of ion-pair association, which reduces the number of charged species as the anion and cation size increases. It should be noted that this is exactly the association pattern found for the same salts in alcohol solutions.¹⁰ As has been pointed out already, negative association constants or association constants smaller than the standard deviation were obtained if the data were processed by eq 2 with the exception of Pr₄NI, Bu₄NI at 25°, and Bu₄NI at 10°. These salts analyzed for an exceedingly small but definite amount of association, as can be seen in Tables IV and V.²⁸

The question must now be asked whether these association constants are real or whether they are artifacts resulting from experimental error or incomplete theory. One simple test that can be applied is to see if eq 2, with its parameters, fits the data better than eq 1. An inspection of $\sigma\Delta$ in Tables IV and V shows that, in general, this is the case for the salts mentioned above. A further test of association lies in plotting Λ' , given by

$$\Lambda' \equiv \Lambda - \Lambda_0 + SC^{1/2} - EC \log C = (J - \theta)C \quad (3)$$

where $\theta = B\Lambda_0$. If association is significant in magnitude, Λ' should not be linear in C but, rather, should

(26) H. O. Spivy and F. M. Snell, *J. Phys. Chem.*, **68**, 2126 (1964).

(27) J. F. Skinner and R. M. Fuoss, *ibid.*, **68**, 1882 (1964).

(28) Levien²³ obtained K_A (Me₄NBr) = 1.4 and K_A (Me₄NI) = 1.8 by setting \bar{d} in eq 2 equal to the crystallographic radii. We have resisted this approach because it gives too strict a physical significance to \bar{d} . Such an interpretation of \bar{d} has not been verified by experiment and could result in association constants that are meaningless. Levien's data when analyzed by eq 1 give $\bar{d} = 1.79 \pm 0.05$ and 1.33 ± 0.04 for the bromide and iodide, respectively, in good agreement with our results in Table IV.

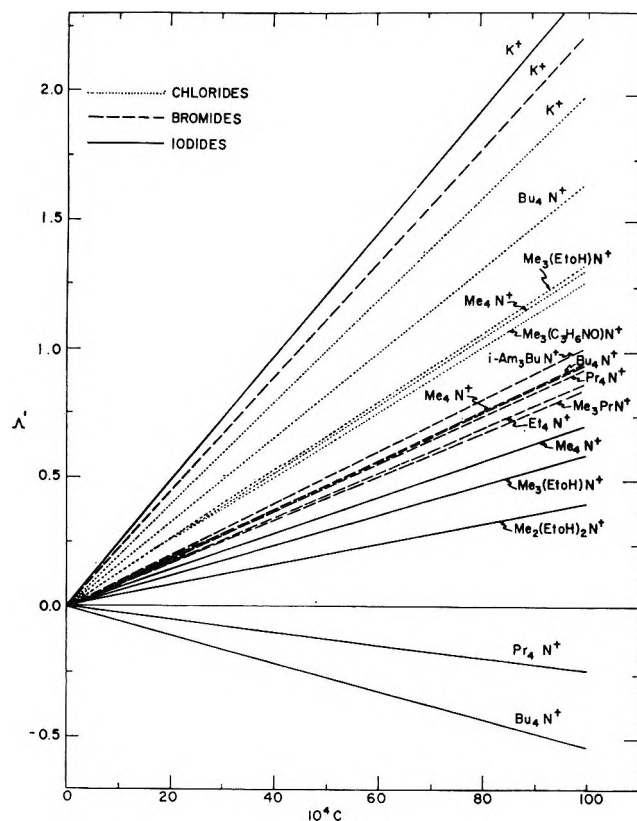


Figure 2. Plot of Λ' (eq 3) showing the opposite dependence on anion size for the quaternary halides as compared to the potassium halides: Me_3PrNBr , $\text{Me}_3(\text{C}_2\text{H}_5\text{NO})\text{NCl}$, and $\text{Me}_3(\text{EtOH})\text{NCl}$, see ref 26; $i\text{-Am}_3\text{BuNBr}$, see ref 27; $\text{Me}_3(\text{EtOH})\text{NI}$ and $\text{Me}_2(\text{EtOH})_2\text{NI}$, J. Varimbe and R. M. Fuoss, *J. Phys. Chem.*, **64**, 1337 (1960).

be curved. Furthermore, the leading term in an expansion of the last term in eq 2 is $K_A\Lambda_0C$, with the next largest but substantially smaller term being a $C^{3/2}$ term. Consequently, since this is a negative term, a small amount of curvature in Λ' requires Λ' to be substantially lower than usual if the curvature is to be attributed to association. In Figure 2, Λ' for the data in Table II at 25° are plotted, along with all the pertinent data that could be found in the literature. The data at 10° were not plotted since they showed the same behavior as the data for 25° . For the sake of clarity only the best straight line through the experimental points is shown in the plot. The most significant feature to be seen in this plot is the fact that Λ' for the quaternary ammonium iodides are much lower than for the other salts and decrease with increasing cation size. The bromides and chlorides are bunched more closely together, but with the chlorides definitely the highest. In contrast, the completely dissociated¹⁷ potassium halides show just the opposite and theoretically correct order in Λ' .

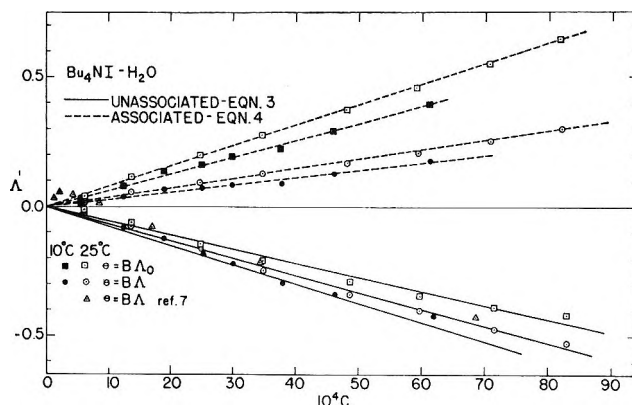


Figure 3. A plot of eq 3 and 4 for Bu_4NI in aqueous solutions at 25 and 10° . The data of Martel and Kraus⁷ are included.

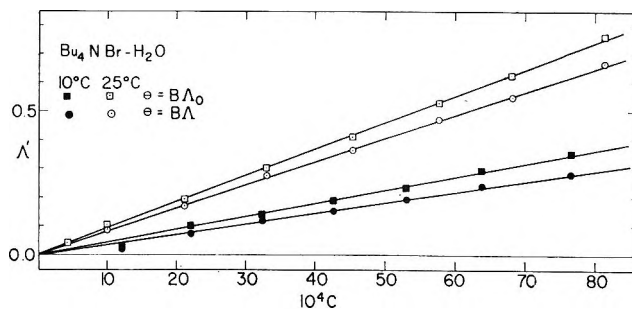


Figure 4. A plot of eq 3 for Bu_4NBr in aqueous solutions at 25 and 10° .

The curvature in the Λ' plot for Bu_4NI at 25 and 10° can be seen in Figure 3. In contrast, Λ' for Bu_4NBr gives a very good straight line with a positive slope as can be seen in Figure 4. The curvature in Λ' for Bu_4NI is verified by the data of Martel and Kraus,⁷ which are included in Figure 3.²⁹ The excellent straight line and large increase in Λ' which results from taking association into account is shown in the top curves in Figure 3. Here, Λ' is given by

$$\Lambda' \equiv \Lambda - \Lambda_0 + S(C\gamma)^{1/2} - EC\gamma \log C\gamma + \theta C + K_A C\gamma \Lambda f^2 = JC\gamma \quad (4)$$

and is plotted vs. $C\gamma$ in Figure 3.

There are at least three other means of introducing some $C^{3/2}$ dependence into eq 1 without assuming association. The very low \hat{a} values obtained here mean that the electrophoretic effect used in the calculation was too large, since an \hat{a} of 5 or 6 would probably be more correct. In the test of this possibility, we re-

(29) The points do not approach zero as the concentration approaches zero, due to the fact that the least-squares computation tends to reduce the curvature in Λ' by splitting the error equally between Λ_0 and J in eq 1.

calculated Λ' using \bar{a} from 0.5 to 6.5 to evaluate the electrophoretic effect, but found that the curvature in Λ' was affected to an insignificant degree.

The second method of producing some $C^{1/2}$ dependence rests in the function used for θ in eq 1. There is no doubt that a viscosity correction must be made since the presence of these large cations affects the solution viscosity to a significant extent. If the correct viscosity correction amounts to multiplying the measured Λ by the ratio of the solution to the solvent viscosity, η/η_0 , then θ can be shown to be equal to $B\Lambda$ in place of the $B\Lambda_0$ as first proposed by Fuoss.³⁰ In this calculation, we assume that the small term resulting from long-range electrostatic interaction between the ions can be neglected. The result of setting θ equal to $B\Lambda$ instead of $B\Lambda_0$ is shown in Figures 3 and 4. The curvature is not affected significantly, and the only result is a lower Λ' . If the same substitution is made in eq 2, the only effect is to decrease \bar{a} by about 0.7 and K_A by 0.4 in the case of Bu_4NI at 25°.

The third method of introducing some $C^{1/2}$ dependence into eq 1 would be to include the $-J_2C^{1/2}$ term contained in the original Fuoss–Onsager equation³¹ or by using the Pitts equation,³² which also contains a $-J_2C^{1/2}$ term. Both of these terms are negative and increase in magnitude with increasing ion size for the systems under investigation here. This is in the correct direction to explain the decreased conductance of the tetraalkylammonium iodides over that of the bromides. This term would be significantly smaller for the much smaller KI and KBr and the reversed order would be found in the conductance of these salts due to the higher J term for the larger KI. However, there is considerable doubt as to the authenticity of this term in the Fuoss–Onsager equation, both on experimental and theoretical grounds. In any case, the magnitude of J_2 required to explain the effect is many times greater than any realistic value of J_2 based on ion sizes. There are indications that the Pitts equation fits conductance data for aqueous solutions better

than the Fuoss–Onsager.³³ However, in order to explain the decrease in the conductance of the iodides over that of the bromides, it would be necessary to attribute a difference in \bar{a} between the iodides and bromides of over 8 Å; that is, the J_2 coefficient in the Pitts equation would have to be unrealistically large.

It should also be pointed out that attributing greater association to the iodide over the bromide due to the greater polarizability of the iodide ion will explain the results for Bu_4NI and Bu_4NBr but will not explain the higher conductance of KI compared to KBr.

Owing to the excellent agreement in λ_0 (Bu_4N^+) obtained from both the iodides and the bromides, we feel that the curvature found in the Λ' plots cannot be attributed to salt impurities which are present in Bu_4NI but which are absent in Bu_4NBr .

Since the same association pattern was found for these salts in the alcohols at low dielectric constant where association can be detected with some confidence, we feel that at least Bu_4NI is exhibiting some ion-pair association in aqueous solution at both 25 and 10°. Whether this is purely electrostatic ion pairing or association that is stabilized by solvent-structural considerations, as used by Wen and Saito⁴ to explain the partial molar volumes of these salts in concentrated solution or by Lindenbaum and Boyd² to explain their activity coefficients, cannot be said with certainty at this point. However, the lack of a significantly greater amount of association at 10° over that at 25° would seem to argue that solvent-structural features are not involved.

Acknowledgment. This work was supported by Contract No. 14-01-0001-359 with the Office of Saline Water, U. S. Department of the Interior.

(30) R. M. Fuoss, *J. Am. Chem. Soc.*, **79**, 3301 (1957).

(31) R. M. Fuoss and L. Onsager, *J. Phys. Chem.*, **61**, 668 (1957).

(32) E. Pitts, *Proc. Roy. Soc. (London)*, **A217**, 43 (1953).

(33) R. Fernández-Frine and J. E. Prue, private communication from J. E. P.

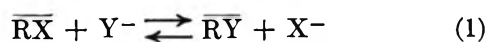
Distribution of Single Anions between Carbon Tetrachloride Solutions of High Molecular Weight Tertiary Ammonium Salts and Aqueous Lithium Chloride Solutions

by G. Scibona, R. A. Nathan, A. S. Kertes, and J. W. Irvine, Jr.

Laboratory for Nuclear Science and Department of Chemistry, Massachusetts Institute of Technology, Cambridge, Massachusetts, and Centro Studi Nucleari, Casaccia, Rome, Italy (Received July 6, 1965)

The distribution of ReO_4^- ions between CCl_4 solutions of tridodecylammonium salts and aqueous solutions of lithium salts has been studied as a function of the ammonium salt and perchlorate ion concentrations. The chloride, bromide, nitrate, and perchlorate ammonium salts have been used. Also, the distribution of Br^- ion between a CCl_4 solution of tridodecylammonium chloride and aqueous LiCl solution has been studied as a function of the ammonium salt and of the bromide ion concentrations. The deviation of the distribution data of some of these systems from a simple mass law model has been interpreted in terms of the formation of the mixed dimer $[(\text{RX})(\text{RY})]$ with $\text{X}^- = \text{Cl}^-$, Br^- , NO_3^- , and $\text{Y}^- = \text{ReO}_4^-$. The $(\text{ReO}_4^*-\text{ClO}_4)$ and (Br^*-Cl) systems are apparently following a simple mass action law, but in the case of the $(\text{ReO}_4^*-\text{ClO}_4)$ system, this effect may not be real.

It is frequently assumed that the following simple anion-exchange process occurs when an organic solution of an alkylammonium salt, $\overline{\text{RX}}$, is equilibrated with an aqueous solution of electrolyte containing the anion Y^-



However, it is known that the alkylammonium salts tend to aggregate in inert solvents of low dielectric constant, so eq. 1 cannot represent all such systems. In order to take into account every polymerization process in the organic phase, the general expression for the distribution coefficient can be derived

$$D = K_{1,\text{X},\text{Y}}(\overline{\text{RX}})(\text{X})^{-1}F^{-1} + \sum_2^J jK_{1,\text{X},\text{Y}}^j K_{j,\text{Y}}(\overline{\text{RX}})^j (\text{Y})^{j-1} (\text{X})^{-j} F^{-j} + \sum_1^A \sum_1^B bK_{1,\text{X},\text{Y}}^b K_{a,b}(\overline{\text{RX}})^{a+b} (\text{Y})^{b-1} (\text{X})^{-b} F^{-b} \quad (2)$$

where J , A , and B indicate the maximum number of units interacting to form polymers, $K_{1,\text{X},\text{Y}}$ is the equilibrium constant of the j -mer formation $j\overline{\text{RY}} \rightleftharpoons (\overline{\text{RY}})_j$,

$K_{a,b}$ is the equilibrium constant of the mixed $(a+b)$ -mer formation $a\overline{\text{RX}} + b\overline{\text{RY}} \rightleftharpoons [(\overline{\text{RX}})_a(\overline{\text{RY}})_b]$, (Y) is the equilibrium aqueous concentration of the anion Y^- , (X) is the equilibrium aqueous concentration of the anion X^- , $(\overline{\text{RX}})$ is the equilibrium monomer concentration of the salt RX in the organic phase, and F is the ratio of the square of the mean activity coefficients, $\gamma_{\pm\text{MX}(\text{MY})}^2 / \gamma_{\pm\text{MY}(\text{MX})}^2$, with $\gamma_{\pm\text{MX}(\text{MY})}$ and $\gamma_{\pm\text{MY}(\text{MX})}$ the mean activity coefficients of the salts MX and MY in the presence of MY and MX , respectively.

In eq. 2 the first term is the expression of the mass action law if only monomers $(\overline{\text{RX}})$ and $(\overline{\text{RY}})$ exist in solution. The second term accounts for the homopolymers $(\overline{\text{RY}})_j$. The third term takes into consideration the formation of the heteropolymers $[(\overline{\text{RX}})_a(\overline{\text{RY}})_b]$. Equation 2 accounts for the deviation of the distribution coefficient from a simple mass action law by considering solute-solute interactions in terms of monomer $\rightleftharpoons n$ -mer equilibria. If the solvent is inert, the solute-solvent interactions can be neglected.

In this work eq. 2 has been used to interpret the distribution of the bromide ion and the perchlorate ion

between aqueous lithium salt solutions and carbon tetrachloride solutions of tridodecylammonium salts.

Experimental Section

Materials. Except for the perchlorate, the tridodecylammonium salts were all prepared as purified crystalline solids. The chloride and bromide salts were prepared by shaking a slight excess of the concentrated aqueous hydrohalic acid with a petroleum ether (bp 35–65°) solution of the amine. The salts were precipitated from the petroleum ether cooling to 0°. The salts were recrystallized at least three times from petroleum ether.

The tridodecylammonium nitrate was prepared in a similar manner, but the solvent was a 1:1 acetone-petroleum ether mixture, and the salt was crystallized by cooling to –78°. The filtration apparatus was pre-cooled to Dry Ice temperature before the salt was filtered out. The salt was recrystallized five times from the acetone-petroleum ether mixture at 0°.

The purity of the salts was checked by chemical analysis, infrared spectra, and melting point determination.

Tridodecylammonium perchlorate was prepared by equilibration of a 0.01 *M* solution of the free amine in CCl₄ with an excess of 0.1 *M* aqueous perchloric acid for 1 hr. The CCl₄ solution was washed once with water and used without isolating the solid salt. Potentiometric titration in methanol showed that the CCl₄ solution contained neither free amine nor free acid.

The tridodecylamine was Eastman White Label, the acids were Du Pont reagent grade, and the carbon tetrachloride and petroleum ether were Fisher reagent grade.

The Br⁸² and Re¹⁸⁶ tracers were prepared by (*n,γ*) reactions in the MIT reactor from NH₄Br and Re metal. The bromide solution was prepared by dissolving the salt in water. The rhenium metal was oxidized to ReO₄[–] with aqua regia, evaporated to dryness, and taken up in water.

Procedure. The studies of the dependence of the distribution coefficient on the ammonium salt concentration were carried out by equilibrating a solution of an ammonium salt (\overline{RX}) in CCl₄ with an aqueous solution of lithium chloride containing the tracer anion. The range of concentration of the ammonium salt was 10^{–4} to 10^{–2} *M*, the tracer anion was less than 10^{–5} *M*, and the supporting electrolyte was 2 *M*. In order to keep the hydrolysis of the ammonium salt below 1%, the lithium chloride solution was adjusted to pH 2 with HCl.

The dependence of the distribution coefficient on (ReO₄[–]) and (Br[–]) was measured by varying the con-

centration of these species in aqueous phase over the range 10^{–4} to 10^{–2} *M* with the ammonium salt concentration 10^{–3} *M* and supporting electrolyte 2 *M*.

Activity Coefficient. Values of the activity coefficients for the supporting electrolyte were taken from the data of Robinson and Stokes.¹ The activity coefficients of the bromide and perrhenate salts in the presence of much larger concentration of the supporting electrolyte were calculated from the Brønsted equation²: $\log \gamma_{\pm MY(MX)} = \frac{1}{2}(\log \gamma_{\pm MY(MY)} + \log \gamma_{\pm MX(MX)})$. In this equation $\gamma_{\pm MY(MY)}$ is the activity coefficient of LiBr or LiReO₄ at 2 *M*, the concentration of the supporting electrolyte. Since the values of activity coefficient for the perrhenate salt are not available in the literature, we have approximated these values with the activity coefficients of the corresponding perchlorate salt. The introduction of this approximation in the calculation of *F* affects only the absolute value of the equilibrium constants.

Results and Discussion

The distribution of (Y) between a CCl₄ solution of a tridodecylammonium salt, \overline{RX} , and an aqueous LiX solution has been determined for the following systems: Y[–] = ReO₄[–], X[–] = Cl[–], Br[–], ClO₄[–]; Y[–] = ReO₄[–], X[–] = NO₃[–] (as the sodium salt); and Y[–] = Br[–], X[–] = Cl[–]. For convenience in referring to these systems, the symbols for tracer will be starred and coupled with the symbol for the macroscopic anion, e.g., (ReO₄^{*}–Cl). The results of these measurements are reported in Tables I–V in terms of distribution coefficient

$$D = (Y)_{org}/(Y)_{aq} \quad (3)$$

The experimental *D* values in Tables I–V, column 2, show that *D* is dependent on \overline{RX} and independent of (Y) (Table VI). The use of $D' = DF$ is more convenient for us since it eliminates *F* in all of the terms of eq. 2 with (*F*) at the first power. Values of *D'* are reported in Tables I–III, column 3. Plots of $\log D'$ vs. $\log \overline{RX}$ for the systems (ReO₄^{*}–Cl) (Figure 1), (ReO₄^{*}–NO₃), and (ReO₄^{*}–Br) give straight lines with slopes >1. For the systems (ReO₄^{*}–ClO₄) (Figure 2) and (Br^{*}–Cl) the plots give straight lines with slopes of 1.

According to eq. 2, a plot of $\log D$ vs. $\log \overline{RX}$ will give a straight line with slope of 1 if only monomeric species are involved. It will give a straight line with

(1) R. A. Robinson and R. H. Stokes, "Electrolyte Solutions," 2nd ed, Academic Press Inc., New York, N. Y., 1959.

(2) H. S. Harned and B. B. Owen, "The Physical Chemistry of Electrolytic Solutions," 3rd ed, Reinhold Publishing Corp., New York, N. Y., 1959.

Table I: System (ReO₄*-Cl)

(RCl), M	D	DF	Q	K'
1 × 10 ⁻⁴	3.7 × 10 ⁻³	3.0 × 10 ⁻³	55	1.0 × 10 ⁴
2 × 10 ⁻⁴	9.3 × 10 ⁻³	7.4 × 10 ⁻³	69.5	7.7 × 10 ⁴
6 × 10 ⁻⁴	4.8 × 10 ⁻²	3.8 × 10 ⁻²	128	1.2 × 10 ⁴
1 × 10 ⁻³	9.5 × 10 ⁻²	4.6 × 10 ⁻²	152	9.8 × 10 ⁴
2 × 10 ⁻³	2.5 × 10 ⁻¹	2.0 × 10 ⁻¹	200	7.3 × 10 ⁴
6 × 10 ⁻³	1.6	1.28	416	6.0 × 10 ⁴
1 × 10 ⁻²	4.3	3.44	620	6.2 × 10 ⁴

Table II: System (ReO₄*-NO₃)

(RNO ₃), M	D	DF	Q	K'
1 × 10 ⁻⁴	4.0 × 10 ⁻⁴	4.1 × 10 ⁻⁴	7.0	5.0 × 10 ³
2 × 10 ⁻⁴	1.1 × 10 ⁻³	9.0 × 10 ⁻⁴	7.3	4.0 × 10 ³
6 × 10 ⁻⁴	4.9 × 10 ⁻³	4.0 × 10 ⁻³	11.5	8.5 × 10 ³
1 × 10 ⁻³	9.4 × 10 ⁻³	7.7 × 10 ⁻³	15	8.5 × 10 ³
2 × 10 ⁻³	2.6 × 10 ⁻²	2.2 × 10 ⁻²	18	4.7 × 10 ³
6 × 10 ⁻³	1.1 × 10 ⁻¹	9.2 × 10 ⁻²	25	3.1 × 10 ³
1 × 10 ⁻²	2.2 × 10 ⁻¹	1.8 × 10 ⁻¹	29	2.2 × 10 ³

Table III: System (ReO₄*-Br)

(RBr), M	D	DF	Q	K'
1 × 10 ⁻⁴	3.4 × 10 ⁻⁴	3.0 × 10 ⁻⁴	6.0	1 × 10 ⁴
2 × 10 ⁻⁴	7.4 × 10 ⁻⁴	6.5 × 10 ⁻⁴	6.5	7.5 × 10 ³
6 × 10 ⁻⁴	3.2 × 10 ⁻³	2.8 × 10 ⁻³	9.3	7.1 × 10 ³
1 × 10 ⁻³	5.8 × 10 ⁻³	6.0 × 10 ⁻³	12.0	7.0 × 10 ³

Table IV: System (ReO₄*-ClO₄)

(RClO ₄), M	D
1 × 10 ⁻⁴	9.6 × 10 ⁻¹
2 × 10 ⁻⁴	2.2 × 10 ⁻⁴
6 × 10 ⁻⁴	5.2 × 10 ⁻⁴
1 × 10 ⁻³	9.3 × 10 ⁻⁴
2 × 10 ⁻³	1.8 × 10 ⁻³
6 × 10 ⁻³	5.5 × 10 ⁻³
1 × 10 ⁻²	9.2 × 10 ⁻³

a slope >1 or a curve whose derivative, $d \log D/d \log (\overline{RX})$, is a function of (\overline{RX}) and has a value >1 when polymeric species are present. The assumption is made in the following discussion of eq. 2 that the concentration of polymeric species, $(\overline{RX})_p$, is negligible in the CCl₄ solution. Although no measurements in this solvent are available, osmometric measurements have

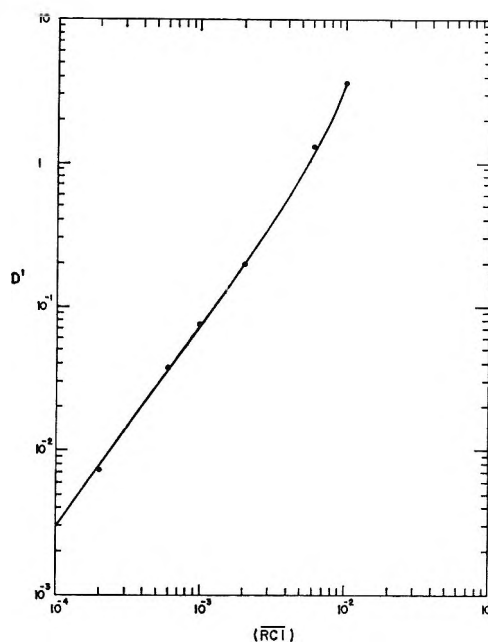
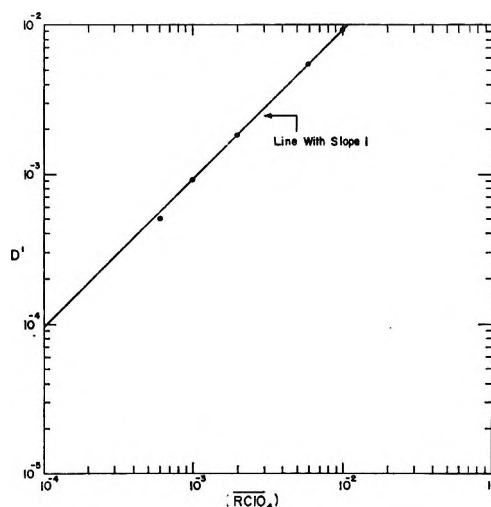

Figure 1. Logarithmic plot of D' vs. (\overline{RCl}) for the system (ReO₄*-Cl). Aqueous phase: 2 M LiCl and 0.02 M H⁺.

Figure 2. Logarithmic plot of D' vs. $(\overline{RClO_4})$ for the system (ReO₄*-ClO₄). Aqueous phase: 2 M LiClO₄ and 0.02 M H⁺.

Table V: System (Br*-Cl)

(RBr), M	D
1 × 10 ⁻⁴	7.3 × 10 ⁻⁴
2 × 10 ⁻⁴	1.3 × 10 ⁻³
6 × 10 ⁻⁴	1.4 × 10 ⁻³
1 × 10 ⁻³	5.5 × 10 ⁻³
2 × 10 ⁻³	1.0 × 10 ⁻³
6 × 10 ⁻³	1.5 × 10 ⁻³
1 × 10 ⁻²	6.4 × 10 ⁻³

Table VI: Distribution Coefficients, D , as Function of the Aqueous ReO_4^- and Br^- Concentrations ($\text{RX} = 10^{-3} M$; $X = 2$; $t = 25^\circ$)

(Y), M	D				
	(Br*-Cl)	(ReO_4^* -Cl)	(ReO_4^* -Br)	(ReO_4^* - NO_3)	(ReO_4^* - ClO_4)
1×10^{-4}	5.0×10^{-3}	1.0×10^{-1}	6.6×10^{-3}	1.0×10^{-2}	
2×10^{-4}	5.0×10^{-3}	1.1×10^{-1}	7.0×10^{-3}	1.0×10^{-2}	9.1×10^{-4}
6×10^{-4}	5.1×10^{-3}	1.0×10^{-1}	6.7×10^{-3}	9.3×10^{-3}	
1×10^{-3}	5.5×10^{-3}	9.5×10^{-2}	6.8×10^{-3}	9.4×10^{-3}	9.3×10^{-4}
2×10^{-3}	5.0×10^{-3}	1.0×10^{-1}	7.05×10^{-3}	9.8×10^{-3}	
6×10^{-3}	5.1×10^{-3}				
1×10^{-2}					

been made for benzene solutions of tridodecylammonium chloride and nitrate.³ In the nitrate case, where polymerization was greatest, it was less than 20% at concentration of the salt $10^{-2} M$.

According to eq. 2 the lack of dependence of D on (Y-), shown in Table VI, along with the slope >1 for the systems (ReO_4^* -Cl), (ReO_4^* - NO_3), and (ReO_4^* -Br), indicates the presence of a mixed dimer [$(\overline{\text{RX}})(\overline{\text{RY}})$] in these systems.

For the further treatment of the data, it is convenient to introduce a new function, Q , obtained by multiplying D of eq. 2 by $(X)(\text{RX})^{-1}(F)$

$$Q = K_{1,x,y} + \sum_2^j j K_{1,x,y}^j K_{j,y} (\overline{\text{RX}})^{j-1} (\text{Y})^{j-1} \times (\text{X})^{-(j-1)} F^{-(j-1)} + \sum_1^A \sum_1^B b K_{1,x,y}^b K_{a,b} \times (\overline{\text{RX}})^{a+b-1} (\text{Y})^{b-1} (\text{X})^{-(b-1)} (F)^{-(b-1)} \quad (4)$$

It follows then from eq. 4 that

$$\lim_{(\overline{\text{RX}}) \rightarrow 0} Q = K_{1,x,y} \quad (5)$$

Since only the mixed dimer is expected from previous considerations, $j = 1$, $a = b = 1$, and eq. 2 and 4 reduce to

$$D = K_{1,x,y} (\overline{\text{RX}}) (\text{X})^{-1} (F)^{-1} + K' (\overline{\text{RX}})^2 (\text{X})^{-1} (F)^{-1} \quad (6)$$

and

$$Q = K_{1,x,y} + K' (\overline{\text{RX}}) \quad (7)$$

with $K' = K_{1,x,y} K_{1,1}$. The dependence of Q on $(\overline{\text{RX}})$ for the systems whose plot of $\log D$ vs. $\log (\overline{\text{RX}})$ has a slope >1 is shown in Figure 3. Values of Q are reported in Tables I-IV, column 4. Using eq. 5 the values of $K_{1,x,y}$ have been calculated and are reported in Table VII. Using eq. 7 with the values of $K_{1,x,y}$ from Table VII, the values of K' are calculated for each $(\overline{\text{RX}})$ concentration. These values

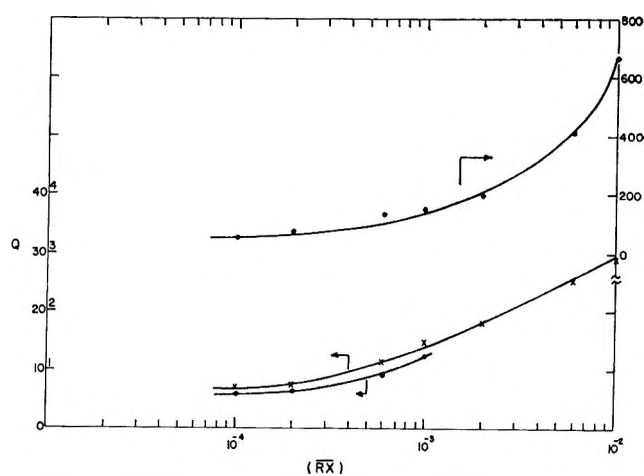


Figure 3. Q plotted against $(\overline{\text{RX}})$ for the systems: (ReO_4^* -Br), bottom curve; (ReO_4^* - NO_3), middle curve; (ReO_4^* -Cl), top curve. The left scale in unit increments refers to the system (ReO_4^* - ClO_4).

are reported in Tables I-III, column 5, and are, of course, fairly constant as expected for the presence of the dimer [$(\overline{\text{RX}})(\overline{\text{RY}})$]. The deviation observed for (ReO_4^* - NO_3) at concentrations of ammonium salt higher than $10^{-3} M$ may be due to the presence of homopolymers (RNO_3).

In the (ReO_4^* - ClO_4) system a simple linear relationship was obtained in plotting $\log D$ vs. $\log (\text{RClO}_4)$

Table VII

System	K'_{av}	$K_{1,x,y}$	$K_{1,1}$
(ReO_4^* -Cl)	7.6×10^4	54	1.4×10^3
(ReO_4^* -Br)	7.2×10^3	5.0	1.4×10^3
(ReO_4^* - NO_3)	5.3×10^3	6.5	9.2×10^2
(ReO_4^* - ClO_4)		1.9	
(Br*-Cl)		10	

(3) G. Scibona, S. Basol, P. Danesi, and F. Orlandini, submitted to *J. Inorg. Nucl. Chem.*

(Figure 2). This line had a slope of 1. It has been determined⁴ that the RClO_4 in benzene solution polymerizes extensively, and consequently we expect that similar polymerization occurs in the CCl_4 solution. Thus, the stoichiometric RClO_4 concentration, from which this straight line was derived, is not a good approximation for the monomeric (RClO_4). This means that the straight line with slope 1 is accidental and that the proper treatment of the ($\text{ReO}_4^*-\text{ClO}_4$) system must be deferred until the degree of polymerization of RClO_4 in CCl_4 has been determined.

The distribution data for the (Br^*-Cl) system indicate simple monomer distribution with no evidence for mixed dimer formation. This agrees with the observation of constancy of the ratio of the activity coefficients of RCl and RBr in the organic phase for the distribution of Br^- between aqueous solutions of alkali chlorides and a 0.1 *M* toluene solution of tri-*n*-octylamine chloride.⁵

In Table VII are reported the average values of K' and $K_{1,1}$ and the values of $K_{1,X,Y}$ for the (ReO_4^*-Cl), (ReO_4^*-Br), and ($\text{ReO}_4^*-\text{NO}_3$) systems. Values of $K_{1,X,Y}$ of the other systems are also reported. The $K_{1,X,Y}$ have been calculated by limit operation from

Figure 3 using eq. 4. The $K_{1,1}$ values have been calculated by using the relation $K' = K_{1,X,Y}K_{1,1}$. When the values of $K_{1,X,Y}$ are known, it should be possible to calculate the equilibrium constant for a given reaction from those of two other reactions. Thus, for example, in the three systems (Br^*-Cl), (ReO_4^*-Cl), and (ReO_4^*-Br), the relationships

$$K_{1,\text{Cl},\text{ReO}_4} = K_{1,\text{Cl},\text{Br}}K_{1,\text{Br},\text{ReO}_4} \quad (8)$$

$$K_{1,\text{Cl},\text{Br}} = K_{1,\text{Cl},\text{ReO}_4}/K_{1,\text{Br},\text{ReO}_4} \quad (9)$$

should be valid.

The following $K_{1,X,Y}$ can be calculated: $K_{1,\text{Cl},\text{ClO}_4} = 29$; $K_{1,\text{Br},\text{ClO}_4} = 27$; $K_{1,\text{NO}_3,\text{ClO}_4} = 3.5$; $K_{1,\text{Cl},\text{NO}_3} = 8.3$; $K_{1,\text{Br},\text{NO}_3} = 0.77$. These $K_{1,X,Y}$ values show the following amine selectivity order: $\text{ReO}_4^- > \text{ClO}_4^- > \text{Br}^- > \text{NO}_3^- > \text{Cl}^-$. This sequence is the same as is found for anion-exchange resins.⁶

(4) (a) J. J. Bucher and R. M. Diamond, *J. Phys. Chem.*, **69**, 1565 (1965); (b) P. Danesi, F. Orlandini, and G. Scibona, unpublished results.

(5) S. Lindenbaum and G. E. Boyd, *J. Phys. Chem.*, **66**, 1383 (1962).

(6) B. Chu, D. C. Whitney, and R. M. Diamond, *J. Inorg. Nucl. Chem.*, **24**, 1405 (1962).

Salts of the Group II-A Metals Dissolved in Nonaqueous or Mixed Solvents.

III. Precision Conductance Data for $\text{Ca}(\text{NO}_3)_2 \cdot 4\text{H}_2\text{O}$, $\text{Mg}(\text{NO}_3)_2 \cdot 6\text{H}_2\text{O}$, or $\text{Be}(\text{NO}_3)_2 \cdot 3\text{H}_2\text{O}$ Dissolved in Methanol or Methanol-Carbon Tetrachloride¹

by W. R. Carper

Department of Chemistry, California State College, Los Angeles, California 90032

and P. A. D. de Maine²

Department of Chemistry, University of California, Santa Barbara, California 93017 (Received July 8, 1965)

Precision conductance data between 10 and 40° are reported for $\text{Be}(\text{NO}_3)_2 \cdot 3\text{H}_2\text{O}$, $\text{Ca}(\text{NO}_3)_2 \cdot 4\text{H}_2\text{O}$, and $\text{Mg}(\text{NO}_3)_2 \cdot 6\text{H}_2\text{O}$ dissolved separately in pure methanol, and for $\text{Be}(\text{NO}_3)_2 \cdot 3\text{H}_2\text{O}$ dissolved in methanol-carbon tetrachloride. Also described are the Janz-McIntyre-type conductance bridge and the thermostated bath used. All data were processed by computer programs containing the self-judgment principle. Compatibility of the data with several equations is discussed.

Introduction

In preceding papers,^{3,4} the literature was reviewed and conductance values reliable to better than 2% were given for several salts of the group II-A metals dissolved separately in nonaqueous solvents. For most systems, plots of the specific conductance *vs.* salt concentrations at a fixed temperature yielded two intersecting straight lines. For each salt at each temperature the concentration at the intersection point was found to be a linear function of the static dielectric constant of the pure solvent.⁴

Discussed here are new conductance data, reliable to 0.1%, for three nitrates of group II-A metals dissolved in methanol or in methanol-carbon tetrachloride at 10, 20, 30, 35, and 40°. Compatibility of these data with various conductance theories was tested by the self-judgment method of curve fitting⁵⁻⁷ in which the preselected limits of reliability for the raw data determine the compatibility of data and the maximum permitted errors associated with each value for each parameter. This curve-fitting method, described in the Data Processing Method section, is free of the ambiguity inherent in "graphical" and "statistical" methods.

Experimental Section

Fisher Spectroanalyzed methanol and CCl_4 were saturated with Matheson anhydrous grade nitrogen (dew point less than -40°) immediately before use. Frequent purity checks, made with an Aerograph Model A-90-P chromatograph with firebrick column and helium as the carrier gas showed less than 0.01% impurity in both solvents. Dielectric constant and conductance data for both solvents agreed with published values.⁸

In analyses of the Fisher purified grade $\text{Be}(\text{NO}_3)_2$

(1) Taken from the Ph.D. Thesis of W. R. Carper, University of Mississippi, 1963.

(2) Address correspondence to this author at the Center for Computer Science and Technology, Institute of Technology, National Bureau of Standards, Washington, D. C. 20234.

(3) W. R. Carper and P. A. D. de Maine, *J. Chem. Eng. Data*, **9**, 316 (1964).

(4) W. R. Carper and P. A. D. de Maine, unpublished data.

(5) P. A. D. de Maine, *Comm. Assoc. Computing Machinery*, **8**, 518 (1965).

(6) P. A. D. de Maine and R. D. Seawright, *Ind. Eng. Chem.*, **55**, No. 4, 29 (1963).

(7) P. A. D. de Maine and R. D. Seawright, "Digital Computer Programs for Physical Chemistry," The Macmillan Co., New York, N. Y.: (a) Vol. I, 1963; (b) Vol. II, 1965.

3H₂O, Fisher Reagent grade Mg(NO₃)₂·6H₂O, and Baker Reagent grade Ca(NO₃)₂·4H₂O the cation content checked to within 0.4% of the theoretical value. The standard solutions used in the calibration of the conductance bridge and cells were prepared from conductance water and calcined Analar grade KCl, both saturated with the dry nitrogen.

Preparation of solutions, filling the conductance cell, and sealing the cell were carried out in a dry nitrogen atmosphere. Resistance measurements were made by the four leads method at 10, 20, 30, 35, and 40° with the precision conductance equipment to be described. For each solution at each temperature the resistances (R_V) measured at 20, 5, 2, and 1 kc (V) were plotted against $1/V$ and the resultant straight line was extrapolated to infinite frequency. Only extrapolated resistances, R_∞ , have been used in our calculations. Resistance measurements with fresh solutions showed reproducibility within 0.1%.

Static dielectric constants for the methanol mixtures were measured at 10, 20, 30, 35, and 40° with the high precision Wissenschaftlich-Technische Werkstätten multidekometer bridge (Type DK-06) described elsewhere.⁹ Viscosity coefficients for the salt solutions at 20° were calculated in the usual manner from flow times measured by means of a free-flow electroviscometer.¹⁰ Concentration ranges for the solutions studied are given in Table I.

Table I: Salt Concentration Range (Scr) and the Per Cent Volume of CCl₄ (near 20°) for the Salt-Methanol-CCl₄ Solutions (G is the Number of Different Salt Concentrations at Which Conductances Were Obtained)

Salt	% CCl ₄	Scr × 10 ⁴ , M	G
Ca(NO ₃) ₂ ·4H ₂ O	0.00	3.682–36.82	9
Mg(NO ₃) ₂ ·6H ₂ O	0.00	4.847–48.47	10
Be(NO ₃) ₂ ·3H ₂ O	0.00	3.989–39.89	10
	0.02	3.989–39.89	10
	0.06	3.989–39.89	10
	0.10	3.989–39.89	10

Description and Calibration of Equipment. The precision conductance bridge was a copy of one already described¹¹ which uses the "four leads method."¹² The central component is a General Radio Co. 1605-A85 impedance bridge. Bridge resistances were carefully checked¹ against resistors obtained from the National Bureau of Standards. Our operational methods have been fully described by Janz and McIntyre.¹¹

Conductance cells were mounted with a Plexiglas collar bound by aluminum strips for easy insertion into

the high-precision thermostated 30-gal capacity oil bath. The constants for the two Sargent (Type S-29815 and S-29885) conductance cells were determined at several temperatures by the method of Lind, Zwolenk, and Fuoss¹³ through use of KCl-H₂O solutions and data in the literature.^{8b} Cell constants were 0.9122 (±0.0004) and 0.002248 (±0.000002).

The constant temperature bath was constructed from a fiber-glass-insulated stainless steel film-developing tank of 35-gal capacity. Heat was supplied by 42 15-w light bulbs mounted on chemically resistant Plexiglas-55 and totally immersed in the 30 gal of Fisher conductance bath oil in the tank. Fifteen switches permitted use of any number of light bulbs. A refrigeration unit, consisting of a compressor (pressure 150–202 psi) containing Freon-12 gas and a 0.25-hp motor, was attached under the tank. The cooling coils lay along two opposite inner sides of the tank and perpendicular to the heating tray of light bulbs. Two high-speed multiple-bladed stirrers, driven by 0.05-hp Dayton Electric Co. 5K002 air-cooled motors and controlled by conventional heavy-duty variacs, were mounted in diagonally opposite corners of the tank in order to maintain temperature uniformity in the bath. A heavy-duty (30-amp) Curtin Model 7600 negative (normally off) mercury relay switch and a mercury-platinum variable thermostat controlled the refrigeration unit to within 0.01° of the desired bath temperature. A Fisher transistor relay (Model 30) and a sensitive mercury-toluene thermostat, constructed in our laboratory, controlled the heating circuit.

The conductance bridge and thermostated oil bath were in an air-conditioned dehumidified room with less than 2° temperature variation over long periods. The bath temperature, frequently checked with a Beckmann differential thermometer which had been calibrated against a National Bureau of Standards thermometer, varied less than 0.005° over several days. This cor-

(8) (a) N. A. Lange, "Handbook of Chemistry," Handbook Publishers Inc., Sandusky, Ohio, 1956; (b) "Handbook of Chemistry and Physics," 41st ed, Chemical Rubber Publishing Co., New York, N. Y., 1960; (c) B. E. Conway, "Electrochemical Data," Elsevier Publishing Co., New York, N. Y., 1952; (d) L. Scheffon and M. B. Jacobs, "The Handbook of Solvents," D. Van Nostrand Co. Inc., New York, N. Y., 1953.

(9) P. A. D. de Maine, J. S. Menendez, and W. C. Herndon, unpublished data.

(10) P. A. D. de Maine and E. R. Russell, *Can. J. Chem.*, **39**, 1929 (1961).

(11) G. J. Janz and J. D. E. McIntyre, *J. Electrochem. Soc.*, **108**, 272 (1961).

(12) F. S. Feates, D. J. G. Ives, and J. H. Pryor, *ibid.*, **103**, 580 (1956).

(13) J. E. Lind, J. J. Zwolenk, and R. M. Fuoss, *J. Am. Chem. Soc.*, **81**, 1557 (1959).

responds to a maximum error in the measured resistance of 0.01% for a temperature coefficient of 2%/°C.

The resistances of all solutions were measured initially at 20° and then the solutions were slowly brought to another temperature by slow changes (less than 2°/hr) in the bath temperature in order to avoid Soret¹⁴ effects. Photochemical effects were eliminated by dyeing the bath oil with croceine scarlet (National Aniline Corp.).

Data Processing Method

In the self-judgment method of curve fitting,⁷ the pre-selected limits of reliability for the raw data, as defined by the instrument reliability factors, are considered an intrinsic part of the experimental information. Values for the ordinates and their associated maximum permitted errors are computed from this information. The self-judgment principle⁶ is used to reject those data points farther than the maximum permitted error from the median curve. Median values for the parameters (P) and their maximum possible (permitted) errors (ΔP) are computed from the G2 accepted data points and their associated maximum permitted errors.

In the description^{7b} of the conductance feeder program 32 (call word FBAAA) the 16 equations tested are described fully.

All salt concentrations and solution densities were computed from weights and/or volumes of the components (measured near 20°) by means of program 5 (call word AAAAE). Ideality of solutions at each temperature was assumed, and density measurements of selected solutions at 40° showed that this assumption was responsible, at most, for an error less than 0.1%.

All conductance-viscosity data were processed with the variable dimensioned programs 32 and 326 (call words FBAAA and ZAAAS)^{7b} which contained the newer definition of maximum possible error (Appendix E of ref 7b). In program 32 the instrument reliability factors selected were as follows: WAC11 = WAC21 = 1.0, lowest (WL21) and highest (WU11, WU21) measured values for specific conductance (WU11) and concentration (WL21, WU21). The two maximum permitted deviations (DEVF1 and DEVF2) were both set equal to 0.5, 0.4, 0.2, and 0.1% in turn. Each of the 16 conductance equations^{7b} was examined for data compatibility. For each equation at each temperature the reject-restore commands⁷ for program 326 were selected after examination of autoplots of data prepared with program 501 (call word AEEEE).

Results and Discussion

With DEVF1 = DEVF2 = 0.005 (*i.e.*, with limits of 0.5%) only three¹⁵ of the 16 conductance equations

listed in Chapter IX of ref 7b were compatible with the new data. Included in the 13 equations which the data do not fit are the second ($L = 3$) and third ($L = 4$) Fuoss-Onsager equations which contain the mean activity coefficient (f) and fraction of salt dissociated (γ).¹⁶

For each salt system at each temperature and for each solvent composition the Walden product, viscosity coefficient (η) times molar conductance (μ), increases markedly as the salt concentration (M) decreases. Values for η , μ , Walden product, and M are given in Table II for methanol systems at 20°. These results

Table II: Values for Molar Conductance (μ), Viscosity Coefficient (η), and Walden Product ($\eta\mu$) at 20° for Methanol Solutions of the Salts at the Indicated Concentrations

Salt	Concn, $M \times 10^4$	μ	η , cp	$\eta\mu$
Ca(NO ₃) ₂ ·4H ₂ O	3.68	108.66	0.576	62.58
	7.36	95.81	0.579	55.48
	11.06	88.70	0.580	51.45
	14.73	83.91	0.581	48.72
	18.41	80.59	0.581	46.82
	25.77	75.15	0.582	43.71
	29.45	74.13	0.582	43.14
	33.14	72.21	0.583	42.07
	36.82	70.33	0.585	41.11
	Be(NO ₃) ₂ ·3H ₂ O	3.99	138.33	0.580
7.98		118.62	0.581	68.89
11.97		110.22	0.581	64.17
15.96		104.02	0.582	60.49
19.95		99.39	0.582	57.82
23.94		95.28	0.582	55.43
27.93		93.51	0.582	54.42
31.91		91.25	0.582	53.13
35.90		89.20	0.583	51.98
39.89		86.32	0.584	50.38
Mg(NO ₃) ₂ ·6H ₂ O	4.85	176.41	0.579	102.16
	9.69	162.58	0.581	94.38
	14.45	153.44	0.582	89.26
	19.39	147.08	0.583	85.69
	24.23	142.95	0.584	83.41
	29.08	139.08	0.584	81.28
	33.93	135.18	0.585	79.12
	38.77	133.75	0.586	78.36
	43.62	129.68	0.587	76.07
	48.47	126.47	0.587	74.28

(14) R. M. Stokes, *J. Phys. Chem.*, **65**, 1277 (1961).

(15) The first Fuoss-Onsager ($L = 2$), the expansion ($L = 5$), and the specific conductance vs. salt concentration ($L = 12$) equations.

(16) Compatibility with these equations was tested by assuming that $\gamma^{0.5}$ and f^2 have the form: $\gamma^{0.5} = a_1 + a_2c^{0.5} + \dots + a_{n+1}c^{n/2}$. With this expansion method,^{7b} actual values for $\gamma^{0.5}$ and f^2 are not required.

Table III: Results of Data-Compatibility Tests by the Self-Judgment Method for the Indicated Salt Dissolved in Methanol at 20° with the Expansion (E) ($\mu = \mu_0 + S_1C^{1/2} - S_2C + S_3C^{3/2} + S_4C^2$) and Fuoss-Onsager (F-O) ($\mu = \mu_0 + S_1C^{1/2} + S_2C \ln C + S_3C$, with $S_2 = E$ and $S_3 = J - F\mu_0$) Equations. Maximum Permitted Errors Are Given in Parentheses and the Selected Maximum Permitted Deviations for the Molar Conductance (μ) and Salt Concentrations (C) Are DEVF1 and DEVF2, Respectively. The Salt Concentration (C) and Relative Location (RL), Beginning at the Lowest C , of Rejected Data Points Are Given in the Last Column. Term. Means That the Calculation Was Terminated Because Less Than Four Data Points Were Accepted

Eq	DEVF1 = DEVF2	$S_1/10^3$	$S_2/10^6$	$S_3/10^6$	$S_4/10^6$	μ_0	$RL (C \times 10^4)$
Ca(NO₃)₂ · 4H₂O^a							
E	0.004	-3.78(0.54)	0.613(0.170)	-4.29(1.70)	0.616(0.315)	161.5(4.4)	6(22.1)
F-O	0.004	-5.06(0.98)	-0.443(0.159)	-0.511(0.242)		168.5(6.70)	6(22.1)
Be(NO₃)₂ · 3H₂O^b							
E	0.005	-8.22(0.93)	1.92(0.29)	-22.12(2.98)	9.77(0.73)	241.8(7.9)	
F-O	0.005	-8.24(1.53)	-0.777(0.238)	-0.931(0.356)		234.5(10.8)	
E	0.004	-8.74(0.59)	2.10(0.17)	-24.61(1.55)	10.90(0.16)	246.8(5.0)	6(23.9)
F-O	0.004	-8.95(1.15)	-0.888(0.180)	-1.10(0.27)		240.3(8.2)	6(23.9)
E	0.002						Term.
F-O	0.002	-7.90(0.75)	-0.733(0.115)	-0.842(0.173)		231.5(5.6)	2(7.95), 6(23.9), 9(36.0)
Mg(NO₃)₂ · 6H₂O							
E	0.005	-0.535(1.243)	-0.602(0.343)	13.52(3.17)	-8.75(0.67)	205.0(12.3)	
F-O	0.005	-4.74(2.06)	-0.372(0.291)	-0.417(0.411)		241.3(16.9)	
E	0.004	-0.535(0.994)	-0.602(0.274)	13.52(2.53)	-8.75(0.53)	205.0(9.8)	
F-O	0.004	-4.42(1.82)	-0.329(0.256)	-0.357(0.359)		238.2(15.2)	8(38.81)
E	0.002	-1.10(1.72)	-0.398(0.604)	10.47(8.63)	-7.13(4.35)	210.5(16.0)	7(33.9), 8(38.7)
F-O	0.002	-4.42(0.91)	-0.329(0.128)	-0.357(0.180)		238.2(7.6)	8(38.7)
E	0.001	-0.773(0.842)	-0.515(0.296)	12.15(4.23)	-7.99(2.13)	207.3(7.85)	5(24.3), 7(33.8), 8(38.7)
F-O	0.001						Term.

^a For DEVF1 = DEVF2 < 0.004 calculations for the expansion and Fuoss-Onsager equations are terminated (*i.e.*, $RL(C) = \text{Term.}$).

^b For DEVF1 = DEVF2 = 0.001 $RL(C) = \text{Term.}$

suggest that the order of cation mobilities is $Mg^{2+} > Be^{2+} > Ca^{2+}$. Elsewhere, it was reported that addition of up to 1 mole % of water to salt-methanol systems yielded maximum changes of 3.0 and 0.5% in the viscosity coefficient¹⁷ and molar conductance,¹⁸ respectively. Thus the unexpected reversal in cation mobilities cannot be attributed to nonideality or partial reversible solvolysis of the ions or to hydrolysis of the cation with formation of hydrogen ions.

Calculations for the dilute solutions show that the equivalent conductance for each salt at each temperature is substantially less than 80% of its limiting value extrapolated from the Fuoss-Onsager or the expansion equations (see below). Thus each of the three salts is only partially ionized in dilute solution ($10^{-4} M$).

The new method of curve fitting (see data-processing method) with DEVF1 = DEVF2 = 0.005, 0.004, 0.002, or 0.001 was used to test compatibility of the

new data with the Fuoss-Onsager equation¹⁹ and with the equation

$$\mu = \mu_0 + S_1C^{0.5} + S_2C + S_3C^{1.5} + S_4C^2$$

Here μ and C are the molar conductance and salt concentration, respectively. In Table III are given details of these tests for methanol solutions at 20°. For the magnesium nitrate the data fit the expansion equation best. For the Ca and Be salts the pattern of rejected data points shows clearly that the poor fits for both the Fuoss-Onsager and expansion equations are not due to uncertainty in the data. Similar results were obtained at each temperature. The

(17) D. O. Johnston and P. A. D. de Maine, *J. Chem. Eng. Data*, **8**, 586 (1963).

(18) M. M. de Maine and P. A. D. de Maine, *J. Miss. Acad. Sci.*, **8**, 294 (1962); D. O. Johnston and P. A. D. de Maine, *J. Electrochem. Soc.*, **112**, 530 (1965).

(19) R. M. Fuoss and L. Onsager, *J. Phys. Chem.*, **61**, 668 (1957).

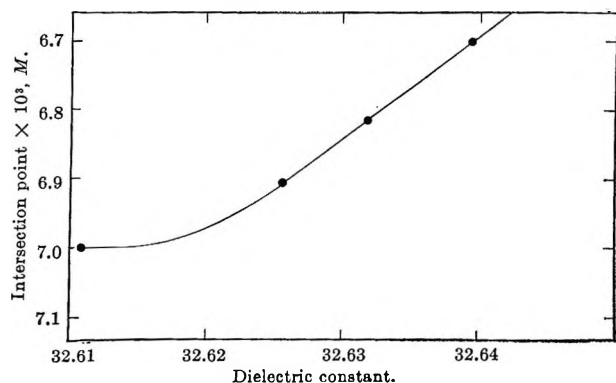


Figure 1. Intersection point *vs.* dielectric constant of methanol-carbon tetrachloride mixture for $\text{Be}(\text{NO}_3)_2 \cdot 3\text{H}_2\text{O}$ at 20° .

comparatively large maximum permitted errors in the limiting molar conductance (μ_0) for precision data illustrate another inherent weakness of conventional curve-fitting methods.

The Fuoss-Onsager equation incorrectly predicts that the limiting molar conductances are in the order $\text{Mg} \approx \text{Be} > \text{Ca}$ salts (Table III). With the expansion equation the expected order ($\text{Be} > \text{Mg} > \text{Ca}$ salts) is obtained. Moreover, the large negative values obtained for S_1 , E , and $J - F\mu_0$ with the Fuoss-Onsager equation appear to be of no real significance physically. Mathematical arguments²⁰ and the fact that the Onsager equation ($\mu = \mu_0 + BC^{0.5}$) is an asymptotic form of the empirical "expansion" equation provide additional justification for its use in computing the limiting molar conductance (μ_0).

For the $\text{Be}(\text{NO}_3)_2 \cdot 3\text{H}_2\text{O} - \text{CH}_3\text{OH} - \text{CCl}_4$ systems, plots of specific conductance *vs.* salt concentration (at fixed temperature and solvent composition)⁴ consist of two intersecting straight lines, each defined by at least four data points. The self-judgment method of curve fitting with $\text{DEVF1} = \text{DEVF2} = 0.002$ was used to obtain median values for the parameters for each pair of lines, and Table IV contains results for the $\text{Be}(\text{NO}_3)_2 \cdot 3\text{H}_2\text{O}$ systems at 20° . Figure 1 shows the salt concentration at the point of intersection (C_I) of the two lines plotted as a function of the static

dielectric constant of the solvent. Plots of similar form were obtained at each of the five temperatures.

Two linear regions in plots of specific conductance *vs.* salt concentration are found for many rare earth, transition metal, and alkaline earth salts dissolved in alcohol or alcohol- CCl_4 .³ The conclusion that for

Table IV: Data for Plots of Specific Conductance *vs.* $\text{Be}(\text{NO}_3)_2 \cdot 3\text{H}_2\text{O}$ Concentration for $\text{CH}_3\text{OH} - \text{CCl}_4$ Solutions at 20° . For the Linear Portions in Two Concentration Regions Are Given Values for the Slope (S) and Intercept (I) on the Ordinate. C_I Denotes the Concentration at Which the Two Linear Sections of Each Plot Intersect. $G1/G = 4/5$ Means That Four of the Five Data Points Were Accepted when $\text{DEVF1} = \text{DEVF2} = 0.002$

% CCl_4 (vol)	Salt concn range, $M \times 10^4$						$C_I \times 10^3$
	3.99 to 19.95		27.93 to 39.89		$G1/G$	$S \times 100$	
0.00	4/5	8.13	3.34	4/4			5.43
0.02	5/5	8.17	3.59	4/4	5.43	21.94	6.80
0.06	5/5	8.15	3.58	4/4	5.40	22.57	6.89
0.10	5/5	8.11	3.59	4/4	5.37	22.78	7.01

each salt concentration region a different ionization process predominates is unacceptable in the continuum model of ionization. However, if this view is accepted, the nonlinearity of the plots of "point of intersection" *vs.* solvent dielectric constant (Figure 1) and similar results for several aliphatic alcohols⁴ indicate that bulk solution and/or solvent properties are not the primary factors in the ionization of these salts in alcohol- CCl_4 solutions. These results can be understood if it is supposed that complex formation and the geometry of the solvent lattice are important precursors to ionization.

Acknowledgment. Sincere thanks are due the donors of the Petroleum Research Fund, administered by the American Chemical Society, for support of this research.

(20) J. B. Scarborough, "Numerical Mathematical Analysis," D. Van Nostrand Co. Inc., New York, N. Y., 1953.

Temperatures of Liquid Crystal Transitions in Cholesteryl Esters

by Differential Thermal Analysis¹

by Edward M. Barrall, II, Roger S. Porter, and Julian F. Johnson

Chevron Research Company, Richmond, California (Received July 8, 1965)

The first differential thermal analysis (d.t.a.) study of liquid crystal phases in cholesteryl esters is reported. Analysis was performed on a series of nine highly purified straight-chain aliphatic esters from formate to stearate. The esters of cholesterol are especially interesting since between the true solid and isotropic liquid at least two mesophases are possible, the smectic and cholesteric. In this study the number of first-order transitions in each ester was found by d.t.a. heating curves. Mesophase transition temperatures observed as endothermal minima by d.t.a. are compared with those available from other techniques. Data obtained from different methods are in generally good agreement concerning transition temperatures and mesophase identification. Several previously unreported solid phases, depending on conditions of crystallization, have been found by d.t.a. In addition, a transition reportedly formed only on cooling in the *n*-nonanoate ester has been found to be a reversible first-order transition. For several esters, speculation is offered concerning the path for mesophase transitions.

The temperature of liquid crystal, *viz.*, mesophase, transitions for esters of cholesterol have been determined. Data have been obtained by controlled-heating studies using calibrated differential thermal analysis (d.t.a.). This technique has been recently applied to the nematic type of mesophase.²

The cholesteric mesophase is found in derivatives of cholesterol but not in cholesterol itself.³ Despite their importance in biological systems, the cholesteric type of mesophase has not, until this time, been studied by d.t.a.⁴ in spite of the fact that the first established liquid crystal behavior was observed for a cholesteryl ester.^{5,6}

Trends with molecular weight in the number and relative magnitude of first-order transitions have been evaluated for a series of nine saturated straight-chain cholesteryl esters from formic to stearic. Relative d.t.a. peak areas are used to estimate relative heats of transition. Quantitative transition heats for cholesteryl esters are the subject of a future study.

The lower molecular weight members of the series have been reported previously to show a single mesophase (cholesteric); whereas, the six highest molecular weight members of the series studied here are reported

to show, in addition, a monotropic smectic type of mesophase. A comparison is made with earlier studies of the mesophases in cholesteryl esters which have been made generally by optical means. The nomenclature for liquid crystal phase types has been adopted from the literature for cholesteryl esters with no specific structure determinations made in this study. The molecules in cholesteric liquid crystals are arranged in layers. The layers are reported to be thin with the long axes of the essentially flat molecules parallel to the plane of the layers.^{7,8}

(1) Part V of a series on order and flow of liquid crystals. Presented in part before the American Physical Society, Kansas City, Mo., March 1965.

(2) (a) E. M. Barrall, II, R. S. Porter, and J. F. Johnson, *J. Phys. Chem.*, **68**, 2810 (1964); (b) H. Martin and F. H. Müller, *Kolloid-Z.*, **187**, 107 (1963).

(3) G. W. Gray, *J. Chem. Soc.*, 3733 (1956).

(4) G. W. Gray, "Molecular Structure and the Properties of Liquid Crystals," Academic Press Inc., New York, N. Y., 1962, p. 114.

(5) F. Reinitzer, *Monatsh.*, **9**, 421 (1888).

(6) G. A. Hulett, *Z. Physik. Chem. (Leipzig)*, **28**, 629 (1899).

(7) J. L. Ferguson, *Sci. Am.*, **211**, 76 (1964).

(8) C. Robinson, *Trans. Faraday Soc.*, **52**, 571 (1956).

Experimental Section

D.t.a. Method. The basic differential thermograph and electronic system employed in these measurements have been described previously.^{9,10} The cell design, a modification of an earlier method,¹⁰ is shown in Figure 1. The present design represents an improvement over previous designs in that temperatures of transition may be read directly from the same thermogram that records the heats of transition. The previously discussed problem of thermal lag has essentially been eliminated.^{2a} The improved sharpness of the endotherms and accuracy of the temperature axis have been effected by making the sample and sample container as small as possible. This lowers the specific heat of the apparatus, improves its sensitivity, and permits the use of very thin samples to avoid heat-transfer problems. The differential thermograph cell compartment was operated after evacuation to a pressure of 1 torr, the residual gas being air.

Sample Preparation. Samples of the cholesteryl esters, the *n*-propionate, myristate, stearate, and palmitate were obtained from Applied Science Laboratories, Inc., State College, Pa. Samples of some of these and other esters were obtained from Columbia Organic Chemicals Co., Inc., Columbia, S. C. These samples were recrystallized three times from boiling ethanol. Carbon-hydrogen analyses are shown in Table I.

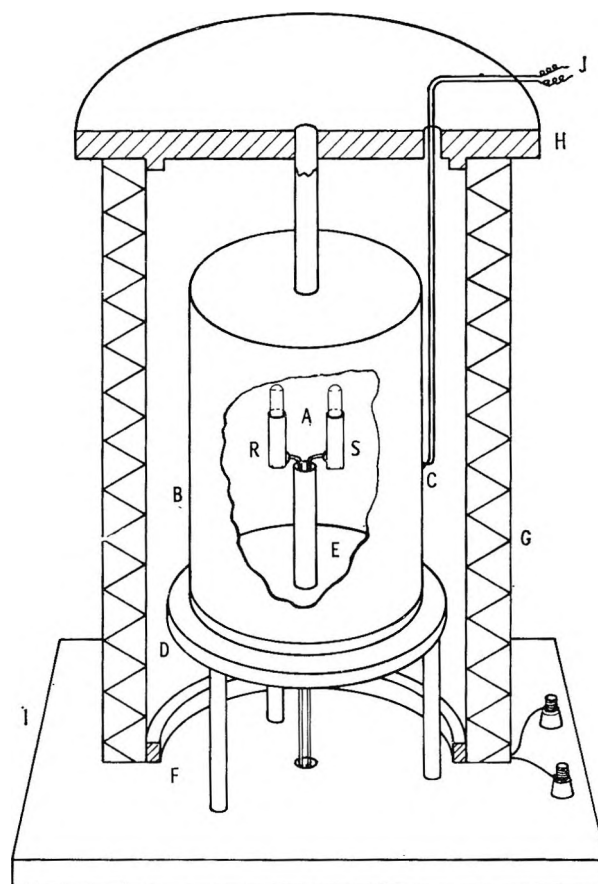


Figure 1. Calorimetric differential thermal analysis cell: A, copper sample (S) and reference (R) cells 0.3 in. by 0.1 in. diameter attached to copper-constantan thermocouples; B, heat shield 1.5 in. in diameter by 2 in. in height; C, program thermocouple attached to B; D, nickel base 1.5 in. in diameter; E, ceramic insulator 0.8 in. high; F, furnace-centering ring; G, furnace 2.5 in. in diameter by 4 in. in height; H, furnace cover; I, transite base; entire apparatus is enclosed in an evacuated bell jar; J, leads to programmer.

Table I: Carbon-Hydrogen Analysis of Cholesteryl Esters

Cholesteryl ester	% calcd.		% found ^a	
	C	H	C	H
Formate	81.2	11.1	81.16	11.08
Acetate	81.3	11.2	81.24	11.20
<i>n</i> -Propionate	81.45	11.3	81.50	11.31
<i>n</i> -Heptylate	81.9	11.65	82.00	11.70
<i>n</i> -Nonanoate	82.1	11.75	82.11	11.79
<i>n</i> -Decanoate	82.2	11.85	82.21	11.90
Myristate	82.55	12.1	82.60	12.10
Palmitate	82.7	12.2	82.70	12.18
Stearate	82.8	12.3	82.78	12.28

^a Average of three determinations.

These analyses indicate a relatively high purity for these compounds and compare with analyses published previously by Gray.³ A 2-mg. portion of the triply recrystallized sample was packed into 1 cm. × 1 mm. i.d. glass capillary tubes and sealed with the flame of a microtorch. Care was exercised not to heat samples with the flame. All weighings were made on a semi-microbalance of 0.01-mg. sensitivity. The samples were melted and remelted in place in the thermograph.

Table II: Calibration Standards for Differential Thermograms

Material	Transition temp., °C.	
	Ref. 11-14	Found
<i>n</i> -Octadecane	28.18	28.21
<i>n</i> -Dotriacontane	69.7	69.00
Ammonium nitrate	125	125.60
	169.0	169.55
Indium	156.4	156.0

(9) E. M. Barrall, II, J. F. Gernert, R. S. Porter, and J. F. Johnson, *Anal. Chem.*, **35**, 1837 (1963).

(10) E. M. Barrall, II, R. S. Porter, and J. F. Johnson, *ibid.*, **36**, 2172 (1964).

Table III: Transition Temperatures for Cholesteryl Esters^a

Cholesteryl ester	D.t.a.			Other workers ¹²⁻¹⁸			Gray ^{3,4}		
	T ₁	T ₂	T ₃	T ₁	T ₂	T ₃	S	C	I
Formate	97.3	(~90)	96.5		(60.5)		97.5
Acetate	44	81-87	118.4	(80-90)	112.8		(94.5)		116.5
<i>n</i> -Propionate	99 ± 1	110?	115.3	93	107.2		102		116
<i>n</i> -Heptylate			114.1	(<92.5)	(95.5)	114
<i>n</i> -Nonanoate	74.0	80.8	93.0	78	79	90.5	(77.5)	80.5	92
<i>n</i> -Decanoate		85.7	91.2		82.2	90.6	(81.5)	85.5	92.5
Myristate	73.6	79.7	85.5	72	78	83	71	81	86.5
Palmitate		79.7			77	81	(78.5)	79	83
Stearate			85.1		74.5	82	(75.5)	(79.5)	83

^a S = smectic; C = cholesteric; I = isotropic liquid; T₁ = lowest transition; T₂ = intermediate transition; T₃ = transition to isotropic liquid; parentheses indicate monotropic metastable transition.

Transition Temperature Determinations

The temperature of the endothermal minimum was determined by measuring the distance from the chart zero to the minimum, converting inches to millivolts (0.25 mv./in.), adding the appropriate bucking voltage value and comparing the resultant sum voltage to a millivolt vs. degree centigrade calibration chart prepared for the copper-constantan thermocouples used. This technique is described in greater detail elsewhere.^{2a,9,10} Some of the calibration data are given in Table II.¹¹⁻¹⁴

The absolute accuracy of the temperatures determined was ±0.1° in all cases. The reproducibility was ±0.05° for an individual sample on successive remeltings. The difference between reproducibility and accuracy is due in part to the movable nature of the cholesteryl ester endotherms—which, in extreme, was found to be ±0.2°. This effect has been reported previously for optical data gained from cooling and heating curves.³

Results

Typical differential thermograms for several cholesteryl esters are shown in Figure 2. These are reproduced to scale directly from the original X-Y recorder. In complex differential thermograms, where all thermal effects are not understood, it is extremely desirable to report actual curves, not smoothed tracings. Data on individual esters are shown with previous literature data in Table III. The best, most recent, and most complete set of transition temperatures for cholesteryl esters have been given by Gray.³ Temperatures for the d.t.a. endothermal minimum, T_m , have been found, as in the case of other liquid crystals, to agree with temperatures of visually observed transitions to within 2°. The transition temperatures obtained by d.t.a. (see Table III) indicate that the triply recrystallized

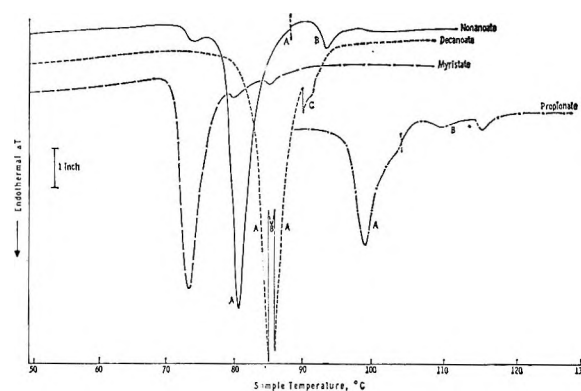


Figure 2. Differential thermograms of cholesteryl esters: *n*-propionate (0.00232 g.) recorded at (A) 0.20 and (B) 0.05°/in. ΔT ; *n*-nonanoate (0.00420 g.) recorded at (A) 0.10 and (B) 0.05°/in. ΔT ; *n*-decanoate (0.00412 g.) recorded at (A) 0.10, (B) 0.20, and (C) 0.05°/in. ΔT ; myristate (0.00343 g.) recorded at 0.20°/in. ΔT . All heating programs at 4°/min.

samples studied here were of relatively high purity. This is also indicated by elemental analyses given in Table II.

Examples of the differential thermograms used in the rate of transformation study on cholesteryl stearate are shown in Figures 2 and 3. The shape of the d.t.a. endotherms is due in part to instrumental parameters.

Discussion

Prior to the discussion of the individual compounds, certain terms and notations in literature use for cholesteryl

(11) American Petroleum Institute Project 44, Critical Constants, 1959.

(12) A. Théorêt and C. Sandorfy, *Can. J. Chem.*, **42**, 57 (1964).

(13) E. S. Watson, M. J. O'Neill, J. Justin, and N. Brenner, *Anal. Chem.*, **36**, 1233 (1964).

(14) "Lange's Handbook of Chemistry and Physics," 9th Ed., Handbook Publishers, Inc., Sandusky, Ohio, 1956, p. 102.

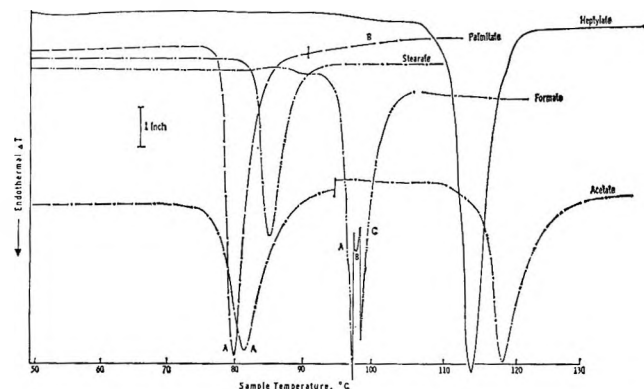
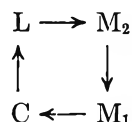
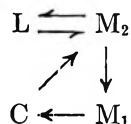


Figure 3. Differential thermograms of cholesteryl esters: formate (0.00342 g.) recorded at (A) 0.10, (B) 0.20, and (C) 0.10°/in. ΔT ; acetate (0.00391 g.) recorded at (A) 0.20 and (B) 0.05°/in. ΔT heated at 8°/min.; *n*-heptylate (0.00409 g.) recorded at 0.10°/in. ΔT ; palmitate (0.00485 g.) recorded at (A) 0.20 and (B) 0.10°/in. ΔT ; stearate (0.00442 g.) recorded at 0.40°/in. ΔT . Heated at 4°/min. unless noted otherwise.

teryl esters must be defined. The notations L, M, and C refer to the isotropic liquid, mesophase (smectic or cholesteric), and solid phases, respectively. Certain mesophases in some cholesteryl esters have been termed monotropic, *i.e.*, metastable. That is, these mesophases characteristically form only on cooling from the isotropic liquid and do not form on heating from the solid. For example



In this hypothetical case a heating process will not show the mesophases M_1 and M_2 . The transition $C \rightarrow L$ will produce a single endotherm by d.t.a. The heat of this transition from equilibrium thermodynamics will equal the sum of the heats for the other transitions in the square. Various combinations of reversibility can exist depending on the ester, for example

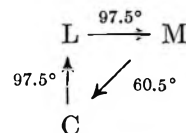


M_2 will not form on heating so that the thermogram will show two endotherms corresponding to $C \rightarrow M_2$ and $M_2 \rightarrow L$. The d.t.a. cooling curves have not been presented. Serious supercooling of the phases is observed. Undercooling has not been observed for low-viscosity, nematic mesophase transitions but has been

previously reported by Vold for viscous mesophases in soaps.¹⁵ Cholesteryl ester transitions observed visually on cooling occur reproducibly in the interval of 0–9° below the transitions observed on heating. Gray considers this is not due to supercooling but to two different textures for the cholesteric phase: the homoeotropic and the focal conic.³ Chistyakov, however, refers to the supercooling of cholesteric mesophase transitions.¹⁶

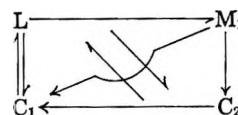
Specific Esters

Cholesteryl Formate. Cholesteryl formate gives a single endothermal minimum at 97.3° irrespective of previous thermal history or solvent used for recrystallization. The smectic–cholesteric transition at 60.5° reported previously by optical means from a cooling curve could not be observed by d.t.a. The mesophases are monotropic with respect to the liquid phase.



Cholesteryl Acetate. The thermographic behavior of the acetate ester is complex. When the acetate is heated, using an ethanol-recrystallized sample, two endothermal minima appear at 81.4 and 118.2°. On a second heating, after rapid quenching of the melt, two endothermal minima at 44.1 and 118.5° appear. After the melt is slowly cooled, 1°/min., three endothermal minima are obtained upon reheating at 43.2, 87.3, and 118.6°. The endothermal differences are not due to the formation of decomposition products since the 81.4 and 118.2° endothermal minima reappear essentially unchanged when the sample is dissolved in ethanol, evaporated to dryness at 30° and 4 torr, and reheated. The procedure was repeated with four different preparations with the same results. These transitions do not compare directly with those observed by Gray³ or by Chistyakov.¹⁶ Neither reports more than a single transition on heating the acetate ester.

Usol'tseva and Chistyakov¹⁷ have summarized the behavior of the acetate as



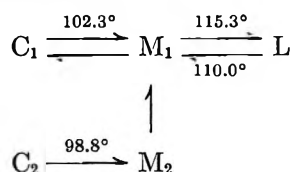
(15) R. D. Vold, *J. Am. Chem. Soc.*, **63**, 2915 (1941).

(16) I. G. Chistyakov, *Kristallografiya*, **8**, 79 (1963).

(17) V. A. Usol'tseva and I. G. Chistyakov, *Russ. Chem. Rev.*, **32**, 495 (1963).

Solid C_2 is monotropic, being unstable relative to solid C_1 . A recent Russian review paper quotes two early and obscure studies which conclude that cholesteryl acetate never forms liquid crystals on heating.¹⁷ Lehmann has reported two mesophases; Gray has reported only one, a monotropic cholesteric mesophase.³ The major endotherm at 118° found by d.t.a. definitely corresponds to a first-order transition to the isotropic liquid. The $43\text{--}44$ and $81\text{--}87^\circ$ endotherms could involve solids C_1 and C_2 , which are formed preferentially from the melt or solution. Either case leads to the conclusion that a mesophase is formed on heating the ester.

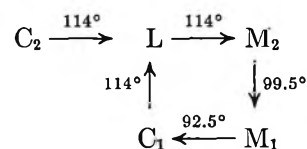
Cholesteryl n-Propionate. When crystals of the propionate ester obtained from ethanol solution are thermographed, three endothermal minima are noted at 98.8 , 110.0 , and 115.3° . A thermogram of material crystallized from the melt showed two endothermal minima at 101.6 and 115.2° . These transitions remained essentially constant on successive reruns. The endotherms produced determine the solid-cholesteric transition at 102 and the cholesteric-isotropic transition at 116° .^{3,4} The solid-cholesteric transition varies in temperature, depending on the conditions of crystallization, *i.e.*, from solution or melt. This indicates the possible existence of two alternative solid phases. The possibility of the melt-recrystallized material being a less ordered form of the solution-recrystallized material is ruled out by the lower transition temperature of the calorically larger solution-crystallized material. The reverse would be expected if the disordered-form proposition were true. The following route of crystallization can be postulated.



where C_1 and M_1 are the solid and cholesteric phases reported by Gray³ and are obtainable from the melt; C_2 and M_2 are solid and liquid crystal phases obtainable only if C_2 is crystallized from solution. It is possible that M_1 may not be identical in both cases. On the basis of transition temperature, the two liquid crystal phases are indistinguishable. The solution-crystallized thermogram could be obtained from a sample previously thermographed by the dissolution of the sample in ethanol or benzene, evaporation to dryness at 4 torr and 30° , and rethermographing. This eliminates the chance that decomposition products or residual solvent are responsible for the thermographic behavior.

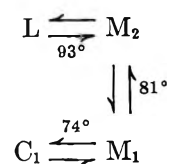
Cholesteryl n-Heptylate. This ester, like the formate, exhibits only a single endotherm on heating. This occurs at 114.1° and is equivalent to the transition reported by Gray.³ The temperature of the endothermal minimum is independent of thermal history, being the same for solution- and melt-recrystallized material.

The heat of fusion on second melting was about 20% higher than for the melting of the original solution-crystallized ester. Since the reported smectic and cholesteric phases for this ester are monotropic,³ a mixture of these phases could occur which would differ, depending on the origin of the solid phase from melt or solution. The following crystallization route can be postulated on the basis of d.t.a. and previous work.³



where C_1 , M_1 , M_2 , and L are the solid, smectic, cholesteric, and isotropic liquid reported by Gray. C_2 is the solid phase obtainable from solution. C_1 is possibly only a more highly ordered form of C_2 and not a completely different solid phase.

Cholesteryl n-Nonanoate. This ester shows three transitions between solid and isotropic liquid. The temperatures and relative heats of transition are independent of the conditions of sample crystallization, from solution or from melt. The first endotherm appears near 74° , the second at 81° , and the third at 93° . The three transitions likely correspond to the solid-smectic, smectic-cholesteric, and cholesteric-isotropic transitions of Gray³ at 77.5 , 80.5 , and 92° . Gray classifies the 77.5° transition as being monotropic. Thus, the solid-smectic transition of cholesteryl nonanoate is the only reportedly monotropic transition to be seen in d.t.a. heating curves. This indicates that the nonanoate solid-smectic transition is indeed not monotropic with respect to either the solid or the liquid phase. In every other monotropic transition of the cholesteryl esters, no endotherm was observable by d.t.a. The following crystallization route can be postulated



where M_1 and M_2 are the smectic and cholesteric phases, respectively.

Cholesteryl n-Decanoate. Two endothermal events are exhibited, at 85.7 and 91.2°, which are independent of conditions of crystallization, from solution or from melt. The 85.7° transition appears as a shoulder on the d.t.a. trace for a major endotherm with a minimum at 91.2°. An attempt was made to resolve the shoulder by carrying out d.t.a. at a very low rate of heating, 0.86°/min. The 85.5° transition persisted as a shoulder. Slower heating rates on other cholesteryl esters showing more than one endothermal process increased peak resolution at the expense of sensitivity. The 85.7° transition compares with Gray's smectic-cholesteric transition at 85.5°. The 91.2° transition compares with the cholesteric-isotropic transition at 92.5°. Since the reported smectic phase is monotropic, the 81.5° solid-smectic transition does not appear on the thermogram.

Chistyakov has noted two transitions by optical means on heating at 82.2 and 90.6°.¹⁶ Since these results were obtained from heating, the monotropic phase does not appear, with the other transitions shifted to lower temperature. Chistyakov's published curves indicate that the 82.2° transition appears as a shoulder at a 1°/min. heating rate. His results are thus consistent with results obtained here except that the earlier study probably involved a less pure ester.

Cholesteryl Myristate. This ester shows no effects due to the origin of the crystals from solvent or from the melt. Three endothermal minima appear at 73.6, 79.7, and 85.5°. These apparently correspond to Gray's solid-smectic transition at 71°, smectic-cholesteric at 81°, and cholesteric-isotropic liquid at 86.5°. No monotropic phases have been reported.³ The d.t.a. thermograms suggest that the calorically large solid-smectic transition continues throughout the transition from solid to isotropic liquid. Slower heating rates and smaller sample sizes had no effect on this possible interpenetration of phases.

Cholesteryl Palmitate. Gray has reported three transitions for the palmitate ester, shown in Table III. The solid-smectic transition is monotropic with the liquid phase. Therefore, only the solid → cholesteric and cholesteric → isotropic liquid transitions should be observable on a heating program. Chistyakov¹⁶ has reported such a sequence. The slopes in his work indicate a large degree of phase interpenetration between the solid and isotropic liquid. The d.t.a. shows

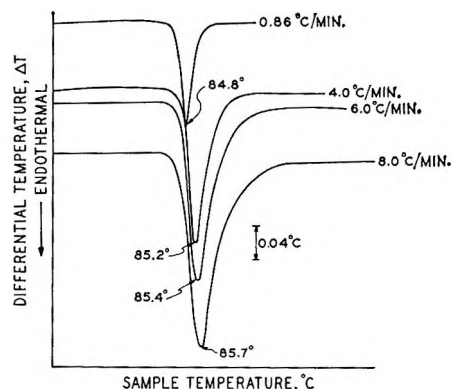


Figure 4. Effect of heating rate on the area and temperature of the endothermal minimum of cholesteryl stearate.

only a single distinct endotherm at 79.7°. This endotherm is probably identical with the solid-cholesteric transition reported by Gray at 79° summed with the 83° cholesteric → isotropic liquid transition. Slower heating rates failed to separate the two transitions as distinct endotherms or shoulders.

Cholesteryl Stearate. This ester shows a single endothermal minimum at 85°. This is to be compared with the literature which indicates a cholesteric-isotropic liquid transition at 82–83°.¹⁸ Reported smectic and cholesteric phases are monotropic, and the transitions cannot be detected upon heating. No effect of melt recrystallization was noted.

Rate of Transformation of Cholesteryl Esters

Owing to the high viscosity of the liquid phases of the cholesteryl esters, it is possible that the rate at which the molecules can convert into alternate forms may be slow with respect to time and heating rate. To test this proposition, a sample of cholesteryl stearate was thermographed at four heating rates. If the transformation is slow from solid to liquid, the endothermal minima should shift to higher temperatures with increasing heating rate due to induced lag in the system. The thermograms of the stearate are shown to scale in Figure 4. The temperature for the endothermal minimum changes by only 0.9° over a heating rate range 0.86–8.0°/min. This small temperature variation is within the limits of instrumental parameters.

(18) R. S. Porter and J. F. Johnson, *J. Appl. Phys.*, **34**, 55 (1963)

The Excess Volume of Binary Mixtures of *trans*-Decalin with Cyclohexane and with *n*-Alkanes

by José D. Gómez-Ibáñez and Tieh Chu Wang

Hall Laboratory of Chemistry, Wesleyan University, Middletown, Connecticut (Received July 18, 1965)

The excess volume of mixing of binary systems of *trans*-decalin with some *n*-alkanes has been determined using both a dilatometric and a pycnometric method. At a given temperature (25.0°), the excess volume increases with increasing length of the alkane chain, from the negative values exhibited by the system *trans*-decalin + *n*-heptane to the slightly positive value observed for the system of *trans*-decalin with *n*-hexadecane. The excess volume seems to be a linear function of $1/(n + 2)$, where *n* is the number of carbons in the aliphatic component. For a given alkane (*i.e.*, *n*-heptane and *n*-nonane), the excess volume increases in magnitude with increasing temperature. Comparison is made with similar alkane-alkane and cyclohexane-alkane binary mixtures previously described. The excess volume of mixtures of *trans*-decalin with hexadecane is also reported.

Reports of excess volume measurements of binary, nonpolar systems are not abundant in the literature although such measurements are of particular interest. Modern theories of solutions^{1,2} emphasize the importance of the excess volume of mixing and its relation to all other excess thermodynamic functions. Moreover, the theories postulate, when dispersion forces are involved, a sign for V^E which depends upon the relative size of the molecular species present in the mixture.

As part of a systematic study of the effects of molecular size and shape on the thermodynamic properties of binary mixtures of nonelectrolytes, we have reported in two previous papers measurements of the excess volumes of binary mixtures of *n*-alkanes³ and of binary mixtures of cyclohexane with some *n*-alkanes.⁴ It seemed of interest to us to extend our study to the binary mixtures of *trans*-decalin (decahydronaphthalene) with *n*-alkanes. Such mixtures, differing from the ones previously studied⁴ by the replacement of cyclohexane by a similar, planar, and nonlinear hydrocarbon, but one which is almost twice as large in one direction, may provide additional and interesting empirical information. We report here the results of measurements of the excess volume of mixing of the following systems: (I) *trans*-decalin (1) + *n*-

heptane (2) at 15.1, 25.0, and 39.5°; (II) *trans*-decalin (1) + *n*-nonane (2) at 25.0 and 39.5°; (III) *trans*-decalin (1) + *n*-dodecane (2) at 25.0°; (IV) *trans*-decalin (1) + *n*-hexadecane (2) at 25.0°; (V) *trans*-decalin (1) + cyclohexane at 25.0°.

Experimental Section

Procedure. The data here reported were obtained using a dilatometer similar to the one described by van der Waals and Desmyter.⁵ The few changes introduced do not modify essentially its design and operation, and reference is made to the original paper for a description of the apparatus. (Details for its operation may be requested from our laboratory.) The errors involved in the dilatometric measurements can be evaluated in terms of temperature fluctuations of the thermostat ($\pm 0.005^\circ$) and the uncertainties in reading the height of the mercury in the measuring capillaries. In a typical experiment mixing *trans*-

(1) I. Prigogine, "The Molecular Theory of Solutions," Interscience Publishers, Inc., New York, N. Y., 1957.

(2) R. L. Scott, *J. Chem. Phys.*, **25**, 193 (1956).

(3) J. D. Gómez-Ibáñez and T.-C. Liu, *J. Phys. Chem.*, **67**, 1388 (1963).

(4) J. D. Gómez-Ibáñez and T.-C. Liu, *ibid.*, **65**, 2148 (1961).

(5) J. H. van der Waals and A. Desmyter, *Rec. Trav. Chim.*, **77**, 53 (1958).

decalin with *n*-heptane at 25°, the linear contraction of the mercury in the capillary (of volume 0.0769 cm.³/cm. of length) was 1.23 cm. at the first mixing and 6.03 cm. at the last. Since the fluctuation in the meniscus reading was constantly ± 0.02 cm., the relative uncertainty in the excess volume was reduced from an initial value of about $\pm 1.7\%$ to a final value of $\pm 0.3\%$. In terms of cm.³/mole, the errors were about ± 0.007 and ± 0.002 cm.³, depending on the molecular weights of the hydrocarbons and the amounts being mixed. The uncertainty in the mole fraction varied from about $\pm 3\%$ in the first mixing to about $\pm 0.4\%$ at the last mixing.

Principally for the purpose of checking the reliability of the dilatometric results, pycnometric measurements were carried out with systems I, II, and V. For this type of measurement, the procedure followed has been described in detail in a previous paper,⁴ which also discusses the errors involved.

Materials. Two samples of *trans*-decalin were used in our study. The first sample was prepared from a 50% *cis-trans* mixture obtained from Matheson Coleman and Bell. The mixture was fractionated in a metal-helices-packed column of about 70 theoretical plates, at a reflux ratio of 5 to 1. The portion boiling between 185 and 187° was collected and fractionated again in the same manner. After four such distillations, final separation was accomplished using a Beckman Megachrome. The purity of the final product was found to be, by v.p.c. analysis, over 99 mole %. The yield was about 10%, and the density of the *trans*-decalin thus obtained was found to be 0.86584 g./cm.³ at 25.0°. Later, a sample of pure *trans*-decalin was obtained from the K & K Laboratories, Inc., which proved to be, by v.p.c. analysis, of about the same purity as the one previously prepared. It had a density of 0.86604 g./cm.³. Both densities quoted here show good agreement with the value of 0.86592 at 25° found in the literature.⁶

All *n*-hydrocarbons and the cyclohexane used were Matheson Coleman and Bell reagents. Cyclohexane and *n*-heptane were spectroquality reagents, *n*-nonane was chromatquality reagent, and all others were labeled as "99% olefin free" reagents. The purification procedure followed was similar to that described in previous papers.^{3,4} The densities of the final materials were determined, and the results, together with those found in the literature,⁷ are summarized in Table I.

Results

The values for the densities of the pure hydrocarbons reported in Table I are each the average of several

Table I: Densities of Some Hydrocarbons

Hydrocarbon	Temp., °C.	<i>d</i> , g./cm. ³ (this work)	Other values in the lit. (ref. 7)	<i>dV/dT</i> , cm. ³ /deg. (25°)	$\alpha \times 10^4$, deg. ⁻¹
<i>trans</i> -Decalin	15.1	0.87363			
	25.0	0.86584			
		0.86604	0.86592 ^a	0.140	0.876
Cyclohexane	39.5	0.85509			
	25.0	0.77396	0.77389		
<i>n</i> -Heptane	15.1	0.68780			
	25.0	0.67969	0.67951	0.186	1.26
<i>n</i> -Nonane	39.5	0.66716			
	25.0	0.71420	0.71364	0.203	1.13
<i>n</i> -Dodecane	39.5	0.70305			
	25.0	0.74504	0.74515		
<i>n</i> -Hexadecane	25.0	0.76967	0.76993		

^a See ref. 6.

measurements and are accurate to within 0.0001 g./cm.³ or better. Comparison is made in the table with other values for the densities available in the literature. In columns 5 and 6 values for *trans*-decalin and for *n*-heptane are given, respectively, for *dV/dT* and for α , the coefficient of thermal expansion at 25°. These values were obtained from a plot of the calculated molar volumes *vs.* the temperature (in both cases yielding a straight line).

The values for the excess volume of mixing obtained for all the systems under study, using the dilatometric method, are summarized in Table II, while in Table III we report the values for systems I, II, and V obtained using the pycnometric method. Using the dilatometric data, equations of the form

$$V^E = x(1-x) \sum_{i=0}^n A_i (1-2x)^i \quad (1)$$

(where *x* always represents the mole fraction of the component other than *trans*-decalin) have been computed for each system by the method of least squares. The first three coefficients in the expansion (1) were considered sufficient to represent the data, and their values, together with their variance or mean-square error, are reported in Table IV.

In general, we consider the pycnometric values somewhat more reliable, but the difference between the pycnometric values and those computed for the same mole fraction by use of eq. 1 amounted to only

(6) D. L. Camin and F. D. Rossini, *J. Phys. Chem.*, **59**, 1173 (1955).

(7) "Selected Values of Physical and Thermodynamic Properties of Hydrocarbons and Related Compounds," American Petroleum Research Project 44, Carnegie Press, Pittsburgh, Pa., 1953.

Table II: Excess of Mixtures of *trans*-Decalin and Some Hydrocarbons (Dilatometric Measurements)

Mole fraction, z_2	$-V^E$, cm. ³ /mole	Mole fraction, z_2	$-V^E$, cm. ³ /mole	Mole fraction, z_2	$-V^E$, cm. ³ /mole
System I					
<i>trans</i> -decalin (1) + <i>n</i> -heptane (2)		0.795	0.519	0.294	0.093
		0.854	0.396	0.368	0.101
				0.449	0.102
				0.594	0.100
				0.730	0.083
				0.818	0.065
System II					
<i>trans</i> -decalin (1) + <i>n</i> -nonane (2)					
		0.135	0.151		
		0.238	0.242		
		0.384	0.321		
		0.473	0.337		
		0.620	0.310		
		0.670	0.292		
		0.753	0.245		
		0.845	0.167		
System IV					
<i>trans</i> -decalin (1) + <i>n</i> -hexadecane (2)					
				0.083	-0.011
				0.157	-0.017
				0.256	-0.026
				0.338	-0.027
				0.413	-0.033
				0.523	-0.037
				0.611	-0.034
				0.709	-0.035
System V					
<i>trans</i> -decalin (1) + cyclohexane (2)					
				0.208	0.028
				0.351	0.038
				0.471	0.057
				0.554	0.068
				0.726	0.084
				0.773	0.089
				0.847	0.075
				0.898	0.061

Table III: Excess Volume of Mixtures of *trans*-Decalin (1) and Some Hydrocarbons (Pycnometric Measurements)

System	Temp., °C.	Mole fraction, z_2	$-V^E$, cm. ³ /mole
I	15.1	0.54839	0.489
		0.29408	0.499
	25.0	0.41845	0.611
		0.56051	0.612
		0.62618	0.575
		0.53871	0.759
II	25.0	0.28289	0.299
		0.41692	0.364
		0.53773	0.351
		0.54557	0.356
		0.62688	0.337
		0.75327	0.273
V	25.0	0.52144	0.418
		0.59901	0.088

± 0.02 to ± 0.03 cm.³/mole. This difference could perhaps be attributed to the "air-free" condition of the components when the dilatometer was used. The dilatometric method offered the additional advantage of providing values for the excess volume of mixing over the whole range of composition in a single operation.

Discussion

The only values in the literature for the type of systems studied here are those reported by Danusso⁸ for the systems *trans*-decalin + *n*-heptane, *trans*-decalin + *n*-hexadecane, and *trans*-decalin + cyclohexane at 30°. For the first system Danusso's values at 30° are not far from our values at 25°. For the second system Danusso reports no change in volume on mixing, while we detect a positive, although small, excess volume. For the system *trans*-decalin + cyclohexane Danusso reports a small and positive excess volume while we have observed equally small but negative values. We should mention, *in passing*, the high value reported by Danusso for the density of the "decalin" used in his work.

In Figures 1 and 2 we have represented by full lines eq. 1 obtained for each system. The curves are practically symmetrical about the composition axis, with the minimum (or maximum) about $x = 0.5$. Systems I and II were studied at more than one temperature, and Figure 1 shows the temperature dependence of V^E for those systems. The contraction observed on mixing increases in magnitude with increasing temperature, but the variation, as shown by the behavior of system I, is not linear. System II

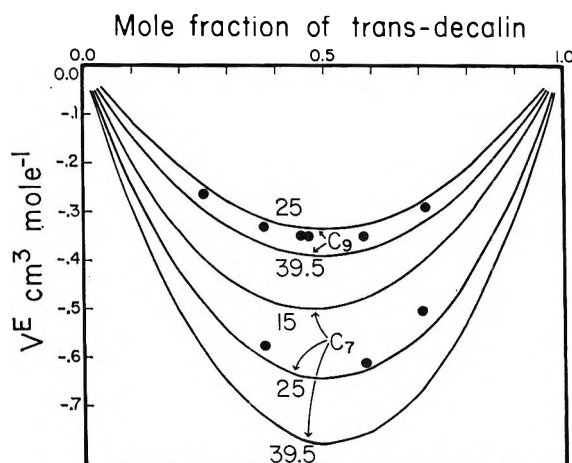
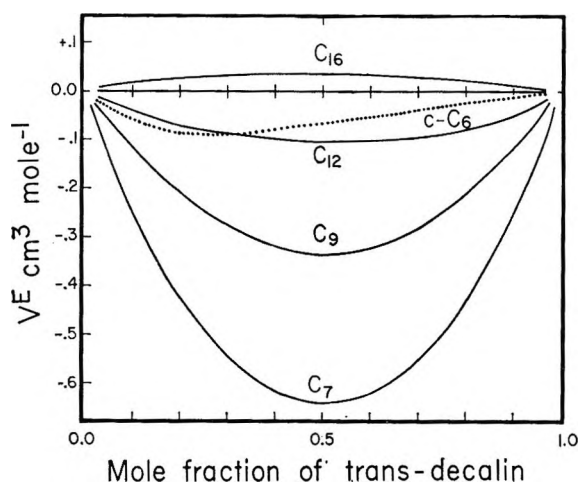
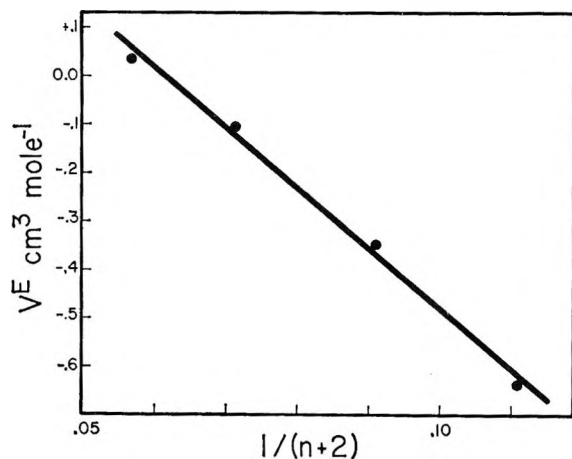


Figure 1. The effect of temperature on the excess volume of mixtures of *trans*-decalin with *n*-heptane and with *n*-nonane. The dots represent pycnometric values (see Table III).

(8) F. Danusso, *Atti Accad. Nazl. Lincei, Rend.*, 13, 131 (1952).

Table IV: Values for the Coefficients and Their Deviations in Eq. 1 for the Excess Volume of Mixtures of *trans*-Decalin and Some Hydrocarbons

System	Temp., °C.	A_0	ΔA_0	A_1	ΔA_1	A_2	ΔA_2
I $C_{10}H_{18} + C_7H_{16}$	15.1	-1.998	0.0078	0.1877	0.0108	-0.0972	0.0204
	25.0	-2.575	0.0121	-0.0467	0.0188	-0.3166	0.0466
	39.5	-3.098	0.0524	-0.1103	0.0733	-0.3794	0.1984
II $C_{10}H_{18} + C_9H_{20}$	25.0	-1.348	0.0069	-0.0238	0.0095	0.1208	0.0238
	39.5	-1.564	0.0061	0.0214	0.0086	0.00012	0.0205
III $C_{10}H_{18} + C_{12}H_{26}$	25.0	-0.406	0.0087	-0.0520	0.0081	-0.1724	0.0198
IV $C_{10}H_{18} + C_{16}H_{34}$	25.0	0.138	0.0040	-0.0456	0.0107	0.0590	0.0192
V $C_{10}H_{18} + c-C_6H_{12}$	25.0	-0.238	0.0066	0.2973	0.0108	-0.2977	0.0237

**Figure 2.** Excess volume of mixtures of *trans*-decalin with *n*-alkanes.**Figure 3.** Relation between excess volume and chain length at $x = 0.5$.

indicates a similar behavior, but the magnitude of the effect shown with this longer paraffin is smaller.

All systems were studied at the common temperature of 25.0°, and the results are plotted in Figure 2 so as to show the effect of the length of the paraffin chain on the excess volume. With increasing chain length, V^E increases from the relatively large negative value (-0.644 at $x = 0.5$), exhibited by *n*-heptane, to the small positive value (+0.035 at the same mole fraction) measured for *n*-hexadecane. The values for *n*-nonane and for *n*-dodecane fall between in the appropriate sequence, and the general pattern is similar to that observed in the corresponding cyclohexane systems. This is shown in Figure 3 where the values for the excess volumes at the maximum ($x = 0.5$) are plotted against the empirical expression $1/(n + 2)$, n being the number of carbons in the paraffin chain. Allowance being made for the experimental errors, the relationship seems to be linear as was the case for the cyclohexane + alkane systems.⁴

The analogies and differences observed in the systems so far studied, alkane + alkane, cyclohexane + alkane, and *trans*-decalin + alkane, are certainly of interest. For the first-mentioned kind of system, the excess volume is shown to be negative, temperature dependent, and increasing in absolute value with increasing difference in the chain length of the two components. The measurements confirmed the fact that the values of V^E for mixtures of *n*-alkanes are consistent with the "principle of congruence"⁹ as shown using the method of representation of Hijmans.¹⁰

(9) J. N. Brønsted and J. Koefoed, *Kgl. Danske Videnskab. Selskab., Mat. Fys. Medd.*, [17] 22, 1 (1946).

(10) J. Hijmans, *Mol. Phys.*, 1, 307 (1958).

The behavior of chain-molecule liquids and their mixtures has been the subject of theoretical studies, the most recent one by Flory, Orwoll, and Vrij,¹¹ who have derived for *n*-paraffin hydrocarbons a reduced equation of state in terms of a segment net volume, an interaction parameter, and the number of degrees of freedom per segment. Their treatment leads to the Brønsted principle of congruence as applied to the excess volume of mixtures of *n*-alkanes.

Mixtures of cyclohexane with *n*-alkanes exhibit a positive excess volume which (in contrast with the systems reported in this paper) is temperature independent over the measured range (15–35°). The excess volume increases in magnitude with increasing length of the alkane and shows a linear dependence with $1/(n + 2)$, as mentioned above.

Two main factors will contribute to determine the excess volume of a mixture. On mixing two liquids, changes may take place in both the intermolecular forces and in the geometrical arrangement of the molecules. As a first approximation, qualitatively, no great differences in the interaction energies between the different segments of the molecules must be expected when, in the systems under consideration, cyclohexane is replaced by *trans*-decalin. Final elucidation of this point requires additional thermodynamic data being gathered.^{12,13} The geometrical factor must then play an important role in determining the sign of V^E . Any arrangement tending to increase the number of contacts between the segments

of the molecules (*i.e.*, the number of nearest neighbors) will be accompanied by a decrease in the volume of mixing. Such must be the case with the mixtures containing heptane and nonane and, to a lesser extent, with those containing dodecane, suggesting, possibly, a coiling of the flexible hydrocarbon chain on the "surface" of the "flat" *trans*-decalin molecule. This "adaptation" will become sterically more difficult as the length of the hydrocarbon increases. In paraffins higher than dodecane the effect of the interacting forces will predominate and account for the expansion on mixing. Because of the smaller size of cyclohexane, the system cyclohexane + *n*-hexane already exhibits a positive excess volume.

A similar explanation may account for the small contraction observed in the cyclohexane + *trans*-decalin system. Or perhaps here we are observing a situation which approaches the "monomer-dimer" effect predicted by Prigogine's corresponding-states theory of mixtures of molecules of different sizes.¹⁴

Acknowledgment. The authors wish to thank the Wesleyan Computer Laboratory and Professor Edward K. Blum for their help with some of the calculations.

(11) P. J. Flory, R. A. Orwoll, and A. Vrij, *J. Am. Chem. Soc.*, **86**, 3507, 3515 (1964).

(12) J. D. Gómez-Ibáñez and J. J. C. Shieh, *J. Phys. Chem.*, **69**, 1660 (1965).

(13) H. Brandt, *Z. Physik. Chem. (Frankfurt)*, **2**, 104 (1954).

(14) See ref. 1, Chapter 17.

Chronopotentiometric Measurements of Chemical Reaction Rates. I.

Programmed Current Studies of the ECE Mechanism¹

by Harvey B. Herman and Allen J. Bard

Department of Chemistry, The University of Texas, Austin, Texas 78712 (Received July 15, 1966)

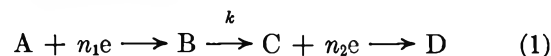
Programmed current chronopotentiometry, specifically current reversal and current decrease, is applied to electrode reactions characterized by a chemical reaction coupled between two charge-transfer reactions, the ECE mechanism. The equations for the transition times are derived and solved. Current-reversal results on systems following the ECE mechanism, *p*-nitrosophenol, *p*-nitrophenol, and *o*-nitrophenol, are in good agreement with those obtained by single transition time chronopotentiometry and potentiostatic investigations. A mechanism is suggested for these electrode and chemical reactions.

Introduction

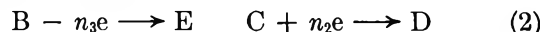
Chronopotentiometry has been recognized as a potentially important tool in the measurement of rate constants of chemical reactions concurrent with the electrode process.² The boundary value problem in chronopotentiometry, unlike that in polarography, can usually be solved explicitly, since the flux at the electrode surface is known. The variation of the chronopotentiometric transition time constant ($i\tau^{1/2}/C$), based only on the first transition time, has been used to calculate the rate constants of chemical reactions, for example, when the starting material is regenerated^{3,4} (a catalytic reaction) or when a chemical reaction is interposed between two charge-transfer reactions^{5,6} (the ECE mechanism). Programmed current techniques have the advantage of allowing calculation of the rate constant without knowing the transition time in the absence of the perturbing chemical reaction or even the concentration, diffusion coefficient, and current density. Many times the latter two variables can only be estimated, severely limiting the accuracy of the calculated rate constant. The value of current-reversal techniques has been demonstrated by current-reversal chronopotentiometry and cyclic chronopotentiometry in the measurement of the rate constants of the hydrolysis of electrochemically generated *p*-quinoneimine^{7,8} and the reaction of electrochemically generated Ti(III) with hydroxylamine.^{3,8,9}

The present study was undertaken with the aim of applying current decrease and current-reversal methods

to compounds following the ECE mechanism. The ECE scheme can be represented by



and on current reversal



The ECE mechanism under consideration in this study is the one in which C is reduced at potentials considerably less cathodic than those required to reduce A, so that upon current reversal, at potentials where B is being oxidized, C continues to reduce. Previous results on the polarographic reduction of *p*- and *o*-nitrophenol and *p*-nitrosophenol were explained by the above scheme.^{2,10} The polarographic diffusion current constant corresponded approximately to a six-electron process (four in the case of the *p*-nitroso compound) at both high and low pH. Intermediate pH measure-

(1) This work supported by the Robert A. Welch Foundation and the National Science Foundation (GP-1921).

(2) P. Delahay, *Discussions Faraday Soc.*, **17**, 205 (1954).

(3) C. Furlani and G. Morpugo, *J. Electroanal. Chem.*, **1**, 351 (1960).

(4) P. Delahay, C. Mattox, and T. Berzins, *J. Am. Chem. Soc.*, **76**, 5319 (1954).

(5) A. C. Testa and W. H. Reinmuth, *ibid.*, **83**, 784 (1961).

(6) G. S. Alberts and I. Shain, *Anal. Chem.*, **35**, 1859 (1963).

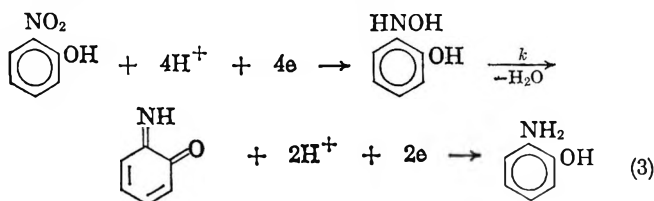
(7) A. C. Testa and W. H. Reinmuth, *ibid.*, **32**, 1512 (1960).

(8) H. B. Herman and A. J. Bard, *ibid.*, **36**, 510 (1964).

(9) J. H. Christie and G. Lauer, *ibid.*, **36**, 2037 (1964).

(10) D. Stočesová, *Collection Czech. Chem. Commun.*, **14**, 615 (1949).

ments revealed that this constant passed through a minimum. While no rate constant was actually calculated—the boundary value problem is quite difficult—the data were interpreted by Stočesová¹⁰ for the system *o*-nitrophenol, to be an acid-base catalyzed decomposition of the product of the first electrode reaction, *o*-hydroxylaminophenol. The product of the chemical reaction, *o*-quinoneimine, was assumed to be further reduced at these potentials giving, if the chemical reaction is fast, an over-all six-electron reduction. The reaction mechanism proposed was



The above mechanism was used by Testa and Reinmuth⁶ in their chronopotentiometric measurements on *o*-nitrophenol and Alberts and Shain⁶ in their measurements on *p*-nitrosophenol. Both authors found comparatively large errors in the ordinary chronopotentiometric determination of the rate constant principally because the data had to be fitted to a two-parameter plot. It appeared likely that a current-reversal technique could circumvent some of these difficulties and allow a more precise measurement of the rate constant of this fairly general chemical reaction.

Theory

Current Decrease. The Murray-Reilley¹¹ current response function has proven quite valuable in the solution of the partial differential equations for chronopotentiometry with programmed current. The availability of solutions for many schemes with kinetic complications¹² allows one to obtain a result for current decrease by using the current response function in a rather straightforward manner. Thus if the concentration at the electrode surface, $C(0, t)$, before the first transition time can be represented by

$$C^0 - C(0, t) = f(t) \quad (4)$$

where C^0 is the original concentration of the electroactive material, the transition time for a current decrease, when the surface concentration of the original material again falls to zero, is obtained by solving

$$f(\tau_1) = f(\tau_1 + \tau_2) - Rf(\tau_2) \quad (5)$$

and

$$R = (i_2 - i_1)/i_1 \quad (6)$$

where τ_1 and τ_2 are the first and second transition times and i_1 and i_2 are the applied currents before and after current decrease.

Testa and Reinmuth¹³ have given $f(t)$ in (4) for the ECE mechanism. The partial differential equations that apply to the ECE scheme are given in the Appendix. Rearranging the solution [eq 21 in ref 14] (see also Appendix) yields

$$f(t) = (i\rho/n_2FD^{1/2}) \left[2t^{1/2}/\pi^{1/2} + (\rho/k^{1/2}) \operatorname{erf}[(kt)^{1/2}] + \frac{a^{1/2}\rho^2 \exp(-at)}{k\pi^{1/2}} \{ \Phi[\rho(at)^{1/2}] + \Phi[(at)^{1/2}] \} \right] \quad (7)$$

where $\Phi(x) = \int_0^x \exp(\mu^2) d\mu$, $a = k/(1 - \rho^2)$, $\rho = n_2/(n_2 + n_1)$, k is the pseudo-first-order rate constant, and the other symbols have their usual meaning.

Equation 4 was solved using (7) as $f(t)$ on a digital computer. The program was similar to the one used to solve for the amount adsorbed on an electrode using current reversal.¹⁴ Solution for the root of any nonlinear equation is possible under the following conditions: the equation has only one positive root and a number less than the root is known. In this case the solution was double valued and the program was modified to solve for both roots. The results are given in Table I. The ratio τ_2/τ_1 in absence of a chemical reaction ($k = 0$) was calculated using a rearranged form of the equation (11)¹³ derived by Testa and Reinmuth.

$$\tau_2/\tau_1 = 4R^2/(R^2 - 1)^2 \quad (8)$$

In both cases, $\rho = 1/2$ and $1/3$, the ratio goes through a maximum. The system is therefore diffusion controlled at both large and small values of $k\tau$; in order to observe the kinetic effect it is necessary to pick an intermediate transition time. Since the solution is double valued, a rate constant cannot be calculated from one measurement; two are needed. Even systems which are completely irreversible, *i.e.*, B is not oxidizable, can be studied by current-decrease techniques. However, a forward transition must be observed, which may prove a disadvantage in systems yielding ill-defined transitions.

Current Reversal. The transition time for current reversal, when the concentration of the electrode

(11) R. W. Murray and C. N. Reilley, *J. Electroanal. Chem.*, **3**, 182 (1962).

(12) C. N. Reilley in "Treatise on Analytical Chemistry," Part I, Vol. IV, I. M. Kolthoff and P. J. Elving, Ed., Interscience Publishers, Inc., New York, N. Y., 1963, p 2151.

(13) A. C. Testa and W. H. Reinmuth, *Anal. Chem.*, **33**, 1320 (1961).

(14) H. B. Herman, S. V. Tatwawadi, and A. J. Bard, *ibid.*, **35**, 2210 (1963).

Table I: Relative Transition Times for ECE Current Decrease

$k\tau_1$	τ_2/τ_1			
	0.20	0.30	0.40	0.50
	R			
	$\rho = 1/2$			
0.0	0.174	0.435	0.907	1.778
0.2	0.264	0.710	1.668	3.928
0.4	0.362	1.052	2.490	5.302
0.6	0.487	1.309	2.807	5.417
0.8	0.569	1.412	2.811	5.211
1.0	0.611	1.420	2.711	4.940
1.2	0.624	1.383	2.582	4.675
1.4	0.619	1.329	2.455	4.434
1.6	0.604	1.272	2.338	4.222
1.8	0.585	1.218	2.233	4.039
2.0	0.565	1.168	2.141	3.880
	$\rho = 1/3$			
0.0	0.174	0.435	0.907	1.778
0.2	0.213	0.549	1.201	2.534
0.4	0.251	0.658	1.462	3.075
0.6	0.286	0.746	1.629	3.295
0.8	0.313	0.806	1.706	3.334
1.0	0.334	0.839	1.728	3.298
1.2	0.348	0.853	1.718	3.235
1.4	0.356	0.855	1.693	3.162
1.6	0.360	0.849	1.661	3.089
1.8	0.360	0.838	1.627	3.021
2.0	0.359	0.826	1.594	2.957

product falls to zero, was obtained using the step-function theorem.¹⁵ Since in the ECE scheme, the flux of B is not constant, the current due to the electrolysis of B must be calculated. The procedure involves defining a new variable whose solution and flux are known, in order to solve for the unknown flux of B. The method is detailed in the Appendix and closely follows the one described by Testa and Reinmuth¹³ and King and Reilley.¹⁶ The result of this calculation yields the surface concentration of B on current reversal

$$C_B(0, t) = g(t, \rho) + (1 - R)g(t - \tau_1, \rho') - g(t - \tau_1, \rho) \quad (9)$$

where

$$g(t, \rho) = (i\rho/n_2FD^{1/2})[k^{-1/2} \operatorname{erf}[(kt)^{1/2}] + (2\rho a^{1/2}/k\pi^{1/2}) \exp(-at) \{ \Phi[(at)^{1/2}] + \Phi[(a - k)^{1/2}t^{1/2}] \}] \quad (10)$$

$\rho = n_2/(n_1 + n_2)$, $\rho' = n_2/(n_2 + n_3)$, $a = k/(1 - \rho^2)$, and $g(t - \tau_1, \rho')$ denotes the same expression as (10) with all t 's replaced by $(t - \tau_1)$ and all ρ 's replaced by ρ' . When $\rho = \rho'$, as in the case of nitrosophenols, (9) simplifies to

$$C_B(0, t) = g(t, \rho) - Rg(t - \tau_1, \rho) \quad (11)$$

When $\rho \neq \rho'$, as in the case of nitrophenols, (10) is approximate (see Appendix). When (10) is multiplied by $\tau_1^{-1/2}$, the equation is in terms of the dimensionless quantity $k\tau_1$. At $t = \tau_1 + \tau_2$, $C_B(0, t) = 0$, and solution of (9) under these conditions yields values of τ_2/τ_1 as a function of $k\tau_1$. The results of such calculations, using the previously mentioned computer program, are given in Table II.

Table II: Relative Transition Times for ECE Current Reversal

$k\tau_1$	$\rho = 1/2$ $\rho' = 1/2$ $R = 2.0$	$\rho = 1/2$ $\rho' = 1/3$ $R = 2.0$	$\rho = 1/2$ $\rho' = 1/3$ $R = 1.5$	$\rho = 1/3$ $\rho' = 1/3$ $R = 2.0$
	τ_2/τ_1	τ_2/τ_1	τ_2/τ_1	τ_2/τ_1
0.00	0.333	0.125	0.333	0.333
0.10	0.281	0.112	0.294	0.293
0.20	0.241	0.101	0.263	0.260
0.30	0.208	0.092	0.236	0.233
0.40	0.182	0.084	0.213	0.210
0.50	0.160	0.076	0.193	0.190
0.60	0.142	0.069	0.175	0.172
0.70	0.127	0.064	0.160	0.157
0.80	0.114	0.059	0.148	0.144
0.90	0.102	0.055	0.136	0.133
1.00	0.093	0.051	0.126	0.123
1.20	0.077	0.044	0.108	0.106
1.40	0.065	0.039	0.095	0.092
1.60	0.056	0.034	0.084	0.081
1.80	0.049	0.030	0.074	0.072
2.00	0.043	0.027	0.066	0.065

In some cases it is necessary to decrease the current on reversal because with equal current densities the transition time ratio may be too small to be measured conveniently.

In the current-reversal technique it is not necessary to reach the first transition time; the current can be reversed at any point along the wave and a rate constant can be calculated. If the first transition time is not well defined, this offers a decided advantage. The solutions are single valued and it appears that the method is experimentally more precise than the current-decrease method.

Results and Discussion

Forward Transition Time Studies. Alberts and Shain,⁶ in a comparison of potentiostatic and chronopotentiometric methods, found that the rate constant

(15) R. V. Churchill, "Operational Mathematics," 2nd ed, McGraw-Hill Book Co., Inc., New York, N. Y., 1958, p 23.

(16) R. M. King and C. N. Reilley, *J. Electroanal. Chem.*, **1**, 434 (1960).

calculated from the first transition time in the reduction of *p*-nitrosophenol exhibited a disturbing trend; at high current densities the calculated rate constant increased. Three sources of error were postulated: (1) the assumption that the concentration product of the chemical reaction, C, was zero at the electrode surface was false; (2) material A was adsorbed on the electrode surface; (3) and/or an appreciable fraction of the current was needed to charge the double layer. These postulates will be examined below.

The chronopotentiometric measurements on *p*-nitrosophenol were repeated under slightly different conditions and the results of Alberts and Shain were confirmed. Table III shows the results on that system and on *p*-nitrophenol. The observed increase in the

Table III: Chronopotentiometric Calculation of the Rate Constant of the Product of the Reduction of *p*-Nitrosophenol and *p*-Nitrophenol^a

$i\tau^{1/2}_{\infty}/i\tau^{1/2}$	τ , sec	k , sec ⁻¹	$i\tau^{1/2}_{\infty}/i\tau^{1/2}$	τ , sec	k , sec ⁻¹
A. 3.0 mM <i>p</i> -nitrosophenol			B. 2.1 mM <i>p</i> -nitrophenol		
1.09	42.6	0.63	1.07	37.4	0.52
1.14	20.2	0.58	1.09	18.35	0.66
1.21	9.34	0.61	1.14	8.73	0.61
1.31	4.03	0.73	1.24	3.75	0.53
1.57	1.24	0.81	1.29	0.788	1.70
1.63	0.59	1.35	1.32	0.373	2.81

^a Conditions: 0.1 M acetic acid, 0.1 M potassium acetate, 0.2 M potassium nitrate, and 20% ethanol (v/v) and at a mercury pool electrode (3.2 cm²), temperature 24.2°.

calculated rate constant becomes apparent at slightly shorter transition times, since the concentration was about three times higher than that used by Alberts and Shain. This suggests that postulates 2 and 3 are more likely. Postulate 1 can be eliminated by examination of the potential-time curves of *p*-nitrosophenol using cyclic chronopotentiometry. A reversible couple corresponding to *p*-nitrosophenol (A) and *p*-hydroxylaminophenol (B) is set up around -0.1 v vs. sce. When wider potential limits are set, another couple is observed very close to the mercury oxidation wave, at least 0.3 v more anodic than the first couple. This corresponds to the reduction of *p*-quinoneimine (C) and the oxidation of *p*-aminophenol (D) and indicates that the concentration of C would indeed be zero at the electrode surface at potentials where A is reduced and B is oxidized.¹⁷

Since the nitro group is reduced in a four-electron step to hydroxylamine, the product of the reduction of

p-nitrophenol is identical with the product of the *p*-nitroso compound. If we are measuring the chemical rate constant of the dehydration of *p*-hydroxylaminophenol, the two compounds should yield the same rate constant. The agreement of the calculated rate constants in Table III suggests that the same intermediate is indeed produced in the two electrode reactions.

To determine if *p*-nitrosophenol is adsorbed on mercury, electrocapillary curves were recorded using drop-time measurements. Addition of *p*-nitrosophenol to the supporting electrolyte caused the drop time to be lowered, indicating adsorption. The amount adsorbed can be calculated from the relationship¹⁸

$$-\Gamma = \partial\sigma/RT \partial \ln C \quad (12)$$

and

$$\Delta\sigma = 38.0\Delta t \quad (13)$$

where Γ is the surface excess, σ is the surface tension, and Δt is the amount the drop time has been lowered. The value calculated for Γ was $(0.13 \pm 0.07) \times 10^{-9}$ mole/cm². The large deviation results from the small change in drop time (a few hundredths of a second) on increasing concentration. Recently, the chronopotentiometric data of Alberts and Shain⁶ were reinterpreted by Evans¹⁹ to account for the increase in the calculated rate constant of *p*-nitrosophenol at short times. He applied an empirical correction factor to the current until the calculated rate constant agreed with the potentiostatic results. The correction factor in millicoulombs corresponded approximately to the estimated amount of charge needed to charge the mercury double layer. However, the voltage range assumed by Evans, 1 v, was probably too large for this system, since the quarter-wave potential is only about -0.1 v vs. sce. In addition, the double-layer capacity is probably further reduced in the presence of adsorption.¹⁸ The amount of adsorption found in this study, even with the large relative deviation, almost exactly accounts for the observed increase in the rate constant. If the adsorbed species is electrolyzed simultaneously with the diffusing species (mechanism 3 in ref 20), the observed transition time will be longer. This effect is more important at short times. If we assume that Γ is the same in both studies, even though the conditions are slightly different, a correction factor of 1.8 μ coulombs is calculated. Evans¹⁹ found em-

(17) Similar results were obtained by R. S. Nicholson and I. Shain, *Anal. Chem.*, **37**, 190 (1965), using stationary electrode polarography.

(18) P. Corbusier and L. Gierst, *Anal. Chim. Acta*, **15**, 254 (1956).

(19) D. H. Evans, *Anal. Chem.*, **36**, 2027 (1964).

(20) S. V. Tatwawadi and A. J. Bard, *ibid.*, **36**, 2 (1964).

pirically that 1.7 μ coulombs gave the best fit to the data.

Programmed Current Studies. Current-decrease chronopotentiometry was performed on *p*-nitrophenol and *o*-nitrophenol at relatively long times (7–10 sec) under the same conditions as in Table III. The second transition time was very poorly defined and good measurements could not be made. The uncertainty in the data made it very difficult to pick the correct value of the rate constant from the double-valued function. The current-decrease results would probably have been better at higher current densities, but current-reversal techniques, described below, were more convenient.

Current-reversal chronopotentiometry was performed on *p*-nitrosophenol, *p*-nitrophenol, and *o*-nitrophenol. The results are shown in Table IV. Again *p*-nitrosophenol and *p*-nitrophenol yielded the

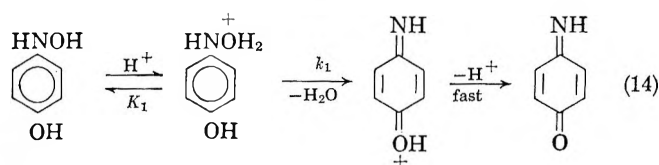
Table IV: Current-Reversal Calculation of the Rate Constant (Conditions Same as in Table III except at Hanging Mercury Drop (Area 0.036 cm², Temperature 24.8°))

τ_1 , sec	τ_2/τ_1	$k\tau_1$	k , sec ⁻¹
A. 2.0 mM <i>p</i> -nitrosophenol, $R = 2.0$			
0.35	0.270	0.13	0.38
0.49	0.216	0.28	0.57
0.68	0.176	0.42	0.62
0.83	0.160	0.50	0.60
1.15	0.143	0.60	0.52
2.40	0.080	1.16	0.48
			Av 0.56 \pm 0.04
B. 1.8 mM <i>p</i> -nitrophenol, $R = 1.5$			
0.162	0.320
0.690	0.220	0.37	0.54
0.870	0.190	0.52	0.60
0.930	0.178	0.58	0.62
3.160	0.078	1.72	0.54
4.200	0.071	1.89	0.45
			Av 0.55 \pm 0.07
C. 1.4 mM <i>o</i> -nitrophenol, $R = 1.5$			
1.43	0.250	0.25	0.18
1.91	0.214	0.40	0.21
2.82	0.187	0.53	0.19
3.33	0.176	0.59	0.18
4.00	0.188	0.53	0.13
4.29	0.166	0.66	0.15
7.38	0.152	0.76	0.11
8.40	0.143	0.83	0.10
8.83	0.170	0.64	0.07
10.53	0.121	1.05	0.10
			Av 0.14 \pm 0.05

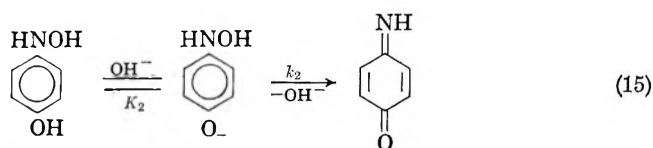
same rate constant as expected. The data for these two systems agree well with the results of single transition time chronopotentiometry and chronoamperometry⁵ with no discernible trend. *o*-Nitrophenol does show a small trend in the calculated rate constant and it may be that, because of the longer times needed to perform the measurement, spherical corrections become more important.

Testa and Reinmuth⁵ determined the mechanism of the reduction of *o*-nitrophenol by chronopotentiometry. In that study they indirectly disproved an alternate hypothesis of a preceding chemical reaction. Current-reversal chronopotentiometry immediately differentiates between the two mechanisms. If a preceding chemical reaction were occurring, the transition time ratio, τ_2/τ_1 , would correspond to diffusion control, since the product is not involved in chemical reaction. For the ECE mechanism, τ_2/τ_1 would vary as described in Table II.

Mechanism. From the pH dependence of the polarographic limiting current, Stočesová¹⁰ suggested that the chemical reaction of *o*-hydroxyphenylhydroxylamine was acid-base catalyzed. A mechanism has already been proposed²¹ to explain the acid-base catalyzed rearrangement of phenylhydroxylamine. This mechanism can be adapted to the catalysis of the product of the reduction of nitrophenols and nitrosophenols. Thus for the *p*-compounds at low pH



and at high pH



If the first-order rate constant is proportional to the concentration of hydrogen ion in the first equilibrium, as is the case in the rearrangement of phenylhydroxylamine,²¹ the acid-base dependence on the rate can be calculated. Thus at low pH

$$dC_B/dt = k_1 K_1 [\text{H}^+][\text{B}] \quad (16)$$

k_1 is the first-order rate constant for the acid-catalyzed

(21) H. E. Heller, E. D. Hughes, and C. K. Ingold, *Nature*, **168**, 909 (1951).

reaction and K_1 is the equilibrium constant for the first equilibrium in (14). At high pH

$$dC_B/dt = k_2 K_2 [\text{OH}^-][\text{BOH}] \quad (17)$$

where k_2 is the first-order rate constant for the base-catalyzed reaction and K_2 is the equilibrium constant for the first equilibrium in (15). In both cases, B and BOH are *p*-hydroxyphenylhydroxylamine. Further studies are being made on the dependence of the rate constant on pH to see if the proposed mechanism is followed.

Experimental Section

The behavior of the first transition time of *p*-nitrosophenol and *p*-nitrophenol at a mercury pool electrode was investigated using the apparatus previously described.⁸ The transition times were measured by starting the digital counter at the instant of applying current and stopping it with a triggered relay at the potential break. Current-decrease measurements were made by modifying the above circuit so that the relay inserted a large resistor in series with the power supply after the first potential break.

The variation of the transition time ratio with the time of current reversal at a hanging mercury drop (area 0.038 cm²) was investigated with an operational amplifier constant current source and potential-sensitive switch.²² The potential-time curves were recorded as before²³ except that the oscilloscope trace was modulated by applying square waves from a low-frequency function generator (Hewlett-Packard Model 202A) in its *Z* input. The transition-time ratios were measured by counting the dots appearing in the trace and multiplying by the reciprocal of the frequency of the generator.

The sodium salt of *p*-nitrosophenol (Eastman Kodak Co.) was purified according to the procedure given by Alberts and Shain.⁶ *p*-Nitrophenol and *m*-nitrophenol (both from Eastman Kodak Co.) were recrystallized from benzene, and *o*-nitrophenol (Eastman Kodak Co.) from water-ethanol mixtures. The *p*-nitrosophenol was weighed into a deaerated solution before measurement. The acetic acid used as supporting electrolyte was standardized by titration with commercially standardized sodium hydroxide. Potassium acetate and potassium nitrate were weighed out directly. The pH of the supporting electrolyte was 4.92.

Electrocapillary curves were determined by the drop-time technique of Corbusier and Gierst¹⁸ using the previously described apparatus.²⁴

Acknowledgment. The authors are grateful for helpful discussions with Nathan Bauld about the mech-

anism and to John Bowman for making some of the experimental measurements.

Appendix

Mathematical Solution of ECE Mechanism Equations for Chronopotentiometry

The mathematical solution of Fick's second-law equations and the appropriate boundary conditions follow essentially the treatment of Testa and Reinmuth.¹³ In order to solve explicitly for the reverse transition time and to indicate approximations in the case where the intermediate product is not oxidized back to the starting material ($\rho \neq \rho'$) a complete derivation of the equations is given.

Forward Transition Time. The ECE mechanism, eq 1, is described by the equations

$$(\partial C_A / \partial t) = D(\partial^2 C_A / \partial x^2) \quad (1a)$$

$$(\partial C_B / \partial t) = D(\partial^2 C_B / \partial x^2) - kC_B \quad (2a)$$

$$(\partial C_C / \partial t) = D(\partial^2 C_C / \partial x^2) + kC_B \quad (3a)$$

$$t = 0, x \rightarrow \infty; \quad C_A = C_A^0, C_B = C_C = 0 \quad (4a)$$

$$x = 0; \quad C_C = 0 \quad (5a)$$

For $t < \tau_1$

$$(\partial C_B / \partial x)_{x=0} = -(\partial C_A / \partial x)_{x=0} \quad (6a)$$

$$n_1(\partial C_A / \partial x)_{x=0} + n_2(\partial C_C / \partial x)_{x=0} = i/FD \quad (7a)$$

The above equations assume that semiinfinite linear diffusion is the sole mode of mass transfer, that the diffusion coefficients of A, B, and C are equal, and that species C is reduced at potentials somewhat less cathodic than those for A, so that (5a) holds at all times. Let $i_j(t)$ represent the instantaneous current involved in the production or consumption of the *j*th species at time *t*, so that (7a) becomes

$$i_A(t) + i_C(t) = i \quad (8a)$$

and (6a) yields

$$i_A(t)/n_1FD = (\partial C_A / \partial x)_{x=0} = -(\partial C_B / \partial x)_{x=0} \quad (9a)$$

Let

$$\phi = C_B + C_C \quad (10a)$$

Combination of (2a), (3a), and (10a) yields

$$(\partial \phi / \partial t) = D(\partial^2 \phi / \partial x^2) \quad (11a)$$

(22) H. B. Herman and A. J. Bard, *Anal. Chem.*, **37**, 590 (1965).

(23) A. J. Bard, *ibid.*, **33**, 11 (1961).

(24) A. J. Bard and H. B. Herman, *ibid.*, **37**, 317 (1965).

Differentiation of (10a) with respect to x , at $x = 0$, and combination with (8a) and (9a) yield

$$(\partial\phi/\partial x)_{x=0} = \frac{i}{n_2FD} - \frac{i_A(t)}{n_2FD} \left(\frac{n_1 + n_2}{n_1} \right) \quad (12a)$$

Combination of (10a) and (4a) shows that

$$\phi(x, 0) = 0 \text{ and } \lim_{x \rightarrow \infty} \phi(x, t) = 0 \quad (13a)$$

Solving (11a), using (12a) and (13a) as boundary conditions gives, in the Laplace transform plane

$$n_2FD^{1/2}[\bar{C}_B(0, s) + \bar{C}_C(0, s)] = -s^{-1/2} \left[i/s - \bar{i}_A(s) \left(\frac{n_1 + n_2}{n_1} \right) \right] \quad (14a)$$

where $\bar{C}_B(0, s)$, $\bar{C}_C(0, s)$, and $\bar{i}_A(s)$ represent the Laplace transforms of $C_B(0, t)$, $C_C(0, t)$, and $i_A(t)$, respectively.

Direct solution of (2a), with boundary conditions (4a) and (9a) yields

$$n_1FD^{1/2}\bar{C}_B(0, s) = \bar{i}_A/(s+k)^{1/2} \quad (15a)$$

Combination of (14a), (15a), and (5a), yields, with some rearrangement

$$\bar{i}_A = \frac{n_1 i \rho}{n_2 s^{3/2}} \left[\frac{s^{1/2}(s+k)^{1/2}}{(s+k)^{1/2} - \rho s^{1/2}} \right] \quad (16a)$$

where $\rho = n_2/(n_1 + n_2)$. Combination of (15a) and (16a) gives an equation for $\bar{C}_B(0, s)$

$$FD^{1/2}\bar{C}_B(0, s) = \frac{i \rho}{n_2 s^{3/2}} \left[\frac{s^{1/2}}{(s+k)^{1/2} - \rho s^{1/2}} \right] \quad (17a)$$

Solution of (1a), using (4a) and (9a) as boundary conditions, and combination with (16a) yield the following expression for $\bar{C}_A(0, s)$ ¹³

$$FD^{1/2} \left[\frac{C_A^0}{s} - \bar{C}_A(0, s) \right] = \frac{i \rho}{n_2 s^{3/2}} \left[\frac{(s+k)^{1/2}}{(s+k)^{1/2} - \rho s^{1/2}} \right] \quad (18a)$$

Inverse transformation of (18a) yields eq 7 in the text.

Current Reversal, $n_1 = n_3$. To calculate the reverse transition time, τ_2 , an expression for \bar{C}_B must be obtained which holds at all times, and then an equation of the form

$$\bar{C}_B(0, s) = \bar{i}(s)\bar{S}(s) \quad (19a)$$

derives, where $\bar{i}(s)$ is the transform of the applied programmed current and $\bar{S}(s)$ is the "system transform,"¹² obtained from the solution of Fick's equations.

For the case in which the oxidation of species B yields A, *e.g.*, the case of the nitrosophenols, so that

$n_1 = n_3$, the boundary conditions that hold on current reversal are (5a) (reduction of C continues at potentials where B is being oxidized), (6a), and

$$n_1(\partial C_B/\partial x)_{x=0} - n_2(\partial C_C/\partial x)_{x=0} = -i/FD \quad (20a)$$

Combination of (20a) and (6a) yields

$$n_1(\partial C_A/\partial x)_{x=0} + n_2(\partial C_C/\partial x)_{x=0} = i/FD \quad (21a)$$

which is the same as (7a). Therefore the same set of equations holds during reversal, and $\bar{C}_B(0, s)$ at any time is given by

$$\bar{C}_B(0, s) = \bar{i}(s) \frac{\rho}{n_2FD^{1/2}} \left[\frac{1}{(s+k)^{1/2} - \rho s^{1/2}} \right] \quad (22a)$$

For current reversal, assuming a constant applied forward current density, i

$$i'(t) = i + S_{\tau_1}(t)(-Ri) \quad (23a)$$

where $R = (i + i_r)/i$, i_r is the constant applied reverse current density, and $S_{\tau_1}(t)$ is the step function

$$S_{\tau_1}(t) = 0 \quad t < \tau_1$$

$$S_{\tau_1}(t) = 1 \quad t > \tau_1$$

The Laplace transform of (23a) is

$$\bar{i}(s) = (i/s)[1 - R \exp(-\tau_1 s)] \quad (24a)$$

Combining (19a) and (24a) and inverse transformation of the result yield an expression for $C_B(0, t)$ any time, t , before or after current reversal.

$$C_B(0, t) = g(t) - S_{\tau_1}(t)Rg(t - \tau_1)$$

where

$$g(t) = \frac{i \rho}{n_2FD^{1/2}} L^{-1} \left\{ \frac{1}{s[(s+k)^{1/2} - \rho s^{1/2}]} \right\} =$$

$$\frac{i \rho}{n_2FD^{1/2}(1 - \rho^2)} \left\{ \frac{2\rho}{(a\pi)^{1/2}} \exp(-at) \Phi[(at)^{1/2}] + \frac{k^{1/2}}{a} \operatorname{erf}[(kt)^{1/2}] + \frac{2(a-k)^{1/2}}{a\pi^{1/2}} \exp(-at) \Phi[(a-k)^{1/2}t^{1/2}] \right\} \quad (25a)$$

where $a = k/(1 - \rho^2)$, $\Phi(x) = \int_0^x \exp(\mu^2) d\mu$, and erf is the error function. At $t = \tau_1 + \tau_2$, $C_B(0, t) = 0$, and solution of (25a) under these conditions yields τ_2/τ_1 as a function of $k\tau_1$.

Current Reversal, $n_1 \neq n_3$. When oxidation of species B yields another species, E (with a different number of electrons involved in this oxidation than in the reduction of A), *e.g.*, the case of nitrophenols, (20a) is replaced by

$$n_3(\partial C_B/\partial x)_{x=0} - n_2(\partial C_C/\partial x)_{x=0} = -i_r/FD \quad (26a)$$

so that different boundary conditions apply during the forward and reverse reactions. Let $i_{jt}(t)$ and $i_{jr}(t)$ represent the instantaneous current involved in the production or consumption of the j th species during forward and backward reaction, respectively, so that

$$i_{Bf}(t) = n_1FD(\partial C_B/\partial x)_{x=0} \quad (27a)$$

$$i_{Br}(t) = n_3FD(\partial C_B/\partial x)_{x=0} \quad (28a)$$

During forward reaction, from (8a)

$$i_C(t) - i_{Bf}(t) = i_f \quad (29a)$$

During reverse reaction, from (26a)

$$i_C(t) - i_{Br}(t) = i_r \quad (30a)$$

Defining ϕ as previously, eq 10a, differentiating with respect to x , at $x = 0$, and using (29a) yield during the forward reaction

$$FD(\partial\phi/\partial x)_{x=0} = i_{Bf}(t)/n_1 + i_f/n_2 + i_{Bf}(t)/n_2 \quad (31a)$$

During reverse reaction, using (30a), one obtains

$$FD(\partial\phi/\partial x)_{x=0} = i_{Br}(t)/n_3 + i_r/n_2 + i_{Br}(t)/n_2 \quad (32a)$$

To obtain an equation which holds during both forward and reverse reactions, so that τ_2 can be obtained in terms of τ_1 through the use of the step-function principle, (31a) and (32a) are combined to yield

$$FD(\partial\phi/\partial x)_{x=0} = i_f/n_2 + i_{Bf}(t)/\rho n_1 - S\tau_1(t) \times \{i_f/n_2 + i_{Bf}(t)/\rho n_1 - i_r/n_2 - i_{Br}(t)/\rho' n_3\} \quad (33a)$$

where $\rho = n_2/(n_1 + n_2)$, $\rho' = n_2/(n_2 + n_3)$, or, with $i_R = Ri$, and $i_f = i$

$$FD(\partial\phi/\partial x)_{x=0} = [1 - RS\tau_1(t)]i/n_2 + [1 - S\tau_1(t)]i_{Bf}(t)/\rho n_1 + S\tau_1(t)i_{Br}(t)/\rho' n_3 \quad (34a)$$

Similarly $(\partial C_B/\partial x)$ can be written

$$FD(\partial C_B/\partial x)_{x=0} = i_{Bf}(t)/n_1 + S\tau_1(t)[i_{Br}(t)/n_3 - i_{Bf}(t)/n_1] \quad (35a)$$

The procedure now follows that for solving for the forward transition time, solution of (34a) and (35a) in the transform plane, finally yielding an expression for $C_B(0, t)$. The Laplace transformation of (35a) is

$$FD(\partial\bar{C}_B/\partial x)_{x=0} = \bar{i}_{Bf}(s)/n_1 + \exp(-\tau_1s)\bar{I}_{Bf}(s, \tau)/n_3 - \exp(-\tau_2s)\bar{I}_{Br}(s, \tau)/n_1 \quad (36a)$$

where

$$\bar{I}_B(s, \tau) = \int_0^\infty \exp(-s\theta)i_B(\theta + \tau) d\theta = L[i_B(\theta + \tau)] \quad (37a)^{25}$$

Similarly the transform of (34a) is

$$FD(\partial\bar{\phi}/\partial x)_{x=0} = [1 - Re^{-\tau_1s}]i/n_2s + \bar{i}_{Bf}(s)/\rho n_1 - \exp(-\tau_1s)\bar{I}_{Bf}(s, \tau)/\rho n_1 + \exp(-\tau_1s)\bar{I}_{Br}(s, \tau)/\rho' n_3 \quad (38a)$$

Solving (11a) using (13a) and (38a) as boundary conditions and noting that (5a) holds yield

$$-FD^{1/2}\bar{C}_B(0, s) = \{[1 - Re^{-\tau_1s}]i/n_2s + \bar{i}_{Bf}(s)/\rho n_1 - \exp(-\tau_1s)\bar{I}_{Bf}(s, \tau)/\rho n_1 + \exp(-\tau_1s)\bar{I}_{Br}(s, \tau)/\rho' n_3\}s^{-1/2} \quad (39a)$$

Similarly solving (2a) with (4a) and (36a) as boundary conditions yields

$$-FD^{1/2}\bar{C}_B(0, s) = (s + k)^{-1/2}\{\bar{i}_{Bf}(s)/n_1 - \exp(-\tau_1s)\bar{I}_{Bf}(s, \tau)/n_1 + \exp(-\tau_1s)\bar{I}_{Br}(s, \tau)/n_3\} \quad (40a)$$

The final equation results from simultaneous solution of (39a) and (40a) to obtain an expression for $\bar{I}_{Bf}(s, \tau)$, substitution of that expression, with expression for \bar{i}_{Bf} and $\bar{I}_{Bf}(s, \tau)$ into (40a) and taking the inverse transform to find $C_B(0, t)$. However, leaving $\bar{I}_{Bf}(s, \tau)$ in its exact form results in fairly intractable integrals on inverse transformation, and it was convenient to use $\bar{i}_{Bf}(s)$ as an approximation for $\bar{I}_{Bf}(s, \tau)$. The range of applicability of this approximation is being investigated and will be discussed in a future communication. With this approximation (39a) and (40a) become

$$-FD^{1/2}\bar{C}_B(0, s) = s^{-1/2}\{[1 - R \exp(-\tau_1s)]i/n_2s + [1 - \exp(-\tau_1s)]\bar{i}_{Bf}(s)/\rho n_1 + \exp(-\tau_1s)\bar{I}_{Br}(s, \tau)/\rho' n_3\} \quad (41a)$$

$$-FD^{1/2}\bar{C}_B(0, s) = (s + k)^{-1/2}\{[1 - \exp(-\tau_1s)] \times \bar{i}_{Bf}(s)/n_1 + \exp(-\tau_1s)\bar{I}_{Br}(s, \tau)/n_3\} \quad (42a)$$

Using (41a) and (42a) to obtain $\bar{I}_{Bf}(s, \tau)$, substituting this value in (42a) and using (16a) ($\bar{i}_{Bf} = -\bar{i}_A$) yields the equation for $\bar{C}_B(0, s)$

$$n_2FD^{1/2}\bar{C}_B(0, s) = \frac{i\rho[1 - \exp(-\tau_1s)]}{s} \times \left\{ \frac{1}{(s + k)^{1/2} - \rho s^{1/2}} \right\} + \frac{(1 - R)i\rho' \exp(-\tau_1s)}{n_3s} \times \left\{ \frac{1}{(s + k)^{1/2} - \rho' s^{1/2}} \right\} \quad (43a)$$

(25) Equation 37a arises from a straightforward application of the Laplace transformation on $i_B(t)$. In general

$$L\{S\tau(t)F(t)\} = \int_\tau^\infty \exp(-st)F(t)dt = \exp(-\tau s) \times L\{F(t + \tau)\}$$

or

$$n_2FD^{1/2}\bar{C}_B(0, s) = \bar{g}(s, \rho) - \exp(-\tau_1 s)\bar{g}(s, \rho) + (1 - R)\exp(-\tau_1 s)\bar{g}(s, \rho') \quad (44a)$$

The inverse transform of (44a) is

$$n_2FD^{1/2}C_B(0, t) = g(t, \rho) - S_{\tau_1}(t)g(t - \tau_1, \rho) + (1 - R)S_{\tau_1}(t)g(t - \tau_1, \rho') \quad (45a)$$

where $g(t, \rho)$ is as given in eq 13 in the text. For $\tau_2 < t < \tau_1$, $S_{\tau_1}(t) = 1$, and eq 12 in the text results.

Electron Spin Resonance Spectra of 9,10-Diphenylanthracene

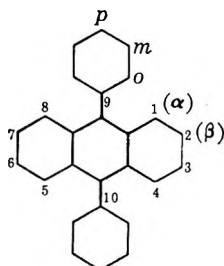
Anion and Cation Radicals

by L. O. Wheeler, K. S. V. Santhanam, and Allen J. Bard¹

Department of Chemistry, The University of Texas, Austin, Texas 78712 (Received August 23, 1965)

The electron spin resonance (esr) spectra of the 9,10-diphenylanthracene radical anion, prepared by electroreduction in N,N-dimethylformamide, and of the cation, prepared by treatment with concentrated sulfuric acid, are given. The experimental coupling constants are compared with those calculated using Hückel molecular orbital theory assuming different angles between the phenyl rings and the anthracene nucleus.

Recent interest in chemiluminescent² and electrochemical³ reactions of 9,10-diphenylanthracene (DPA) prompted an investigation of anion and cation radicals of DPA. Additional interest in DPA radicals centers on the nonplanarity of the parent molecule caused by interactions of the *o*-hydrogens on the phenyls in the 9 and 10 positions and hydrogens on the anthracene



nucleus at positions 1, 4, 5, and 8. By comparing the coupling constants obtained from experimental spectra with those calculated by molecular orbital methods, an estimation of the angle between the phenyl rings and the anthracene nucleus can be obtained.

Brunner and Dörr⁴ reported the esr spectrum of DPA anion radical in liquid ammonia at -40° , produced by reaction of DPA with alkali metal. They obtained a 17-line spectrum with a total width of 5.3 gauss and concluded that no conjugation with the phenyl rings occurred and that a very large spin density was present on the 9 and 10 positions. An abstract of a paper mentioning an esr spectrum of DPA radicals has appeared,⁵ but details of this work are unavailable.

(1) To whom all correspondence and requests for reprints should be directed.

(2) (a) E. A. Chandross and F. I. Sonntag, *J. Am. Chem. Soc.*, **86**, 3179 (1964); (b) K. S. V. Santhanam and A. J. Bard, *ibid.*, **87**, 139 (1965); (c) R. Visco and E. A. Chandross, *ibid.*, **86**, 5350 (1964).

(3) K. S. V. Santhanam and A. J. Bard, to be submitted for publication.

(4) V. E. Brunner and F. Dörr, *Ber. Bunsenges. Physik. Chem.*, **68**, 468 (1964).

(5) T. W. Chiu, N. Y. Wang, and S. H. Chang, *Yao Hsueh Hsueh Pao*, **19**, 583 (1963); *Chem. Abstr.*, **60**, 8803 (1964). The Library of Congress is the only listed receiver of this journal and they had not received this issue. The reported resolution in the abstract is well below that of this work.

We report here the spectra of the anion radical of DPA produced by controlled-potential electroreduction in *N,N*-dimethylformamide and the cation radical produced in concentrated sulfuric acid.

Results and Discussion

Anion Radical. The esr spectrum of DPA anion is shown in Figure 1. A computer-simulated spectrum is shown based on the following coupling constants (in gauss): $a_H(\alpha) = 2.76 \pm 0.05$, $a_H(\beta) = 1.38 \pm 0.03$, $a_H(o) = a_H(p) = 0.28 \pm 0.01$; a line width (between the maxima and minima of the first derivative presentation) of 0.1 gauss (Lorentzian line shape) is also shown. Of the 67 theoretical lines 63 are observed experimentally. The total width of the spectrum is 17.2 gauss.

Cation Radical. The esr spectrum of DPA cation radical produced by dissolving DPA in hexane and treating with concentrated sulfuric acid is shown in Figure 2. A computer-simulated spectrum is shown based on the following coupling constants (in gauss):

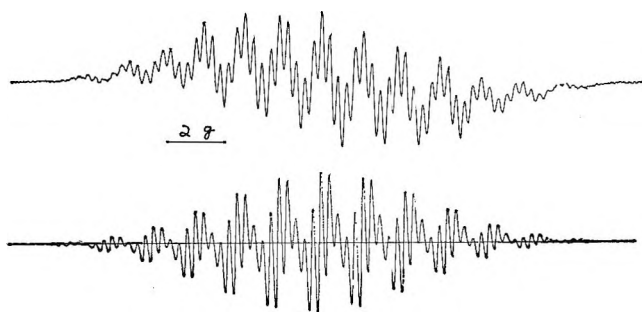


Figure 1. Top: derivative esr spectrum of DPA anion radical produced by electroreduction of 10^{-3} M DPA solution containing 0.1 M tetra-*n*-butylammonium iodide in *N,N*-dimethylformamide. Spectrometer conditions: modulation amplitude, 0.1 gauss; power, 10 db; sweep time, 25 min. Bottom: calculated spectrum using constants in text.

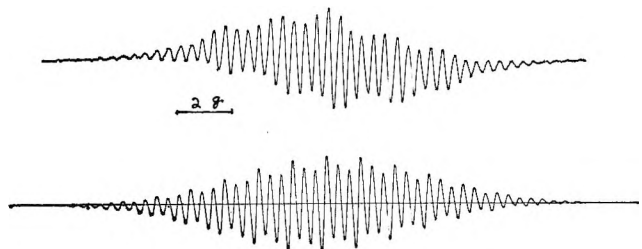


Figure 2. Top: derivative esr spectrum of DPA cation radical produced by treating a 5×10^{-3} M DPA solution in hexane with concentrated sulfuric acid. Spectrometer conditions: modulation amplitude, 0.07 gauss; power, 20 db; sweep time, 25 min. Bottom: calculated spectrum using constants in text.

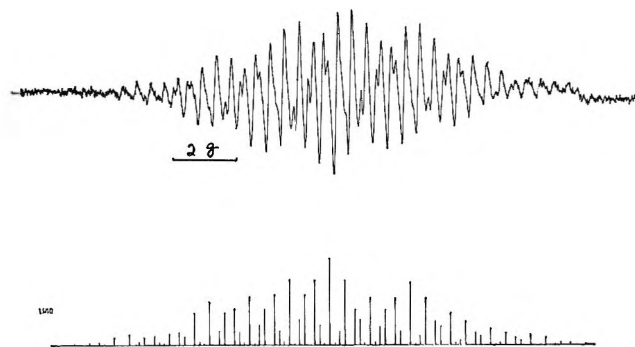


Figure 3. Top: derivative esr spectrum resulting from dilution of solution of DPA cation radical with concentrated sulfuric acid. Spectrometer conditions: modulation amplitude, 0.04 gauss; power, 20 db; sweep time, 25 min. Bottom: calculated spectrum.

$a_H(\alpha) = 2.46 \pm 0.03$, $a_H(\beta) = 1.23 \pm 0.02$, $a_H(o) = a_H(p) = 0.41 \pm 0.01$; a line width of 0.16 gauss is also shown. All 41 theoretical lines can be seen experimentally. On continually decreasing the concentration of the radical ion by dilution with concentrated sulfuric acid and operating at power levels of about 20 db, a more highly resolved spectrum can be obtained (Figure 3). This corresponds to coupling constants of $a_H(\alpha) = 2.45 \pm 0.03$, $a_H(\beta) = 1.22 \pm 0.02$, and $a_H(o) = a_H(p) = 0.45 \pm 0.01$ gauss.

HMO Calculations. Simple Hückel molecular orbital (HMO) calculations⁶ were performed, assuming different angles (θ) between the phenyl rings and the anthracene nucleus and assuming that the resonance integral, β , varied as the cosine of θ .⁷ The resulting spin densities (ρ) are shown as a function of θ in Figure 4. The ratios of the coupling constants for the anion radical correspond most closely to calculated spin densities for θ near 68° . The cation radical shows a larger coupling constant for the *o*- and *p*-phenyl hydrogens, indicating a larger amount of conjugation with the phenyl rings and thus a smaller θ (61°). Jones⁸ estimated a θ of at least 57° , based on molecular models.

Bolten⁹ has given the following equation for relating

$$A_H = -[Q \pm K\rho]\rho$$

spin densities to proton coupling constants for HMO calculated spin densities where Q and K are empirically determined constants based on measurements of a number of aromatic hydrocarbons and are taken to have the values of 27 and 12 gauss, respectively. The

(6) J. D. Roberts, "Molecular Orbital Calculations," W. A. Benjamin, Inc., New York, N. Y., 1962.

(7) M. J. S. Dewar, *J. Am. Chem. Soc.*, **74**, 3345 (1952).

(8) R. N. Jones, *ibid.*, **67**, 2127 (1945).

(9) J. R. Bolton, *J. Chem. Phys.*, **43**, 309 (1965).

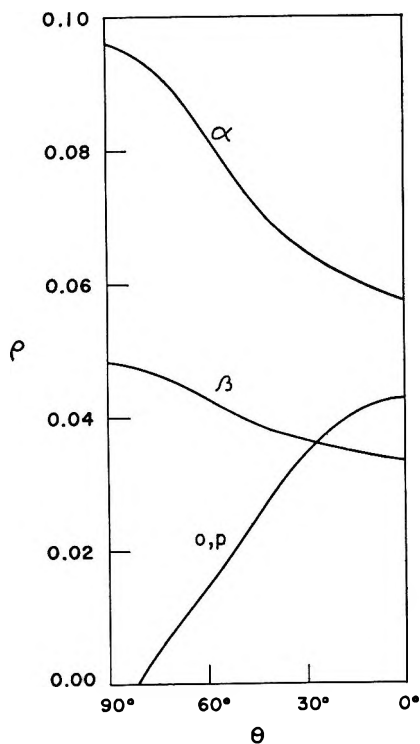


Figure 4. Variation of the spin density (ρ) with angle between phenyl rings and anthracene nucleus (θ) as calculated by HMO theory.

sign in the equation corresponds to the charge on the radical. The calculated coupling constants for the anion radicals using $\theta = 68^\circ$ for calculation of ρ and based on this equation are $a_H(\alpha) = 2.27$, $a_H(\beta) = 1.17$, and $a_H(o) = a_H(p) = 0.26$ gauss. For the cation radical using $\theta = 61^\circ$, they are $a_H(\alpha) = 2.15$, $a_H(\beta) = 1.13$, and $a_H(o) = a_H(p) = 0.45$ gauss. Coupling constants based on a single Q for each radical or the original equation given by Colpa and Bolton,¹⁰ in which $Q = 31.2$ and $K = 17$, are in better agreement with experimental results. Although the usual results for hydrocarbon radicals indicate that larger proton coupling constants are found with cation radicals, this is not the case here for the α and β protons. This may be caused by a difference in angle in the anion and cation radicals.

The results obtained in this study differ from those obtained by Brunner and Dörr⁴ in liquid ammonia. Specific solvent effects for hydrocarbon radicals are probably small since the esr spectra of 9,10-dimethylanthracene anion radical are very similar in both liquid ammonia⁴ and dimethoxyethane.¹¹ Even for the phenyl rings rotated perpendicular to the anthracene nucleus ($\theta = 90^\circ$), a wider spectrum would be expected, assuming no extreme dependence of Q on tem-

perature. Since some commercial samples of DPA have been known to contain anthraquinone,¹² Brunner and Dörr may have been observing the radical anion of this substance which has appreciable spin density on the oxygens and which produces a narrow esr spectrum.¹³

Experimental Section

A Varian Associates V-4502 spectrometer employing 100-kc field modulation was used. A Varian V-153C klystron (output 300 mw) was used; attenuation levels represent attenuation of the output of this klystron in a standard Varian bridge. Samples were contained in the flat Varian aqueous sample cell.

The anion radical was prepared by controlled-potential electroreduction of DPA at a mercury cathode in a solution of *N,N*-dimethylformamide containing 0.1 *M* tetra-*n*-butylammonium iodide. The solution was degassed, and the reduction and transfer to the esr cell were carried out on a vacuum line.³ The solution of the anion radical produced under these conditions was stable for at least 4 hr. The radical anion is very unstable in the presence of traces of oxygen or impurities, however.

The cation radical was prepared by dissolving DPA in 2-3 ml of hexane and treating this solution with about 10 ml of concentrated sulfuric acid. Similar results were obtained by dissolving the DPA in acetonitrile and *N,N*-dimethylformamide before treating with sulfuric acid. Spectra of samples treated by this procedure were always better than those obtained by dissolving the DPA directly in concentrated sulfuric acid.

The HMO calculations were done on a Control Data Corp. 1604 computer. The theoretical simulated spectra were also calculated on the CDC 1604 computer and were then plotted on the CDC 160 plotter.

Acknowledgment. The support of this research by the Robert A. Welch Foundation and the National Science Foundation (Grant No. GP-1921) is gratefully acknowledged. The esr instrument was purchased with funds provided by the National Science Foundation (Grant No. GP-2090).

(10) J. P. Colpa and J. R. Bolton, *Mol. Phys.*, **6**, 273 (1963).

(11) (a) J. R. Bolton, A. Carrington, and A. D. McLachlan, *ibid.*, **5**, 31 (1962); (b) D. Bachmann, *Z. Physik. Chem. (Frankfurt)*, **43**, 198 (1964).

(12) R. N. Adams, University of Kansas, private communication.

(13) (a) M. Adams, M. S. Blois, and R. H. Sands, *J. Chem. Phys.*, **28**, 774 (1958); (b) G. Vincow and G. K. Fraenkel, *ibid.*, **34**, 1333 (1961).

Reversing Hydrogen Isotope Effect on the Rate of the Gas Phase

Decomposition of Oxalic Acid

by Gabriel Lapidus,¹ Donald Barton,² and Peter E. Yankwich

Noyes Laboratory of Chemistry, University of Illinois, Urbana, Illinois 61803 (Received July 16, 1965)

The decomposition of oxalic acid- d_2 vapor at an initial pressure of 0.8 mm has been studied between 127 and 156°. The decomposition appears to be first order with respect to oxalic acid; observed Arrhenius parameters are: $E = 34.5 \pm 0.9$ kcal mole⁻¹ and $\log A$ (sec⁻¹) = 14.3 ± 0.5 . Comparison of these results with those for oxalic acid reveals a small hydrogen isotope effect which inverts within the experimental temperature range and which has very great temperature dependence for its magnitude. The size of the temperature dependence seems explainable by combination of kinetic, equilibrium (between cyclic and noncyclic structures), and tunneling isotope fractionation effects. The magnitude of the observed isotope effect can be explained if there is impressed on this combination a virtually temperature-independent inverse isotope effect such as that described and observed by Rabinovitch and his co-workers.

Introduction

Recently,³ we reported the results of experiments on the kinetics and stoichiometry of the decomposition of oxalic acid in the gas phase. The Arrhenius activation energy was found to be about 30 kcal mole⁻¹, and the preexponential factor was found near 10^{12} . After comparison of these results with those obtained from the related decompositions in a variety of solvents, we argued that they were consistent with a unimolecular mechanism proceeding *via* a cyclic activated complex and suggested that the rate-determining step was intramolecular hydrogen atom transfer from one carboxyl group to the carbonyl oxygen of the other.

To permit more detailed exposure of the reaction mechanism, we have carried out experiments on oxalic acid- d_2 and report the results in this paper.

Experimental Section

Reagent. Fisher Analytical grade anhydrous oxalic acid was purified by vacuum sublimation at 110°, labeled by three or four evaporations to dryness from deuterium oxide (99.5 atom % D; Stuart Oxygen Co.), dried *in vacuo* at 40°, and stored in a vacuum desiccator over magnesium perchlorate; the final product was at least 99.3 atom % D in both carboxyl groups. Permanganate titrations showed the material to be pure within an analytical error of approximately 0.02%.

Apparatus and Procedure. The apparatus and procedures were identical with those employed to obtain data on the decomposition of oxalic acid.³ Special care was used to establish identity of the reaction temperatures. Although no parallel study was carried out to determine the vapor pressure of oxalic acid- d_2 , we did observe from the material balance results that the vapor pressure of this substance at about 130° (the "injection" temperature) is slightly less than that of the ordinary acid. Blank experiments showed that the correction for decomposition upon injection was $-1.3 \pm 0.4\%$ here; a slightly lower correction, $-1.2 \pm 0.3\%$, was applied to the data for the decomposition of oxalic acid.

Results

As with the ordinary acid, the stoichiometry of the decomposition of oxalic acid- d_2 under these low-pressure, moderate-temperature conditions is simple. The formic acid- d_2 product found averages $99.5 \pm 0.5\%$ of the carbon dioxide produced. Equivalence in amount of the carbon dioxide product and the oxalic

(1) Research Associate, 1960-1963.

(2) Visiting assistant professor, 1960-1962.

(3) G. Lapidus, D. Barton, and P. E. Yankwich, *J. Phys. Chem.*, **68**, 1863 (1964).

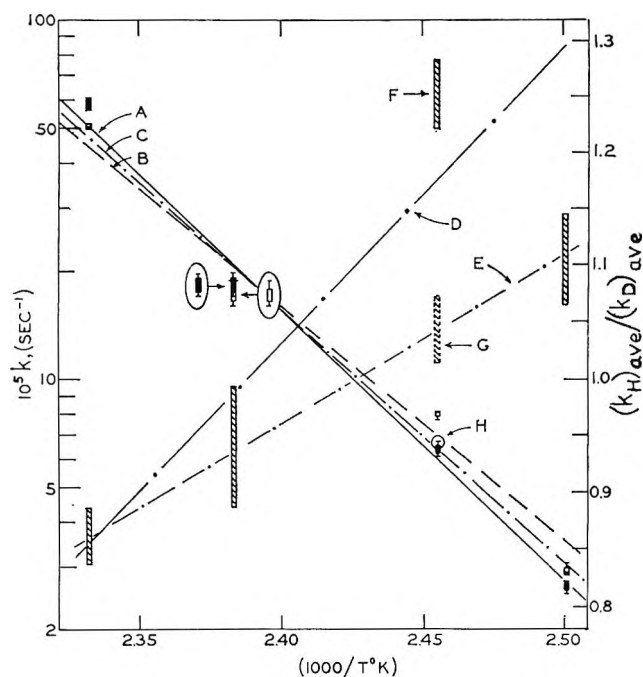


Figure 1. Temperature dependence of rate constants and rate constant ratios in the gas phase decomposition of oxalic acid and oxalic acid- d_2 . Left ordinate: $10^5 k$ (sec^{-1}); right ordinate: $(k_H)_{\text{ave}}/(k_D)_{\text{ave}}$. Open points are for $(\text{COOH})_2$, solid points for $(\text{COOD})_2$. Vertical rectangles encompass average deviations from the mean; horizontal bars indicate maximum and minimum results observed. At 146.4° , the points for k_H and k_D are partly superimposed; for clarity, they are separated in the ovals at either side of this point. Line A, —, k_D from Table I; line B, ---, k_H from ref 3; line C, — · —, k_H with "first runs" correction applied to $(k_H)_{\text{ave}}$ at 134.1° (point H); line D, — · —, $(k_H)_{\text{ave}}/(k_D)_{\text{ave}}$ with original data ratio at 134.1° (point F); line E, · — ·, $(k_H)_{\text{ave}}/(k_D)_{\text{ave}}$ with corrected $(k_H)_{\text{ave}}$ used to form ratio at 134.1° (point G).

acid decomposed is demonstrable within a mean-composite analytical error (of titrations and manometry) of 1%; material balance can be proved to $\pm 1.4\%$.

The Discussion of the kinetics results is based on data from 19 runs at temperatures between 126.6 and 155.6° ; in each case the initial pressure of oxalic acid- d_2 vapor in the reactor was 0.82 ± 0.02 mm (0.88 ± 0.02 for oxalic acid). Examination of the data indicates that the rate is first order with respect to oxalic acid; the quality of the results is such that the accuracy of this order is approximately ± 0.1 . Individual and average values of the apparent first-order specific rate constants, k_D (sec^{-1}), are shown in Table I and plotted as the solid points in Figure 1; the only correction applied to the input data is for the small decomposition during injection. Line A is the least-squares fit of these data; the related activation

Table I: Rate of Decomposition of Oxalic Acid- d_2 Vapor

Run temp, $^\circ\text{C}$	Time, sec	Degree of decompn, cor	$10^5 k_D$, sec^{-1}
126.6	28,920	0.546	2.73
	32,400	0.574	2.63
	33,900	0.578	2.55
			Av 2.64 ± 0.07
134.1 ^a	4,800	0.276	6.72
	10,800	0.493	6.29
		0.493	6.28
	18,000	0.673	6.20
		0.676	6.26
	23,400	0.777	6.42
	25,200	0.803	6.45
			Av 6.38 ± 0.13
146.4	1,500	0.255	19.64
	2,700	0.375	17.42
	4,200	0.544	18.71
	7,200	0.738	18.61
	13,440	0.898	16.97
			Av 18.3 ± 0.8
155.6	900	0.422	60.9
	1,800	0.637	54.3
	2,400	0.756	58.8
			Av 58.7 ± 1.6

^a Four additional runs at 134.1° yielded k_D values of 6.86, 7.17, 7.26, and $8.11 \times 10^{-5} \text{ sec}^{-1}$ for 0.10–0.17 decomposition. All four of these results are excluded from later consideration to maintain consistency with the oxalic acid results, in which similar data for low decomposition at this temperature were rejected.

parameters are listed in column A of Table II; in column B of Table II are shown the corresponding quantities for k_H as reported in a previous paper,³ and line B in Figure 1 is the least-squares fit of those results (open points).

Comparison of the plotted average values of k_D with those for k_H shows that the deviations from the fitted lines are greater in the case of the latter. The hatched points in Figure 1 are $(k_H)_{\text{ave}}/(k_D)_{\text{ave}}$ at each temperature, and line D is least-squares-fitted to those ratios; the large separation of point F from line E suggests that there may be an anomaly in the results reported earlier³ for k_H at 134.1° .

While a careful review of the data upon which the earlier publication was based does not preclude a different origin, we believe this possible anomaly could have arisen in an effect noticed not infrequently in

Table II: Calculated Activation Parameters

	A (COOD) ₂	B (COOH) ₂ orig	C (COOH) ₂ cor
Log $A(\text{sec}^{-1})$	14.3 ± 0.5	11.9 ± 0.7	12.7 ± 0.5
E^a	34.5 ± 0.9	30.0 ± 1.3	31.5 ± 0.8
ΔH^{*a}	33.7 ± 0.9	29.2 ± 1.3	30.7 ± 0.8
ΔS^{*b}	$+4.3 \pm 2.1$	-6.6 ± 3.0	-2.9 ± 2.1
ΔF^{*a}	31.9 ± 1.2	31.9 ± 1.8	32.0 ± 1.1
Mean dev of least-squares log k	± 0.038	± 0.065	± 0.035
Est'd inversion temp, H/D isotope effect		$145 \pm 13^\circ$	$139 \pm 9^\circ$

^a Kcal mole⁻¹. ^b Kcal mole⁻¹ °K⁻¹.

gas kinetics studies⁴: the nine runs at 134.1° using oxalic acid as reagent were the first carried out in the apparatus; any failure to *season* or *age* the reactor or *condition* its surfaces could have resulted temporarily in a rate being observed which was different from that which would have been observed after an appropriate number of experiments had been completed in the apparatus. Problems of this kind must contribute to the much lower accuracy of isotope effect results based on isotope *comparative* experiments (as here) as opposed to isotope *competitive* experiments.

For purposes of discussion, we assume that the smallest temperature dependence of k_H/k_D implied by our combined data is that based upon the results at temperatures other than 134.1°, line E.⁵ The best use of the other seven nonsuspect sets of data can be made by adoption of the corollary that the true value of $(k_H)_{av}/(k_D)_{av}$ at 134.1° is shown by the dashed point G, which is equivalent to the notion that the correct value of k_H at this temperature is approximately as shown by the circular point H.⁶ In column C of Table II we give the Arrhenius parameters and the transition state theory activation quantities calculated using this interpolated $(k_H)_{av}$; these are closer to those in column A than are those in column B, and the lessened differences seem appropriate for the level of the apparent hydrogen isotope effect, which is rather small.

Discussion

In our earlier paper³ we suggested that the oxalic acid decomposition proceeded *via* a cyclic activated complex, there being intramolecular hydrogen atom transfer from one carboxyl group to the carbonyl oxygen of the other. Whatever the sense of the re-

lated hydrogen kinetic isotope effect, its magnitude would depend upon the changes in bonding about the hydrogen atom incident upon activation. Maintenance of nearly constant total bond order about hydrogen would generate a small hydrogen kinetic isotope effect, perhaps as small as that observed here. However, no anomalous temperature dependence is expected on such a model, and certainly no inversion.

If the hydrogen isotope effect is secondary instead of primary, a magnitude of 10–20% is entirely reasonable⁷; but, once again, one would not expect the temperature effects observed.

Earlier Experiments on Isotopic Oxalic Acids. The only previous comparison of the rates of decomposition of hydrogen isotopic oxalic acids is in the work of Lütgert and Schröer,⁸ who determined k_H for solutions in ordinary water, k_D in D₂O, and both in ordinary dioxane. The water solution experiments were carried out at five temperatures between 132.2 and 173.6°; the results correspond to a reverse isotope effect at low temperatures which decreases with increasing temperature (and would be expected to invert in the neighborhood of 300°). Experiments in dioxane were at only two temperatures: $k_H/k_D = 0.974$ at 120.0°, and 0.997 at 152.5°. Though the results are few, a reverse isotope effect is indicated which appears to approach inversion to normal at about 155°.

Temperature Dependence of Kinetic Isotope Effects. In the remainder of this Discussion, we examine the possible sources of a hydrogen isotope effect as strongly temperature dependent as that represented by line E. One would expect inversion of the isotope effect were large temperature dependence coupled with small magnitude; but, as will be shown, the limitations imposed by a conventional theoretical description are severe in this regard. Any explanation or model

(4) *E.g.*: D. Brearley, G. B. Kistiakowsky, and C. H. Stauffer, *J. Am. Chem. Soc.*, **58**, 44 (1936); D. H. R. Barton and P. F. Onyan, *Trans. Faraday Soc.*, **45**, 725 (1949); J. B. Peri and F. Daniels, *J. Am. Chem. Soc.*, **72**, 424 (1950); F. O. Rice and K. F. Herzfeld, *J. Phys. Chem.*, **55**, 975 (1951).

(5) It seems only fair to examine the situations which would obtain were this assumption made, in turn, at each one of the other reaction temperatures (as if the first runs had been made at some temperature different from 134.1°). It is apparent from Figure 1 that elimination of any other point would suggest a best-fit line of slope equal to or greater than that of line D. In any case, the temperature dependence over the short experimental range of 29° is so large as to imply the inversion of the isotope effect even had it not been observed directly.

(6) That is, instead of using a pair of rate data for computation of the isotope effect, we employ an interpolated value of the isotope effect to calculate the numerator of the isotopic rate constant ratio.

(7) A secondary hydrogen isotope effect of this size in this reaction would seem to imply important changes upon activation in the adjacent C–O bond.

(8) I. Lütgert and E. Schröer, *Z. Physik. Chem.*, **A187**, 133 (1940).

which fails for line E must fail for a plot of higher slope, such as D.

The ratio k_H/k_D is the product of a temperature-independent factor (TIF) arising in the reaction coordinate motion and a temperature-dependent factor (TDF) due to the mass dependence of the genuine vibrations in the normal molecules and activated complexes; it is to the latter that one must look first for an explanation of a kinetic isotope effect which reverses with increasing temperature.

Except for the missing terms due to the reaction coordinate, TDF has the form of an isotopic exchange reaction equilibrium constant. Urey,⁹ in his Liver-side lecture, mentions that reversal (with respect to unity) of such equilibrium constants, though not general, is not uncommon. The reversal "will occur if the difference in the sum of differences of (isotopic) frequencies has the same sign as the differences in the sums of the fractional differences of frequencies"—a condition rather difficult to predict.

In attempting to account for earlier observations on the kinetics of the decomposition of ordinary oxalic acid in the gas phase,³ it was proposed that the reaction was unimolecular and that the mechanism involved intramolecular hydrogen transfer through formation of a cyclic activated complex.¹⁰⁻¹⁴ In this regard, it is important to note that there are apparently reversing isotope effects in several equilibria which involve hydrogen bonding not dissimilar to that proposed for the transition state of the oxalic acid decomposition. The ratios of the isotopic association constants for the monomer-dimer equilibria in the gas phase for the following pairs of carboxylic acids all show temperature dependence which should lead to reversal of the isotope effect: $\text{CH}_3\text{CH}_2\text{COOH}-\text{CH}_3\text{CH}_2\text{COOD}$,^{15,16} $\text{CH}_3\text{COOH}-\text{CD}_3\text{COOD}$,¹⁷ and $\text{CF}_3\text{COOH}-\text{CF}_3\text{COOD}$ ¹⁸; the senses with respect to unity of K_H/K_D at low temperature and estimated inversion temperatures ($t^\circ\text{C}$) are, respectively: >1 (70°), <1 (210°), and >1 (265°). The largest temperature dependence is exhibited by the propionic acid equilibria; across a 30° span centered on the inversion temperature (similar to the conditions of our experiments), K_H/K_D falls from 1.08 to 0.94. Even this large change with temperature is much smaller than that observed in the decomposition of the isotopic oxalic acids.

Some appreciation for the magnitude of the variation with temperature of k_H/k_D can be gained by comparing it with that of the most strongly temperature-dependent equilibrium constant tabulated by Urey⁹ for hydrogen-deuterium exchange. For the exchange of these isotopes between potassium hydride and water vapor, the ratio of equilibrium constants at 127 and

156° is 1.13; for k_H/k_D reported here, the corresponding ratio is 1.28 for line E and 1.48 for line D.

Similar equilibrium constant calculations for hydrogen-deuterium exchange between noncyclic, monocyclic, and bicyclic oxalic acid molecules (cyclization being through hydrogen bonding of oxygens in different carboxyl groups) have been carried out in our laboratory.¹⁹ Single cyclization can contribute to the observed k_H/k_D a factor of 1.100 at 127° and 1.095 at 156° , while double cyclization can contribute factors of 1.210 and 1.199, respectively; the ratios of these factors at the temperature extremes of our experiments are 1.0046 for single cyclization and 1.0092 for double cyclization—both far too small to explain the temperature dependence of k_H/k_D .

Another source of large temperature dependence in a hydrogen-deuterium kinetic isotope effect is hydrogen tunneling; a classic example of the application of this approach is contained in the paper of Sharp and Johnston²⁰ on the reaction of methane with trifluoromethyl radical. Though unimolecular instead of bimolecular, the model proposed for the oxalic acid transition state is similar in many respects to that studied by Sharp and Johnston. Tunnel effect factor calculations depend not only upon the molecular model but also upon the choice of computation method. Typically, for a hydrogen transfer of the type considered here, hydrogen tunneling might contribute the factors 2.04 and 1.89 to k_H/k_D at 127 and 156° , respectively; their ratio is 1.08. If the ordinary kinetic isotope effect contribution to k_H/k_D is a factor of 2.00 at 127° (a reasonable value for an intramolecular hydrogen transfer),¹⁹ the ratio of such contributions at 127 and 156° would be about 1.05, typically. If we combine the effects of single cyclization (*i.e.*, assume that a

(9) H. C. Urey, *J. Chem. Soc.*, 562 (1947).

(10) K. J. Pedersen, *J. Am. Chem. Soc.*, **51**, 2098 (1929); **60**, 595 (1938).

(11) A. Dinglinger and E. Schröer, *Z. Physik. Chem.*, **A179**, 401 (1937).

(12) M. R. F. Ashworth, R. P. Daffern, and D. L. Hammick, *J. Chem. Soc.*, 809 (1939).

(13) F. H. Westheimer and W. A. Jones, *J. Am. Chem. Soc.*, **63**, 3283 (1941).

(14) J. A. King, *ibid.*, **69**, 2738 (1947).

(15) M. D. Taylor and J. Bruton, *ibid.*, **74**, 4151 (1952).

(16) R. C. Herman and R. Hoistadter, *J. Chem. Phys.*, **7**, 460 (1939).

(17) A. E. Potter, Jr., F. Bender, and H. L. Ritter, *J. Phys. Chem.*, **59**, 250 (1955).

(18) M. D. Taylor and M. B. Templeton, *J. Am. Chem. Soc.*, **78**, 2950 (1956).

(19) W. E. Buddenbaum and P. E. Yankwich, unpublished calculations.

(20) T. E. Sharp and H. S. Johnston, *J. Chem. Phys.*, **37**, 1541 (1962).

monocyclic form of oxalic acid is the actual reactant), hydrogen tunneling, and kinetic isotope fractionation, we would estimate $k_H/k_D = 4.49$ at 127° and 3.94 at 156° , the ratio of these figures being 1.14.

It is possible to increase somewhat the temperature dependence of this estimated isotope effect, without altering similarly its average value near 140° , by adjusting the parameters of the molecular model and the method of calculating the tunnel effect. However, even extreme variations of these kinds are capable only marginally of lifting the temperature dependence so high that the ratio of k_H/k_D at 127 and 156° is in the neighborhood of 1.2. A complex model such as this, however, yields an estimated isotope effect of large magnitude and provides no explanation for the observed isotope effect being small. To rationalize the experimental results we require that the temperature dependence of the complex model described above be preserved, while some temperature-independent phenomenon depress its magnitude so that a small isotope effect, inverting over a limited temperature range, would be observed.

Our experiments on the oxalic acid decompositions were carried out at a single pressure for each of the isotopic compounds, these pressures being in the neighborhood of 1 mm. We know nothing of the relative collision efficiencies of oxalic acid *vs.* carbon dioxide + formic acid, but it may be that they are so similar as to mask effectively apparent second-order behavior of the kinetics as determined from decomposition measurements at different time intervals where the pressure is this low.

Recently, Rabinovitch and his associates²¹⁻²⁵ have detailed some effects of frequency lowerings and of differential quantal effects on nonequilibrium falloff behavior (and on other characteristics) of thermal systems. The effect of possible interest in the present

discussion is statistical-weight inversion of an intermolecular kinetic isotope effect. The system studied by Schneider and Rabinovitch²⁵ was the isomerization of methyl- d_3 isocyanide. It was observed that the inverse isotope effect could be large, a factor of 0.28 in k_H/k_D and, important to our discussion, that the temperature dependence of this effect was *very small*.

We have not yet carried out detailed calculations for the oxalic acid intermolecular isotope effect using the techniques of Rabinovitch and his co-workers, but a phenomenon with the characteristics they describe seems required to explain the gross features of our observations and is consistent with them. As indicated above, such an explanation is plausible only if at about 1 mm the oxalic acid decomposition is well over into the falloff region. As yet, there is no evidence on this point. Carbon-13 isotope effect results which we have obtained²⁵ may permit a stringent test of the notions discussed above even in the absence of information about the low-pressure kinetics of this reaction; such a test is presently under way.

Acknowledgments. We are indebted for much helpful discussion to our colleagues Prof. R. A. Marcus and Drs. L. B. Sims and W. E. Buddenbaum. This research was supported by the U. S. Atomic Energy Commission.

(21) B. S. Rabinovitch, D. W. Setser, and F. W. Schneider, *Can. J. Chem.*, **39**, 2609 (1961).

(22) B. S. Rabinovitch and J. H. Current, *ibid.*, **40**, 557 (1962).

(23) F. W. Schneider and B. S. Rabinovitch, *J. Am. Chem. Soc.*, **84**, 4215 (1962).

(24) J. H. Current and B. S. Rabinovitch, *J. Chem. Phys.*, **38**, 1967 (1963).

(25) F. W. Schneider and B. S. Rabinovitch, *J. Am. Chem. Soc.*, **85**, 2365 (1963).

(26) G. Lapidus, D. Barton, and P. E. Yankwich, unpublished experiments.

Modified General Theory of Charge-Transfer Electrode Kinetics

by Sidney Barnartt

Edgar C. Bain Laboratory for Fundamental Research, United States Steel Corporation, Research Center, Monroeville, Pennsylvania (Received July 19, 1965)

The kinetic theory of electrode reactions contained several unsatisfactory aspects. The modified general equations derived here largely eliminate these drawbacks. A rigorous thermodynamic treatment of the activation process shows that the activity of the activated complex at the electrode in its standard state is a definite quantity not open to arbitrary selection. The activity coefficient of the complex can be eliminated under specified conditions. The modified rate equations yield energies of activation which are determined primarily by the variation with temperature of the concentration of the activated complex at the reversible electrode, with no dependence upon the reference zero potential.

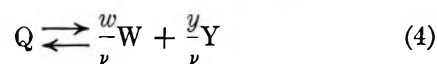
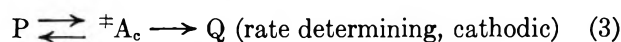
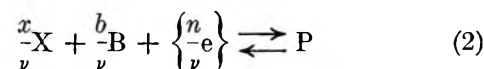
Introduction

The charge-transfer kinetics of electrode reactions have been interpreted most extensively by the theory of absolute reaction rates.¹⁻³ There are, however, some unsatisfactory aspects of the present rate equations: (1) the energy of activation depends upon a reference zero potential which is not accessible experimentally⁴⁻⁶; (2) the reaction rate may be expressed in terms of the concentration of the activated complex in its standard state, whereas the standard state is open to arbitrary selection⁶; (3) the activity coefficient of the activated complex is usually assumed to be unity, but it may have a profound influence on predicted rates and on allowable reaction mechanisms.⁷ The theory is modified below in an attempt to eliminate these drawbacks. A rigorous thermodynamic treatment is given for the activity of the activated complex. This requires definite values for the activity of the complex at the standard electrode and leads to new expressions for the concentration of the complex and reaction rates, in which all terms are independent of reference potential.

The generalized electrode reaction utilized by Parsons³ will be treated with little change in notation. The over-all electrode reaction is written

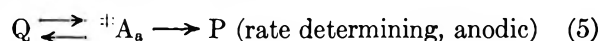


where either B and Y are both ionic, or only one is ionic ($z = 0$ or $bz = n$). The reaction may occur as a series of consecutive reaction steps. In the cathodic direction the component reactions are formulated as



where ν is the stoichiometric number. The total number, n/ν , of electrons is placed in braces to signify that the number of electrons used up in forming each of the intermediate states P, ${}^{\pm}A_c$, and Q is not fixed.

The anodic reaction steps are the same, but in the reverse direction, with (3) rewritten



The cathodic activated complex ${}^{\pm}A_c$ has the same chemical constitution as the anodic, but its velocity along the reaction coordinate is in the opposite direction. At a given moment the concentration ${}^{\pm}c_c$ of the cathodic complex at the metal-solution interface will generally differ from ${}^{\pm}c_a$, the concentration of the

(1) H. Eyring, S. Glasstone, and K. J. Laidler, *J. Chem. Phys.*, **7**, 1053 (1939).

(2) S. Glasstone, H. Eyring, and K. J. Laidler, "Theory of Rate Processes," McGraw-Hill Book Co., Inc., New York, N. Y., 1941.

(3) R. Parsons, *Trans. Faraday Soc.*, **47**, 1332 (1951).

(4) P. Delahay, "New Instrumental Methods in Electrochemistry," Interscience Publishers, Inc., New York, N. Y., 1954, p. 42.

(5) J. O'M. Bockris, *Mod. Aspects Electro-Chem.*, **1**, 180 (1954).

(6) T. Hurlen, *Electrochim. Acta*, **7**, 653 (1962).

(7) J. Horiuti and H. Sugawara, *J. Res. Inst. Catalysis, Hokkaido Univ.*, **4**, 1 (1956); J. Horiuti, *ibid.*, **4**, 55 (1956).

anodic complex. The fundamental rate equations of the absolute reaction rate theory² may be written

$$r_c = \frac{kT}{h} \kappa_c^\ddagger c_c \quad r_a = \frac{kT}{h} \kappa_a^\ddagger c_a \quad (6)$$

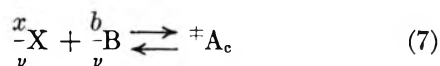
where r_c and r_a are the cathodic and anodic rates and κ_c and κ_a are the transmission coefficients (assumed constant).

Electrical work done during the formation of intermediate P from the cathodic reactants will be designated as p , and that done during the formation of Q from the products will be q . The quantities p and q will be restricted by the following conditions. (a) There may be portions of p and of q which depend on T and composition, hence which vary with the reversible potential, but which are independent of charge-transfer polarization η . (Note that Parsons³ described these portions as independent of any change in single-electrode potential.) (b) The remainder of p and q is directly proportional to the electrode potential, the proportionality constant being independent of T and composition. (c) The rate-determining step involves a finite quantity of electrical work; hence $p - q$ is less than the total electrical work involved in the over-all reaction; either p or q or both may be zero.

An inherent difference from Parsons' treatment has been introduced to simplify discussion of the concepts being modified: the reaction sequence (2) to (4) includes only mechanisms for which the cathodic complex is formed from X and B in the ratio given by (1), thus excluding possible mechanisms in which the complex is formed from the same constituents in other proportions, or from B without X, etc.

Thermodynamics of the Activation Process

The over-all cathodic activation process is represented by the equilibrium (omitting the electrons involved)



The first and second laws of thermodynamics applied to this process at constant T and P give ${}^\ddagger\Delta U_c = T{}^\ddagger\Delta S_c - (P{}^\ddagger\Delta V_c + {}^\ddagger u_c)$, or

$$-{}^\ddagger\Delta G_c = {}^\ddagger u_c \quad (8)$$

where ${}^\ddagger\Delta U_c$, ${}^\ddagger\Delta S_c$, ${}^\ddagger\Delta V_c$, and ${}^\ddagger\Delta G_c$ are the changes in internal energy, entropy, volume, and Gibbs free energy, respectively, and ${}^\ddagger u_c$ is the total electrical work done during cathodic activation

$${}^\ddagger u_c = p + u_{(P \rightarrow \ddagger A)} \quad (9)$$

The last term is a quantity not directly accessible experimentally. It can be expressed, following Horiuti

and Polanyi,⁸ as a fraction β of the electrical work done in the rate-determining step

$$u_{(P \rightarrow \ddagger A)} = \beta u_{(P \rightarrow Q)} = \beta \{ (n/\nu) F \Delta \phi - p + q \} \quad (10)$$

where $\Delta \phi$ is the total potential change across the electrode-solution reaction zone. With (9) and (10), eq 8 becomes

$$-{}^\ddagger\Delta G_c = \beta (n/\nu) F \Delta \phi + (1 - \beta) p + \beta q \quad (11)$$

Here one introduces a fundamental assumption of electrode kinetic theory that the "transfer coefficient" β ($0 < \beta < 1$) is independent of T and P , of electrode potential, and of the concentration of any reactant or product of the electrode reaction. This constancy prevails for the range of conditions within which the reaction mechanism is invariant. The same assumption is applied to the transmission coefficients.

The energy change $(n/\nu) F \Delta \phi$ is not experimentally accessible and not an absolute quantity; hence, the related free energy of activation, ${}^\ddagger\Delta G_c$, is also not absolute. Since ions are involved, these quantities depend upon a reference level for ionic free energies. For consistency with tabulated thermodynamic data based upon the universally accepted rules for selection of standard states, these energy changes are based upon zero free energy of formation for hydrogen ion and upon the standard hydrogen electrode as the reference zero for single-electrode potentials. Therefore $\Delta \phi$ in (11) may be replaced by the electrode potential ε

$$-{}^\ddagger\Delta G_c = \beta (n/\nu) F \varepsilon + (1 - \beta) p + \beta q \quad (12)$$

for both $\Delta \phi$ and ε represent the measured voltage of an isothermal cell made by combining the test electrode and s.h.e., provided the measurement excludes any appreciable IR drop or liquid junction potential.

With the boundary conditions assigned above to p and q , one may use Parsons' equation

$$(1 - \beta) p + \beta q = \gamma (n/\nu) F \varepsilon + \delta \quad (13)$$

to define γ and δ . The proportionality constant γ is assumed to remain constant over the same range of conditions as β , but γ unlike β may be negative. The quantity δ is independent of η but may vary with T and composition. Equation 12 may now be rewritten

$$-{}^\ddagger\Delta G_c = (\beta + \gamma) (n/\nu) F \varepsilon + \delta \quad (14)$$

Let the concentrations of the electrode components be adjusted such that reaction 1 occurs with each in-

(8) J. Horiuti and M. Polanyi, *Acta Physicochim. URSS*, 2, 505 (1935).

dependently variable reactant or product J in its standard state (activity $a^{\circ}_J = 1$). The standard state is conventionally the state of the pure substance at 1 atm for those reactants which may be present as solvent or pure substances in a separate phase. For dissolved solutes the standard state is given by $a^{\circ}_J = 1$ under the condition of unit activity coefficient at infinite dilution, *i.e.*, $a_J \rightarrow c_J$ as $c_J \rightarrow 0$. If the reaction is carried out reversibly at $a^{\circ}_J = 1$, we have the defined standard electrode at potential ε° , and the standard free energy of activation becomes from (14)

$$-\ddagger\Delta G_{c,s} = (\beta + \gamma)(n/\nu)F\varepsilon^{\circ} + \delta_s \quad (15)$$

where δ_s is the value of δ for the standard electrode.

The activated complex, like any other dissolved solute, has its standard state defined by $\ddagger a^{\circ}_c = 1$ under the infinite dilution condition for solutes: $\ddagger a_c \rightarrow \ddagger c_c$ as $\ddagger c_c \rightarrow 0$. The free energies of activation in (14) and (15) are related by

$$\ddagger\Delta G_c = \ddagger\Delta G_{c,s} + RT \ln \left[\frac{\ddagger a_c}{\ddagger a_{c,s}} \left(\frac{a^{\circ}_X}{a_X} \right)^{z/\nu} \left(\frac{a^{\circ}_B}{a_B} \right)^{b/\nu} \right] \quad (16)$$

where $\ddagger a_{c,s}$ is the activity of the cathodic activated complex at the standard electrode. Since each independently variable component J is at fixed (unit) activity at the standard electrode, the latter is completely defined, and therefore the equilibrium which exists between reactants and activated complex determines the chemical potential of the latter without further arbitrariness. It follows that the activity $\ddagger a_{c,s}$ of the complex at the standard electrode is a definite value established by the nature of the electrode system. It is not equal to the standard state value, $\ddagger a^{\circ}_c = 1$. The fact that $\ddagger a_{c,s}$ has a definite value for a given electrode system negates the validity of an arbitrary calculation of $\ddagger a_{c,s}$, such as the one recently proposed,⁶ which does not take into consideration the detailed atomistic mechanism of the electrode reaction.

The two conditions, thermodynamic reversibility and electrode potential ε° , are necessary but not sufficient to establish the activity of the complex at the definite value $\ddagger a_{c,s}$. The reversible electrode potential is given by

$$\varepsilon_r = \varepsilon^{\circ} + \frac{RT}{nF} \ln \frac{a_X^x a_B^b}{a_W^w a_Y^y} \quad (17)$$

from which it is evident that one may obtain $\varepsilon_r = \varepsilon^{\circ}$ at values $a_X \neq 1$ and/or $a_B \neq 1$ by adjusting the activities of the denominator substances to keep the activity product ratio unity. If the reversible potential ε° is set up in this manner for $a_B \neq 1$ (and/or $a_X \neq 1$),

the activity $\ddagger a_c$ which results from equilibrium 7 must differ from the value of $\ddagger a_{c,s}$ which develops at the standard electrode where $a^{\circ}_X = a^{\circ}_B = 1$. The latter condition is thus the third requirement for establishing $\ddagger a_{c,s}$.

From eq 16 one obtains, after substituting the expressions given in (14) and (15) for $\ddagger\Delta G_c$ and $\ddagger\Delta G_{c,s}$ and unity for a°_X and a°_B

$$\frac{\ddagger a_c}{\ddagger a_{c,s}} = (a_X^x a_B^b)^{1/\nu} \exp \left[(\beta + \gamma) \frac{n}{\nu} \epsilon (\varepsilon^{\circ} - \varepsilon) + \frac{\delta_s - \delta}{RT} \right] \quad (18)$$

where $\epsilon \equiv F/RT$. Then with $\varepsilon = \varepsilon_r + \eta$, where η is the charge-transfer polarization and ε_r is given by (17), one obtains

$$\ddagger a_c / \ddagger a_{c,s} = \Pi \exp [-(\beta + \gamma)(n/\nu)\epsilon\eta + (\delta_s - \delta)/RT] \quad (19)$$

where Π denotes the activity product

$$\Pi = (a_X^x a_B^b)^{(1-\beta-\gamma)/\nu} (a_W^w a_Y^y)^{(\beta+\gamma)/\nu} \quad (20)$$

The thermodynamics of the anodic activation process may be treated in the same manner as above. Here the electrical work $u_{(Q \rightarrow \ddagger A)}$ is the complementary fraction, $1 - \beta$, of the total for the rate-determining step. With this modification it is readily shown that the corresponding equations for anodic activation are

$$\ddagger\Delta G_a = (1 - \beta - \gamma)(n/\nu)F\varepsilon - \delta \quad (21)$$

$$\ddagger\Delta G_a = \ddagger\Delta G_{a,s} + RT \ln \left[\frac{\ddagger a_a}{\ddagger a_{a,s}} \left(\frac{1}{a_W} \right)^{w/\nu} \left(\frac{1}{a_Y} \right)^{y/\nu} \right] \quad (22)$$

$$\ddagger a_a / \ddagger a_{a,s} =$$

$$\Pi \exp [(1 - \beta - \gamma)(n/\nu)\epsilon\eta + (\delta_s - \delta)/RT] \quad (23)$$

where the activity product Π is identical with that for the cathodic activation (eq 20).

Concentration of the Activated Complex

The surface concentration of the activated complex will always be very small. This follows directly from (6) since kT/h is very large (6.2×10^{12} at 300°K). For example, the value of $\ddagger c$ corresponding to rapid discharge of a univalent ion at 1.0 A/cm² is 1.0×10^6 molecules/cm² for $\kappa = 1$. Since a uniform electrode surface will present roughly 10^{15} adsorption sites/cm², this value of $\ddagger c$ corresponds to a fractional surface coverage $\ddagger\theta = 10^{-9}$. Even with changes of three orders of magnitude in discharge rate, in transmission coefficient, or in available surface sites, $\ddagger\theta$ will remain very small.

If the activated complex is the only species specifically adsorbed, the infinite dilution condition that $\dagger a \rightarrow \dagger c$ as $\dagger c \rightarrow 0$ permits replacement of the activity ratio in (18), (19), and (23) with the corresponding concentration ratio. This replacement will be valid also where other species are adsorbed, each to surface concentrations greater than $\dagger c$, provided the total surface coverage by all remains small with respect to unity. This may be shown by use of the statistical thermodynamic treatment of a localized monolayer. Following Fowler and Guggenheim,⁹ one may express the activity ratio as

$$\frac{\dagger a}{\dagger a_s} = \frac{\dagger \theta}{1 - \Sigma_i \theta_i} \bigg/ \frac{\dagger \theta_s}{1 - \Sigma_i \theta_{i,s}} = \left(\frac{\dagger \theta}{\dagger \theta_s} \right) \left(\frac{1 - \Sigma_i \theta_{i,s}}{1 - \Sigma_i \theta_i} \right) \quad (24)$$

for the condition of no mutual interactions between adsorbed molecules. Here $\Sigma_i \theta_i$ is the total fractional coverage of electrode surface sites by all specifically adsorbed species, both charged and uncharged, for any given set of solution conditions and potential ϵ ; $\Sigma_i \theta_{i,s}$ is the corresponding quantity at the standard electrode. For electrode systems which maintain $\Sigma_i \theta_i \ll 1$, eq 24 reduces to

$$\dagger a / \dagger a_s = \dagger \theta / \dagger \theta_s = \dagger c / \dagger c_s \quad (25)$$

since the activity coefficient ratio approaches unity

$$\dagger f / \dagger f_s = (1 - \Sigma_i \theta_{i,s}) / (1 - \Sigma_i \theta_i) = 1 \quad (26)$$

The activity coefficient ratio is unity also at electrodes which maintain $\Sigma \theta_i = \Sigma \theta_{i,s}$; here each activity coefficient, at a given value of $\dagger \theta$, will be greater than unity.

At electrodes where relatively large fractions of the surface are covered by specifically adsorbed species and mutual interactions between adsorbate molecules occur, the $\dagger a$ ratio will deviate from the corresponding $\dagger \theta$ ratio in a complicated manner.⁹ In the following development of charge-transfer kinetics the simple relation (25) will be utilized. The resulting rate equations will be strictly applicable only to electrode systems included in the three categories: (C-1) there is no specific adsorption except for the activated complex; (C-2) coverage by all adsorbed species is a small fraction of the total surface; (C-3) total surface coverage remains constant with no mutual interaction by adsorbed molecules.

Replacement of the activity ratio in (19) with the concentration ratio yields

$$\dagger c_c / \dagger c_{c,s} = \Pi \exp[-(\beta + \gamma)(n/\nu)\epsilon\eta + (\delta_s - \delta)/RT] \quad (27)$$

The concentration $\dagger c_{c,r}$ at the reversible potential is then

$$\dagger c_{c,r} / \dagger c_{c,s} = \Pi \exp[(\delta_s - \delta)/RT] \quad (28)$$

Similarly, for the anodic direction

$$\dagger c_a / \dagger c_{a,s} = \Pi \exp[(1 - \beta - \gamma)(n/\nu)\epsilon\eta + (\delta_s - \delta)/RT] \quad (29)$$

and

$$\frac{\dagger c_{a,r}}{\dagger c_{a,s}} = \Pi \exp\left[\frac{\delta_s - \delta}{RT}\right] = \frac{\dagger c_{c,r}}{\dagger c_{c,s}} \quad (30)$$

Rate Equations

The rate equations are obtained by substituting $\dagger c$ from (27) and (29) into (6)

$$r_c = (kT/h)\kappa_c \dagger c_{c,s} \Pi \exp[-(\beta + \gamma)(n/\nu)\epsilon\eta + (\delta_s - \delta)/RT] = i_c / (n/\nu)F \quad (31)$$

$$r_a = (kT/h)\kappa_a \dagger c_{a,s} \Pi \exp[(1 - \beta - \gamma)(n/\nu)\epsilon\eta + (\delta_s - \delta)/RT] = i_a / (n/\nu)F \quad (32)$$

where i_c and i_a are the rates expressed as current densities. The rate in either direction is proportional to Π ; hence, both rates have the same dependence on the activity of any substance taking part in reaction 1 whether reactant or product.

In the present formulation of the reaction rate, the activity coefficient of the activated complex enters as the ratio $\dagger f_s / \dagger f$, which is unity for all of the reaction categories treated. In the previous formulation^{2,3,6} this term appeared as a single activity coefficient, and, hence, within category C-3 (activity coefficient > 1) it would affect the reaction rate. The use of eq 24 to evaluate $\dagger a / \dagger a_s$ implies that the adsorbed species on the electrode surface obey the Langmuir isotherm. If another isotherm were obeyed instead (Parsons¹⁰ describes 10 common isotherms), the activity coefficient term could not generally be neglected. Here, it would be sufficient to derive $\dagger a / \dagger a_s$ and thence $\dagger f_s / \dagger f$ for the particular isotherm and insert the latter as a multiplying factor in the expressions for concentration of the complex (eq 27, 29) and reaction rate (eq 31, 32).

In contrast with previous formulations, the present one clearly demonstrates the independence of reaction rate on the reference zero of potential. The reaction rate is proportional to $\dagger c$ (eq 6) or to $\dagger a$, and the

(9) R. Fowler and E. A. Guggenheim, "Statistical Thermodynamics," Cambridge University Press, London, 1939, p 421.

(10) R. Parsons, "Proceedings of the Fourth Soviet Conference on Electrochemistry, 1956," Consultants Bureau, New York, N. Y., 1961, p 18.

latter was shown (eq 18) to be determined by the difference between two values of the single electrode potential, as well as by $\ddagger a_s$ which has a definite value fixed by the nature of the electrode reaction. Therefore the rate equations (31) and (32), which derive directly from (18), are independent of the selected reference potential level. The activation energy for the reaction, obtained from the variation of the rate constant with T (see below), must also be independent of reference potential level.

The effect of δ on reaction rate is now different from that derived by Parsons.³ The latter treatment yielded rates proportional to $\exp[-\delta/RT]$, so that δ affected the rate as long as its value was an appreciable fraction of RT . It is clear from the present formulation that δ can be large and still have little or no effect on the reaction if variations in T or composition produce relatively small changes in δ .

Exchange Currents

At the reversible potential $i_c = i_a = i_0$, the exchange current density; hence

$$\frac{i_0}{(n/\nu)F} = \frac{kT}{h} \kappa_c \ddagger c_{c,s} \Pi \exp\left[\frac{\delta_s - \delta}{RT}\right] = \frac{kT}{h} \kappa_a \ddagger c_{a,s} \Pi \exp\left[\frac{\delta_s - \delta}{RT}\right] \quad (33)$$

If the electrode is in its standard state, $\Pi = 1$, $\delta = \delta_s$, and the rate in either direction is given by the standard exchange current density $i_{0,s}$

$$i_{0,s}/(n/\nu)F = (kT/h)\kappa_c \ddagger c_{c,s} = (kT/h)\kappa_a \ddagger c_{a,s} \quad (34)$$

whence

$$\kappa_c \ddagger c_{c,s} = \kappa_a \ddagger c_{a,s} \quad (35)$$

Equation 33 may now be rewritten

$$\frac{i_0}{i_{0,s}} = \Pi \exp\left[\frac{\delta_s - \delta}{RT}\right] = (a_X^x a_B^b)^{(1-\beta-\gamma)/r} (a_W^w a_Y^y)^{(\beta+\gamma)/\nu} \exp\left[\frac{\delta_s - \delta}{RT}\right] \quad (36)$$

By combining (36) with (30) one obtains

$$i_0/i_{0,s} = \ddagger c_{c,r}/\ddagger c_{c,s} = \ddagger c_{a,r}/\ddagger c_{a,s} \quad (37)$$

and this with (35) gives

$$\ddagger c_{c,r}/\ddagger c_{a,r} = \ddagger c_{c,s}/\ddagger c_{a,s} = \kappa_a/\kappa_c \quad (38)$$

The last result expresses two conclusions concerning the electrode at any reversible potential. (1) The concentration of the cathodic activated complex will be equal to that of the anodic complex only when the transmission coefficients are equal. (2) The ratio of

these two concentrations is not changed by change in T or composition.

The concentration of the complex at the standard electrode, $\ddagger c_{c,s}$ or $\ddagger c_{a,s}$, may be considered the fundamental parameter of this modified general theory. Therefore a successful atomistic mechanism of a specific electrode reaction should be able to predict $\ddagger c_s$ and its temperature variation. The standard rate constant $i_{0,s}/(n/\nu)F$, which is proportional to $\ddagger c_s$ (eq 34), may be identified with the quantity $k_{s,h}$ introduced in 1954 by Delahay.¹¹

The rate equations may be written in terms of the standard exchange current density

$$i_c = i_{0,s} \Pi \exp[(\delta_s - \delta)/RT] \times \exp[-(\beta + \gamma)(n/\nu)\epsilon\eta] \quad (39)$$

$$i_a = i_{0,s} \Pi \exp[(\delta_s - \delta)/RT] \times \exp[(1 - \beta - \gamma)(n/\nu)\epsilon\eta] \quad (40)$$

For η negative, the net (positive) cathodic current density is $i = i_c - i_a$, or

$$i = i_{0,s} \Pi \exp\left[\frac{\delta_s - \delta}{RT}\right] \times \exp\left[-(\beta + \gamma)\frac{n}{\nu}\epsilon\eta\right] \left\{1 - \exp\left(\frac{n}{\nu}\epsilon\eta\right)\right\} \quad (41)$$

For η positive, the net (positive) anodic current density is $i = i_a - i_c$, or

$$i = i_{0,s} \Pi \exp\left[\frac{\delta_s - \delta}{RT}\right] \times \exp\left[-(\beta + \gamma)\frac{n}{\nu}\epsilon\eta\right] \left\{\exp\left(\frac{n}{\nu}\epsilon\eta\right) - 1\right\} \quad (42)$$

These equations are readily simplified for the following two groups of mechanisms. (A) All of the electrical work preceding and following the rate-determining step is proportional to the single electrode potential; $\delta = 0$ and (41) reduces to

$$i = i_{0,s} \Pi \exp\left[-(\beta + \gamma)\frac{n}{\nu}\epsilon\eta\right] \left\{1 - \exp\left(\frac{n}{\nu}\epsilon\eta\right)\right\} \quad (41A)$$

(B) No electrical work is involved in the steps preceding and following the rate-determining step; $\gamma = \delta = 0$ and

$$i = i_{0,s} \Pi' \exp\left[-\beta\frac{n}{\nu}\epsilon\eta\right] \left\{1 - \exp\left(\frac{n}{\nu}\epsilon\eta\right)\right\} \quad (41B)$$

where

$$\Pi' = (a_X^x a_B^b)^{(1-\beta)/r} (a_W^w a_Y^y)^{\beta/\nu}$$

(11) P. Delahay, ref 4, p 35.

Reaction Order

The exchange current density given by (36) is the basic experimental quantity for determining the order of the reaction, ω_J , with respect to any reactant J taking part in the reduction or the reverse (oxidation) reaction. Thus, for ion B

$$\omega_B = \left(\frac{\partial \ln i_0}{\partial \ln a_B} \right)_{T, a_{J \neq B}} = \frac{b(1 - \beta - \gamma)}{\nu} - \frac{1}{RT} \left(\frac{\partial \delta}{\partial \ln a_B} \right)_{T, a_{J \neq B}} \quad (43)$$

The anodic and cathodic reaction rates exhibit exactly the same dependence

$$\omega_B = \left(\frac{\partial \ln i_c}{\partial \ln a_B} \right)_{\eta, T, a_{J \neq B}} = \left(\frac{\partial \ln i_a}{\partial \ln a_B} \right)_{\eta, T, a_{J \neq B}} \quad (44)$$

Here it must be understood that values of i_c and i_a utilized in (44) are the total cathodic or anodic current densities, which for fast reactions at small η are not the experimentally observed net current densities. If activity coefficients of B are unknown, one may determine i_0 in solutions containing excess inert electrolyte in which the activity coefficient remains constant; then the concentration c_B may be substituted for a_B in (43) without error.

The reaction order with respect to reactant Y of the oxidation reaction is from (36)

$$\omega_Y = \frac{y(\beta + \gamma)}{\nu} - \frac{1}{RT} \left[\frac{\partial \delta}{\partial \ln a_Y} \right]_{T, a_{J \neq Y}} \quad (45)$$

The reaction order with respect to X or W is obtained similarly from i_0 . If one of the substances J has little effect on δ the reaction order reduces to the first term of the appropriate equation. The alternative definition of reaction order in terms of constant ($\epsilon_r + \eta$), *e.g.*, by Vetter,¹² leads to different values depending on whether the order is obtained from i_c or from i_a , an unnecessary complication. The experimental procedure for constant ($\epsilon_r + \eta$) is admittedly more direct since the reaction rate can be followed potentiostatically while incremental concentration changes are made to the solution. Only a minor change in procedure, however, may be required to obtain the measurements at constant η , namely, a corresponding change in potentiostat setting of $\Delta\epsilon_r$ applied as each concentration change is made.

The reaction order can also be determined experimentally by galvanostatic measurements. It is readily shown from (39) that, for an applied constant cathodic current in the Tafel region, the effect of varying the activity of any reactant, for example, ion B, is given by

$$\left(\frac{\partial \eta}{\partial \ln a_B} \right)_{i_0, T, a_{J \neq B}} = \frac{\omega_B}{(\beta + \gamma)(n/\nu)\epsilon} \quad (46)$$

where ω_B is the reaction order as determined potentiostatically. Similarly for constant anodic current in the Tafel region, the effect of any reactant, such as Y, is

$$\left(\frac{\partial \eta}{\partial \ln a_Y} \right)_{i_a, T, a_{J \neq Y}} = \frac{-\omega_Y}{(1 - \beta - \gamma)(n/\nu)\epsilon} \quad (47)$$

Activation Energy

The exchange current density is also the basic experimental quantity for determination of the characteristic activation energy

$$\left(\frac{\partial \ln i_0}{\partial T} \right)_{II} = \frac{E_{act}}{RT^2} \quad (48)$$

With (33) and (30) one obtains

$$E_{act} = RT + RT^2 \left(\frac{\partial \ln \ddagger c_{c,r}}{\partial T} \right)_{II} = RT + RT^2 \left(\frac{d \ln \ddagger c_{c,s}}{dT} \right) - (\delta_s - \delta) + T \left[\frac{\partial (\delta_s - \delta)}{\partial T} \right]_{II} \quad (49)$$

where $\ddagger c_{c,r}$ and $\ddagger c_{c,s}$ may be replaced by $\ddagger c_{B,r}$ and $\ddagger c_{A,s}$, respectively, without effect. This expression is quite different from that given by Bockris¹³ for the "virtual heat of activation," and unlike the latter it yields values independent of the reference potential level. Equation 49 shows that the experimental energy of activation may vary with solution composition. For the electrode in its standard state, $\delta = \delta_s$, and one obtains the standard activation energy

$$E_{act,s} = RT + RT^2 \left(\frac{d \ln \ddagger c_{c,s}}{dT} \right) \quad (50)$$

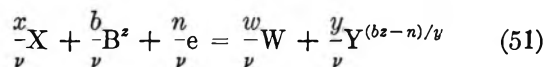
Other Mechanisms

The family of mechanisms to which the above development applies was restricted by specifying that the activated complex contain reactants X and B in the ratio $x:b$ and also that p and q comprise potential-dependent and composition-dependent portions having properties defined by the quantities γ and δ . In this section these restrictions will be removed to permit analysis of other classes of mechanisms.

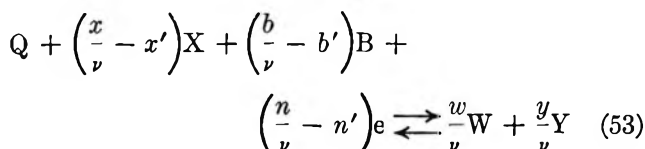
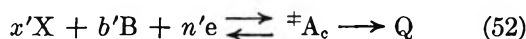
The over-all electrode reaction per mole of activated complex may be written

(12) K. J. Vetter, "Transactions of the Symposium on Electrode Processes," John Wiley and Sons, Inc., New York, N. Y., 1961, p 47.

(13) J. O'M. Bockris, *Mod. Aspects Electro-Chem.*, 1, 197 (1954).



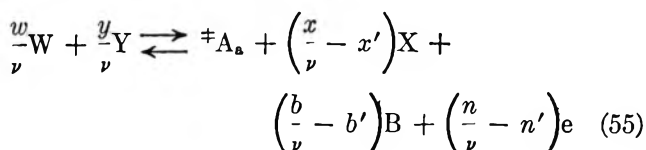
We will now permit the cathodic complex to be formed by reaction of $x' \leq x/\nu$ molecules of X, $b' \leq b/\nu$ molecules of B, and $n' \leq n/\nu$ electrons



The electrical work done in the rate-determining step, P \rightarrow Q, may be either finite (case A) or zero (case B). In either case the free energy of activation becomes, for the cathodic process

$$\ddagger \Delta G_c = \ddagger \Delta G_{c,s} + RT \ln \left[\left(\frac{\ddagger a_c}{\ddagger a_{c,s}} \right) a_X^{-x'} a_B^{-b'} \right] \quad (54)$$

For the anodic activation equilibrium



$$\ddagger \Delta G_a = \ddagger \Delta G_{a,s} + RT \ln \times \left[\left(\frac{\ddagger a_a}{\ddagger a_{a,s}} \right) a_X^{(x/\nu) - x'} a_B^{(b/\nu) - b'} a_W^{-w/\nu} a_Y^{-y/\nu} \right] \quad (56)$$

Case A. The electrical work done in the rate-determining step is finite. The free energy change for the equilibrium in (52) is still given by (12)

$$-\ddagger \Delta G_c = \beta(n/\nu)F\epsilon + (1 - \beta)p + \beta q \quad (57)$$

$$-\ddagger \Delta G_{c,s} = \beta(n/\nu)F\epsilon^\circ + (1 - \beta)p_s + \beta q_s \quad (58)$$

where p_s and q_s are the values of p and q when the electrode is in its standard state. With (57), (58), and (17) one obtains from (54)

$$\frac{\ddagger a_c}{\ddagger a_{c,s}} = \Pi'' \exp \frac{(1 - \beta)(p_s - p)}{RT} \times \exp \frac{\beta(q_s - q)}{RT} \exp \left[-\beta \frac{n}{\nu} \epsilon \eta \right] \quad (59)$$

where

$$\Pi'' = a_X^{x' - (\beta x/\nu)} a_B^{b' - (\beta b/\nu)} a_W^{\beta w/\nu} a_Y^{\beta y/\nu} \quad (60)$$

After equating this activity ratio to the concentration ratio and combining with (6) and (34), one obtains the cathodic rate equation

$$i_c = i_{0,s} \Pi'' \exp \frac{(1 - \beta)(p_s - p)}{RT} \times \exp \frac{\beta(q_s - q)}{RT} \exp \left[-\beta \frac{n}{\nu} \epsilon \eta \right] \quad (61)$$

For the reverse reaction

$$i_a = i_{0,s} \Pi'' \exp \frac{(1 - \beta)(p_s - p)}{RT} \times \exp \frac{\beta(q_s - q)}{RT} \exp \left[(1 - \beta) \frac{n}{\nu} \epsilon \eta \right] \quad (62)$$

At the reversible potential $p = p_r$, $q = q_r$, and the exchange current density given by (61) or (62) is

$$i_0 = i_{0,s} \Pi'' \exp \left[\frac{(1 - \beta)(p_s - p_r)}{RT} \right] \exp \left[\frac{\beta(q_s - q_r)}{RT} \right] \quad (63)$$

The rate equations, rewritten in terms of i_0 , become

$$i_c = i_0 \exp \left[\frac{(1 - \beta)(p_r - p)}{RT} \right] \times \exp \left[\frac{\beta(q_r - q)}{RT} \right] \exp \left[-\beta \frac{n}{\nu} \epsilon \eta \right] \quad (64)$$

$$i_a = i_0 \exp \left[\frac{(1 - \beta)(p_r - p)}{RT} \right] \times \exp \left[\frac{\beta(q_r - q)}{RT} \right] \exp \left[(1 - \beta) \frac{n}{\nu} \epsilon \eta \right] \quad (65)$$

A specific mechanism will dictate expressions for the exponentials containing p or q in terms of experimentally accessible parameters.

Case A-1. *Modified Frumkin Equation.* As an illustration we will apply these rate equations to the diffuse double layer effect treated by Frumkin,¹⁴ with discharge of ion B^{z+} as the rate-determining step. Here electrical work p results only from the movement of b/ν ions B through the diffuse double layer potential ψ , so that $p = bzF\psi/\nu$, where ψ will generally vary with the polarization η as well as with T and composition.¹⁵ Similarly, q results only from the movement of y/ν ions Y through the same potential difference; hence $q = (bz - n)F\psi/\nu$. Substitution for p and q in (61) and (62) yields

$$i_0 = i_{0,s} \Pi'' \exp[(bz - \beta n)(\epsilon/\nu)(\psi_s - \psi)] \times \exp[-\beta(n/\nu)\epsilon\eta] \quad (66)$$

(14) A. N. Frumkin, *Z. Physik. Chem.*, **A164**, 121 (1933).

(15) R. Parsons, *Advan. Electrochem. Electrochem. Eng.*, **1**, 1 (1961).

$$i_a = i_{0,s} \Pi'' \exp[(bz - \beta n)(\epsilon/\nu)(\psi_s - \psi)] \times \exp[(1 - \beta)(n/\nu)\epsilon\eta] \quad (67)$$

If ψ varies appreciably with η , the electrode reaction rates will not obey the Tafel equation. These rate equations are not identical with the generalized Frumkin equations given by Parsons,¹⁵ the principal modification being that the quantity ψ in Parsons' equations is now replaced by $(\psi_s - \psi)$. Thus, for a range of solution composition over which $\psi_s - \psi$ remains small, even though ψ itself may be large, the diffuse double layer will have negligible effect on reaction rate.

At the reversible potential, $\psi = \psi_r$ and the exchange current density is

$$i_0 = i_{0,s} \Pi'' \exp[(bz - \beta n)(\epsilon/\nu)(\psi_s - \psi_r)] \quad (68)$$

In terms of i_0 the cathodic current density becomes

$$i_c = i_0 \exp[(bz - \beta n)(\epsilon/\nu)(\psi_r - \psi)] \times \exp[-\beta(n/\nu)\epsilon\eta] \quad (69)$$

and an analogous expression may be written for i_a .

The reaction order with respect to a given reactant may be obtained from (68). Thus, for ion B

$$\omega_B = b' - \beta b/\nu - (bz - \beta n)(\epsilon/\nu) \left[\frac{\partial \psi_r}{\partial \ln a_B} \right]_{T, a_{j \neq B}} \quad (70)$$

The experimental energy of activation, defined by (48), is also obtained from (68)

$$E_{act} = RT + RT^2 \left(\frac{d \ln i_{c,s}}{dT} \right) - \left(\frac{bz - \beta n}{\nu} \right) F \left[T \left\{ \frac{\partial(\psi_s - \psi_r)}{\partial T} \right\}_{T'} - \psi_s + \psi_r \right] \quad (71)$$

and is seen to vary with ψ_r , *i.e.*, with the particular solution composition selected for study.

Case B. The rate-determining step involves no electrical work; hence

$$p - q = (n/\nu)F\epsilon \quad (72)$$

This condition simplifies eq 8 to $-\ddagger\Delta G_c = p$; also

$-\ddagger\Delta G_{c,s} = p_s$. Substitution of these quantities into (54) yields

$$\ddagger a_c / \ddagger a_{c,s} = a_X^{x'} a_B^{b'} \exp \frac{p_s - p}{RT} \quad (73)$$

which leads to the cathodic rate equation

$$i_c = i_{0,s} a_X^{x'} a_B^{b'} \exp \frac{p_s - p}{RT} \quad (74)$$

Similarly for the anodic reaction $-\ddagger\Delta G_a = q$ and $-\ddagger\Delta G_{a,s} = q_s$; these values substituted into (56) yield

$$i_a = i_{0,s} a_X^{x' - (x/\nu)} a_B^{b' - (b/\nu)} a_W^{w/\nu} a_Y^{y/\nu} \exp \frac{q_s - q}{RT} \quad (75)$$

In this case also a specific mechanism will determine experimentally accessible expressions for the exponential term in each of the rate equations. These terms may be converted immediately if either $p = 0$ or $q = 0$. Thus, for $q = 0$ all of the electrical work of the reaction is given by $p = (n/\nu)F\epsilon$, so that (74) and (75) simplify to

$$i_a = i_{0,s} a_X^{x' - (x/\nu)} a_B^{b' - (b/\nu)} a_W^{w/\nu} a_Y^{y/\nu} = i_0 \quad (76)$$

$$i_c = i_0 \exp[-n\epsilon\eta/\nu] \quad (77)$$

Electrical work is done only during the cathodic activation; hence, only the cathodic current density depends upon the charge-transfer polarization. The reaction order, defined as in (43), for each participating substance is given by the exponent of the corresponding activity in (76). Similarly for $p = 0$ the rate equations become

$$i_c = i_{0,s} a_X^{x'} a_B^{b'} = i_0 \quad (78)$$

$$i_a = i_0 \exp(n\epsilon\eta/\nu) \quad (79)$$

and only the anodic current density is polarization dependent. Here the reaction order is simply x' with respect to X, b' with respect to B, and zero with respect to W or Y.

Acknowledgments. The author gratefully acknowledges fruitful discussions with Drs. L. S. Darken, R. P. Frankenthal, and R. A. Oriani of this laboratory.

Photocurrents at a Flash-Irradiated Mercury-Electrolyte Interface

by Paul Delahay^{1,2} and V. S. Srinivasan

Coates Chemical Laboratory, Louisiana State University, Baton Rouge, Louisiana 70803
(Received July 23, 1965)

Photocurrents at a flash-irradiated mercury-electrolyte interface were studied from potential-time variations under coulstatic conditions. Electrons, after thermalization and solvation, reacted with hydrogen ions as scavenger in acid solution. The Barker-Gardner dependence of the photocurrent on scavenger concentration was confirmed. The influence of the electrode potential is discussed qualitatively in terms of a field effect. The effect of the double layer structure was significant but did not lend itself to a Frumkin type of correction. The influence of the nature of the electrode was investigated for the thallium amalgam and was interpreted on the basis of the shift of the point of zero charge.

Introduction

At least two effects can be distinguished with a mercury-electrolyte interface upon ultraviolet irradiation of sufficiently short wavelength: (a) production of radicals, excited states, etc., in solution with subsequent electrode processes that do not occur in the absence of irradiation; (b) electron emission with subsequent reactions in solution. The first effect was studied in this laboratory³ by flash irradiation in 1955, but results could not be interpreted satisfactorily. More recent work, particularly by Berg (*cf.* bibliography⁴) has been more successful, and the problem is of current interest in several laboratories.^{5,6} The phenomena associated with electron emission were recently interpreted with great insight by Barker and Gardner.⁷ (See also Berg and Schweiss.⁴) An earlier interpretation⁸ based on a supposed effect of irradiation on the kinetics of hydrogen evolution at a mercury electrode was disproved by these authors, and results were interpreted, correctly it would seem, by a mechanism involving solvated electrons. The subject is of interest in relation to current extensive work on the solvated electron (*cf. e.g.,* Hart's review⁹), and the work reported here represents an attack by a novel approach.

The approach is as follows. A mercury electrode of constant area, in contact with the electrolyte being studied, is polarized with a potentiometer at an adjustable potential at which there is no significant faradaic process. The potentiometer circuit is opened, and the electrode is immediately flash-irradiated. The poten-

tial-time variations are measured at open circuit with a cathode-ray oscilloscope. (Reinmuth independently is using the same technique.¹⁰) Interference by the small drift of potential at open circuit, as a result of spurious faradaic processes, is virtually eliminated by a differential technique using the above flash-irradiated electrode and a similar nonirradiated electrode. The drift of potential is practically the same for both electrodes in the absence of irradiation, and a zero reading is observed. This approach is a natural outgrowth of coulstatic studies of electrode kinetics. The charging pulse, instead of being supplied by an outside source, as is done in electrode kinetics, is now generated by electron emission.

Experimental Section

Chemicals. Analytical reagents were used. Solu-

(1) Department of Chemistry, New York University, New York, N. Y. 10003.

(2) Send correspondence to this author.

(3) P. Delahay and W. Vielstich, unpublished work.

(4) H. Berg and H. Schweiss, *Electrochim. Acta*, **9**, 425 (1964).

(5) T. Kuwana, personal communication.

(6) R. A. Marcus, personal communication.

(7) G. C. Barker and A. W. Gardner, paper presented at the Moscow meeting of the International Committee of Electrochemical Thermodynamics and Kinetics (CITCE), Sept 1963. Some of this work was done a few years before 1963. These authors modulated irradiation and measured photocurrents with a square-wave polarographic technique.

(8) F. P. Bowden, *Trans. Faraday Soc.*, **28**, 505 (1931).

(9) E. J. Hart, *Science*, **146**, 19 (1964).

(10) W. H. Reinmuth, personal communication. No reference was made to the differential technique used here.

tions were prepared with double-distilled water and were treated by purified activated charcoal (Barker technique) to remove traces of adsorbable impurities. Oxygen was removed by Matheson high-purity nitrogen. Mercury was triple distilled. Thallium amalgams were prepared by electrolysis from $TlNO_3$ and were handled under nitrogen. They were analyzed as in a previous study.¹¹ The temperature was $25 \pm 2^\circ$.

Cell. The cell comprised two compartments—one with the flash-irradiated mercury pool in a cup (2.42 cm^2), the other with a nonirradiated mercury pool in a cup of approximately the same size. (The area need not be the same for both electrodes, as decay of potential at open circuit is independent of the electrode area for a plane electrode.) The cups were silicone coated and provided with an inlet for filling them with mercury. These two compartments were connected to a central compartment (no fritted-glass separators), the latter being connected by a bridge to a saturated calomel electrode which served as reference and counterelectrode. This electrode was prepared with KCl in all experiments except with perchlorate solutions, in which case NaCl was used. The three compartments were provided with inlets and outlets for deaeration by nitrogen. Care was taken between consecutive flashes to destroy any concentration gradient in solution by nitrogen bubbling.

Apparatus. The flash was generated by a General Electric Co. flash lamp (glass envelope removed), Type FT-503, connected to a Graflex (Rochester, N. Y.) Multistrob II unit. (This unit which was used in our 1955 work is no longer in production.) The flash intensity decayed somewhat irregularly and had practically died out in a few milliseconds. This rather long irradiation was of no consequence in this work. The power output of the flash unit was not known exactly but did not exceed 200 to 300 joules. Distance between the end of the lamp and the pool was approximately 10 cm.

The variation, Q , of the electrode charge caused by flashing was determined with the circuit of Figure 1. Flash experiments were run with S' open. The potential of e_1 and e_2 was set on P_1 with switch S in position 1. As S was turned from 1 to 2, the cells e_1 - e_3 and e_2 - e_3 were at open circuit; the flash unit and CRO were triggered simultaneously, an internal delay of approximately 1.5 msec prevailing in the flash unit. The resulting potential-time curve, during and after the flash, was observed on CRO (Figure 2). Photographic recording was not necessary in general as a constant potential was reached after a few milliseconds. The variation of potential, which was as

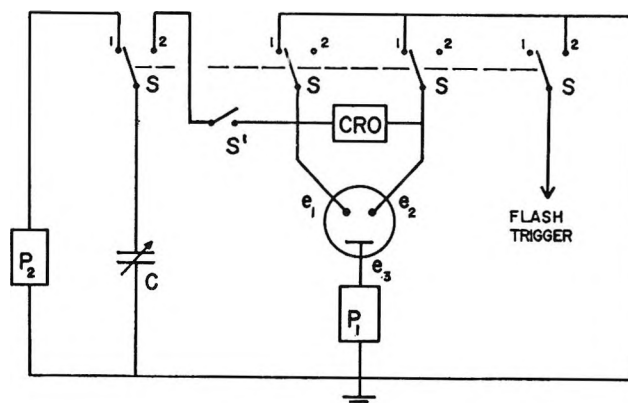


Figure 1. Circuit: e_1 , flash-irradiated mercury (amalgam) pool; e_2 , mercury (amalgam) pool; e_3 , reference electrode; P_1 , 0-2 v potentiometer; P_2 , 0-6 v potentiometer; S , quadruple-pole switch; CRO, Tektronix 535 oscilloscope with D plug-in unit; C , General Radio decade capacitor, Type 219-K.

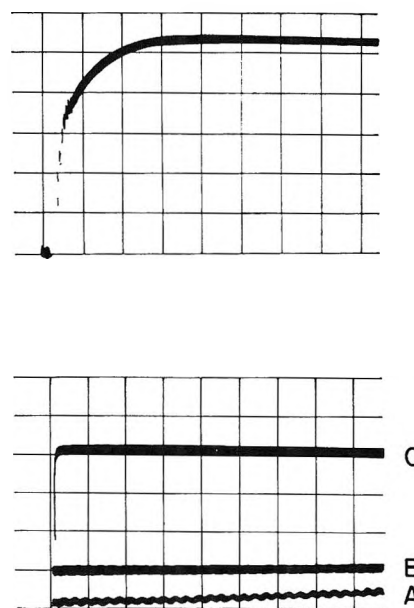


Figure 2. Top: tracing of oscillogram of potential-time variations with flash for 0.1 M HCl + 0.4 M NaCl at -0.5 v vs. sce. Scales: 0.5 msec and 10 mv per division, respectively. Bottom: same as top but for 0.01 M HCl + 0.49 M KCl at -0.7 v vs. sce. Scales: 50 msec and 20 mv per division, respectively. A, potential of e_1 against e_3 (Figure 1) without flash; B, differential signal between e_1 and e_2 without flash; C, same as B but with flash. This is an early oscillogram, in which ΔE exceeded the 50-mv limit discussed under the Experimental Section.

large as 50 mv for the highest photocurrent, resulted in some uncertainty about the actual potential to

(11) P. Delahay and M. Kleinerman, *J. Am. Chem. Soc.*, **82**, 4509 (1960).

which the Q reading pertained. All reported potentials are the initial values before flashing.

The charge was determined as follows. Switch S' was closed, and the flash unit was disconnected from the triggering circuit. The potentials of e_1 and e_2 , with switch S in position 1, were exactly the same as before flash irradiation. Turning S from 1 to 2 now caused the pulsing of e_1 by discharge of C . The known charge on C was adjusted, and pulsing was repeated until the potential variations caused by flashing or by charge pulsing were the same. Determination of the double-layer capacity was avoided in this method, and Q could be determined even when the double-layer capacity varied appreciably over the range of potentials being covered. The double layer capacity is not supposed to change significantly during photoemission. The effect of a variation of capacity caused by adsorption of impurities also canceled out since the same double-layer capacity prevailed in both determinations with and without flash. (Impurity adsorption, of course, would probably affect the phenomena being observed!) This technique could be developed in a zero-signal method by simultaneous flashing and charge pulsing causing compensating variations of potential. Compensation would be achieved after flashing because equal charges of opposite signs are supplied. However, compensation would not prevail during flashing because the time dependences of the two compensating effects are not the same, and the uncertainty about potential, referred to above, would not be avoided. The only simple solution seems to limit the variations of potential to 10 to 15 mv.

Results and Discussion

Dependence on Concentration of Solvated Electron Scavenger. The variation, Q , of the electrode charge during flashing was determined at different potentials for a solution containing hydrogen ion as solvated electron scavenger (Figure 3). (Photocurrent-potential curves having the same general shape as those of Figure 3 were reported by Berg and Schweiss.⁴) The maximum photocurrent density for Figure 3 is roughly 10^{-4} to 10^{-3} amp cm^{-2} , *i.e.*, about 10 to 100 times larger than the current densities measured by Barker and Gardner⁷ under continuous irradiation. Berg and Schweiss⁴ reported currents up to $3 \mu\text{a}$ with a flash-irradiated dropping-mercury electrode, *i.e.*, approximately 10^{-4} amp cm^{-2} . Higher current densities would be feasible with more powerful flashes, but care should be taken to avoid significant depletion of the solvated electron scavenger near the electrode under strong irradiation. A rough estimate showed that no

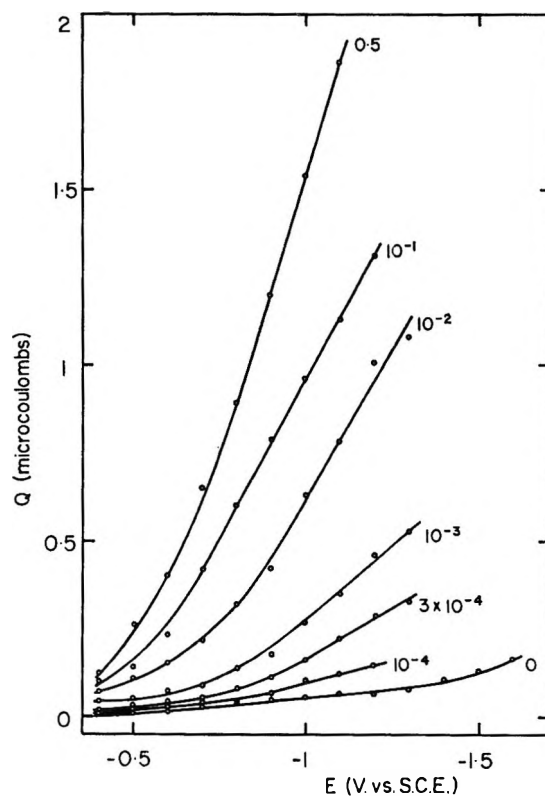
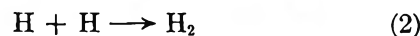
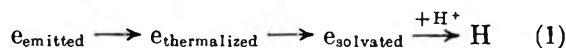


Figure 3. Variation of the charge on the electrode, caused by flashing, with potential for different concentrations of HCl (M). Total concentration is $0.5 M$, as made up with KCl.

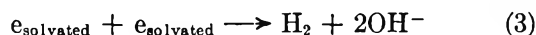
depletion prevailed in this work, even for the lowest acid concentration.

The dependence of Q at constant E on acid concentration can be interpreted on the basis of the following sequence according to Barker and Gardner⁷



Reaction 2 is so rapid that little, if any, H is lost by back-diffusion toward the electrode and subsequent anodic oxidation. H_2 cannot (thermodynamically) be oxidized at the prevailing potentials. The essential feature of this scheme is the removal of the product of the scavenger-solvated electron reaction by an *irreversible* process. If the product of this reaction were sufficiently stable and were oxidizable at the electrode, the photocurrent would be much smaller since the loss of electrons by the electrode during the flash would be compensated in a major part by an anodic process.

The blank is accounted for by: (a) scavenger impurities (notably O_2), (b) the H^+ from H_2O dissociation, and (c) the second-order decay of solvated electrons according to



The kinetics of this reaction is known.⁹ Q in this case is much lower than with acid present since most solvated electrons diffuse back to the electrode and are oxidized.

Barker and Gardner⁷ calculated the steady-state photocurrent by assuming thermalization of electrons at a fixed distance δ of the electrode (see Appendix). This treatment is similar to polarographic theory. Their result is immediately transposed to Q since this quantity is simply the integral of the photocurrent during the flash. Thus

$$\frac{Q}{Q^s - Q} = \delta \left(\frac{kc}{D} \right)^{1/2} \quad (4)$$

where Q^s is the saturation value of Q that would be observed for $c \rightarrow \infty$ (all emitted electrons reacting with the scavenger); k is the rate constant for the forward reaction between the solvated electron and H^+ ; c is the bulk H^+ concentration; and D is the diffusion coefficient of the solvated electron. The backward reaction between H^+ and the solvated electron is neglected. No mass transfer complication is supposed to prevail, *i.e.*, c at the electrode is independent of Q .

The model of Barker and Gardner⁷ is approximate, as they fully realized, since thermalization occurs over a range of distances from the electrode. Further, eq 4 applies to steady-state conditions, but this is really not a restriction for the conditions prevailing here because the reaction half-lives are very short in comparison with the flash duration. We solved the problem for transient response for an exponentially decaying flash, but the final result is quite cumbersome, and, at any rate, the actual flash decay was not truly exponential. We shall use eq 4, keeping in mind the restrictions just stated.

It follows from eq 4 that Q is proportional to $c^{1/2}$ for $Q \ll Q^s$. This is the case at different potentials, and the slope of the lines in Figure 4 is indeed 0.5 at the lower concentrations. As c increases, Q approaches Q^s , and the curves of Figure 4 level off. The value of Q^s was taken to be that of Q for $c = 0.5 M$ at each potential, as it was found that Q became virtually independent of c at higher concentrations. Actually, Q for $5 M \text{ HCl}$ was slightly lower than for $0.5 M$. A single line should be obtained according to eq 4 provided δ is independent of potential. (However, see below.) This is nearly the case and the slope is indeed 0.5 except for the highest concentration. The curvature near the highest concentration may be due in part to the uncertainty on Q^s . This curvature is certainly caused, at least in part, by the variation of

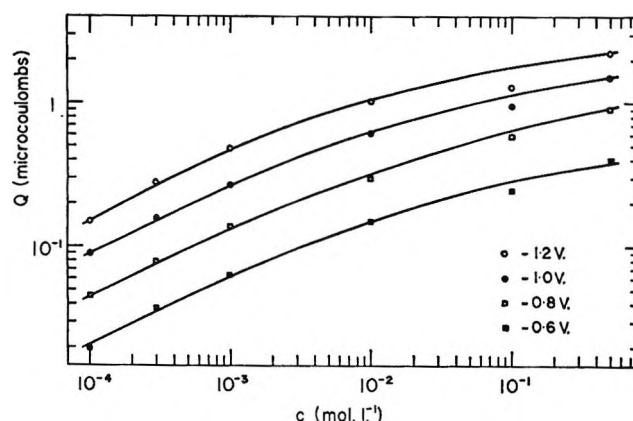


Figure 4. Log Q against log c at different E values (v vs. sce) for the data of Figure 3.

potential during the flash (see Experimental Section). The Q values in Figure 3 correspond to the initial E values before flashing whereas the actual potentials were somewhat ($\Delta E \leq 50$ mv) more positive. Since Q decreased when E became less negative, the values of Q in Figures 3 to 5 are too low, particularly for the higher Q values.

These results indicate excellent agreement between experiment and the Barker-Gardner equation.

Field Dependence. Figure 3 shows a gradual increase of Q as E becomes more negative, Q becoming measurable with sufficient precision for $E < -0.4$ v vs. sce for this particular solution. This observation agrees with previous work^{4,7} except that Barker and Gardner⁷ reported a decrease in the steepness of the photocurrent-potential curve at the more negative E values. Barker¹² pointed out that the tendency for dQ/dE to decrease at the more negative potentials may not be observed with polychromatic light if the incident energy decreases rapidly with decreasing wavelength in the 2500-3000-Å range. Our results, which are plotted as $Q^{1/2}$ vs. E in Figure 6, show hardly any decrease of dQ/dE except for the 0.1 and 0.5 M curves. The decrease for these two concentrations is due, in part or perhaps totally, to the experimental artifact discussed in connection with Figure 5, *i.e.*, the variation of E during the flash.

At least two reasons can be invoked for the field dependence: (a) space-charge effects and (b) influence of the field on photocurrents. Space-charge-limited currents do lead to a quadratic dependence on the field in some instances,¹³ but transposition of theory,

(12) G. C. Barker, private communication to P. D.

(13) A. Rose, "Concepts in Photoconductivity and Allied Problems," Interscience Publishers, Inc., New York, N. Y., 1963, pp 69-81.

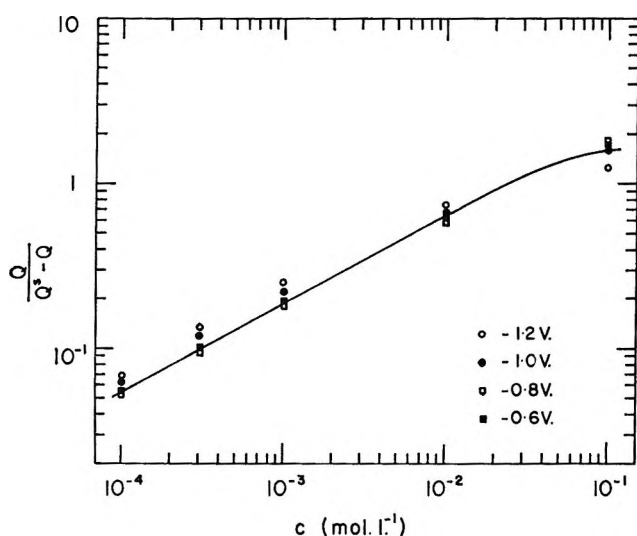


Figure 5. Plot of the data in Figure 3 according to eq 4. The Q values for $c = 0.5 M$ HCl were taken as Q^0 values.

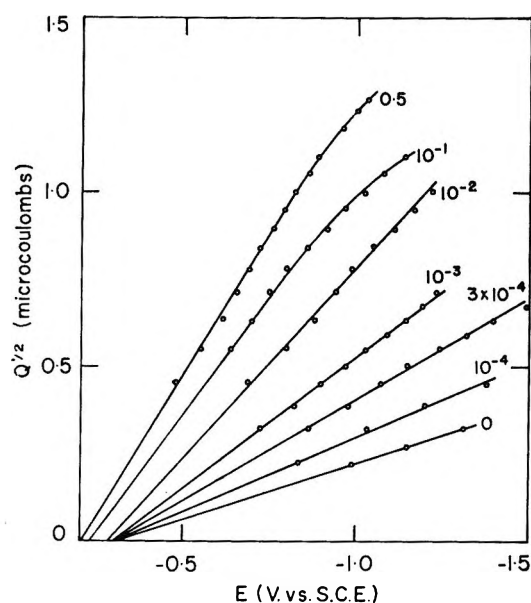


Figure 6. Plot of $Q^{1/2}$ against E for the data of Figure 3. Concentrations in moles per liter.

developed for dielectrics sparingly populated with charge carriers, to the metal-electrolyte interface does not seem justified. It is unlikely that the potential distribution be drastically affected by the photoemitted electrons. Field dependence of the photocurrent appears a more satisfactory explanation. Theory was worked out by Fowler¹⁴ for photoemission by a metal under vacuum and monochromatic irradiation. His predictions are borne out by experiment as was shown by Juenker and co-workers for accelerating

potentials. (See ref 15 as a source for other papers.) Experimental conditions in this work differ from those in the Fowler theory at least on two points: (a) emission in an aqueous electrolyte and (b) polychromatic irradiation. Thus, modification in theory may be necessary, and experiment with *monochromatic* radiation seems to be required. No particular significance can be attached at this time to the apparently quadratic field dependence as suggested in Figure 6. Likewise, no interpretation will be given of the intercept for $Q = 0$ in Figure 6 at this time. Further work toward the elucidation of the field dependence is planned.

Effect of Double-Layer Structure. The effect of the double-layer structure on photocurrents depends on the relative magnitude of two parameters: the distance δ defined in connection with eq 4 and the reciprocal Debye length $1/\kappa$ characterizing the diffuse double-layer structure. If $\delta \gg 1/\kappa$, no significant double-layer effect would be expected; *i.e.*, Q for a given scavenger concentration would be essentially independent of the supporting electrolyte concentration. Conversely, if δ were close to the distance of closest approach, a correction analogous to the Frumkin correction of electrode kinetics should apply. The situation is similar to double-layer effects in electrode processes with a coupled chemical reaction.¹⁶

A rather pronounced double-layer effect was observed in perchlorate medium. This electrolyte was selected to minimize specific adsorption. Results are displayed as plots of $Q^{1/2}$ against E in Figure 7. These plots are linear, just as in Figure 6. (The inversion of the 10^{-3} and $10^{-2} M$ lines is unexpected but is of no particular significance in view of the following comments.) The increase of Q , as the electrolyte concentration decreased, is to be expected since there is then increasing attraction of H^+ ions in the diffuse double layer. A decrease of Q similar to that in Figure 7 was also observed for $10^{-3} M$ HCl when electrolyte was added ($0.5 M$ KCl). This seems to rule out an interpretation based on inhibition by ClO_4^- or Cl^- or by some impurity.

These results are analyzed by analogy with the Frumkin correction and plots of $Q^{1/2} \exp[(F/4RT)\phi_2]$ against $E - \phi_2$ were prepared. There, ϕ_2 is the potential in the plane of closest approach and R , T , and F are as usual. A single line would have been expected

(14) R. H. Fowler, *Phys. Rev.*, **38**, 45 (1931).

(15) R. C. Jaklevic and D. W. Juenker, *J. Appl. Phys.*, **23**, 562 (1962).

(16) See, *e.g.*, P. Delahay, "Double Layer and Electrode Kinetics," Interscience Publishers, Inc., New York, N. Y., 1965, pp 207, 208, 227.

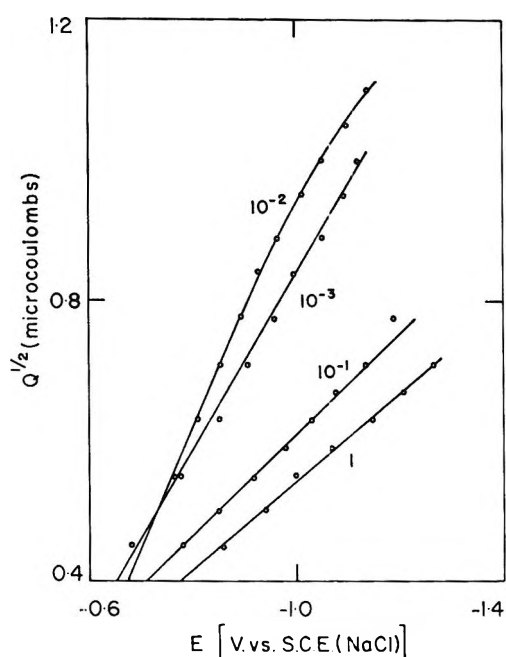


Figure 7. Plot of $Q^{1/2}$ against E for $10^{-3} M$ $HClO_4$ in $NaClO_4$. The number on each line is the total concentration in moles per liter.

at all concentrations, had the Frumkin correction been applicable. The resulting plots were not any closer to each other than in Figure 7. Plotting of $Q^{1/2}$ against $E - \phi_2$ did not result in any improvement. It is concluded that a double-layer effect must be reckoned with but that the Frumkin correction cannot be transposed. This is not unexpected since δ , according to Barker and Gardner,⁷ is possibly between 10 and 100 Å.

Because of the failure of the double-layer correction, we simply used E in the plot of Figure 6 rather than $E - \phi_2$. Logically, $E - \phi_2$ would give a better linearity with the field in the compact double layer than E , and the $Q^{1/2}$ vs. $E - \phi_2$ plots are indeed linear. When E is not near the point of zero charge (E_z), $|\phi_2| \ll |E - E_z|$ for an electrolyte which is not too dilute, and furthermore ϕ_2 does not vary rapidly with E . This is why we selected E rather than $E - \phi_2$ in Figure 6, as experimental errors, at this stage, prevent one from finding out whether E or $E - \phi_2$ ought to be used. Anyhow, theoretical work is necessary.

Influence of the Nature of the Electrode. Investigation was limited to the thallium amalgam for which the point of zero charge E_z can be varied by as much -0.4 v by adjustment of the thallium concentration.^{17,18} One would expect the shift of E_z toward more negative values to result in a corresponding shift of the plot of $Q^{1/2}$ against E . This was indeed the case,

and shifts of that order were observed with concentrated amalgams. However, results for the more negative potentials were quite erratic and the drift of potential at open circuit and without flash was much higher than for pure mercury, possibly because of hydrogen evolution on a somewhat contaminated electrode. (This could also result in a shift of the $Q^{1/2}$ vs. E line.)

Conclusion

Two aspects of this work appear of interest for future investigations: (a) the field dependence of photocurrents and (b) the application to the kinetics of scavenger-solvated electrons reactions. The first aspect has theoretical connotations and may be of interest in the study of the compact double layer. The kinetic aspect is of interest because of the simplicity of apparatus and the possibility of electrochemical study of reaction products. However, the more conventional approach involving electron irradiation with spectroscopic examination of kinetics is more straightforward (no complication caused by a heterogeneous interface). Anyhow, the kinetic aspects must be understood if field effects are to be examined. This work is continuing, and numerous problems posed by this and previous studies^{4,7} are or will be attacked: effect of the electrode, of the electrolyte, and of the solvent (nonaqueous solvents and molten salts), kinetics, field effect, wavelength, etc. In brief, this work poses some interesting problems; it gives a way of attacking them, and it provides some insight into what happens.¹⁹

Acknowledgment. This work was supported by the National Science Foundation. The authors are indebted to Dr. G. C. Barker for an extended abstract of his paper.⁷ Dr. A. M. Giuliani made the double-layer measurements and calculations for the experiment in perchlorate medium. P. D. is indebted to Professor M. Pope, Physics Department, New York University, for a most helpful discussion of field effects.

Appendix

Since the derivation of Barker and Gardner is available only in an unpublished extended abstract,⁷ their treatment leading to eq 4 above will be outlined.

(17) A. N. Frumkin and A. Gorodetskaya, *Z. Physik. Chem.*, **A136**, 451 (1928).

(18) J. N. Butler, *J. Electroanal. Chem.*, **9**, 149 (1965).

(19) NOTE ADDED IN PROOF. Theoretical calculations have now been made of the photocurrent and tunneling current and of the corresponding transmission coefficients (G. G. Susbielles and P. Delahay, unpublished investigation).

They write Fick's equation for diffusion with the additional term $-kcc_e$ where c_e is the concentration of the solvated electron and k and c are defined above. They assume that solvated electrons diffuse toward the solution from a plane at the fixed distance δ from the electrode and obtain for the steady-state photocurrent

$$i = Fc_e^\delta(kcD)^{1/2} \quad (5)$$

where F is the faraday, c_e is the value of c_e in the plane at the distance δ , and D is the diffusion coefficient of the solvated electron. The main simplifications made

in arriving at eq 5 are mentioned in connection with eq 4.

The concept of saturation current i^s , *i.e.*, the current for $kc \rightarrow \infty$, is then introduced, and c_e is calculated as a function of i^s by the same approach as in polarography. Thus

$$c_e^\delta = \frac{\delta}{FD}(i^s - i) \quad (6)$$

Since eq 5 and 6 correspond to steady-state conditions, Q and Q^s of eq 4 are proportional to i and i^s , respectively, and eq 4 follows immediately.

The Conductance of Dilute Solutions of Lithium in Liquid Ammonia at -71° ^{1,2}

by E. Charles Evers and Frederick R. Longo

The John Harrison Laboratory of Chemistry, University of Pennsylvania, Philadelphia, Pennsylvania
(Received July 26, 1965)

The conductance of solutions of lithium in liquid ammonia at -71° has been measured from 0.000309 to 0.14 *N*. The results are compared with the data for sodium in liquid ammonia at -34° and for lithium in methylamine at -78° . A mechanism for conduction based on the inversional motion of the ammonia molecule is proposed for dilute metal solutions.

The properties of metal-amine solutions have been investigated extensively for many years. Unfortunately, because these systems are metastable and the reaction between metal and ammonia is subject to catalysis, it has been difficult to obtain precise data in very dilute solutions; however, such data are essential since these solutions represent a region in which the systems exhibit quasi-electrolytic properties that gradually transform into those representing a metallic system as the metal concentration is increased. If we may assume that the metal solutions at low concentrations do conform to laws which govern the behavior of normal electrolytes, then, by measurement of various physical properties, it should be possible to establish some mode of the electrical interactions which occur among the species. One method of approaching this

problem is to study the conductance of these systems as a function of solute concentration, for, in the case of electrolytes, we have a fairly comprehensive theory of the interaction of ions subject to various parameters such as temperature and dielectric constant.

Precise conductance data have been reported for very dilute sodium in ammonia solutions by Kraus³ and lithium in methylamine solutions by Berns, Evers, and Frank.⁴ These data have been analyzed^{4,5} using a

(1) Taken in part from a thesis by F. R. Longo, presented in partial fulfillment of the requirements of the Ph.D. degree, Dec 1962.

(2) Sponsored in the main by the Office of Ordnance Research, U. S. Army, and partially by the Advanced Research Project Agency, Contract SD-69.

(3) C. A. Kraus, *J. Am. Chem. Soc.*, **43**, 749 (1921).

(4) D. S. Berns, E. C. Evers, and P. H. Frank, Jr., *ibid.*, **82**, 310 (1960).

conductance function based upon a modified form of the Shedlovsky⁶ equation for conductance and a mass action model proposed by Becker, Lindquist, and Alder.⁷ An equation relating the conductance to the two equilibrium constants for the reactions proposed by Becker, *et al.*, is

$$\frac{1}{\Lambda S(Z)} = \frac{1}{\Lambda_0} + \frac{S(Z)Nf^2\Lambda}{\Lambda_0^2k_1} \left[1 + \frac{2k_2^2\Lambda^2S(Z)^2N^2f^2}{k_1\Lambda_0^2} \right]$$

where Λ is the equivalent conductance, Λ_0 is the equivalent conductance at infinite dilution, $S(Z)$ includes mobility corrections as defined by Shedlovsky, f is the mean ionic activity coefficient for the ionized metal, N is the normality, k_1 is the equilibrium constant for the ionization, $M = M^+ + e^-$, and k_2 is the equilibrium constant for the dimerization, $M = 0.5 M_2$.

More recently, Dewald and Dye⁸ have reported a conductance study of dilute solutions of alkali metals in ethylenediamine at room temperature. They noted that solutions in this solvent are less stable than those in ammonia or methylamine. The data were treated by the Shedlovsky analysis, and values for Λ_0 and the ionization constant were obtained for solutions of cesium, potassium, and rubidium. These values were compared with those calculated by Evers, *et al.*, for Na in NH₃ and Li in MeNH₂. Dewald and Dye⁹ augmented their conductance studies with a spectral investigation and, on the basis of this work, have concluded that amine solutions differ essentially from ammonia solutions.¹⁰ They postulate the existence of "gaslike covalent dimers and electrons trapped by one-electron bonded M_2^+ ions," in addition to the species which are generally accepted as being present in ammonia solutions.

In order to obtain further, precise data for dilute solutions it was decided to measure the conductance of solutions of lithium in liquid ammonia. At -34° decomposition was so rapid in dilute solutions that it was not possible to obtain reproducible results; hence, the measurements were finally made at -71° . The data obtained are compared with the data for sodium in liquid ammonia at -34° and for lithium in methylamine at -78° .

Experimental Section

At -71.0° the rate of decomposition was negligible provided that extreme care was taken to guarantee the cleanliness of the equipment, but even at this low temperature it was noted that the shiny platinum electrodes became blackened during some experiments. The black material could not be removed by strong mineral acids or by alcoholic KOH. However, it

was found that the electrodes could be cleaned by electrolysis in concentrated HCl solutions.

The conductance cells used in this investigation were large enough to accommodate 1 l. of solution. The bright platinum ball electrodes, previously described by Hnizda and Kraus,¹¹ were small in area, and the cell constants varied from 1 to 2 cm⁻¹. The cell was filled with a 50 vol % mixture of concentrated sulfuric acid and fuming red nitric acid and steamed out before using. The cell constants are determined by established procedures.¹²

A thermocouple well was sealed through the body of the cell in such a way that the temperature could be measured close to the electrodes. A 23-mm Pyrex tube rose vertically from the top of the cell and communicated with a "doser" stopcock assembly which was used to provide the cell with weighed samples of lithium. The cell also communicated with the vacuum system through this tube. The entire cell, including electrodes, was sealed through a desiccator-like lid. The lid was then cemented with black Apiezon wax to a large jar which served as a bath for temperature control. Details concerning construction may be found in the thesis by Longo.¹

Measurements were made at $-71.00 \pm 0.03^\circ$. This temperature was maintained by controlling the vapor pressure of CHF₂Cl (Freon 22), which was distilled into the bath around the conductance cell. The bath was stirred by permitting a stream of Freon vapor to pass through the liquid at all times. The vapor pressure of this liquid was controlled at approximately 145 ± 0.05 mm with the use of a Micro-Set Manostat (Catalog No. 63273, Precision Scientific Co.). A copper-constantan thermocouple was used for temperature measurements in conjunction with a Leeds and Northrup portable precision potentiometer, Model No. 8662.

Lithium was obtained from the Lithium Corp. of America, (analysis: Li, 99.95; Na, 0.005; K, 0.01; Cu, 0.002; N, 0.01; Fe, 0.01; Si, 0.002; Cl, 0.001%). Metal samples were cut under argon-saturated mineral oil in a heavy petri dish. The cut samples were taken from the mineral oil with forceps and placed in a

- (5) E. C. Evers and P. H. Frank, Jr., *J. Chem. Phys.*, **30**, 61 (1959).
- (6) T. Shedlovsky, *J. Franklin Inst.*, **225**, 739 (1938).
- (7) E. Becker, R. H. Lindquist, and B. J. Alder, *J. Chem. Phys.*, **25**, 971 (1956).
- (8) R. R. Dewald and J. L. Dye, *J. Phys. Chem.*, **68**, 128 (1964).
- (9) R. R. Dewald and J. L. Dye, *ibid.*, **68**, 121 (1964).
- (10) R. R. Dewald and J. L. Dye, *ibid.*, **68**, 135 (1964).
- (11) V. F. Hnizda and C. A. Kraus, *J. Am. Chem. Soc.*, **71**, 1956 (1949).
- (12) E. C. Evers and A. G. Knox, Jr., *ibid.*, **73**, 1739 (1951).

bottle, where the mineral oil was washed away with dry toluene by a procedure described by Longo.¹

After being washed, the lithium samples were transferred under argon into weighing bottles which were designed to fit on a vacuum system. The toluene was pumped off, the samples were weighed under vacuum, and transferred into the four doser stopcocks under an argon atmosphere. For solutions of higher concentration, a large metal sample was sealed in a side arm above the cell. It was pushed into the cell with a glass-covered magnet.

Ammonia was obtained from the National Ammonia Co. (The company furnished the following analysis: H₂O, 50 to 100 ppm; hydrocarbon oils, 3 ppm; non-volatiles, 1 ppm.) It was purified in a manner which was previously found successful for monomethylamine.⁴

The bath was filled with Freon 22 by distillation from a commercial cylinder. Ammonia was condensed in the cell from a weighed storage can and was stirred by an externally driven glass-covered magnet. The vapor pressure of the Freon was adjusted, and the ammonia came to temperature equilibrium within 1 hr after the distillations.

The lithium samples were dropped individually from the four doser stopcocks. The resistances of the resulting solutions were measured at 2000 cps with a Leeds and Northrup Jones bridge using earphones as a null detector.

The concentration of metal is reported in g-atoms of metal per liter of solvent. For the calculation of solvent volume, the density data of Cragoe and Harper¹³ were used.

In order to apply the method of Evers and Frank⁵ it was necessary to know the dielectric constant and viscosity coefficient of the solvent. The dielectric constant was obtained by a graphical interpolation of data in the literature covering the temperature range from -77.70 to 35° .¹⁴ At -71.0° , the dielectric constant, D , is 25.1. Using the method of Nissan,¹⁵ we calculated the viscosity at -71° by extrapolation of the data of Fredenhagen¹⁶; at -71.0° , $\eta = 0.00500$ poise.

Discussion

Figure 1 is a plot of Λ vs. \sqrt{N} for the conductance of Li in liquid ammonia at -71° . At the lowest concentration measured, $0.000309 N$, the value of Λ is 445 Kohlrausch units. The equivalent conductance decreases sharply with increasing metal concentration until it reaches a minimum value of about 220 at approximately $0.025 N$. From this point it rises to a value of 304 at $0.14 N$, the concentration at which a

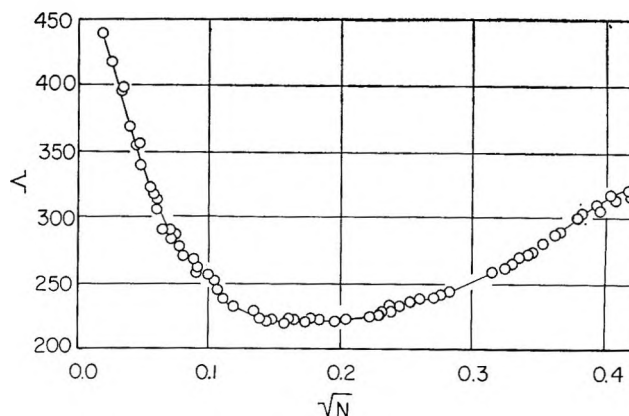


Figure 1. Λ vs. \sqrt{N} for Li in liquid NH₃ at -71° .

second liquid phase was observed to separate.¹⁷ A plot of the conductance data for this system at concentrations below the minimum is formally similar to that obtained for other metal-amine systems which have been studied and for normal electrolytes. The method of Evers and Frank⁵ was applied to the conductance data. A fit of the data to their function requires that $\Lambda_0 = 558.70 \pm 15.90$, $k_1 = 1.28 \pm 0.16 \times 10^{-3}$, and $k_2 = 4.33 \pm 1.29$.

A comparison of the experimental data with calculations from the above function is shown graphically in curve 2, Figure 2, where Λ/Λ_0 is plotted vs. the square root of the concentration. The solid line was calculated from the function, and the open circles are experimental data. The agreement is fairly good up to $0.02 N$, the highest concentration shown. The significance of the other plots in Figure 2 will be discussed below.

Also given in Figure 2 are plots for sodium in liquid ammonia at -34° , curve 1, and for lithium in liquid methylamine at -78° , curve 3.

Table I summarizes some of the important results derived from conductance measurements in various systems, which have been treated according to the method of Evers and Frank. In this table are presented the equivalent conductance at infinite dilution,

(13) C. S. Cragoe and R. Harper, National Bureau of Standards, Scientific Papers, No. 420, U. S. Government Printing Office, Washington, D. C., 1921, p 313.

(14) National Bureau of Standards Circular 514, U. S. Government Printing Office, Washington, D. C.

(15) A. H. Nissan, *Phil. Mag.*, **32**, 441 (1941).

(16) K. Fredenhagen, *Z. Anorg. Allgem. Chem.*, **186**, 1 (1930).

(17) P. D. Schettler, Jr., and A. Patterson, Jr., *J. Phys. Chem.*, **68**, 2865 (1964), have recently reported results of a phase study of the Li-NH₃ system. They found that at -70° , the concentration at which a second liquid phase appears is $1.6 M$. Furthermore, Sienko, "Metal-Ammonia Solutions," G. Lepoutre and M. J. Sienko, Ed., W. A. Benjamin, Inc., New York, N. Y., 1964, has reported that separation occurs at about $2 M$ at this temperature.

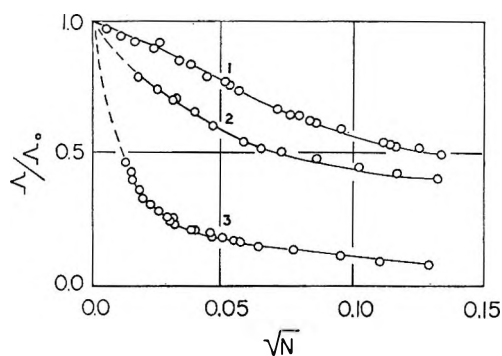


Figure 2. Curve 1: Na in NH₃ at -34°. Curve 2: Li in NH₃ at -71°. Curve 3: Li in CH₃NH₂ at -78°.

Λ_0 , the equilibrium constants for the ionization and dimerization processes, k_1 and k_2 , and the Walden product $\Lambda_0\eta_0$. Also listed are properties of the solvents, the viscosity coefficient η , and the dielectric constant D .

Table I: Constants Derived from Conductance Data

	System		
	Na-NH ₃ , -34°	Li-MeNH ₂ , -78°	Li-NH ₃ , -71°
Λ_0	1022.0	228.3	558.7
Concn. at minimum	0.04	0.13	0.025
Λ minimum	540	17	220
10^3k_1	7.23	0.0479	1.28
k_2	27.0	5.42	4.33
Solvent $\eta \times 10^3$	2.54	9.12	5.00
Solvent D	22	17.12	25.1
$\Lambda_0\eta_0$	2.6	2.1	2.8

The conductance of sodium in ammonia at -34° is approximately twice the conductance of lithium in ammonia at -71° at corresponding metal concentrations, a result not evident from the plot because the values of Λ have been divided by the respective Λ_0 values. The slope of the curve in the dilute region is steeper at -71°. Another important aspect is the position of the minimum. For sodium in ammonia at -34°, it occurs at 0.04 N and for Li in ammonia at -71° it occurs at 0.025 N . In an attempt to interpret these observations, we have assumed that dilute lithium and sodium solutions possess identical electrical properties at -34° since data which are available³ for lithium indicate that the conductance values are approximately equal; also the equivalent conductance curves are approximately parallel. These data suggest that at -34° the values of k_1 for sodium and lithium solutions are approximately equal.

The fact that the conductance is higher at the higher temperature indicates that the system is predominantly nonmetallic. This conforms to the idea of quasi-electrolytic behavior where conductance is enhanced by an increase in temperature. This is also supported by the fact that the data seem to be in fair agreement with Walden's rule; *i.e.*, $\Lambda_0\eta_0$ is fairly constant for these systems, suggesting that the conductance mechanism is viscosity dependent at infinite dilution.

The steeper slope for the curve for lithium in ammonia at -71° (Figure 2) indicates that the efficiency of conduction is decreasing more rapidly with concentration at this temperature. This may be interpreted as being due to different causes depending upon the model considered. Using the model of Becker, *et al.*, and discounting the concentration of dimers in this dilute region, one may contend that the equilibrium $M = M^+ + e^-$ determines the state of the system. According to Becker, *et al.*,⁷ this ionization is endothermic by about 0.1 eV, and therefore the equilibrium constant, $k_1 = (\text{slope } \Lambda_0^3)^{-1}$, should be lower at -71° than at -34°. It is not possible to compare the constants k_1 (-34°) and k_1 (-71°) because data for lithium in ammonia at -34° are not available at sufficiently low concentrations. However, since there is not too great a difference between the conductance of sodium and lithium solutions at -34°, one might use Evers' value for sodium-ammonia at -34°. He found k_1 (-34°) = 7.23×10^{-3} , and from this investigation k_1 (-71°) = 1.28×10^{-3} . The values of k_1 can be used to obtain the energy of ionization. The result is 0.2 eV and is in fair agreement with the value of Becker, *et al.*

The behavior of the three systems is in qualitative agreement with predictions based on electrolyte theory for dilute solutions. Table I and Figure 2 show that parameters such as temperature, viscosity, and dielectric constant affect the conductance in a manner which we would predict to be normal for electrolytes of classes such as weak acids in water, *e.g.*, HIO₃. However, we feel that the minimum must be attributed to causes other than those ascribed to electrolytic solutions. We agree with others that this may be attributed to the onset of metallic character which depends upon a relatively small separation of metal ions and a fairly regular, periodic-potential field. The minimum value of Λ found in this investigation occurs at 0.025 N which corresponds to an average distance between metal atoms of approximately 37 Å. This distance is too great to allow ordinary metallic conduction, but the separation of a golden phase at low concentration (0.14 N) suggests that "cybotactic metallic groups" are present before phase separation is observed.

If these groups begin to form well below 0.025 *N*, the minimum and the eventual increase in Λ are easily understood since the electrical conductance of such groups would be very high.

Conductance minima occur, respectively, at concentrations of 0.025, 0.04, and 0.13 *N* in Li-NH₃ (-71°), Na-NH₃ (-34°), and Li-MeNH₂ (-78°). This is exactly what might be expected if one considers the effect of temperature and the nature of the solvent molecules on the formation of a metallic structure. A lower temperature would favor order, but the unsymmetrical MeNH₂ molecules would oppose this. Hence, metallic structure is more easily achieved in NH₃ than in MeNH₂ and more readily at -71° than at -34°.

The values of k_2 calculated from the Evers and Frank⁵ conductance function must be suspected since the dimerization equilibrium becomes important only above concentrations where the calculated activity coefficients and the mobility corrections apply. However, if the relative values of k_2 are meaningful, they indicate that lithium solutions in methylamine at -78° and in ammonia at -71° have a smaller tendency to dimerize than the sodium-ammonia solutions at -34°. This is not in disagreement with paramagnetic susceptibility data^{18,19} which indicate that the atomic susceptibility of lithium solutions is very high.

A Model for the Dilute Region

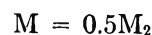
The nuclear magnetic resonance (nmr) investigations of McConnell and Holm²⁰ on solutions of sodium in ammonia at room temperature indicate a substantial Knight shift for the nitrogen nuclei and a definite, but much smaller, shift for sodium nuclei, whereas proton shifts are very small. Their data also indicate that in dilute solution the contact interaction between nitrogen nuclei and electrons is independent of metal concentration, but the interaction between sodium nuclei and electrons increases with increasing concentration.

The above considerations, together with others which will be discussed below, have suggested to us a conductance mechanism based on a cavity model in which the electron is in a molecular orbital on the nitrogen nuclei adjacent to the cavity. Our mechanism is based on an accepted molecular motion of the ammonia molecule, namely, inversion. When an ammonia molecule at the cavity wall undergoes inversion with the nitrogen atom moving toward the center of a trap, two events occur simultaneously: (1) the trap tends to collapse, and (2) an adjacent one tends to form. If the bulk solvent molecules near

the cavity are favorably oriented at the time of inversion the electron can be transported quickly and trapped in the new cavity adjacent to the collapsing one. Since several solvent molecules are involved in the cavity unit, the probability of this type of transport may be large.

Some support for the inversion mechanism comes from the fact that the inversional frequency ($4.5 \times 10^{10} \text{ sec}^{-1}$) is about equal to perturbation frequency ($3.5 \times 10^{10} \text{ sec}^{-1}$), as calculated by Kaplan and Kittel²¹ and by Pollak²² for rotation and diffusion of ammonia molecules at the cavity wall. Hence, if these workers had used inversional motion as the perturbation of the electron-nitrogen interaction, they would have obtained equally good agreement with experiment.

As the metal concentration increases from infinite dilution, it becomes probable that some of the ammonia molecules which normally are involved in the cavity unit are also participating in metal ion solvation. Metal ion solvation should impede the inversional motion of the ammonia molecule, and the equivalent conductance would be reduced. The aggregate of the cavity and metal ion is the formal equivalent of the monomer of Becker, Lindquist, and Alder⁷ and is very similar to the monomer proposed by Gold, Jolly, and Pitzer.²³ In dilute solution the monomer is considered to be participating in two equilibria, a dissociation and a dimerization



In the dimer some of the molecules which solvate a particular metal ion are present at two cavity walls.

It is obvious from the above equilibria that the success of the method of Evers and Frank⁵ in analyzing the conductance data can be explained equally well by this cavity model or by the model proposed by Becker, Lindquist, and Alder⁷ since the equilibria proposed are formally identical. Our model also conforms to the nmr implications which Pitzer²⁴ has discussed: the model must permit rapid exchange of

(18) A. Charru, *Compt. Rend.*, **247**, 195 (1958).

(19) R. A. Levy, *Phys. Rev.*, **102**, 31 (1957).

(20) H. McConnell and C. Holm, *J. Chem. Phys.*, **26**, 1517 (1957).

(21) J. Kaplan and C. Kittel, *ibid.*, **21**, 1856 (1953).

(22) V. L. Pollak, *ibid.*, **34**, 864 (1961).

(23) M. Gold, W. L. Jolly, and K. S. Pitzer, *J. Am. Chem. Soc.*, **84**, 2264 (1962).

(24) K. S. Pitzer, "Metal-Ammonia Solutions," G. Lepoutre and M. J. Sienko, Ed., W. A. Benjamin, Inc., New York, N. Y., 1964, p 193.

electrons between monomer and e^- species, and the monomer must be of such a nature that it will bring

the Na^{23} nucleus in contact with electrons without making an appreciable change in N^{14} -electron contact.

The Conductances, Viscosities, and Densities of Solutions of

Tetra-*n*-pentylammonium Thiocyanate in Nitrobenzene at 25^o

by Frederick R. Longo, James D. Kerstetter,
Thomas F. Kumosinski, and E. Charles Evers

Chemistry Department, Drexel Institute of Technology, Philadelphia, Pennsylvania, and
Harrison Laboratory of Chemistry, University of Pennsylvania, Philadelphia, Pennsylvania
(Received August 17, 1965)

The equivalent conductance of solutions of tetra-*n*-pentylammonium thiocyanate in nitrobenzene have been measured from 6.839×10^{-5} to 1.8275 *N*. The data for the dilute region were analyzed by the Fuoss-Onsager theory. The viscosity coefficients were determined between 0.03062 and 1.8513 *N*. The results are discussed in terms of the prevailing theory of electrolyte solutions.

Dilute electrolyte solutions have been studied quite thoroughly, both experimentally and theoretically for many years, and our understanding of such systems is quite good. However, only a few studies have been made of the physical properties of electrolyte solutions covering concentrations ranging from extremely dilute regions to the limit of solubility in one system.²⁻⁹

Recently,^{8,9} mechanisms have been proposed which qualitatively account for the properties of dilute and concentrated solutions in the nonpolar solvents benzene and *p*-xylene. An investigation in nitrobenzene would serve as a test of the generality of these ideas for, unlike benzene and *p*-xylene, nitrobenzene is polar and has a moderately high dielectric constant. Furthermore, since nitrobenzene is easily purified and has a low vapor pressure and a high resistivity, it is possible to obtain precise data in very dilute solutions where modern electrolyte theory may be used to interpret the behavior of the system.

Accumulating data on completely miscible systems seems to be the necessary first step in developing a good, phenomenological description which would be

adequate for a theoretical interpretation of the behavior of electrolyte solutions at higher concentrations. Therefore, we have initiated a project to study the physical properties of certain electrolyte solutions in nitrobenzene over as wide a range of concentrations

(1) Taken in part from research performed by J. D. Kerstetter in an undergraduate project supported by the National Science Foundation at Drexel Institute of Technology and from a thesis presented to the Graduate School of the University of Pennsylvania by F. R. Longo, 1962. F. R. L. wishes to acknowledge partial support from the Laboratory for Research on the Structure of Matter, University of Pennsylvania, during initial stages of this research.

(2) A. N. Campbell, A. P. Gray, and E. M. Kartzmark, *Can. J. Chem.*, **10**, 128 (1952).

(3) A. N. Campbell, A. P. Gray, and E. M. Kartzmark, *ibid.*, **13**, 617 (1953).

(4) M. L. Miller, *J. Phys. Chem.*, **60**, 189 (1956).

(5) R. P. Seward, *J. Am. Chem. Soc.*, **71**, 515 (1951).

(6) R. P. Seward, *ibid.*, **77**, 905 (1955).

(7) R. P. Seward, *J. Phys. Chem.*, **62**, 758 (1958).

(8) L. C. Kenausis, E. C. Evers, and C. A. Kraus, *Proc. Natl. Acad. Sci.*, **48**, 121 (1962).

(9) L. C. Kenausis, E. C. Evers, and C. A. Kraus, *ibid.*, **49**, 141 (1963).

Table I: The Conductance and Conductance-Viscosity Product for Tetra-*n*-pentylammonium Thiocyanate in Nitrobenzene at 25°

<i>N</i>	Λ	$10^2\Lambda\eta$	<i>N</i>	Λ	$10^2\Lambda\eta$
1.8275	0.3751	18.41	0.30916	8.084	19.16
1.8010	0.4084	18.26	0.26483	8.865	20.48
1.6826	0.5661	17.80	0.25755	9.013	20.64
1.6750	0.5816	17.80	0.21093	10.04	22.28
1.5406	0.7876	17.30	0.18057	10.84	23.51
1.5187	0.8248	17.24	0.15564	11.61	24.61
1.4145	1.046	16.90	0.13386	12.39	25.76
1.3718	1.154	16.66	0.11447	13.21	27.08
1.3395	1.241	16.65	0.10167	13.82	28.06
1.2615	1.458	16.62	0.091349	14.391 ^a	28.78
1.2338	1.533	16.48	0.088021	14.57	29.15
1.2109	1.611	16.45	0.074877	15.04	29.79
1.1531	1.801	16.14	0.069129	15.40	30.34
1.1090	2.001	16.39	0.053608	16.389 ^a	31.96
1.0890	2.083	16.31	0.043143	17.369 ^a	33.52
1.0490	2.228	16.31	0.041156	17.640 ^a	33.69
1.0027	2.370	16.31	0.034734	18.403 ^a	34.78
0.97773	2.482	16.25	0.034679	18.508 ^a	34.98
0.95414	2.602	16.29	0.029810	19.284 ^a	36.25
0.90540	2.834	16.35	0.026373	19.715 ^a	37.06
0.90104	2.844	16.27	0.026103	19.946 ^a	37.50
0.85765	3.082	16.37	0.020344	21.143 ^a	39.54
0.81586	3.296	16.25	0.015321	22.455 ^a	41.99
0.78049	3.509	16.28	0.013803	22.801 ^a	42.64
0.14045	3.755	16.15	0.011726	23.612 ^a	44.15
0.69592	4.061	16.32	0.0081622	25.032 ^a	46.56
0.68582	4.118	16.27	0.0056960	26.292 ^a	48.90
0.64673	4.401	16.55	0.0037258	27.604 ^a	51.07
0.59312	4.836	16.44	0.0028720	28.300 ^a	52.35
0.57091	4.983	16.59	0.0012525	29.821 ^a	55.17
0.51424	5.535	16.83	0.00068375	30.742 ^a	56.87
0.46947	5.969	16.77	0.00040663	31.517 ^a	58.31
0.44501	6.254	16.88	0.00019099	32.200 ^a	59.57
0.38206	6.999	17.71	0.000068394	32.643 ^a	60.39
0.38084	7.030	17.65	0	33.24	61.63
0.31380	8.031	19.19			

^a Resistance measured with the Jones bridge.

and temperatures as is experimentally attainable. This report concerns investigations carried out at 25°.

Experimental Section

Tetra-*n*-pentylammonium thiocyanate was prepared in 70 to 90% yields from the commercially available iodide salt by ion exchange on Amberlite resin (I.R.A.-400). This resin, supplied in the chloride form, was converted to the thiocyanate by treatment with aqueous NaSCN or KSCN, followed by elution with 96% ethanol. The desired product was obtained by the ion-exchange reaction with an ethanolic solution of the iodide. The thiocyanate was recrystallized to a constant melting point 50.5° from ethyl acetate-hexane mixtures at Dry Ice temperatures and was then stored in a vacuum desiccator.⁸

Fisher reagent grade nitrobenzene was purified by treatment with activated alumina according to a procedure described elsewhere.^{10a} The method produced a solvent having a specific conductance of 8 to 30 × 10⁻¹¹ ohm⁻¹ cm⁻¹.

The conductances of the solutions were measured in two different cells. An erlenmeyer cell having a cell constant of 0.10656 cm⁻¹ was used over the concentration range of 6.84 × 10⁻⁵ to 9.483 × 10⁻² *N*. A U-shaped cell,^{10b} whose constant was 14.72 cm⁻¹ was used over a higher range, 5.124 × 10⁻² to 1.83 *N*. This cell had facilities which permitted nitrogen gas mixing of the solution. A Leeds and Northrup Jones

(10) (a) F. R. Longo, Doctoral Thesis, University of Pennsylvania, (1962); (b) J. A. O'Malley, Doctoral Thesis, University of Pennsylvania, 1963, p 36.

conductivity bridge was used in conjunction with the erlenmeyer cell, while a Wayne Kerr universal bridge, Model No. B211, was used with the U-shaped cell. The cell constants were determined by the method of Lind, Zwolenik, and Fuoss.¹¹

Viscosities were determined with precalibrated Cannon-Ubbelohde viscometers, and flow times were measured with an electric timer to ± 0.05 sec. Densities were measured using a Christian-Becker specific gravity balance to ± 0.0002 density unit.

All measurements were made in oil baths at 25° with the temperature controlled to $\pm 0.01^\circ$. The solutions were prepared by weighing and were diluted to change the concentrations. At least two complete runs were made over the same concentration range for each kind of measurement.

Results

In Table I are presented the values of the equivalent conductance, Λ , and the product, $\Lambda\eta$, given at the normality, N , at which Λ was actually determined; $\Lambda\eta$ was calculated from the experimental value of Λ , and a value of the viscosity coefficient was interpolated from a large-scale plot. In Table II are given the experimental values of η .

The density of the solution is adequately described by the equation $d = 1.1974 - 0.1058N - 0.002163N^{3/2}$. This function was obtained by a least-squares analysis of 42 density determinations between $N = 0.00$ and $N = 1.8479$. The average deviation (of the calculated densities) from the experimental densities is 0.0003 density unit.

Discussion

A plot of equivalent conductance, Λ , vs. the square root of the concentration, \sqrt{N} (not shown), reveals that Λ is a linear function of \sqrt{N} up to approximately 0.006 N . Employing values of 0.018451 for the viscosity coefficient and 34.82¹² for the dielectric constant the Onsager equation for a completely dissociated electrolyte in nitrobenzene at 25° becomes $\Lambda = \Lambda_0 - (0.884\Lambda_0 - 45.6)\sqrt{N}$. Using the value of $\Lambda_0 = 33.44$ obtained from extrapolation of Λ vs. \sqrt{N} to $N = 0$, the theoretical slope is -75.17 , whereas the experimental slope is -95.17 . Thus, although Λ vs. \sqrt{N} is linear in dilute solution, short-range interactions occur between the ions giving rise to equilibria between ions and ion pairs. Kraus^{16,17} observed this behavior in nitrobenzene solutions of organic salts when one of the ions was relatively small, e.g., tetramethylammonium and tetra-*n*-butylammonium picrates.

A Shedlovsky¹³ analysis of the data yielded values

Table II: The Viscosity Coefficients for Tetra-*n*-pentylammonium Thiocyanate in Nitrobenzene at 25°

N	$10^3\eta$
1.8513	53.241
1.6326	27.139
1.4622	18.002
1.3275	13.008
1.2214	10.533
1.0891	7.8225
0.99731	6.7478
0.89012	5.5950
0.78660	4.6111
0.70653	4.0193
0.50815	3.0022
0.40684	2.5164
0.25903	2.2506
0.18036	2.0635
0.030618	1.8891
1.8334	49.937
1.7861	42.329
1.7592	38.278
1.7115	34.310
1.5276	21.638
1.4167	16.887
1.2603	11.844
0.94440	6.3006
0.86255	5.5102
0.60783	3.5195
0.35003	2.4853
0.17014	1.9811
0.000	1.8541

of 33.65 for Λ_0 and 62.7 for K_A , the association constant. Since K_A was less than 100, we analyzed the data on an IBM 1620 computer using Kay's Fortran program¹⁴ for the solution of the Fuoss-Onsager equation¹⁵ for associated electrolytes

$$\Lambda = \Lambda_0 - S(N\gamma)^{1/2} + EN\gamma \log N\gamma + \frac{JN\gamma - K_A\Lambda_0^2N\gamma}{JN\gamma - K_A\Lambda_0^2N\gamma}$$

From this analysis, we obtained values of $\Lambda_0 = 33.26$, $K_A = 37.02$, and $a = 6.1 \text{ \AA}$. (Also, $S = 69.47$, $E = 65.75$, $J = 588.6$, and $\partial J/\partial a = 74.80$.) The concentration range covered in this analysis was from 0.000068394 to 0.0056960 N .

(11) J. Lind, J. Zwolenik, and R. M. Fuoss, *J. Am. Chem. Soc.*, **83**, 1557 (1959).

(12) A. Maryott and E. Smith, "Tables of Dielectric Constants of Pure Liquids," National Bureau of Standards Circular 514, U. S. Government Printing Office, Washington, D. C.

(13) T. Shedlovsky, *J. Franklin Inst.*, **225**, 739 (1938).

(14) Dr. R. L. Kay of the Mellon Institute, Pittsburgh, Pa., kindly provided the Fortran program which was used in the analysis of our data.

(15) R. M. Fuoss and F. Accascina, "Electrolyte Conductance," Interscience Publishers, Inc., New York, N. Y., 1959.

We would expect a Fuoss-Onsager analysis of the data for $(n\text{-C}_4\text{H}_9)_4\text{NBr}$ to give results almost identical with those of $(n\text{-C}_5\text{H}_{11})_4\text{NSCN}$ since the values of Λ_0 and K_A as reported by Witschonke and Kraus¹⁶ are virtually equal to the values which we obtained from the Shedlovsky analysis of the data for the thiocyanate.

The values of many single-ion conductances at infinite dilution in nitrobenzene have been estimated previously.¹⁶⁻¹⁸ The value for $(n\text{-C}_5\text{H}_{11})_4\text{N}^+$ is 10.0 and therefore, from our study, Λ_0^- for SCN^- is 22.3, which is approximately equal to the values found for other small ions, like Cl^- , Br^- , I^- , NO_3^- , and BF_4^- , in nitrobenzene.

Figure 1 shows a plot of $\log \Lambda$ vs. $\log N$ over the range 6.839×10^{-5} to $1.827 N$. The equivalent conductance decreases sharply as the concentration increases above $0.01 N$ and drops to a value of 0.3751 near the limit of solubility.

Figure 2 is a plot of the $\Lambda\eta$ product as a function of concentration. The maximum value is 0.6163 at infinite dilution. The product drops sharply in dilute solution, reaching a minimum of approximately 0.163 at $0.6 N$; it then remains constant up to $1.2 N$. The value of $\Lambda\eta$ gradually increases to 0.184 near the limit of solubility. The general shape of the curve is not unusual except for the virtual linearity of the product over such a wide range. Miller⁴ has investigated concentrated aqueous solutions of NaSCN , NaI , and NaClO_4 at three temperatures and has reported that $\Lambda\eta$, plotted against concentration, goes through a minimum. He suspected that this was a result of the significant increase in the sodium ion transport number as the concentration increased near and above the minimum.

The conductance-viscosity studies of Seward⁵⁻⁷ on aqueous and nonaqueous systems over wide concentration ranges have shown that the behavior of the product as reported by Miller is quite general. Also, for solutions of tetra-*n*-butylammonium picrate at 90° , he found that the $\Lambda\eta$ product at infinite dilution was approximately equal to the value for the fused salt. He interpreted this as support for the hypothesis¹⁹ that fused electrolytes are completely dissociated and that addition of solvent to the pure, ionic liquid causes association.

The value of the Walden product at infinite dilution for *t*-pentylammonium thiocyanate in nitrobenzene at 25° is 0.6163. It would be interesting to compare this with the value for the fused salt, but this is impossible because the salt melts at 50.5° . However, the value of the Walden product for liquid $(n\text{-C}_5\text{H}_{11})_4\text{NSCN}$ supercooled to 25° can be estimated by ex-

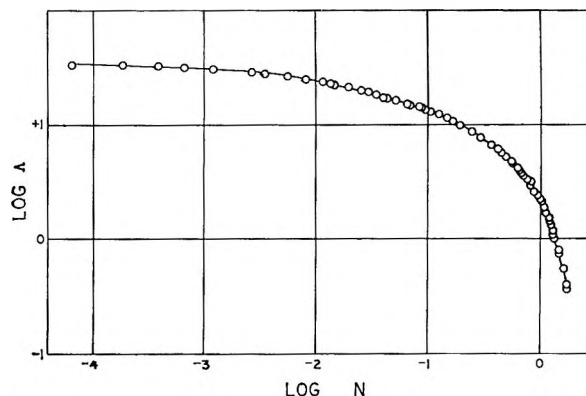


Figure 1. A plot of $\log \Lambda$ vs. $\log N$ for tetra-*n*-pentylammonium thiocyanate in nitrobenzene at 25° .

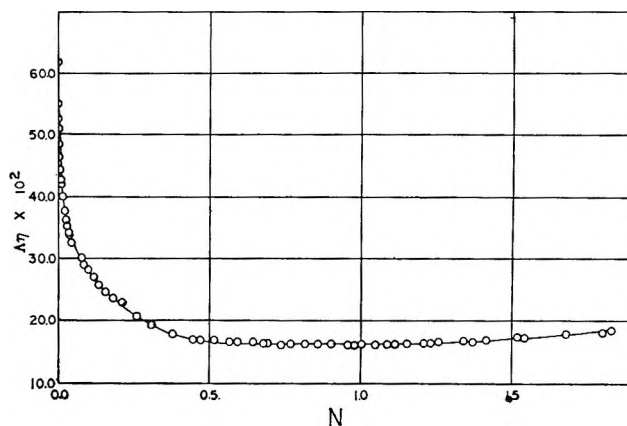


Figure 2. A plot of $\Lambda\eta$ vs. N for tetra-*n*-pentylammonium thiocyanate in nitrobenzene at 25° .

trapolation, using an equation given by Kenausis, Evers, and Kraus for this salt

$$\log \Lambda\eta = \frac{93.85}{T} - 0.6885$$

which gives $\Lambda\eta = 0.424$ at 25° . Hence, it is seen that the values of $\Lambda\eta$ for the fused salt and for its solution at infinite dilution are probably significantly different, which means Seward's observations may not be general. This is not surprising, for, if the equality of the Walden products for infinite dilution and the fused electrolyte infers that the fused electrolyte is completely dissociated, it seems reasonable that there would generally be a nonequality; the degree of dissociation of fused

(16) C. R. Witschonke and C. A. Kraus, *J. Am. Chem. Soc.*, **69**, 2472 (1947).

(17) E. G. Taylor and C. A. Kraus, *ibid.*, **69**, 1731 (1947).

(18) J. F. Coetzee and G. P. Cunningham, *ibid.*, **87**, 2529 (1965).

(19) L. E. Strong and C. A. Kraus, *ibid.*, **72**, 166 (1950).

electrolytes would depend on temperature and on the nature of the ions: their constitution, size, and charge. Seward studied solutions of tetra-*n*-butylammonium picrate, a 1-1 electrolyte in which both ions are relatively large and, therefore in which association would be less favorable. Kraus¹⁷ showed that this salt is a strong electrolyte in dilute nitrobenzene solutions, whereas we have shown that $(n\text{-C}_5\text{H}_{11})_4\text{NSCN}$ is appreciably associated under the same conditions. Therefore, it would be reasonable to assume that ionic interactions in fused $(n\text{-C}_5\text{H}_{11})_4\text{NSCN}$ at 25° would be greater than in fused $(n\text{-C}_4\text{H}_9)_4\text{NPI}$ at 90°.

Kenausis, Evers, and Kraus⁹ have investigated the system of tetra-*n*-pentylammonium thiocyanate in *p*-xylene at 52 and at 90°. They have attempted to explain the behavior of electrolyte solutions at very high concentration on the basis of a new mechanism:

in ultraconcentrated solutions (moles of solvent to moles of salt, N/n , equals 0.0 to 0.4), they proposed that the presence of a solvent molecule enhances ion-pair formation by distorting the symmetry of the fields about the ions. The fact that the ion-pair fraction in ultraconcentrated regions of their solutions is a linear function of N/n and is independent of temperature supports this idea. Unfortunately, the results of the present investigation cannot be a test of this mechanism since we could not reach the ultraconcentrated region due to solubility limitations. We have begun a study of nitrobenzene and *t*-pentylammonium thiocyanate solutions above the melting point of the electrolyte so that we might compare the effects of polar and nonpolar solvent molecules on ion-pair formation at very high concentrations. The results of this study will be reported shortly.

Heats of Immersion in the Thorium Oxide-Water System. II.

Net Differential Heats of Adsorption¹

by H. F. Holmes, E. L. Fuller, Jr., and C. H. Secoy

Reactor Chemistry Division, Oak Ridge National Laboratory, Oak Ridge, Tennessee (Received August 3, 1965)

Net differential heats of adsorption for water on thorium oxide were obtained from the integral heats of immersion of samples containing known amounts of presorbed water. The samples were prepared by the thermal decomposition of thorium oxalate and were carefully characterized as to purity, calcining temperature, particle size, and crystallite size. Surface areas ranged from 1.2 to 14.7 m²/g. Initial net differential heats of adsorption at low surface coverages ranged from -20 to -30 kcal/mole. In no case did the net differential heat of adsorption decrease to zero with the completion of the first adsorbed monolayer. The results are interpreted in terms of chemisorption involving the formation of surface hydroxyl groups with possibly additional contributions from hydrogen bonding. The samples showed marked dissimilarities with respect to surface heterogeneity.

Introduction

Previous work² has demonstrated that the heat of immersion of thorium oxide in water is dependent in a complex but reproducible manner on the specific surface area and crystallite size. A detailed investigation of this phenomenon requires the determination of the differential heat of adsorption as a function of the amount of adsorbed water. A convenient and conventional method for obtaining differential heats of adsorption is to measure the adsorption isotherms at two or more temperatures and then to apply the Clausius-Clapeyron equation to the adsorption data. However, heat data obtained from adsorption isotherms are often rendered invalid by such complicating factors as very low equilibrium pressures, irreversibility, extremely slow kinetics, and adsorption-desorption hysteresis. These factors become increasingly more difficult in those cases where chemisorption is involved. All of these difficulties have been shown to be present in the thorium oxide-water system.³

Heat of immersion calorimetry normally circumvents these difficulties. This technique involves measuring the integral heat of immersion as a function of the amount of presorbed immersion liquid. Differentiation of the resulting curve will then provide unambiguous values for the net differential heats of adsorption. The scope, advantages, and limitations of this type of

measurement have been reviewed by Zettlemyer and Chessick.^{4,5} A convenient classification of the various types of heat of immersion curves as a function of the amount of presorbed immersion liquid has been provided by these same authors.^{4,5} As examples of the success of this technique in systems similar to the present one, the determination of the differential heats of adsorption of water on alumina,⁶ silica,⁷ and titania^{8,9} may be cited.

Experimental Section

The calorimeter and its associated instrumentation and techniques were described in detail in a preceding publication.²

Materials. Samples A, B, C, and D were prepared

(1) Research sponsored by the U. S. Atomic Energy Commission under contract with Union Carbide Corp.

(2) H. F. Holmes and C. H. Secoy, *J. Phys. Chem.*, **69**, 151 (1965).

(3) E. L. Fuller, Jr., H. F. Holmes, and C. H. Secoy, to be published.

(4) A. C. Zettlemyer and J. J. Chessick, *Advances in Chemistry Series*, No. 43, American Chemical Society, Washington, D. C., 1964, p 88.

(5) J. J. Chessick and A. C. Zettlemyer, *Advan. Catalysis*, **11**, 263 (1959).

(6) R. L. Venable, W. H. Wade, and N. Hackerman, *J. Phys. Chem.*, **69**, 317 (1965).

(7) J. W. Whalen, *ibid.*, **65**, 1676 (1961).

(8) C. M. Hollabaugh and J. J. Chessick, *ibid.*, **65**, 109 (1961).

(9) W. D. Harkins and G. Jura, *J. Am. Chem. Soc.*, **66**, 919 (1944).

Table I: Properties of ThO₂ Samples

	Sample				
	A	B	C	D	E ^a
Calcining temperature, °C	650	800	1000	1200	1600
Nitrogen surface area, m ² /g	14.7	11.5	5.64	2.20	1.24
Geometric mean particle diameter, μ ^b	2.63	2.67	2.72	2.97	1.20
Crystallite size, Å ^c	194	220	682	1700	>2500

^a Impurities (in ppm) in sample E: NO₃, <10; SO₄, <10; PO₄, 10; Si, 20; Cl, <10; Fe, 30; Ni, 10; Cr, <10; Pb, <10; Na, <10; K, <10; Li, <10; Cu, <10. Impurities in remaining samples are listed in ref 2. ^b Equivalent Stokes diameter for a sphere. From sedimentation rates. See ref 13 for method. ^c From X-ray line broadening. Uncertainty is about 5% below 500 Å and 10% above 500 Å.

by thermal decomposition from the same lot of thorium oxalate and are the samples used in the previous study.² Pertinent physical properties of these samples are repeated in Table I.¹⁰ Sample E was also prepared¹¹ by the thermal decomposition of thorium oxalate, but from a different lot. The small specific surface area and relatively large crystallite size for sample E are characteristic of the higher calcining temperature. However, the significantly smaller particle size for this sample is probably related to the particle size of the parent thorium oxalate material.¹² The influence of various factors on the physical properties of thorium oxide prepared by thermal decomposition of the oxalate has been discussed elsewhere.¹³

Sample Preparation. Samples which were not dosed with water prior to the immersion experiments were outgassed at elevated temperatures according to the previous procedure.² All of the samples were outgassed for 24 hr to an ultimate pressure of 10^{-5} torr and were sealed off under vacuum at the end of the outgassing period. Those samples which were dosed with water prior to the immersion experiments were outgassed in the special sample holder shown in Figure 1. All of these samples were outgassed for 24 hr at 500° prior to dosing with water.

Two methods were used for dosing the outgassed samples with water. The first of these involved exposing the sample to a known water vapor pressure which was controlled by a saturated salt solution. After outgassing and sealing off, the ball-joint in Figure 1 was sealed (with hard vacuum wax) to a reservoir containing a saturated salt solution. The salt solution was then degassed by repeated freezing with liquid nitrogen, evacuating to approximately 1×10^{-5} torr, and melting under vacuum. After at least three such cycles the frozen salt solution was sealed off under vacuum. The entire assembly was then allowed to stand for several days at room temperature with

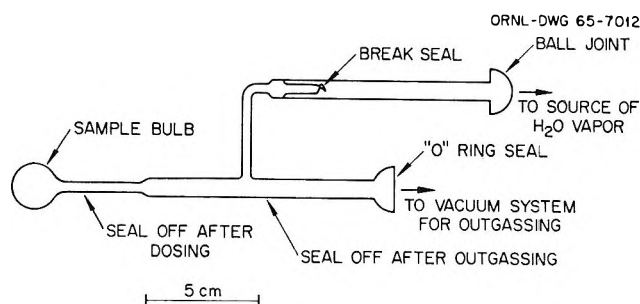


Figure 1. Sample holder for outgassing and dosing ThO₂ samples.

frequent magnetic stirring to ensure saturation of the solution with the salt which had precipitated during the freezing process. The break-seal isolating the sample was then broken with a glass-covered magnet and the entire assembly was immersed in a water bath which was controlled at 25.0°. After an equilibration period of 72 hr, the sample bulb was sealed off slowly while still immersed just below the water level in order to avoid heating the sample. The component parts of the sample-holder assembly were weighed before and after exposure to water vapor to give the amount of water adsorbed by the sample. The saturated salt solutions used in this study gave relative pressures (P/P_0) ranging from 0.120 to 0.969.¹⁴

The main disadvantage of the method of sample preparation just described is that it cannot be used

(10) The data in Table I were obtained by the Analytical Chemistry Division of Oak Ridge National Laboratory.

(11) ORNL Lot No. DT-9 prepared by the Chemical Technology Division of Oak Ridge National Laboratory.

(12) R. Beckett and M. E. Winfield, *Australian J. Sci. Res.*, **4A**, 644 (1951).

(13) V. D. Allred, S. R. Buxton, and J. P. McBride, *J. Phys. Chem.*, **61**, 117 (1957).

(14) A. Wexler and S. Hasegaura, *J. Res. Natl. Bur. Std.*, **53**, 19 (1954).

to prepare samples containing very small amounts of presorbed water. There are two reasons for this. The first is that the very low water vapor pressures required cannot be achieved with saturated salt solutions. Secondly, the amount of adsorbed water is determined by the difference in sample weight before and after equilibration and is therefore relatively inaccurate for small amounts of presorbed water (low specific surface area and/or low equilibrium pressures). Accordingly, a new technique for sample preparation was devised in which the ThO_2 samples were dosed directly with a known amount of water. After outgassing the sample and sealing off under vacuum, the ball-joint of the sample holder was connected (with hard vacuum wax) to a vacuum manifold containing calibrated volumes. After evacuation of the manifold, a selected volume was filled with water vapor. The desired water vapor pressures were maintained by a degassed liquid water reservoir controlled at a selected temperature below ambient. The ThO_2 sample was then immersed in a liquid nitrogen bath to a point below the seal-off point, the break-seal was broken with a glass-covered magnet, and the water vapor reservoir was exposed to the sample. After condensation of the water vapor onto the sample, the sample bulb was sealed off while still at liquid nitrogen temperature. Blank experiments showed that the liquid nitrogen bath reduced the water vapor pressure to a negligible value in less than 5 min. The amount of adsorbed water was readily calculated from the pressure, volume, and temperature of the vapor reservoir. The amount of water vapor in the void space of the sample bulb was negligible because of the very low equilibrium pressures and small void volume (approximately 3 cm^3) in the sample bulb.

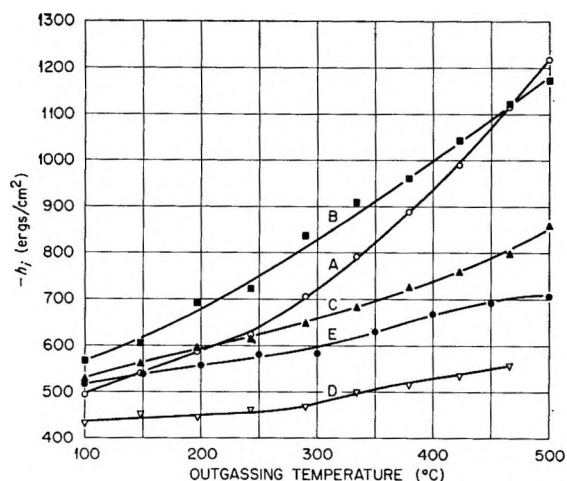


Figure 2. Heat of immersion of ThO_2 in water at 25.0° .

After dosing and sealing off, both types of samples were stored at room temperature for periods of time ranging from 3 weeks to 3 months before being used in an immersion experiment. No detectable difference was noted between samples which had been stored for different lengths of time.

All of the immersion experiments were performed at 25.0° . Sample bulbs and the heat of bulb-breaking correction were described in the previous publication.² Accuracy of the calorimetric measurements is estimated to be about 1%. Total heat evolution during an immersion experiment varied from about 1.4 to 55 joules. The calorimeter was calibrated electrically for each loading. Results were reduced to a unit area basis by means of the measured nitrogen surface areas.

Results and Discussion

Effect of Outgassing Temperature. The integral heats of immersion (h_i) for all five samples are shown in Figure 2 as a function of the outgassing temperature. These results for samples A through D were reported in the previous publication² and are repeated here for two reasons. The obvious reason is to obtain a comparison with the results for sample E. Secondly, the outgassing temperatures listed in the preceding paper² are in error due to an incorrectly applied thermometer stem correction. This resulted in error of approximately 34° at the highest temperature but decreased with temperature and was negligible at 100° . The magnitude of this error can be seen from the results for sample D in Figure 2 where the spacing between data points was erroneously given as 50° in the earlier report.² It should be emphasized that this error in no way invalidates any of the previous conclusions. However, at the highest outgassing temperature used (500°) the heats of immersion of samples A, B, C, and D are now in the same order as their specific surface areas. This is opposite to the behavior observed for the heats of immersion of TiO_2 ,¹⁵ SiO_2 ,¹⁶⁻¹⁸ and Al_2O_3 ¹⁹ in water.

When one considers sample E, however, the dependence of the heat of immersion on specific surface area and crystallite size is opposite to that observed with the remaining four samples. According to the previous

(15) W. H. Wade and N. Hackerman, *J. Phys. Chem.*, **65**, 1681 (1961).

(16) W. H. Wade, R. L. Every, and N. Hackerman, *ibid.*, **64**, 355 (1960).

(17) A. C. Makrides and N. Hackerman, *ibid.*, **63**, 594 (1959).

(18) J. W. Whalen, *Advances in Chemistry Series*, No. 33, American Chemical Society, Washington, D. C., 1961, p 281.

(19) W. H. Wade and N. Hackerman, *J. Phys. Chem.*, **64**, 1196 (1960).

behavior, sample E, having a lower specific surface area and a larger crystallite size, should have a smaller heat of immersion than sample D. Obviously this is not the case although the dependence of the heat of immersion of the two samples on outgassing temperature is very similar as can be seen from the shapes of the two curves. The difference can possibly be attributed to a particle size effect, rather than effects due to specific surface area and/or crystallite size. From the data in Table I it can be seen that the mean particle size for sample E is less than five times as large as the crystallite size while the mean particle size of sample D is some 17 times as large as the crystallite size. Thus, any effect of particle size on the heat of immersion would be greatly enhanced in the case of sample E. Obviously, what is needed to resolve the important question of the dependence of the heat of immersion on specific surface area, particle size, and crystallite size are samples in which the particles themselves are single crystals. Unfortunately, such samples are not available at the present time.

Effect of Presorbed Water. Heats of immersion for samples A, B, and E are shown in Figures 3, 4, and 5, respectively, as a function of the amount of presorbed water (adsorbed prior to the immersion experiments but after outgassing at 500°). These studies were not done with samples C and D because of exhaustion of available material. Results for sample B were limited to relatively small quantities of presorbed water for the same reason. As can be seen from the open and closed data points in Figures 3 and 5, the agreement between results from the two methods of sample preparation is very good. The horizontal lines in Figures 3 and 5 which are labeled h_L correspond to the surface enthalpy (118.5 ergs/cm²) of water at 25.0°. The significance of this quantity and its relationship to the experimental results will be discussed in a subsequent section.

The general shape of the curve shown in Figure 3 has frequently been observed for the immersion of polar solids in polar liquids. Except for the initial small linear portion, this type of curve has been classified by Zettlemoyer and Chessick^{4,5} as being indicative of a heterogeneous surface, *i.e.*, the adsorption sites have a wide distribution of energies.

The data shown in Figure 3 provided additional insight as to the mechanism responsible for the slow heat of immersion observed with samples A, B, and C.² As much as 18% of the total heat of immersion was not released immediately upon immersion of highly porous, high surface area thoria. Briefly, it was postulated that the slow heat release was due to the slow diffusion of liquid water into the porous structure of the particles.

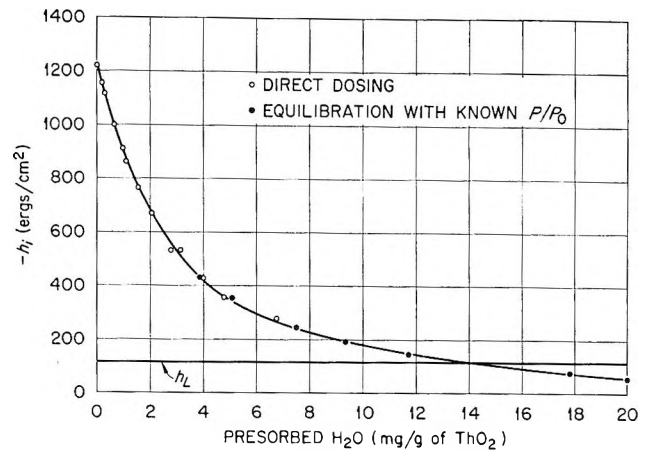


Figure 3. Heat of immersion of ThO₂ (sample A) containing presorbed H₂O.

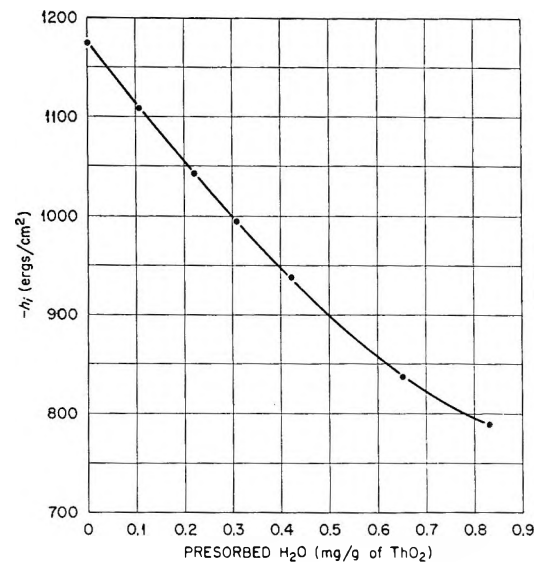


Figure 4. Heat of immersion of ThO₂ (sample B) containing presorbed H₂O.

In the present study, samples of A which had been equilibrated at relative water vapor pressures as high as 0.54 still had a readily detectable slow heat of immersion. Samples which were equilibrated at relative water vapor pressures of 0.70 and above gave no measurable slow heat. The transition point for the disappearance of the slow heat of immersion must be at a relative pressure between these two values. Chemisorption (which should be complete during preadsorption at much lower relative pressures) cannot be responsible for a phenomenon which is readily observable at relative pressures as high as 0.54, especially in view of the fact that there was no difference between samples stored for 3 months and 3 weeks prior to the immersion experiments. The conclusion is that the

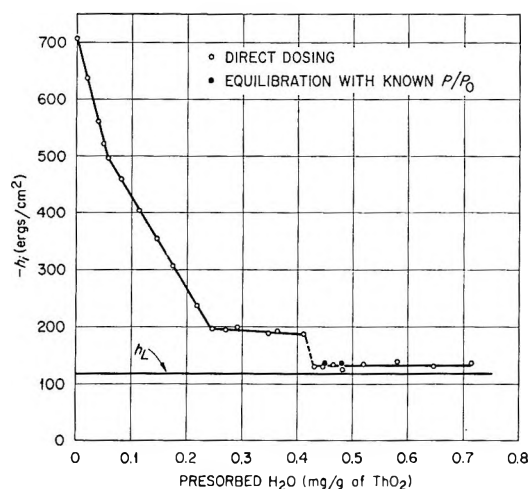


Figure 5. Heat of immersion of ThO_2 (sample E) containing presorbed H_2O .

slow heat phenomenon must be due to slow diffusion of water into the pores of the oxide particles. As confirmation of this, the water vapor adsorption isotherm for sample A exhibits a capillary condensation hysteresis loop which does not close until one reaches relative pressures corresponding to pores of two molecular diameters in dimension.³

Harkins and Jura²⁰ established the utility of heats of immersion of samples equilibrated at high relative pressures as a means for an absolute surface area measurement. Briefly their method involves the thermodynamically sound assumption that the heat of immersion (on a unit area basis) of a solid covered with a multimolecular layer of water is equal to the surface enthalpy of water. The results in Figure 3 were reduced to a unit area basis by means of the measured nitrogen surface area of $14.7 \text{ m}^2/\text{g}$. According to Harkins and Jura's method, if the film-covered solid actually had a surface area of $14.7 \text{ m}^2/\text{g}$, the heat of immersion values should not have fallen below $118.5 \text{ ergs}/\text{cm}^2$. One sample (not shown in Figure 3) which was equilibrated at a relative pressure of 0.969 gave a heat of immersion of only $21 \text{ ergs}/\text{cm}^2$ when calculated on the basis of $14.7 \text{ m}^2/\text{g}$. Obviously, either the absolute method for measuring surface area is in error or the available surface area actually decreases with increasing amounts of adsorbed water. The fact that the latter reason is correct has been confirmed by adsorption measurements made in this laboratory.³ This finding is not surprising in view of the porous structure of this sample and the associated slow heat phenomenon since the Harkins-Jura absolute method measures only the surface area of the adsorbed film-vapor interface and not that of the outgassed solid.

This same effect has been noted and explored in more detail in the case of the alumina-water system.^{21,22} This phenomenon is not limited to polar systems as it has also been observed in the graphite-benzene system.²³

Adsorption data from the preparation of samples of A by exposure to known pressures of water vapor gave a typical Type II isotherm showing multilayer adsorption. The BET surface area estimated from the adsorption data was approximately $28 \text{ m}^2/\text{g}$ (using 10.6 \AA^2 for the area²⁴ of an adsorbed water molecule.) This is roughly twice the surface area as determined by nitrogen adsorption and indicates that chemisorption of water is occurring on the outgassed surface of the ThO_2 . This discrepancy between water and nitrogen surface area has previously been noted in the case of ThO_2 .²⁵ Later work³ in this laboratory has demonstrated that the conditions used in preparing the calorimetric samples were not sufficient to obtain a reversible equilibrium isotherm. For this reason the adsorption data referred to here cannot be used for thermodynamic calculations. It should be emphasized that this in no way affects the validity of the calorimetric measurements. Indeed, it is not even necessary to know the equilibrium water vapor pressure⁵ in order to obtain meaningful heat of adsorption data by the method used in the present study.

The calorimetric data for sample B (Figure 4) are also indicative of a heterogeneous surface.^{4,5} As mentioned previously, the data for sample B do not extend to the degree of surface coverage investigated in the case of sample A. This fact prevented us from obtaining the relative water vapor pressure corresponding to the disappearance of the slow heat of immersion (all samples of B were prepared by the direct dosing technique). However, all of the calorimetric samples of B gave a slow heat of immersion, the quantity of which decreased with increasing amounts of presorbed water. For the same reason, we were unable to determine if the heat of immersion of sample B would ultimately fall below the surface enthalpy of water, given a sufficient quantity of presorbed water. The quantitative behavior of sample B, as compared to sample A, leads us to believe that this would be the case.

(20) W. D. Harkins and G. Jura, *J. Am. Chem. Soc.*, **66**, 1362 (1944).

(21) W. H. Wade, *J. Phys. Chem.*, **68**, 1029 (1964).

(22) N. Hackerman and W. H. Wade, *ibid.*, **68**, 1592 (1964).

(23) C. Pierce, J. Mooi, and R. E. Harris, *ibid.*, **62**, 655 (1958).

(24) H. K. Livingston, *J. Am. Chem. Soc.*, **66**, 569 (1944).

(25) M. E. Winfield, *Australian J. Sci. Res.*, **3A**, 290 (1950).

The heat of immersion data for sample E (Figure 5) are both interesting and unusual. Heat of immersion curves which have a linear dependence on the amount of presorbed immersion fluid have been cited as evidence for a homogeneous surface.^{4,5} Such linearity has been found, for example, in the asbestos-water system.²⁶ However, the two sharp breaks and an apparent discontinuity in Figure 5 indicate abrupt changes in the energy of adsorption and further, that these changes are from one type of homogeneous adsorption to a second type of homogeneous adsorption. At the larger amounts of presorbed water in Figure 5, the heat of immersion of sample E differed from the surface enthalpy of water by a constant 14 ergs/cm². One sample of E which was equilibrated at a relative water vapor pressure of 0.969 (and containing 2.66 mg of H₂O/g of ThO₂) gave a measured heat of immersion of 112 ergs/cm² based on the nitrogen surface area. The combined uncertainty in the calorimetric measurements and the nitrogen surface area indicates no significant difference between the nitrogen surface area (1.24 m²/g) and that obtained by the Harkins-Jura absolute method (1.17 m²/g). Rather, we tend to believe that these two values are quite compatible and that the ThO₂ particles of sample E are relatively nonporous and, as a result, suffer little or no loss of available surface area with increasing amounts of adsorbed water. Additional credence is given to this viewpoint by the fact that no slow heat of immersion was ever observed with sample E under any conditions. The nonporosity of this sample has not, as of yet, been confirmed by adsorption measurements.

Net Differential Heats of Adsorption. The net differential heats of adsorption (ΔH_a) were obtained by graphical differentiation of the integral heat of immersion as a function of the amount of presorbed water. Prior to the differentiation, the heat of immersion data were plotted in units of calories per gram of ThO₂ rather than on a unit area basis. This procedure obviates any questions associated with the decrease in available surface area with increasing amounts of adsorbed water such as was observed with sample A (see later discussion). Presentation of the data in this manner is just as thermodynamically sound as on a unit area basis and is probably less ambiguous in the case of powdered samples where the surface area decreases in an unknown manner.²² The resulting net differential heats of adsorption as a function of the amount of adsorbed water are depicted in Figures 6, 7, and 8 for samples A, B, and E, respectively. These derived quantities are believed to represent the true net differential heats of adsorption with an accuracy of about 5%. These net heats are relative

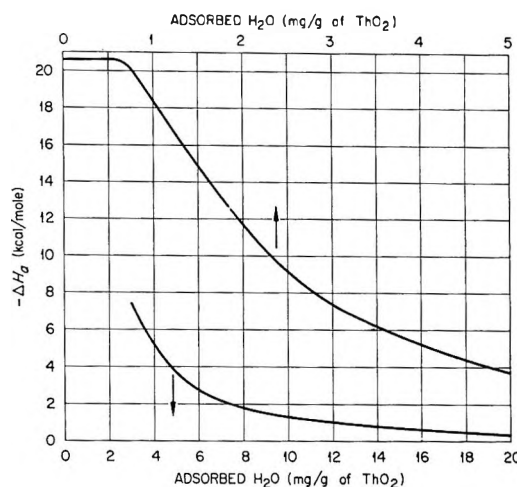


Figure 6. Net differential heat of adsorption of H₂O on ThO₂ (sample A).

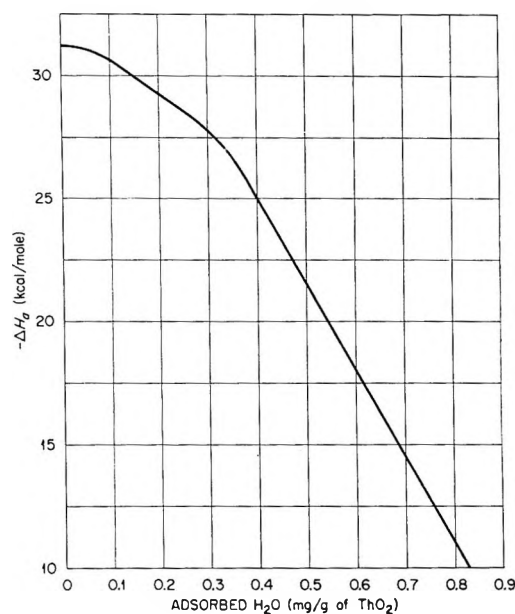


Figure 7. Net differential heat of adsorption of H₂O on ThO₂ (sample B).

to the liquid state and are less than the conventional isosteric heats of adsorption by the molar heat of vaporization of water.

Heat of adsorption data are almost universally displayed as a function of the fraction of the surface covered. This procedure permits correlation of the thermodynamic functions with the completion of various monolayers, of which the first is the most important. This practice has not been followed for

(26) A. C. Zettlemoyer, G. J. Young, J. J. Chessick, and F. H. Healey, *J. Phys. Chem.*, **57**, 649 (1953).

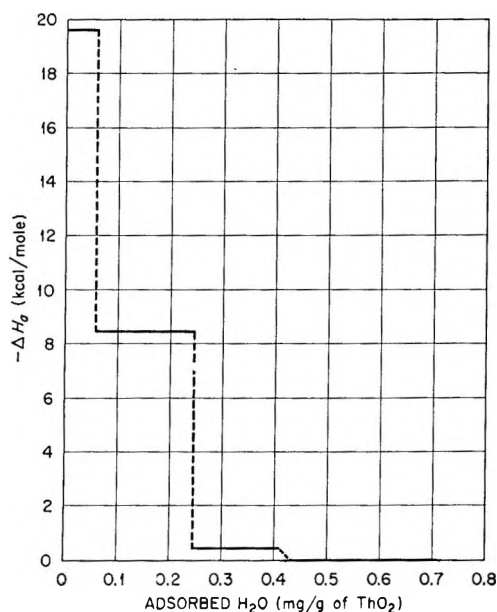


Figure 8. Net differential heat of adsorption of H_2O on ThO_2 (sample E).

several reasons. Pertinent to this discussion is the fact that zero on the adsorbed water axis in Figures 6, 7, and 8 represents the sample weight under high vacuum at 500° . These outgassing conditions are not sufficient to remove all of the water from the surface of thorium oxide.^{2,27} In order to dehydrate the surface of ThO_2 completely, it is necessary to outgas at 900 to 1000° or, according to the infrared study of surface hydroxyl groups by Wadsworth *et al.*,²⁸ heat the sample to 1300° under atmospheric conditions. Such treatment would drastically alter the surfaces of samples A and B as their original calcining temperatures were only 650 and 800° , respectively, and is impossible with Pyrex sample bulbs.

The relatively large net differential heats of adsorption are a very good indication that chemisorption of water is occurring. Chemisorption is not surprising in view of the wide variety of evidence indicating that the surfaces of polar oxides are populated with surface hydroxyl groups. One is immediately faced with the question of assigning a monolayer capacity for chemical adsorption based on a surface area which is usually determined by the physical adsorption of nitrogen. Of course, one can select the original outgassing temperature on the basis of the best compromise between complete removal of physically adsorbed water while leaving the chemisorbed water intact. Unfortunately, in the usual case, the borderline between physical adsorption and chemisorption is not distinct enough to permit an unambiguous selection of outgassing con-

ditions. Furthermore, if one does attempt to choose such outgassing conditions he is abandoning study of the chemisorption process. In so doing, one is losing one of the strong points of the heat of immersion technique, namely the ability to determine heats of adsorption for both chemical and physical adsorption, even for those cases where the adsorption isotherms are experimentally unattainable.

Not to be ignored are those cases in which the available surface area decreases with increasing amounts of adsorbed water. One must decide what fraction of the surface is covered when each additional increment of adsorbate decreases the total available surface area of the adsorbent. This condition is certainly occurring with sample A of the present study and also the alumina samples studied by Venable, Wade, and Hackerman,⁶ as was noted by them. The present authors feel that the points discussed in the preceding paragraphs are important factors to be considered in the interaction of any polar adsorbate with a polar adsorbent.

Nevertheless, if for comparison purposes only, one can estimate monolayer capacities for the adsorption of water on these samples. This procedure is warranted only if one realizes that these are estimates and understands the assumptions involved in the estimates. The estimated quantity of water necessary to form a monolayer on these samples of ThO_2 are given in Table II. The basic assumption is that the measured nitrogen surface area is the true surface area of the bare surface. The capacity for a monolayer of chemisorbed water was estimated on the basis of the number of sites for surface hydroxyl groups on the 100 plane of a ThO_2 crystal (one water molecule forms two OH groups and is equivalent to 15.6 \AA^2). The physically adsorbed monolayer capacity was estimated by assuming that one physically adsorbed water molecule occupies an area²⁴ of 10.6 \AA^2 . Admittedly these monolayer capacities are rough estimates, especially in the case of sample A, but perhaps they can be taken as upper limits for the amount of water in a monolayer on these surfaces.

There are several significant features of the curve for the net differential heat of adsorption of water on sample A (Figure 6). Of obvious significance are the initial high values of net differential heats of adsorption, which are much too large to be associated with the

(27) E. L. Fuller, Jr., H. F. Holmes, and C. H. Secoy, "Vacuum Microbalance Techniques," Vol. IV, Plenum Press, New York, N. Y., 1965, p 109.

(28) M. E. Wadsworth, *et al.*, "The Surface Chemistry of Thoria," Progress Report, AEC Subcontract 2176 under W-7405-eng-26, University of Utah, Salt Lake City, Utah, Jan. 31, 1959. Available from CFSTI, Springfield, Va.

Table II: Estimated Monolayer Capacities

Sample	Chemical, mg of H ₂ O/g of ThO ₂	Physical, mg of H ₂ O/g of ThO ₂
A	2.818	4.148
B	2.205	3.245
C	1.081	1.592
D	0.422	0.621
E	0.238	0.350

normal process of physical adsorption. The two most plausible mechanisms for the chemisorption of water on this surface are the rehydroxylation of surface oxide groups which were formed by dehydroxylation during the outgassing procedure and very strongly hydrogen bonded water. It seems unlikely that a water molecule could form enough hydrogen bonds to account for a net heat of adsorption of -20 kcal/mole. Since the existence of hydroxyl groups on oxide surfaces has been demonstrated by infrared spectroscopy,²⁹ one must conclude that at least the initial portion of the net differential heat curve in Figure 6 is due to the formation of surface hydroxyl groups.

Except for the initially constant value for the net differential heat of adsorption, the exponential-like decrease is typical of adsorption (either chemical or physical) on a heterogeneous surface. A constant net differential heat of adsorption, as observed in the initial part of the curve, is indicative of either a constant site energy with a constant (possibly zero) contribution from lateral interaction or a functionally changing site energy combined with an exactly compensating functional contribution from lateral interaction. A possible situation fulfilling these conditions would be the formation of surface hydroxyl groups on equally energetic sites with no interaction between adjacent hydroxyl groups or, since interaction in this case would presumably be hydrogen bonding, that hydrogen bonding is energetically equal during that range of surface coverage corresponding to a constant net differential heat of adsorption. Since we are certain that there are still hydroxyl groups remaining on the surface after outgassing at 500° , we tend to favor the latter viewpoint. It is conceivable that the point at which the net differential heat of adsorption starts to decrease corresponds to a surface which is completely covered with hydroxyl groups (work is in progress using infrared spectroscopy to prove this point). The shape of the curve shown in Figure 6 is somewhat similar to that obtained by Hollabaugh and Chessick⁸ for the adsorption of water on

TiO₂. It is interesting that the initial constant differential heats of adsorption in the two cases differ by only about 2 kcal/mole. These authors also explain their data in terms of chemisorption with the formation of surface hydroxyl groups.

A comparison of Figure 6 with the estimated monolayer capacities in Table II clearly shows that the net differential heat of adsorption does not, as it is often assumed, fall to zero with the first adsorbed monolayer. This point has also been observed in the TiO₂-water system.^{8,9} These observations indicate the presence of longer range forces than are normally assumed to exist in adsorption processes, perhaps an ordering effect in the adsorbed water layers (probably through hydrogen bonding to surface hydroxyl groups). Again, it would take a tool for structure determination to establish this point firmly, although some degree of orderliness in the initial layers of water adsorbed on ThO₂ has been demonstrated by nuclear magnetic resonance and dielectric measurements.³⁰

In all fairness, it should be pointed out that the decrease in available surface area with increasing amounts of adsorbed water may account for the existence of a nonzero net differential heat of adsorption even after the completion of the equivalent of five physically adsorbed monolayers. This possibility arises because the surface energy of water (118.5 ergs/cm²) is equivalent to 1.81 kcal/mole when calculated on the basis of a physically adsorbed monolayer (10.6 Å²/molecule). Several workers^{6,22,31-33} have observed minima and maxima in the differential heat curves in the region of capillary condensation when working with samples having a narrow pore size distribution. Relatively small amounts of adsorbed water can cause a drastic reduction in available surface area and this has actually been observed in the case of the alumina gel sample used by Hackerman and Wade.²² As pointed out by Kiselev,³¹ differential heat curves for samples having a wide pore size distribution have, at best, only a vague maximum. It is known that sample A has a wide pore size distribution.³ The supposition is that the energy involved in reduction of the available surface area appears over a wide range of adsorbed water and not as a sharp maximum. Kington and Smith³³ conclude, and we agree, that the reduction in

(29) A. V. Kiselev and V. I. Lygin, *Russ. Chem. Rev.*, **31**, 175 (1962).

(30) K. D. Lawson, Ph.D. Thesis, University of Florida, 1963.

(31) A. V. Kiselev, "Proceedings of the Second World Congress on Surface Activity," Vol. II, Academic Press, New York, N. Y., 1957, p 189.

(32) G. L. Kington and P. S. Smith, *Trans. Faraday Soc.*, **60**, 705 (1964).

(33) G. L. Kington and P. S. Smith, *ibid.*, **60**, 721 (1964).

available surface area is more important than any hydrostatic pressure effects in the capillaries. These conclusions do not invalidate the concept of a heat of adsorption, but indicate that the mechanism responsible for the energy release is different for the case under discussion than for physical adsorption on a flat surface. In either case, this energy release on adsorption is real and measurable. However, any effect due to a reduction in available surface area is not nearly large enough to account for a nonzero net differential heat of adsorption after completion of the first monolayer in the case of sample A.

Net differential heats of adsorption of water on sample B are shown in Figure 7. Although the data for sample B extend over only about 40% of an estimated chemisorbed monolayer (Table II) compared to a much larger range of coverages for sample A, it is evident that the energetics of water adsorption on the two samples are markedly different. One of the most significant facts is that the initial net differential heats of adsorption are some 50% greater for sample B than those observed with sample A. The decline of the net differential heats with increasing coverage indicates a heterogeneous surface, but there is no evidence for a region of surface homogeneity such as was found with sample A. Perhaps such a region would be found if the measurements were extended to smaller surface coverages (by outgassing at temperatures greater than 500°). These differences are not unexpected since the integral heats of immersion for sample A and B as a function of outgassing temperature (Figure 2) are also different. A more detailed comparison of samples A and B would require quantitative information on the degree of dehydration as a function of the outgassing temperature. Such information will be presented in a subsequent publication.

The surprising and unusual results for the net differential heat of adsorption of water on sample E are shown in Figure 8. The net differential heats up to about 0.25 mg of H₂O/g of ThO₂ are certainly indicative of chemisorption. In sharp contrast to samples

A and B, sample E exhibits four distinct regions in which each succeeding molecule of water is adsorbed with the same net heat of adsorption. It is somewhat difficult to conceive of an adsorption process which could account for a net differential heat curve such as shown in Figure 8. Perhaps the most logical explanation would be the formation of successive homogeneous, immobile monolayers. It is interesting to compare the ranges of surface coverage corresponding to the constant net differential heats of adsorption of 8.4 and 0.4 kcal/mole. These are 0.188 and 0.185 mg of H₂O/g of ThO₂, respectively, with a small amount of uncertainty in the latter value due to the apparent discontinuity. Although these are somewhat smaller than the estimated monolayer capacity for chemisorption given in Table II, their near equality lends support to the idea of successive homogeneous monolayers. Chances for observing such a phenomenon would certainly be better in the case of sample E because of its relatively large crystallite size. However, as is well known, net differential heat data taken alone are not sufficient to delineate an adsorption model. Additional work on this same sample is clearly indicated.

Literature data for the isosteric heat of adsorption of water on thorium oxide are rather scanty. The available data^{25,34,35} show considerable variation with outgassing conditions and sample preparation but all are large enough to indicate chemisorption. Data in the present paper reinforce the opinion⁴ that the adsorption of water on polar oxide surfaces activated at high temperatures is not necessarily a simple process of physical adsorption. In particular, as emphasized previously,³⁶ one should always consider hydroxylation of surface oxide groups and hydrogen bonding.

(34) A. G. Oblad, S. W. Weller, and G. H. Mills, "Proceedings of the Second World Congress on Surface Activity," Vol. II, Academic Press, New York, N. Y., 1957, p 309.

(35) A. L. Draper and W. O. Milligan, "Structure and Surface Chemistry of Thorium Oxide," The Rice Institute, Houston, Texas, 1959.

(36) L. G. Ganichenko, V. F. Kiselev, and V. V. Murina, *Kinetika i Kataliz*, **2**, 977 (1961).

The Pulse-Sampling Technique for the Study of Electron-Attachment Phenomena

by W. E. Wentworth, Edward Chen,¹ and J. E. Lovelock

Department of Chemistry, University of Houston, Houston, Texas (Received August 6, 1965)

A study of the parameters characterizing the electron-capture detector operated in the pulse-sampling mode was carried out. The pulse width, $\sim 0.4 \mu\text{sec.}$, applied voltage, -50 v. , and the pulse period $\sim 1000 \mu\text{sec.}$, necessary to collect all of the electrons and to achieve a steady state when argon-10% methane is used as a carrier gas were determined. It was assumed that the electrons acquired a thermal distribution when no potential was applied to the cell and that the results were independent of the pulse potential examined up to 80 v. A kinetic model of the processes occurring within the electron-capture detector operated in the pulse-sampling mode has been proposed. For the case in which the electron-capturing species is capable of forming a stable negative ion (in contrast to dissociative electron capture), the system of differential equations has been solved using the steady-state approximation. From this solution, one can obtain the previously defined electron capture coefficient in terms of the rate constants for the processes proposed in the model. In certain cases one can obtain values for the rate constants and/or the electron affinity of the molecule from the temperature dependence of this electron-capture coefficient. Evidence is given for the validity of the proposed model, and the magnitude of the rate constants and the electron affinities are given for several aromatic hydrocarbons.

Introduction

The phenomena associated with the attachment of electrons to molecules in the gaseous state has long been a subject for experimental and theoretical studies. The scope of these studies can be seen from the numerous reviews of this subject in monographs, such as those by Loeb,² Massey and Burhop,^{3a} Massey,^{3b} Healy and Reed,⁴ etc., and also from the numerous articles appearing in the literature. However, none of these studies has been carried out under conditions of atmospheric pressure, low fields, with low energy electrons, and in the presence of complex organic molecules. These are precisely the conditions under which the Lovelock electron-capture detector⁵⁻¹¹ operates when the pulse-sampling mode is employed. Therefore, the interpretation of the physical processes occurring within the detector would clarify the phenomena associated with the attachment of electrons to molecules under these unique conditions.

In view of the many highly developed and accurate techniques already described,²⁻⁴ the introduction of a new method of measurement in electron-attachment studies would seem to need more than usual justifica-

tion. The pulse-sampling method arose not from a perverse desire for novelty but as a simple and inexpensive qualitative detector for gas chromatography. Its later consideration as a potential method for electron-attachment studies was made not because it was

(1) A portion of this work was done in partial fulfillment of the requirements of the Ph.D. degree, University of Houston, 1965.

(2) L. B. Loeb, "Basic Processes of Gaseous Electronics," University of California Press, Berkeley, Calif., 1961.

(3) (a) H. S. W. Massey and E. H. S. Burhop, "Electronic and Ionic Impact Phenomena," Oxford University Press, New York, N. Y., 1952; (b) H. S. W. Massey, "Negative Ions," Cambridge University Press, New York, N. Y., 1950.

(4) R. H. Healy and J. W. Reed, "The Behavior of Slow Electrons in Gases," Amalgamated Wireless Press (Australasia) Ltd., Sydney, 1941.

(5) J. E. Lovelock, *Anal. Chem.*, **33**, 162 (1961).

(6) J. E. Lovelock, *Nature*, **139**, 729 (1961).

(7) J. E. Lovelock and A. Zlatkis, *Anal. Chem.*, **33**, 1958 (1961).

(8) J. E. Lovelock and N. L. Gregory, "Gas Chromatography," N. Brenner, Ed., Academic Press, New York, N. Y., 1962, p. 219.

(9) J. E. Lovelock, A. Zlatkis, and R. S. Becker, *Nature*, **193**, 540 (1962).

(10) J. E. Lovelock, *Anal. Chem.*, **35**, 474 (1963).

(11) J. E. Lovelock, P. G. Simmonds, and W. J. A. VandenHeuvel, *Nature*, **197**, 249 (1963).

better able to perform the physical measurements, but because none of the methods previously described are able to satisfy the severe chemical constraints imposed during measurements of weakly volatile, highly polar, and possibly impure organic compounds, for example, steroids. The method is dynamic and designed for the observation of brief pulses of ultrapure, dilute vapor emerging from a chromatograph column. Static methods of observing electron attachment, although adequate with pure permanent gases, are quite unsuited for this purpose.

The original electron-capture detector described by Lovelock and Lipsky¹² was operated on the basis of a constant applied voltage, but it was soon discovered that the pulse-sampling technique offered many advantages over the original d.c. system.⁶ These advantages were briefly discussed, and the electron-capture coefficients for several compounds relative to that of chlorobenzene as unity were obtained using the pulse-sampling technique and were given in the references cited earlier. A more complete discussion of the advantages and a more detailed description of the pulse-sampling mode of operation is given by Lovelock.¹⁰ However, the exact physical mechanisms occurring within the electron-capture detector were deferred to a later date since they were still being studied.

In a preliminary article, Wentworth and Becker¹³ have interpreted the electron-capture coefficients obtained for several aromatic hydrocarbons by using the pulse-sampling mode in terms of the electron affinities of the molecules by assuming an equilibrium between the attachment and detachment of thermal electrons to the aromatic hydrocarbon. This interpretation was supported by a correlation with the half-wave reduction potentials of the aromatic hydrocarbons, and a comparison of the experimental values with those calculated by Hoyland and Goodman.¹⁴ In a later article, Becker and Wentworth¹⁵ correlated the measured electron affinities and the 0-0 frequency of the aromatic hydrocarbons and also substantiated the theoretical prediction made by Hush and Pople¹⁶ that the sum of the ionization potential and the electron affinity should be a constant for alternant hydrocarbon molecules and radicals. Scott and Becker¹⁷ used the ω technique to calculate electron affinities for several aromatic hydrocarbons. The calculated values were in good agreement with the experimental values. Wentworth and Chen¹⁸ correlated the change in free energy for formation of complexes of *p*-xylene with different aromatic hydrocarbons and the electron affinities determined by the pulse-sampling technique. These studies, taken together, represent a formidable

body of evidence in favor of the interpretation of the electron-capture coefficients in terms of the electron affinities of the aromatic hydrocarbons.

Much of the existing information concerning the electron affinities of complex organic molecules has been summarized in ref. 13, 14, 15, 17, and 18. In addition, Briegleb¹⁹ has recently given a comprehensive review of the subject and has extended many of the techniques for estimating electron affinities of molecules. However, Briegleb applied the calculation of electron affinities from electron-capture coefficients indiscriminately to dissociative and nondissociative compounds. In the earlier reference,¹³ it was emphasized that the interpretation was only applicable to compounds which were clearly nondissociative, such as the aromatic hydrocarbons. However, it was not clearly stated how one could distinguish between these two processes for all types of molecules. Results from this paper will assist in making the decision but will not in itself distinguish between nondissociative and dissociative electron capture.

The purpose of this paper is to present a detailed model of the physical processes occurring in the electron-capture cell operating in the pulse-sampling mode and to verify this model with experimental observations. Except for the consideration of a few experiments with chlorobenzene where dissociative electron capture is used diagnostically to test for the presence of hyperthermal electrons, this discussion will be restricted to molecules which form stable negative ions upon electron attachment in contrast to compounds which undergo dissociative electron capture.

Experimental Section

During the course of these studies, a variety of equipment was used, *i.e.*, different electrometers, recorders, ovens, etc. Since these variations in the ancillary equipment did not affect the results obtained, only one of the systems will be described in detail as an example of the type of apparatus used. The electron-capture cell and the electrical schematic were described in references cited earlier. An Applied Physics Corp. Cary Model 31 vibrating-reed electrometer with the

(12) J. E. Lovelock and S. R. Lipsky, *J. Am. Chem. Soc.*, **82**, 431 (1960).

(13) W. E. Wentworth and R. S. Becker, *ibid.*, **84**, 4263 (1962).

(14) J. R. Hoyland and L. Goodman, *J. Chem. Phys.*, **36**, 21 (1962).

(15) R. S. Becker and W. E. Wentworth, *J. Am. Chem. Soc.*, **85**, 2210 (1963).

(16) N. S. Hush and J. A. Pople, *J. Chem. Phys.*, **51**, 600 (1955).

(17) D. R. Scott and R. S. Becker, *J. Phys. Chem.*, **66**, 2713 (1962).

(18) W. E. Wentworth and E. Chen, *ibid.*, **67**, 2201 (1963).

(19) G. Briegleb, *Angew. Chem.*, **76**, 326 (1964).

turret input was used. The voltage source was a Rutherford Model B78 square wave pulse generator. The signal was recorded on a 1-mv. Texas Instruments Servoriter recorder. A Tektronix Type RM35A oscilloscope was used to measure the pulse characteristics.

One of the chromatographs used was a modified Aerograph Autoprep. The temperature in the detector cell was measured with a thermometer rather than the thermocouple which was provided. The chromatographic column used was packed with 1% SF96 on glass beads, in 4 ft. of 0.25-in. copper tubing. The operating temperature on the column varied with the compounds but was held constant for a given compound. The flow rate was 135 ml./min. of argon through the column and 15 ml./min. of methane added to the system between the column and the electron-capture detector. The flow rates were measured with a stopwatch and a bubble flow meter. The argon was obtained from the Big Three Welding Co. and C.P. grade methane was obtained from the Matheson Co. The gases were passed through an Illinois Institute Dri Pak, filled with Molecular Sieve Type 5A 0.07-in. pellets, before going through the column or to the detector.

Except for naphthalene, triphenylene, phenanthrene, and azulene, the remaining aromatic hydrocarbons used in this work were obtained from Dr. R. S. Becker, and the purity of these materials has been given in an earlier paper.²⁰ The triphenylene and phenanthrene was obtained from Dr. M. S. Newman through Dr. Becker. The naphthalene was Baker and Adamson's reagent grade, and the azulene was obtained from K and K Laboratories, Inc. The solvent used was Eastman's spectroquality benzene. All of these compounds were used without prior purification since they were passed through the gas chromatographic column before going to the detector.

The material was weighed out on a Cahn Electrobalance, and the solutions were prepared in a 10- or 5-ml. volumetric flask. Further dilutions were made volumetrically. The samples were injected with a Hamilton 10- μ l. syringe with 0.2- μ l. divisions. The areas under the chromatographic peaks were obtained by triangulation and conversion of the signal.

Preliminary Experiments

The parameters applicable to the pulsed voltage are the applied voltages, V_A , the width of the pulse, t_w , and the pulse period or essentially the time between pulses, t_p . The current arising from the electron capture cell is measured as a voltage drop, V_M , across a known input resistance. This current is actually an average value of the current obtained in each in-

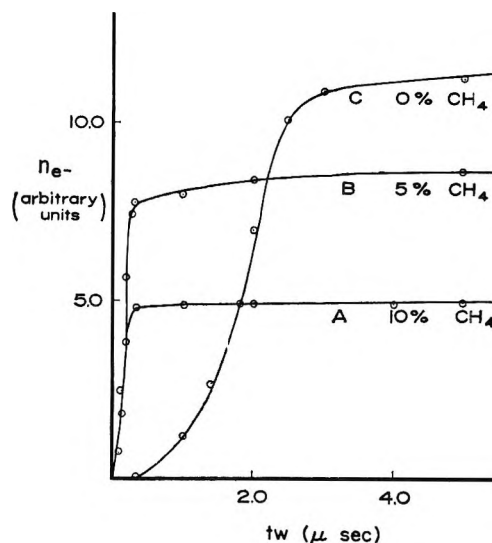


Figure 1. Electron concentration vs. pulse width at various argon-methane ratios.

dividual pulse; thus, the product, $V_M t_P$, is proportional to the number of electrons collected per pulse, n_{e-} , or if the reaction volume is constant, then $V_M t_P$ is proportional to the electron concentration [e^-] within the reaction zone. It will soon be shown that only electrons are collected and that other negative molecular ions could not be collected during the time, t_w .

The negative charge carriers when argon, or argon with methane added, is ionized are free electrons and these presumably are the species collected. This is confirmed by the evidence shown in Figure 1 in which n_{e-} is plotted against the width of the applied pulse, t_w . Curve A is for argon-10% methane, curve B is for argon-5% methane, and curve C is for pure argon. The electron drift velocities in argon-methane and argon can be estimated in the following manner. The electron cloud extends approximately 2 mm. from the tritium foil, and since the metal gauze (electron collector) is separated by 1.0 cm. from the foil, the mean distance for electron travel is 0.9 cm. The time necessary for the collection of the maximum concentration of electrons (greatest first derivative of the curve in Figure 1) is 2.0 μ sec. in argon and 0.15 μ sec. in argon-5% methane. Thus, the drift velocities, calculated under the above assumptions, at 40 v. and 1 atm., are approximately 6.0 cm./ μ sec. in argon-5% methane and 0.45 cm./ μ sec. in argon and are in fair agreement with the previously measured drift velocities in argon,²¹⁻²³ 0.2 cm./ λ sec., and in argon-5% meth-

(20) R. S. Becker, I. S. Singh, and E. A. Jackson, *J. Chem. Phys.*, **38**, 2144 (1963).

ane^{21,24} 3.5 cm./ μ sec., measured at 0.06 v. cm.⁻¹ mm.⁻¹. The drift velocity in argon-10% methane is approximately the same as it is in argon-5% methane. These values quoted from the literature were read from graphs and consequently are not extremely accurate, but the general agreement is good and the difference between the values in argon and in argon-methane are obviously significant. The high value in argon is almost certainly due to trace impurities which can profoundly alter the drift velocity in this gas. Thus, it is certain that the current being measured is due to the free electrons generated primarily during the time that the voltage is not being applied.

Figure 2 shows the variation of n_e with pulse width at several voltages for argon-10% methane at a pulse time of 1000 μ sec. The appearance of a plateau on the graphs shown in Figures 1 and 2 is an indication that all of the free electrons have been collected. The plateaus are not perfectly flat but the increase in the current in the plateau region can be ascribed to the fact that the electrons produced during the pulse are no longer negligible. As a result, some of these electrons which would otherwise recombine with the positive species or react with radicals are collected. Furthermore it is obvious from the common plateau for the curves shown in Figure 2 that the degree of ionization is independent of the applied voltage.

In order to determine the dimensions of the reaction zone, the current was measured as a function of the pulse time at different electrode spacings. The curves are essentially the same up to a distance of 2 mm., which indicates that this is approximately the depth of the reaction zone or at least represents a maximum value for the depth. This is also in agreement with the limited range of the weak β 's from tritium.

The value of the half thickness for tritium β 's at 1 atm. pressure in helium has been determined to be 2.75 mm.²⁵ It is to be expected that the value in argon would be smaller. The cross-sectional area of the reaction zone can be taken as the area of the tritium foil.

One important factor which must be considered before the electrons can be completely characterized is the average energy of the electrons. The β particles released from the tritium have a maximum energy of 17.6-18.9 kev. as summarized in a paper by Strominger, *et al.*²⁶ However, these particles rapidly lose their energy by ionization of the argon and methane until their energy is less than that necessary for formation of an ion pair. The electrons produced by the β 's will initially have an energy in excess of thermal energies, but it is assumed that they will rapidly lose

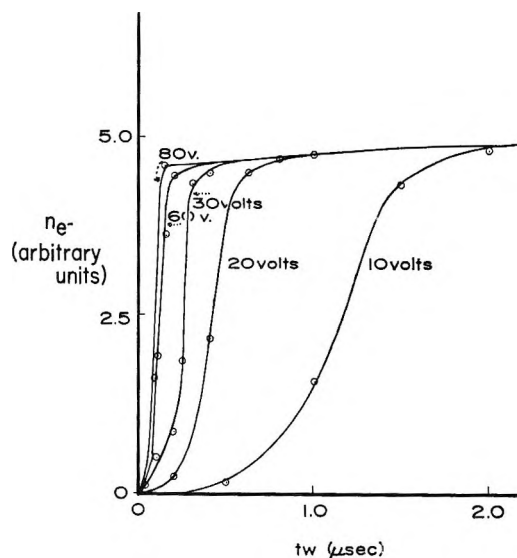


Figure 2. Electron concentration vs. pulse width at various voltages.

energy in collisions, primarily with methane, until their average energy is thermal. In pure argon, only elastic collisions can take place once the energy is below the excitation level of argon. However, in the presence of methane there are other possible modes for the loss of energy, such as vibrational and rotational excitation of methane. This difference is reflected in the large difference in the drift velocity of electrons in argon and argon-methane (see Figure 1).

In argon-10% methane the collision frequency, ν_c , at STP is about 3×10^{11} collisions/sec., and the fractional energy loss per collision, f , for elastic collisions is $2m/M = 2.73 \times 10^{-4}$, where m is the mass of an electron and M is the mass of an argon atom. If these quantities are constant, then the following formulas²⁷ can be used to calculate the time necessary to cool an electron of energy u_0 to near thermal energies.

$$\frac{du}{dt} = -f \left(u - \frac{kT}{\epsilon} \right) \nu_c \quad (1)$$

where ϵ is the electronic charge. Integration under the assumption above gives

(21) T. Nagy, L. Nagy, and S. Desi, *Nucl. Instr. Methods*, **8**, 327 (1960).

(22) T. E. Bortner, G. E. Hurst, and W. G. Stone, *Rev. Sci. Instr.*, **28**, 103 (1957).

(23) L. Coli and W. Facchini, *ibid.*, **23**, 39 (1959).

(24) W. N. English and G. C. Hanna, *Can. J. Phys.*, **31**, 768 (1953).

(25) W. F. Libby, *Phys. Rev.*, **103**, 1900 (1956).

(26) D. Strominger, J. M. Hollaander, and G. T. Seaborg, *Rev. Mod. Phys.*, **30**, 585 (1958).

(27) A. V. Phelps, O. T. Fundingsland, and S. C. Brown, *Phys. Rev.*, **84**, 559 (1951).

$$t = \frac{1}{f\nu_c} \ln \frac{u_0 - \frac{kT}{\epsilon}}{u_t - \frac{kT}{\epsilon}} \quad (2)$$

This value for f is certainly a lower limit, and the difference in the drift velocities in argon and argon-methane indicates that it should be higher. However, using these figures one obtains a value of 0.076 $\mu\text{sec.}$ to cool a 10-e.v. electron to 10% above thermal energies. This is much shorter than the pulse periods, t_p , used in these studies. Although this calculation does not rigorously prove there is a thermal distribution, it would seem reasonable to assume that in the period of 1000 $\mu\text{sec.}$ with no voltage applied that a thermal distribution could well be obtained.

Another important parameter which must be considered is the average energy of the electrons during the application of the pulse. A very rough approximation to this can be obtained from the Langevin expression

$$\bar{E} = 0.33 \frac{\lambda^2 X^2 \epsilon}{v^2 m} \quad (3)$$

where λ is the Ramsauer free path, X is the field strength, and v is the drift velocity. The free path is a function of the energy so that the energy must be estimated in order to choose the free path. Loeb² states that data derived from this method should be good to 20%. Since it is anticipated that the average energy is going to be approximately thermal, the free path is chosen to be that at thermal energies. The free path is not known for argon-10% methane but is known for pure argon to be $1/2.1P$.²⁷ Using this value at atmospheric pressure, the average energy is 0.038 e.v., which is not much above thermal energies. The approximate nature of the free path used in this calculation does not warrant iteration. If the value for the drift velocity in pure argon is used, the average energy is 3.8 e.v., demonstrating that the methane does lower the average energy considerably. The latter point is in agreement with the calculations made by Uman,²⁸ which demonstrated that traces of molecular gases in argon lower the average energy of electrons in the presence of an electric field.

An additional study of the effect of the energy of the electrons during the pulse with respect to electron capture was carried out. The capture coefficient for anthracene was measured as a function of voltage in argon and argon-10% methane. The value with the argon-10% methane and the pure argon did not vary as a function of voltage from 10 to 80 v., indicating that the portion of the reaction taking place during the

application of the voltage is either negligible or coincidentally the same as the capture of electrons when an electric field is not applied.

In addition, the ratio of capture coefficient of chlorobenzene to that of azulene was measured as a function of voltage, methane concentration, and pulse time. Chlorobenzene probably undergoes dissociative capture in an endothermic process, while azulene probably forms a stable negative ion in a thermoneutral or exothermic process of attachment. Under these assumptions it would be expected that the capture of electrons by chlorobenzene would vary quite considerably with electron energy while that of azulene would be relatively insensitive. In Figure 3, this ratio is plotted as a function of voltage at a fixed pulse time and pulse width for different carrier gas mixtures. For pure argon, this ratio reaches a maximum at 50 v., whereas it remains relatively constant for argon plus methane. This type of behavior is qualitatively in agreement with the work of Stockdale and Hurst,²⁹ who have recently observed that the cross section for the dissociative capture of electrons by chlorobenzene peaks at a mean energy of 0.5 e.v. This substantiates the claim that the mean energy of the

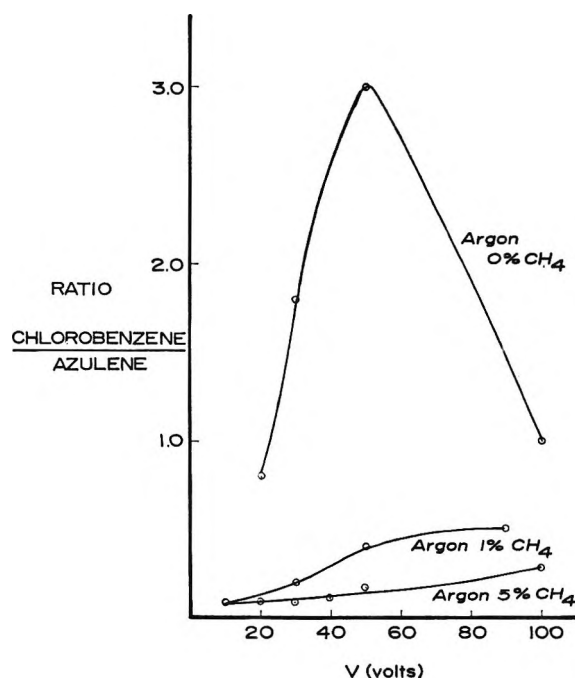


Figure 3. Ratio of the response of chlorobenzene to the response of azulene vs. voltage applied for different argon-methane ratios.

(28) M. A. Uman, *Phys. Rev.*, **133**, A1266 (1964).

(29) J. A. Stockdale and G. S. Hurst, *J. Chem. Phys.*, **41**, 255 (1964).

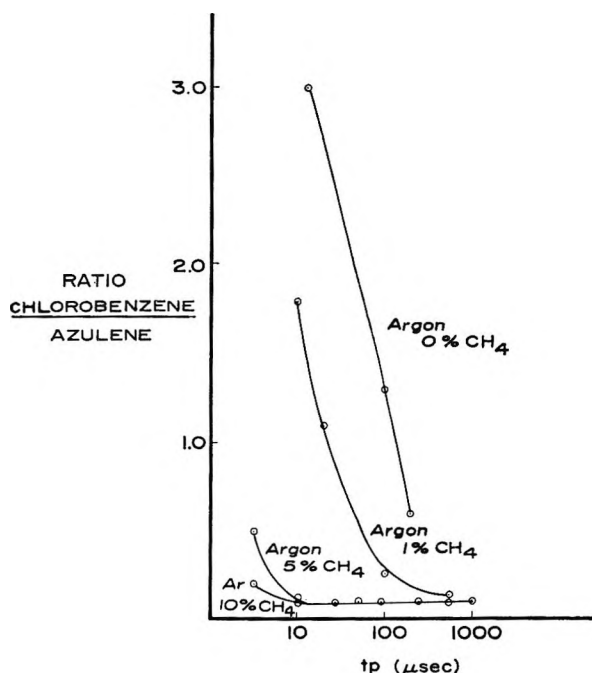


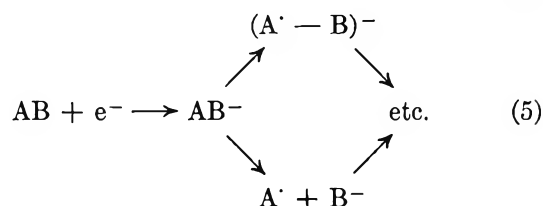
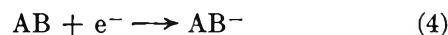
Figure 4. Ratio of the response of chlorobenzene to the response of azulene vs. the time between pulses for different argon-methane ratios.

electrons is higher than thermal in pure argon but is lowered by the addition of methane. Figure 4 shows the variation in the same ratio as a function of pulse time at a fixed pulse width and a fixed voltage for several carrier gases. The difference in the curves for pure argon and argon-10% methane clearly emphasizes the previous point. In addition, this illustration demonstrates that the reaction taking place during the application of the pulse is negligible since, after 10 μ sec. pulse time, the relative response remains constant.

Another indication of the presence of thermal electrons is the value of the probability for the attachment of an electron to a neutral molecule at thermal energies. It will be seen in a later section that an estimate of this value can be obtained for some compounds and that this value is approximately unity. Higman and Fox,³⁰ for SF₆, and more recently, Asundi and Craggs,³¹ for SF₆ and C₇F₁₃, have shown that the cross section for attachment in these gases reaches a maximum value corresponding to approximately unit probability around thermal energies and remains high for a narrow range of energies.

In addition to the electrons, the β particles also produce positive species. In the case of argon-10% methane as the carrier gas, these are probably CH₂⁺, CH₃⁺, and Ar⁺.³² Thus, if only the carrier gas is

present and no field is applied, the loss of electrons can be due to recombination, diffusion, or attachment. The effect of diffusion is small as can be seen by consulting ref. 2, p. 203. With a capturing species present, two types of electron attachment may take place.



In the first case, a stable negative ion is formed which will only recombine with the positive species or react with the radicals. In the second case, the negative ion dissociates and forms radicals and ions or a radical-ion which can subsequently react further.

Description of the Model

The description of the model for the events occurring within the electron capture cell in the pulse-sampling mode is probably best initiated by a discussion of the assumptions made in the model. As will be seen shortly, the justification for most of these assumptions can be found in the results of the experiments just described.

The first assumption to be made is that the rate of production of thermal electrons is a constant which is not affected by the presence of the added capturing species. Next, it is assumed that the reaction zone is localized in the region about 1 to 2 mm. from the tritium foil. The reaction zone includes a cloud of ions, electrons, and radicals in addition to the argon-methane mixture and the electron-capturing species. Since the electrons are being continuously removed by the application of the pulse and the positive species are only removed by the much slower flow out the end of the cell or by being collected at the other electrode, it is assumed that the cloud is not neutral but rather has an excess of positive species. In addition, it is assumed that there is an excess of radicals in the cloud. The cloud is considered to be homogeneous, or if localized clusters of ions exist, the kinetics are valid in the localized region. The reaction zone can be treated as a static system with respect to the electron concentration since the flow out of the cell is much slower than

(30) W. M. Higman and R. E. Fox, *J. Chem. Phys.*, **25**, 642 (1956).

(31) R. K. Asundi and J. D. Craggs, *Proc. Phys. Soc. (London)*, **83**, 611 (1964).

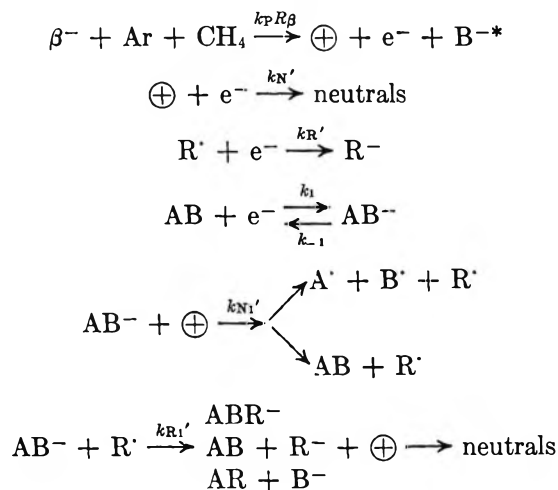
(32) F. H. Field, N. H. Head, and J. L. Franklin, *J. Am. Chem. Soc.*, **84**, 1118 (1962).

the pulse times. The slow removal of material occurs by the flow of the carrier gas approximately parallel to the face of the tritium foil.

The primary mode for the loss of electrons in the presence of carrier gas alone is the recombination of the electrons with the positive species and/or the reaction of electrons with radicals. It is assumed that diffusion losses are minor. It is not necessarily assumed that electron capture by an impurity in the carrier gas is absent. However, if such an impurity is present, it is assumed that the concentration of such a species is constant. This may arise, for example, from a small amount of bleeding from a gas chromatographic column or from O₂ in the carrier gas. In the presence of an electron-capturing species which has been deliberately added, electrons will be lost by the capture of electrons to form negative ions. If the negative ions are stable, then detachment of the electrons can occur or the negative ions can recombine with the positive species. If the negative ions dissociate, then a host of subsequent reactions are possible. The final assumption is that the amount of material which undergoes electron capture is small in comparison to the total amount of material present.

The rate constant, $k_p R_\beta$, will be used to represent a composite process for thermal electron production. This process includes ionization of carrier gas by β particles followed by numerous electron-carrier gas molecule collisions. Other variables are defined as: a , the concentration of the capturing species, AB; b , the concentration of electrons in the absence of a capturing species; $[e^-]$, the concentration of electrons in the presence of AB; $[\oplus]$, the concentration of the positive species; $[R^\cdot]$, the concentration of the radicals.

The processes taking place in the cloud and their respective rate constants can be described as



In the absence of a capturing species and assuming

$[\oplus] \gg [e^-]$, the following differential equations can be written

$$\frac{d[e^-]}{dt} = k_p R_\beta - k_{N'}[\oplus][e^-] - k_R'[R^\cdot][e^-] \quad (6)$$

$$\frac{d[\oplus]}{dt} \approx 0 \quad (7)$$

If $[R^\cdot] \approx cst$, eq. 6 can be solved directly to give

$$b = \frac{k_p R_\beta}{k_R'[R^\cdot] + k_{N'}[\oplus]} (1 - e^{-(k_{N'}[\oplus] + k_R'[R^\cdot])t}) \quad (8)$$

In the presence of a capturing species AB which does not dissociate and again assuming $[\oplus] \gg [e^-]$ and $[\text{AB}] = a - [\text{AB}^-] \approx a$, $[R^\cdot] \approx cst$, eq. 6 becomes

$$\begin{aligned} \frac{d[e^-]}{dt} &= k_p R_\beta - k_{N'}[\oplus][e^-] - \\ &\quad k_1 a [e^-] + k_{-1} [\text{AB}^-] - k_R'[R^\cdot][e^-] \quad (9) \end{aligned}$$

The equation for the rate of formation of $[\text{AB}^-]$ is

$$\begin{aligned} \frac{d[\text{AB}^-]}{dt} &= k_1 a [e^-] - k_{-1} [\text{AB}^-] - \\ &\quad k_{N'}[\ominus][\text{AB}^-] - k_R'[R^\cdot][\text{AB}^-] \quad (10) \end{aligned}$$

or with the following definitions

$$k_L = k_{N1}'[\oplus] + k_{R1}'[R^\cdot] \quad (11)$$

$$k_D = k_{N'}[\oplus] + k_R'[R^\cdot] \quad (12)$$

eq. 9 and 10 become

$$\frac{d[e^-]}{dt} = k_p R_\beta - k_D [e^-] - k_1 a [e^-] + k_{-1} [\text{AB}^-] \quad (13)$$

$$\frac{d[\text{AB}^-]}{dt} = k_1 a [e^-] - k_{-1} [\text{AB}^-] - k_L [\text{AB}^-] \quad (14)$$

These equations can be solved simultaneously to give

$$\begin{aligned} [e^-] &= \frac{k_p R_\beta}{k_D \left(\frac{k_L k_1 a}{k_D (k_L + k_{-1})} + 1 \right)} + \\ &\quad \frac{k_p R_\beta (K_1 + k_{-1} + k_L) e^{K_1 t}}{K_1 (\sqrt{\quad})} - \frac{k_p R_\beta (K_2 + k_{-1} + k_L) e^{K_2 t}}{K_2 (\sqrt{\quad})} \quad (15) \end{aligned}$$

$$K_1 = \frac{-[k_1 a + k_{-1} + k_L + k_D] + \sqrt{\quad}}{2} \quad (16)$$

$$K_2 = \frac{-(k_1 a + k_{-1} + k_L + k_D) - \sqrt{\quad}}{2} \quad (17)$$

$$\sqrt{\quad} = \sqrt{(k_1a + k_{-1} + k_L + k_D)^2 - 4\{(k_L)(k_1a + k_D) + k_1k_D\}} \quad (18)$$

K_1 and K_2 are both negative quantities so that at time infinity, eq. 15 becomes

$$[e^-]_{t=\infty} = \frac{k_p R_\beta}{k_D \left(\frac{k_L k_1 a}{k_D (k_L + k_{-1})} + 1 \right)} \quad (19)$$

and eq. 8 becomes

$$b_{t=\infty} = \frac{k_p R_\beta}{k_D} \quad (20)$$

then

$$\frac{b - [e^-]}{[e^-]_{t=\infty}} = \frac{k_L k_1 a}{k_D (k_L + k_{-1})} \quad (21)$$

Equation 21 can also be obtained from eq. 13 and 14 by applying the steady-state criteria to the species $[AB^-]$ and $[e^-]$. In that case

$$\frac{d[e^-]}{dt} = 0 = k_p R_\beta - k_D [e^-] - k_1 a [e^-] + k_{-1} [AB^-] \quad (22)$$

$$\frac{d[AB^-]}{dt} = 0 = k_1 a [e^-] - k_{-1} [AB^-] - k_L [AB^-] \quad (23)$$

or solving eq. 23 for AB^- gives

$$[AB^-] = \frac{k_1 a [e^-]}{k_{-1} + k_L} \quad (24)$$

or substituting in eq. 22 and solving for $[e^-]$ gives

$$[e^-] = \frac{k_p R_\beta}{k_D \left(\frac{k_L k_1 a}{k_D (k_L + k_{-1})} + 1 \right)} \quad (25)$$

which is identical with eq. 19.

In a gas chromatographic system there is often bleeding of the liquid phase from the column, or when the temperature of the column is increased, there is bleeding of materials accumulated on the column from the numerous injections at the lower temperature. In addition, there may be impurities in the carrier gas which come through the column and pass through the detector. Thus, it is necessary to see how impurities of this type would affect the response of the detector for a particular compound.

If the species is the same as the capturing species being studied, then no new processes would have to be considered. When a constant concentration of

AB , designated as a_0 , is bleeding into the gas stream the concentration of the electrons, b , is given by

$$b = \frac{k_p R_\beta}{k_D \left(\frac{k_1 k_L a_0}{(k_D (k_L + k_{-1}))} + 1 \right)} \quad (26)$$

If the impurity is different from the species being studied, then the processes of attachment, detachment, and recombination must also be considered for this species. Designating the impurity as C , the rate constants for these three processes can be symbolized by k_{1C} , k_{-1C} , k_{LC} . It is assumed that the exchange of electrons between species C and AB is negligible. In this case, b , the concentration of electrons before the addition of AB is given by

$$b = \frac{k_p R_\beta}{k_D \left(\frac{k_{LC} k_{1C} C}{k_D (k_{LC} + k_{-1C})} + 1 \right)} \quad (27)$$

In both cases, the steady-state criteria lead to the equation

$$\frac{b - [e^-]}{[e^-]} = \frac{k_L k_1 a}{k_D (k_L + k_{-1})} \frac{b}{b_0} = K a \frac{b}{b_0} \quad (28)$$

where b_0 is the maximum concentration of electrons and is given by

$$b_0 = \frac{k_p R_\beta}{k_D} \quad (29)$$

Thus, if the standing current varies owing to bleeding from the column, it is possible to correct the response to the maximum standing current from eq. 28. It must be emphasized that changes in the standing current due to variations in the degree of ionization or changes in performance of electronic apparatus should not be corrected in this manner. The correction is also valid if C has a large electron affinity so that if electron transfer occurs, it only occurs from AB^- to C .

In each of these three cases, the corrected response is proportional to the concentration of the electron capturing species which is being studied. Thus, the capture coefficient, K , can be determined from the slope of the linear graph of corrected response *vs.* concentration of the capturing species.

Since the capture coefficient, K , contains the term $(k_L + k_{-1})$ (eq. 21), it is convenient to consider the case where $k_L \gg k_{-1}$ and the case when $k_{-1} \gg k_L$, in order to examine the type of temperature dependency to be expected. If the temperature variation for the forward rate is slight, corresponding to no energy of activation for the addition of an electron, and if the

electron affinity of the molecule is appreciable, then the backward rate constant, k_{-1} , must have a significant temperature variation. Thus, it is quite likely that there would exist a region at low temperatures where k_L , which is relatively temperature insensitive, would be greater than k_{-1} and a region at higher temperatures where the opposite would be true. In the latter region, designated α , it is assumed that $k_{-1} \gg k_L$ so that eq. 21 becomes

$$\frac{b - [e^-]}{[e^-]} = Ka = \frac{k_L}{k_D} \frac{k_1}{k_{-1}} a = \frac{k_L}{k_D} K_{eq} a \quad (30)$$

or assuming an ideal gas and using the statistical mechanical expression for K_{eq}

$$K = \frac{k_L}{k_D} K_{eq} = \frac{k_L}{k_D} A T^{-3/2} \exp(EA/kT) \quad (31)$$

or

$$\ln(KT^{3/2}) = \ln \frac{k_L}{k_D} + \ln A + \frac{EA}{kT} \quad (32)$$

If it is assumed that k_L/k_D is temperature independent, then $\ln KT^{3/2}$ is a linear function of $1/T$ with a slope of EA/k and an intercept of $\ln k_L/k_D + \ln A$. In the former region, designated β , it is assumed that $k_L \ll k_{-1}$ so that k_{-1} can be neglected in comparison to k_L and eq. 21 becomes

$$\frac{b - [e^-]}{[e^-]} = Ka = \frac{k_1}{k_D} a \quad (33)$$

If there is no energy barrier to the addition of an electron, then K should be relatively insensitive to temperature in this region.

Results

Figure 5 shows the variation of the electron concentration, n_{e^-} , as a function of time at different proportions of argon-methane as the carrier gas. The measurements were carried out at room temperature at fixed pulse width. This function should fit the expression given in eq. 8, $b = k_p R_\beta / k_D (1 - e^{-k_D t})$. The general variation is correct; however, the occurrence of the maximum at about 200 μsec . is not in agreement with eq. 8. If the contribution of the radical reactions is small, this can be explained by considering a change in the concentration of the positive species at different times, which in turn could be attributed to a different manner by which the positive species are lost. At lower pulse times, where the voltage is on about 1% of the time, the primary mode for the loss of the positive species is presumably by the collection at the negative electrode. At longer

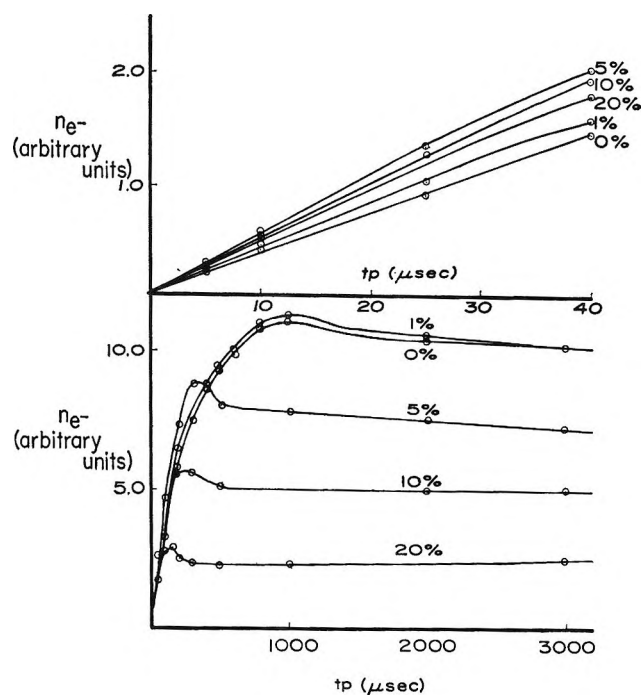


Figure 5. Electron concentration vs. time between pulses for several argon-methane ratios.

times, the loss could be due primarily to flow out of the cell. Figure 6 shows the variation of k_D as a function of time, or essentially the variation of the positive species, which is necessary to correct the electron concentration curves to a pure exponential. The curve is not defined at lower times since the limiting expression for the electron concentration is given by

$$b_{t \rightarrow 0} = k_p R_\beta \quad (34)$$

which is independent of k_D . It should be emphasized at this point that although the concentration of the positive species can vary from time to time, it is assumed to be constant at a given time. The curves given in Figure 6 are relatively insensitive to temperature.

Using eq. 34 it is possible to estimate the rate of production of the thermal electrons, $k_p R_\beta$, from the limiting slope at lower pulse times. With this information and the b value in the plateau region, it is possible to estimate the pseudo-first-order rate constant, k_D , from eq. 20. Then with an order of magnitude estimate of the second-order recombination rate constant, it is possible to obtain a rough approximation for the concentration of the positive species if the electron-radical reactions are neglected. These results are given in Table I.

The points to be noted in this table are: (1) the rate of ionization is increased by the addition of the methane

Table I

% CH ₄	$k_p R \beta$, mole/l. sec.	$k_D(t=1000)$, sec. ⁻¹	k'_N , l./mole sec.	$[\Theta]_{(t=1000\mu\text{sec})}$, mole/l.	$[e^-]_{(t=1000\mu\text{sec})}$, mole/l.
0	3.73×10^{-10}	6.5×10^2	2×10^{13}	1.8×10^{-10}	1.1×10^{-13}
1	4.35×10^{-10}	7.2×10^2			1.2×10^{-13}
5	6.06×10^{-10}	1.7×10^3			0.8×10^{-13}
10	5.96×10^{-10}	2.4×10^3			0.5×10^{-13}
20	5.59×10^{-10}	4.6×10^3			0.25×10^{-13}

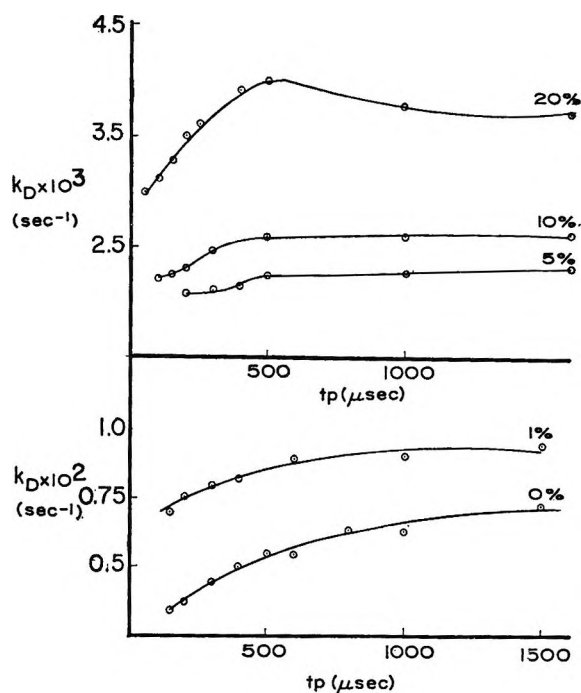


Figure 6. Pseudo rate constant for the loss of electrons *vs.* time between pulses for different argon-methane ratios.

as has been observed earlier;³³ (2) the pseudo-first-order rate constant, k_D , is higher with the methane present than with pure argon; and (3) the concentration of positive species is much greater than the electron concentration. This increase of k_D can be due to two possible factors: (1) a higher concentration of positive species and radicals, and (2) an increase in the second-order rate constants for recombination and/or radical reaction. Actually, both factors probably contribute to this effect, since the increased ionization would favor a higher concentration of the positive species, and the presence of vibrational and rotational modes of energy loss with the positive species and/or radicals formed in the presence of methane would favor higher intrinsic rate constants.

The infinite time assumption or the equivalent steady-state assumption was tested by measuring the response for a capturing species at different pulse times.

The results show a general qualitative agreement with the function given by eq. 15, increasing at shorter pulse times and reaching a constant value at longer times.

The concentration dependency of the corrected response according to eq. 28 is given in terms of the instantaneous concentration of the capturing species; however, only the total amount of sample injected is actually known, making it necessary to integrate the corrected response with respect to the volume of gas passed through the cell. Rearranging eq. 28 gives

$$\frac{b_0 b - [e^-]}{b [e^-]} = Ka \quad (35)$$

Integration with respect to volume gives

$$\frac{b_0}{b} \int \frac{b - [e^-]}{[e^-]} dV = Ka \quad (36)$$

or

$$\frac{b_0}{b} \int \frac{b - [e^-]}{[e^-]} dx = \frac{S}{F} KMZ \quad (37)$$

where x is the chart distance in inches, S is the chart speed in inches per minute, F is the flow rate in milliliters per minute, and A is the total number of moles injected and is equal to the molar concentration of the solution injected, M , times the sample size, Z , in liters. Figure 7 shows several plots of the corrected area *vs.* sample size injected for several different compounds at approximately the same temperature. Similar linear results are obtained at other temperatures. The data were reduced by a weighted least-squares procedure with the slope and intercept taken as parameters. The integration was carried out by drawing triangles and transforming the heights. This procedure is quite suitable at lower percentages of capture but must be modified at higher percentages. In future work, the integrations will be carried out using a digital or analog computer calculating $(b - [e^-])/[e^-]$ at each point before integration. In the triangu-

(33) W. P. Jesse, "Penetration of Charged Particles in Matter," E. A. Uehling, Ed., Publication 752 National Academy of Sciences, National Research Council, Washington, D. C., 1960.

lation procedure, the greatest error is in the width. In the least-squares adjustment, the error in the area arises primarily from the width measurement which is assumed to be constant. The error in the area was thus

$$\sigma_A^2 = \left(\frac{\partial \text{area}}{\partial W} \right)^2 \sigma_W^2 = (1/2h\sigma_W)^2 = \left(\frac{\text{area}}{W} \sigma_W \right)^2 \quad (38)$$

The error in the sample size was also assumed to be constant and equal to 0.1 μl . The points were then weighted in the following manner

$$W_A = \frac{\sigma_A^2}{\sigma_0^2} = \left(\frac{\text{area}}{W} \right)^2 \frac{\sigma_W^2}{\sigma_0^2} \quad (39)$$

$$W_Z = \frac{\sigma_Z^2}{\sigma_0^2} = 1 \quad (40)$$

The lines shown in Figure 7 are the lines obtained from the least-squares adjustment and support the proposed mechanisms. The slopes determined in this manner are proportional to the capture coefficient. The ratio b_0/b can be obtained by lowering the temperature on the column or by eliminating the column entirely. The variation in this quantity was small for the different compounds studied. The error in the capture coefficient is obtained by the normal propagation of error using the error in the slope obtained from the least-squares adjustment and using constant errors in the flow rate, concentrations, and chart speed.

In Figure 8, $\ln KT^{3/2}$ (see eq. 32) is plotted as a function of $1/T$. The two types of regions are quite obvious, but in the cases of naphthalene, phenanthrene, triphenylene, and chrysene, there is no β region. In the α region, the slope is proportional to the electron affinity from eq. 32 and the intercept is $\ln A + \ln k_L/k_D$. The curves shown in Figure 8 for this region are calculated from the least-squares estimates of the slope and intercept. The values for the intercepts and the electron affinities obtained from the slope can be found in columns 1 and 2 of Table II.

The value of $\ln A$ is 12.5 and the average value for the intercept is 14.3, so that $k_L \approx 8k_D$. Since the deviations from the average value of the intercept are small, the ratio k_L/k_D is approximately constant. Initially, it appeared strange that $k_L \approx 8k_D$ since the velocity of the electron is so much greater than the velocity of a negative ion. However, if one considers the fact that a species which is traveling faster must approach closer to the positive species or radicals in order to become permanently attached, then the fact that the two pseudo rate constants are within an order of magnitude is reasonable. This fact is also confirmed by other studies. For example, the electron-positive

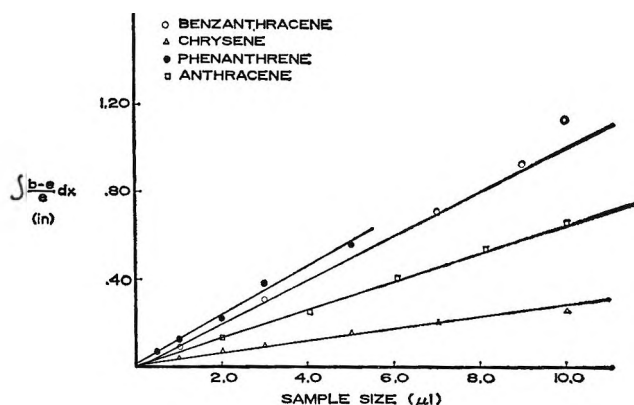


Figure 7. Integrated response vs. sample size for several different compounds.

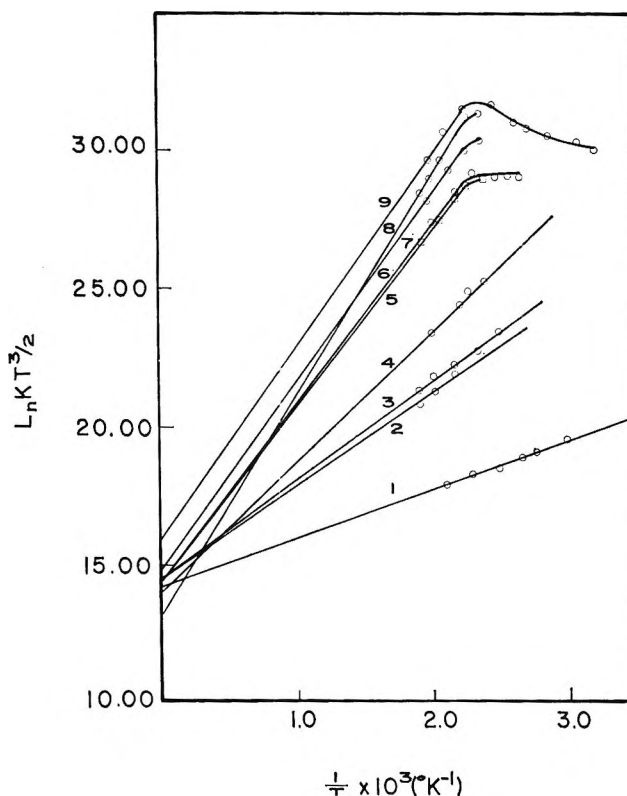


Figure 8. $\log KT^{3/2}$ vs. $1/T$. The K values are referenced to the maximum standing current: 1, naphthalene; 2, triphenylene; 3, phenanthrene; 4, chrysene; 5, benzo(c)phenanthrene; 6, anthracene; 7, pyrene; 8, benzantracene; 9, azulene.

ion recombination rate constant in argon was determined by Oskam and Middlestadt³⁴ to be $6.7 \pm 0.5 \times 10^{-7}$ cm^3/sec ., at 9–35 mm. and 300°K. while the recombination rate constant, k_0 , for the reaction

(34) H. J. Oskam and V. R. Middlestadt, *Phys. Rev.*, **132**, 1445 (1963).

Table II

Compound	Electron affinity, slope, e.v. $\pm \sigma_{e.a.}$, e.v.	Intercept $\pm \sigma$ intercept	E.a., fixed intercept, e.v. $\pm \sigma_{e.a.}$, e.v.	E.a., ref. 13, e.v.	E.a., ref. 14, e.v.
Naphthalene	0.152 \pm 0.016	14.21 \pm 0.51	0.148 \pm 0.006		
Triphenylene	0.284 \pm 0.020	14.38 \pm 1.54	0.285 \pm 0.008	0.14	
Phenanthrene	0.308 \pm 0.024	14.33 \pm 0.63	0.307 \pm 0.007	0.20	0.25
Chrysene	0.419 \pm 0.036	13.98 \pm 0.92	0.397 \pm 0.007	0.33	
Benzo(c)phenanthrene	0.542 \pm 0.040	14.44 \pm 0.97	0.545 \pm 0.008	0.33	
Anthracene	0.552 \pm 0.061	14.44 \pm 1.52	0.556 \pm 0.008	0.42	0.61
Pyrene	0.579 \pm 0.064	14.66 \pm 1.58	0.591 \pm 0.008	0.39	0.55
Benz(a)anthracene	0.696 \pm 0.045	12.94 \pm 1.03	0.630 \pm 0.008	0.46	
Azulene	0.587 \pm 0.065	16.06 \pm 1.29	0.656 \pm 0.008		

$\text{NO}^+ + \text{NO}_2^- \rightarrow$ neutrals was determined to be $3.8\text{--}4.0 \times 10^{-7}$ cm.³/sec., in argon at 41 mm. and 298°K. by Mahan and Person.³⁵ Thus the two constants are of comparable magnitude.

The electron affinities have also been calculated assuming a fixed intercept and are included in column 3 of Table II. These values were calculated by using all of the data for the aromatic hydrocarbons and the data for six aromatic aldehydes and ketones (data to be published later) to determine the best value for the fixed intercept and the best values for the slopes according to the least-squares criteria. This would normally entail solving an $n + 1$ by $n + 1$ matrix, but a simplified technique which involves solving a two by two matrix $2n$ times has been developed and will be reported shortly.³⁶ These values obtained by assuming a fixed intercept probably give the best value of the electron affinity for compounds in which the intercept and slope are poorly defined. However, the errors which are quoted may be optimistic in light of the additional assumptions which must be made. The assumption of a constant intercept implies that k_L/k_D is the same for all compounds and that all of the corrections for secondary capturing species have been correctly taken into account. The first implication is probably the most serious one, especially when one considers the fact that the forward rate of attachment of an electron, as will be shown shortly, does vary. The latter point could become critical if, for example, there are drifts in the electronics or if the activity of the tritium varies significantly. The latter technique is the same as was used to calculate the electron affinities in ref. 13. The electron affinities given in that article are also listed in column 4 of Table II. It can be seen that the values obtained from the slope are generally about 0.1–0.2 e.v. higher than the earlier values.¹³ The reasons for this difference are: (1) the data were

referenced to an absolute value of the capture coefficient for anthracene determined in the β region, and (2) the reference capture coefficient was determined at short pulse times.

In order to support the interpretation of the electron capture coefficients in terms of the electron affinities, the earlier values were compared to other experimental estimates of the electron affinities, such as the half-wave reduction potential,¹³ the 0–0 frequency, and the ionization potential of the aromatic hydrocarbons.¹⁶ Since the values determined from the slope differ from the earlier values by a constant, the same general trends will still be valid. In the earlier paper, the experimental results were also compared with the theoretical calculation by Hoyland and Goodman,¹⁴ which are also shown in Table II. The agreement between the values obtained from the slope and these values is also quite good.

Before leaving the subject of the determination of electron affinities, it should be emphasized that the variation of the capture coefficient with temperature is necessary before any estimate of the electron affinity can be made. As pointed out earlier, Briegleb¹⁹ estimated the electron affinities of several compounds using the method given earlier in ref. 13 and using capture coefficients published in ref. 5–12. No distinction was made between compounds which dissociate and compounds which form stable negative ions.

Some preliminary work has been done on dissociative compounds. The fact that these compounds actually dissociate would best be shown by obtaining the products of the reaction and determining their composition. This type of study is being initiated in this

(35) B. C. Mahan and J. C. Person, *J. Chem. Phys.*, **40**, 392 (1964).

(36) W. E. Wentworth, W. Hirsch, and E. Chen, in preparation.

Table III

Compound	k_D , sec. ⁻¹	k_L , sec. ⁻¹	k_1 , l./mole sec.	k_{-1} , sec. ⁻¹
Anthracene	2.4×10^3	2.0×10^4	2.7×10^{12}	$8.0 \times 10^8 T^{3/2} \exp(-0.552/kT)$
Benzo(c)phenanthrene	2.4×10^3	2.0×10^4	2.5×10^{12}	$4.5 \times 10^8 T^{3/2} \exp(-0.542/kT)$
Pyrene	2.4×10^3	2.0×10^4	7.5×10^{12}	$1.6 \times 10^7 T^{3/2} \exp(-0.597/kT)$
Benzantracene	2.4×10^3	2.0×10^4	3.6×10^{13}	$6.0 \times 10^8 T^{3/2} \exp(-0.696/kT)$

laboratory presently. However, the dissociative compounds can also be differentiated by considering the energies of the processes which are postulated in the reaction or by considering the chemical nature of the compounds. In addition, the results which have been obtained for compounds which are thought to be dissociated with regard to the temperature dependency of the capture coefficient are quite different from the results obtained for the compounds which form stable negative ions. For compounds which apparently are dissociative, the capture coefficients either increase with increasing temperature or show no temperature dependency. The results obtained by Briegleb¹⁹ for the chloro, bromo, and iodo compounds are probably invalid since dissociation most likely occurs upon electron attachment.

In addition, the values for the compounds which do form stable negative ions given by Briegleb¹⁹ are inaccurate (1) because the temperature of the measurements of the capture coefficients, except for the aromatic hydrocarbons, were not specified in the original references, and (2) because the type of temperature variation was not determined. For example, studies of the capture coefficients of nitrobenzene as a function of temperature indicate that up to 225°, there is no temperature variation so that nitrobenzene could possibly be in the β region up to that temperature, if it forms a stable negative ion. Under these conditions the data in the β region place a lower limit upon the electron affinity of nitrobenzene of 0.8 e.v. This value is even higher than the value given by Briegleb¹⁹ for the electron affinity of trinitrobenzene obtained from charge-transfer data which should be greater than that of nitrobenzene; therefore, this implies that Briegleb's values are all consistently low. This point will be pursued further in future studies by measuring the electron affinity of compounds which are common acceptors in charge-transfer complexes.

At low temperatures, when a compound enters a β region, the ratio, k_1/k_D can be determined, or if no β region is exhibited, a lower limit for that ratio can be estimated; the ratio k_1/k_{-1} as a function of temperature can be determined from the α region; the

ratio k_L/k_D can be estimated from the intercept, and k_D can be estimated from the variation of the current as a function of pulse time. In this manner, all of the rate constants can be determined. In this calculation, it has been assumed that the preexponential term for the rate constant k_{-1} has a $T^{3/2}$ dependency. The intrinsic second-order rate constants cannot be determined because the concentrations of the positive species and the radicals are not known. The results for the aromatic hydrocarbons are given in Table III. The average value of k_L/k_D was used in these calculations.

From this analysis, it can be seen that the rate constant for the addition of an electron to a molecule is not constant but varies over a range of an order of magnitude. The molecule, azulene, is unique in that in the β region, there is an exponential temperature dependence with an activation energy of about 0.15 e.v., indicating a possible barrier to the addition of an electron. Such a barrier could conceivably be due to a promotion of the azulene molecule to an excited vibrational level to which the addition of the electron would be more probable than in the ground state.

The magnitude of the forward rate constants is approximately that to be expected for the number of collisions between electrons and the molecule indicating that the electron is attached with every collision. This would correspond to a unit probability for attachment. The major problem with this type of interpretation is the difficulty in defining a collision between an electron and a molecule. In other words, the theoretical cross section is not well known.

Conclusions

The pulse-sampling technique as applied to the electron capture detector is a valuable tool for studying phenomena associated with the attachment of thermal electrons to molecules. The unique opportunity of observing these phenomena in conjunction with a gas chromatographic separation allows one to carry out these studies on small and very pure samples.

The model for the processes occurring in the electron capture cell in the presence of a molecule which forms

a stable negative ion agrees with the experimental data. Using the results of the steady state or "infinite time" treatment of the kinetics of the model for the compounds which form stable negative ions, the electron affinity can be determined if the compounds exhibit an α region. If the compounds also exhibit a β region, the rate constant for the attachment of an electron to the molecule, k_1 , and that for the detachment of an electron from a negative ion, k_{-1} , can be determined. In addition, the pseudo-first-order rate constants for the recombination of positive species with an electron and/or radical reactions, k_D , and with a negative ion, k_L , can be de-

termined. The rate of production of thermal electrons can also be determined.

Acknowledgments. The contributions to this paper by W. E. Wentworth and E. Chen were supported financially by the Robert A. Welch Foundation. The investigation carried out by J. E. Lovelock was supported by a research grant, AP 00308-01, from the Public Health Service of the U. S. Department of Health, Education, and Welfare. E. Chen was also a NASA Predoctoral Fellow during the latter portion of these studies. The authors also wish to acknowledge the helpful discussions with Dr. J. L. Franklin, Dr. D. C. Conway, and Dr. R. S. Becker.

Green's Function Analysis of the In-Plane Vibrations of Some Isotopic Ethylenes^{1a}

by S. J. Cyvin^{1b}

Department of Chemistry, Oregon State University, Corvallis, Oregon (Received August 11, 1965)

The theory of Green's function applied to molecular vibrations of isotopic molecules is re-formulated and expressed in what is believed to be a more conventional notation than that of deWames, *et al.* A detailed account on the concept of "mixing parameters" is included. The theory is applied to the planar vibrations of some isotopic ethylenes. Here for the first time a symmetry block of 3×3 appears in the "unperturbed" molecule treated by this method. The Teller-Redlich product rules for symmetric substitutions are reevaluated, along with some new frequency sum rules. Squared mixing parameters for ethylene are reported from (a) a force-constant calculation with adjusted frequencies and (b) the Green's function method with observed frequencies. The latter calculations (b) gave imaginary mixing parameters, demonstrating the necessity of adjusting the observed fundamentals.

I. Introduction

In some recent papers^{2,3} deWames, *et al.*, have presented the application of Green's function to problems in the field of harmonic vibrations of polyatomic molecules. The new method of treating the vibrations of "perturbed molecules" is very interesting and seems to have a powerful applicability. It is felt, however, that the investigators have exaggerated its usefulness in some aspects, on which it shall be commented in the following.

1. In ref 2a the authors claim that the Teller-Redlich product rule in their version (for a triatomic

(1) (a) This project has been supported by the National Science Foundation under Grant GP-2830. (b) Fulbright-Hays Research Scholar; on leave from Technical University of Norway, Trondheim, Norway.

(2) (a) R. E. deWames and T. Wolfram, *J. Chem. Phys.*, **40**, 853 (1964); (b) C. D. Bass, L. Lynds, T. Wolfram, and R. E. deWames, *ibid.*, **40**, 3611 (1964).

(3) T. Wolfram, C. D. Bass, R. E. deWames, and L. Lynds, to be published.

molecule) is considerably simpler than usual when derived from Green's function, since then it is not necessary to know the moments of inertia of the molecules. The same result is, however, obtained much simpler and still without explicit use of moments of inertia by means of the \mathbf{G} matrix determinants in the method of Wilson.⁴

In the present application of Green's function to ethylenes, moments of inertia (and total molecule masses) do appear in the derived Teller-Redlich product rules, but these quantities have merely been introduced as suitable abbreviations in the course of the computations.

2. In the applications communicated by deWames, *et al.*,^{2,3} the symmetry block dimensions of the unperturbed molecules never exceed 2. Hence the treatment becomes comparatively simple, because only one mixing parameter is associated with each 2×2 block. The evaluation of arithmetic expressions is expected to increase rapidly in complexity as the block dimension increases.

In the present work the method of Green's function was successfully applied to the totally symmetric 3×3 block in ethylene. There does not seem to be a principal limitation of the method on account of block dimensions, but the practical applicability is more limited as the arithmetic evaluations constitute an essential part of the method. To the writer's opinion the exact arithmetic forms of certain frequency sum rules and related equations represent the most valuable results obtained by the method of Green's function. These equations contain the mixing parameters (*cf.* section V) and allow for their computation directly from vibrational frequencies, without using the force constants.

3. A further application of Green's function needs some comments. In ref 2a it is stated, "Once the mixing parameter [for H₂O] is known the Green's function can be constructed exactly and the frequencies of all other isotopes can be calculated without even employing a force constant model." As a matter of fact, the problem is already determined by the mixing parameters (calculated by some method or another) along with the frequencies of the "unperturbed" molecule. The frequencies of all isotopic ("perturbed") molecules may then equally well be calculated using the standard methods⁴ and following the steps: "unperturbed" \mathbf{L} matrix, force constants, "perturbed" \mathbf{L} matrices and frequencies. The final results from either of the methods must be precisely the same. It feels important to stress this point here because the arguments of deWames, *et al.*, easily may be misunderstood. In particular, the following state-

ment from ref 2b seems to be substantially wrong on the basis of the above discussion. "It [the Green's function method] has proved most successful and convenient for assignment of a complex spectrum where standard normal coordinate calculations would have been quite tedious, if not impossible."

II. Notation

The notation of deWames, *et al.*,^{2,3} deviates largely from that of Wilson, Decius, and Cross⁴ and other standard works on spectroscopy. It was found worthwhile to transcribe the main symbols and some of the important relations, of which the result is given in Table I. The present notation is in the right-hand column of the table, which includes the conventional symbols from Wilson, Decius, and Cross⁴ and other sources, along with related symbols devised for the purpose. The presently adopted notation will be clarified further through the comprehensive theoretical approach given in the following sections.

III. Some Coordinate Transformations

First consider the transformations between Cartesian displacement coordinates (\mathbf{X}) and sets of internal sym-

Table I: Comparison of Symbols and Relations

deWames, <i>et al.</i> ^{2,3}	Present
F (also F^c)	\mathbf{F}^x
\mathbf{M}	\mathbf{M}
\mathbf{D}	\mathbf{F}^q or \mathbf{D}
$(X_1, X_2), (Q_1, Q_2)$	(Q_1, Q_2)
(S_1, S_2)	(S_1^q, S_2^q)
$G(\omega^2)$	$g(\lambda)$
U	\mathbf{l}_{vr}'
\mathbf{X}	\mathbf{X}
α	\mathbf{R}
S_t	\mathbf{S}_{vr}^q
δ_r	\mathbf{S}
\mathbf{F}^w	\mathbf{F}
$\mathbf{T}(\delta_r = \mathbf{T}\mathbf{X})$	$\mathbf{B}(\mathbf{S} = \mathbf{B}\mathbf{X})$
δ	\mathbf{U}'
$\mathbf{f}(\mathbf{F}^w = \delta' \mathbf{f} \delta)$	$\mathbf{f}(\mathbf{F} = \mathbf{U}\mathbf{F}\mathbf{U}')$
\mathbf{S}	\mathbf{u}_{vr}'
\mathbf{D}^s	$\mathbf{u}_{vr} \mathbf{D} \mathbf{u}_{vr}'$ or $\mathbf{u} \mathbf{D} \mathbf{u}'$
$\mathbf{B} = \{\mathbf{T}\mathbf{M}^{1/2}\mathbf{S}\}$ truncated	$\mathbf{k} = \mathbf{B}\mathbf{M}^{-1/2}\mathbf{u}'$
$\mathbf{B}^{-1}(\mathbf{F}^w = (\mathbf{B}')^{-1}\mathbf{D}^s\mathbf{B}^{-1})$	$\mathbf{k}^{-1} = \mathbf{u}\mathbf{M}^{1/2}\mathbf{A}$
	$(\mathbf{F} = \mathbf{A}'\mathbf{M}^{1/2}\mathbf{u}'\mathbf{D}\mathbf{u}\mathbf{M}^{1/2}\mathbf{A})$
$\mathbf{B}\mathbf{B}' = \mathbf{G}$	$\mathbf{k}\mathbf{k}' = \mathbf{B}\mathbf{M}^{-1}\mathbf{B}' = \mathbf{G}$
\mathbf{A}	α or α_{vr}
$\mathbf{\Lambda}$	$\mathbf{\Lambda}$ or $\mathbf{\Lambda}_{vr}$
\mathbf{H}	$\mathbf{L}(\mathbf{S} = \mathbf{L}\mathbf{Q})$
$\mathbf{H} = \mathbf{B}\mathbf{A}$	$\mathbf{L} = (\mathbf{B}\mathbf{M}^{-1/2}\mathbf{u}')\alpha = \mathbf{k}\alpha$

(4) E. B. Wilson, Jr., J. C. Decius, and P. C. Cross, "Molecular Vibrations," McGraw-Hill Book Co., Inc., New York, N. Y., 1955.

metry coordinates, where \mathbf{Q} represents the normal coordinates

$$\mathbf{S} = \mathbf{B}\mathbf{X}; \quad \mathbf{X} = \mathbf{A}\mathbf{S} \quad (1)$$

$$\mathbf{Q} = \mathbf{b}\mathbf{X}; \quad \mathbf{X} = \mathbf{a}\mathbf{Q} \quad (2)$$

Hence $\mathbf{B}\mathbf{A} = \mathbf{b}\mathbf{a} = \mathbf{E}_{(3N-6) \times (3N-6)}$. Notice that \mathbf{B} and \mathbf{b} have the dimensionality of $(3N - 6) \times 3N$, while \mathbf{A} and \mathbf{a} are $3N \times (3N - 6)$ matrices. From the transformation conventionally denoted as $\mathbf{S} = \mathbf{L}\mathbf{Q}$ one obtains the connections

$$\mathbf{b} = \mathbf{L}^{-1}\mathbf{B}; \quad \mathbf{a} = \mathbf{A}\mathbf{L} \quad (3)$$

A useful relation connecting \mathbf{A} and \mathbf{B} is due to Crawford and Fletcher⁵ and reads

$$\mathbf{A} = \mathbf{M}^{-1}\mathbf{B}'\mathbf{G}^{-1} \quad (4)$$

where \mathbf{M} is the $3N \times 3N$ matrix of atomic masses, and \mathbf{G} the Wilson \mathbf{G} matrix associated with the coordinates \mathbf{S} . Similarly, one has

$$\mathbf{a} = \mathbf{M}^{-1}\mathbf{B}'(\mathbf{L}')^{-1} = \mathbf{M}^{-1}\mathbf{b}' \quad (5)$$

The mass-weighted Cartesian displacements are introduced as

$$\mathbf{q} = \mathbf{M}^{1/2}\mathbf{X}; \quad \mathbf{X} = \mathbf{M}^{-1/2}\mathbf{q} \quad (6)$$

The transformation between the coordinates \mathbf{q} and normal coordinates is of special interest. It may be written

$$\mathbf{Q} = \mathbf{l}\mathbf{q}; \quad \mathbf{q} = \mathbf{l}'\mathbf{Q} \quad (7)$$

Notice $\mathbf{l}\mathbf{l}' = \mathbf{E}$. One has

$$\mathbf{l} = \mathbf{b}\mathbf{M}^{-1/2}, \quad \mathbf{l}' = \mathbf{M}^{1/2}\mathbf{a} = \mathbf{M}^{-1/2}\mathbf{b}' \quad (8)$$

If the six external coordinates are added to each set of internal coordinates, we will write

$$\mathbf{S}_{vr} = \mathbf{B}_{vr}\mathbf{X}; \quad \mathbf{X} = \mathbf{A}_{vr}\mathbf{S}_{vr}; \quad \mathbf{Q}_{vr} = \mathbf{b}_{vr}\mathbf{X}, \text{ etc.}$$

Then all the matrices \mathbf{B}_{vr} , \mathbf{A}_{vr} , \mathbf{b}_{vr} , etc., become square (dimension $3N \times 3N$), and one has

$$\mathbf{B}_{vr}\mathbf{A}_{vr} = \mathbf{A}_{vr}\mathbf{B}_{vr} = \mathbf{E}_{3N \times 3N}; \quad \mathbf{b}_{vr}\mathbf{a}_{vr} = \mathbf{a}_{vr}\mathbf{b}_{vr} = \mathbf{E}_{3N \times 3N} \quad (9)$$

i.e., \mathbf{A}_{vr} and \mathbf{a}_{vr} are the inverse of \mathbf{B}_{vr} and \mathbf{b}_{vr} , respectively. The important transformation of

$$\mathbf{Q}_{vr} = \mathbf{l}_{vr}\mathbf{q}; \quad \mathbf{q} = \mathbf{l}'_{vr}\mathbf{Q}_{vr} \quad (10)$$

appears to be orthogonal ($\mathbf{l}_{vr}\mathbf{l}'_{vr} = \mathbf{l}'_{vr}\mathbf{l}_{vr} = \mathbf{E}_{3N \times 3N}$).

IV. Transformation of Force Constants and Green's Function

The potential function in external coordinates may be written⁶

$$2V = \mathbf{X}'\mathbf{F}^X\mathbf{X} = \mathbf{q}'\mathbf{D}\mathbf{q} = \mathbf{Q}_{vr}'\mathbf{\Lambda}_{vr}\mathbf{Q}_{vr} \quad (11)$$

$\mathbf{\Lambda}_{vr}$ is the diagonal matrix containing the $3N - 6$ frequency parameters λ and six zeros for the external coordinates. Consequently, the following transformations of the force-constant matrices exist.

$$\mathbf{F}^X = \mathbf{b}_{vr}'\mathbf{\Lambda}_{vr}\mathbf{b}_{vr}; \quad \mathbf{D} = \mathbf{M}^{-1/2}\mathbf{F}^X\mathbf{M}^{-1/2} = \mathbf{l}_{vr}'\mathbf{\Lambda}_{vr}\mathbf{l}_{vr} \quad (12)$$

Green's function, $\mathcal{G}(\lambda)$, may be evaluated according to the transformation

$$\mathcal{G}(\lambda) = (\lambda\mathbf{E} - \mathbf{D})^{-1} = \mathbf{l}_{vr}'\mathcal{G}^Q(\lambda)\mathbf{l}_{vr} \quad (13)$$

where

$$\mathcal{G}^Q(\lambda) = (\lambda\mathbf{E} - \mathbf{\Lambda}_{vr})^{-1} \quad (14)$$

V. Mixing Parameters

External symmetry coordinates may be constructed as an orthogonal transformation of the mass-weighted Cartesian displacements

$$\mathbf{S}_{vr}^q = \mathbf{u}_{vr}\mathbf{q}; \quad \mathbf{q} = \mathbf{u}_{vr}'\mathbf{S}_{vr}^q \quad (15)$$

The transformation between the coordinates \mathbf{S}_{vr}^q and normal coordinates define the mixing parameter matrix α_{vr} . It is important to notice also that this transformation is orthogonal. One has

$$\mathbf{S}_{vr}^q = \alpha_{vr}\mathbf{Q}_{vr}; \quad \mathbf{Q}_{vr} = \alpha_{vr}'\mathbf{S}_{vr}^q \quad (16)$$

where

$$\alpha_{vr} = \mathbf{u}_{vr}\mathbf{l}'_{vr} \quad (17)$$

Let \mathbf{S}^q , \mathbf{u} , and α (without subscripts) denote the vibrational parts of the appropriate matrices. One finds

$$\alpha = \mathbf{u}\mathbf{l}' \quad (18)$$

Equation 18 is analogous to eq 17, which consequently holds for the vibrational part separately.

Let us explain the idea of introducing the "mixing parameters" by the example of two symmetry coordinates (S_1, S_2) belonging to the same species. The vibrational problem of this kind, as far as small harmonic vibrations are concerned, is determined by three independent constants, for instance the symmetrized force constants F_{11}, F_{22}, F_{12} . The same result may be represented by the two frequencies (λ_1, λ_2) in addition to the \mathbf{L} matrix block for the coordinates in question.

(5) B. L. Crawford, Jr., and W. H. Fletcher, *J. Chem. Phys.*, **19**, 141 (1951).

(6) It would be sensible to use the symbol \mathbf{F}^q instead of \mathbf{D} for the force-constant matrix in terms of the coordinates \mathbf{q} , but we have here adopted the symbol \mathbf{D} from deWames, *et al.*,²⁸ because of the importance of this matrix in the definition of Green's function.

This block contains four elements, but its number of unknowns is reduced by means of $\mathbf{L}\mathbf{L}' = \mathbf{G}$ to one parameter. In general, the number of unknown parameters in \mathbf{L} will be the same as if the matrix were orthogonal, *viz.* $1/2i(i-1)$, where i is the block dimension. The "mixing parameter" matrix α is in fact an orthogonal matrix which contains the desired information. It has naturally a close connection to the \mathbf{L} matrix, which is to be considered in the following. By combining the various transformations already defined, one obtains

$$\mathbf{S} = \mathbf{B}\mathbf{M}^{-1/2}\mathbf{u}'\mathbf{S}^q = \mathbf{B}\mathbf{M}^{-1/2}\mathbf{u}'\alpha\mathbf{Q} \quad (19)$$

Hence

$$\mathbf{L} = \mathbf{B}\mathbf{M}^{-1/2}\mathbf{u}'\alpha \quad (20)$$

One finds conversely that

$$\alpha = \mathbf{u}\mathbf{M}^{-1/2}\mathbf{B}'(\mathbf{L}')^{-1} \quad (21)$$

Also the following relation may be noticed.

$$(\mathbf{u}\mathbf{D}\mathbf{u}')\alpha = \alpha\Lambda \quad (22)$$

In other words, the mixing parameter matrix α diagonalizes the matrix product given in parentheses (eq 22), which is equivalent to the force-constant matrix in terms of the \mathbf{S}^q coordinates and has the frequency parameters λ as eigenvalues.

VI. Relations for Force-Constant and Compliance-Constant Matrices

The conventional symmetrized force-constant matrix⁴ \mathbf{F} may be expressed with the aid of the mixing parameter matrix in the following way.

$$\mathbf{F} = (\mathbf{L}')^{-1}\Lambda\mathbf{L}^{-1} = \mathbf{A}'\mathbf{M}^{1/2}\mathbf{u}'\alpha\Lambda\alpha'\mathbf{u}\mathbf{M}^{1/2}\mathbf{A} \quad (23)$$

The corresponding relation for the compliance matrix⁷ (inverse of \mathbf{F}) reads

$$\mathbf{F}^{-1} = \mathbf{L}\Lambda^{-1}\mathbf{L}' = \mathbf{B}\mathbf{M}^{-1/2}\mathbf{u}'\alpha\Lambda^{-1}\alpha'\mathbf{u}\mathbf{M}^{-1/2}\mathbf{B}' \quad (24)$$

VII. Application of Green's Function

The definition of Green's function has already been given; see eq 13. We now write

$$\mathcal{G}_0(\lambda) = (\lambda\mathbf{E} - \mathbf{D}_0)^{-1} = (\lambda\mathbf{E} - \mathbf{M}_0^{-1/2}\mathbf{F}_0^X\mathbf{M}_0^{-1/2})^{-1} \quad (25)$$

where all the quantities refer to an "unperturbed" molecule. The frequencies of this molecule are obtainable from the secular determinant

$$|\mathcal{G}_0(\lambda)^{-1}| = 0 \quad (26)$$

Consider a "perturbed" molecule with masses and force constants given by

$$\mathbf{M} = \mathbf{M}_0 + \Delta\mathbf{M} \quad (27)$$

$$\mathbf{F}^X = \mathbf{F}_0^X + \Delta\mathbf{F}^X \quad (28)$$

For Green's function of this molecule one has found

$$\mathcal{G}(\lambda) = \mathbf{M}^{1/2}\mathbf{M}_0^{-1/2}[\mathbf{E} + \mathcal{G}_0(\lambda)(\lambda\Delta\mathbf{M}\mathbf{M}_0^{-1} - \Delta\mathbf{D})]^{-1}\mathcal{G}_0(\lambda)\mathbf{M}_0^{-1/2}\mathbf{M}^{1/2} \quad (29)$$

and the secular determinant^{2a}

$$|\mathbf{E} + \mathcal{G}_0(\lambda)(\lambda\Delta\mathbf{M}\mathbf{M}_0^{-1} - \Delta\mathbf{D})| = 0 \quad (30)$$

Here

$$\Delta\mathbf{D} = \mathbf{M}_0^{-1/2}\Delta\mathbf{F}^X\mathbf{M}_0^{-1/2} \quad (31)$$

Notice that $\Delta\mathbf{D}$ is *not* equal to $\mathbf{D} - \mathbf{D}_0$, but

$$\mathbf{D} - \mathbf{D}_0 =$$

$$\Delta\mathbf{D} + \mathbf{M}^{-1/2}\mathbf{F}^X\mathbf{M}^{-1/2} - \mathbf{M}_0^{-1/2}\mathbf{F}^X\mathbf{M}_0^{-1/2} \quad (32)$$

For isotopic substitution where $\Delta\mathbf{F}^X = 0$, one has $\Delta\mathbf{D} = 0$ as well (but $\mathbf{D} - \mathbf{D}_0$ does *not* vanish). If we furthermore assume that only one type of atoms has been subjected to isotopic substitution, the $\Delta\mathbf{M}\mathbf{M}_0^{-1}$ matrix will be of the form

$$\Delta\mathbf{M}\mathbf{M}_0^{-1} = \begin{bmatrix} \epsilon\mathbf{E} & \mathbf{0} \\ \mathbf{0} & \mathbf{0} \end{bmatrix} \quad (33)$$

where

$$\epsilon = (m^* - m)/m \quad (34)$$

Here m and m^* denote the masses of the original and isotopic atoms, respectively. The dimension of the submatrix \mathbf{E} is in general three times the number of substituted atoms. From the theory of partitioning of secular equations,^{8,9} it appears that the secular determinant for the frequencies of the presently considered case of perturbed molecule reads

$$|\mathbf{E} + \epsilon\lambda\mathcal{G}_0(\lambda)^*| = 0 \quad (35)$$

Here the asterisk indicates that only the part of the Green's function associated with the perturbation needs be taken into account. \mathbf{E} in eq 35 has the same dimensionality as \mathbf{E} in eq 33.

VIII. In-Plane Vibrations of the Ethylene Molecule Model

The theory has been applied to the in-plane vibrations of deuterated ethylenes, using ethylene itself as the unperturbed molecule. For the appropriate planar X_2Y_4 molecule model (symmetry group \mathbf{D}_{2h}), see Figure 1. Below are given the external symmetry

(7) J. C. Decius, *J. Chem. Phys.*, **38**, 241 (1963).

(8) P.-O. Löwdin, *J. Math. Phys.*, **3**, 969 (1962).

(9) G. W. Lehman and R. E. deWames, *Phys. Rev.*, **131**, 1008 (1963).

coordinates in terms of the mass-weighted Cartesian displacements, *viz.*

$$\xi_i = (m_Y)^{1/2}x_i; \quad \eta_i = (m_Y)^{1/2}y_i \quad i = 1, 2, 3, 4$$

$$\xi_i = (m_X)^{1/2}x_i; \quad \eta_i = (m_X)^{1/2}y_i \quad i = 5, 6$$

m_X and m_Y denote the masses of the atoms X and Y, respectively. The equations below define the transformation matrix \mathbf{u}_{vt} of eq 15.

$$S_1^a = 1/2(\xi_1 + \xi_2 - \xi_3 - \xi_4)$$

$$S_2^a = 2^{-1/2}(\xi_5 - \xi_6)$$

$$S_3^a = 1/2(\eta_1 - \eta_2 - \eta_3 + \eta_4)$$

$$S_5^a = (L/2K)(-\xi_1 + \xi_2 + \xi_3 - \xi_4) + (R/K)(\eta_1 + \eta_2 - \eta_3 - \eta_4) \sin A$$

$$S_6^a = (RD/K)(m_X/2I)^{1/2}(\xi_1 - \xi_2 - \xi_3 + \xi_4) \sin A + (LD/2K)(m_X/2I)^{1/2}(\eta_1 + \eta_2 - \eta_3 - \eta_4) + K(m_Y/2I)^{1/2}(-\eta_5 + \eta_6)$$

$$S_9^a = 1/2(\xi_1 - \xi_2 + \xi_3 - \xi_4)$$

$$S_{10}^a = (m_X/2M)^{1/2}(\eta_1 + \eta_2 + \eta_3 + \eta_4) - (2m_Y/M)^{1/2}(\eta_5 + \eta_6)$$

Species B_{1g}

$$\begin{bmatrix} -m_Y^{-1/2} \cos A & (2/m_X)^{1/2} \cos A & m_Y^{-1/2} \sin A \\ 0 & -(2/m_X)^{1/2} & 0 \\ -(D/R)m_Y^{-1/2} \sin A & (D/R)(2/m_X)^{1/2} \sin A & -(D/R)m_Y^{1/2} \cos A \end{bmatrix} \quad (39)$$

$$\begin{bmatrix} (2R + D \cos A)K^{-1}m_Y^{-1/2} & K^{-1}(2I/m_X m_Y) \sin A \\ (D^2/RK)m_Y^{-1/2} \sin A & -(2R + D \cos A)(RK)^{-1}(2I/m_X m_Y)^{1/2} \end{bmatrix} \quad (40)$$

Species B_{2u}

$$\begin{bmatrix} -m_Y^{-1/2} \cos A & (M/2m_X m_Y) \sin A \\ -(D/R)m_Y^{-1/2} \sin A & -(D/R)(M/2m_X m_Y)^{1/2} \cos A \end{bmatrix} \quad (41)$$

Species B_{3u}

$$S_{11}^a = (m_X/2M)^{1/2}(\xi_1 + \xi_2 + \xi_3 + \xi_4) - (2m_Y/M)^{1/2}(\xi_5 + \xi_6)$$

$$S_{12}^a = 1/2(\eta_1 - \eta_2 + \eta_3 - \eta_4)$$

$$T_x^a = (m_Y/M)^{1/2}(\xi_1 + \xi_2 + \xi_3 + \xi_4) + (m_X/M)^{1/2}(\xi_5 + \xi_6)$$

$$T_y^a = (m_Y/M)^{1/2}(\eta_1 + \eta_2 + \eta_3 + \eta_4) + (m_X/M)^{1/2}(\eta_5 + \eta_6)$$

$$R_z^a = R(m_Y/I)^{1/2}(-\xi_1 + \xi_2 + \xi_3 - \xi_4) \sin A + (L/2)(m_Y/I)^{1/2}(-\eta_1 - \eta_2 + \eta_3 + \eta_4) + (D/2)(m_X/I)^{1/2}(-\eta_5 + \eta_6) \quad (36)$$

Here R and D denote the interatomic XY and XX distances, respectively. One has introduced the abbreviations

$$K = (4R^2 + D^2 + 4RD \cos A)^{1/2};$$

$$L = D + 2R \cos A; \quad M = 2m_X + 4m_Y;$$

$$I = m_Y K^2 + 1/2 m_X D^2 \quad (37)$$

M and I denote the total mass of the molecule and the moment of inertia with respect to the z axis, respectively. The interbond YXY angle is $2A$.

A set of internal symmetry coordinates is given in the legend of Figure 1. This set differs from that of Cyvin and Cyvin^{10,11} only in a trivial change of the constant factor multiplying the bending coordinates, which presently has been chosen as D .¹²

IX. Force Constants and Mixing Parameters for Ethylene

The matrix connecting the mixing parameters (α) and the \mathbf{L} matrix (*cf.* eq 21) will be considered. The matrices α and \mathbf{L} are based on the presently adopted external and internal symmetry coordinates, respectively. We introduce a matrix \mathbf{k} as

$$\mathbf{k} = \mathbf{B}\mathbf{M}^{-1/2}\mathbf{u}'; \quad \alpha = \mathbf{k}'(\mathbf{L}')^{-1} \quad (38)$$

and specify its explicit form in the following.

Species A_g \mathbf{k} matrix block

(10) B. N. Cyvin and S. J. Cyvin, *Acta Chem. Scand.*, **17**, 1831 (1963).

(11) B. N. Cyvin and S. J. Cyvin, *Kgl. Norske Videnskab. Selskabs Skrifter*, in press.

(12) In the cited papers^{10,11} this factor is $(RD)^{1/2}$. Accordingly, the differing \mathbf{G} matrix elements in the previously used system (\mathbf{G}') may be transformed to the present system (\mathbf{G}) by

$$G_{jj} = (D/R)G_{jj}'; \quad G_{ij} = (D/R)^{1/2}G_{ij}' \quad (i \neq j)$$

for $j = 3, 6, 10, 12$. Correspondingly, for the force constants

$$F_{jj} = (R/D)F_{jj}'; \quad F_{ij} = (R/D)^{1/2}F_{ij}'$$

$$\begin{bmatrix} -(M/2m_x m_y) \cos A & m_y^{-1/2} \sin A \\ -(D/R)(M/2m_x m_y)^{1/2} \sin A & -(D/R)m_y^{-1/2} \cos A \end{bmatrix} \quad (42)$$

Notice the relations

$$\mathbf{k}'\mathbf{G}^{-1}\mathbf{k} = \mathbf{E}; \quad \mathbf{k}\mathbf{k}' = \mathbf{G} \quad (43)$$

The mixing parameter matrix α is orthogonal, and shall be identified in its general form by the following blocks.

Species A_g

$$\begin{bmatrix} \alpha_a & \alpha_b & \alpha_c \\ \alpha_d & \alpha_e & \alpha_f \\ \alpha_g & \alpha_h & \alpha_i \end{bmatrix}$$

B_{1g}

B_{2u}

B_{3u}

$$\begin{bmatrix} \cos \beta & \sin \beta \\ -\sin \beta & \cos \beta \end{bmatrix} \begin{bmatrix} \cos \gamma & \sin \gamma \\ -\sin \gamma & \cos \gamma \end{bmatrix} \begin{bmatrix} \cos \delta & \sin \delta \\ -\sin \delta & \cos \delta \end{bmatrix} \quad (44)$$

In the 3×3 block of species A_g there are three independent parameters.¹³ Each of the 2×2 blocks is determined by one parameter. We shall use the notation

$$\beta_s = \sin \beta; \quad \gamma_s = \sin \gamma; \quad \delta_s = \sin \delta \quad (45)$$

Wolfram, *et al.*,³ have pointed out the possibility of giving explicit equations for the force constants with aid of the mixing parameters. Such equations are easily obtained from the here-reported matrices according to (cf. eq 23 and 24)

$$\mathbf{F}^{-1} = \mathbf{k}\alpha\Lambda^{-1}\alpha'\mathbf{k}'; \quad \mathbf{F} = (\mathbf{k}')^{-1}\alpha\Lambda\alpha'\mathbf{k}^{-1} \quad (46)$$

Since the explicit expressions are rather lengthy, they will not be reproduced here.

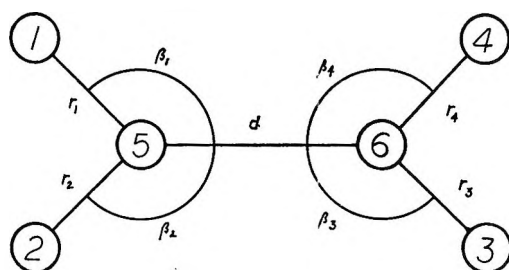


Figure 1. Planar X_2Y_4 molecule model (symmetry D_{2h}). Internal symmetry coordinates for in-plane vibrations are specified below. Species A_g : $S_1 = 1/2(r_1 + r_2 + r_3 + r_4)$; $S_2 = d$; $S_3 = 1/2D(\beta_1 + \beta_2 + \beta_3 + \beta_4)$. Species B_{1g} : $S_5 = 1/2(r_1 - r_2 + r_3 - r_4)$; $S_6 = 1/2D(\beta_1 - \beta_2 + \beta_3 - \beta_4)$. Species B_{2u} : $S_8 = 1/2(r_1 - r_2 - r_3 + r_4)$; $S_{10} = 1/2D(\beta_1 - \beta_2 - \beta_3 + \beta_4)$. Species B_{3u} : $S_{11} = 1/2(r_1 + r_2 - r_3 - r_4)$; $S_{12} = 1/2D(\beta_1 + \beta_2 - \beta_3 - \beta_4)$.

In the method of deWames, *et al.*,² the mixing parameters are obtained from the frequencies of isotopic molecules using Green's function. The close connection between the mixing parameters and the \mathbf{L} matrix has already been pointed out. As a consequence, the mixing parameters are readily obtainable if the force constants for the molecule are known. Presently, a force field previously established for ethylene¹² has been used to calculate the mixing parameters. The result is given in Table II. In later sections we shall consider the equations relating mixing parameters directly to the frequencies of isotopic molecules, without employing the force constants.

Table II: Force Constants (F in mdynes/A) and Mixing Parameters (α) for In-Plane Vibrations of Ethylene

Species	F			α		
A_g	5.500	1.020	-0.066	0.487	0.578	0.655
		10.634	1.337	-0.176	0.799	-0.575
			0.812	-0.856	0.165	0.491
B_{1g}	5.159	0.168		0.885		-0.466
		0.353		0.466		0.885
B_{2u}	5.174	0.029		0.492		0.870
		0.253		-0.870		0.492
B_{3u}	5.182	-0.094		0.542		0.841
		0.737		-0.841		0.542

X. Green's Function for Ethylene

Green's function is a symmetric matrix, in which the elements are functions of λ , *viz.* (cf. eq 13 and 14)

$$\mathcal{G}(\lambda)_{ij} = \sum_{k=1}^{3N} l_{ki} l_{kj} / (\lambda - \lambda_k) \quad (47)$$

The explicit form of $\mathcal{G}(\lambda)$ for ethylene is rather complicated. The 12×12 elements associated with the in-plane vibrations are specified in the Appendix.

XI. $X_2^*Y_4$ -Type Ethylene

In the present application of Green's function, the simplest case corresponds to an isotopic substitution

(13) One may, for instance, introduce the three Euler's angles for three-dimensional rotation and write

$$\begin{aligned} \alpha_a &= \cos \alpha_1 \cos \alpha_2 \\ \alpha_b &= \sin \alpha_1 \cos \alpha_3 + \cos \alpha_1 \sin \alpha_2 \sin \alpha_3 \\ \alpha_c &= \sin \alpha_1 \sin \alpha_3 - \cos \alpha_1 \sin \alpha_2 \cos \alpha_3 \\ \alpha_d &= -\sin \alpha_1 \cos \alpha_2 \\ \alpha_e &= \cos \alpha_1 \cos \alpha_3 - \sin \alpha_1 \sin \alpha_2 \sin \alpha_3 \\ \alpha_f &= \cos \alpha_1 \sin \alpha_3 + \sin \alpha_1 \sin \alpha_2 \cos \alpha_3 \\ \alpha_g &= \sin \alpha_2 \\ \alpha_h &= -\cos \alpha_2 \sin \alpha_3 \\ \alpha_i &= \cos \alpha_2 \cos \alpha_3 \end{aligned}$$

of both of the central X atoms, e.g., $C^{12}_2H_4 \rightarrow C^{13}_2H_4$. Equation 35 gives the determinant (cf. eq A8 of Appendix)

$$\begin{vmatrix} 1 + \epsilon_X \lambda \mathcal{G}_{99} & 0 & \epsilon_X \lambda \mathcal{G}_{9,11} & 0 \\ 0 & 1 + \epsilon_X \lambda \mathcal{G}_{10,10} & 0 & \epsilon_X \lambda \mathcal{G}_{10,12} \\ \epsilon_X \lambda \mathcal{G}_{9,11} & 0 & 1 + \epsilon_X \lambda \mathcal{G}_{99} & 0 \\ 0 & \epsilon_X \lambda \mathcal{G}_{10,12} & 0 & 1 + \epsilon_X \lambda \mathcal{G}_{10,10} \end{vmatrix} = 0 \quad (48)$$

Here

$$\epsilon_X = (m_{X^*} - m_X)/m_X \quad (49)$$

where m_{X^*} refers to the X^* atomic mass of the substituted molecule. The determinant gives rise to the following four equations.

$$\begin{aligned} 1 + \epsilon_X \lambda (\mathcal{G}_{99} \pm \mathcal{G}_{9,11}) &= 0; \\ 1 + \epsilon_X \lambda (\mathcal{G}_{10,10} \pm \mathcal{G}_{10,12}) &= 0 \end{aligned} \quad (50)$$

The Green's function elements are given in Appendix. As a result, the following frequency product and sum rules have been deduced.

Species A_g

$$\lambda_1' \lambda_2' \lambda_3' = \lambda_1 \lambda_2 \lambda_3 (1 + \epsilon_X)^{-1} \quad (51)$$

$$\begin{aligned} \lambda_1' \lambda_2' + \lambda_2' \lambda_3' + \lambda_1' \lambda_3' = \\ (\lambda_1 \lambda_2 + \lambda_2 \lambda_3 + \lambda_1 \lambda_3) (1 + \epsilon_X)^{-1} + \\ \epsilon_X (1 + \epsilon_X)^{-1} [\lambda_1 \lambda_3 + \alpha_d^2 \lambda_3 (\lambda_2 - \lambda_1) + \\ \alpha_f^2 \lambda_1 (\lambda_2 - \lambda_3)] \end{aligned} \quad (52)$$

$$\begin{aligned} \lambda_1' + \lambda_2' + \lambda_3' = (\lambda_1 + \lambda_2 + \lambda_3) (1 + \epsilon_X)^{-1} + \\ \epsilon_X (1 + \epsilon_X)^{-1} [\lambda_1 + \lambda_3 + \alpha_d^2 (\lambda_2 - \lambda_1) + \\ \alpha_f^2 (\lambda_2 - \lambda_3)] \end{aligned} \quad (53)$$

Species B_{1g}

$$\lambda_5' \lambda_6' = \lambda_5 \lambda_6 (I'/I) (1 + \epsilon_X)^{-1} \quad (54)$$

$$\begin{aligned} \lambda_5' + \lambda_6' = (\lambda_5 + \lambda_6) (I'/I) (1 + \epsilon_X)^{-1} + \\ (K^2 m_Y / I) \epsilon_X (1 + \epsilon_X)^{-1} [\lambda_5 + \beta_s^2 (\lambda_6 - \lambda_5)] \end{aligned} \quad (55)$$

Species B_{2u}

$$\lambda_9' \lambda_{10}' = \lambda_9 \lambda_{10} (M'/M) (1 + \epsilon_X)^{-1} \quad (56)$$

$$\begin{aligned} \lambda_9' + \lambda_{10}' = (\lambda_9 + \lambda_{10}) (M'/M) (1 + \epsilon_X)^{-1} + \\ (4m_Y / M) \epsilon_X (1 + \epsilon_X)^{-1} [\lambda_9 + \gamma_s^2 (\lambda_{10} - \lambda_9)] \end{aligned} \quad (57)$$

Species B_{3u}

$$\lambda_{11}' \lambda_{12}' = \lambda_{11} \lambda_{12} (M'/M) (1 + \epsilon_X)^{-1} \quad (58)$$

$$\begin{aligned} \lambda_{11}' + \lambda_{12}' = (\lambda_{11} + \lambda_{12}) (M'/M) (1 + \epsilon_X)^{-1} + \\ (4m_Y / M) \epsilon_X (1 + \epsilon_X)^{-1} [\lambda_{12} + \delta_s^2 (\lambda_{11} - \lambda_{12})] \end{aligned} \quad (59)$$

Here the marked symbols refer to quantities of the substituted molecule. In particular (cf. eq 37)

$$M' = 2m_{X^*} + 4m_Y; \quad I' = m_Y K^2 + 1/2 m_{X^*} D^2 \quad (60)$$

The equilibrium structure is assumed not to be affected by the isotope substitution. Equations 51, 54, 56, and 58 are the ordinary Teller-Redlich product rules. Each of the other equations contain some mixing parameters (cf. section V, especially eq 44 and 45) and allow for the precise determination of their squared values, if the required isotopic frequencies are known. The situation is particularly interesting for species A_g . One observes (eq 52 and 53) that the squares of α_d and α_f are obtainable. Since $\alpha_d^2 + \alpha_e^2 + \alpha_f^2 = 1$, the squared mixing parameters of the whole second row in the appropriate matrix block (see eq 44) may be found by this method, while the other parameters remain unknown. This result is in perfect agreement with the well-known fact that the frequencies of two isotopic molecules do not provide sufficient information to solve the vibrational problem for a 3×3 block. It is not immediately clear, however, why the second row, and none of the others, has the preference in the here-considered calculation of mixing parameters. This feature may perhaps be traced back to the fact that the corresponding external symmetry coordinate (*viz.* S_2^9) is the only one associated with the central atoms exclusively (cf. eq 36).

XII. X_2Y_4 -Type Ethylene

The isotopic substitution of all Y atoms in X_2Y_4 is exemplified by the most familiar deuteration of ethylene, *viz.* $C_2H_4 \rightarrow C_2D_4$. Equations corresponding to (51-59) are most easily obtained by the scaling process, outlined by deWames, *et al.*² One performs the substitutions $m_X \rightarrow m_X m_Y^* / m_Y$, $m_Y \rightarrow m_Y^*$, $m_{X^*} \rightarrow m_X$, $\lambda_i \rightarrow \lambda_i m_Y / m_Y^*$, and $\lambda_i' \rightarrow \lambda_i^*$; where λ_i^* refers to the frequency parameters of the $X_2Y_4^*$ molecule. On introducing the notation

$$\epsilon_Y = (m_{Y^*} - m_Y) / m_Y \quad (61)$$

and

$$M^* = 2m_X + 4m_{Y^*}; \quad I^* = m_{Y^*} K^2 + 1/2 m_X D^2 \quad (62)$$

one has obtained the following set of equations.

Species A_g

$$\lambda_1^* \lambda_2^* \lambda_3^* = \lambda_1 \lambda_2 \lambda_3 (1 + \epsilon_Y)^{-2} \quad (63)$$

$$\begin{aligned} \lambda_1^* \lambda_2^* + \lambda_2^* \lambda_3^* + \lambda_1^* \lambda_3^* = \\ (\lambda_1 \lambda_2 + \lambda_2 \lambda_3 + \lambda_1 \lambda_3) (1 + \epsilon_Y)^{-1} - \\ \epsilon_Y (1 + \epsilon_Y)^{-2} [\lambda_1 \lambda_3 + \alpha_d^2 \lambda_3 (\lambda_2 - \lambda_1) + \\ \alpha_f^2 \lambda_1 (\lambda_2 - \lambda_3)] \end{aligned} \quad (64)$$

$$\lambda_1^* + \lambda_2^* + \lambda_3^* = \lambda_1 + \lambda_2 + \lambda_3 - \epsilon_Y(1 + \epsilon_Y)^{-1}[\lambda_1 + \lambda_3 + \alpha_d^2(\lambda_2 - \lambda_1) + \alpha_f^2(\lambda_2 - \lambda_3)] \quad (65)$$

Species B_{1g}

$$\lambda_5^* \lambda_6^* = \lambda_5 \lambda_6 (I^*/I)(1 + \epsilon_Y)^{-2} \quad (66)$$

$$\lambda_5^* + \lambda_6^* = (\lambda_5 + \lambda_6)(I^*/I)(1 + \epsilon_Y)^{-1} - (K^2 m_Y / I) \epsilon_Y (1 + \epsilon_Y)^{-1} [\lambda_5 + \beta_s^2 (\lambda_6 - \lambda_5)] \quad (67)$$

Species B_{2u}

$$\lambda_9^* \lambda_{10}^* = \lambda_9 \lambda_{10} (M^*/M)(1 + \epsilon_Y)^{-2} \quad (68)$$

$$\lambda_9^* + \lambda_{10}^* = (\lambda_9 + \lambda_{10})(M^*/M)(1 + \epsilon_Y)^{-1} - (4m_Y / M) \epsilon_Y (1 + \epsilon_Y)^{-1} [\lambda_9 + \gamma_s^2 (\lambda_{10} - \lambda_9)] \quad (69)$$

Species B_{3u}

$$\lambda_{11}^* \lambda_{12}^* = \lambda_{11} \lambda_{12} (M^*/M)(1 + \epsilon_Y)^{-2} \quad (70)$$

$$\lambda_{11}^* + \lambda_{12}^* = (\lambda_{11} + \lambda_{12})(M^*/M)(1 + \epsilon_Y)^{-1} - (4m_Y / M) \epsilon_Y (1 + \epsilon_Y)^{-1} [\lambda_{12} + \delta_s^2 (\lambda_{11} - \lambda_{12})] \quad (71)$$

It was attempted to use the equations obtained here to calculate the squared mixing parameters from the observed frequencies for C₂H₄ and C₂D₄, quoted in ref 11. The results turned out to be critically dependent on differences between comparatively large numbers of almost the same magnitude, and consequently very sensitive to the applied frequency parameters. Table III shows the two sets of frequency

Table III: Values of λ ($= 0.588852 \times 10^{-6} \omega^2$, Where ω is in cm⁻¹) for In-plane Vibrations of C₂H₄ and C₂D₄

No.	C ₂ H ₄		C ₂ D ₄	
	λ (calcd) ^a	λ (obsd)	λ (calcd) ^a	λ (obsd)
1	5.588	5.393	2.920	3.008
2	1.556	1.550	1.361	1.357
3	1.047	1.061	0.574	0.571
5	5.667	5.668	3.144	3.142
6	0.893	0.879	0.593	0.602
9	5.760	5.679	3.196	3.238
10	0.396	0.402	0.204	0.201
11	5.364	5.263	2.801	2.851
12	1.238	1.227	0.679	0.684

^a Force-constant calculations of ref 11.

parameters (λ) used in the calculations, *viz.* those from the force-constant calculations of ref 11, and those representing the observed frequencies. The resulting squared mixing parameters are shown in

Table IV. The two sets are seen to deviate largely. In particular, the negative value of α_f^2 (*i.e.*, imaginary α_f) which appears in the last column of Table IV is not acceptable.

Table IV: Squared Mixing Parameters for Ethylene, According to Calculations by Green's Function Method

Species	Symbol	Adjusted frequency ^a	Observed frequency
A _g	α_d^2	0.031	0.069
	α_f^2	0.330	-0.099
B _{1g}	β_s^2	0.217	0.230
B _{2u}	γ_s^2	0.757	0.969
B _{3u}	δ_s^2	0.706	0.313

^a Consistent with Table II.

XIII. Other Isotopic Ethylenes

The method of Green's function could also in principle be applied to other isotopic ethylenes, *e.g.*, C₂-H₃D, C₂HD₃, and the three dideuterated species. It was found that the arithmetic computations for each of these cases would be rather tedious, but not impossible. They were not found worthwhile performing at the present stage of the work, mainly due to the conclusions of the preceding section.

XIV. Conclusion

The present application of Green's function to ethylenes has led to new and interesting isotopic frequency sum rules. In principle, the derived equations make it possible to compute the mixing parameters, and hence the **L** matrix and force constants, of ethylene for the species B_{1g}, B_{2u}, and B_{3u}. In species A_g only two of the three independent mixing parameters can be computed using the simplest isotopic substitution. The numerical calculation of mixing parameters from the observed frequencies resulted in an imaginary mixing parameter. This shows the necessity of using adjusted frequencies in the vibrational analysis; such frequencies are involved in the reported calculations using force constants. It was not found worth the while to extend the computations to further isotopic species of ethylene.

There is, however, another topic which might be worthwhile investigating with the aid of Green's function, namely the study of substituted ethylenes by atoms other than isotopes. Allowance should then be made for changes in the force field. For this type of application of Green's function, which has not been

treated in this paper, reference is made especially to a quite recent article of Wolfram and deWames.¹⁴

Appendix

The Complete Green's Function for Ethylene In-Plane Vibrations

Because of many regularities, it is possible to specify the elements of $\mathfrak{G}(\lambda)$ for the in-plane vibrations of ethylene (*cf.* section X) in a fairly compact way. In the first place, it is sufficient to give only the terms with $i \leq j$ because of the symmetry. We introduce the abbreviations

$$\begin{aligned}\beta_a &= (L/2K) \cos \beta + (RD/K)(m_X/2I)^{1/2} \sin A \sin \beta \\ \beta_b &= (L/2K) \sin \beta - (RD/K)(m_X/2I)^{1/2} \sin A \cos \beta \\ \beta_c &= (R/K) \sin A \cos \beta - (LD/2K)(m_X/2I)^{1/2} \sin \beta \\ \beta_d &= (R/K) \sin A \sin \beta + (LD/2K)(m_X/2I)^{1/2} \cos \beta\end{aligned}\quad (\text{A1})$$

Moreover

$$\begin{aligned}A_1 &= 1/4[\alpha_a^2(\lambda - \lambda_1)^{-1} + \alpha_b^2(\lambda - \lambda_2)^{-1} + \alpha_c^2(\lambda - \lambda_3)^{-1}] \\ A_2 &= 1/4[\alpha_g^2(\lambda - \lambda_1)^{-1} + \alpha_h^2(\lambda - \lambda_2)^{-1} + \alpha_i^2(\lambda - \lambda_3)^{-1}] \\ A_{12} &= 1/4[\alpha_a\alpha_g(\lambda - \lambda_1)^{-1} + \alpha_b\alpha_h(\lambda - \lambda_2)^{-1} + \alpha_c\alpha_i(\lambda - \lambda_3)^{-1}] \\ B_1 &= \beta_a^2(\lambda - \lambda_5)^{-1} + \beta_b^2(\lambda - \lambda_6)^{-1} \\ B_2 &= \beta_c^2(\lambda - \lambda_5)^{-1} + \beta_d^2(\lambda - \lambda_6)^{-1} \\ B_{12} &= \beta_a\beta_c(\lambda - \lambda_5)^{-1} + \beta_b\beta_d(\lambda - \lambda_6)^{-1} \\ C_1 &= 1/4[(\lambda - \lambda_9)^{-1} \cos^2 \gamma + (\lambda - \lambda_{10})^{-1} \sin^2 \gamma] \\ C_2 &= (m_X/2M)[(\lambda - \lambda_9)^{-1} \sin^2 \gamma + (\lambda - \lambda_{10})^{-1} \cos^2 \gamma] \\ C_{12} &= 1/2(m_X/2M)^{1/2}[(\lambda - \lambda_9)^{-1} - (\lambda - \lambda_{10})^{-1}] \sin \gamma \cos \gamma \\ D_1 &= (m_X/2M)[(\lambda - \lambda_{11})^{-1} \cos^2 \delta + (\lambda - \lambda_{12})^{-1} \sin^2 \delta] \\ D_2 &= 1/4[(\lambda - \lambda_{11})^{-1} \sin^2 \delta + (\lambda - \lambda_{12})^{-1} \cos^2 \delta] \\ D_{12} &= 1/2(m_X/2M)^{1/2}[(\lambda - \lambda_{11})^{-1} - (\lambda - \lambda_{12})^{-1}] \sin \delta \cos \delta \\ E &= m_Y/M\lambda \\ F_1 &= (R^2m_Y/I\lambda) \sin^2 A \\ F_2 &= L^2m_Y/4I\lambda \\ F_{12} &= (RLm_Y/2I\lambda) \sin A\end{aligned}\quad (\text{A2})$$

With these symbols the various elements of Green's function corresponding to the four Y atoms may be expressed in the following way.

$$\mathfrak{G}(\lambda)_{ii} = A_1 + B_1 + C_1 + D_1 + E + F_1; \quad i = 1, 3, 5, 7 \quad (\text{A3})$$

$$\begin{aligned}\mathfrak{G}(\lambda)_{13} &= \mathfrak{G}(\lambda)_{57} = A_1 - B_1 - C_1 + D_1 + E - F_1 \\ \mathfrak{G}(\lambda)_{35} &= \mathfrak{G}(\lambda)_{17} = -A_1 + B_1 - C_1 + D_1 + E + F_1\end{aligned}\quad (\text{A4})$$

$$\begin{aligned}\mathfrak{G}(\lambda)_{15} &= \mathfrak{G}(\lambda)_{37} = -A_1 - B_1 + C_1 + D_1 + E - F_1 \\ \mathfrak{G}(\lambda)_{14} &= A_2 + B_2 + C_2 + D_2 + E + F_2; \quad i = 2, 4, 6, 8 \quad (\text{A5})\end{aligned}$$

$$\begin{aligned}\mathfrak{G}(\lambda)_{24} &= \mathfrak{G}(\lambda)_{68} = -A_2 + B_2 + C_2 - D_2 + E + F_2 \\ \mathfrak{G}(\lambda)_{46} &= \mathfrak{G}(\lambda)_{28} = A_2 - B_2 + C_2 - D_2 + E - F_2 \\ \mathfrak{G}(\lambda)_{26} &= \mathfrak{G}(\lambda)_{48} = -A_2 - B_2 + C_2 + D_2 + E - F_2\end{aligned}\quad (\text{A6})$$

$$\begin{aligned}\mathfrak{G}(\lambda)_{12} &= \mathfrak{G}(\lambda)_{56} = -\mathfrak{G}(\lambda)_{34} = -\mathfrak{G}(\lambda)_{78} = \\ &A_{12} - B_{12} - C_{12} - D_{12} + F_{12} \\ \mathfrak{G}(\lambda)_{23} &= \mathfrak{G}(\lambda)_{67} = -\mathfrak{G}(\lambda)_{14} = -\mathfrak{G}(\lambda)_{58} = \\ &A_{12} + B_{12} + C_{12} - D_{12} - F_{12} \\ \mathfrak{G}(\lambda)_{45} &= \mathfrak{G}(\lambda)_{18} = -\mathfrak{G}(\lambda)_{36} = -\mathfrak{G}(\lambda)_{27} = \\ &A_{12} + B_{12} - C_{12} + D_{12} - F_{12} \\ \mathfrak{G}(\lambda)_{47} &= \mathfrak{G}(\lambda)_{38} = -\mathfrak{G}(\lambda)_{26} = -\mathfrak{G}(\lambda)_{16} = \\ &A_{12} - B_{12} + C_{12} + D_{12} + F_{12}\end{aligned}\quad (\text{A7})$$

The 4×4 submatrix of $\mathfrak{G}(\lambda)$ associated with the two X atoms is comparatively simple and has the form

$$\begin{bmatrix} \mathfrak{G}_{99} & 0 & \mathfrak{G}_{9,11} & 0 \\ 0 & \mathfrak{G}_{10,10} & 0 & \mathfrak{G}_{10,12} \\ \mathfrak{G}_{9,11} & 0 & \mathfrak{G}_{99} & 0 \\ 0 & \mathfrak{G}_{10,12} & 0 & \mathfrak{G}_{10,10} \end{bmatrix}\quad (\text{A8})$$

Here

$$\begin{aligned}\mathfrak{G}_{99} &= A' + D' + E'; \\ \mathfrak{G}_{9,11} &= -A' + D' + E'; \\ \mathfrak{G}_{10,10} &= B' + C' + E' + F'; \\ \mathfrak{G}_{10,12} &= -B' + C' + E' - F'\end{aligned}\quad (\text{A9})$$

where

(14) T. Wolfram and R. E. deWames, to be published.

$$\begin{aligned}
 A' &= 1/2[\alpha_d^2(\lambda - \lambda_1)^{-1} + \alpha_e^2(\lambda - \lambda_2)^{-1} + \alpha_f^2(\lambda - \lambda_3)^{-1}] \\
 B' &= (K^2m_Y/2I)[(\lambda - \lambda_5)^{-1} \sin^2 \beta + (\lambda - \lambda_6)^{-1} \cos^2 \beta] \\
 C' &= (2m_Y/M)[(\lambda - \lambda_9)^{-1} \sin^2 \gamma + (\lambda - \lambda_{10})^{-1} \cos^2 \gamma] \\
 D' &= (2m_X/M)[(\lambda - \lambda_{11})^{-1} \cos^2 \delta + (\lambda - \lambda_{12})^{-1} \sin^2 \delta] \\
 E' &= m_X/M\lambda \\
 F' &= D^2m_X/4I\lambda
 \end{aligned}
 \tag{A10}$$

There remains to specify the rest of the last four columns of $\mathcal{G}(\lambda)$. One may introduce the following abbreviations.

$$\begin{aligned}
 A_1' &= 8^{-1/2}[\alpha_a\alpha_d(\lambda - \lambda_1)^{-1} + \alpha_b\alpha_c(\lambda - \lambda_2)^{-1} + \alpha_e\alpha_f(\lambda - \lambda_3)^{-1}] \\
 A_2' &= 8^{-1/2}[\alpha_d\alpha_g(\lambda - \lambda_1)^{-1} + \alpha_e\alpha_h(\lambda - \lambda_2)^{-1} + \alpha_f\alpha_i(\lambda - \lambda_3)^{-1}] \\
 B_1' &= 1/2L(m_Y/2I)^{1/2}[(\lambda - \lambda_5)^{-1} - (\lambda - \lambda_6)^{-1}] \sin \beta \cos \beta + (RD/2I)(m_Xm_Y)^{1/2} \sin A [(\lambda - \lambda_5)^{-1} \sin^2 \beta + (\lambda - \lambda_6)^{-1} \cos^2 \beta] \\
 B_2' &= R(m_Y/2I)^{1/2} \sin A [(\lambda - \lambda_5)^{-1} - (\lambda - \lambda_6)^{-1}] \sin \beta \cos \beta - (LD/4I)(m_Xm_Y)^{1/2} [(\lambda - \lambda_5)^{-1} \sin^2 \beta + (\lambda - \lambda_6)^{-1} \cos^2 \beta] \\
 C_1' &= (m_Y/2M)^{1/2} [(\lambda - \lambda_9)^{-1} - (\lambda - \lambda_{10})^{-1}] \sin \gamma \cos \gamma
 \end{aligned}$$

$$\begin{aligned}
 C_2' &= (m_Xm_Y)^{1/2}M^{-1}[(\lambda - \lambda_9)^{-1} \sin^2 \gamma + (\lambda - \lambda_{10})^{-1} \cos^2 \gamma] \\
 D_1' &= (m_Xm_Y)^{1/2}M^{-1}[(\lambda - \lambda_{11})^{-1} \cos^2 \delta + (\lambda - \lambda_{12})^{-1} \sin^2 \delta] \\
 D_2' &= (m_Y/2M)^{1/2}[(\lambda - \lambda_{11})^{-1} - (\lambda - \lambda_{12})^{-1}] \sin \delta \cos \delta \\
 E'' &= (m_Xm_Y)^{1/2}/M\lambda \\
 F_1' &= [RD(m_Xm_Y)^{1/2} \sin A]/2I\lambda \\
 F_2' &= DL(m_Xm_Y)^{1/2}/4I\lambda
 \end{aligned}
 \tag{A11}$$

Then the submatrix in question may be given by

$$\begin{bmatrix} \mathcal{G}_1(\lambda) & \mathcal{G}_2(\lambda) \\ \mathcal{G}_2(\lambda) & \mathcal{G}_1(\lambda) \end{bmatrix}
 \tag{A12}$$

where

$$\mathcal{G}_1(\lambda) = \begin{bmatrix} A_1' - D_1' + E'' & -(B_1' - C_1' - F_1') \\ A_2' + D_2' & B_2' - C_2' + E'' + F_2' \\ A_1' - D_1' + E'' & B_1' - C_1' - F_1' \\ -(A_2' + D_2') & B_2' - C_2' + E'' + F_2' \end{bmatrix}
 \tag{A13}$$

and

$$\mathcal{G}_2(\lambda) = \begin{bmatrix} -A_1' - D_1' + E'' & B_1' + C_1' - F_1' \\ -(A_2' - D_2') & -B_2' - C_2' + E'' - F_2' \\ -A_1' - D_1' + E'' & -(B_1' + C_1' - F_1') \\ A_2' - D_2' & -B_2' - C_2' + E'' - F_2' \end{bmatrix}
 \tag{A14}$$

The Strontium–Strontium Hydride Phase System¹

by D. T. Peterson and R. P. Colburn

*Institute for Atomic Research and Department of Metallurgy, Iowa State University, Ames, Iowa
(Received August 12, 1965)*

The Sr–SrH₂ phase diagram was studied by thermal analysis, chemical analysis of equilibrated phases, and X-ray diffraction. The maximum solubility of SrH₂ in strontium metal is 38 mole % at the peritectic temperature of 880°. Strontium metal undergoes an allotropic transformation at 555° and melts at 768°. A second transformation was found, at about 240°, in samples containing hydrogen. Strontium hydride was found to have an allotropic transformation at 855°.

Introduction

The strontium–hydrogen system has not been investigated extensively. Strontium was shown by Zintl and Harder² to form SrH₂, which is a saltlike hydride with an orthorhombic lattice and a structure which has a slightly distorted hexagonal closest packing of the metal atoms. The enthalpy of formation of strontium hydride has been reported by Guntz and Benoit³ to be 42.2 kcal/mole. Strontium metal has been reported to exist in three allotropic forms. The stable phase at room temperature is face-centered cubic. Sheldon and King,⁴ Hirst, *et al.*,⁵ and Schottmiller, *et al.*,⁶ reported that at about 215° the face-centered-cubic phase transforms to a hexagonal closest-packed phase and that this phase transforms at about 605° to a body-centered-cubic phase which is stable to the melting point. These results were obtained by a high-temperature X-ray diffraction investigation of finely divided strontium metal. Rinck⁷ reported a phase transition at 540° on the basis of thermal arrests in cooling curves and a transition at 235° on the basis of slight changes in the electrical resistance and thermal expansion coefficients.

In view of the pronounced effect of hydrogen on the phase transitions of calcium metal reported by Peterson and Fattore⁸ and the large solubility of hydrogen in barium metal reported by Peterson and Indig,⁹ this investigation of the strontium–strontium hydride system was undertaken. Thermal analysis and analysis of equilibrated phases were used to establish the phase relationships, and X-ray diffraction was used to a limited extent to confirm the results.

Experimental Procedures

Materials. Strontium metal obtained from King Laboratories, Syracuse, N. Y., was purified by distillation at 825° under 8 mm of argon pressure. Semi-quantitative spectrochemical analysis indicated the principal metallic impurities as: less than 1000 ppm barium, less than 1000 ppm calcium, and less than 500 ppm magnesium. A typical chemical analysis showed 60 ppm N₂, 200 ppm C, 15 ppm Fe, 50 ppm Mn, 20 ppm Ni, and 10 ppm Cr. The average hydrogen content of the material was 350 ppm hydrogen or 1.5 mole % SrH₂ as determined by a vacuum fusion. In order to obtain strontium with a lower hydrogen content, a quantity of the distilled material was placed in a sealed tantalum capsule and held under dynamic vacuum at 800° for 48 hr. This procedure reduced the hydrogen content to 0.4 mole % strontium hydride. The oxygen content was not determined owing to the lack of a suitable analytical method. The strontium

(1) Work was performed at the Ames Laboratory of the U. S. Atomic Energy Commission. Contribution No. 1282.

(2) E. Zintl and H. Harder, *Z. Elektrochem.*, **41**, 33 (1935).

(3) A. Guntz and F. Benoit, *Ann. Chim.*, **20**, 5 (1923).

(4) E. A. Sheldon and A. J. King, *Acta Cryst.*, **6**, 100 (1953).

(5) R. G. Hirst, A. J. King, and F. A. Kanda, *J. Phys. Chem.*, **60**, 302 (1956).

(6) J. C. Schottmiller, A. J. King, and F. A. Kanda, *ibid.*, **62**, 1446 (1958).

(7) E. Rinck, *Compt. Rend.*, **234**, 845 (1952).

(8) D. T. Peterson and V. G. Fattore, *J. Phys. Chem.*, **65**, 2062 (1961).

(9) D. T. Peterson and M. Indig, *J. Am. Chem. Soc.*, **82**, 5645 (1960).

metal was handled in a glove box under a helium atmosphere reported to be 99.99% pure.

Differential Thermal Analysis. Thermal analysis capsules 6 cm long and 2 cm in diameter were made from Type 304 stainless steel. The capsules had a 1.5-mm wall thickness. A thermocouple well was welded into the base of the capsule. The chromel-alumel thermocouples used in this investigation were periodically calibrated at the melting points of a National Bureau of Standards aluminum sample and a sample of electrolytic silver. The thermal analysis samples were prepared by weighing out approximately 10 g of the metal in a helium-filled glove box into a partially closed thermal analysis capsule. The capsule was placed in a quartz tube which was closed at one end and sealed with Apiezon W wax to a stopper with a stopcock at the other end. This closed tube was transferred from the drybox to the hydrogen-charging apparatus which was then evacuated and closed off. In this apparatus, the sample was heated to 450° and allowed to react with a measured quantity of hydrogen. Very pure hydrogen was obtained from the thermal dissociation of uranium hydride. Following the charging of the sample to a known hydride composition, the capsule was welded shut in an inert atmosphere glove box with the lower part of the capsule cooled in a metal block to prevent the loss of hydrogen. The sealed capsules were then transferred to the differential thermal analysis apparatus. The loss of hydrogen by diffusion through the capsule walls during thermal analysis was measured by observing the pressure in the closed thermal analysis apparatus. This loss was found to be negligible in all cases. The free volume inside the thermal analysis capsule was about 12 cc, and, if the hydrogen pressure inside the capsule had been as high as 1 atm, the composition of the condensed phases would have been changed only 0.05 mole %. A differential thermocouple located in an empty stainless steel capsule immediately above the sample was used to give greater sensitivity in observing the thermal arrests. Even at heating and cooling rates up to 10°/min, excellent agreement between the temperatures of thermal arrests upon heating and cooling was obtained.

Isothermal Equilibration. The solubility limit of strontium hydride in strontium metal was determined by analysis of specimens of strontium that had been held at temperature in contact with strontium hydride. Distilled strontium, cast into rods and machined to specimens 3 cm long and 1.25 cm in diameter, was heated to the desired temperature and allowed to react with a limited amount of hydrogen sufficient to form a coating of strontium hydride about 0.5 mm thick

on the outside of the rod after the strontium core was saturated. At temperature, hydrogen diffused from the surface into the strontium metal until the hydrogen content of the metal reached the solubility limit. The time at temperature varied from 2 hr at the higher temperatures to 48 hr at the lowest temperatures. These times were estimated to be several times as long as necessary to approach saturation. This estimate was based on the rate of diffusion of hydrogen in calcium metal. The specimens equilibrated below 450° were first heated to 600° under vacuum and cooled to the desired temperature before adding hydrogen. This was done to destroy a surface layer, probably strontium hydroxide as indicated by the work of Svec and Staley,¹⁰ which prevented reaction of the metal with hydrogen below 450°. After cooling to room temperature, the specimens were placed in a glove box and sampled. The strontium hydride layer at the surface was completely removed, and the core was cut into a number of samples. Each set of samples contained several from near the surface of the core and several from the center. Failure to achieve saturation would be indicated by a higher concentration near the surface. In no case was a significant difference between samples from these two regions observed. The hydrogen content was determined by the vacuum fusion technique described by Peterson and Fattore.¹¹

This method of establishing the solubility limits of strontium hydride in strontium was used in preference to that based on measurement of equilibrium hydrogen pressures because it could be used at lower temperatures where the hydrogen pressures are not measurable. The measurement of hydrogen equilibrium pressures in the strontium-hydrogen system is complicated by the volatility of strontium in this temperature range.

X-Ray Diffraction. This method was used in the temperature range from 25 to 300° to find a phase transformation reported in this temperature range. Differential thermal analysis data did not show a thermal arrest in this temperature range although several authors using X-ray powder methods have reported a transformation in pure strontium metal in the temperature range from 213 to 235°.^{4-6,11} Diffraction of an X-ray beam incident at a small angle to the surface of a solid sample was used in this investigation in preference to the more conventional powder sample methods because of the possibility of

(10) H. J. Svec and H. G. Staley, *J. Electrochem. Soc.*, **105**, 121 (1958).

(11) D. T. Peterson and V. G. Fattore, *Anal. Chem.*, **34**, 579 (1962).

serious contamination of the sample in the latter method. The massive sample was placed in a Vycor tube which had a thin hemispherical Vycor window at the end. The sample was positioned so that a collimated X-ray beam penetrated the window and impinged on the sample surface at a small angle. The diffraction patterns were recorded on a flat photographic plate. Experimental difficulties made accurate measurement of the lattice parameters impossible, but the reported fcc to hcp transition could be clearly recognized. The samples were loaded into the Vycor tube in a helium-filled glove box. After removal from the drybox, the tube was evacuated for the remainder of the experiment. Electrical resistance windings around the Vycor tube allowed the sample to be heated up to 300°. The sample temperature was measured by a thermocouple inserted in a hole in the specimen and located approximately 1 mm beneath the diffracting surface.

Results

The strontium-strontium hydride phase diagram is shown in Figure 1. This system is quite similar to the calcium-calcium hydride system and the barium-barium hydride system. A sample containing 0.4 mole % strontium hydride had a melting point of 768° which is in good agreement with the current values reported for pure strontium in the literature. Schottmiller⁶ reported the melting point to be 774°, Hirst, *et al.*,⁵ reported 768°, and Rinck⁷ reported 770°. The correction for the increase in melting point of this sample based on the 0.4 mole % strontium hydride content, and the slope of the melting temperature *vs.* composition curve would be only 1.1°; this is less than the probable error in the melting point measurement. With increasing hydrogen content the melting point of metallic strontium slowly increased to a peritectic at 880°, where the maximum solubility of strontium hydride in solid strontium metal was 38 mole %.

An allotropic transformation at 557° was indicated by a thermal arrest on heating in the 0.4 mole % strontium sample. The correction for the residual hydrogen content of this specimen would give a transformation temperature on heating of 555°. The thermal arrests on cooling for this transformation were always about 15 to 25° lower than the arrests on heating. The heating arrests were more reproducible and were used in plotting the phase diagram. The thermal arrest at the slowest cooling rates was found at 540° which is in excellent agreement with the transformation temperature reported by Rinck on the basis of cooling curves. The temperature of the allotropic transformation increased with increasing hydrogen content until

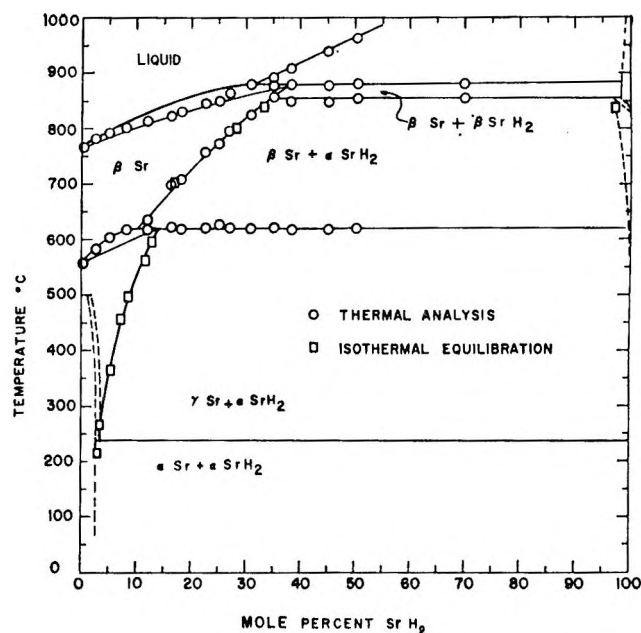


Figure 1. The strontium-strontium hydride phase system.

a peritectoid was reached at 620° with a maximum solubility of 14 mole % strontium hydride in the lower temperature metal phase. This peritectoid temperature is very close to the temperature reported by Schottmiller,⁶ Hirst, *et al.*,⁵ and Sheldon, *et al.*,⁴ for the allotropic transformation of hcp strontium to bcc strontium.

Differential thermal analysis also revealed a thermal arrest at 855° in samples containing more than 38 mole % strontium hydride which was attributed to an allotropic transformation in strontium hydride. This interpretation was supported by the increasing duration of this thermal arrest, relative to the thermal arrest at the peritectic temperature, with increasing hydrogen content. Similar allotropic transformations occur in barium hydride at 600°⁹ and calcium hydride at 780°.⁸ The melting point of strontium hydride was not determined because of the high dissociation pressure of this material above 1000°.

The solubility of strontium hydride in solid strontium metal at various temperatures was determined by isothermal equilibration studies. This was done to confirm the interpretation of the thermal analysis data and to provide data on the solubility of strontium hydride in the lower temperature phases of strontium metal where no thermal arrests were obtained. Excellent agreement between solubilities indicated by the thermal analysis data and the isothermal equilibration data was obtained in those regions of the system where both methods could be employed. This study was also useful in giving the composition of the hy-

hydride phase, which had almost exactly the composition SrH₂ when equilibrated with strontium metal at temperatures below 500°. At higher temperatures, analysis of the hydride phase showed a slightly lower hydrogen content. The solubility strontium hydride in strontium metal is shown in Table I.

Table I: Solubility of Strontium Hydride in Strontium Metal

Temp, °C	Solubility limit, mole % SrH ₂
810	33.4
802	27.8
740	17.4
668	13.0
595	11.5
562	11.5
497	7.9
456	7.1
365	5.3
263	3.3
212	2.5

A plot of the solubility of strontium hydride in strontium metal *vs.* the reciprocal of the absolute temperature is shown in Figure 2. An abrupt change in slope was found to occur in the region of the γ - to β -transformation temperature. The data for the solubility of α -SrH₂ in β -Sr metal indicate an enthalpy of solution of $+15,900 \pm 2000$ cal/mole of strontium hydride by a least-squares treatment of 22 solubility measurements. The solubility of α -SrH₂ in the γ phase indicates an enthalpy of solution of $+3560 \pm 150$ cal/mole of strontium hydride by a similar treatment of 25 data points. No evidence was obtained from either thermal analysis or solid solubility of the phase change reported at about 215°. Two samples were studied by X-ray diffraction from room temperature up to 286°. The first sample contained 3.27 mole % strontium hydride, which is above the solid solubility limit in this temperature range. A reversible transformation from a fcc to a hcp lattice was observed between 236 and 244° in this specimen. The second sample contained 0.40 mole % strontium hydride. This sample was examined from room temperature to 286°, the highest temperature that could be obtained with the present apparatus, and no crystallographic transformation was observed.

Discussion

The question of the allotropy of strontium has not been completely clarified by this investigation. The transition, presumed to be to the bcc structure, in

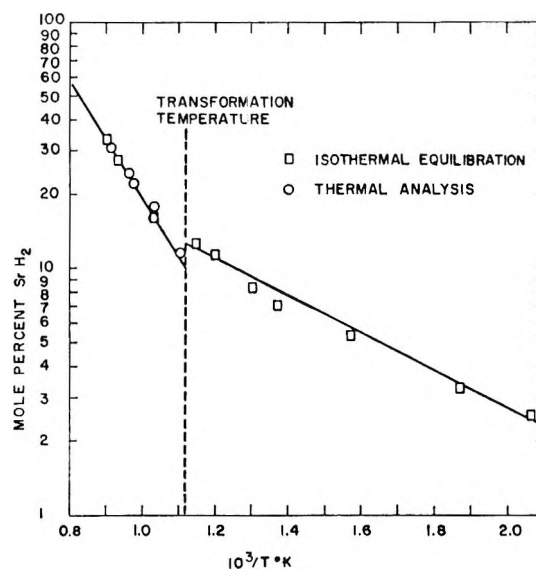


Figure 2. Solubility of SrH₂ in strontium *vs.* reciprocal temperature.

pure strontium at about 555° is quite well established by the concordance of the results of this investigation and those of Rinck. The raising of this transformation by hydrogen in solution to a peritectoid at about 620° would explain the transformation reported at about 605° if the powdered X-ray specimens contained hydrogen as an impurity. The lower transition is not well established although it certainly occurs at about 215 to 235° in specimens containing sufficient hydrogen, and additional investigations with very low hydrogen content strontium should be made. This transformation may be similar to the transformations from one close-packed structure to another in cobalt and in lanthanum which occur by a dislocation mechanism. These transformations are often incomplete and result in structures with numerous stacking faults.

As in the barium-barium hydride system and the calcium-calcium hydride system, hydrogen has a greater solubility in the solid metal phase than in the liquid phase, and increasing the concentration of hydrogen increases the melting temperatures of these metals. Also characteristic of the calcium-calcium hydride, strontium-strontium hydride, and barium-barium hydride system is the extensive endothermic solubility of the hydride in the metal phase. The maximum solubility increases from calcium to strontium to barium, respectively. Thus, it is seen that the position of strontium between calcium and barium in the alkaline earth family of metals is clearly reflected in the character of its metal-hydride phase system.

Absorption Spectra of Alkali Metal Tellurides and of Elemental Tellurium in Molten Alkali Halides¹

by D. M. Gruen, R. L. McBeth, M. S. Foster, and C. E. Crouthamel

Argonne National Laboratory, Argonne, Illinois (Received August 16, 1965)

Absorption spectra of solutions of Li_2Te in molten LiCl and LiCl-LiF and of Cs_2Te in molten CsCl have been measured in the range 40,000 to 4000 cm^{-1} . The Li_2Te and Cs_2Te spectra are characterized by absorption bands with maxima at 21,250 and 18,200 cm^{-1} ; widths at half-maximum of 7100 and 7400 cm^{-1} , and oscillator strengths of 0.86×10^{-3} and 2.00×10^{-2} , respectively. The absorption bands are interpreted as arising from $5p \rightarrow 6p$ atom-like transitions centered on tellurium. The spectrum of Te metal in molten CsCl has also been measured and is characterized by two overlapping absorption bands with maxima at 15,500 cm^{-1} and 20,800 cm^{-1} having a total oscillator strength of 3.87×10^{-2} . The solubility of Te in molten CsCl at 671° is 1.28×10^{-2} wt %, in molten KCl at 802° is 3.50×10^{-2} wt %, and in molten LiCl at 627° is estimated at less than 5×10^{-4} wt %.

Introduction

Solutions of intermetallics in molten salts were studied by Heymann and his co-workers,^{2,3} who investigated distribution equilibria with reference to the stability of intermetallic compounds in melts. Recently, spectral data on solutions of Li_3Bi in molten LiCl-LiF were reported.⁴ The present study concerns itself with solutions of alkali metal tellurides and of tellurium metal in alkali chlorides. In view of the paucity of information concerning solutions of this type, it is of interest to study their spectra in order to gain more insight into the nature of the species present in these systems.

Experimental Section

Materials. Tellurium used to prepare the various alkali metal tellurides was obtained from the American Smelting and Refining Co., South Plainfield, N. J. The metal was melted in a helium atmosphere and filtered through a fine-porosity fritted disk. The sources of the alkali metals were the following: lithium metal, Foote Mineral Co., Philadelphia, Pa.; sodium metal, Allied Chemical, New York, N. Y.; potassium metal, J. T. Baker Chemical Co., Phillipsburg, N. J.; and cesium metal, Dow Chemical Co., Midland, Mich. No further purification of these metals was

attempted, but only bright metal pieces were used and the metal was stored in the helium-atmosphere box.

Solvents of LiCl-LiF (80 mole % LiCl , mp 505°), LiCl-KCl (59 mole % LiCl , mp 352°), and LiCl (mp 607°) were made from reagent grade material and purified by the method of Maricle and Hume.⁵ Cesium chloride, as the 99.9% material, was obtained from Atomergic Chemetals Co., Carle Place, N. Y., and was used after filtering through a quartz fritted disk. Potassium chloride (mp 776°), NaCl-NaF (50 mole % NaCl , mp 675°), and NaCl (mp 801°) were also used after filtering the reagent grade materials through a quartz fritted disk.

The alkali metal tellurides were prepared directly by combining stoichiometric quantities of the elements. Lithium telluride (Li_2Te) was prepared in a

(1) Based on work performed under the auspices of the U. S. Atomic Energy Commission. Presented in part at the 148th National Meeting of the American Chemical Society, Chicago, Ill., Sept. 1964.

(2) E. Heymann and H. P. Weber, *Nature*, **141**, 1059 (1938); *Trans. Faraday Soc.*, **34**, 1492 (1938).

(3) E. Heymann, R. J. L. Martin, and M. F. R. Mulcahy, *J. Phys. Chem.*, **47**, 473 (1943).

(4) M. S. Foster, C. E. Crouthamel, D. M. Gruen, and R. L. McBeth, *ibid.*, **68**, 980 (1964).

(5) D. L. Maricle and D. N. Hume, *J. Electrochem. Soc.*, **107**, 354 (1960).

BeO crucible at 950°, but sodium telluride (Na_2Te) and potassium telluride (K_2Te) were prepared in alumina crucibles at 950 and 725°, respectively. Cesium telluride (Cs_2Te) was prepared in either alumina or quartz crucibles at 600°.

The solubility of tellurium metal in LiCl, KCl, and CsCl was determined by equilibrating 1 g of the metal with 10 g of the salt in the appropriate container for several hours with occasional agitation at 627, 802, and 671°, respectively. The saturated solutions were then dipped from the crucible with a small quartz container and solidified for analysis and subsequent use in spectral measurements.

Apparatus and Procedure. Solutions of the telluride in molten salts were prepared in the helium box by heating the telluride and salt together, usually in the same container used to prepare the telluride. These solutions, too concentrated for use in spectrophotometric measurements, were decanted from the undissolved telluride, solidified, and crushed. An aliquot of the concentrated solution was diluted with an appropriate amount of the purified salt used as a solvent. Approximately 6 g of this mixture was then added to the cell apparatus used in obtaining the absorption spectrum at elevated temperatures.

The cell apparatus consisted of a Fisher-Porter 1-cm path length cell sealed to a 45-cm length of 12-mm o.d. quartz tubing which contained a fine-porosity quartz frit 15 cm above the cell. To obtain shorter path lengths for the study of more concentrated solutions, suitable quartz cell spacers were employed. A standard-taper joint attached to the open end of the tube completed the cell-frit apparatus. By using appropriate vacuum line techniques, the diluted mixture was melted and filtered into the absorption cell, sealed off under 0.5 atm of argon, and transferred to the spectrophotometer furnace.

Absorption spectra measurements were made from 300 to 2500 $m\mu$ in a Cary Model 14 H spectrophotometer at temperatures up to 1000°. A description of the furnace and temperature controller has been given elsewhere.⁶ In place of the standard tungsten source, a high-intensity Sylvania DXL quartz halogen tungsten lamp (original Sun Gun lamp) was installed. This modification enables one to use more highly absorbing samples with improved resolution.

After the spectral measurements had been obtained, the cell was withdrawn from the furnace and the melt was allowed to solidify along the walls of the container. The cell was broken open inside the helium box and the solid was removed for analysis. The amount of tellurium present was determined by a colorimetric procedure using an extraction of the

diethyldithiocarbamate complex into carbon tetrachloride. Knowing the tellurium content and the density of the various solvents as a function of temperature, the molar extinction coefficients, ϵ , were calculated.

Results

Spectra of Li_2Te in LiCl-LiF . Solutions of Li_2Te in LiCl-LiF (80 mole % LiCl , mp 505°) are burgundy red and were studied spectrophotometrically at 525°. The spectrum (Figure 1, curve A) is characterized by an absorption band with a maximum at 21,250 cm^{-1} and a half-width of 7000 cm^{-1} . To calculate the oscillator strength of the transition, the band envelope at energies less than 21,250 cm^{-1} was symmetrically reproduced at energies greater than 21,250 cm^{-1} . The edge of what is presumed to be a charge-transfer band was obtained by subtraction of the dashed band-envelope curve from the measured absorption in the 22,000–29,000- cm^{-1} region.

Three different Li_2Te concentrations were studied. At 0.07, 0.10, and 0.13 M Li_2Te concentrations, the molar absorptivities at 21,250 cm^{-1} were found to be 25.1, 24.0, and 33.4, respectively. The major uncertainty in these measurements is in the analyses for the Li_2Te content of the melts. The differences in the values of the molar absorptivities of the three solutions are within the limits of error of the measurements and are probably not an indication of a breakdown of Beer's law. The molar absorptivities given in curve A (Figure 1) represent an average over the three determinations, and lead, by integration over the wavelength range 30,000 to 12,500 cm^{-1} , to an oscillator strength $f = 0.86 \times 10^{-3}$ for the transition. The low oscillator strength of the band implies that it is due to a forbidden transition.

Spectra of Cs_2Te in CsCl . Solutions of Cs_2Te in molten CsCl also are red in color. The absorption spectrum of such a solution obtained at 675° (Figure 2) is characterized by an absorption band with a maximum at 18,200 cm^{-1} , a half-width of 7400 cm^{-1} , and a molar absorptivity at the maximum of 581. By symmetrically reproducing the band envelope on the high-energy side of the maximum (dashed curve) and integrating from 9000 to 27,500 cm^{-1} , the oscillator strength of the transition was found to be $f = 2.0 \times 10^{-2}$. Although about 23 times as intense as the analogous transition in the Li_2Te solutions, the low oscillator strength of the Cs_2Te absorption band strongly implies that it too originates from a forbidden transition.

(6) D. M. Gruen and R. L. McBeth, *J. Phys. Chem.*, **66**, 57 (1962).

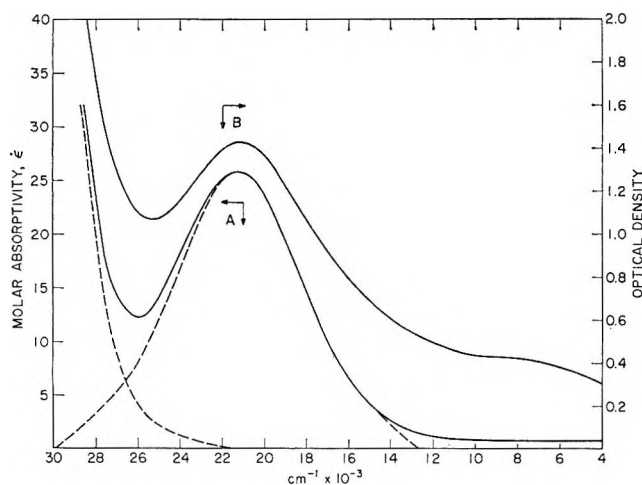


Figure 1. Curve A, Li_2Te in LiCl-LiF at 525° ; curve B, Li_2Te in LiCl at 650° .

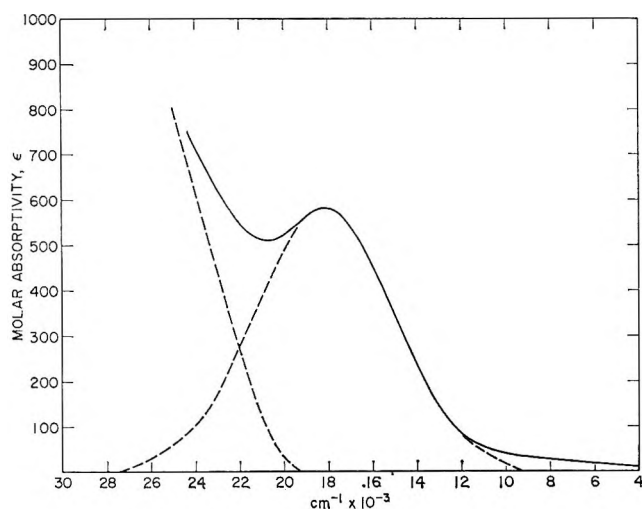


Figure 2. Cs_2Te in CsCl at 675° .

Experiments that were performed early in this investigation gave spectra which appeared to change with changing Cs_2Te concentration. In particular at low initial Cs_2Te concentrations, an entirely different spectrum was obtained which later measurements showed to be the spectrum of Te metal (see below). The cause of the difficulty was traced to an impurity present in the CsCl used as a solvent in the early experiments. Although the impurity was not identified, it reacted with Cs_2Te to give Te metal. At high Cs_2Te concentrations, all of the impurity was removed in this way but since Cs_2Te was present in large excess, its spectrum could be measured by using short path-length cells. At low Cs_2Te concentrations only the Te metal spectrum was observed. However, in later experiments using the high-purity CsCl (Atomergic

Chemetals material) as a solvent, we were able to measure the Cs_2Te spectrum at the $10^{-3} M$ concentration level. The spectrum shown in Figure 2 was obtained on a solution of Cs_2Te in high-purity CsCl .

Spectra of Li_2Te in CsCl and of Cs_2Te in LiCl-LiF . The possibility that the alkali metal tellurides do not exchange with solvent cations cannot be ruled out *a priori*. To test this admittedly remote possibility, spectra of solutions of Li_2Te in CsCl and of Cs_2Te in LiCl-LiF were measured. The spectra were identical with those obtained on solutions of Li_2Te in LiCl-LiF and of Cs_2Te in CsCl , respectively. It was thus demonstrated that the overwhelming concentration of solvent cations causes replacement of the initial alkali metal constituent and ensures that the alkali metal nearest neighbors surrounding tellurium are derived from the cations of the solvent. The nature of the solute species will be more fully discussed in a later section.

Effects of Temperature on the Absorption Spectra of the Alkali Metal Tellurides. Effects of temperature on the telluride spectra were first encountered in a study of a solution of Li_2Te in LiCl-KCl eutectic and are graphically represented in Figure 3. At 400° , the eutectic melt has the typical red color of the telluride solutions and the spectrum (curve A, Figure 3) has a band maximum at $20,400 \text{ cm}^{-1}$. Raising the temperature to 600° has the effect of shifting the band energy to the slightly lower value, $20,000 \text{ cm}^{-1}$. The edge of the charge-transfer band, however, shifts $\sim 2500 \text{ cm}^{-1}$ to lower energies (curve B).

The effect on the spectrum of going to 800° is shown in curve C. The absorption intensity has dropped and a broad band with considerable absorption intensity in the $12,000\text{-}17,000\text{-cm}^{-1}$ region has developed. This band is quite similar to the absorption spectrum of Te metal (see below). Indeed, on raising the temperature to 1000° , Te metal distilled out of the solution depositing in the unheated portion of the quartz tube. The remaining liquid had the spectrum shown in curve D. The low absorption intensity remaining in the visible region indicated that the Li_2Te solute had been removed from solution. After cooling the melt and washing it out of the optical cell, examination of the quartz surface showed that it had been etched.

The sequence of events deduced to explain these spectral changes can be summarized as follows. In the $400\text{-}700^\circ$ region, the telluride solution in LiCl-KCl eutectic is stable with respect to reaction with the quartz container. Beginning at about 800° , the telluride solute species reacts with the quartz of the container liberating Te metal which then volatilizes out of the solution at the still higher temperature of 1000° .

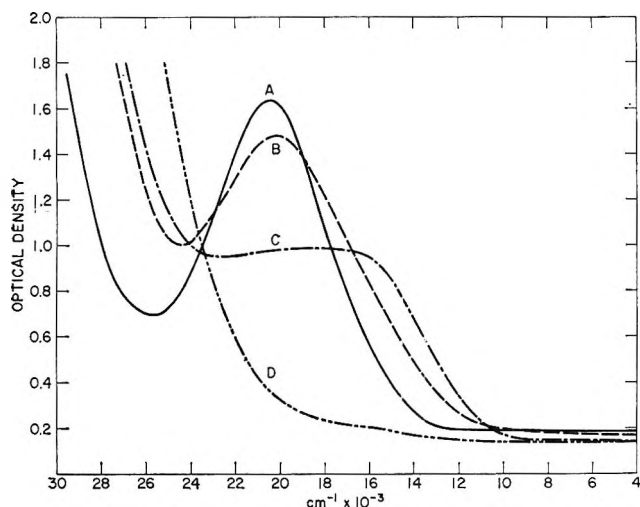


Figure 3. Li_2Te in LiCl-KCl eutectic: A, 400° ; B, 600° ; C, 800° ; D, 1000° .

At 800° , the solubility of Te metal in KCl is responsible for the increased absorption in the $12,000\text{--}17,000\text{-cm}^{-1}$ region.

Attempts to obtain the spectra of Na_2Te in molten NaCl and of K_2Te in molten KCl were only partially successful presumably because of reaction of the tellurides with the quartz at the lowest temperature ($\sim 800^\circ$) at which measurements can be performed on these liquids.

A qualitative spectrum of Li_2Te in molten LiCl at 650° (curve B, Figure 1) was obtained. Etching and reaction with the cell wall occurred at a lower temperature in this solvent because of the more corrosive nature of pure LiCl compared with LiCl-KCl eutectic.

Spectrum of Tellurium Metal in CsCl. In the course of this work, as has been mentioned, similar spectra were obtained on telluride solutions whose composition had been altered either by reaction with an impurity in the solvent (Cs_2Te in CsCl) or by reaction with the quartz container (Li_2Te in LiCl-KCl above 800°). It seemed likely that the new spectra were due to Te metal produced as a product of the reactions. To test this hypothesis, molten CsCl was equilibrated with Te metal, and the spectrum of the resultant blue solution was measured at 675° . The spectrum shown in Figure 4 was indeed found to be virtually identical with those obtained on the telluride solutions which had undergone chemical reactions, thus lending support to the hypothesis.

The Te metal spectrum (Figure 4) is characterized by a broad complex absorption band stretching from $27,000\text{ cm}^{-1}$ to about $10,000\text{ cm}^{-1}$ and having an oscillator strength of 3.9×10^{-2} . A resolution of this complex band into two overlapping bands with maxima

at $15,500$ and $20,800\text{ cm}^{-1}$ is suggested by the dashed curves. Subtraction of these dashed curves from the measured absorption band yields the edge (dotted) of a very intense absorption band.

In the course of this work, Te metal was equilibrated not only with molten CsCl, but also with molten LiCl and KCl. The saturation solubilities in these alkali halides were found from subsequent analyses for Te metal content to be 1.28×10^{-2} wt % in CsCl at 671° ; 3.5×10^{-2} wt % in KCl at 802° ; less than 5×10^{-4} wt % in LiCl at 627° , the lower limit of detection of Te by our analytical method.

Discussion

Absorption Spectra of Li_2Te in LiCl-LiF and of Cs_2Te in CsCl. In attempting an interpretation of the alkali metal telluride spectra, we are cognizant of the fact that it is based on the observation of a single absorption band per spectrum. It is nonetheless instructive to consider a very simple model which takes as its point of departure the forbiddenness of the $21,250\text{-cm}^{-1}$ transition of Li_2Te ($f = 0.86 \times 10^{-3}$) and of the $18,200\text{-cm}^{-1}$ transition of Cs_2Te ($f = 2.00 \times 10^{-2}$).

The compound Li_2Te has the antifluorite structure with 4:8 coordination such that each tellurium is surrounded by eight lithiums at the corners of a cube.⁷ It is likely that Cs_2Te has the anti- CdCl_2 structure by analogy with the structure of Cs_2O . In that event, each tellurium would be surrounded by six cesiums at the corners of an octahedron. On the assumption that similar coordination conditions prevail in the melts, the solution species could be formulated as

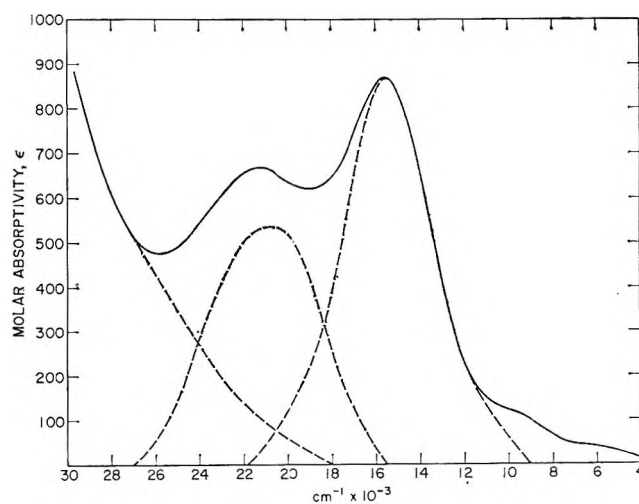


Figure 4. Tellurium metal in CsCl at 675° .

(7) A. F. Wells, "Structural Inorganic Chemistry," The Clarendon Press, Oxford, 1962, p 459.

so as to keep the reaction temperature at 60°. The effluent gas passed through a reflux condenser to retain the methanol and through water to remove the last traces of methanol. Finally, the gas was dried with Drierite. A gas chromatogram showed the gas to be over 99% C₂F₄ with only two impurities. A distillation at -126° effectively eliminated these impurities. Ozone was prepared by the electrodeless discharge of research grade oxygen.

The reaction cell was of Pyrex and had a Teflon stopcock with Viton O rings. Salt windows were at either end of the cell to permit *in situ* infrared analysis. The vacuum seal between the cell and the windows was made with Viton O rings lubricated with Kel F grease. The cell was situated in the sample beam of a Beckman IR-4 spectrophotometer.

Pure ozone was allowed to stand in the cell. It decomposed slowly but measurably. Thus, all runs were done by adding the ozone last, so that its decomposition would have negligible effect.

The olefin was degassed at -196° and placed in the cell at known pressure. The ozone was then degassed at -196° outside the reaction cell, and the stopcock to the cell was quickly opened and closed. The total pressure was then measured on a suitably calibrated Alphatron gauge. The rate of growth of a product peak (either the 5.12- μ band of CF₂O or the 5.30- μ band of CF₃CFO) was monitored, and the initial rate of growth was obtained by extrapolation to zero time. In some cases, after the run, the pressure of gas non-condensable at -196° (*i.e.*, O₂) was measured.

III. Results

The products of the reaction are CF₂O, CF₃CFO, and O₂. No other products were found. In the C₂F₄ experiments, careful checks were made for CF₂CF₂O and CF₃CFO, and they were definitely absent. Furthermore, some runs of the C₂F₄-O₃ system with excess O₃ were taken to completion, and the CF₂O pressure was twice the initial C₂F₄ pressure. The O₂ formed could come from either the ozone-perfluoroolefin reaction or the background decomposition of O₃ or both. From our results it is difficult to ascertain the situation.

The initial rates of product formation $R\{RO\}$, where RO is either CF₂O or CF₃CFO, are shown in Tables I through V. At any perfluoroolefin (hereafter referred to as R₂) pressure, $R\{RO\}$ increases linearly with (O₃) at small O₃ pressures but then levels off or even drops as (O₃) continues to rise. For the region where $R\{RO\}$ is linear with (O₃), the ratio $R\{RO\}/(O_3)$ rises with the R₂ pressure, as shown in Figures 1

Table I: CF₂O Production from C₂F₄-O₃ Reaction

(C ₂ F ₄), mm	(O ₃), mm	$R\{CF_2O\}$, μ/sec
0.20	0.73	14
0.22	2.1	35
0.22	5.7	27
0.20	14.6	20
0.22	24	26
0.63	1.07	39
0.54	1.85	47
0.66	4.7	128
0.58	11.3	83
0.61	17	78
1.10	1.7	123
1.03	18	190
2.2	2.4	165
2.2	9.8	370
2.2	22	280
5.7	6.2	340

Table II: CF₂O Production from C₃F₆-O₃ Reaction

(C ₃ F ₆), mm	(O ₃), mm	$R\{CF_2O\}$, μ/sec
0.22	4.7	7.6
0.23	14.8	7.8
0.46	2.0	17
0.48	2.0	23
0.41	4.9	21
0.36	6.5	10.1
0.41	14.7	20
0.70	2.1	16
0.73	4.5	30
0.70	9.3	34
1.07	2.4	26
1.14	4.3	44
1.07	14.0	150
2.0	1.9	23
2.0	7.4	200
7.0	10.6	615

Table III: CF₃CFO Production from C₃F₆-O₃ Reaction

(C ₃ F ₆), mm	(O ₃), mm	$R\{CF_3CFO\}$, μ/sec
0.186	5.0	~2.5
0.43	4.7	3.9
0.75	4.2	8.4
1.02	4.2	10.4
1.96	2.1	9.3
1.89	7.9	38
5.5	6.2	88

through 3. Under all conditions, the ratio of $R\{CF_2O\}$ to $R\{CF_3CFO\}$ remains constant at 4.0 in the C₃F₆ runs and 2.8 in the C₄F₈ runs.

Table IV: CF₂O Production from C₄F₈-O₃ Reaction

(C ₄ F ₈), mm	(O ₃), mm	R{CF ₂ O}, μ/sec
0.19	39	1.8
0.19	85	3.5
0.39	46	6.0
0.84	9.9	4.8
0.86	33	19
1.31	4.0	7.2
1.29	11.3	18
1.33	19.4	25
1.33	24.5	30
1.28	37	27
1.31	65	33
2.6	11.9	31
5.3	6.0	37

Table V: CF₃CFO Production from C₄F₈-O₃ Reaction

(C ₄ F ₈), mm	(O ₃), mm	R{CF ₃ CFO}, μ/sec
0.19	33	0.65
0.22	63	1.45
0.33	37	1.44
0.46	9.6	0.71
0.42	37	2.2
0.70	28	4.2
0.88	20	3.8
0.82	40	5.0
1.07	20	7.7
1.09	27	6.1
1.28	3.9	1.48
1.32	12.8	5.0
2.2	16	12.0
2.3	20	13.9
3.5	1.3	1.75
3.4	7.0	9.1
3.5	16	17.2
6.7	5.6	12.5

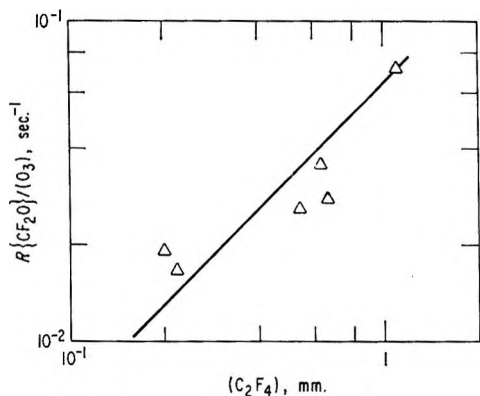


Figure 1. Plot of R{CF₂O}/(O₃) vs. (C₂F₄).

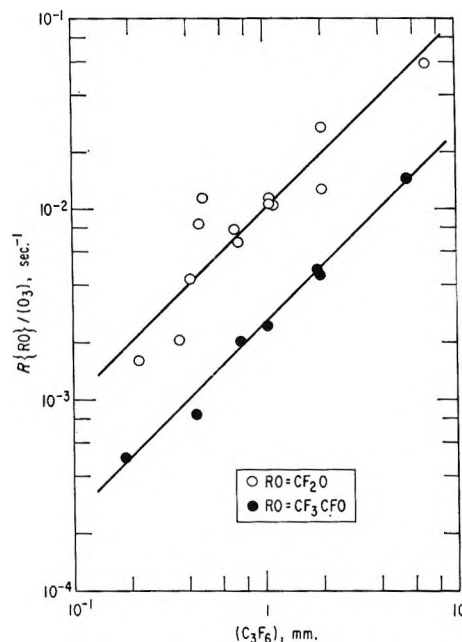


Figure 2. Plots of R{RO}/(O₃) vs. (C₃F₆).

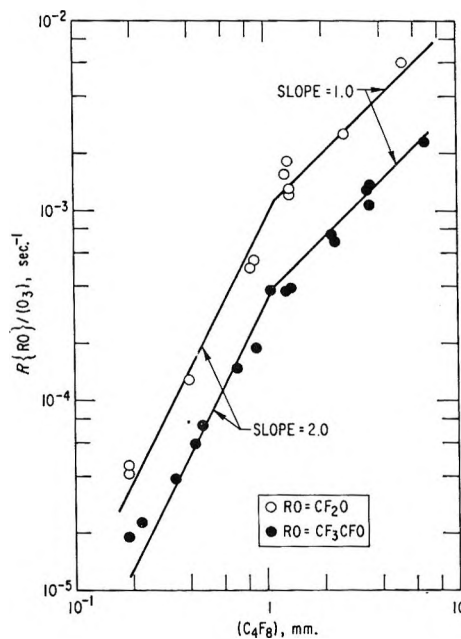


Figure 3. Plots of R{RO}/(O₃) vs. (C₄F₈-2).

IV. Discussion

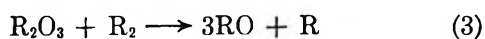
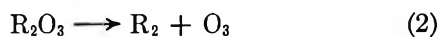
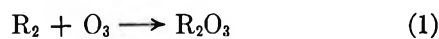
At low reactant pressures, the rate of reaction should be slow and diffusional mixing of reagents should be fast. On the other hand, at high reactant pressures, the reverse is true. Thus, at low pressures, the chemical reaction should be rate controlling, but at high pressures diffusion should be rate controlling.

Table VI: Rate Constant Ratios

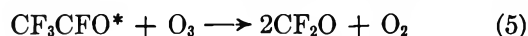
Olefin	k_1		k_1k_2/k_2		$R\{CF_2O\}/R\{CF_3CFO\}$
	$mm^{-1} sec^{-1}$	$M^{-1} sec^{-1}$	$mm^{-2} sec^{-1}$	$M^{-2} sec^{-1}$	
C_2F_4	16×10^{-3}	81×10^3	>0.08	$>2.0 \times 10^{12}$	∞
C_3F_6	2.5×10^{-3}	13×10^3	>0.012	$>0.13 \times 10^{12}$	4.0
C_4F_8	0.22×10^{-3}	1.1×10^3	1.9×10^{-4}	4.8×10^9	2.8

Our results conform to this model. At low pressures, $R\{RO\}$ increases linearly with (O_3) at any R_2 pressure, thus indicating that the chemistry controls the rate. However, at high O_3 pressures (which is then similar to the total pressure), $R\{RO\}$ becomes independent of (O_3) or actually falls as the (O_3) is enhanced. This effect is most marked in the C_2F_4 system where chemical reaction is the fastest and is least noticeable in the C_4F_8 system where chemical reaction is the slowest. Clearly, diffusion must be the controlling step. The effect is so pronounced in the C_2F_4 system that there is only a very limited experimentally accessible region where the chemistry controls. We are only interested in the region in which chemistry controls, so that all of the ensuing discussion will be limited to the region where $R\{RO\}$ is proportional to (O_3) .

The mechanism that most easily explains the results is



where R_2O_3 is the unstable ozonide intermediate. Reaction 3 cannot be a one-step process for its reverse would be quadrimolecular. Perhaps the intermediates are $(RO)_2$ and R_2O . The $(RO)_2$ would fall apart to $2RO$, and R_2O could either decompose to $RO + R$ or react directly with O_3 to yield $2RO + O_2$. In the latter case reaction 4 would not be needed. Apparently, since CF_2O is the principal product even in the C_4F_8 experiments, some fraction of the CF_3CFO formed has sufficient energy to react further with ozone



where CF_3CFO^* represents those CF_3CFO molecules with sufficient energy to react *via* (5).

The mechanism predicts that

$$R\{CF_3CFO\} + \frac{1}{2}R\{CF_2O\} = \frac{\alpha k_1 k_3 (O_3) (R_2)^2}{k_2 + k_3 (R_2)} \quad (6)$$

$$\frac{R\{CF_2O\}}{R\{CF_3CFO\}} = \text{constant} \quad (7)$$

where α is 2, 3, or 4, respectively, for C_2F_4 , C_3F_6 , or C_4F_8 . Thus, the quantities $R\{RO\}/(O_3)$ should be independent of the ozone pressure and rise linearly with (R_2) at high R_2 pressures or with $(R_2)^2$ at low R_2 pressures. The appropriate plots are shown in Figures 1 through 3.

For C_2F_4 , only very limited data are available, but the log-log plot (Figure 1) can be represented by a straight line of unit slope. From the intercept, a value for k_1 of $81 \times 10^3 M^{-1} sec^{-1}$ is obtained.

The data for C_3F_6 are shown in Figure 2, and the log-log plots can be well fitted by a line of slope 1. The ratio $R\{CF_2O\}/R\{CF_3CFO\}$ is 4.0, and k_1 is $13 \times 10^3 M^{-1} sec^{-1}$.

For neither C_2F_4 nor C_3F_6 is the pressure sufficiently low to enter the second-order region, but the situation is considerably different for C_4F_8 , as shown by Figure 3. Both the first- and second-order regions are readily apparent. The ratio $R\{CF_2O\}/R\{CF_3CFO\}$ is 2.8, k_1 is $1.1 \times 10^3 M^{-1} sec^{-1}$, and k_1k_2/k_2 is $4.8 \times 10^9 M^{-2} sec^{-1}$.

The rate constant data for the perfluoroolefins are summarized in Table VI, and they are comparable to those for the hydrocarbon analogs. However, contrary to the hydrocarbons, the reactivity increases in the perfluoroolefin series from C_4F_8 to C_2F_4 corresponding to the diminution of the double-bond strength for this series.

Acknowledgment. The author wishes to thank Mr. Dennis Saunders for preparation of C_2F_4 and Mrs. Barbara Peer for assistance with the manuscript.

A Nuclear Magnetic Resonance Study of Diethylamine Hydrogen Bonding¹

by Charles S. Springer, Jr., and Devon W. Meek

Department of Chemistry, The Ohio State University, Columbus, Ohio 43210 (Received August 23, 1965)

The concentration dependence of the chemical shift of the diethylamine NH proton was studied both in the hydrogen-bonding solvent acetonitrile and in the nonhydrogen-bonding solvent cyclohexane. In the cyclohexane solutions the N-H...N bonds in pure diethylamine break upon dilution and the resonance position of the N-H peak changes toward higher magnetic fields, whereas in acetonitrile solutions the N-H resonance changes systematically toward lower fields as the concentration of amine decreases. Thus, the N-H group of diethylamine forms a stronger hydrogen bond with acetonitrile than with itself. Rapid exchange of the diethylamine N-H proton appears to result from trace amounts of water present in acetonitrile and cyclohexane.

Introduction

The self-association of liquid amines *via* hydrogen bonds has been studied by infrared spectroscopy in both the N-H fundamental² and overtone regions,³ by nmr in carbon tetrachloride,^{4,5} and by the enthalpy of mixing of diethylamine with monoethylamine and triethylamine.⁶ Since the N-H chemical shift of tris(2-N-methylaminoethyl) borate, B(OCH₂CH₂NH-CH₃)₃, was strongly dependent on concentration in acetonitrile,⁷ an investigation of the proton nuclear magnetic resonance of the "model" compound, (C₂H₅)₂NH, was undertaken in order to determine the behavior of the N-H group in the hydrogen-bonding solvent acetonitrile.

Experimental Section

Reagents. Acetonitrile was purified and the water content was determined as reported previously.⁷ Cyclohexane was refluxed overnight over calcium hydride and then fractionated. The middle portion was stored in a desiccator and opened only in a drybox which was continuously flushed with nitrogen. Eastman White Label diethylamine was distilled from anhydrous BaO and protected from moisture. The middle fraction was stored in a desiccator and opened only in the drybox.

Nmr Spectra. A Varian A-60 nmr spectrometer with a 60-Mc probe was operated at 40°. All nmr samples were prepared in a drybox as described previously.⁷ All spectra were calibrated internally with tetramethylsilane. The near-infrared spectra were

obtained with a Cary Model 14 recording spectrophotometer using a set of matched 1-cm quartz cells.

Results and Discussion

Diethylamine in Acetonitrile. The significant portions of the nmr spectra of diethylamine in acetonitrile (that of the CH₃ and NH groups) are shown in Figure 1, and the data are given in Table I. A plot of the N-H resonance position, in τ units, as a function of concentration in acetonitrile is shown in Figure 2. The resonance position of the N-H peak shifts systematically to lower τ values as the concentration of diethylamine is decreased in acetonitrile, indicating that the solute-solvent hydrogen bonds are stronger than those between diethylamine molecules, that is, that acetonitrile is a stronger hydrogen-bond acceptor than diethylamine. Since only one sharp NH peak is seen, the equilibrium between (C₂H₅)₂NH--HN(C₂H₅)₂ and (C₂H₅)₂NH--N≡C-CH₃ must be very rapid, so that the spectrometer records the average resonance.

(1) Grateful acknowledgment is made to the donors of the Petroleum Research Fund, administered by the American Chemical Society, for the grant (1518-A1,3) which supported this research.

(2) A. G. Moritz, *Spectrochim. Acta*, **17**, 365 (1961).

(3) K. B. Whetsel and J. H. Lady, *J. Phys. Chem.*, **68**, 1010 (1964).

(4) V. P. Bystrov and V. P. Lezina, *Opt. i Spektroskopiya*, **16**, 790 (1964); *Chem. Abstr.*, **61**, 4186a (1964).

(5) J. Feeney and L. H. Sutcliffe, *J. Chem. Soc.*, 1123 (1962).

(6) H. J. Bittrich, G. Duering, and G. Linke, *Wiss. Z. Tech. Hochsch. Chem. Leuna-Merseburg*, **4**, 245 (1962); *Chem. Abstr.*, **59**, 3371d (1963).

(7) D. W. Meek and C. S. Springer, Jr., *Inorg. Chem.*, in press.

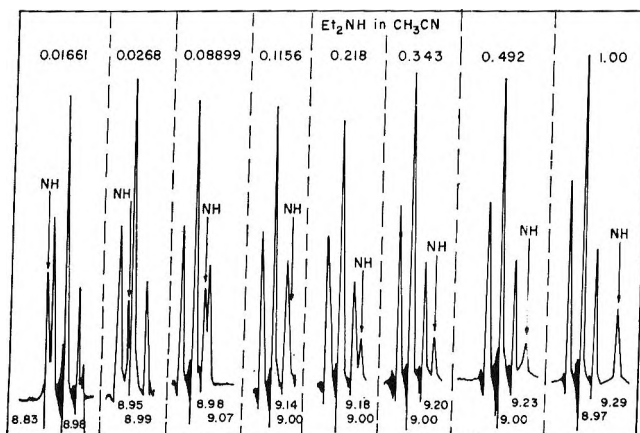


Figure 1. The CH_3 and N-H regions from eight different proton nmr spectra of diethylamine in acetonitrile at 40° . Concentration of diethylamine (given in mole fraction) increases from left to right. Assignments of the resonance positions are given by the numbers at the bottom of each spectrum. Resonance of the CH_3 group is at τ 8.97–9.00, whereas the N-H resonance varies systematically from τ 8.83 to 9.29.

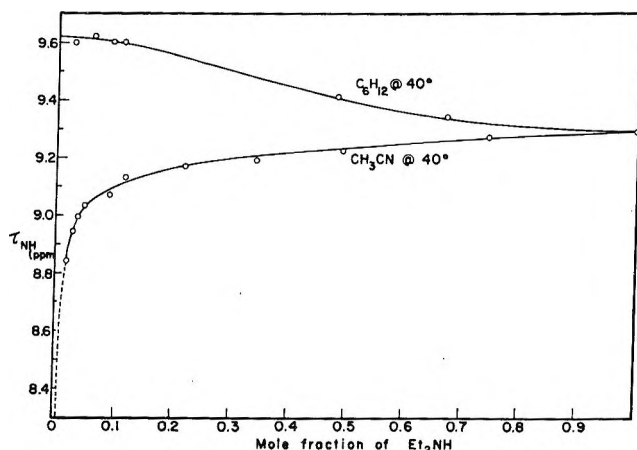


Figure 2. Concentration dependence of the NH resonance position (τ_{NH}) in the proton nmr spectrum of diethylamine in both acetonitrile and cyclohexane at 40° .

The sharp peaks can be attributed to rapid exchange of the amino proton caused by a trace of water in the hygroscopic solvent, acetonitrile.

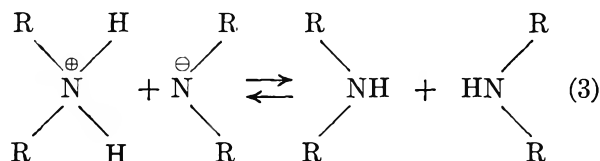
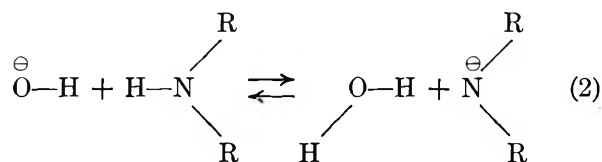
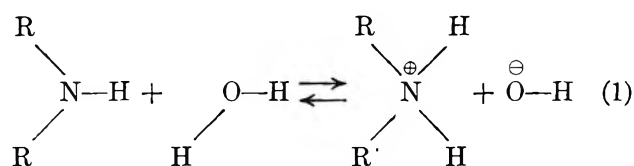
The rapid exchange of the labile amine proton eliminates the quadrupole broadening effect of N^{14} , thus resulting in a sharp resonance peak. Ogg⁸ reports that only 0.1 ppm of water is necessary to give a sharp NH resonance peak for liquid ammonia. If the forms of the $(\text{C}_2\text{H}_5)_2\text{NH}$ molecule in which it is hydrogen bonded, either to itself or to the solvent, are in rapid equilibrium with the free amine species, an exchange scheme, in which water acts as an acid toward

Table I: Proton Nmr Data^{a,b} of Diethylamine in Acetonitrile as a Function of Concentration

Concn, mole fraction of $(\text{C}_2\text{H}_5)_2\text{NH}$	CH_3 triplet, τ , ppm	CH_2 quartet, τ , ppm	NH singlet, τ , ppm
0.0166 ^a	8.98	7.44	8.83
0.0268	8.99	7.43	8.95
0.0330	8.99	7.42	8.99
0.0665	8.99	7.45	9.03
0.0889	8.98	7.43	9.07
0.1156	9.00	7.44	9.14
0.2180	9.00	7.43	9.18
0.3430	9.00	7.43	9.20
0.4920	9.00	7.45	9.23
0.7440	9.02	7.43	9.27
1.0000 ^b	8.97	7.41	9.29

^a At the mole fraction 0.0166 the total area under the peaks assigned as $\text{CH}_3 + \text{NH}$ is 7.11 relative to 4.00 for the area of the methylene peaks (theory = 7.0:4.0). ^b In pure diethylamine the areas of the CH_3 and CH_2 peaks are 6.14 and 4.12 relative to the N-H = 1.00 (theory = 6.0 and 4.0:1.0, respectively).

the amine molecule, can be represented by the equations



Most of the exchange which involves an ionic intermediate probably occurs by route 1.

Huyskens and Huyskens^{9,10} observed a rapid proton exchange between primary and secondary amines with alcohols. They discounted the possibility that the exchange occurred *via* ionic intermediates and proposed a simultaneous exchange of two hydrogens through a

(8) R. A. Ogg, Jr., *J. Chem. Phys.*, **22**, 560 (1954).

(9) P. Huyskens and T. Z. Huyskens, *Bull. Soc. Chim. Belges*, **69**, 267 (1960).

(10) T. Z. Huyskens, P. Huyskens, and P. Van Tiggelen, *ibid.*, **70**, 386 (1961).

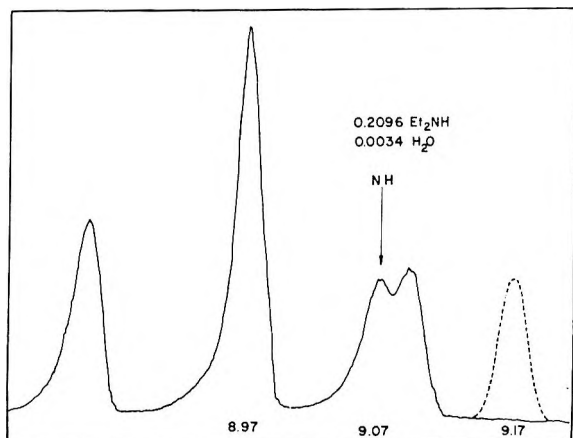


Figure 3. The CH_3 and NH region of the proton nmr spectrum of diethylamine in wet acetonitrile at 40° . The solution contained 0.2096 and 0.0034 mole fraction of diethylamine and water, respectively. The dashed curve at τ 9.17 represents the N-H resonance peak of a solution containing no added water. The magnetic field axis is expanded to ten times that shown in Figure 1. Methyl triplet is centered at τ 8.97.

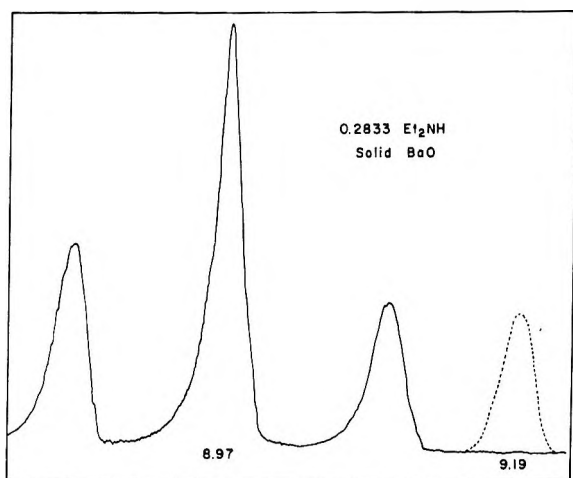


Figure 4. Part of the proton nmr spectrum of diethylamine in acetonitrile containing solid anhydrous BaO . The dashed curve at τ 9.19 represents the interpolated N-H peak for a solution containing 0.2833 mole fraction diethylamine. The scale of the magnetic axis is the same as in Figure 3. Methyl triplet is centered at τ 8.97.

powdered barium oxide in the bottom of the sample tube. The solution was dried sufficiently so that not enough water was present to cause rapid exchange of the NH peak, and no sharp N-H peak was seen. However, the CH_3 peaks remain sharp and characteristic of the methyl group.

Diethylamine in Cyclohexane. Since liquid diethylamine is associated *via* hydrogen bonding with itself,²⁻⁵ the peak position of the amine proton given in Figure

1 for pure liquid $(\text{C}_2\text{H}_5)_2\text{NH}$, τ 9.29, is not the resonance position of the unbonded NH . This value can be found only at infinitely high dilution of $(\text{C}_2\text{H}_5)_2\text{NH}$ in an inert solvent. The chemical shift of the N-H changes to higher fields as the concentration of diethylamine in cyclohexane decreases. This is opposite to the behavior in acetonitrile, but it is just the behavior expected when a self-associating compound is diluted with a nonassociating solvent. The plot of $\tau_{\text{N-H}}$ against concentration in cyclohexane is presented in Figure 2. The N-H resonance position of diethylamine, extrapolated to infinite dilution in cyclohexane, occurs at τ 9.60. Since this represents a change in the chemical shift of only 0.3 τ unit over the entire concentration range, the amine can be associated only very weakly in the pure liquid. In fact, shifts of nearly this magnitude (0.3 τ unit) were observed for nonhydrogen-bonded protons on dilution.¹³ Since all measurements were made at a temperature of 40° , the observed values do not correspond to the maximum hydrogen-bond shifts that would be obtained for diethylamine just above the melting point. However, this is not serious for the present comparison because each system was measured under closely similar conditions.

The method used for determination of the association constant of diethylamine in cyclohexane was that devised by Saunders and Hyne¹⁴ from the theory of Gutowsky and Saika.¹⁵ The exchange process between hydrogen-bonded and nonhydrogen-bonded species is sufficiently rapid to prevent observation of separate resonance peaks. If one assumes that the time-averaged resonance results from exchange between the monomer and a single polymeric species, then the ratio of monomer to polymer in equilibrium can be calculated from the equations

$$\nu = \frac{\nu_1 M_1 + n \nu_n K_n M_1}{C} \quad (4)$$

$$C = M_1 + n K_n M_1^n \quad (5)$$

where M_1 is the concentration of the monomeric form, C is the total amount of all forms, and ν is the observed frequency of the hydrogen-bonded proton.

By tabulating arbitrary values of M_1 , which appears in both eq 4 and 5, and approximating ν_1 , ν_n , and K_n , values of C and ν can be determined for each M_1 . One varies the parameters until a plot of $\log C$ against ν fits the experimental curve.

(13) J. D. Roberts, "Nuclear Magnetic Resonance," McGraw-Hill Book Co., Inc., New York, N. Y., 1959, p 24.

(14) M. Saunders and J. B. Hyne, *J. Chem. Phys.*, **29**, 1319 (1958).

(15) H. S. Gutowsky and A. Saika, *ibid.*, **21**, 1688 (1953).

Table II gives the experimental values for diethylamine in cyclohexane. The experimental circled points are plotted as $\log C$ against ν_{NH} in Figure 5. The heavy line in Figure 5 is the best fitting theoretical curve. It is obtained from assuming a tetrameric equilibrium, $n = 4$, and the values $\nu_1 = 576.3$ cps, $K_4 = 1.75 \times 10^{-3} M^{-3}$, and $\nu_4 = 529.1$ cps.

Table II: Concentration Dependence of the N-H Resonance of Diethylamine in Cyclohexane (TMS = 10 ppm = 600 cps)

Concn		τ_{NH} , ppm	ν_{NH} , cps
Mole fraction	Molarity		
0.02606	0.2413	9.60	576
0.05986	0.5553	9.62	577
0.09204	0.8552	9.60	576
0.1109	1.031	9.60	576
0.4815	4.560	9.41	565
0.6710	6.414	9.34	560
1.000	9.718	9.29	557

The value of ν_1 was taken to be the average of the four lowest concentration points (576.3 cps). It can be seen from Figure 2 that this part of the curve is nearly horizontal, and it was assumed that the intermolecular hydrogen bonds are broken below a mole fraction of 0.1 in C_6H_{12} and the resonance at 576.3 cps is characteristic of the monomer. The values of K_4 and ν_4 were changed arbitrarily until the theoretical curve could be fitted to the experimental points. Table III shows the final theoretical data.

The value of K_4 is in reasonable agreement with that of Feeny and Sutcliffe,⁵ who determined $K_4 = 2.5 \times 10^{-4} M^{-3}$ for diethylamine in carbon tetrachloride at

Table III: Theoretical Concentration Dependence of Nmr Spectrum of Diethylamine in Cyclohexane at 40°^a

M_1, M	C, M	ν, cps
0.20	0.2000	576.3
0.40	0.4002	576.3
0.80	0.8029	576.1
1.00	1.007	576.0
2.00	2.112	573.8
3.00	3.567	570.1
3.50	4.550	565.4
4.00	5.792	561.7
5.00	9.375	554.3

^a The following values were the results of arbitrarily varying the parameters in eq 4 and 5: $\nu_1 = 576.3$ cps, $K_4 = 1.75 \times 10^{-3} M^{-3}$, and $\nu_4 = 529.1$ cps.

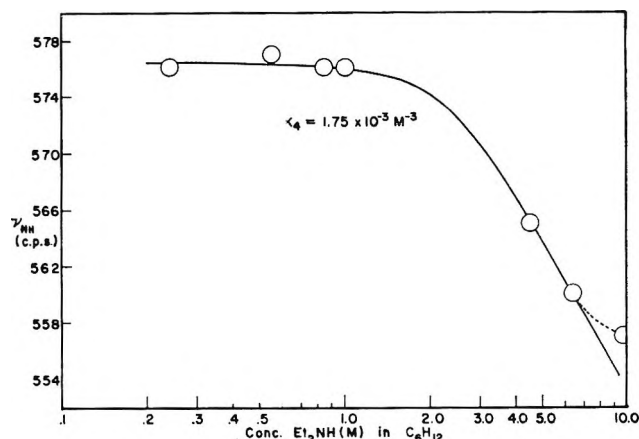
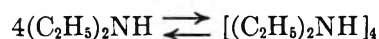


Figure 5. Concentration dependence of NH resonance position (ν_{NH} cps) in the proton nmr spectrum of diethylamine in cyclohexane at 40°. Circles are experimental values. Solid line is the theoretical curve assuming $\nu_1 = 576.3$ cps, $\nu_4 = 529.1$ cps, and $K_4 = 1.75 \times 10^{-3} M^{-3}$.

25° by the same method. Both the solvent and temperature are known to have an effect on the association constant, and the difference between the solvents and the temperatures could account for the difference in the equilibrium constants.

The agreement of the theoretical curve with the experimental points is excellent except for the point corresponding to pure diethylamine. However, this deviation is actually predicted since, in this limit of high concentration, polymers higher than tetramers are expected. Indeed, the direction of deviation of the experimental point is exactly that predicted for higher polymers. The excellent fit for the rest of the curve, however, is a good indication that the monomer-tetramer equilibrium



dominates through the intermediate and low concentration regions.

Infrared work by Feeny and Sutcliffe⁵ seems to indicate that these tetramers are cyclic in nature. Cohen and Reid¹⁶ claim that alcohols and many other hydrogen-bonded species tend to form trimers and tetramers instead of dimeric species because of the cyclic stability associated with a six- or eight-membered ring. It should be noted that with an assumption of $n = 3$, it was impossible to get as good a fit no matter how ν_3 and K_3 were varied. This method is somewhat insensitive for curves of $n > 4$ so that the presence of polymers greater than tetramers cannot be excluded. However, the excellent fit of the theoretical curve

(16) A. D. Cohen and C. Feid, *J. Chem. Phys.*, **25**, 790 (1956).

with the experimental points strongly supports the tetramer as the predominate polymeric species.

Near-Infrared Spectra. An investigation was carried out on the first overtone band of the N-H stretch in the near-infrared absorption spectra of diethylamine in both acetonitrile and cyclohexane. In cyclohexane, two peaks at 1536 (N-H stretch of the free amine) and 1544 $m\mu$ (N-H hydrogen bonded) are present, whereas

only the 1544- $m\mu$ peak is observed in acetonitrile over the concentration range of 0.01–0.05 mole fraction. Thus, the 1544- $m\mu$ peak appears to be characteristic of the hydrogen-bonded form, but is insensitive to whether the proton acceptor is the nitrogen atom of an NH_2 or $C\equiv N$ group. Therefore, for this system, nmr spectroscopy is more sensitive to hydrogen-bonding interaction than infrared spectroscopy.

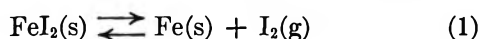
Thermodynamic Properties of Iron(II) Iodide(s) from Equilibrium Studies

by Wayne E. Zaugg and N. W. Gregory

Department of Chemistry, University of Washington, Seattle, Washington 98105 (Received August 23, 1965)

Thermodynamic properties of $FeI_2(s)$ have been evaluated from an equilibrium study of its decomposition to the elements over the temperature interval 498–585°. Values of $\Delta H_f^\circ = -24 \pm 1$ kcal mole⁻¹ and $S^\circ = 41 \pm 2$ cal deg⁻¹ mole⁻¹ at 298.2°K are derived.

Certain of the transition metal iodides have small enough free energies of formation to allow study of the equilibrium between the compounds and the elements at moderate temperatures. We find this to be the case for iron and have applied the transpiration method to determine thermodynamic properties of $FeI_2(s)$. An estimate of its entropy has previously been reported.¹ The enthalpy of formation has been evaluated indirectly from a series of heat of reaction and heat of solution measurements involving iron carbonyl iodides and iron(II) iodide.² It was anticipated that a direct study of reaction 1 would give more reliable values for



these quantities. The entropy is of particular interest because of the unknown contribution associated with antiferromagnetic–paramagnetic transition reported in the vicinity of 10°K.³

Experimental Section

The transpiration apparatus and procedure, with argon as the carrier gas, were essentially the same as described earlier.^{4,5} A mixture of $FeI_2(g)$ and iodine

was introduced into an argon stream by passing the gas, at *ca.* 1000 torr, over a preliminary sample of $FeI_2(s)$, placed in a compartment adjacent to the equilibration vessel and maintained at nearly the same temperature. In one series of runs the equilibration vessel itself was also packed with initially pure FeI_2 , and in another series it was packed with an approximately 4:1 *M* mixture of $FeI_2(s)$ and iron wire. Equilibrium was established readily when approached by decomposition of FeI_2 but only slowly by reaction of excess iodine with iron. In the former case reproducible pressures of iodine were obtained at flow rates between 16 and 47 cm³ min⁻¹, calculated at the reaction tem-

(1) K. K. Kelley and E. G. King, U. S. Bureau of Mines Bulletin 592, U. S. Government Printing Office, Washington, D. C., 1961.

(2) F. D. Rossini, D. D. Wagman, W. H. Evans, S. Levine, and I. Jaffe, National Bureau of Standards Circular 500, U. S. Government Printing Office, Washington, D. C., 1952.

(3) H. Bizette, C. Terrier, and B. Tasi, *Compt. Rend.*, **245**, 507 (1957).

(4) R. R. Richards and N. W. Gregory, *J. Phys. Chem.*, **68**, 3089 (1964).

(5) For details, see the Ph.D. thesis of W. E. Zaugg, University of Washington, 1965.

perature and pressure. These were taken as equilibrium values.

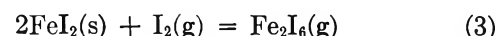
As the gas mixture left the equilibrium vessel, the iron(II) iodide vapor condensed in the exit tube in the cooler regions adjacent to the furnace; iodine vapor was collected in a following trap, cooled with liquid oxygen, and argon was collected in a second trap, cooled with liquid nitrogen. At the conclusion of a run the quantity of argon was determined from its pressure after isolation and expansion into a calibrated volume. While maintaining a positive pressure and flow of argon in the system to minimize contact of the main sample with air, the iodine trap was removed by breaking the exit tube; the iodine was subsequently dissolved in KI solution and determined by "dead-stop" titration with sodium thiosulfate.⁶ The part of the exit tube extending into the furnace, which contained the FeI₃ deposit, was removed (*via* a Viton O ring connector), and the system was quickly reevacuated prior to setting up for another run. The condensate was dissolved in water, and the ferrous ion was determined colorimetrically as the 1,10-phenanthroline complex.⁷

FeI₂ was prepared by reaction of Fisher Reagent grade electrolytic iron powder with Mallinckrodt Reagent grade iodine in a Pyrex vacuum system. Iodine vapor, originating from solid iodine at room temperature, was pumped continuously over the iron powder at 450°. The FeI₂ sublimed to cooler portions of the reaction vessel and was subsequently transferred to the transpiration tube in a nitrogen-filled drybox.

Apparent decomposition pressures of iodine $P(\Sigma I_2)$ were calculated from the number of moles collected, $n(I_2)$, and the number of moles of argon, $n(\text{Ar})$, passing through the vessel during a given run: $P(\Sigma I_2) = n(I_2)P/n(\text{Ar})$. P is the measured pressure of argon during the experiment; since argon constituted more than 99.5% of the gas mixture, $n(\text{Ar})$ was taken as the total number of moles of gas. The apparent pressure of iodine actually consists of contributions from a number of species: $P(\Sigma I_2) = P(I_2) + \frac{1}{2}P(I) + \frac{1}{2}P(\text{FeI}_3) + P(\text{Fe}_2\text{I}_6)$. The $I_2 = 2I$ equilibrium is well known, and values of the equilibrium constant at various temperatures are conveniently tabulated in the JANAF tables.⁸ The contributions $P(\text{FeI}_3)$ and $P(\text{Fe}_2\text{I}_6)$ arise from the decomposition of FeI₃ and Fe₂I₆, respectively, which occur in the equilibrium vapor. Ferric iodide, under conditions of this study, is unstable in the solid phase and on condensation decomposes to FeI₂ and iodine. Schäfer and Hönes⁹ have determined equilibrium constants for the reactions



and



Hence, $P(I)$, $P(\text{FeI}_3)$, and $P(\text{Fe}_2\text{I}_6)$ can be expressed in terms of known equilibrium constants and $P(I_2)$, and the value of $P(I_2)$ can be calculated from each measured $P(\Sigma I_2)$.

Slight etching of the quartz transpiration tube in regions of contact with crystalline FeI₂ was observed after prolonged reaction periods. A black deposit was also observed on portions of the vessel. In addition, traces of silicon were detected in the iodine solution washed out of the iodine collector. No silicon was found in the FeI₂ condensate. This suggests that quartz and FeI₂ may react to form products such as SiI₄ and FeO, but insufficient data are available to calculate the partial pressure of SiI₄ which might be expected. To test the dependence of the results on the nature of the container a transpiration tube with an alumina liner and exit tube was constructed. After adequate baking to remove adsorbed water, iodine pressures were obtained which were found to agree with those obtained in quartz at the higher temperatures. At lower temperatures, iodine pressures were slightly below those from the quartz reactor; this may have been caused by adsorption of iodine on the cooler portions of the unglazed alumina tube at the lower temperatures. The similarity of the results in alumina and quartz at higher temperatures was taken to indicate that the slight reaction of FeI₂ with quartz had no significant effect upon the calculated equilibrium constants for the primary reaction.

Results and Discussion

The equilibrium constants of Schäfer and Hönes⁹ were refined for use in this work. They studied reactions 2 and 3 by a transpiration method in which iodine at various partial pressures in nitrogen was passed over FeI₂(s). They subtracted the amount of FeI₂ which vaporized when no iodine was added to the nitrogen from the total transported in the presence of iodine and attributed the remainder to FeI₃ and Fe₂I₆. From the dependence of the amount transported on the iodine pressure they calculated equilibrium constants for (2) and (3).

(6) C. W. Foulk and A. T. Bawden, *J. Am. Chem. Soc.*, **48**, 2045 (1926).

(7) E. B. Sandell, "Colorimetric Determination of Traces of Metals," Vol. 3, Interscience Publishers, Inc., New York, N. Y., 1959, p 541.

(8) "JANAF Thermochemical Tables," revised ed, The Dow Chemical Co., Midland, Mich., 1963.

(9) H. Schäfer and W. J. Hönes, *Z. Anorg. Allgem. Chem.*, **288**, 62 (1956).

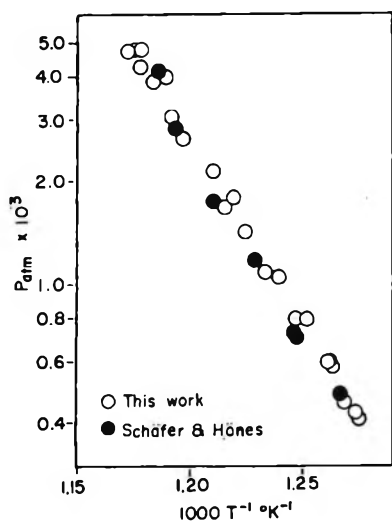


Figure 1. Amounts of iron iodide, expressed as an apparent pressure of $\text{FeI}_2(\text{g})$, in equilibrium with $\text{FeI}_2(\text{s})$.

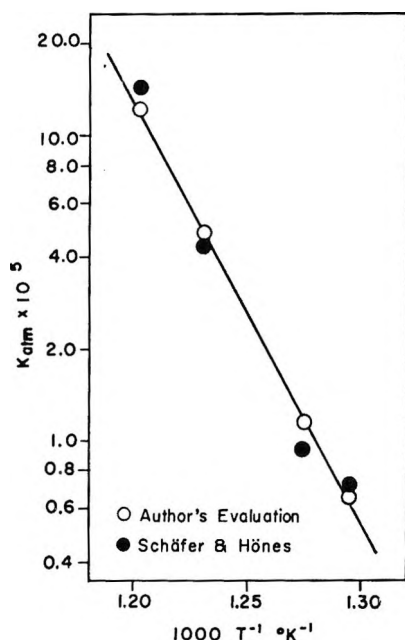


Figure 2. Equilibrium constants for $2\text{FeI}_2(\text{s}) + \text{I}_2(\text{g}) \rightleftharpoons 2\text{FeI}_3(\text{g})$.

In this work the amount of iron iodide transported when pure FeI_2 is heated in a stream of inert gas without addition of excess iodine was also determined. Our results are in good general agreement with those of Schäfer and Hönes (see Figure 1). Since we have also determined the iodine pressure in this system, it is possible to calculate the importance of FeI_3 and of Fe_2I_6 in these experiments. Because the iodine pressures are so small, the amount of FeI_3 is small and its contribution to the total iron is very small but the

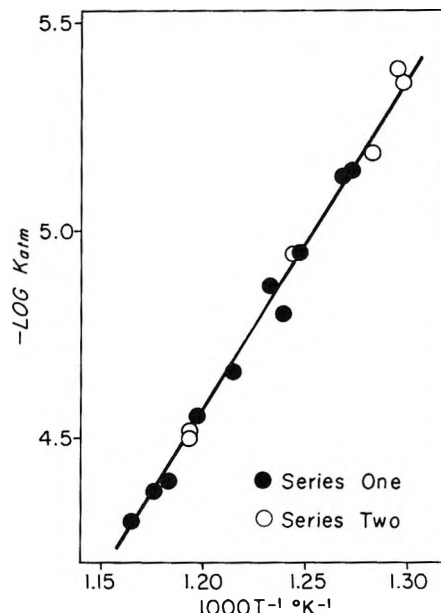


Figure 3. Equilibrium constants for $\text{FeI}_2(\text{s}) = \text{Fe}(\text{s}) + \text{I}_2(\text{g})$.

iodine it releases is a significant part of the total iodine collected. The amount of Fe_2I_6 is negligibly small. If we then correct the total amount of iodine and iron transported for the presence of the iron(III) species, a refined equilibrium constant for (2) can be obtained. Through an iteration process, consistent values of the equilibrium constants and the iodine pressures were finally reached. The results are shown in Figure 2. It is seen that the constants reported by the original authors are essentially correct, but the refinement eliminates the curvature in the plot of the uncorrected values. The average thermodynamic constants derived from the line drawn are not perceptibly changed from the result one gets if the curvature in the original data is ignored.

The data shown in Figure 1 will not be treated further at this time; the vapor of the iron(II) species is found to be a mixture of FeI_2 and Fe_2I_4 and will be discussed in detail in a subsequent paper.

The results of the study are shown in Table I.

A plot of equilibrium constants (iodine pressures) for reaction 1 is shown in Figure 3. Results from series I and series II are indistinguishable; we take this as evidence that significant solid solution of iron in $\text{FeI}_2(\text{s})$ did not occur. Such an effect should manifest itself in higher iodine pressures in the experiments initiated with pure FeI_2 (series II).

The standard enthalpy and entropy of reaction 1, calculated from a van't Hoff treatment, are $\Delta H^\circ_{813^\circ\text{K}} = 36.5 \pm 0.7 \text{ kcal mole}^{-1}$ and $\Delta S^\circ_{813^\circ\text{K}} = 22.9 \pm 0.8 \text{ cal deg}^{-1} \text{ mole}^{-1} (\text{eu})$. The latter gives a value of

Table I: Decomposition Pressures (atm) of Iodine above Ferrous Iodide and Iron

t , °C	$P(\Sigma I_2)$ $\times 10^6$	$1/2P(FeI_2)$ $\times 10^6$	$P(Fe_2I_4)$ $\times 10^6$	$P(I_2)$ $\times 10^6$
Series I				
512	1.77	0.445	1.3	0.710
516	1.89	0.525	1.5	0.738
529	2.69	0.914	3.5	1.13
534	3.99	1.22	5.8	1.59
538	3.73	1.22	5.5	1.34
550	5.99	2.08	13.1	2.18
562	8.22	3.13	24.2	2.80
572	11.81	4.66	44.4	4.01
577	13.01	5.36	55.9	4.23
585	16.09	6.94	82.5	5.00
Series II				
498	1.06	0.253	0.5	0.438
499	1.03	0.258	0.5	0.408
506	1.58	0.396	1.0	0.666
530	3.01	0.94	3.6	1.13
565	8.96	3.47	28.0	3.01
565	9.21	3.51	29.2	3.14

$S^\circ_{813^\circ K} = 62.2$ eu for $FeI_2(s)$.^{1,10} Using enthalpy and entropy increments calculated from heat capacity data (from Kelley¹⁰ for Fe and I_2 ; from Oetting and Gregory¹¹ for FeI_2), one obtains 38.6 kcal mole⁻¹ and 27.0 eu, respectively, as the values of $\Delta H^\circ_{298^\circ K}$ and $\Delta S^\circ_{298^\circ K}$. From the standard values for $I_2(g)$ and $Fe(s)$,¹² the standard enthalpy of formation and standard entropy of $FeI_2(s)$ at 298°K are found to be -23.7 kcal mole⁻¹ and 41.8 eu, respectively.

Earlier work in this laboratory has revealed a minor transition in $FeI_2(s)$ in the vicinity of 370°.¹¹ Subsequent studies¹³ have shown the occurrence and magnitude of the transition to be sensitive to trace amounts of impurities, but the nature of the transition has not been clearly established. The enthalpy and entropy changes associated with the transition are only of the order of a tenth of a kilocalorie and a few tenths of an entropy unit, respectively. However the results of Wydeven on samples in which the magnitude of the transition was diminished by the presence of trace amounts of impurities gave heat capacities between room temperature and the transition temperature slightly larger than observed in the earlier work.¹¹ The two studies give values of the entropy increment between room temperature and our reaction temperature of 20.5 eu¹¹ and 21.0 eu¹³; if one takes a mean value of 20.7 eu, the value of $S^\circ_{298^\circ K}$ becomes 41.5 eu. The uncertainty in the enthalpy increment is only a few tenths of a kilocalorie.

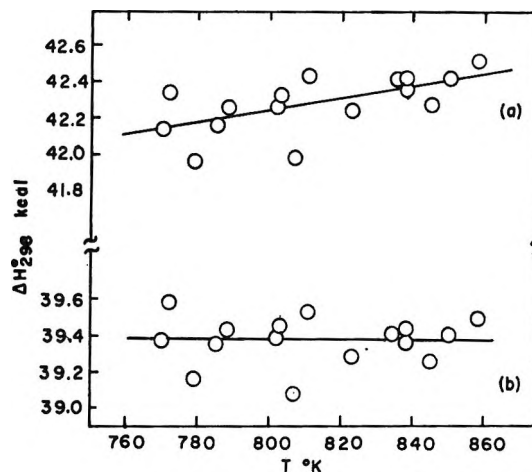


Figure 4. Third-law treatment of equilibrium data for $FeI_2(s) \rightleftharpoons Fe(s) + I_2(g)$ based on two choices of S°_{298} for $FeI_2(s)$: (a) 36.8, (b) 40.5 eu.

Kelley and King¹ list a value of 36.8 ± 2 eu for $FeI_2(s)$ which they state was estimated from an inadequate set of low-temperature heat capacity data. This estimate does not appear to include a contribution associated with a magnetic transition at 10°K.³ Our enthalpy of formation is appreciably less than the -30 kcal mole⁻¹ listed in NBS tables² and based on earlier heat of solution work.

A third-law treatment of the data, in which $\Delta H^\circ_{298^\circ K}$ was evaluated from the expression $T(-R \ln K - \Delta(G^\circ - H^\circ_{298^\circ K})/T)$ and the free energy functions from the relation $(G^\circ - H^\circ_{298^\circ K})/T = (H^\circ_T - H^\circ_{298^\circ K})/T - (S^\circ_T - S^\circ_{298^\circ K}) - S^\circ_{298^\circ K}$, gave results shown in Figure 4. Enthalpy and entropy increments were evaluated from heat capacity data.^{10,11} The uncertainty of increments for $FeI_2(s)$ has been discussed above. The results show that calculated values of $\Delta H^\circ_{298^\circ K}$ are consistent only if a larger value than Kelley and King's estimate of $S^\circ_{298^\circ K}$ for $FeI_2(s)$ is used. With $S^\circ_{298^\circ K}$ for $FeI_2(s)$ as 36.8 eu, an average value of 42.3 kcal for $\Delta H^\circ_{298^\circ K}$ was obtained, with values changing systematically with temperature (Figure 4a). A choice of $S^\circ_{298^\circ K}$ for $FeI_2(s)$ of 40.5 eu yields the results shown in Figure 4b; the results no longer show a trend with temperature and give an

(10) K. K. Kelley, U. S. Bureau of Mines Bulletin 584, U. S. Government Printing Office, Washington, D. C., 1960.

(11) F. L. Oetting and N. W. Gregory, *J. Phys. Chem.*, **65**, 173 (1961).

(12) G. N. Lewis and M. Randall, "Thermodynamics," revised by K. S. Pitzer and L. Brewer, McGraw-Hill Book Co., Inc., New York, N. Y., 1961.

(13) T. J. Wydeven, Ph.D. Thesis, University of Washington, Seattle, Wash., 1964.

average value of $\Delta H^\circ_{298^\circ\text{K}}$ of 39.4 kcal in good agreement with 38.6 kcal obtained from the van't Hoff plot. When $S^\circ_{298^\circ\text{K}}$ was taken as 41.5 eu, a slight downward trend of $\Delta H^\circ_{298^\circ\text{K}}$ values was noted.

On this basis the values -24 ± 1 kcal mole⁻¹ and 41 ± 2 eu are proposed for the standard enthalpy of

formation and standard entropy, respectively, of FeI₂(s) at 298.2°K.

Acknowledgment. This work was supported in part by grants from the National Science Foundation and the U. S. Army Research Office (Durham) which we acknowledge with thanks.

Thermodynamic Properties of FeI₂(g) and Fe₂I₄(g)

by W. E. Zaugg and N. W. Gregory

Department of Chemistry, University of Washington, Seattle, Washington 98105 (Received August 27, 1965)

A transpiration study of the interaction of iron and iodine has given equilibrium constants for the formation of FeI₂(g) and Fe₂I₄(g). Thermodynamic constants derived are compared with previous estimates for FeI₂, and a reinterpretation of earlier vapor pressure data is presented.

In a preceding paper we have reported results of an equilibrium study of the decomposition of FeI₂(s) into its elements.¹ This work has been extended to investigate the equilibrium at iodine pressures below that necessary to stabilize the solid phase, in which case the equilibrium formation reaction of the iodide vapor species can be investigated. The total pressure of iron(II) iodide species in the vapor phase is found markedly dependent on the iodine pressure. It has been found possible to correlate the data by assuming the iron(II) constituents to be FeI₂ and Fe₂I₄. On this basis thermodynamic constants for the reactions



and



were evaluated. Earlier evidence for the existence of Fe₂I₄ has been reported by Schoonmaker, Friedman, and Porter.² Their study at a single temperature, based on mass spectrometric evidence, indicated that dimerization occurs in the saturated vapor of FeI₂(s) to the extent of 16% at 441°.

Experimental Section

The transpiration apparatus, procedure, and source of materials have been described earlier.^{1,3,4} It was found kinetically more favorable to approach the equilibrium by introducing a higher partial pressure of FeI₂ into the vapor stream than can exist at the temperature and iodine pressure in the equilibration chamber. This was done by placing a sample of FeI₂(s) in a portion of the transpiration vessel adjacent to and just preceding the main equilibration region. The latter was maintained at a slightly higher temperature and contained iron wire. The FeI₂ vapor and iodine in the argon stream then equilibrated with the iron. The iodine pressure could be increased independently of FeI₂(g) by permitting the argon to flow, prior to entering the heated portions of the system, over a trap filled with crystalline iodine, held at various

(1) W. E. Zaugg and N. W. Gregory, *J. Phys. Chem.*, **70**, 486 (1966).

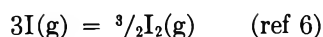
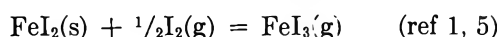
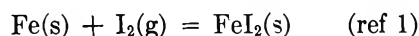
(2) R. C. Schoonmaker, A. H. Friedman, and R. F. Porter, *J. Chem. Phys.*, **31**, 1586 (1959).

(3) R. R. Richards and N. W. Gregory, *J. Phys. Chem.*, **68**, 3089 (1964).

(4) W. E. Zaugg, Ph.D. Thesis, University of Washington, 1965.

temperatures. Furnace temperatures were controlled within $\pm 0.5^\circ$. The quantities of iodine, iron iodide, and argon leaving the equilibration zone were determined as described previously.¹ Flow rates were varied from 5 to 50 $\text{cm}^3 \text{min}^{-1}$ (calculated at equilibration temperature); partial pressure ratios, in the form of the equilibrium constants, determined from experiments in which equilibrium was approached from the FeI_2 side, were independent of flow rate in this range. When an excess of iodine was introduced, only the slowest flow rates gave equilibrium mixtures. The study extended over the range 591 to 751 $^\circ$.

From the total number of moles of iron transported, $n(\text{Fe})$, apparent iron(II) iodide pressures, $P(\text{Fe}^{\text{II}})$, were first calculated from the relation $P(\Sigma\text{Fe}) = n(\text{Fe})P/n(\text{Ar}) = P(\text{Fe}^{\text{II}}) + P(\text{FeI}_3)$, where P is the pressure of argon and $n(\text{Ar})$ is the number of moles of argon passing through the equilibration chamber during the run. $P(\text{FeI}_3)$, the contribution of FeI_3 , may be calculated from the results of Schäfer and Hönes,^{1,5} the decomposition pressures of iodine above $\text{FeI}_2(\text{s})$,¹ and the $\text{I}_2(\text{g}) = 2\text{I}(\text{g})$ equilibrium,⁶ as seen from the equations



which add to give



The expression $\log K_3 = -6.811 + 13,024T^{-1}$ (pressures in atmospheres) was derived for the temperature dependence of the equilibrium constant for reaction 3. Hence, the partial pressure of FeI_3 can be expressed in terms of K_3 and the partial pressure of iodine atoms. At the low iodine pressures used, the partial pressure of Fe_2I_6 may be neglected.⁵

From the number of moles of iodine collected $n(\text{I})$, the corresponding apparent pressures $P(\Sigma\text{I})$ of atomic iodine may be calculated. These values are a composite of several contributions: $P(\Sigma\text{I}) = n(\text{I})P/n(\text{Ar}) = P(\text{I}) + 2P(\text{I}_2) + P(\text{FeI}_3)$. Under conditions of these experiments FeI_3 decomposes into FeI_2 and iodine on condensation.

Thus, we may write $P(\Sigma\text{Fe}) = P(\text{Fe}^{\text{II}}) + K_3 \times (P(\text{I}))^3$ and $P(\Sigma\text{I}) = P(\text{I}) + 2(P(\text{I}))^2/K + K_3(P(\text{I}))^3$ where K is the equilibrium constant for the $\text{I}_2(\text{g}) = 2\text{I}(\text{g})$ reaction. The last equation can be solved for the actual pressure of atomic iodine $P(\text{I})$, and then the preceding expression can be solved for $P(\text{Fe}^{\text{II}})$. $P(\text{Fe}^{\text{II}})$ was assumed to consist of the contributions $P(\text{FeI}_2) + 2P(\text{Fe}_2\text{I}_4)$. Hence, in terms of the equi-

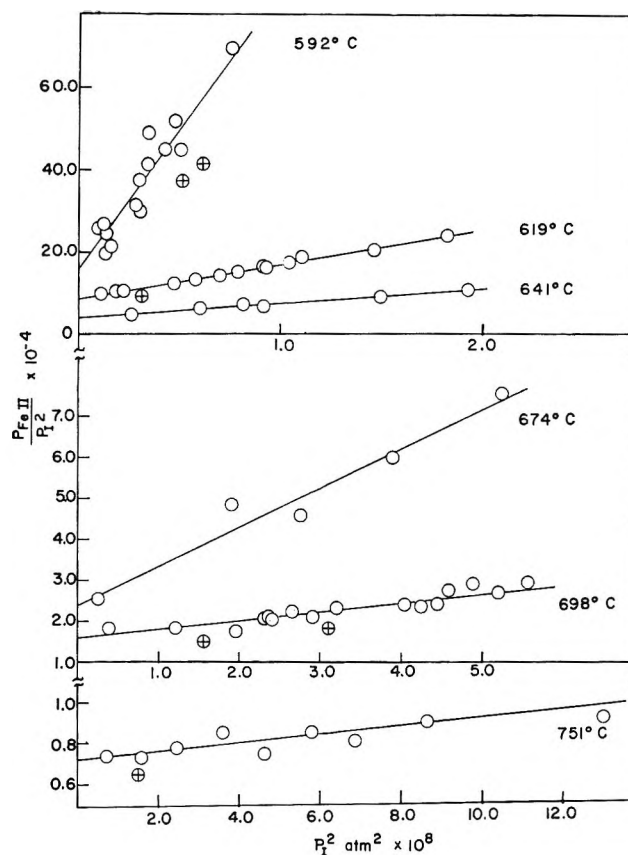


Figure 1. Equilibrium isotherms for the iron-iodine-ferrous iodide system. Pressures are in atmospheres. Note the various scales.

librium constants for reactions 1 and 2, represented as K_2 and K_4 , respectively, where the subscripts indicate the number of iodine atoms in the molecule, for the experimentally determined $P(\text{Fe}^{\text{II}})$, we may write $P(\text{Fe}^{\text{II}}) = K_2(P(\text{I}))^2 + 2K_4(P(\text{I}))^4$ or, rearranging, $P(\text{Fe}^{\text{II}})/(P(\text{I}))^2 = K_2 + 2K_4(P(\text{I}))^2$. If this interpretation is correct, a plot of $P(\text{Fe}^{\text{II}})/(P(\text{I}))^2$ vs. $(P(\text{I}))^2$ should give a straight line; the intercept at $P(\text{I}) = 0$ should be K_2 , and the slope should be $2K_4$.

Results and Discussion

Graphs of $P(\text{Fe}^{\text{II}})/(P(\text{I}))^2$ as a function of $(P(\text{I}))^2$ are shown in Figure 1.⁷ The lines drawn represent a least-squares fit to a linear equation. Several points, designated by crosses, deviated, for inexplicable reasons, by appreciably more than the average scatter from the least-squares line and were weighted one-half in the

(5) H. Schäfer and W. J. Hönes, *Z. Anorg. Allgem. Chem.*, **288**, 62 (1956).

(6) "JANAF Thermochemical Tables," revised ed, the Dow Chemical Co., Midland, Mich., 1953.

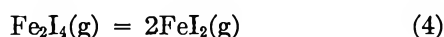
(7) See ref 4 for detailed tables of data.

least-squares treatment. Values of K_2 and K_4 derived are listed in Table I, and plots of $\log K_2$ and $\log K_4$

Table I: Equilibrium Constants (Pressure in atm) for the Iron-Iodine System

$10^{-4}K_2$	$10^{-11}K_4$	10^2K_D	$1000T^{-1}$, °K ⁻¹
15.7 ± 1.7	388 ± 23	0.729 ± 0.12	1.156
8.7 ± 0.19	41.9 ± 1.1	1.81 ± 0.07	1.121
4.16 ± 0.24	18.3 ± 1.0	0.95 ± 0.1	1.094
2.45 ± 0.22	4.76 ± 0.34	1.26 ± 0.2	1.056
1.61 ± 0.03	1.06 ± 0.04	2.44 ± 0.1	1.030
0.712 ± 0.02	0.095 ± 0.012	5.36 ± 0.7	0.976

K_4 vs. T^{-1} are shown in Figure 2. Values of K_D for the reaction



derived from K_2 and K_4 are listed as well as the probable errors indicated by least-squares treatment for each equilibrium constant. Figure 3 shows the results for K_D are in good general agreement with the one point determined by Schoonmaker, Friedman, and Porter.² The latter was included in the least-squares treatment for K_D . The temperature dependence of the equilibrium constants, as given by the least-squares treatment, are represented in Table II together with the corresponding mean values of the enthalpy and entropy changes for reactions 1, 2, and 4.

Table II

	$\Delta H^\circ_{938^\circ\text{K}}$, kcal mole ⁻¹	$\Delta S^\circ_{938^\circ\text{K}}$, cal deg ⁻¹ mole ⁻¹
(1) $\log K_2 =$ $-3.550 + 7540T^{-1}$	-34.5 ± 1.5	-16.3 ± 2
(2) $\log K_4 =$ $-8.751 + 19213T^{-1}$	-87.8 ± 3	-40.0 ± 3.5
(4) $\log K_D =$ $2.557 - 5006T^{-1}$	22.9 ± 4	12 ± 4

The absolute entropy of $\text{FeI}_2(\text{g})$, obtained by combining the experimental value of ΔS° for reaction 1 with the absolute entropies of $\text{Fe}(\text{s})$ and $\text{I}(\text{g})$,^{8,9} is $S^\circ_{938^\circ\text{K}} = 96 \pm 2$ cal deg⁻¹ mole⁻¹. The value based on the estimated molecular constants and ionic model for the electronic contributions of Brewer, Somayajulu, and Brackett¹⁰ is 101 eu. The difference of 5 eu, while only 5%, is larger than can reasonably be attributed to a change in the estimated vibrational

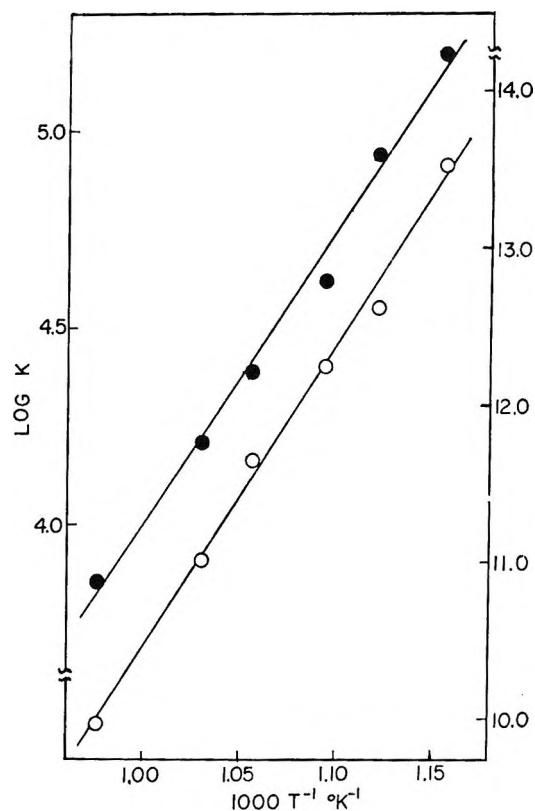


Figure 2. Equilibrium constants for $\text{Fe}(\text{s}) + 2\text{I}(\text{g}) = \text{FeI}_2(\text{g})$ (solid circles) and $2\text{Fe}(\text{s}) + 4\text{I}(\text{g}) = \text{Fe}_2\text{I}_4(\text{g})$ (open circles).

frequencies. Part of the discrepancy may be an overestimate of the electronic contribution, based on the ionic model, of 6.1 eu. It will be shown that the experimental entropy derived from this study is consistent with that derived from vapor pressure data.

A value of $S^\circ_{938^\circ\text{K}}(\text{Fe}_2\text{I}_4(\text{g})) = 185 \pm 4$ eu is indicated by the experimental value of ΔS° for reaction 2. Since estimates of the vibrational frequencies for the dimer involve large uncertainties, no attempt was made to test the consistency of the equilibrium constant data for K_4 by a third-law calculation.

The monomer-dimer equilibria in the saturated vapor of a number of similar substances have been studied, and comparison of results reported¹¹⁻¹³ can

(8) K. K. Kelley, U. S. Bureau of Mines Bulletin 584, U. S. Government Printing Office, Washington, D. C., 1960.

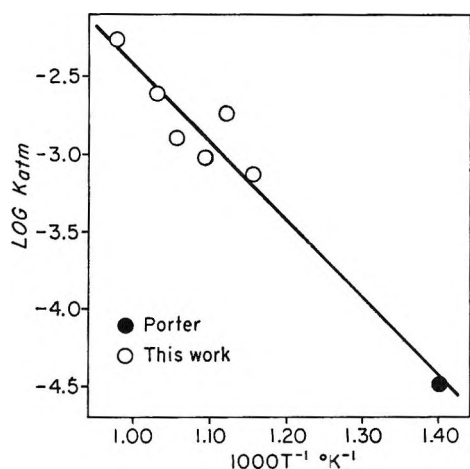
(9) K. K. Kelley and E. G. King, U. S. Bureau of Mines Bulletin 592, U. S. Government Printing Office, Washington, D. C., 1961.

(10) L. Brewer, G. R. Somayajulu, and E. Brackett, *Chem. Rev.*, **63**, 111 (1963).

(11) H. Schäfer, *Z. Anorg. Chem.*, **259**, 53 (1949).

(12) W. Kangro and H. Bernstorff, *Z. Anorg. Allgem. Chem.*, **263**, 316 (1950).

(13) R. R. Hammer, Doctoral Dissertation, University of Washington, 1963.

Figure 3. Equilibrium constants for Fe₂I₄(g) = 2FeI₂(g).

be made with this work. The standard enthalpy and entropy of dissociation of the dimer into monomer, ΔH_D° and ΔS_D° , found for ferrus iodide are smaller than corresponding values for the other iron halides, as shown in Table III. Thallous bromide is reported to have an unusually small entropy of dissociation.

Table III: Dimer Dissociation Enthalpies and Entropies

Compd	T, °K	ΔH_D° , kcal mole ⁻¹	ΔS_D° , cal mole ⁻¹ deg ⁻¹	Ref
Fe ₂ Cl ₆	573	36 ± 8	32 ± 2	11, 12, 13
Fe ₂ Br ₆	573	33.2 ± 0.8	31.4	14
Fe ₂ Cl ₄	640	32 ± 3	23 ± 6	15
Fe ₂ Br ₄	640	34.7 ± 4	23 ± 5	16
Fe ₂ I ₄	938	22.9 ± 1.6	11.8 ± 4.4	This work
Tl ₂ Cl ₂	1000	17.0 ± 0.8	13.3 ± 1.2	17
Tl ₂ Br ₂	1000	-2 ± 5	2 ± 4	18

Vapor Pressure Considerations

The equilibria studied in this work and vapor pressure data, together with results discussed in ref. 1, provide independent paths for the determination of the heat of formation and entropy of FeI₂(g). Sime and Gregory¹⁹ have reported a torsion effusion vapor pressure study of FeI₂(s) over the temperature range 400 to 470°. Transpiration vapor pressure measurements were carried out by Schäfer and Hönes⁵ and by the present authors¹ in the range 517 to 577°.

The contributions of iodine vapor and of Fe₂I₄, not known at the time of the torsion effusion study, must be subtracted from the reported vapor pressure to obtain the contribution of FeI₂(g). One may write $P(\text{FeI}^\text{II}) = P_{\text{TE}} - P(\text{I}_2) - P(\text{I}) = P(\text{FeI}_2) +$

$P(\text{Fe}_2\text{I}_4)$, where P_{TE} is the reported torsion effusion vapor pressure (torsion pressures are not dependent on molecular weight). The iodine pressures are known from ref. 1. Introducing K_D and rearranging, one obtains

$$P(\text{FeI}_2) = (K_D/2) \left(-1 + \sqrt{1 + \frac{4P(\text{FeI}^\text{II})}{K_D}} \right)$$

Monomer pressures calculated are shown in Table IV.

Table IV: Ferrous Iodide Monomer Pressures (atm)

1000T ⁻¹	From torsion effusion measurements		
	10 ⁶ P _{TE}	10 ⁶ P(Fe ^{II})	10 ⁶ P(FeI ₂)
1.502	1.95	1.67	1.46
1.491	2.41	2.07	1.81
1.478	3.37	2.94	2.52
1.464	4.39	3.83	3.24
1.462	4.71	4.13	3.47
1.453	5.68	5.00	4.15
1.448	6.54	5.79	4.74
1000T ⁻¹	From transpiration measurements		
	10 ³ P _t	10 ³ P(Fe ^{II})	10 ³ P(FeI ₂)
1.266	0.481	0.470	1.61
1.247	0.696	0.678	2.22
1.245	0.713	0.694	2.27
1.228	1.18	1.15	3.32
1.210	1.75	1.70	4.54
1.193	2.85	2.78	6.55
1.192	2.83	2.76	6.54
1.176	4.16	4.05	8.81

Schäfer and Hönes⁵ assumed FeI₂(g) to be the only important species in the saturated vapor of ferrous iodide. However, in the temperature range of their investigation appreciable dimerization occurs. In addition, a small amount (less than 3% of the total iron iodide) of FeI₃(g) is formed. The apparent transpiration vapor pressure, P_t , should then be written $P_t = P(\text{FeI}_2) + 2P(\text{Fe}_2\text{I}_4) + P(\text{FeI}_3) = P'(\text{FeI}^\text{II}) + P(\text{FeI}_3)$, where $P(\text{FeI}_3)$ can be evaluated as discussed previously,¹ and the FeI₂(g) contribution (see Table IV) can be derived from the expression

(14) R. O. MacLaren, Doctoral Dissertation, University of Washington, 1954.

(15) R. C. Schoonmaker and R. F. Porter, *J. Chem. Phys.*, **29**, 116 (1958).

(16) R. F. Porter and R. C. Schoonmaker, *J. Phys. Chem.*, **63**, 626 (1959).

(17) D. Cubicciotti, *ibid.*, **68**, 1528 (1964).

(18) D. Cubicciotti, *ibid.*, **68**, 3835 (1964).

(19) R. J. Sime and N. W. Gregory, *ibid.*, **64**, 86 (1960).

$$P(\text{FeI}_2) = \frac{K_D}{4} \left(-1 + \sqrt{1 + \frac{8P'(\text{FeI})}{K_D}} \right)$$

A Σ function for $\text{FeI}_2(\text{g})$ was defined in the usual manner

$$\Sigma = -\log P + \frac{\Delta C_P^\circ}{R} \log T$$

and ΔC_P° was taken as $-5.9 \text{ cal mole}^{-1} \text{ deg}^{-1}$ over the temperature range of the measurements.^{10,20} A least-squares analysis of data (see Figure 4) gave the equation for the temperature dependence of the monomer partial pressures P_M in the saturated vapor: $\log P_M(\text{atm}) = [-9435T^{-1} - 2.969 \log T + 16.742] \pm 0.010$; and for the heat of sublimation of $\text{FeI}_2(\text{g})$ in this temperature interval it gave: $\Delta H^\circ_T(\text{kcal/mole}) = 43.2 - 5.9 \times 10^{-3}T$, where ΔH° at 750°K , the mean temperature, is 38.8 kcal/mole . $\Delta S^\circ_{750^\circ\text{K}}$ is $31.6 \text{ cal deg}^{-1} \text{ mole}^{-1}$.

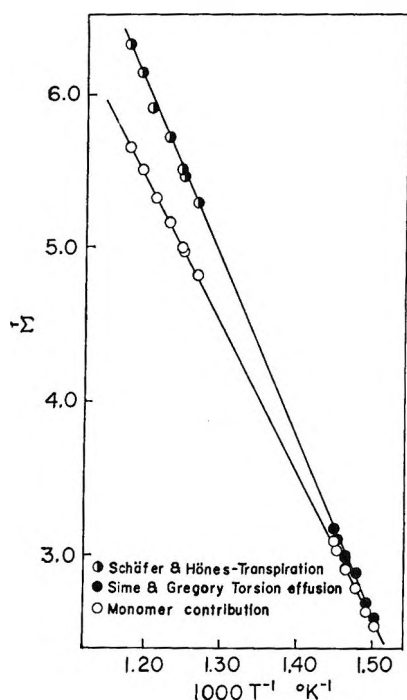
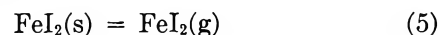


Figure 4. Σ plot for the vapor pressure of iron(II) iodide.

The over-all consistency of the results can now be tested. A temperature of 813°K , the mean for the

study of the decomposition of $\text{FeI}_2(\text{s})$ and intermediate between 938°K , the mean for reaction 1, and 750°K , the mean for reaction 5, will be used. ΔC_P°



for (5) was taken as -5.9 and for (1) as $-4.1 \text{ cal deg}^{-1} \text{ mole}^{-1}$. We find

	$\Delta H^\circ_{813^\circ\text{K}}$, kcal mole ⁻¹	$\Delta S^\circ_{813^\circ\text{K}}$, cal mole ⁻¹ deg ⁻¹	$\Delta H^\circ_{298^\circ\text{K}}$, kcal mole ⁻¹
$\text{FeI}_2(\text{s}) = \text{FeI}_2(\text{g})$	38.4	31.2	41.3
$\text{Fe}(\text{s}) + \text{I}_2(\text{g}) = \text{FeI}_2(\text{s})$	-36.5	-22.9	-38.6
$2\text{I}(\text{g}) = \text{I}_2(\text{g})$	-36.7	-25.1	-36.1
(1) $\text{Fe}(\text{s}) + 2\text{I}(\text{g}) = \text{FeI}_2(\text{g})$	-34.8	-16.8	-33.4

For the direct study of (1) we obtain $-33.9 \text{ kcal mole}^{-1}$ for $\Delta H^\circ_{813^\circ\text{K}}$, $-15.7 \text{ cal mole}^{-1} \text{ deg}^{-1}$ for $\Delta S^\circ_{813^\circ\text{K}}$, and $-33.2 \text{ kcal mole}^{-1}$ for $\Delta H^\circ_{298^\circ\text{K}}$. This indicates for the absolute entropies at 813°K : $\text{FeI}_2(\text{s})$, 62.5 ± 1 ; $\text{FeI}_2(\text{g})$, 93.7 ± 1 ; and $\text{Fe}_2\text{I}_4(\text{g})$, $181 \pm 4 \text{ cal mole}^{-1} \text{ deg}^{-1}$. The values of $\Delta H^\circ_{298^\circ\text{K}}$ involve an estimate of the heat capacity of $\text{FeI}_2(\text{g})$. The standard enthalpy of formation of $\text{FeI}_2(\text{g})$ at 298°K is $17.8 \text{ kcal mole}^{-1}$.

In view of the complexity of the system, the general agreement of the results is quite good. As can be seen in Figure 4, the correction of the vapor pressure data for the presence of dimer changes the heat of sublimation of the monomer from an apparent value of *ca.* 47 to $38 \text{ kcal mole}^{-1}$. The upper line, Figure 4, indicates the apparent pressure (given by the original workers) when monomer is assumed to be the only species present.

The $\Delta H^\circ_{298^\circ\text{K}}$ value for (1) corresponds to an average bond energy for the $\text{FeI}_2(\text{g})$ molecule of 68 kcal , which may be compared with 95 and 82 kcal reported for $\text{FeCl}_2(\text{g})$ and $\text{FeBr}_2(\text{g})$, respectively.¹⁹ The total bond energy for $\text{Fe}_2\text{I}_4(\text{g})$ is $289 \text{ kcal mole}^{-1}$. If a two-iodine bridge model is assumed for the dimer and the two nonbridging iron-iodine bonds are given the same bond energy as in FeI_2 , the average bond energy for the four bridge bonds is $38 \text{ kcal mole}^{-1}$.

Acknowledgments. This work was carried out with financial support from a grant by the National Science Foundation which we acknowledge with thanks.

(20) F. L. Oetting and N. W. Gregory, *J. Phys. Chem.*, **65**, 173 (1961).

The Use of the First-Order Rate Equation in Treating Kinetic Data¹

by DeLos F. DeTar and Victor M. Day

Department of Chemistry and the Institute of Molecular Biophysics of the Florida State University,
Tallahassee, Florida (Received August 26, 1965)

A detailed analysis is presented of the use of the first-order rate equation with data which only approximate to first order. Rather large departures from first-order kinetics may be undetectable within a single run. The relationship between the parameters of the first-order equation and the true rate constants and factors affecting the precision of the rate constant are considered. By proper use of the apparent first-order rate constants, it is possible to get a reliable estimate of the first-order component of a reaction which does not deviate further from first order than the examples cited (*e.g.*, 25% of second order) or of the second-order rate constant for the reaction $A + B$ with B present in moderate excess. The approach has its limitations, and for complete treatment other methods of calculation must be used which assume the correct kinetic form.

Few actual chemical systems yield rate data which follow a simple reaction order.² It is, nevertheless, often fruitful to use the first-order expression for data which are approximately first order. This is now particularly convenient since good computer programs are available for finding parameters adjusted by the least-squares criterion.¹ The best ways of finding parameters for the first-order equation for data which conform accurately to first order have been discussed.^{3,4}

The gross deviations are well known. If data conforming to a second-order expression are fitted to the first-order equation, the resulting compromise underestimates the amount of reactant which has disappeared during the early part of the reaction and overestimates the amount in later stages. Corresponding treatment of data for a zero-order reaction produces the converse effect.

Of more immediate interest is definite information about reactions which deviate only slightly from first order kinetics. The following points are of practical importance.

(1) For a given precision of analysis for reactants or products, how far must a reaction depart from first order before this departure can be clearly demonstrated?

(2) Assuming that a departure has been demonstrated or is suspected, what is the best way to treat the data so as to obtain correct values for the rate constants? More explicitly, for given known departures

from first-order kinetics, what is the relationship between the parameters of the best first-order equation and the exact parameters?

It is tedious and not very useful to work out these quantitative relationships in explicit form but quite practical to use an empirical approach. We have done this for two classes of reaction. The first involves a single reactant, A , and has three subdivisions: (a) first plus second order: $-dA/dt = k_1A + k_2A^2$; (b) first plus three-halves order: $-dA/dt = k_1A + k'A^{3/2}$; (c) first plus half order: $-dA/dt = k_1A + k'A^{1/2}$.

Certain known reactions approximate to these various subdivisions.⁵ Furthermore, traditional "salt effects" can be approximated by such expressions. The second class involves a clean second-order reaction: $-dA/dt = k_2AB$. It is assumed that B is present in considerable but not overwhelming excess.

(1) This work was supported by the United States Air Force, Office of Aerospace Research, under Grant AF-AFOSR 629-64. All computations were performed by LSK1N1 written by D. F. DeTar and C. E. DeTar.

(2) Many general treatments are available, *e.g.*, A. A. Frost and R. G. Pearson, "Kinetics and Mechanism," 2nd ed., John Wiley and Sons, Inc., New York, N. Y., 1963.

(3) D. F. DeTar, *J. Am. Chem. Soc.*, **78**, 3911 (1956); D. F. DeTar and A. R. Ballentine, *ibid.*, **78**, 3916 (1956).

(4) C. J. Collins, *Advan. Phys. Org. Chem.*, **2**, 1 (1963).

(5) K. Nozaki and P. D. Bartlett, *J. Am. Chem. Soc.*, **68**, 1686 (1946); B. Barnett and W. E. Vaughan, *J. Phys. Chem.*, **53**, 926, 945 (1949).

We have obtained values of A as a function of time for a number of examples of both classes. In some cases we introduced a known error into these A values by use of standard tables so that the data would approximate more closely those obtained experimentally.⁶ The resulting data were then fitted to the first-order expression, eq. 1. For this purpose we used the com-

$$A = A_{\infty} + (A_0 - A_{\infty})e^{-kt} \quad (1)$$

puter program LSKIN1, which has a variety of options and permits use of any of several types of weighting required. In general, A_0 , A_{∞} , and k were all treated as disposable parameters, and the scalar error in A was minimized. The effect of minimizing the scalar error when the relative error (dA/A or $d \ln A$) is normally distributed and the converse have a relatively minor effect in the applications under discussion, but proper weight is necessary if the highest precision is required. It is also possible to take either A_0 or A_{∞} or both as accurately known. The main effect of this approach is to extend the range of reaction covered by the data.

The Magnitude of the Systematic Error

Figures 1-6 summarize the answers to the first point, the question of how small a departure from accurate first-order kinetics is detectable. All of these figures represent a plot of the residuals, $(A_{\text{obsd}} - A_{\text{calcd}})$ vs. per cent of reaction. These are presented in control chart form. The inner pair of dashed lines represents one standard deviation, and the outer pair (where shown) represents about two standard deviations. Roughly half of the points should be within the inner pair and 95% of the points within the outer pair. If the data conform to the first-order expression, there should be no trend. Figure 1 is a typical example. It represents accurate first-order data upon which have been imposed a scalar error in A which is nominally 0.001; $A_0 = 1.000$.

Figure 2 shows what happens if the reaction is not first order but instead has a second-order component. The data in Figure 2 correspond to an ideal case. The accuracy (standard deviation) with which A can be determined was taken as ± 0.001 , and the initial concentration was 1.000. The reaction has been followed from 0-99%. The fraction of second-order reaction of course decreases as the reaction proceeds. Initially the second-order component was 5%. Under these almost ideal conditions the deviation from first-order kinetics shows up plainly as an S curve. Initially A disappears faster than expected for a first-order process, and toward the end of the reaction it disappears more slowly. Such a result is, of course, exactly that

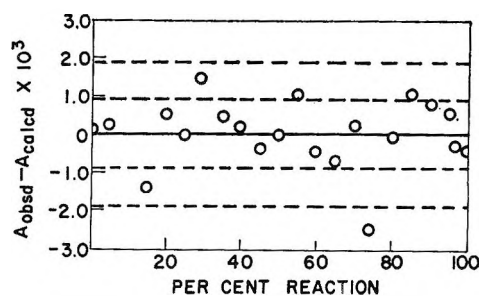


Figure 1. Exact first-order data; standard deviation of A nominal 0.001, actual 0.00094. $A_0 = 1.000$.

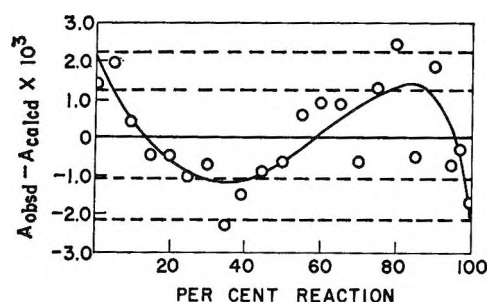


Figure 2. Initial reaction 5% second order, 95% first order. Points represent nominal standard deviation of 0.001. Line is drawn through exact values. $A_0 = 1.000$.

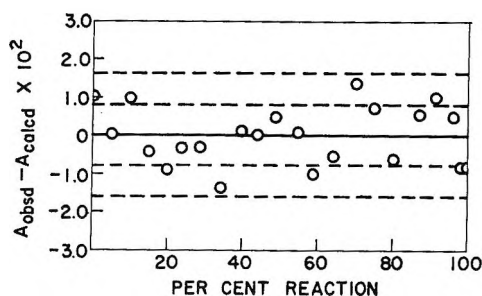


Figure 3. Initial reaction 25% second order, 75% first order. Points represent nominal standard deviation of 0.01. $A_0 = 1.00$.

expected for a reaction somewhat greater than first order.

If it is more difficult to analyze accurately for A , then a large amount of second-order component may escape detection. This is shown in Figure 3. Here the initial reaction is 25% second order, and A is determined with an initial accuracy of 1%. Such accuracy might be better than actually attainable from infrared spectral data, for example.

(6) W. E. Deming, "The Statistical Adjustment of Data," John Wiley and Sons, Inc., New York, N. Y., 1943, Appendix. We used 10% larger values than those in the table since these gave actual errors more nearly in accord with the nominal error.

Figure 4 shows a reaction which is first plus three-halves order with the three-halves order component 10% initially. As in Figure 2, the accuracy of determining A (scalar error) is 0.1% of its initial value. Figure 5 shows a reaction which is first plus half order. The trend of the deviation in Figure 5 is the converse of the trend in those cases where the reaction has a component higher than first order. It should be noted that any reaction which is less than first order comes to an abrupt stop at some finite time.

Figure 6 shows the result of following a reaction over a more restricted range. This is often forced upon the experimenter because of side reactions. Considerably larger extents of nonfirst-order component will readily escape detection.

The deviation for a second-order reaction between A and B gives curves which look very much like those for the case in which A disappears by both first- and second-order steps as in Figure 3.

To define the situation more precisely, we note that there are two contributions to the observed standard deviation of A , errors arising from the analysis for A and systematic errors from the nonfirst-order part of the reaction. The reliable detection of departures from first-order kinetics depends upon having the systematic error relatively large compared with the analytical error.

While it is possible to develop statistical criteria to test for systematic error, unless the systematic error is large enough to show up plainly as in Figures 4 and 5, such tests are not of much practical use. Anyone with experience in kinetics knows that the most reliable way to determine reaction orders is to study the behavior of k_{obsd} , preferably the initial rate, as initial concentrations are varied. It is, however, most useful to know how the two types of error interact to produce an over-all error pattern.

We have, therefore, used exact values of the variable, A , corresponding to known kinetics in order to determine the contribution of the nonfirst-order component. The situation is complicated by the fact that these deviations are a complex function of the extent of reaction covered by the data. As a reference point we take the ideal case in which the reaction has been followed from 0 to 99%. Representative values are then presented for other extents of reaction.

The results are summarized in Table I for the first class of reaction and in Table II for the A-B second-order class. It is seen that for a first- plus second-order reaction, the systematic part of the error in A varies from 0.0012 for $A_0 = 1.000$ with 5% of second-order component to 0.0065 for 25% of second-order component. It turns out, however, that, if the

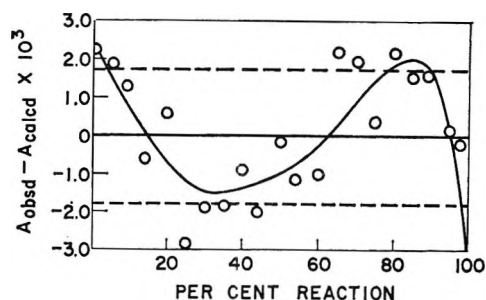


Figure 4. Initial reaction 10% three-halves order, 90% first order. Points represent nominal standard deviation of 0.001. Line is drawn through exact values. $A_0 = 1.000$.

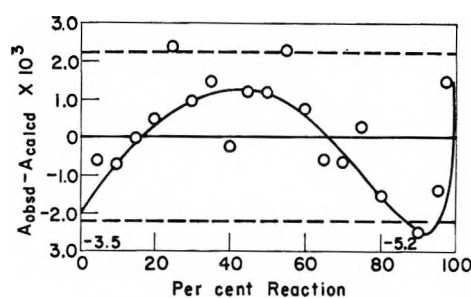


Figure 5. Initial reaction 5% half order, 95% first order. Points represent nominal standard deviation of 0.001. Line is drawn through exact values. $A_0 = 1.000$.

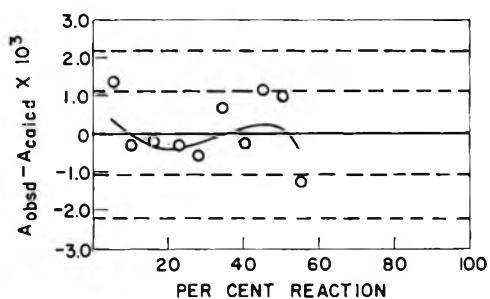


Figure 6. Initial reaction 25% second order. Points represent a nominal standard deviation of 0.001 with $A_0 = 1.000$. Theoretical deviation shown by solid line is much too small to be detectable. Compare Figure 2.

nominal analytical error in A is 0.01, for $A_0 = 1.000$, then the calculated standard deviation for A is 0.008–0.01 for all examples in Table I. See footnote *b*.

Table II shows the corresponding data for the second-order reaction. Roughly speaking, a reaction following first- plus second-order kinetics with a 25% second-order component is equivalent in behavior to a true second-order reaction in which the initial $A:B$ ratio is 1:4.

The effect of using points that cover various extents of reaction is, in general, quite complex. The ex-

Table I: Effect of Nonfirst-Order Component on Error in Variable and on the Apparent Rate Constant

Reaction type	Extent followed, %	Error in variable from non-first-order ^a	Obsd. ^b rate const. $\times 10^3$
10% 2	0-99	0.24	4.85
10% 2	5-91	0.12	4.95
10% 2	5-72	0.04	5.09
10% 2	5-53	0.01	5.20
5% 2	0-99	0.12	4.93
25% 2	0-99	0.65	4.62
25% 2	0-92	0.32	4.85
25% 2	0-75	0.11	5.20
5% 3/2	0-99	0.08	4.96
10% 3/2	0-99	0.16	4.93
10% 3/2	0-90	0.06	5.00
25% 3/2	0-99	0.41	4.82
5% 1/2	0-99	0.16	5.03
10% 1/2	0-98	0.21	5.00
25% 1/2	0-96	0.45	4.95

^a This table refers to data in which the scalar error in the variable is normally distributed and has been minimized. The systematic error due to the nonfirst-order component is treated as though it were a random error and has been tabulated as the percentage of the initial value. ^b The true initial k in every case was 5.00×10^{-3} . The observed or apparent k depends both upon the per cent of nonfirst-order component and upon the extent of reaction covered. Taking the nominal standard deviation of the variable as 1% of its initial value, the standard deviation of k was 0.1×10^{-3} (2% of k) for all k values in this table. The error arising from the systematic deviation (column 3) has practically no effect at the levels present here. Why this is so, can be seen from an example. Thus, the over-all error for line 6 is nominally $(0.65^2 + 1.0^2)^{1/2} = 1.2$, and there is a considerably larger random variability in the standard deviation from its nominal value than the difference between 1 and 1.2.

amples in Tables I and II all start with 0 or 5% of reaction and go to various extents. The effect of ignoring part of the data is to reduce the extent to which the data deviate from first-order kinetics. The first four entries in Table I and the latter part of Table II show the magnitude of the effect.

For a trend in the residuals to be clearly discernible, it is necessary that the standard deviation of the analysis for the variable be smaller than the systematic error for the variable given in Tables I and II.

Factors Affecting the Standard Deviation of the Rate Constant

The standard deviation of the rate constant is determined by the standard deviation of the observed variable and by a propagation of error term. This

Table II: Relationship between Parameters of First-Order Equation and True Second-Order Values ($B_0 = 0.1000$, $k = 5.00 \times 10^{-3}$)

$10^3 A_0$	% reaction	Std. dev. in A due to 2nd order ^a	$10^4 k_{\text{obsd}}^b$
5.0	0-99	0.11	4.93
10.0	0-99	0.23	4.86
20.0	0-99	0.46	4.74
25.0	0-99	0.58	4.68
5.0	0-51	...	5.12
10.0	0-52	0.01	5.23
20.0	0-53	0.04	5.48
25.0	0-54	0.03	5.62
4.0	1-40	0.00	5.10
10.0	1-41	0.00	5.31
20.0	1-43	0.00	5.63

^a Tabulated as per cent of A_0 although scalar error in A was minimized. ^b True initial kB_0 was 5.00×10^{-4} for all runs.

term is obtained from the reciprocal matrix of the normal equations.⁷ By concentrating on the contribution from the propagation of error term, it is possible to form conclusions which concern a property of the first-order equation itself. These are independent of departures from first-order kinetics.

However, the way in which the standard deviation of the variable enters depends on how the error is treated. If the normally distributed error is scalar in the variable, then an analytical accuracy in which the standard deviation is 1% of the initial value gives one over-all result. On the other hand, if the normally distributed error is the relative error in the variable, then an analytical accuracy in which the standard deviation is 1% of the variable gives a different over-all result, for in effect the analysis is much more accurate. A normally distributed error in per cent T gives still another result which depends further upon the specific per cent T values covered.

While it is desirable for best results to minimize the proper error, this is a weighting problem which has only indirect bearing on the above point. Data usually do not conform rigorously to a particular form of weighting. The effect of calculating by an improper procedure is to give somewhat poorer estimates of k but not the gross differences which appear in Tables III and IV. As experience with a given technique accumulates, each calculation produces an estimate of the error in the variable appropriate to the mode of calculation used (*i.e.*, which error is minimized), and it

(7) See ref. 6, p. 167.

is this error estimate which is to be used to get correct error estimates of the parameters.

To illustrate these factors, representative results are shown in Tables III and IV. Table III refers to the special case in which product formation is observed spectrophotometrically and the error in per cent T is minimized. The initial T was 95%, and the final T was 3.5%. For purpose of tabulating, it was assumed that the standard deviation of T was 1%. The standard deviation of k is directly proportional and can readily be calculated for any other assumed error.

Table III: Relationship between Error in Rate Constant and Extent of Reaction Covered^a

Reaction points, % reaction	Std. dev. of k , % ^b
50, 75, 87	97
1, 75, 94	31
30, 60, 90	30
30, 50, 70	56
20, 50, 80	28
10, 50, 90	19
5, 50, 95	16
1, 50, 99	14
2-97, "best"	5

^a Except for the last run which included 20 points, all runs involved just three. ^b Based on 1% scalar accuracy in per cent T measurements: $T_0 = 97\%$; $T_\infty = 3.5\%$.

Table IV: Relationship between Error in Rate Constant and Extent of Reaction Covered

% reaction covered ^a	Std. dev. of k , % ^b
0-99 (22)	1.9 ^b
5-91 (18)	3.5 ^b
5-72 (14)	8.4 ^b
5-53 (10)	22 ^b
0-98 (22)	0.3 ^c

^a Number of evenly spaced points taken is given in parentheses. ^b Based on scalar error in the variable of 1% of the initial value. Scalar error minimized. ^c Based on 1% relative error in the variable; relative error minimized.

In order to show clearly the effect of including various extents of reaction, each "run" utilized just three points. As a standard, the "best" run used 20 points with optimum distribution (at eighth-life intervals). Of course, three points provide no error estimate for the variable, but they do provide the propagation of error term, and the error estimate for the variable was supplied independently.

The pronounced falloff in the standard deviation of k as the per cent of reaction covered is reduced from 8 half lives to 7 to 6 to 1 is shown in Table IV. The ratio of 6 in the standard deviation for the first and last lines in Table IV gives an idea of the improvement in analytical accuracy involved in having a 1% relative error in the variable rather than a scalar error in the variable which is 1% of the initial value. There is not too much difference between the 1% scalar error and the 1% error in per cent T (last line in Table III), particularly in view of the fact that the final stages of the reaction in Table III are subject to very large relative error owing to the particular range of T values used.

It is possible to get highly precise estimates of a first-order rate constant, but extreme precautions are essential if better than about 1% accuracy is to be achieved. The precision of measuring the values of the variable within a run is clearly only part of the story.

Relationship between Apparent First-Order Rate Constant and True Rate Constants

In actual systems departures from first-order kinetics may relate to no simple analytical expression. It is necessary to consider limiting cases, however, in order to show how typical departures can be treated.

Tables I and II show that the apparent first-order rate constant obtained for a given set of data depends systematically on the extent of reaction covered. This is to be expected since the higher order terms contribute more heavily to the initial part. In general, the rate constants are lower than the true value if the reaction is followed over 7 or 8 half lives and higher than the true value if followed to a considerably smaller extent of reaction.

In general, with proper procedures, it is possible to get a reliable (2-4%) estimate of the first-order rate constant of a reaction of first plus some other order and of the second-order rate constant, in the A-B case. However, there seems to be no elegant way to obtain a reliable estimate of the nonfirst-order terms from the apparent first-order rate constants alone.

The correct procedure for obtaining the rate constants is a small but essential variant on the standard way: the apparent first-order rate constant is plotted as a function of A_0 for a series of values of A_0 . For a reaction of first plus second order the abscissa involves A_0 , for first plus three-halves order it involves $A_0^{1/2}$, and for first plus half order it involves $A_0^{-1/2}$. For the A-B second order reaction, a plot of k/B_0 vs. A_0/B_0 gives a straight line which gives the correct value of k ($B_0 = 1$) where $A_0/B_0 = 0$.

The key point is that in making these plots it is essential that all data refer to the same extent of reaction within a few per cent. It is obvious from Table II that it would be futile to attempt to combine data covering 5-99% reaction with data covering 5-50%. However, the 5-50% data are not incompatible with the 0-40% data, and some leeway is therefore available.

The optimum extent of reaction to use in applying the first-order equation is not immediately obvious in view of the fact that the standard deviation of k must go through a minimum at some extent of reaction. Fortunately, this point needs to be answered only in rather general terms. In most cases it is advantageous to cover as large a fraction of reaction as possible. The effect is shown by comparing the first

four entries in Table I with the entries in Table IV. If the accuracy in determining the variable is 0.1% of its initial value, then the standard deviation of k is $0.24 \times 1.9 = 0.46\%$ for 0-99% reaction, $0.17 \times 3.5 = 0.6\%$ for 5-91%, and about $0.1 \times 8.4 = 0.8\%$ for 5-72% reaction. In the first two cases, the error in k arises primarily from systematic error while in the latter case it arises from the analytical error. The larger the analytical error, the greater the advantage in covering as great an extent of reaction as possible.

In conclusion, the proper application of the first-order equation to reactions deviating only moderately from first-order kinetics can be a very powerful tool in analyzing sets of data and in obtaining the correct rate constants. The approach has its limitations, and for complete treatment other methods of calculation must be used which assume the correct kinetic form.

Heats of Solution of Some Trifluoroacetates, Tetraphenylborates, Iodides, and Perchlorates in Water and in Propylene Carbonate and the Relative Enthalpies of Solvation of the Alkali Metal Ions in Propylene Carbonate

by Yung-Chi Wu and Harold L. Friedman¹

IBM Watson Research Center, Yorktown Heights, New York (Received August 30, 1965)

The enthalpies of transfer of the alkali metal ions from water to propylene carbonate (dielectric constant 65.1) at 25° have been determined calorimetrically with the following results for the ΔH relative to that for Na⁺: Li⁺, 3.17; Na⁺, 0; K⁺, -2.80; Rb⁺, -3.43; Cs⁺, -3.96 kcal./mole. Each of these values has been derived from two independent sets of data with the disparity between independently determined values being, at most, 0.26 kcal./mole. The solvation enthalpies and their correlation, by means of the theory of Latimer, Pitzer, and Slansky, are derived and discussed. Lithium trifluoroacetate is a very weak electrolyte in propylene carbonate, Λ/Λ^0 being only 0.6 in 0.001 *M* solution. The association produces not only ion pairs but also a large proportion of a larger aggregate.

1. Introduction

The energetics of ion solvation processes are poorly known in solvents other than water although these quantities are of fundamental importance. The situation is somewhat worse for solvation enthalpies than free energies, and it seems of value to determine these enthalpies, at least for some series of ions and some solvents that are of special interest. A calorimeter for this purpose has recently been constructed,² and the first measurements are reported here. Recently, Held and Criss³ have reported some measurements with similar objectives, although on different systems.

Propylene carbonate was chosen for our initial study because its high dielectric constant tends to minimize difficulties due to ion association and because in the anhydrous state it is resistant to reduction by alkali metals.⁴ On the basis of these observations, it seems likely that the standard potentials of the alkali metals may easily be determined in this solvent. The resulting data would lead to the free energies of solvation and, with the present data, to solvation entropies.

There have been only a few studies made of propylene carbonate as a solvent for ionic solutions. Harris⁴ has measured several properties of the pure liquid and of ionic solutions in propylene carbonate and other

cyclic carbonates. Watanabe and Fuoss⁵ have made some precise conductivity studies in propylene carbonate, and Kempa and Lee⁶ have made extensive dielectric measurements on various cyclic carbonates at 40°. From various sources, we have collected the list of solvent properties given in Table I.

In the present work the procedure is to determine the heat of solution of a salt MX in propylene carbonate and in water, extrapolate each of these values to infinite dilution of the final solution, and then, by difference, obtain the standard enthalpy of transfer of MX from water to propylene carbonate. The standard enthalpy is, of course, the sum of the separate enthalpies of transfer of M⁺ and X⁻ from water to propylene carbonate. The determination is made for a number of salts of the same anion, and the relative heats of transfer of the metal ions are obtained by difference.

(1) Department of Chemistry, State University of New York at Stony Brook, Stony Brook, N. Y.

(2) H. L. Friedman and Y. C. Wu, *Rev. Sci. Instr.*, **36**, 1236 (1965).

(3) R. P. Held and C. M. Criss, *J. Phys. Chem.*, **69**, 2611 (1965).

(4) W. S. Harris, Ph.D. Thesis, University of California, Berkeley, Calif., 1958, UCRL Report 8381.

(5) M. Watanabe and R. M. Fuoss, *J. Am. Chem. Soc.*, **78**, 527 (1956).

(6) R. Kempa and W. H. Lee, *J. Chem. Soc.*, 1936 (1958).

Table I: Physical Properties of Propylene Carbonate at 25°

Property	Units	"Best" value	Ref.
ϵ , dielectric constant	...	65.1	5
$d \ln \epsilon / dT$	deg. ⁻¹	-0.0037	5, 6
ρ , density	g./cm. ³	1.198	4
$d \ln \rho / dT$	deg. ⁻¹	-1×10^{-3}	4
η , viscosity	cp.	2.530	4
$d \ln \eta / dT$	deg. ⁻¹	-0.018	4

These may be combined with the relative *hydration* enthalpies of the same ions to obtain the relative solvation enthalpies in propylene carbonate.

The principal problem in this work is to find salts that dissolve fast enough so that our instrument gives a heat measurement of useful accuracy. We work at final electrolyte concentrations of a few millimolal, and our requirement is that the finely ground solid electrolyte dissolve to give a solution of this concentration in less than 20 min. with moderate stirring. We find it to be commonplace that many electrolytes, whose solubility is 10 mm or more, do not meet this condition, not only in propylene carbonate but also in other organic solvents as well.⁷ The salts studied here are exceptional in this respect.

A second requirement for salts to be used in this work is that the anion be the conjugate base of a strong acid. This is to minimize the tendency of the anion to associate with the alkali metal ion. This consideration is based on the assumption that strongly basic anions can bind even alkali metal ions covalently. At any rate, in the work reported here the only difficulty with ion association occurs with lithium trifluoroacetate, and trifluoroacetate is the most basic anion studied.

2. Experimental Section

The calorimeter and sample handling have been described elsewhere.² In all of the measurements of heats of solution in water, the final concentration is less than 10 mm, and the measured heats are corrected to standard heats by assuming that the excess enthalpy of the dilute solution is the same as that of a KCl solution of the same total concentration. The error in this procedure is less than 5 cal./mole, judging by the known excess enthalpies of solutions of single electrolytes⁸ and known heats of mixing at constant ionic strength.^{9,10} Similarly, in reducing measurements of the heats of precipitation in water, the heat of mixing at constant ionic strength was assumed to be negligible.

Conductivity water was used for all of the measurements in aqueous solutions and in the preparation of various salts. Propylene carbonate (Eastman Kodak, White Label) was purified by distillation at 1.5 torr in a five-plate Oldershaw column. The middle cut, which had a specific conductivity κ of 2×10^{-8} /ohm-cm. was used immediately after collection. The conductivity increased on standing at a rate of about 10^{-9} /ohm-cm. hr.⁻¹. This increase in κ on standing was observed to be about the same for wet (40 mm H₂O) propylene carbonate as for dry. Water also enhances the conductivity of propylene carbonate, roughly 10^{-9} /ohm-cm. per increment of 1 mm water, but this dependence does not seem to be very linear. By Karl Fischer titration the water content of a sample of purified propylene carbonate was found to be less than 0.6 mm. Finally, a sample of propylene carbonate to which water had been added to a level of 2.43 mm was used for calorimetric experiments like those described in section 3. Two samples of sodium trifluoroacetate were dissolved. For the first, giving a final salt concentration of 0.446 mm, $\Delta H = 2.95$ kcal./mole while for the second, giving an increase in salt concentration of 0.500 mm, $\Delta H = 3.41$ kcal./mole. These were some of the first calorimetric experiments we did in propylene carbonate and are of lower accuracy than the later work, but they do serve to indicate that accidental water in the solvent in the millimolal range would lead to greater concentration dependence of the heat of solution than we actually observed except in the case of LiClO₄ and LiO₂CCF₃.

The alkali metal trifluoroacetates¹¹ were prepared by treating reagent grade carbonates with an equivalent amount of trifluoroacetic acid and drying *in vacuo* at 70 to 100°. In some cases, treatment with trifluoroacetic anhydride was used to facilitate the drying process, but this treatment did not work as well as expected because of a tendency for compound formation between the salts and either trifluoroacetic anhydride or acid. One effect of this sort has been studied by Klemperer and Pimentel.¹²

For analysis, samples of these salts were converted to sulfates and weighed with the results (weight of

(7) J. L. Hawes and R. L. Kay, *J. Phys. Chem.*, **69**, 2420 (1965).

(8) V. B. Parker, "Thermal Properties of Aqueous Uni-Univalent Electrolytes," U. S. National Bureau of Standards NSRDS-NBS2, Washington, D. C., 1965.

(9) R. H. Wood and R. W. Smith, *J. Phys. Chem.*, **69**, 2974 (1965).

(10) Y. C. Wu, M. B. Smith, and T. F. Young, *ibid.*, **69**, 1873 (1965).

(11) R. Hara and G. H. Cady, *J. Am. Chem. Soc.*, **76**, 4285 (1954).

(12) W. Klemperer and G. C. Pimentel, *J. Chem. Phys.*, **22**, 1399 (1954).

sulfate/weight calculated from weight of trifluoroacetate): Li, 0.9998; Na, 0.9999; K, 0.9997; Rb, 0.9992; Cs, 0.9998. As another check on the composition, samples of the trifluoroacetates were dissolved in water to form solutions in the range 2 to 15 mm, and the conductivities were measured at 25.00°. The limiting ionic conductivity of CF_3CO_2^- was taken as 40.00,¹³ while values for Li^+ , Na^+ , and K^+ were taken from Robinson and Stokes,¹⁴ Rb^+ from Kunze, Fuoss, and Owen,¹⁵ and Cs^+ from Justice and Fuoss.¹⁶ Equivalent conductivities at infinite dilution were estimated from the measured conductivities by the empirical equation¹⁴ $\Lambda^0_{\text{estd}} = \Lambda_{\text{measd}} + S\sqrt{c}/[1 + \sqrt{c}]$ where S is the Onsager slope and c is the molarity. This equation usually gives Λ^0 within 0.2% for 1-1 electrolytes in this concentration range. Our observations for $\Lambda^0_{\text{estd}}/\Lambda^0_{\text{lit}}$ for the various trifluoroacetates follow: Li, 1.0095; Na, 1.017; K, 1.011; Rb, 1.017; Cs, 1.015. Each of these is the average of three measurements which differ among themselves by, at most, 0.3%. Our tentative conclusion is that Λ^0 for CF_3CO_2^- is about 41.0. Then only the conductance of the rubidium salt is off by more than 0.5%. The rubidium salt was also analyzed for metallic impurities by arc and flame spectroscopy. The chief impurity was found to be Ca, but its amount, compared to Rb, was less than 5 atoms/1000. A second sample of rubidium trifluoroacetate was later prepared having substantially less Ca impurity. It gave the same heat of solution in water as the first but a different heat in propylene carbonate, as noted below.

Sodium and potassium tetraphenylborates were purified as described by Kunze and Fuoss.¹⁷ Rubidium and cesium tetraphenylborates were precipitated from aqueous solutions of the sodium salt and recrystallized from acetone by adding petroleum ether or from propylene carbonate by adding water. These salts were all dried under vacuum at 100° before use.

LiCl , KCl , NaI , and KI , of reagent grade, were dried at 350° and used without further purification.

LiClO_4 was prepared from lithium carbonate and perchloric acid and dried at 100° *in vacuo* for 2 days. A sample was converted to sulfate, dried, and weighed with the result: weight of sulfate/weight calculated = 0.9993.

LiI was prepared from reagent grade $\text{LiI} \cdot 3\text{H}_2\text{O}$ by dehydrating at 240° in a stream of nitrogen and then purified by zone-refining in a stream of forming gas containing a little I_2 vapor. A sample converted to sulfate and weighed gave 0.9993 of the calculated weight. As another check on the purity the heat of solution in water was measured and compared with earlier work^{8,18} (Table II).

Table II: Heats of Solution in Water at 25°

Salt	ΔH° , kcal./mole	
	This research ^a	Lit.
LiI	-14.95	-15.13, ^b -14.47 ^c
RbCl	4.04	4.13, ^b 4.17 ^d
CsCl	4.15, 4.16	4.25, ^b 4.14 ^e

^a Each entry is the result of a single measurement in which the final concentration is less than 10 mm, and the correction for the heat of dilution is made as described in section 2. ^b See ref. 8. ^c Lange and Martin¹⁸ value combined with estimated heat of dilution⁸ ($\Delta H = -124$ cal./mole) from 0.20 *m*. ^d Lange and Martin¹⁸ value combined with estimated heat of dilution⁸ ($\Delta H = -67$ cal./mole) from 0.157 *m*. ^e Lange and Martin¹⁸ value combined with heat of dilution⁸ ($\Delta H = -24$ cal./mole) from 0.267 *m*.

RbCl and CsCl were prepared from 99.9% carbonates (supplied by Eastern Chemical Co.) by treatment with HCl , drying, and fusing in platinum. The equivalent conductivity of aqueous solutions, estimated from measurements on our preparations as described above for the trifluoroacetates, were ($\Lambda^0_{\text{estd}}/\Lambda^0_{\text{lit}}$) 0.9955 and 0.9969 for RbCl and CsCl , respectively.^{15,16} The heats of solution of these materials in water were measured and compared with earlier work (Table II). The heat of dilution of aqueous RbCl was also measured for this work; the results will be reported elsewhere.

3. Trifluoroacetates

The heats of solution in water are reported in Table III. Each individual value in the "present work" column is the result of a separate experiment. Replicate determinations were only made in cases where there was disagreement with the earlier work. These differences seem to be due to impurities in the samples investigated earlier. It is remarkable that the results are so sensitive to impurities.

The heats of solution in propylene carbonate are reported in Table IV. To get ΔH° of solution from these data we require the heats of dilution from the final concentration to zero concentration. From the temperature coefficient of the dielectric constant and the density of the solvent (Table I) we estimate that the Debye-Hückel limiting law contribution to the

(13) A. L. Henne and C. J. Fox, *J. Am. Chem. Soc.*, **73**, 2321 (1951).

(14) R. A. Robinson and R. H. Stokes, "Electrolyte Solutions," Butterworths Scientific Publications, London, 1959.

(15) R. W. Kunze, R. M. Fuoss, and B. B. Owen, *J. Phys. Chem.*, **67**, 1719 (1963).

(16) J.-C. Justice and R. M. Fuoss, *ibid.*, **67**, 1707 (1963).

(17) R. W. Kunze and R. M. Fuoss, *ibid.*, **67**, 385 (1963).

(18) E. Lange and W. Martin, *Z. Elektrochem.*, **42**, 667 (1936).

Table III: Heats of Solution of Trifluoroacetates in Water

Metal	ΔH° , kcal./mole		
	Present work	Earlier work ^a	Best value
Li	-6.32, -6.34, -6.26	-5.55 ± 0.05	-6.33
Na	-2.00	-1.96 ± 0.12	-1.99
K	1.24	1.24 ± 0.03	1.24
Rb	1.84, 1.92, 1.90	1.36 ± 0.03	1.89
Cs	1.52	1.56 ± 0.03	1.53

^a K. H. Hu and H. L. Friedman, unpublished results with an earlier version of the calorimeter used in the present work. The uncertainties indicate the maximum deviation from the average of three or more determinations. Analysis of the materials used after the calorimetry was completed, revealed over 1% impurity in the Li, Rb, and Cs salts.

heat of dilution is $\Delta H_{DHL} = -90\sqrt{c}$ cal./mole. The magnitude of this effect is only 7 cal./mole at 6 mm, the highest concentration in this work, and this is negligible compared to the experimental errors.

Table IV: Heats of Solution of Trifluoroacetates in Propylene Carbonate

Metal	Initial concn., mm	Final concn., mm	ΔH , kcal./mole	ΔH° , kcal./mole, best value
Li	0	1.29	-0.09	2.36 ± 0.4
	1.29	2.78	-1.75	
	2.78	5.36	-2.14	
	0	0.95	0.17	
	0.95	2.60	-1.66	
	2.60	4.80	-2.10	
Na	0	0.90	3.32	3.32
	0.90	2.01	3.33	
K	0	0.91	3.76	3.73
	0.91	2.08	3.73	
	2.08	3.44	3.51	
Rb	0	0.93	2.84	3.78
	0.93	4.59	2.93	
	0.63	1.21	3.79	
	1.21	2.10	3.76	
Cs	0	0.75	3.11	3.04
	0.75	2.36	2.97	
	2.36	6.24	3.03	

Therefore, for strong electrolytes we expect ΔH of solution to be independent of concentration within the accuracy of the present work, and this is consistent with the observations for all the trifluoroacetates but that of lithium.

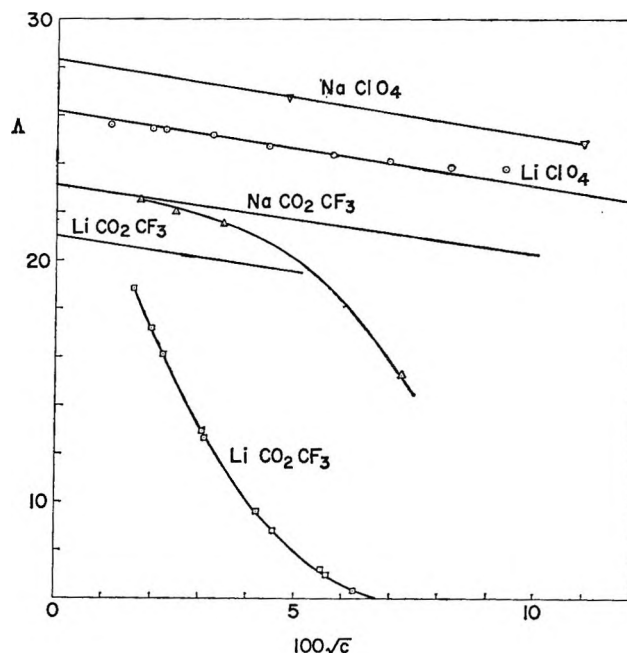


Figure 1. Phoreograms for various salts in propylene carbonate at 25°. Here c is the molar concentration. The straight lines are calculated Onsager slopes for the various salts. The curved lines serve only to connect data for the same salts and are without theoretical significance.

The strong concentration dependence of the heat of solution of the lithium salt suggests that an ion association process with a substantial heat effect is contributing to the heat. Attempts to fit the concentration dependence of ΔH on the basis of an ion association equilibrium led to the tentative conclusion that an association complex of four ions was involved. In order to elucidate this, the electrical conductivities of some of the solutions were measured with the results shown in Figure 1. Λ^0 for LiCO_2CF_3 cannot be determined by extrapolating the phoreogram, and at lower concentrations than those investigated the solvent conductance interferes. The conductivities of the other salts shown in Figure 1 were determined to get Λ^0 for LiCO_2CF_3 by Kohlrausch's law, with the result shown on Figure 1. Apparently, NaCO_2CF_3 is also a weak electrolyte in propylene carbonate, but its association is not very significant in the concentration range of the calorimetric measurements.

It was found to be impossible to calculate the phoreogram for LiCO_2CF_3 on the basis of association to form either an ion pair or an ion-pair dimer. Presumably, both association processes are occurring in this concentration range, which would be consistent with the concentration dependence of ΔH .

If we make the approximation that only one (un-

specified) association process is occurring and if the degree of dissociation at molality m be designated $\alpha(m)$, then the molar heat of solution of the salt to form a final solution of concentration m is of the form

$$\Delta H(m) = \Delta H^\circ + [1 - \alpha(m)]\Delta H_a \quad (3.1)$$

where ΔH_a is the molar enthalpy increase in the association process. In this equation, as in the preceding discussion of this problem, we have neglected the long-range interionic effects that determine the Debye-Hückel and Debye-Hückel-Onsager limiting laws. That this is reasonable may be seen from Figure 1, where the limiting-law contributions to the conductances of the perchlorates are seen to be only a moderate fraction of the total conductance. These long-range interionic effects will, of course, be even smaller for the weak electrolytes at a given stoichiometric concentration.

If we neglect the long-range interionic effects, then in any given solution $\alpha(m) = \Lambda/\Lambda^0$. Thus, according to eq. 3.1, a plot of ΔH as a function of Λ/Λ^0 should yield a straight line whose intercept is ΔH° and whose slope is ΔH_a . This is demonstrated in Figure 2. The observed small curvature of the data when plotted is presumably due to the fact that there are two association processes playing a role in this concentration range, and they do not have the same ΔH_a . The linear extrapolation is regarded as yielding a provisional value of ΔH° for this system.

The two sets of values for rubidium trifluoroacetate in Table IV were obtained from the two different preparations of the material described in the Experimental Section. The second set is much more in accord with the rest of the data, and, on this basis, it is presumed that the first set reflects a sizeable heat effect due to some impurity. This illustrates again the sensitivity of these heats to impurities and the need for independent checks in this work.

The ΔH° values from Tables III and IV may be combined to obtain the standard enthalpies of transfer of the trifluoroacetates from water to propylene carbonate (Table V). These heats of transfer are composed of additive ionic contributions, and this affords an opportunity to test their accuracy by investigating other salts as described in the following sections.

4. Tetraphenylborates

The heat of solution of sodium tetraphenylborate in water was measured directly, while the salts of K, Rb, and Cs were studied by measuring the heat of the precipitation reaction which ensues when a solution of $\text{NaB}(\text{C}_6\text{H}_5)_4$ is mixed with, respectively, KCl solu-

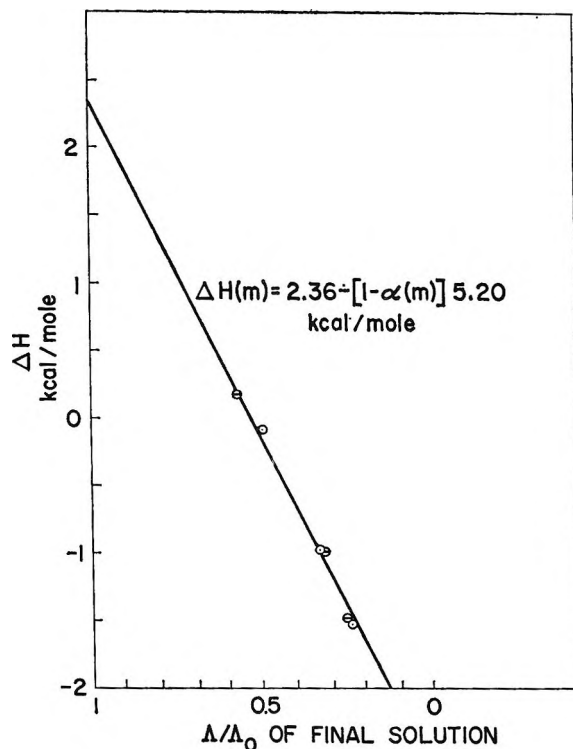


Figure 2. Integral ΔH of solution of LiCO_2CF_3 in propylene carbonate. The plain and barred circles represent two series of determinations.

Table V: Standard Heats of Transfer from Water to Propylene Carbonate

Metal	$\Delta H^\circ(\text{MX})$, kcal./mole	$\Delta H^\circ(\text{MX}) - \Delta H^\circ(\text{NaX})$, kcal./mole
Trifluoroacetates		
Li	8.69	3.34
Na	5.35	0
K	2.52	-2.83
Rb	1.89	-3.46
Cs	1.52	-3.83
Tetraphenylborates		
Na	-5.93	0
K	-8.67	-2.74
Rb	-9.32	-3.39
Cs	-10.02	-4.09
Perchlorates		
Li	-3.16	3.21
Na	-6.37	0
Iodides		
Li	-0.10	3.12
Na	-3.22	0

tion, RbCl solution, or crystalline CsCl. Further details and the results are given in Table VI.

Table VI: Heats of Solution of Tetraphenylborates in Water

Metal	Initial MCl concn., <i>m</i>	Initial B(C ₆ H ₅) ₄ ⁻ concn., <i>mm</i>	Final B(C ₆ H ₅) ₄ ⁻ concn., <i>mm</i>	Kcal./mole				ΔH° soln., best value
				ΔH^a precip.	Sol. ^b cor.	Dil. ^c cor.	ΔH° soln.	
Na		0	0.82			0.010	-4.79	-4.79
		0.82	1.53			0.005	-4.80	
		1.53	2.06			0.002	-4.75	
K	3.06	2.06	1.32	-8.79	-0.19	-0.29	9.27	9.41
	1.99	21.64	20.65	-9.32	-0.02	-0.17	9.51	
	1.99	20.65	18.38	-9.27	-0.01	-0.17	9.46	
Rb	3.37	18.38	17.27	-11.17	0	-0.40	11.57	11.73
	3.37	17.27	15.61	-11.49	0	-0.40	11.89	
Cs	Crystal	10.70	9.51	-8.13	0	-4.16	12.29	12.40
	Crystal	9.51	7.38	-8.30	0	-4.16	12.46	
	Crystal	7.38	4.83	-8.29	0	-4.16	12.45	

^a This is the molar heat of the precipitation reaction, corrected for the heat of breaking the sample bulb. ^b This is the correction to allow for the incomplete precipitation of MB(C₆H₅)₄. The estimate for KB(C₆H₅)₄ is based on a value of 3.3×10^{-8} for the solubility product (W. Rudoff and H. Zaunier, *Z. Naturforsch.*, **8b**, 611 (1953)). The solubility products for RbB(C₆H₅)₄ and CsB(C₆H₅)₄ are assumed to be, at most, half this value. ^c This is a correction to standard states. In the case of KCl (ref. 8) and RbCl (Wu and Friedman, unpublished results), it is the molar heat of dilution of the initial MCl solution. In the case of CsCl it is the standard heat of solution of the crystal in water.

The heats of solution of the tetraphenylborates in propylene carbonate were measured directly, with the results given in Table VII, and used to calculate the heats of transfer from water to propylene carbonate (Table V).

Table VII: Heats of Solution of Tetraphenylborates in Propylene Carbonate

Metal	Initial concn., <i>mm</i>	Final concn., <i>mm</i>	ΔH , kcal./mole	ΔH° , kcal./mole, best value
Na	0	0.20	-10.92	-10.72
	0.20	0.30	-10.52	
K	0	0.55	0.74	0.74
	0.55	0.77	0.74	
Rb	0	0.57	2.41	2.41
	0.57	1.14	2.41	
Cs	0	0.14	2.41	2.38
	0	0.18	2.38	

5. Iodides

The solubility of KI in propylene carbonate is 0.23 *m*, but the rate of solution is not large enough to permit measurement of the heat of solution with our instrument. The same is presumably true of the Rb and Cs salts, but the Li and Na salts dissolve readily and

rapidly enough, and the heats were measured with the results given in Table VIII. It proved to be more difficult to get reproducible results with the iodides than with the other salts reported here, apparently because of heat effects due to the interaction of iodide ion with traces of impurities in propylene carbonate. Heats differing by several kilocalories per mole from those reported here were obtained in other experiments in which less care was used in purifying the salts and handling the solvent.

Table VIII: Heats of Solution in Propylene Carbonate

Salt	Initial concn., <i>mm</i>	Final total concn., <i>mm</i>	ΔH , kcal./ mole	ΔH° , kcal./mole, best value
LiI	0.85 ^a	3.39	-15.04	-15.05
	0	0.76	-14.93	
	0.76	1.82	-15.14	
NaI	3.39 ^a	8.83	-5.00	-5.04
	8.83	10.58	-5.00	
	1.82 ^a	2.76	-5.16	
	2.76	3.79	-5.01	
LiClO ₄	0	1.64	-9.33	-9.51
	1.64	5.24	-8.43	
	5.24	14.26	-6.99	
NaClO ₄	See ref. 2			-3.05

^a Initial concentration of LiI solution.

The heat of solution of LiI in water is given in Table II while for NaI the corresponding quantity is -1.81^8 or -1.82^{18} kcal./mole. With these data and those in Table VIII we calculate the heats of transfer given in Table V.

6. Perchlorates

For these salts the solubility situation is similar to that for iodides in propylene carbonate, and heats of solution were measured only for the Li and Na salts (Table VIII). Conductance measurements (Figure 1) indicate that LiClO₄ and NaClO₄ in propylene carbonate are strong electrolytes in the concentration range of interest here. However, the heat data for LiClO₄ depend strongly on the molality, the magnitude of the concentration dependence being as large as for LiCO₂CF₃. From these data we may calculate $\Delta H(m)$, the enthalpy change on dissolving the salt in pure solvent to form a solution of final molality m , with the result $\Delta H(m) = -9.51 + 14.30m \pm 0.10$ kcal./mole, where the uncertainty given is the maximum deviation. This differs from the concentration dependence for ΔH for LiCO₂CF₃ in two important respects. First, the dependence is linear for the perchlorate, implying that, if an association process were responsible, the degree of association would be small in the experimental range and the molar heat of association would be astronomical. Second, the sign of the concentration dependence is positive here. Therefore, the predominant ion-ion interaction is endothermic, rather than exothermic as for the trifluoroacetate.

For solution in water we have⁸ $\Delta H^\circ = -6.35$ kcal./mole for LiClO₄, and 3.32 kcal./mole for NaClO₄.¹⁸ Combining the heats in water and propylene carbonate, we obtain the heats of transfer given in Table V.

7. Other Attempted Studies and Miscellaneous Observations

We examined several other processes which at first seemed promising for determining heats of solution in propylene carbonate.

The alkali halides are relatively easy to obtain in pure form, but for the most part they dissolve only slowly in propylene carbonate, and their solubilities are quite low.⁴ A possible approach seems to be to dissolve the alkali halide in the presence of an agent, previously added to the propylene carbonate, to complex the halide ion and thus compensate for the presumed poor solvating power of the solvent for these ions. FeCl₃ is such a complexing agent for chloride,¹⁹ and it was found that FeCl₃ enhances the solubility of KCl in propylene carbonate and that FeCl₄⁻ is formed in the process. However, even this process proved

to be too slow to be investigated in our calorimeter although a measurement was obtained with LiCl and FeCl₃.

For FeCl₃ dissolving in propylene carbonate $\Delta H = -17.3$ kcal./mole for a final concentration of 7 *mm*. When LiCl dissolves in this solution $\Delta H = -3.3$ kcal./mole for a final Li⁺ concentration of 2.6 *mm*.

An attempt was made to enhance the rate of solution of the iodides of the heavier metals by employing I₂ as a complexing agent since the process I₂ + I⁻ = I₃⁻ is expected to proceed readily. Again the equilibrium prediction was correct, but the rate of solution of KI was too small even in the presence of excess I₂.

For H₂O(l) dissolving in propylene carbonate, we find $\Delta H = 2.00$ kcal./mole for a final concentration of 2.35 *mm*.

Several solubilities in propylene carbonate were determined with the following results: LiI, 0.020 *m* (1.365 *m*); NaI, 1.10 *m* (1.11 *m*); KI, 0.23 *m* (0.206 *m*); CsB(C₆H₅)₄, 0.016 *m*. The figures in parentheses are the results of Harris.⁴ We have not analyzed the solid phases in equilibrium with the solution, but the above results suggest that at least LiI(c) becomes solvated in equilibrium with propylene carbonate.

8. Solvation Energies

The various independent determinations of the heats of transfer relative to sodium ion, listed in Table V, are considered to be in good agreement in view of the fact that each entry in the last column of the table is the combination of four separate ΔH° determinations, each with an uncertainty of at most 30 cal./mole for aqueous solutions and 50 cal./mole for propylene carbonate solutions. Simple averages of these determinations are taken as best values given in Table IX, except that the LiCO₂CF₃ data have been neglected because of the uncertainty in the extrapolation in Figure 2.

In Table IX we also list the standard enthalpies of hydration of the alkali metal ions. These may be combined with the heats of transfer to obtain the relative solvation enthalpies in propylene carbonate, given in the last column of the table.

The range of enthalpies of solvation is smaller for these ions in propylene carbonate than in water, which implies that the magnitudes of the solvation energies are smaller as well. In fact, they are smaller than expected on the basis of the difference in dielectric constant alone. This may be seen in the following way.

(19) H. L. Friedman, *J. Am. Chem. Soc.*, **74**, 5 (1952).

Table IX: Heats of Transfer Relative to Na⁺ (kcal./mole)

	ΔH° , aq. \rightarrow P.C. ^a	ΔH° , ^b aq. \rightarrow gas	ΔH° , P.C. \rightarrow gas
Li ⁺	3.17	26.28	23.11
Na ⁺	0	0	0
K ⁺	-2.80	-20.18	-17.38
Rb ⁺	-3.43	-26.09	-22.66
Cs ⁺	-3.96	-30.61	-26.65

^a P.C. = propylene carbonate. ^b Calculated from the heats of formation of gaseous and aqueous ions tabulated in "Selected Values of Chemical Thermodynamic Properties," National Bureau of Standards Circular 500, U. S. Government Printing Office, Washington, D. C., with the following exceptions: Li⁺(aq), $\Delta H^\circ = -66.706$ kcal./mole from H. L. Johnson and T. W. Bauer, *J. Am. Chem. Soc.*, **73**, 1119 (1951); Cs⁺(aq), $\Delta H^\circ = -62.6$ kcal./mole, reported by H. L. Friedman and M. Kahlweit, *J. Am. Chem. Soc.*, **78**, 243 (1956).

We begin with the Latimer, Pitzer, and Slansky²⁰ formula for the free energy of solvation of an ion of charge e_i and Pauling crystal radius r_i in a solvent of dielectric constant ϵ

$$F_i = -e_i^2[1 - 1/\epsilon]/2[r_i + \delta] \quad (8.1)$$

where δ is a parameter depending on the sign of the ion and on the solvent. This is a modification of the Born equation for the solvation energy in which the parameter δ accommodates a number of effects suppressed in the derivation of the Born equation, where the solvent is considered only in the role of a dielectric continuum with properties independent of field strength and pressure.^{20,21} Although it seems surprising that such diverse effects as molecular structure and pressure dependence and electric field strength dependence of solvent properties can all be accommodated by a single parameter δ , Latimer, Pitzer, and Slansky found that, for aqueous solutions, eq. 8.1 gave good agreement with experiment if $\delta = 0.85$ Å. for cations and $\delta = 0.10$ Å. for anions.²² On this basis, it seems to us that the δ parameters may be useful for characterizing and correlating the ability of various media to solvate ions.²³

By differentiating eq. 8.1 we obtain the corresponding enthalpy of solvation

$$H_i = F_i \left[1 - \frac{T \partial \epsilon / \partial T}{\epsilon(\epsilon - 1)} + \frac{T}{r_i + \delta} \frac{\partial \delta}{\partial T} \right] \quad (8.2)$$

To the extent that $\partial \delta / \partial T$ is negligible this gives the same dependence on $[r_i + \delta]^{-1}$ as eq. 8.1 except for the slope. For the rest, we explicitly neglect $\partial \delta / \partial T$ (which amounts to including a portion of its effect, if any, in δ) and fit the solvation enthalpies in water

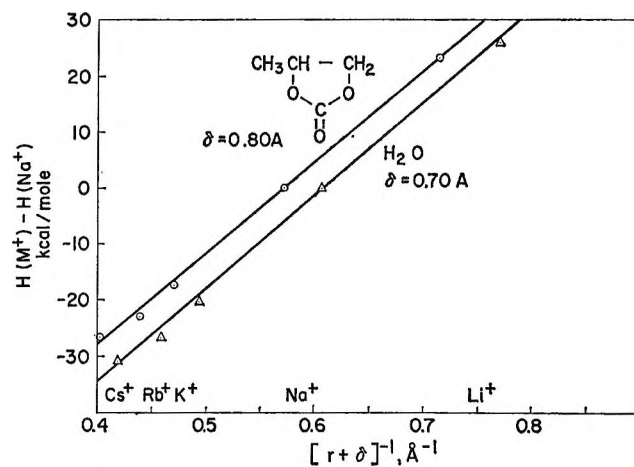


Figure 3. Ionic solvation enthalpies relative to sodium ion at 25°.

and in propylene carbonate to the abbreviated equation, with the results shown in Figure 3.

The linearity of the plots in Figure 3 is about as good as for the free energy of hydration.²⁰ It would be premature to conclude from the fact that the linearity is a little better for propylene carbonate than for water that the former is a more nearly "ideal" ionic solvent. We do conclude from the significant difference in δ values that the former is not so good a solvent for these ions as the latter, even after allowing for the difference in dielectric properties.

It seems appropriate to rest with this primitive interpretation of the data until the corresponding free energies and entropies are known.

9. Ion Association Processes

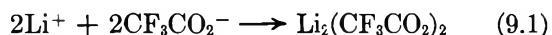
In the course of this work we have found some evidence for the association process

(20) W. M. Latimer, K. S. Pitzer, and C. M. Slansky, *J. Chem. Phys.*, **7**, 108 (1939).

(21) K. J. Laidler and M. Pegis, *Proc. Roy. Soc. (London)*, **A241**, 80 (1957).

(22) On the other hand, it has been claimed²¹ that eq. 8.1 is in error because it implies that the ion has radius $r_i + \delta$ in the gas phase as well as in solution. This seems to be wrong. Equation 8.1 may be derived by calculating the free energy of the electric field outside of the ion in the gas phase and in solution and taking the difference. If the ion is a spherically symmetric charge distribution with all of the charge within a radius $l_i \leq r_i + \delta$, then the electric field in the shell between l_i and $r_i + \delta$ does not change when the ion is solvated. The field outside of this shell is the same as the field outside of a conducting sphere having radius $r_i + \delta$ and the same charge as the ion. This is all that is needed for the familiar derivation of eq. 8.1. This equation does assume that the charge distribution of the ion is the same in the gas phase as in solution. An alternative model has been investigated by R. H. Stokes, *J. Am. Chem. Soc.*, **86**, 979 (1964).

(23) One of the possible refinements of this equation is to apply it only to the difference of the ionic solvation energy and the solvation energy of a real or equivalent uncharged body. See H. L. Friedman and G. R. Haugen, *J. Am. Chem. Soc.*, **76**, 2060 (1954), and R. M. Noyes, *ibid.*, **86**, 971 (1964).



in propylene carbonate.

It seems that the greater part of the electrolyte is associated to the ion-pair dimer at all concentrations in excess of 10 *m*. A possible structure of the ion-pair dimer is that of a carboxylic acid dimer with the protons in the hydrogen bonds replaced by lithium ions.

As a check that these effects are not due to impurities in LiCO_2CF_3 , we have studied the change in conductivity on mixing a LiClO_4 solution with an equal volume of NaCO_2CF_3 solution, both having $c = 4.59 \text{ mM}$. The equivalent conductance of the mixture was 16.32 while that estimated from the mixing ratio and the conductivities of the end solutions, assuming linearity, was 19.62. This confirms that the lithium ion and the trifluoroacetate ion have an exceptional affinity for each other in propylene carbonate. In another experiment small amounts of water were added to a 5 *mM* LiCO_2CF_3 solution. Up to 1 *m* water added increases the equivalent conductance only slightly.

The great stability of the ion association products, especially the ion-pair dimer, seem surprising to us, but we are unable to propose an alternative interpretation of our observations. This situation implies

that for some reason the solvation of trifluoroacetate ion by propylene carbonate is much poorer than that of other ions in other solvents. Support for this view may be found in the fact that the heats of transfer of neutral salts from water to organic solvents are generally exothermic, but this is not so for trifluoroacetates in propylene carbonate. Some examples of the general rule may be found in Table V; others have been reported by Held and Criss.³

The conductance data for NaCO_2CF_3 (Figure 1), although sparse, indicate that appreciable ion association occurs in this case too, but at higher concentrations than used in the calorimetry of this salt. On the other hand, the conductivity data for lithium and sodium perchlorates in propylene carbonate give no evidence for ion association although, as pointed out in section 6, the heat effect indicates a very large ionic interaction in LiClO_4 solutions.

Acknowledgment. The authors are grateful to Miss T. I. Sun for the preparation and analysis of the trifluoroacetates, to Mr. E. J. Petrillo for assistance in operating the calorimeter, to Dr. W. Reuter and Mr. B. L. Olsen for carrying out many of the chemical analyses, and to Dr. R. W. Dreyfus and Mr. K. W. Asai for zone-refining the lithium iodide.

Experimental Free Energy and Enthalpy of Formation of the α Helix¹

by Jan Hermans, Jr.²

*The Department of Biochemistry, University of North Carolina, Chapel Hill, North Carolina
(Received August 30, 1965)*

The free energy of the reaction—uncharged random coil to uncharged α helix—has been determined at several temperatures for poly-L-glutamic acid and poly-L-lysine, by an accurate determination of the titration curve. The following values have been determined at 25°: $\Delta F^\circ = -105$ cal/mole, $\Delta H^\circ = -1120$ cal/mole for polyglutamic acid, and $\Delta F^\circ = -80$ cal/mole, $\Delta H^\circ = -885$ cal/mole for polylysine. It is pointed out that theoretical values of this magnitude can be obtained as the sum of contributions from hydrogen bonds, from hydrophobic bonds, and from the freezing in of rotational motions, using acceptable values of ΔF° and ΔH° for each of these interactions.

Introduction

Many globular proteins are known to have considerable fractions of their total chain length arranged in the form of α helices. Interaction between the side chains of the amino acids and of those parts of the main chain which are not forming an α helix further stabilize the structure of proteins. Recently, there has been much theoretical work done to understand why proteins take up their particular conformation and to estimate the magnitude of the free energy terms contributed by the various interactions present. It is therefore of interest to examine experimental data on the α helix, which has a very simple structure compared with native proteins, in the light of these results.

To do this it was first necessary to obtain precise experimental values for the free energy contributed by the addition of one amino acid residue to the α helix. Zimm and Rice³ have indicated how $\Delta F^\circ_{\text{hel}}$ values can be obtained by analyzing titration data for ionizable polypeptides which are randomly coiled, *i.e.*, denatured, when the ionizable groups are charged, and helical when the ionizable groups are not charged. The value of $\Delta F^\circ_{\text{hel}}$ obtained is that for the reaction—uncharged coil to uncharged helix—and does not contain a contribution from the repulsion of charged groups (even though this repulsion is sufficiently strong to make the coil more stable than the helix when many of the groups are charged). Thus, one obtains values which should be comparable to those for α helices containing nonionizable side chains, *dissolved in water*.

Zimm and Rice used experimental data of Wada⁴

on poly-L-glutamic acid to illustrate the approach and showed that $\Delta F^\circ_{\text{hel}}$ is approximately -100 cal/mole. More recent titrations of polyglutamic acid were performed by Nagasawa and Holtzer⁵ and by Appel and Yang.^{6,6a} Polylysine was studied by Applequist and Doty.⁷ From their results one can easily calculate an approximate value of $\Delta F^\circ_{\text{hel}}$ for polylysine, which is also about -100 cal/mole.

The work reported in this paper was done to obtain accurate values of $\Delta F^\circ_{\text{hel}}$ for polylysine and polyglutamic acid and, by determining $\Delta F^\circ_{\text{hel}}$ as a function of temperature, to obtain values of $\Delta H^\circ_{\text{hel}}$, the enthalpy of helix formation.

(1) This work was supported by a research grant (GM-12175) from the National Institutes of Health.

(2) Research Career Development Awardee of the U. S. Public Health Service.

(3) (a) B. H. Zimm and S. A. Rice, *Mol. Phys.*, **3**, 391 (1960); (b) S. A. Rice and M. Nagasawa, "Polyelectrolyte Solutions," Academic Press Inc., New York, N. Y., 1961, Section 7.7.

(4) A. Wada, *Mol. Phys.*, **3**, 409 (1965).

(5) M. Nagasawa and A. Holtzer, *J. Am. Chem. Soc.*, **86**, 538 (1964).

(6) P. Appel and J. T. Yang, *Biochem.*, **4**, 1244 (1965).

(6a) NOTE ADDED IN PROOF. At the time of submission of this article, a paper was published by W. G. Miller and R. E. Nylund, *J. Am. Chem. Soc.*, **87**, 3542 (1965), which gives values of $\Delta F^\circ_{\text{hel}}$ and $\Delta H^\circ_{\text{hel}}$ for poly-L-glutamic acid obtained in the same manner. These values are in rough agreement with ours. However, Miller and Nylund's experiments covered a smaller temperature range and therefore our enthalpy value is more accurate. Their conclusion that the poly-L-glutamic acid helix is stable at temperatures below 90° is in contradiction to the results obtained here.

(7) J. Applequist and P. Doty in "Polyamino Acids, Polypeptides and Proteins," M. A. Stahmann, Ed., University of Wisconsin Press, Madison, Wis., 1962, p 161.

Experimental Section

Materials. The sodium salt of poly-L-glutamic acid (type III) and poly-L-lysine hydrobromide (type I) were obtained from Sigma Chemical Co. (Lot No. 74B-1720 and 54B-0930).

Titrations. Titrations were carried out in a thermostated vessel. In each experiment 10 ml of solution contained 0.1 *M* KCl and from 40 to 60 mg of polymer. The water used to make the solutions was CO₂ free. A flow of CO₂-free nitrogen was used to prevent CO₂ from dissolving in the solution during the experiment. When prepared in that way, the solutions were approximately neutral. Some base (polyglutamic acid) or acid (polylysine) was then added, and the solutions were titrated with 1 *N* HCl or 1 *N* CO₂-free KOH, respectively, using a micrometer buret. The pH was measured after the addition of each aliquot with a Radiometer Type 4 pH meter, using a 202B glass electrode and a K 100 calomel electrode, which contained 3 *M* KCl for experiments below room temperature. The tip of the calomel electrode was made very narrow, so that a very small flow of KCl solution would suffice. The pH meter was initially standardized at several pH values with buffers prepared according to Bates.⁸ For the titrations 0.05 *M* potassium acid phthalate was used to standardize the meter; a polypeptide solution was then titrated, followed by the titration of 10 ml of 0.1 *M* KCl, after which the pH of the buffer was again read. In most cases the drift of the meter was only a few thousandths of a pH unit in this interval. The blank titration data were interpolated and subtracted from the titration data for the polymer solution.

Results

After the trivial correction for the titration of the solvent, the data obtained are in the form: volume of acid (base) added as a function of pH. The free energies which we wish to calculate are obtained by applying the equation^{9,10}

$$\Delta F^\circ = -RT \int \alpha d \ln a_H \quad (1)$$

where a_H is the hydrogen ion activity and α is the degree of ionization of the polypeptide. Equation 1 is applied twice, namely (a) to the equilibrium mixture of random coil and helix (these are the experimental data) and (b) to the pure random coil. Then the two integrals are subtracted to give ΔF°_{hel} . The integration is extended over a sufficiently large pH range that α goes from nearly zero to nearly unity, and the difference between the two integrals is, except for the factor RT , equal to the area between two titration curves: the curve for the equilibrium mixture and the

(hypothetical) titration curve for the random coil. The data for the random coil are obtained by extrapolation, using a formula of the type

$$pK_{app} = pH - \log [\alpha_{coil}/(1 - \alpha_{coil})] = pK^\circ + W_1\alpha \quad (2)$$

for polyglutamic acid and

$$pK_{app} = pH - \log [\alpha_{coil}/(1 - \alpha_{coil})] = pK^\circ - W_2(1 - \alpha) \quad (3)$$

for polylysine, where the W 's are constants and the pK° 's are the intrinsic pK values of the carboxyl and amino groups, respectively. (Nagasawa and Holtzer⁵ have shown that the extrapolations are indeed linear at ionic strengths of 0.1 *M* and higher.)

As a consequence of the form of eq 2 and 3, a plot of $pH - \log [\alpha/(1 - \alpha)]$ as a function of α is more informative than the titration curve α vs. pH. Moreover, Zimm and Rice³ have been able to show that the area between the two curves plotted in this new fashion is equal to the area between the two curves when these are plotted as α vs. pH.

Figure 1 shows the titration data of polyglutamic acid plotted in this manner. Obviously our measurements are quite precise, at least over short pH intervals, all points, except those at the extremes of pH (and of α), lying within a few thousandths of a unit of pK or of α from the curve best fitting the points. It should, however, be pointed out that over greater intervals of pH, the precision of the measurement with the glass electrode should not be considered better than ± 0.01 unit.

The curve shown in Figure 1 clearly demonstrates that, when $\alpha > 0.75$, the random coil is the only form present. The curve is linear in this range, and the slope, W , is smallest. These data can be extrapolated to $\alpha = 0$ with considerable confidence.⁵ When α drops below 0.75, a mixture of helix and random coil exists, and, from the fact that the plot again becomes linear when $\alpha = 0.3$, one concludes that for $\alpha < 0.3$ all of the material is present in the helical form. The data for the helix are also easily extrapolated to $\alpha = 0$, and it is noted that the values of pK° for the random coil and helix are equal within experimental error. Finally, one notes an irregularity at $\alpha = 0.17$, which coincides with the formation of a precipitate at low pH. When the precipitate is completely formed

(8) R. G. Bates, "Determination of pH," John Wiley and Sons, Inc., New York, N. Y., 1964.

(9) F. E. Harris and S. A. Rice, *J. Phys. Chem.*, **58**, 725 (1954).

(10) J. Hermans and H. A. Scheraga, *J. Am. Chem. Soc.*, **83**, 3283 (1961).

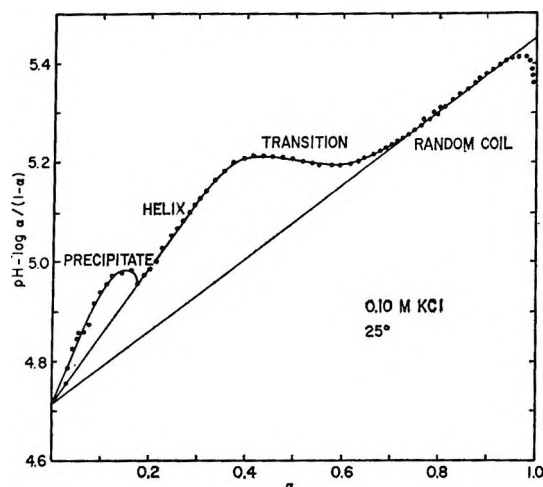


Figure 1. The apparent pK of poly-L-glutamic acid as a function of the degree of ionization. Circles are experimental points. The solid curves are: a curve best fitting the points and three linear extrapolations, corresponding to the titration of, from right to left, the random coil, the α helix, and the precipitate.

($\alpha < 0.12$), the curve is again roughly linear and extrapolates to the same pK° .

When α is to be calculated, the values of the volume of titrant added where $\alpha = 0$ and where $\alpha = 1$ are introduced. Since these numbers are used to calculate each value of pK_{app} , an error in them may produce a significant systematic error, and it may not be immediately obvious that such an error has been made. In fact, the accuracy of the ΔF_{hel}° values obtained from the type of graph shown in Figure 1 is limited almost exclusively by the uncertainty in the choice of these two limits. Hence, we have spent some effort in determining criteria for the proper choice of these limits.

The choice of the limit where the titration begins, *ca.* pH 7 for both polymers, is usually evident from the titration data within 1μ , which corresponds to about 0.3% of the volume needed to titrate all of the polymer present. The difficulty lies in determining the limit at very low (very high) pH, where large corrections must be made for the blank titration. To obtain readings which are within 0.3% of the limit, one must go to a pH 2.5 units below (above) pK° , *i.e.*, to pH 2.2 for polyglutamic acid and to pH 12.7 for polylysine; but at these pH values the error in the blank titration is 1 and 6μ for an error of 0.005 in pH. Thus, under the most favorable conditions, an accurate limit can be obtained directly for polyglutamic acid, as was, for example, the case for the data of Figure 1. However, for polylysine and for titrations of polyglutamic

acid which are less precise for other reasons (*e.g.*, high or low temperature), the limit has to be found from the data at pH values where the titration is incomplete. The procedure which we adopted was to calculate the values of pK_{app} and α for a few points at the extremes of the titration curves and to see which choice of limits would give the straightest plots since an error of even 1μ will make the plot curve noticeably at the very end, as can be seen in Figure 1 for values of α near unity. The precipitation occurring in the polyglutamic acid solutions at low pH makes this procedure somewhat less reliable. However, it is with polylysine that one relies exclusively on this treatment, and here precipitation occurred only in the experiment at 40° , and that at a value of $\alpha > 0.9$.

Plots of pK_{app} as a function of pH for polyglutamic acid at 4, 15, 25, 40, and 55° and for polylysine at 4, 15, 25, and 35° are shown in Figures 2 and 3. Only the curves best fitting the points and the extrapolations have been drawn. It is important to notice that the slopes of the extrapolations for the random coil of the individual polypeptides and the slopes of the extrapolation for the α helix of both polypeptides are very nearly the same at all temperatures. The area bounded by the extrapolations for random coil and helix, the titration curve itself in the coil to helix transition region, and the ordinate was determined by graphical integration. Multiplied by $-RT \ln 10$, it gives us a value for ΔF_{hel}° . The values obtained are shown in Figure 4.^{11,11a}

Finally, values of pK° for helical and randomly coiled polyglutamic acid and polylysine follow from the curves of Figures 2 and 3. While it is interesting to notice that the temperature dependence of pK° of polyglutamic acid is not the same for the helix and the coil, so that pK° for helix and coil are significantly different at 55° , the values which we obtain for pK° and for the heat of ionization, following from the temperature dependence of pK° , lie in the range expected for normally ionizing carboxyl and ϵ -amino groups.¹²

(11) In calculating the areas for the titrations of polyglutamic acid at 40 and 55° , the triangular area between the $pH - \log [\alpha/(1-\alpha)]$ axis and the intersection of the extrapolations for helix and random coil is, of course, subtracted from the larger area to the right of the intersection.

(11a) NOTE ADDED IN PROOF. The large positive free energy required to initiate the helix in each molecule (ΔF_{in}°) has not been taken into account in these values. These are, therefore, too high by an amount $\Delta F_{in}^\circ/n$, where n is the degree of polymerization. For our sample, $n = 450$, while ΔF_{in}° is estimated to be 5500 cal/mole.³ Thus, the correction to be applied is quite small.

(12) E. J. Cohn and J. T. Edsall, "Proteins, Amino Acids and Peptides as Dipolar Ions," Reinhold Publishing Corp., New York, N. Y., 1943.

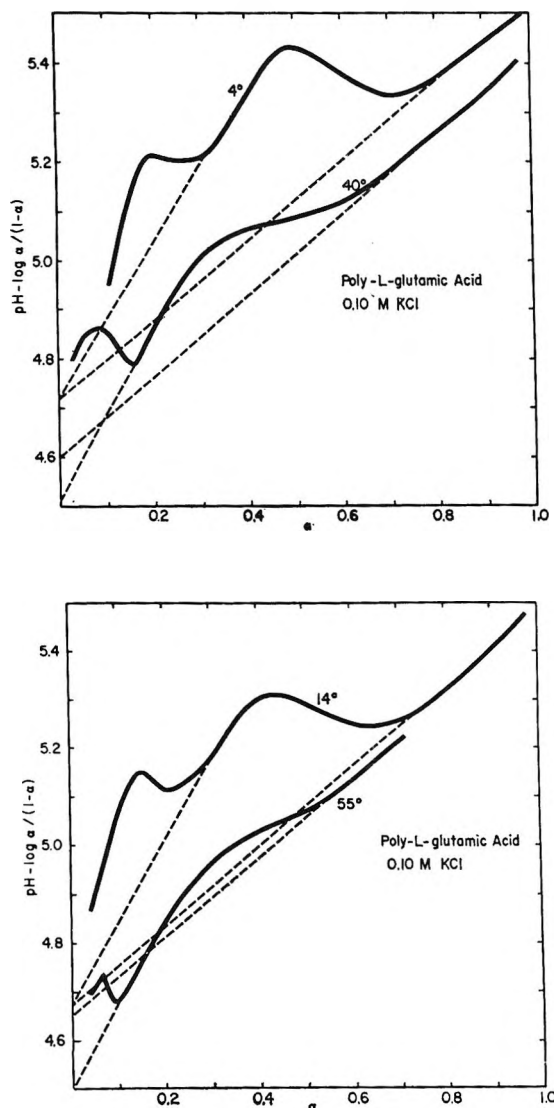


Figure 2. Titration data for poly-L-glutamic acid at four different temperatures, plotted in the manner of Zimm and Rice:^{3a} solid curves, experimental data; dashed lines, extrapolation for random coil (right) and helix (left).

Discussion

The data of $\Delta F^\circ_{\text{hel}}$ as a function of temperature shown in Figure 4 can be fitted with straight lines for both polypeptides. Their slope is, of course, equal to $-\Delta S^\circ_{\text{hel}}$, and a value of $\Delta H^\circ_{\text{hel}}$ can therefore also be calculated. The values calculated are

$$\Delta F^\circ_{\text{hel}} = -105 \text{ cal/mole} \quad (4a)$$

$$\Delta S^\circ_{\text{hel}} = -3.43 \text{ eu} \quad (4b)$$

and

$$\Delta H^\circ_{\text{hel}} = -1120 \text{ cal/mole} \quad (4c)$$

for polyglutamic acid, and

$$\Delta F^\circ_{\text{hel}} = -80 \text{ cal/mole} \quad (5a)$$

$$\Delta S^\circ_{\text{hel}} = -2.7 \text{ eu} \quad (5b)$$

and

$$\Delta H^\circ_{\text{hel}} = -885 \text{ cal/mole} \quad (5c)$$

for polylysine. These values are fairly close, and in first approximation one might say that they characterize the formation of the α helix in 0.1 M KCl. This would not be so if specific contributions to ΔF° or ΔH° from the side chains were present. However, the near equality of ΔF° and ΔH° for polyglutamic acid and polylysine and the normal value of pK° for the carboxyl and amino groups indicate that neither hydrophobic bonding nor hydrogen bonding by the side chains plays an important role.

Of course, this argument does not rule out a contribution of the β - and α - CH_2 groups, which are present in the side chains of both glutamic acid and lysine, to the free energy of formation of the α helix. The

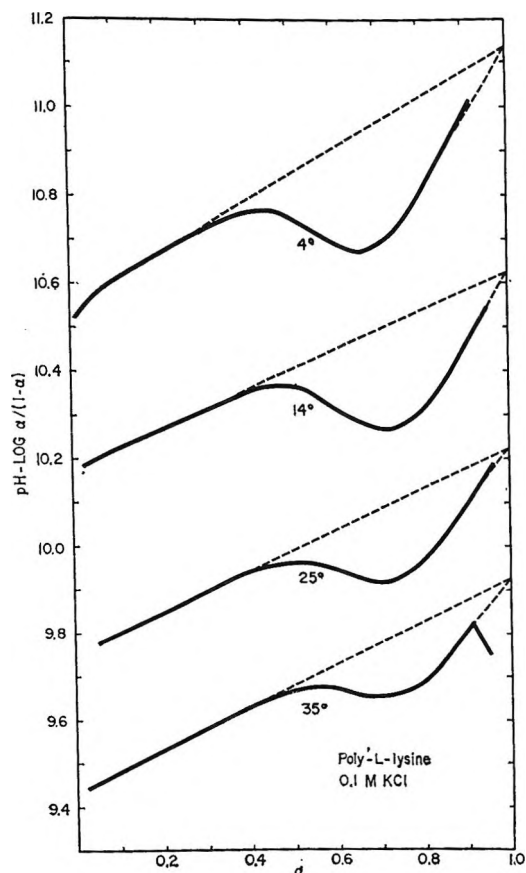


Figure 3. Titration data for poly-L-lysine: solid curves, experimental data; dashed lines, extrapolation for random coil (left) and helix (right).

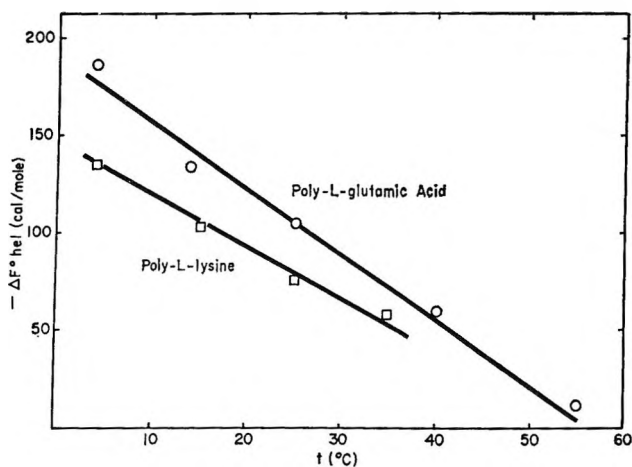


Figure 4. Standard free energies for the formation of the uncharged α helix from the uncharged random coil for poly-L-glutamic acid and poly-L-lysine, as a function of temperature. Values are expressed in calories per mole of monomer unit.

contribution of the side chain to the entropy of the helix-coil transition has been investigated theoretically by Némethy, Leach, and Scheraga.¹³ They obtain a value for the change in $\Delta S^\circ_{\text{hel}}$ due to the presence of the side chain of less than 0.5 eu. While this effect is certainly not negligible, it is less than the difference in $\Delta S^\circ_{\text{hel}}$ for polyglutamic acid and polylysine, and, it will be seen below, it is also less than the limit of error which we must place on any theoretical estimate of $\Delta S^\circ_{\text{hel}}$.

An interesting consequence of the data shown in Figure 4 must be briefly mentioned. Since $\Delta F^\circ_{\text{hel}}$ extrapolates to positive values for temperatures greater than 55°, uncharged polyglutamic acid and polylysine should show a reversible transition from helix to random coil in this temperature range. Unfortunately the insolubility of both polymers at higher temperatures makes the observation of any transition impossible. G. Fasman (private communication) has studied the precipitation of uncharged poly-L-lysine in detail. He comes to the conclusion that the rate of precipitate formation shows a sudden increase with temperature at about 50°. According to Fasman, the precipitate contains intermolecular hydrogen bonds involving the peptide CO and NH groups (and perhaps the side-chain NH₂ group) of nonhelical molecules. These observations can be satisfactorily explained by assuming that the rate-limiting step in the precipitation is the relatively slow transition from α helix to random coil below 50° but not above 50° since above this temperature the helix is not stable according to our extrapolation.

In the light of the expected instability of the α helix when $t > 55^\circ$, it is surprising that Gratzer and Doty¹⁴ could not convert a water-soluble block copolymer of sodium D, L-glutamate, and L-alanine from helix to random coil by bringing the temperature of the solution to 95°. This would mean that the polyalanine helix is more stable than the polyglutamic acid helix by at least 200 cal/mole. It is not clear which structural feature underlies this extra contribution.^{14a}

We shall now conclude this article with an attempt at analyzing the values of $\Delta F^\circ_{\text{hel}}$ and $\Delta H^\circ_{\text{hel}}$ in terms of a very simple model in which the contributions by hydrogen bonds, hydrophobic bonds, and loss of rotational freedom are counted separately and then added. The choice of this simple model is not unreasonable since the α helix was first proposed on the basis of the unstrained bond angles and distances present in it, both for the covalent bonds and for the hydrogen bond.¹⁵ Further, Ramachandran, *et al.*,¹⁶ and Liquori, *et al.*,¹⁷ have recently shown that the van der Waals interactions in the α helix are very favorable, also. Thus, Schellman's¹⁸ and Poland and Scheraga's¹⁹ estimates for the strength of the peptide hydrogen bond and Némethy and Scheraga's²⁰ estimate for the strength of a favorable packed hydrophobic bond should apply. Furthermore, the estimate of Laskowski and Scheraga²¹ for the free energy change upon the freezing of rotations about primary valence bonds may be taken as a first approximation. In Table I we show the magnitude of the estimates from the literature of ΔF° and ΔH° for each interaction and our estimates of the number of times each interaction is present in the α helix. Obviously, this is once for the peptide hydrogen bond and twice for the loss of primary

(13) G. Némethy, S. J. Leach, and H. A. Scheraga, *J. Phys. Chem.*, in press.

(14) W. B. Gratzer and P. Doty, *J. Am. Chem. Soc.*, **85**, 1193 (1963).

(14a) NOTE ADDED IN PROOF. D. C. Poland and H. A. Scheraga, *Biopolymers*, **3**, 305 (1965), have recently proposed an explanation of the high melting temperature of poly-L-alanine helices in which it is assumed that the helices are not straight but fold back on themselves several times.

(15) L. Pauling, R. B. Corey, and H. R. Branson, *Proc. Natl. Acad. Sci. U. S.*, **37**, 205 (1951).

(16) G. N. Ramachandran, C. Ramakrishnan, and V. Sasisekharan, *J. Mol. Biol.*, **7**, 95 (1963).

(17) P. De Santis, E. Giglio, A. M. Liquori, and A. Ripamonti, *Nature*, in press.

(18) J. A. Schellman, *Compt. Rend. Trav. Lab. Carlsberg*, **29**, 223, 230 (1956).

(19) D. C. Poland and H. A. Scheraga, *Biopolymers*, **3**, 275 (1965).

(20) G. Némethy and H. A. Scheraga, *J. Phys. Chem.*, **66**, 1773 (1962).

(21) M. Laskowski and H. A. Scheraga, *J. Am. Chem. Soc.*, **76**, 6305 (1954).

valence bond rotation of the backbone. The strength of the hydrophobic bond is expressed in terms of the number of water molecules present in contact with hydrophobic surfaces in the randomly coiled polymer, which are not in contact with these surfaces in the α helix. This number we estimate to be 6.²² Thus

$$\Delta F^\circ_{\text{hel}} = \Delta F^\circ_{\text{pep}} + 2\Delta F^\circ_{\text{rot}} + 6\Delta F^\circ_{\text{w}} \quad (6)$$

with a similar equation for the enthalpies. The subscripts pep, rot, and w clearly refer to the three types of interactions taken into consideration.

The values of $\Delta F^\circ_{\text{hel}}$ and $\Delta H^\circ_{\text{hel}}$ thus calculated are -420 cal/mole and -1320 cal/mole. In view of the number of assumptions made in obtaining the estimates of Table I, the agreement between theoretical and experimental values is surprisingly good.

Table I: Contributions to the Heat and Free Energy of Formation of the α Helix

	Lit estimates		No. of times counted per residue
	ΔF°	ΔH°	
Peptide H bond	-1500^a	-1500^a	1
Loss of bond rotation	$+900^b$	-600^b	2
Hydrophobic bond (per water molecule)	-120^c	$+230^c$	6

^a From ref 18 and 19. ^b From ref 21. ^c From ref 20.

By taking the loss of the rotational freedom of the side chain into account,¹³ the theoretical value of ΔF° could be made to lie closer to the experimental one. However, one should not try too hard to remove discrepancies of the order of a few hundred calories per mole by taking additional contributions into account since the three major contributions cannot be estimated that closely. Also, the differences in the experimental values of $T\Delta S^\circ_{\text{hel}}$ and $\Delta H^\circ_{\text{hel}}$ for polylysine and polyglutamic acid are of this order of magnitude, whereas, on the basis of the simple model here investigated, much closer agreement was to be expected.

Since it may be difficult to obtain closer theoretical estimates of $\Delta F^\circ_{\text{pep}}$, $\Delta F^\circ_{\text{rot}}$, and $\Delta F^\circ_{\text{w}}$, it would appear useful to obtain reliable experimental values. This could in principle be done by analyzing several other types of molecules (which would presumably have to be proteins) in the way here done for the α helix and solving several equations of the type of (6), for example, for the unknowns. The possibility of doing this is now being investigated.

Acknowledgment. The author is grateful to Professor H. A. Scheraga for a discussion of this work and for the communication of unpublished results.

(22) The decision to include a hydrophobic bond in this manner was arrived at by considering the fact that it is to be expected that the NH and CO groups lose most of their polar character when they are hydrogen-bonded to another dipole. A disturbance of the water structure by the presence of these groups should then be present. Of course, it is rather questionable if the estimate by Némethy and Scheraga²⁰ for the strength of the hydrophobic bond between hydrocarbon side chains should apply here.

Normal Stress Effect in Dilute Polymer Solutions. I.

Polystyrene in Dioctyl Phthalate

by Mikio Tamura, Michio Kurata, Kunihiko Osaki, and Katsuhisa Tanaka

Department of Industrial Chemistry and Institute for Chemical Research,
Kyoto University, Kyoto, Japan (Received August 30, 1965)

Normal stresses of a series of polystyrene solutions in dioctyl phthalate (poor solvent) were measured with a parallel-plate rheogoniometer in the range of concentration, 0.8~2.0 wt %. The shear stress and dynamic moduli were also measured in the same range of concentration with a coaxial cylinder rheometer. It was found that the incremental normal stress attributable to the polymer was primarily exerted in the flow direction and that $\sigma_{11} - \sigma_{33}$ was proportional to κ^2 and c/M over a wide range of variables. Here σ_{11} is the normal stress in the flow direction, σ_{33} is the normal stress in the direction perpendicular both to the flow line and the sheared plane, κ is the rate of shear, c is the polymer concentration in grams per cubic centimeter, and M is the molecular weight.

1. Introduction

Measurements of the dynamic mechanical properties of dilute polymer solutions have recently been reported by several groups of investigators. Ferry and co-workers measured the storage (G') and loss (G'') shear moduli of dilute solutions of polystyrene and other polymers in the range of relatively low frequencies (0.016–400 cps) by using very viscous liquids as solvents, and they presented a map of the so-called "hydrodynamic interaction parameter" h as a function of polymer concentration and molecular weight.^{1–5} The result shows that the value of h changes progressively from ∞ (Zimm behavior⁶) to 0 (Rouse behavior⁷) with increasing concentration, increasing molecular weight, and increasing solvent power. Lamb and co-workers measured G' and G'' of dilute solutions of polystyrene in various ordinary solvents (actually in toluene, butanone, and cyclohexane) using torsional quartz crystals resonant at 40 and 73 kc/sec, and they found a very similar dependence of h on molecular weight and solvent power as above.^{8,9} A similar investigation has also been carried out by Furuichi and co-workers.^{10,11} The success of these studies in obtaining detailed information on the hydrodynamic interaction between polymer segments has awakened our interest in measuring the normal stress components in steady shearing flow in dilute polymer solutions.

The normal stress effect in concentrated polymer solutions has been extensively studied by many investigators with use of the cone-plate or parallel-plate type of apparatus.^{12–15} In dilute solutions, however, the effect generally becomes too small in magnitude to

- (1) R. B. DeMallie, M. H. Birnboim, J. E. Frederick, N. W. Tschoegl, and J. D. Ferry, *J. Phys. Chem.*, **66**, 537 (1962).
- (2) N. W. Tschoegl and J. D. Ferry, *ibid.*, **68**, 867 (1964).
- (3) N. W. Tschoegl and J. D. Ferry, *Kolloid-Z.*, **189**, 37 (1963).
- (4) J. E. Frederick, N. W. Tschoegl, and J. D. Ferry, *J. Phys. Chem.*, **68**, 1974 (1964).
- (5) J. E. Frederick and J. D. Ferry, *ibid.*, **69**, 346 (1965).
- (6) B. H. Zimm, *J. Chem. Phys.*, **24**, 266 (1956).
- (7) P. E. Rouse, *ibid.*, **21**, 1272 (1953).
- (8) G. Harrison, J. Lamb, and A. J. Matheson, *J. Phys. Chem.*, **68**, 1072 (1964).
- (9) J. Lamb and A. J. Matheson, *Proc. Roy. Soc. (London)*, **A281**, 207 (1964).
- (10) H. Tanaka, A. Sakanishi, and J. Furuichi, *Rept. Progr. Polymer Phys. Japan*, **7**, 145 (1964).
- (11) A. Sakanishi, H. Tanaka, M. Kaneko, and J. Furuichi, *ibid.*, **8**, 191 (1965).
- (12) H. Markovitz and R. B. Williamson, *Trans. Soc. Rheol.*, **1**, 25 (1957); H. Markovitz, *ibid.*, **1**, 37 (1957).
- (13) W. Philippoff, *ibid.*, **1**, 95 (1957); J. G. Brodnyan, F. H. Gaskins, and W. Philippoff, *ibid.*, **1**, 105 (1957).
- (14) M. Tamura, M. Kurata, and T. Kotaka, *Bull. Chem. Soc. Japan*, **32**, 471 (1959); T. Kotaka, M. Kurata, and M. Tamura, *J. Appl. Phys.*, **30**, 1705 (1959).
- (15) T. Kotaka, M. Kurata, and M. Tamura, *Rheol. Acta*, **2**, 179 (1962).

be detected by an ordinary apparatus, and no measurement has been reported for solutions with concentration less than about 2 wt % so far as we are aware. This difficulty may be solved if we adopt a very viscous liquid as solvent such as those used in the recent work by Ferry, *et al.*¹⁻⁵ Such a possibility is tested here.

In the present paper, we report the normal stress data as well as the steady shear viscosity and the complex modulus data which were obtained for polystyrene in dioctyl phthalate in the range of polymer concentration between 0.8 and 2.0 wt %. This combination of polymer and solvent was chosen as an example of poor-solvent systems; actually, the Θ temperature was designated as 12° by Ferry, *et al.*,⁴ while the measurement was performed at 20°. Effects of polymer concentration and molecular weight on the normal and shear stresses were investigated in detail, and they were compared with the predictions of the existing molecular theories.

2. Theory

We first summarize the results of the theory of normal stress effect for dilute polymer solutions, which were obtained by Ikeda¹⁶ and Williams.¹⁷ The polymer model used in their theories is the so-called Rouse-Zimm chain which consists of $N + 1$ identical beads connected by Gaussian springs. The hydrodynamic interaction between beads is taken into account in the form of the isotropic average of the Oseen tensor (Kirkwood-Riseman approximation¹⁸). With the model and approximation, the increments of stress components caused by the presence of polymer molecules are given as

$$\begin{aligned}\sigma_{12} - \sigma_{12}^{\circ} &= nkT(\Sigma_p \tau_p) \kappa \\ \sigma_{13} - \sigma_{13}^{\circ} &= \sigma_{23} - \sigma_{23}^{\circ} = 0 \\ \sigma_{11} - \sigma_{11}^{\circ} &= 2nkT(\Sigma_p \tau_p^2) \kappa^2 \\ \sigma_{22} - \sigma_{22}^{\circ} &= \sigma_{33} - \sigma_{33}^{\circ} = 0\end{aligned}\quad (1)$$

where n is the number of polymer molecules per unit volume, k is the Boltzmann constant, T is the absolute temperature, and κ is the rate of shear. The suffixes 1, 2, and 3 attached to σ and σ° denote the directions parallel to the flow line, perpendicular to the plane of shear, and perpendicular to both 1 and 2, respectively. τ_p represents the relaxation time relating the p th mode of cooperative segmental motion. The distribution of τ_p depends on the strength of the hydrodynamic interaction which is usually represented by the parameter h

$$h = \zeta N^{1/2} / 6^{1/2} \pi^{3/2} a \eta_s \quad (2)$$

Here ζ is the friction constant of a bead, a is the root-

mean-square length of a spring, and η_s is the solvent viscosity. In the case of $h \ll 1$, the values of τ_p are given as⁷

$$\tau_p = 6(\eta_0 - \eta_s) / \pi^2 p^2 nkT \quad (p = 1, 2, \dots, N) \quad (3)$$

while in the case of $h \gg 1$, they are given as⁶

$$\tau_p = 1.71(\eta_0 - \eta_s) / \lambda_p nkT \quad (4)$$

with

$$\begin{aligned}\lambda_p &= 4.04, 12.79, 24.2, 37.9, \dots \\ &\text{(for } p = 1, 2, 3, 4, \dots)\end{aligned}\quad (5)$$

The former case is often called the free-draining limit, and the latter is the nonfree-draining limit. For intermediate values of h , Tschoegl has recently tabulated values of τ_p ^{19,20} (not reproduced here). Substitution of eq 3 or 4 into eq 1 gives¹⁷

$$\begin{aligned}\Sigma \tau_p^2 / (\Sigma \tau_p)^2 &= (nkT/2) [(\sigma_{11} - \sigma_{11}^{\circ}) / (\sigma_{12} - \sigma_{12}^{\circ})^2] \\ &= 0.206 \text{ for } h = \infty \\ &= 0.400 \text{ for } h = 0\end{aligned}\quad (6)$$

which may be used for estimation of the hydrodynamic interaction parameter h from the normal and shear stress data. In the same notations, the storage and loss moduli in shear, G' and G'' , are written as

$$\begin{aligned}G' &= nkT \Sigma_p [\omega^2 \tau_p^2 / (1 + \omega^2 \tau_p^2)] \\ G'' &= nkT \Sigma_p [\omega \tau_p / (1 + \omega^2 \tau_p^2)] + \omega \eta_s\end{aligned}\quad (7)$$

where ω is the angular frequency.

Turning to the phenomenological theory of the normal stress effect, we may refer to the recent theory of Coleman and Noll for the second-order viscoelastic fluids.²¹ In this theory, components of stresses in steady shear flow are given as second-order terms in the rate of shear

$$\begin{aligned}\sigma_{12} &= \eta_0 \kappa \\ \sigma_{11} - \sigma_{22} &= -2\gamma \kappa^2 \\ \sigma_{22} - \sigma_{33} &= (\beta + 2\gamma) \kappa^2\end{aligned}\quad (8)$$

where η_0 , β , and γ are the material constants. In terms of the same constants, G' and G'' are given (again with second-order terms in ω)²²

(16) Y. Ikeda, *Kobunshi*, **5**, 635 (1957).

(17) M. C. Williams, *J. Chem. Phys.*, **42**, 2988 (1965).

(18) J. G. Kirkwood and J. Riseman, *ibid.*, **16**, 565 (1948).

(19) N. W. Tschoegl, *ibid.*, **39**, 149 (1963).

(20) In a good-solvent system, the excluded volume effect also affects the distribution of τ_p . See N. W. Tschoegl, *J. Chem. Phys.*, **40**, 473 (1964).

(21) B. D. Coleman and W. Noll, *Arch. Rational Mech. Anal.*, **6**, 355 (1960); *Ann. N. Y. Acad. Sci.*, **89**, 672 (1961).

$$\begin{aligned}\lim_{\omega \rightarrow 0} (G'/\omega^2) &= -\gamma \\ \lim_{\omega \rightarrow 0} (G''/\omega) &= \eta_0\end{aligned}\quad (9)$$

As will be shown later, eq 8 and 9 offer a possibility of separate determination of $\sigma_{11} - \sigma_{33}$ and $\sigma_{22} - \sigma_{33}$ which are measured only in a combined form in typical normal stress measurements.

3. Materials

The polystyrene used in the present study was prepared by thermal polymerization at 95°. Fractionation was performed at 30° from a 0.5% benzene solution using methanol as precipitant. Three fractions, F1, F3, and F4, were used for measurement. Their viscosity-average molecular weights were 5.0×10^6 , 1.2×10^6 , and 6.6×10^5 , respectively, as evaluated by²³

$$[\eta] = 1.13 \times 10^6 M_v^{0.73} \quad (\text{benzene, } 25^\circ) \quad (10)$$

Commercial dioctyl phthalate (DOP; Nakarai Chemicals, Ltd., CP grade) was used as a solvent without further purification. The viscosity was 1.10 poises at 20°. According to Ferry, *et al.*,⁴ the Θ temperature is about 12°.

Polymer solutions were prepared by storing weighed amounts of polymer and solvent at 50° with occasional stirring with a spatula. Several weeks were necessary for obtaining homogeneous solutions. Evaporation of the solvent was negligible.

4. Apparatus and Method

Measurements of the normal stress effect were carried out with a parallel-plate rheogoniometer. Details of this apparatus have been reported previously.¹⁴ The radial distribution of the pressure exerted normal to the stationary (upper) plate was measured. This is related to the normal stress components as

$$-(\partial P/\partial \ln r) = \sigma_{11} - \sigma_{33} + [\partial(\sigma_{22} - \sigma_{33})/\partial \ln \kappa] \quad (11)$$

with

$$\kappa = r\Omega/l \quad (12)$$

Here r is the radial distance from the axis of rotation, Ω is the angular velocity of the rotating (lower) plate, and l is the gap between two plates.

Measurements of the shear stress were carried out with a coaxial cylinder rheometer with rotating outer cylinder. The single-bob method of Krieger and Maron was used for determination of the steady shear viscosity.²⁴

The dynamic shear moduli, G' and G'' , were also

measured with the same rheometer. Details of the method for measurement were given in the previous report by Kotaka and Osaki.²⁵

For separate determination of two normal stress differences, $\sigma_{11} - \sigma_{33}$ and $\sigma_{22} - \sigma_{33}$, we used the following procedure. The substitution of eq 8 into eq 11 yields

$$-\partial P/\partial \ln r = (3\beta + 4\gamma)\kappa^2 \quad (13)$$

Then, from eq 8, 9, and 13, we obtain

$$\begin{aligned}\frac{1}{\kappa^2} \left(-\frac{\partial P}{\partial \ln r} \right) - 2 \lim_{\omega \rightarrow 0} \left(\frac{G'}{\omega^2} \right) = \\ 3(\beta + 2\gamma) = 3(\sigma_{22} - \sigma_{33})/\kappa^2\end{aligned}\quad (14)$$

This equation allows us to evaluate $\sigma_{22} - \sigma_{33}$ through the comparison of the normal pressure P with the storage modulus G' .²⁶ Application of the method is of course limited to the range of sufficiently small κ where the second-order fluid approximation remains valid.

5. Results and Discussion

Comparison of the stresses in steady shear with the dynamic shear moduli are illustrated in Figure 1 where the data obtained for a 2 wt % solution of polystyrene F1 in DOP at 20° are shown by various types of circles and lines. The thin line represents the log-log plot of the incremental shear stress attributable to the polymer, $\sigma_{12} - \kappa\eta_s$, against the rate of shear κ . The plots of the corresponding dynamic data, *i.e.*, $\log(G'' - \omega\eta_s)$ vs. $\log \omega$, are shown by the small white circles. The large white circles represent the log-log plots of $-(1/2)(\partial P/\partial \ln r)$ against κ , and the large black circles represent those of G' against ω . Thus, the observed features of these properties are as follows.

(i) The incremental shear stress $\sigma_{12} - \kappa\eta_s$ is proportional to κ over the whole observed range of κ .

(ii) The normal pressure gradient $-(\partial P/\partial \ln r)$ is proportional to κ^2 in the range of κ smaller than about 20 sec⁻¹.

(iii) $G'' - \omega\eta_s$ is also proportional to ω over a wide range of ω . The proportional constant $(G'' - \omega\eta_s)/\omega$ is compatible with the prediction of the second-order fluid theory that

(22) B. D. Coleman and H. Markovitz, *J. Appl. Phys.*, **35**, 1 (1964).

(23) W. R. Krigbaum and P. J. Flory, *J. Polymer Sci.*, **11**, 37 (1953).

(24) I. M. Krieger and S. H. Maron, *J. Appl. Phys.*, **23**, 147 (1952).

(25) T. Kotaka and K. Osaki, *Bull. Inst. Chem. Res. Kyoto Univ.*, **39**, 331 (1961).

(26) A test of the method has recently been made by the present authors for concentrated polymer solutions: K. Osaki, M. Tamura, T. Kotaka, and M. Kurata, *J. Phys. Chem.*, **69**, 3642 (1965).

$$\lim_{\omega \rightarrow 0} (G'' - \omega\eta_s)/\omega = (\sigma_{12} - \kappa\eta_s)/\kappa = \eta - \eta_s \quad (15)$$

(iv) G' is proportional to ω^2 in the range of ω smaller than about 2 sec^{-1} . In the limit of small κ and ω , two quantities G'/ω^2 and $(-1/2\kappa^2)(\partial P/\partial \ln r)$ come into coincidence within experimental error.

The last finding shows that, for this system, $\sigma_{22} - \sigma_{33}$ is very much less than $\sigma_{11} - \sigma_{33}$ in the range of κ where $-\partial P/\partial \ln r$ is proportional to κ^2 . Thus, in this range of κ , our measurements appear consistent with the molecular theory (eq 1).²⁷

Figure 2 shows the log-log plot of $\sigma_{12} - \kappa\eta_s$ and $-\partial P/\partial \ln r$ against κ for a series of polystyrene (F1) solutions in DOP with various concentrations. $\sigma_{12} - \kappa\eta_s$ is proportional to κ for all solutions over the whole range of variables. The value of κ at which $-\partial P/\partial \ln r$ begins to deviate from the κ^2 dependence increases with decreasing concentration. At concen-

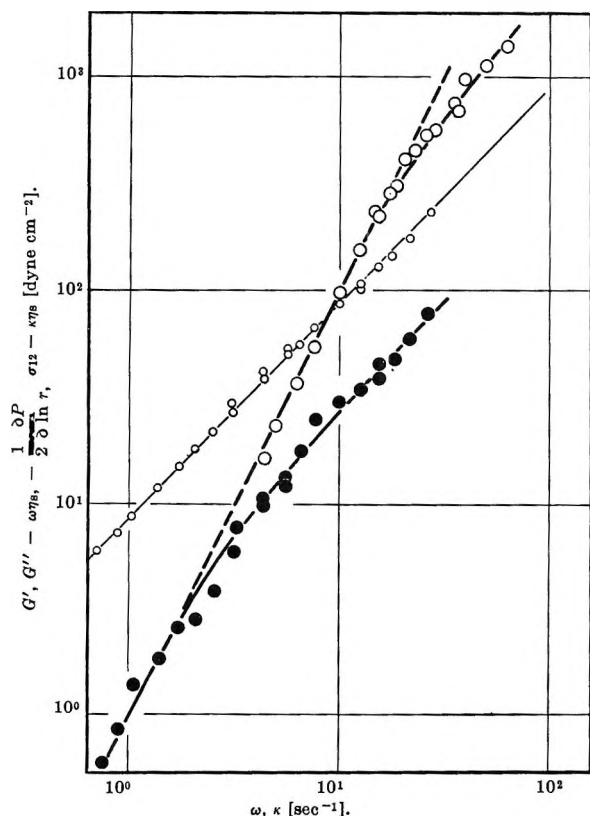


Figure 1. Comparison between stresses in steady shear and dynamic moduli of a 2 wt % solution of polystyrene (F1) in dioctyl phthalate at 20°C: thin line, incremental steady shear $\sigma_{12} - \kappa\eta_s$ plotted against rate of shear κ ; large white circles, normal stresses measured as $-(1/2)(\partial P/\partial \ln r)$ and plotted against κ ; small white circles, loss moduli $G'' - \omega\eta_s$ plotted against angular frequency ω ; large black circles, storage moduli G' plotted against ω ; broken line, limiting κ^2 dependence of the quantity $-(1/2)(\partial P/\partial \ln r)$.

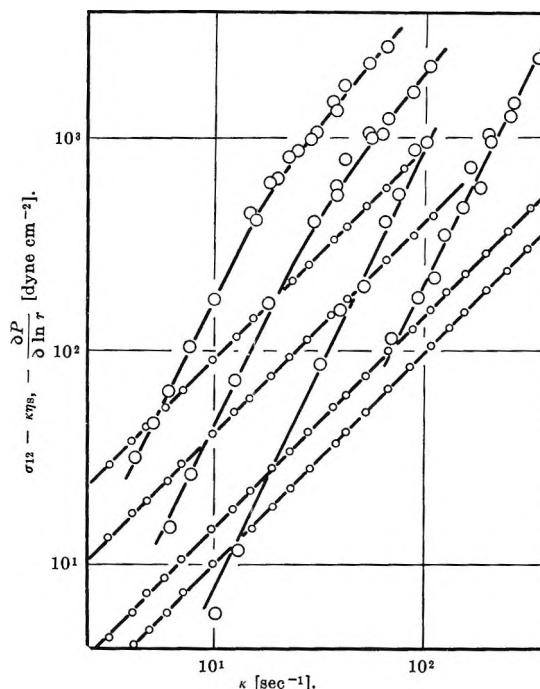


Figure 2. Effect of concentration on normal and shear stresses in solutions of polystyrene F1 in dioctyl phthalate at 20°C. Concentrations are 2, 1.5, 1, and 0.8% in weight from left to right, respectively. Small white circles represent $\sigma_{12} - \kappa\eta_s$, and large white circles represent $-\partial P/\partial \ln r$.

trations below 1%, the normal stress $\sigma_{11} - \sigma_{33}$ is proportional to κ^2 over the whole range of κ observed.

Figure 3 illustrates the effect of molecular weight on the normal and shear stresses. A series of 2% solutions of polystyrene F1, F3, and F4 in DOP was tested.

Now, the most important prediction by eq 1 is that both $\sigma_{12} - \kappa\eta_s$ and $\sigma_{11} - \sigma_{11}^0$ are proportional to the number of polymer molecules n in unit volume and, hence, to the ratio of the weight concentration and the molecular weight, c/M . Here c is expressed in grams per cubic centimeter. If this same relationship holds for all M and all concentrations it would predict that all data obtained for the solutions with different combinations of c and M could be superposed on a composite curve in the plot of $(-\partial P/\partial \ln r)M/c$ against $\kappa(\eta - \eta_s)M/c$. This prediction is roughly supported by the present data as is shown in Figure 4. This is in sharp contrast to the case of concentrated polymer solutions, in which the superposition of the normal stress data was possible only within a very limited range of small κ and the reduction factor was M^0/c^2 , or simply c^{-2} , instead of M/c .¹⁵

(27) This result does not necessarily imply that $\sigma_{22} = \sigma_{33}$. However, the difference between σ_{22} and σ_{33} , if any, is so small that the present measurements cannot detect it at low rate of shear.

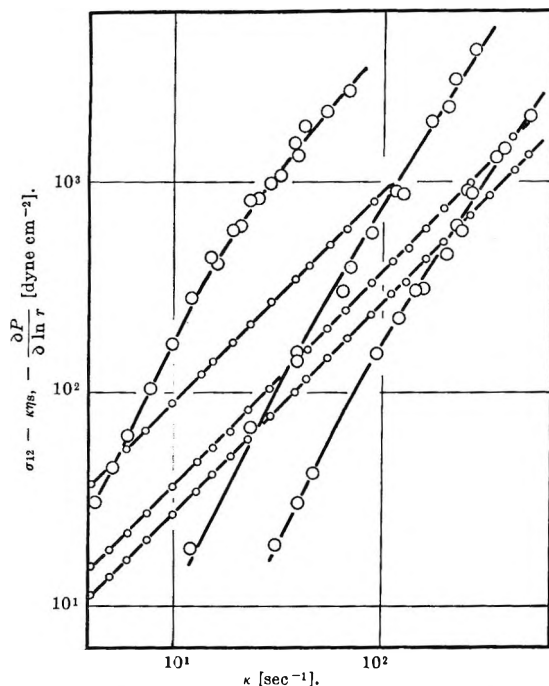


Figure 3. Effect of molecular weight on normal and shear stresses in 2 wt % solutions of polystyrene F1, F3, and F4 (from left to right) in dioctyl phthalate at 20°. Molecular weights are 5.0×10^5 for F1, 1.2×10^6 for F3, and 6.6×10^5 for F4, respectively. Small white circles represent $\sigma_{12} - \kappa\eta_s$, and large white circles represent $-\partial P/\partial \ln r$.

From the data obtained, we can estimate the steady shear compliance or, more conveniently, the quantity $\Sigma_p \tau_p^2 / (\Sigma_p \tau_p)^2$ by the formula

$$\gamma = \frac{\Sigma_p \tau_p^2}{(\Sigma_p \tau_p)^2} = \frac{1}{2} \frac{cRT}{M} \frac{(-\partial P/\partial \ln r)}{(\sigma_{12} - \kappa\eta_s)^2} \quad (16)$$

The observed value of this ratio was about 1.1 or, more precisely, 1.10, 1.34, and 1.06 for F1, F3, and F4 polymers, respectively. These values are about 5 or 2.5 times as large as the theoretical values 0.206 (non-free-draining case) or 0.400 (free-draining case; see eq 6). An analogous result was also obtained by Frederick, *et al.*, in the study of the dynamic moduli for dilute polystyrene solutions in DOP.⁴

The ratio γ is strongly affected by the heterogeneity in molecular weight. The correction factor is given as²⁸

$$\begin{aligned} \gamma_{\text{hetero}}/\gamma_{\text{homo}} &= M_z M_{z+1}/M_w M_v \quad (\text{free-draining case}) \\ &= M_z M_w^3 / (\overline{M}^{1.5})^2 M_v \quad (\text{nonfree-draining case}) \end{aligned} \quad (17)$$

where M_v , M_w , M_z , and M_{z+1} are the viscosity-average, weight-average, z -average, and $(z + 1)$ -average molecular weight, respectively. $\overline{M}^{1.5}$ is defined by

$$\overline{M}^{1.5} = \int_0^\infty M^{1.5} \varphi(M) dM \quad (18)$$

where $\varphi(M)$ is the distribution function of M in number. Then, assuming the Schulz exponential distribution for $\varphi(M)$ approximating M_v by M_w , we obtain from the observed value $\gamma = 1.10$

$$\begin{aligned} M_w/M_n &= 1.81 \quad (\text{freedraing case}) \\ &= 1.83 \quad (\text{nonfree-draining case}) \end{aligned} \quad (19)$$

where M_n is the number-average molecular weight. It is notable that an almost identical estimate for M_w/M_n was obtained irrespective of the assumptions on the strength of hydrodynamic interaction, $h = 0$ or ∞ . This implies that for polydisperse samples, the ratio γ could be a convenient measure for the

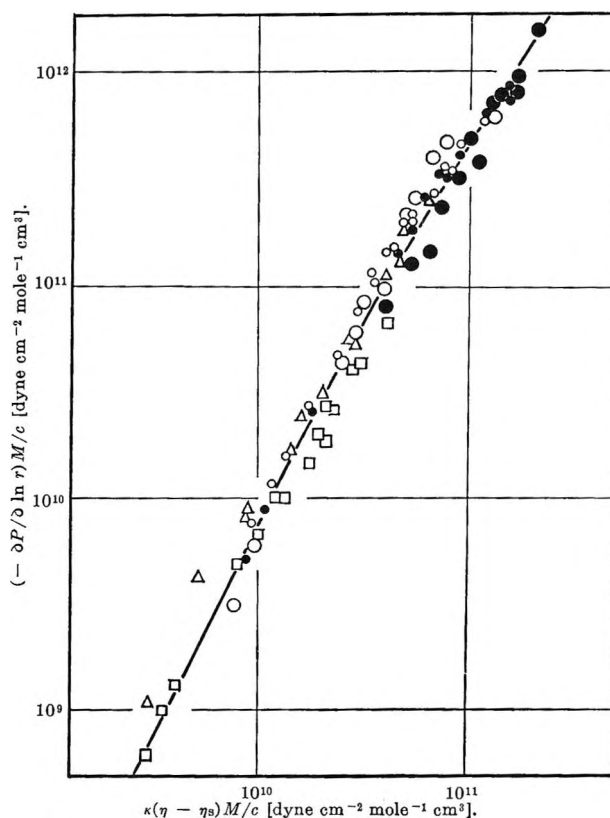


Figure 4. Reduced plot of the normal stress obtained for polystyrene in dioctyl phthalate with various combinations of M and c : small white circles, F1 with $c = 1.96 \times 10^{-2}$ g/cc (or 2 wt %); small black circles, F1 with $c = 1.47 \times 10^{-2}$ (or 1.5 wt %); large white circles, F1 with $c = 0.98 \times 10^{-2}$ (or 1 wt %); large black circles, F1 with $c = 0.785 \times 10^{-2}$ (or 0.8 wt %); triangles, F3 with $c = 1.96 \times 10^{-2}$; squares, F4 with $c = 1.96 \times 10^{-2}$; solid line, composite curve corresponding to $\gamma = 1.10$ (see eq 16).

(28) S. E. Lovell and J. D. Ferry, *J. Phys. Chem.*, **65**, 2274 (1961).

heterogeneity in molecular weight, but not for the strength of the hydrodynamic interaction h .

In conclusion, in the present system near the Θ temperature, the normal stress component $\sigma_{11} - \sigma_{33}$ was proportional to κ^2 and c/M over a wide range of variables, and the component $\sigma_{22} - \sigma_{33}$ was negligible.

The effect of solvent power on the normal stresses will be studied in the following paper.

Acknowledgment. We are indebted to Professor Tadao Kotaka for his kind advice and stimulating discussions. Thanks are also tendered to the Ministry of Education of Japan for a grant-in-aid.

Ion-Exchange Processes in Aqueous Dimethylformamide Mixtures¹

by A. Ghodstinat, J. L. Pauley, Teh-hsuen Chen,² and M. Quirk³

Department of Chemistry, Kansas State College of Pittsburg, Pittsburg, Kansas (Received August 30, 1965)

Lithium-sodium, potassium-sodium, cesium-sodium, and sodium-cesium exchange on Dowex 50W X-1 in 0, 5, 10, 25, 50, 75, and 90% dimethylformamide-water mixtures were studied. In general, the logarithm of the exchange coefficients varied with the reciprocal of the dielectric constant as would be predicted for coulombic interactions. However, a minimum was observed for the potassium-sodium and the cesium-sodium exchanges with increasing dimethylformamide concentration. The sodium-cesium exchange showed a corresponding maximum. Radioactive tracer techniques were used to determine exchange coefficients. Solvent uptake and solvent distribution data were also obtained. In general, water is preferred in the resin phase. The preference decreases with higher dimethylformamide concentrations. Total solvent uptake also decreased with increasing dimethylformamide concentration, although much less markedly for the Li resin than for the others.

Introduction

Nonaqueous solvents as ion-exchange media have been investigated in recent years by several authors.⁴⁻⁸ In general, mixed solvents using water as one component have been used rather than strictly nonaqueous media for systems using organic exchangers. Equilibrium is reached very slowly in most pure organic solvents. In the present investigation, the dimethylformamide-water (DMF-H₂O) system was chosen since this system provided reasonably good salt solubilities, a good range of dielectric constants, and water-like properties. A low cross-linked exchanger was used to facilitate attainment of equilibrium in the DMF-rich mixtures where resin swelling was limited.

Experimental Section

Materials. Solutions were prepared using reagent

grade DMF and ion-free water. Potassium chloride, sodium chloride, lithium chloride, and cesium chloride were all reagent grade and were dried under vacuum before use. The radioactive sodium-22 and cesium-134 were carrier free in the chloride form. The ex-

(1) Presented before the Division of Physical Chemistry of the American Chemical Society at the Southwest Regional Meeting, Shreveport, La., Dec 1964.

(2) Taken in part from the dissertation of Teh-hsuen Chen to the Graduate School of Kansas State College of Pittsburg in partial fulfillment of the requirements for the Master of Science degree.

(3) National Science Foundation undergraduate research participant.

(4) R. G. Fessler and H. A. Strobel, *J. Phys. Chem.*, **67**, 2562 (1963).

(5) P. C. Huang, A. Mizany, and J. L. Pauley, *ibid.*, **68**, 2575 (1964).

(6) R. Gable and H. Strobel, *ibid.*, **60**, 513 (1956).

(7) D. D. Bonner and J. C. Moorefield, *ibid.*, **58**, 555 (1954).

(8) A. Materova, Zh. L. Verts, and G. P. Grinberg, *Zh. Obshch. Khim.*, **24**, 953 (1954).

changer used was Dowex 50W X-1 (50–100 mesh) obtained in the hydrogen form from Bio-Rad Corp. The resins were converted to the appropriate salt form with the hydroxide or chloride of the desired salt as convenient. Resin capacities were determined by adding excess base and back titrating the excess. Capacities in milliequivalents per dry gram of resin were 5.20, 5.00, 4.66, 4.34, and 3.08 for the hydrogen, lithium, sodium, potassium, and cesium exchangers, respectively. Samples of the various salt forms of the exchanger were spiked with carrier-free sodium-22 or cesium-134 (activity approximately 10^6 counts/min per g) and dried under vacuum at 120° before use.

Equilibrium Systems. Weighed samples of approximately 1 g of the dry, spiked exchanger in the salt form were transferred to glass serum bottles and permitted to equilibrate at 30° with 25 ml of an approximately 0.1 M solution of the salt corresponding to the ionic form of the resin. When equilibrium had been reached, aliquots of the solution phase were taken and counted to determine radioactivity eluted from the resin phase. Later aliquots were counted to determine that equilibrium had truly been reached. A total activity balance was determined in several cases to assure that there were no losses of activity due to adsorption.

Selectivities. Selectivities calculated corresponded to the exchange $A^+ + B^*R = AR + B^{*+}$, where A^+ was sodium, lithium, potassium, or cesium and B^* was radioactive sodium or cesium. Selectivity coefficients were calculated according to

$$K_{B}^A = \frac{(AR, \text{ mequiv/g})(B^{*+}, \text{ counts/min per ml})}{(B^*R, \text{ counts/min per g})(A^+, \text{ mequiv/ml})}$$

The normality of the metal salt solution, (A^+), and the capacity of the resin, (AR), were assumed to remain constant during the exchange. The activity of the resin phase was corrected for the activity in the equilibrium solution phase.

Rate Determinations. To determine the rates of reaction, the same procedure was used as for the equilibrium studies except that samples were withdrawn periodically, centrifuged, and the aliquots were counted to determine tracer activity in the solution phase.

Solvent Distribution. Solvent distribution between the resin and solution phases was obtained by equilibrating the appropriate salt form of the resin with the various solvent mixtures. The excess solvent was then removed by filtration, followed by blotting the resin phase. The solvent retained in the resin phase was removed by distillation under vacuum. The composition of the distillate was determined by measuring its refractive index.

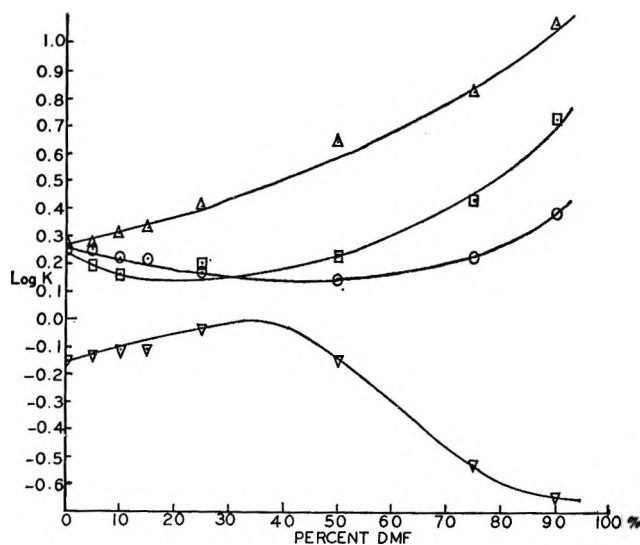


Figure 1. Logarithm of selectivity coefficient for exchange reactions vs. composition of the DMF-H₂O solvent mixture: Δ , Na-Li exchange; \square , K-Na exchange; \circ , Cs-Na exchange; ∇ , Na-Cs exchange. The points (Δ) for Na-Li exchange represent the inverse of the experimentally determined selectivity coefficients for the Li-Na exchange using radioactive sodium as the tracer element.

Swelling. A weighed amount of the dry resin in the appropriate salt form was equilibrated with the solvent mixture in a stoppered vessel. The swollen resin was then filtered, patted dry of excess solvent, and weighed. Swelling was calculated in terms of grams of solvent per milliequivalent of resin. These values appeared to be more reproducible and more easily interpreted than volume ratios.

Results

Equilibrium results for several exchanges are shown in Figure 1, in which the logarithm of the selectivity coefficient is plotted against solvent composition. In the case of the Li-Na exchange, the reciprocals of experimental exchange coefficients, corresponding to the calculated coefficient for the Na-Li exchange, are plotted for convenience in comparing the results for the various systems. In the case of Na-Li, K-Na, and Cs-Na exchanges, there is an increase of $\log K$ in going from water to high concentrations of DMF. This corresponds to the change expected for ion-ion interactions since the dielectric constant decreases rather regularly with increasing DMF concentration.

In the cases of the Cs-Na and K-Na exchanges, however, a minimum was observed in the plot of $\log K$ vs. concentration of DMF. To investigate the reality of the minimum, the Na-Cs exchange was also investigated, and a maximum was observed at about the

Table I: Dielectric Constant as a Function of Composition for the H₂O-DMF System.

Compn, % DMF	Dielectric constant, <i>D</i>	$1/D \times 10^2$
0	78.2	1.18
10	72.2	1.38
25	63.7	1.57
50	56.7	1.76
75	46.8	2.14
90	40.0	2.50
100	36.7	2.73

same solvent composition as the minimum for the Cs-Na system. Plots were made also of $\log K$ vs. the reciprocal of the dielectric constant of the solvent mixtures. The general shapes of the curves were the same.

The increase of K with decreasing dielectric constant agrees generally with the effects noted by Fessler and Strobel⁴ for exchanges in methanol-water and ethanol-water mixtures. For the Na-Li exchange they noted no maximum as solvent composition varied although a leveling off of K values was observed at higher methanol concentrations. They noted maxima for all exchanges involving hydrogen ion at dielectric constants of about 40 and 29 for ethanol-water mixtures and methanol-water mixtures, respectively.

The presence of a minimum or maximum in selectivity coefficients as the per cent of DMF increases implies the operation of two opposing factors. The decrease in dielectric constant accompanying the increase in per cent of DMF would be expected to result in a regular increase of selectivity for the preferred ion. However, if ionic solvation changed in an opposing manner as the solvent composition changed, the observed minima or maxima could be accounted for on the basis of a relatively simple electrostatic interaction model⁹ or on the basis of competition between coulomb interaction and ionic solvation as proposed by Eisenman.¹⁰ It may be of interest to note that at low DMF concentrations the solvent distribution results (Table II) suggest that the cesium resin does not selectively absorb water as effectively as do the potassium and sodium resins. It is possible that at these concentrations the cesium ion on the resin is at least partially solvated by the larger DMF molecules while potassium and sodium ions are either solvated only by water, or at least are less solvated by DMF. This would result in a change of relative, solvated ionic sizes in the direction required to account for the observed results. It can be seen from Table II that above

about 50% DMF there seems to be little difference in selectivities of each of these ions for water over DMF. If this reflects attainment of a relatively stable solvated state, dielectric constant effects should again become dominant which would lead to the observed increase of selectivity with increasing DMF concentration.

The reversal of selectivity for potassium and cesium which occurs above about 25% DMF may be related to the observed changes in order of solvent absorption as shown in Table II. Below about 25% DMF the order of solvent absorption is as expected: Li > Na > K > Cs. Above about 25% DMF the order is Li > Na > Cs > K. This may suggest a relative change in the solvation of the ions which would account for the reversal of selectivities.

The fact that there may be differences in composition in the solvent composition in the solution and resin phases has not been generally considered for systems of mixed solvents. It can be seen from Table II and would be expected from work on solvent exclusion processes that the resin phase has a significantly higher affinity for water than for DMF. This is particularly true at low DMF concentrations. The Li resin seems to have a much less marked preference for water in the middle region of the composition of solvent. Similarly, as seen from solvent uptake data, the Li resin is swollen to a much larger degree by the solvent mixtures high in DMF than the other resins. This may suggest at least weak complex formation of the lithium ion with the DMF somewhat analogous to complexes formed with lithium ions and ethylenediamine. Plots of $\log K$ vs. composition of the solution in the resin phase were also made. However, the nature of the plots was not significantly different from plots of $\log K$ vs. composition of the external solution phase although the slopes changed slightly and the maxima or minima were shifted slightly toward lower DMF concentrations.

Rate data were obtained for the Li-Na exchange in 10% DMF-H₂O, 90% DMF-H₂O, and pure DMF solution.¹¹ As would be anticipated, the rate of exchange decreased with increasing DMF concentration. Equilibrium was reached within 1 hr in 10% DMF and in less than 2 hr in 90% DMF. However, it is doubtful if a true equilibrium was reached in pure DMF even after 3 days. A plot of the function $B(t)$ as suggested

(9) J. L. Pauley, *J. Am. Chem. Soc.*, **76**, 1422 (1954).

(10) G. Eisenman, "Membrane Transport and Metabolism," A. Klienzzeller and A. Kotyk, Ed., Academic Press Inc., New York, N. Y., 1961, p 163.

(11) F. Helfferich, "Ion Exchange," McGraw-Hill Book Co., Inc., New York, N. Y., 1962, p 302 ff.

Table II: Swelling and Changes in Solvent Composition in the Resin and Solution Phases for Li, Na, K, and Cs Resins as a Function of the Composition of the Solution Phase

Compn of soln phase, % DMF	LiR		NaR		KR		CsR	
	A	B	A	B	A	B	A	B
0	0	1.1	0	0.97	0	0.95	0	0.96
5	2.5	...	1.5	...	2.0	...	2.5	...
10	4.5	1.1	4.0	1.1	4.0	0.96	6.0	0.06
25	23	1.1	14	0.91	14	0.92	19	0.96
50	46	0.99	35	0.81	37	0.67	41	0.79
75	73	0.95	66	0.60	66	0.15	67	0.24
90	88	0.91	84	0.24	89	0.12	85	0.12

by Reichenberg^{12,13} indicated that the rate is diffusion controlled as appears to be the case in water.

Conclusion

As shown by this and other investigations, the solvent does significantly affect both the selectivities and the rates of ion-exchange processes. The present results agree with the conclusion of other investigations that the dielectric constant of the media is a most significant factor in solvent effects. However, other effects, including ionic solvation, do play a significant

role as evidenced by the existence of maxima or minima in plots of selectivity coefficients *vs.* solvent composition. These effects appear also to be reflected by changes in solvent composition in the resin and solution phases and by resin swelling results. These observations suggest that further studies may be of value in improving understanding of the interaction of ionic materials as a function of solvent composition.

(12) D. J. Reichenberg, *J. Am. Chem. Soc.*, **75**, 589 (1953).

(13) G. E. Boyd, A. W. Adamson, and L. S. Myers, Jr., *ibid.*, **69**, 2836 (1947).

Catalytic Exchange of Methane with Deuterium on Palladium-Gold Alloys

by D. W. McKee

General Electric Research & Development Center, Schenectady, New York (Received August 31, 1965)

The rates of the exchange reaction between CH_4 and D_2 have been measured on a series of Pd-Au alloy powders in the temperature range 90 to 200°. Stepwise exchange was the dominant mechanism in every case and the specific activity of the alloys at 100° showed a small maximum at a composition of about 10 atom % Au. Increasing concentrations of Au gave rise to a rapid decrease in exchange rate which became immeasurably small at about 30 atom % Au. The apparent activation energy for the exchange reaction varied between 14 and 23 kcal/mole and showed a shallow minimum at about 20 atom % Au. Possible reasons for this behavior are discussed.

Introduction

One potentially fruitful approach to the understanding of catalytic behavior and particularly to the evaluation of the role of electronic factors in catalysis lies in the systematic study of activity variations in alloy systems. For this purpose a simple test reaction should be used and the binary alloy system chosen should preferably have a wide range of mutual solubility between the components so that the surface phase remains homogeneous over a considerable range of alloy composition.

The exchange reaction between CH_4 and D_2 has recently proved useful in studies of the behavior of binary alloys of the Pt-group metals, among which wide variations in catalytic behavior are encountered.^{1,2} Palladium in particular shows a lower activity for this reaction than would be expected on the basis of its electronic structure although its activity can be enhanced considerably by alloying with Ru.³ There is also evidence that the activity of Pd for hydrogen atom recombination⁴ and for parahydrogen conversion⁵ can be increased to some extent by alloying with a small amount of Au. This alloy system involves a continuous range of solid solutions between a metal of group VIII and group IB and is therefore ideal for an investigation of the influence of d-band vacancies in catalytic reactions. Rates of CH_4 - D_2 exchange have been measured as a function of temperature and alloy composition for a series of homogeneous Pd-Au powders. It was hoped to relate the results of this study to previously published information on

hydrogen equilibration and exchange over similar alloy catalysts.

Experimental Section

The alloy samples were prepared from Fisher reagent grade gold chloride and Engelhard pure palladium chloride by reduction in solution with 5% sodium borohydride solution, as described previously.³ The alloys were washed thoroughly, dried slowly in air, then ground to -325 mesh. X-Ray diffraction patterns showed the products to be homogeneous solid solutions in every case. Homogeneous Pd-Au alloy powders have also been obtained by Holt⁶ using a similar method.

Alloy samples were sealed into the apparatus described previously^{1,2} and reduced *in situ* with H_2 for 2 hr at 150°. Following evacuation at this temperature for 4 hr, the temperature was raised to that of the subsequent exchange experiment. The sample was then treated with D_2 for 1 hr and evacuated to a pressure less than 10^{-6} torr before admission of the CH_4 - D_2 mixture.

The reaction mixture was adjusted to an initial composition of 80 mm of CH_4 and 40 mm of D_2 , amount-

(1) D. W. McKee and F. J. Norton, *J. Phys. Chem.*, **68**, 481 (1964).

(2) D. W. McKee and F. J. Norton, *J. Catalysis*, **3**, 252 (1964).

(3) D. W. McKee, *Trans. Faraday Soc.*, **61**, 2273 (1965).

(4) P. G. Dickens, J. W. Linnett, and W. Palczewska, *J. Catalysis*, **4**, 140 (1965).

(5) A. Couper and D. D. Eley, *Discussions Faraday Soc.*, **8**, 172 (1950).

(6) E. L. Holt, *Nature*, **203**, 857 (1964).

ing to 3.5×10^{19} molecules of CH_4 and 1.7×10^{19} molecules of D_2 at the start of the exchange experiment. The B.E.T. surface area of the sample was also determined in each case; this was found to remain constant during the course of the exchange experiments.

Phillips research grade methane, 99.57 mole % pure, was used. Deuterium (General Dynamics Corp., 96% pure) and hydrogen for reduction purposes were purified by passage through Pd diffusion tubes before use. Samples of the four deuteriomethanes were obtained from Merck Sharp and Dohme (Canada) Ltd., and had minimum purities of 98 mole %.

Results

The initial exchange rates were determined as functions of temperature and alloy composition by utilizing the first-order equations developed by Kemball.⁷

The initial rate of substitution of H by D in 100 molecules of CH_4 in unit time was calculated from the relation

$$-\log(\phi_\infty - \phi) = \frac{k_\phi t}{2.303\phi_\infty} - \log \phi_\infty \quad (1)$$

ϕ being defined by

$$\phi = \sum_{i=1}^4 ix_i$$

where x_i is the percentage of the isotopic species containing i D atoms present after time t and ϕ_∞ is the equilibrium value of ϕ . The value of ϕ_∞ was generally obtained from the composition of the gas phase after 60 min.

The initial rate of disappearance of light CH_4 , in percentage per unit time, was obtained from the equation

$$-\log(X - X_\infty) = \frac{kt}{2.303(100 - X_\infty)} - \log(100 - X_\infty) \quad (2)$$

where X and X_∞ are the percentages of CH_4 present in the gas phase after t min and at equilibrium (60 min), respectively.

The rate constants k and k_ϕ are related by the equation

$$k_\phi/k = M$$

where M is the average number of H atoms being replaced initially by D. A value of M around unity implies that the hydrogens in the CH_4 molecule are being replaced successively by D, a process referred to as "stepwise exchange." Under certain conditions, relatively high proportions of highly deuterated species

are formed initially by the process of "multiple exchange." In this case the value of M may approach 3 or 4.

Equations 1 and 2 were found to fit the exchange data quite well in the initial stages of the reaction when the proportion of deuterated products in the gas phase was small. Values of the over-all exchange rate k and the ratio M were obtained over a range of temperature for each alloy sample. The initial rate of stepwise exchange R_1 was also calculated from the rate of CH_3D formation. By definition, R_1 is related to the rate of multiple exchange R_2 and to the over-all exchange rate k by the equation

$$k = R_1 + R_2$$

Previous work with pure noble metals^{2,8} has indicated that the ability to promote $\text{CH}_4\text{-D}_2$ exchange decreases in the order $\text{Pt} > \text{Rh} > \text{Pd} > \text{Ru}$, although the sequence depends on temperature to some extent. Rh and Ru generally give rise to substantially more multiple exchange than to Pt and Pd under the same conditions.

Typical exchange runs are illustrated in Figures 1 and 2 for two different alloy samples, the isotopic composition of methane in the gas being plotted as a function of time. In the first case, the mechanism is mainly that of stepwise exchange, the value of M being close to unity and the concentrations of CHD_3 and CD_4 in the products remaining low. These species are formed slowly by readsorption and further exchange of desorbed CH_3D . Increasing evidence of multiple exchange is found in Figure 2 where the initial concentrations of CH_3D and CH_2D_2 are almost equal, the value of M being close to 2 in this case. At temperatures below 150° , stepwise exchange was the dominant mechanism in all cases. A plot of the first-order eq 1 and 2 is shown in Figure 3 for a typical exchange run. The physical properties of the alloys and typical exchange results over a range of temperature are shown in Table I. Columns 1 and 2 give the atomic composition and lattice constant of the samples. Owing to the small particle size of the alloys and the resulting diffuse character of the X-ray lines, the values of a_0 are probably accurate only to within ± 0.01 A. However, they agree fairly well with the published data of Maeland and Flanagan.⁹ The B.E.T. surface area (obtained from the adsorption of nitrogen at -195°) during the exchange runs is shown in column 3. For any given alloy the value of M increased with increasing

(7) C. Kemball, *Advan. Catalysis*, **11**, 228 (1959).

(8) D. W. McKee and F. J. Norton, *J. Catalysis*, **4**, 510 (1965).

(9) A. Maeland and T. B. Flanagan, *Can. J. Phys.*, **42**, 2364 (1964).

Table I: CH₄-D₂ Exchange over Pd-Au Alloys (3.5×10^{19} Molecules of CH₄ + 1.7×10^{19} Molecules of D₂ Initially)

Alloy composition, atom % Pd	Lattice constant a_0 , Å	Surface area, m ² /g	Temp., °C	Log k (molecules/sec cm ²)	Log R_1	M	ΔE , kcal/mole	Log A (A in molecules/sec cm ²)
100	3.890	6.82	96.5	10.686	10.663	1.0	21.6	23.51
			105	10.977	10.935	1.1		
			116.5	11.344	11.297	1.2		
			125	11.539	11.447	1.4		
			147	11.857	11.602	1.7		
95.2	3.890	7.32	96	10.700	10.672	1.1	16.8	20.68
			129	11.516	11.362	1.2		
			139	11.957	11.663	2.1		
90.1	3.892	9.27	104	11.100	11.000	1.1	15.8	20.27
			114.8	11.344	11.265	1.2		
			123	11.617	11.415	1.4		
			133	11.749	11.463	1.5		
83.6	3.895	7.67	99	10.902	10.857	1.2	14.1	19.22
			126	11.260	11.176	1.2		
			139	11.826	11.491	1.9		
			151	11.920	11.623	2.1		
78.3	3.920	9.21	97	10.532	10.507	1.1	22.8	24.05
			106	10.879	10.813	1.1		
			118	11.258	11.182	1.2		
			131	11.420	11.272	1.5		
69.4	3.890	4.66	109	10.842	10.785	1.1	19.3	21.92
			126	11.316	11.253	1.1		
			147	11.748	11.540	1.3		
			166	11.810	11.559	2.0		
			202	12.107	11.724	2.2		
53.1	3.983	5.53	101.5	10.025	10.000	1.1	19.3	21.33
			114.5	10.403	10.386	1.1		
			129	10.726	10.663	1.1		
			134.5	10.937	10.892	1.1		
			151	11.295	11.201	1.2		
46.0	3.987	4.76	155	10.772	10.732	1.1	21.9	21.99
			175.5	11.286	11.188	1.1		
33.8	4.008	3.63	197	9.124	9.10	1.1	~22	~19.4
16.7	4.042	2.20	197		

temperature, indicating increasing contributions of multiple exchange. The rate of exchange fell rapidly for alloys containing more than 40 atom % Au. For the sample with 66.2 atom % Au, exchange was very slow at 197°, whereas for the 90.2 atom % Au alloy no exchange was detectable after 60 min at this temperature.

It was noticed in every case that the first exchange run with a fresh alloy sample was always somewhat slower than expected. Subsequent runs were quite reproducible after evacuation at the reaction temperature, however, and it is possible that the initial slow rate was due to the presence of a desorbable impurity

on the alloy surface. The nature of this impurity is not known, but it is possible that such an effect could account for the acceleration of the exchange rate noted by Coekelbergs and others¹⁰ for CH₄-D₂ exchange over evaporated films of Mo and Ni.

From the linear portions of the Arrhenius plots, the apparent activation energy for over-all exchange ΔE and the corresponding frequency factors, A , were calculated for the alloy series. The results are included in Table I, the frequency factors being given in logarith-

(10) R. Coekelbergs, Y. Delaunois, A. Frennet, and G. Lienard, *J. Chim. Phys.*, **61**, 1174 (1964).

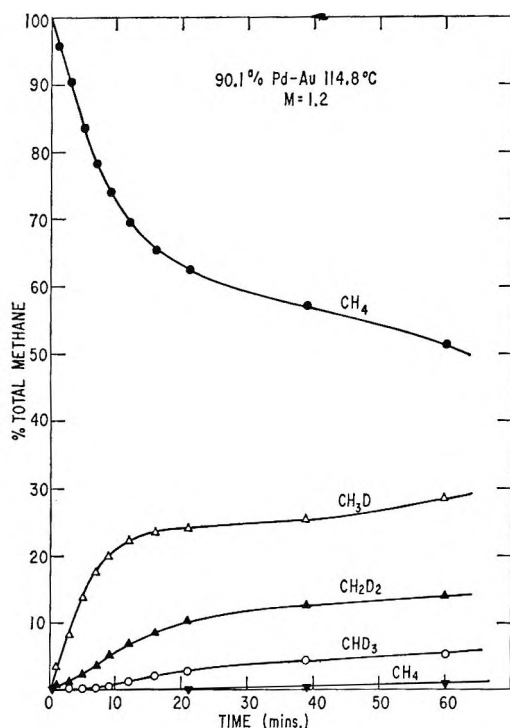


Figure 1. CH_4 - D_2 exchange on 90.1 atom % Pd-Au 114.8°. Total area of alloy = 11.63 m².

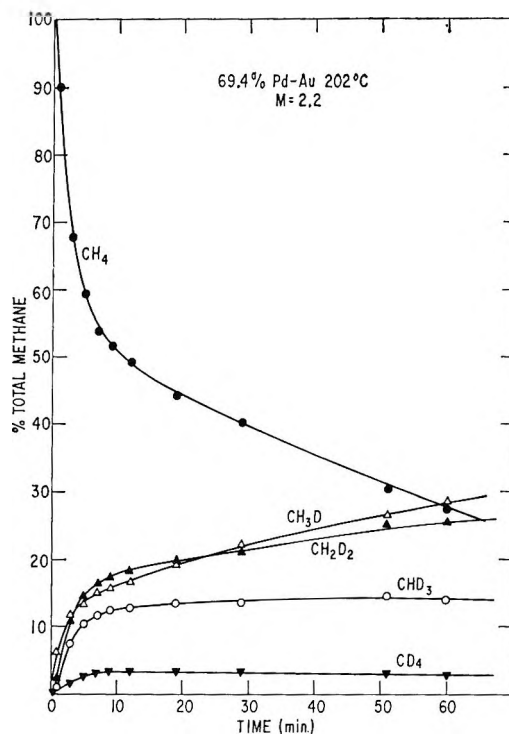


Figure 2. CH_4 - D_2 exchange on 69.4 atom % Pd-Au 202°. Total area of alloy = 7.07 m².

mic form, where A is expressed in molecules/sec cm². As in previous work, a well-defined compensation effect was observed between the activation energies and the corresponding frequency factors for the different alloys.

Using the kinetic parameters in Table I, the specific over-all rate of the exchange reaction was compared for all the alloy samples at a temperature of 100°, as shown in Figure 4. Also shown in Figure 4 is a plot of sample surface area against alloy composition.

Discussion

The following main conclusions may be drawn from these results.

(a) Stepwise exchange was the most important mechanism with all the alloy samples, although multiple exchange became more evident with increasing temperature. There was also a tendency for multiple exchange to become less important with increasing Au content.

(b) The addition of Au to Pd caused a small increase in specific reaction rate up to about 10 atom % Au. At higher Au concentrations the exchange rate fell off sharply, becoming essentially zero at 60 atom % Au. The decrease in rate between 90 and 40% Pd was about four orders of magnitude.

(c) The apparent activation energy for exchange

showed a shallow minimum at an alloy composition of about 20 atom % Au.

Although no previous information is available for the CH_4 - D_2 exchange reaction on Pd-Au alloys, similar catalytic activity patterns have been reported for the p- H_2 conversion and H-atom recombination reactions. In the former case, Couper and Eley⁵ demonstrated that on addition of Au to Pd a maximum activity occurred at about 30 atom % Au, the activity at this composition being 5–10 times greater than that of pure Pd. With increasing Au content the activity of the alloys rapidly decreased and at about 60 atom % Au a sudden increase in activation energy was observed. These results have been widely quoted as illustrating the electronic factor in catalysis, the vacant d-orbitals of the Pd being held responsible for the catalytic activity of the pure metal. On addition of Au, donation of s electrons occurs so that the d-band of the alloy becomes progressively filled, until at a composition of about 60 atom % Au, the d-band is complete and the alloy becomes diamagnetic.

Unlike Pd, Au appears to lack the ability to catalyze the dissociation of molecular hydrogen at low temperatures, although there is evidence that chemisorption of atomic hydrogen can occur.¹¹ Also from studies of H_2 - D_2 exchange Mikovsky, Boudart, and Taylor conclude that chemisorption of hydrogen can occur on

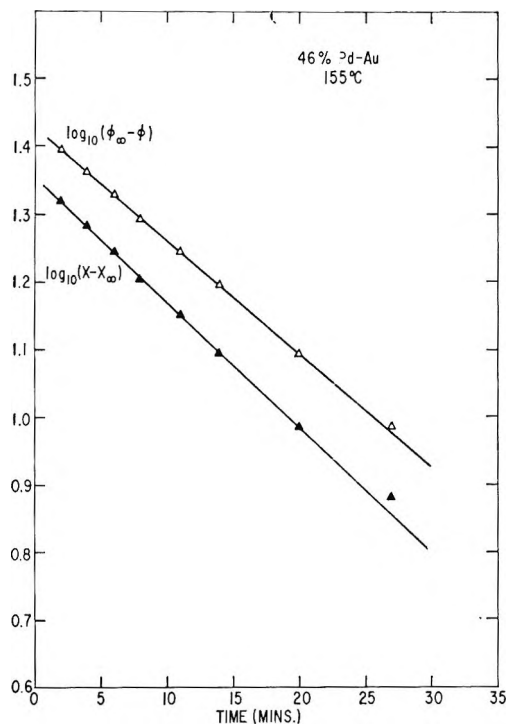


Figure 3. First-order plots, eq 1 and 2, for $\text{CH}_4\text{-D}_2$ exchange on 46 atom % Pd-Au, 155°.

Au above 300°, presumably as a result of d-s promotion at high temperature.¹² From the results of an electrochemical study of hydrogen coverage on Pd-Au alloys at room temperature, Gray, Rozelle, and Soeder¹³ were unable to detect chemisorbed hydrogen on alloys containing more than 60 atom % Au, whereas alloys with less Au chemisorbed copious amounts. It seems likely that the decrease in $\text{CH}_4\text{-D}_2$ exchange rate with increasing Au content can be accounted for on the same basis. Because of the filling of the d-band of Pd and the intrinsic inactivity of Au in this temperature range, alloys containing more than 60% Au are unable to dissociate the D_2 molecule and initiate exchange. However, it is also possible that the ability to catalyze dissociation of C-H bonds also decreases with increasing Au content and it is not known which factor is responsible for the observed fall in exchange activity.

The observed maximum activity at low Au concentrations is more difficult to account for and although similar effects have been noted before for other reactions, few explanations have been offered. Commenting on the maximum found by Couper and Eley for p- H_2 conversion, Bond¹⁴ has suggested that as the d-band is filled, the strength of binding of chemisorbed H decreases and the surface species becomes more labile. It is possible that the unexpectedly low activ-

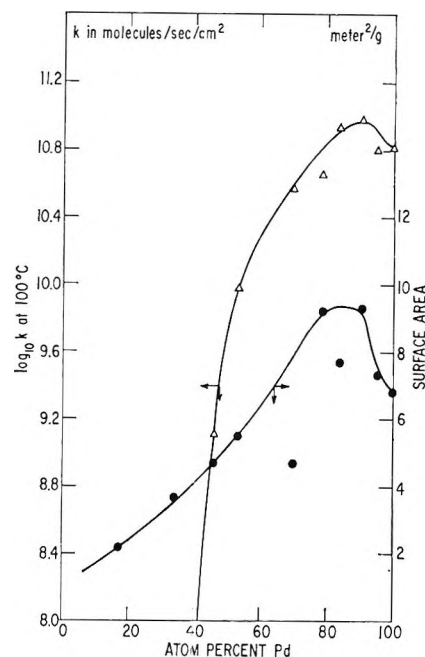


Figure 4. Variation of $\log k$ at 100° and surface area with alloy composition.

ity of Pd in dehydrogenation and exchange reactions can be attributed to a poisoning effect of chemisorbed H. Adsorption of H by Pd results in a decrease in magnetic susceptibility of the bulk metal suggesting donation of electrons to the vacant d-orbitals; however, it is possible that migration of H occurs into the bulk metal so that filling of the d-orbitals is not carried to completion in the surface layer as in the case of alloying with Au.

A maximum in the activity of Pd-Au catalysts supported on silica has been found for benzene hydrogenation and the dehydrogenation of cyclohexane.¹⁵ In the present case, the enhanced activity of 10 atom % Au-Pd was small (about 1.5 times that of pure Pd at 100°) and was similar in magnitude to the effect found by Dickens, Linnett, and Palczewska⁴ and by Wood and Wise¹⁶ for the H recombination reaction over Pd-Au alloys, the maximum in the latter case

(11) H. Wise and K. M. Sancier, *J. Catalysis*, **2**, 149 (1963); W. M. H. Sachtler and J. Fahrenfort, *Actes Congr. Intern. Catalyse*, **2°**, Paris, **1**, 831 (1960).

(12) R. J. Mikovsky, M. Boudart, and H. S. Taylor, *J. Am. Chem. Soc.*, **76**, 3818 (1954).

(13) T. J. Gray, R. B. Rozelle, and M. L. Soeder, *Nature*, **202**, 181 (1964).

(14) G. C. Bond, "Catalysis by Metals," Academic Press, London, 1962, p 171.

(15) A. A. Alchudzhan and M. A. Mantikyan, *Izv. Akad. Nauk Armyan SSR*, **12**, 153 (1959).

(16) B. Wood and H. Wise, *J. Phys. Chem.*, **65**, 1976 (1961).

occurring at around 30% Au. The maximum in exchange rate disappears at higher temperatures and rates calculated at 130° from the kinetic parameters of the alloys show only a steady decrease with increasing Au content.

The similarity between the variation in exchange rate and alloy surface area shown in Figure 4 is worthy of comment. Au-rich samples had appreciably lower surface areas than those containing high concentrations of Pd and the maximum areas were associated with the maximum specific exchange rate. In a previous study of the catalytic activity of Pt black,¹⁷ it was shown that the dehydrogenation activity decreased more rapidly during sintering of the black than would be expected from the loss in surface area alone. This suggested that the sintering process eliminated active sites or defects responsible for the catalytic

activity. The decrease in density of active sites was also accompanied by an increase in activation energy for the dehydrogenation reaction. The exchange results indicate that alloys containing about 10 atom % Au have a greater resistance to sintering than Pd alone so that the density of catalytically active sites may be higher at this composition. In a recent study of the electrochemical formation and reduction of oxygen layers on Pt-Au alloys,¹⁸ a similar maximum in activity was observed at a composition of about 20 atom % Au. It is interesting that this effect was attributed to an increase in roughness factor of the Pt-rich phase.

(17) D. W. McKee, *J. Phys. Chem.*, **67**, 841 (1963).

(18) M. W. Breiter, *ibid.*, **69**, 901 (1965).

A Method to Estimate the Bulk Modulus and the Thermal Expansion Coefficient of Liquids

by A. Bondi

Shell Development Company, Emeryville, California (Received August 31, 1965)

Simple corresponding states correlations are presented for the thermal expansion coefficient and for the zero pressure bulk modulus of liquids and polymer melts.

Purpose and Scope

The improved theory of solutions by Flory and co-workers¹ requires as input information equation of state data derivable from the thermal expansion coefficient and the zero pressure bulk modulus of the solvent and the solute. While the former is often available from the literature and can, if necessary, be determined in a comparatively simple experiment with the accuracy required by the Flory calculations, the bulk modulus data are less readily accessible.

Isothermal zero pressure bulk moduli (K_0) of fair accuracy can be obtained by extrapolation from high

pressure p - v - t data.² A more plentiful source is the sound velocity of liquids (and polymers).³⁻⁵ These data have the advantage of comparatively safe extrapolation to higher and lower temperature because

(1) P. J. Flory, *et al.*, *J. Am. Chem. Soc.*, **86**, 3515 (1964); **87**, 1833, 1838 (1965).

(2) S. D. Hamann, bibliography in "Physico Chemical Effects of High Pressure," Academic Press, Inc., New York, N. Y., 1957.

(3) L. Bergmann, "Der Ultraschall," Hirzel, 1954, 1957.

(4) V. F. Nozd'rev, "Use of Ultrasonics in Molecular Physics," Pergamon Press Inc., New York, N. Y., 1965.

(5) W. P. Mason, "Physical Acoustics," Vol. II, Academic Press Inc., New York, N. Y., 1964, 1965.

the sound velocity changes linearly with temperature over wide ranges. The major source of uncertainty can be the absence of expansion coefficient and specific heat data, required for conversion of the adiabatic to isothermal bulk modulus. Here a 10% uncertainty in the expansion coefficient or in the heat capacity causes 4 to 5% and 2 to 3% uncertainty, respectively, in the bulk modulus. If the ideal gas heat capacity of the compound in question is known, the conversion to liquid phase heat capacity by known methods⁶ could hardly introduce errors in excess of $\pm 5\%$. However, the crude guesses which may be made in the absence of gas-phase information could lead to errors in C_p as large as 20% since there are at present no reliable simple methods available to estimate the heat capacity of liquids. Hence there is a need for additional estimation methods for the p - v - t properties of liquids and polymer melts. The present work constitutes an attempt to provide simple estimation methods for the thermal expansion coefficient and the zero pressure bulk modulus.

The scope of the work is set by the desire to use molecular structure information as the sole data input, yet retain the option to produce a more accurate result by additional experimental data, especially of the density. The assumptions underlying the correlations used limit the validity to temperatures below the atmospheric boiling point for simple substances and to above the glass transition temperature for polymers.

General Principles

The basis of the present work is a corresponding-states correlation⁶ developed from the theory of Prigogine, *et al.*,⁷ for the equilibrium properties of liquid polymers. That theory is a forerunner of the recent equation of state for polymeric liquids by Flory, *et al.*,⁸ which has provided some of our correlating criteria. The main difference between the theories and the corresponding states correlation is the supply of the reference volume and the reference temperature (potential energy parameter) from independent experimental information in the correlation, whereas the theories derive these reference parameters from the p - v - t data.

The dimensionless properties to be correlated are the packing density $\rho^* = V_w \rho / M$, reduced temperature $T^* = ZcRT/2E^\circ$, and reduced zero pressure bulk modulus $K_0^* = K_0 V_w / E^\circ$ where V_w is the van der Waals volume derived from X-ray diffraction data,⁹ E° is the energy of vaporization defined as $E^\circ = \Delta H_{\text{vap}} - RT$ at that temperature at which $\rho^* = 0.588$; the number of nearest neighbors Z is taken as 10, and $3c$ is the number of external degrees of freedom per molecule including those due to internal rota-

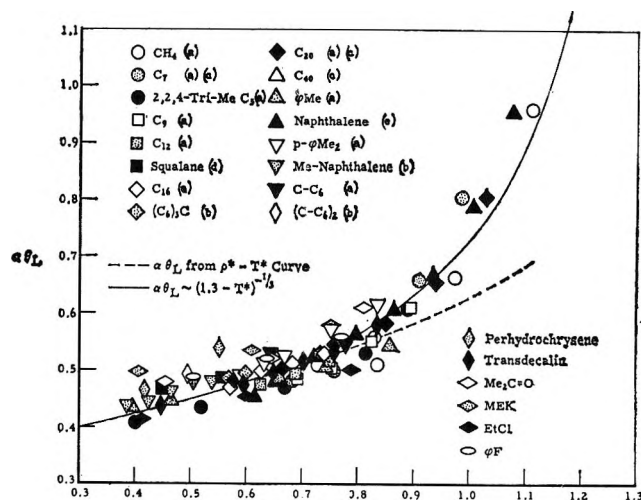


Figure 1. Plot of reduced expansion coefficient vs. temperature. References: (a) API-Res. Project 44, Tables; (b) API-Res. Project 42, Tables; (c) A. K. Doolittle, *et al.*, *A.I.Ch.E. J.*, 6, 150, 157 (1960); (d) see ref 22; (e) D. I. Juravlev, *Russ. J. Phys. Chem.*, 9, 875 (1937).

tion excited in the liquid state in the temperature range under consideration.

One finds that the reduced density-temperature curve of most liquids with $M \geq 150$ can be represented by the relation

$$\rho^* = 0.726 - 0.249T^* - 0.019T^{*2} \quad (1)$$

The center of gravity of experimental points is at about $\rho^* = 0.555$ corresponding to $T^* = 0.652$. Hence this point is taken as reference point, and c is calculated from the observed density and energy of vaporization as $c = 0.652E^\circ/5RT(1.8)$, where $T(1.8)$ is the temperature ($^\circ\text{K}$) at which $\rho^* = 0.5556$. For rigid non-linear polyatomic molecules, of course, $3c = 6$. Empirical correlations for estimating $3c$ and for calculating E° from increments for flexible molecules have been presented elsewhere^{10,11} so that the reference temperature $\theta_L = 5cR/E^\circ$ can be estimated from molecular structure information. When density data are available, one obtains directly $\theta_L = T(1.8)/0.652$. The correlations are not applicable to alcohols with fewer than four carbon atoms per hydroxyl group.

(6) A. Bondi and D. J. Simkir, *A.I.Ch.E. J.*, 6, 191 (1960).

(7) I. Prigogine, *et al.*, *J. Chem. Phys.*, 26, 741 (1957).

(8) P. J. Flory, *et al.*, *J. Am. Chem. Soc.*, 86, 3507 (1964).

(9) A. Bondi, *J. Phys. Chem.*, 68, 441 (1964).

(10) A. Bondi, *A.I.Ch.E. J.*, 8, 610 (1962).

(11) A. Bondi in "Rheology," Vol. 4, F. R. Eirich, Ed., Academic Press, Inc., New York, N. Y., 1965.

The Thermal Expansion Coefficient

The generalized expansion coefficient $\alpha^* = \alpha\theta_L \equiv 1/\rho^*(\partial\rho^*/\partial T^*)$ can be obtained by differentiation of the generalized density-temperature curve over the range for which the latter has been plotted.^{12a} The data in Figure 1 show that, as expected, only the low-temperature region is adequately represented in this fashion. Representation of the steep increase of α^* as T_c is approached requires inclusion of T_c into the equation. Since for many substances $T_c^* \approx 1.30$, an equation in T^* could be used as indicated in Figure 1.

The meaning of the structure insensitive generalized expansion coefficient $\alpha^* = \alpha E^0/5cR$ is basically that the expansion coefficient is proportional to the ratio of the configurational heat capacity to the "lattice" energy of liquids, a well-known result of the theory of lattice vibrations in crystals. For the expansion coefficient of van der Waals liquids composed of rigid molecules, Wall and Krigbaum obtained the very similar result that $\alpha \sim R/\Delta H_{\text{vap}}$.^{12b}

In Figure 1, one can discern certain small but systematic deviations from the average behavior. However, in evaluating these differences one should keep in mind that few density measurements are sufficiently precise to assign significance to differences of 10% or less in expansion coefficients. The scatter of the data points is of that order of magnitude. Within this scatter there is a trend for highly branched paraffins to exhibit smaller than average values of α^* , and several polar compounds show not only a slightly higher than average value of α^* but also somewhat smaller than average variations of α^* with temperature. The latter trend, of course, deals with a second derivative of density with respect to temperature and all comparisons can note "trends" at best.

The rather good fit of the data of flexible molecules onto the general curve suggests that the parameter "c" in the reducing temperature $E^0/5cR$ accounts adequately for the effect of internal rotation on the thermal expansion coefficient.

In the reduced temperature range $0.3 < T^* < 0.7$ high polymer melts are very near their glass transition (T_g) temperature. The more rapid change in the number of excited external degrees of freedom over a given temperature interval near T_g is probably responsible for the fact that some polymer melts exhibit a thermal expansion coefficient in excess of expectation from their low molecular weight analogs. The characteristic difference between the thermal expansion of amorphous polymers at $T > T_g$ and of simple liquids is apparent from the data of Figure 2. In view of the notorious difficulty of dilatometric measurements on

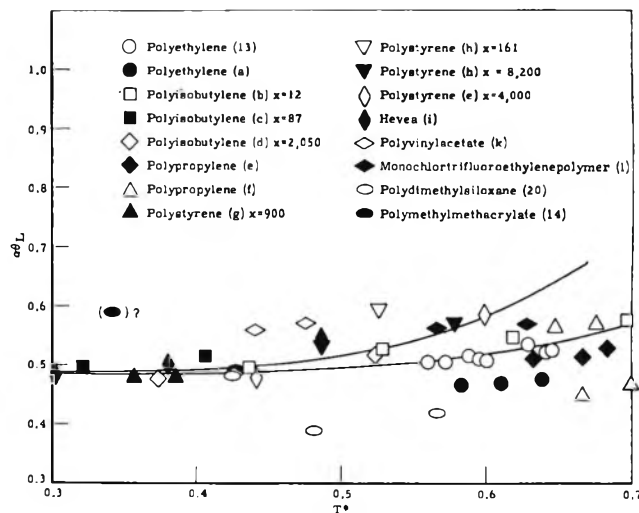


Figure 2. Reduced thermal expansion coefficient of polymer melts as a function of reduced temperature. References:

- (a) L. D. Moore, *J. Polymer Sci.*, **36**, 155 (1959);
 (b) D. Bradbury, Ph.D. Thesis, Harvard University, 1950;
 (c) G. S. Parks and J. D. Ferry, *J. Chem. Phys.*, **4**, 70 (1936);
 (d) T. G. Fox and P. J. Flory, *J. Phys. Colloid Chem.*, **55**, 221 (1951); (e) F. Danusso, *et al.*, *Chim. Ind. (Milan)*, **41**, 748 (1959); (f) Equals ref 13; (g) T. G. Fox and P. J. Flory, *J. Appl. Phys.*, **21**, 581 (1950); (h) K. Ueberreiter and G. Kanig, *Z. Naturforsch.*, **6a**, 551 (1951); (i) N. Bekkedahl, *Rubber Chem. Technol.*, **14**, 347 (1941);
 (k) A. Kovacs, *J. Polymer Sci.*, **30**, 131 (1958);
 (l) S. Furuya and M. Honda, *ibid.*, **20**, 587 (1956).

polymers, one should perhaps not try to rationalize the relations between the data of Figure 2 and molecular structure. It is noteworthy that the very accurate data on polyethylene melts by Pals¹³ fall very near the curve for simple liquids.

A question can arise regarding the appropriate expansion coefficient for the polymeric solute at $T < T_{g(\text{polymer})}$. The coefficient for polymeric glasses is nearly independent of molecular structure, $\alpha_g \approx (2.2 \pm 0.1) \times 10^{-4} \text{ }^\circ\text{K}^{-1}$.¹⁴ However, the thermal expansion coefficient of the partial specific volume of polymer solutes at $T < T_{g(\text{polymer})}$ is within a fairly wide error margin about $0.9 \alpha_L$,^{15,16} just as the partial specific volume is more nearly like the extrapolated liquid density than like that of the glass.¹⁷ One may

(12) (a) The Flory theory predicts for the similar reduced expansion coefficient (at $p = 0$) $\alpha T_0 = (3\bar{V}^{1/3}) / [(1 - 3\bar{V}^{1/3}) - 1]$, i.e., a function of \bar{V} , or T , only; (b) F. T. Wall and W. R. Krigbaum, *J. Chem. Phys.*, **17**, 1274 (1949).

(13) D. T. F. Pals, unpublished information.

(14) A. J. Kovacs, *Fortschr. Polymer. Forsch.*, **3**, 394 (1964).

(15) G. V. Schulz and M. Hoffmann, *Makromol. Chem.*, **23**, 220 (1957).

(16) A. Schmitt and A. J. Kovacs, *Compt. Rend.*, **255**, 677 (1962).

(17) A. Horth, *et al.*, *J. Polymer Sci.*, **39**, 189 (1959).

conclude from these observations that the appropriate p - v - t properties assigned to the polymer in the range $T_{g(\text{polymer})} > T > T_{g(\text{solution})}$ are those extrapolated from its melt properties. The properties of polymer solutions at $T < T_{g(\text{solution})}$ are only beginning to be examined.¹⁸ Hence generalizations cannot yet be made.

Due to the compensating effect of opposing temperature trends one finds that the product $\alpha\rho = (\partial\rho/\partial T)_p$, the temperature coefficient of density, is independent of temperature over the wide range $0.4 < T^* < 0.8$. This very useful fact had been known to petroleum chemists,^{19,20} but is not widely appreciated. The incorrect notion that $(\partial v/\partial T)_p$ is constant is rather widespread. Examples for the constancy of $(\partial\rho/\partial T)_p$ and the lack thereof with $(\partial v/\partial T)_p$ are given in Figure 3 for simple liquids as well as polyethylene melts. The data by Murphy, *et al.*, show the constancy of $(\partial\rho/\partial T)_p$ for many nonhydrocarbon liquids as well. It should be noted, however, that the above indicated rise in expansion coefficient of polymer melts near T_g leads to $(\partial v/\partial T)_p = \text{constant}$ as one approaches T_g to within about 50° . Long extrapolation of density or specific volume, as practiced in crystallinity determination, should therefore be carried out with caution.

Bulk Modulus of Liquids

The bulk modulus of liquids K_0 (at atmospheric pressure) is far more sensitive to molecular structure than is the thermal expansion coefficient. Yet, as suggested by Flory's theory²¹ and confirmed by the data in Figure 4, $K_0^* = K_0 V w / E^\circ$ is a simple function of ρ^* or T^* for a wide variety of substances, indicating that K_0 is primarily a function of E° and V_w , *i.e.*, of the cohesive energy density, besides T^* .

The highly anisometric structure of long-chain compounds and the related anisotropy of "molecular" compressibility requires special consideration. The internal compressibility, E_p^{-1} , of these molecules is only about $1/100$ as large as the compressibility (K_i^{-1}) of the intermolecular space. Hence, in the limit of $M \rightarrow \infty$ the bulk modulus of the polymer liquid is given by

$$\frac{1}{K_0} = \frac{2}{3K_i} + \frac{1}{3E_p} \approx \frac{2}{3} \frac{1}{K_i}$$

i.e., the compression takes place only in two dimensions, normal to the axis of the long molecule. For molecules of finite length, one has to consider also the compressibility of intermolecular space between ends of molecules, and the arithmetic becomes a bit more complicated

$$K_0^*(L) = K_0 \left\{ \frac{V_w}{E^\circ} \left[\frac{2}{3} \left(1 + \frac{1}{N_s} \right) \right] + \frac{1}{3E_p} \left(1 - \frac{1}{N_s} \right) \right\}$$

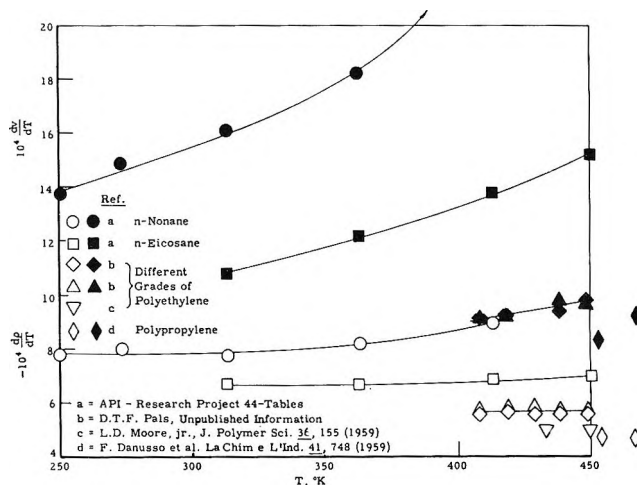


Figure 3. Comparison of the temperature coefficients of density (open circles) with those of specific volume (solid symbols) for n -paraffins, polyethylenes, and polypropylene melts.

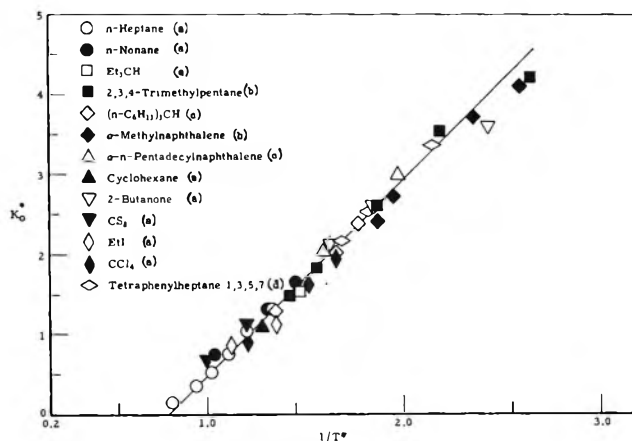


Figure 4. Plot of generalized bulk modulus of liquids vs. temperature. References: (a) ref c of Figure 1 and ref 3 and 4; (b) H. Geelen, Ph.D. Thesis, Delft, 1956; (c) ref b of Figure 1; (d) J. W. M. Boelhouwer, private communication.

The general shape of the relation is indicated in Figure 5. Typical E_p data have been assembled in Table I.

Polymers with *cis* configuration in the repeating unit of the backbone chain do not lose van der Waals compressibility parallel to the chain axis. Their bulk modulus in the melt state is therefore correlated as

- (18) K. Ueberreiter and W. Bruns, *Ber. Bunsenges.*, **68**, 541 (1964).
 (19) M. R. Lipkin and S. S. Kurtz, *Ind. Eng. Chem. Anal. Ed.*, **13**, 291 (1941).
 (20) C. M. Murphy, *et al.*, *Trans. ASME*, **71**, 561 (1949).
 (21) According to which at $p = 0$

$$\bar{K}_0 = \frac{1 - 3(\bar{V}^{1/3} - 1)}{3\bar{V}^2(\bar{V}^{1/3} - 1)}$$

Table I: Spectroscopic Elastic (Young's) Modulus E_p of Various Polymer Molecules (All in 10^{10} dynes/cm²)

Polymer	E_p (calcd) ^a	E_p (obsd) ^b
Polyethylene	182, ^d 340	260
Polytetrafluoroethylene	160	
Polyvinylchloride (syndiotactic)	160 (or 230?)	
Polyvinylidene chloride		41.5
Polyoxymethylene	220	54
Polyisobutylene	70-84	
Polypropylene (isotactic)	49	42
Polystyrene		12
Polyvinyl alcohol		255
Polyethylene terephthalate	122, ^d 146 ^c	76 ^c
Nylon 66	196, ^d 157 ^c	
Cellulose I		137
Cellulose II		90
Polyethylene glycol ($M \rightarrow \infty$)	4.8	
Poly-3,3-bis(fluoromethyl)oxacyclobutane	110	
Poly-3,3-bis(chloromethyl)oxacyclobutane	100	
Poly-3,3-bis(bromomethyl)oxacyclobutane	92	
Poly-3,3-bis(iodomethyl)oxacyclobutane	77	

^a From the spectroscopic force constants; M. Asahina, *et al.*, *J. Polymer Sci.*, **59**, 93, 101, 113 (1962). ^b By X-ray diffraction analysis of crystallite extension; I. Sakurada, *et al.*, *ibid.*, **57**, 651 (1962); *Makromol. Chem.*, **75**, 651 (1964). ^c F. W. Dalmage and L. E. Contois, *J. Polymer Sci.*, **28**, 275 (1958), find 140×10^{10} dynes/cm² by the same technique. ^d L. F. G. Treloar, *Polymer*, **1**, 95, 279, 290 (1960). ^e W. J. Lyons, *J. Appl. Phys.*, **29**, 1429 (1958).

K_0 , *i.e.*, like that of a monomeric liquid, however, on the polymer correlation curve.

The equations for the two cases shown in Figures 4 and 5 are quite similar, for simple liquids

$$K_0^* = \frac{2.00}{T^*} - 1.60 \quad (2)$$

and for long-chain compounds and polymer melts

$$K_0^* (L) = \frac{2.30}{T^*} - 1.98 \quad (3)$$

Both equations are strictly empirical and are probably valid only in the range $1.0 > T^* > 0.4$. At the low-temperature end there is an indication of a slower than $1/T^*$ rise of K_0^* . At the high-temperature end the point $K_0^* = 0$ is attained at $T^* = 1.25$ which is somewhat less than the critical temperature, which as a rule is at $T^* \approx 1.3$. Hence exact expressions for both systems yield S-shaped curves rather than straight

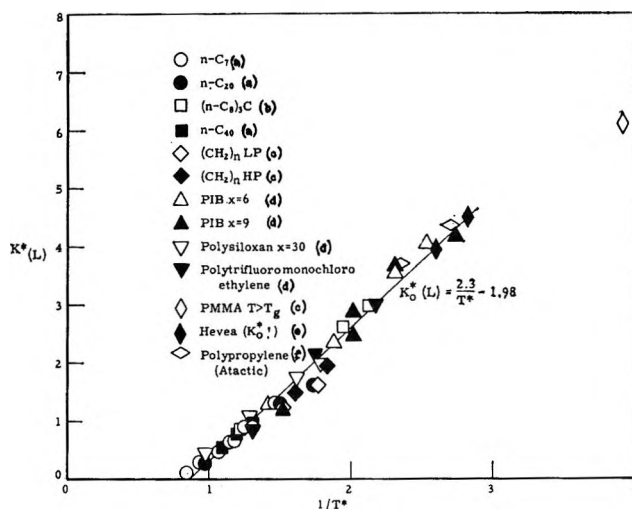


Figure 5. Plot of generalized bulk modulus of liquids, including polymer melts, composed of flexible chain molecules. References: (a) ref c of Figure 1; (b) ref b of Figure 1; (c) K. H. Hellwege, *et al.*, *Kolloid-Z.*, **183**, 110 (1962); (d) ref b of Figure 2; (e) L. A. Wood and G. M. Martin, *J. Res. Natl. Bur. Std.*, **68A**, 259 (1964); (f) E. Passaglia and G. M. Martin, *ibid.*, **68A**, 273 (1964).

lines. While this deficiency is not a serious problem with most monomeric liquids because they are used largely in the temperature range in which the straight line is a good approximation, it may well become a problem when one is concerned with solutions of polymers at or below their glass transition temperature. The example of poly(methyl methacrylate) in Figure 5 illustrates this point.

Since the thermal pressure coefficient $\gamma (=K_0\alpha)$ can presumably be measured more accurately than it can be calculated from the independently measured K_0 and α , an attempt has been made to correlate γ directly. Two routes have been tried, as $P_i^* \equiv \gamma TV_w/E^\circ$ and as P_i^*/ρ^{*2} because the latter is often claimed to be temperature independent, at least at low temperatures.²² A few spot checks of room temperature measurements yield data in tolerable agreement with each other. However, data taken over an extended temperature range by several well-known investigators are in striking disagreement as shown by the curves of Figure 6. The other data in that figure offer little encouragement for the discovery of a universal correlation of P_i^*/ρ^{*2} vs. T^* , since the properties of *n*-paraffins are generally most amenable to correlation. Convergence of all curves into a single curve is indicated only for the higher molecular weight alkanes ($N_c \geq 16$) at low temperatures ($T^* \leq 0.7$). Numerical values of P_i^*/ρ^{*2} have been obtained for various com-

(22) G. Allen, *et al.*, *Polymer*, **1**, 467 (1960).

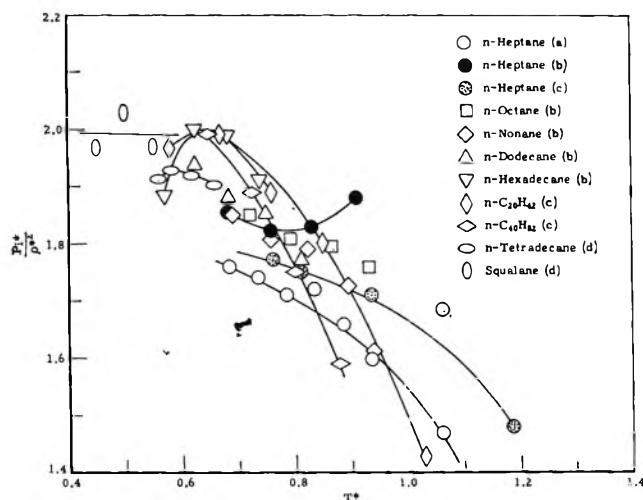


Figure 6. Plot of reduced internal pressure function vs. reduced temperature for several alkanes. References: (a) J. S. Rowlinson, "Liquids and Liquid Mixtures," Academic Press, New York, N. Y., 1959; (b) J. W. M. Boelhouwer, *Physica*, **26**, 1021 (1960); (c) see ref c of Figure 1; (d) see ref 22.

pounds and were found to cover too broad a range even within given chemical series to offer much hope for useful correlation. This lack of simple trends appears to hold even within data series obtained by single and very careful investigators.

Comparison of the reducing parameters V^* and T^* of Flory's generalized equation of state with the corresponding independently determined properties used in the present correlation yields the following results. The volume V^* can be compared directly with V_w , and $T_F = s\eta/2\nu^*cR = (\bar{\nu}E_0/Nrc'R)_F$ can be compared with $\theta_L = E^\circ/5cR$, where the two energy terms E° and E_0 are not identical by definition, but are likely to be very similar in numerical magnitude. Flory's rc' is only one-half of our c . Hence T_F^*/θ_L should be of the order $10\bar{\nu}$. This turns out to be the case. Specifically, while the temperature drift of V^* prevents a constant ratio, $V_w/V_F^* \approx 0.70 \pm 0.02$, which is of the order of the packing density at 0°K . Typical comparisons with zero-point volume V_0 are shown in Table II. The same table also shows the ratio T_F^*/θ_L and the almost universal constant factor $\rho^*T_F^*/\theta_L$, indicating how the two methods of correlation can be interchanged.

Limitations of the Methods

Inspection of Figure 1 shows that prediction of the expansion coefficient of monomeric liquids for a generalized curve might be good only to within $\pm 10\%$. This uncertainty can often be reduced to $\pm 3\%$ by starting with a known expansion coefficient of a com-

Table II: Comparison of Flory's Reducing Temperature T_F^* with That of the Present Work (θ_L) and of Flory's Reducing Volume V_F^* with V_0^a

Substance	t , $^\circ\text{C}$	T_F^*/θ_L	$\rho^*T_F^*/\theta_L$	V_F^*/V_0
CCl ₄	0	10.9	5.70	0.996
	70	11.5	5.75	1.02
Cyclohexane	0	10.3	5.90	1.01
	70	10.65	5.60	1.03
Methylcyclohexane	65	11.5	6.0	
Benzene	0	10.4	5.77	0.99
	70	11.0	5.61	1.01
Diphenyl	70	9.47	5.60	
n-Hexane	20	12.1	6.31	1.02
n-Heptane	20	11.6	6.20	1.03
n-C ₆ F ₁₄	20	10.0	5.05	
CF ₃ ·cyclo-C ₆ F ₁₁	65	9.90	5.02	

^a V_0 = zero point volume, W. Biltz, "Raumchemie der festen Stoffe," 1934.

pound similar to that under consideration, e.g., a member of the same homologous series. Its experimental value of $\alpha\theta_L$ vs. T^* then locates the curve of $\alpha\theta_L \sim (1.30 - T^*)^{-1/3}$ for the compound under consideration. The E° increments required for this calculation can be found in ref 10 and 11. The thermal expansion coefficients of polymer melts should be estimated from the correlation of Figure 2. However, care should be taken not to extrapolate into the immediate neighborhood of or below T_g^* where rather different relations prevail.^{14,23}

The average error of the bulk modulus correlations within the linear range discussed earlier appears to be of the order of $\pm 5\%$, and the maximum error range may be of the order of $\pm 15\%$. Here again the error range can be sharply reduced by sacrificing generality and specializing the correlations for families of compounds.

Conclusions

The corresponding-states correlations presented here permit an estimate of the thermal expansion coefficient and of the bulk modulus of liquids and polymer melts to within $\pm 10\%$. This error limit can be reduced to less than 3% by specializing the correlations for particular series of compounds. Further reduction of this error limit is probably unrealistic because few experimental data have a smaller error limit. The alternative route to the bulk modulus *via* the sound velocity is open only if heat capacity data with uncertainties of $\leq 10\%$ are available.

(23) A. Bondi, *J. Polymer Sci.*, **A2**, 3159 (1964).

Diffusion of Silver Nitrate in Concentrated Aqueous Solutions

by G. J. Janz, G. R. Lakshminarayanan, M. P. Klotzkin, and G. E. Mayer

Department of Chemistry, Rensselaer Polytechnic Institute, Troy, New York (Received September 2, 1965)

The diffusion coefficients of AgNO_3 in aqueous solutions, obtained by Stokes diaphragm technique, are reported for the range of concentrations from 0.1 to 9.0 M at 25°. Application of the extended Hartley-Crank analysis, modified for hydrated and associated 1:1 electrolytes, clearly indicates the ion-pair formation in aqueous AgNO_3 solutions. The marked difference of diffusion results of AgNO_3 and related 1:1 electrolytes, *e.g.*, LiNO_3 and NH_4NO_3 , is considered in the light of ion-association and ion-solvent interactions.

Introduction

While there is a relatively large amount of conductance data for 1:1 electrolytes in moderately concentrated and concentrated regions, little information exists for the diffusion of salts in such aqueous solutions, while in nonaqueous media the data are virtually nonexistent. AgNO_3 has a high solubility in water (>10 moles/l) and in nonaqueous solvents such as acetonitrile (12 moles/l) and benzonitrile (>4 moles/l). The conductance and viscosity of aqueous AgNO_3 solutions up to 10 M have already been investigated¹ and more recently results in nonaqueous media have been reported.² The only diffusion results for aqueous AgNO_3 available are those of Harned and Hildreth³ in the dilute region (0.007 M). In the course of the present study, Firth and Tyrrell⁴ reported on the diffusion of AgNO_3 up to concentrations of 4 M in which the Stokes method⁵ of computing the differential diffusion coefficients from the integral diffusion coefficients was used. A different technique, using solutions of finite concentrations in the upper compartment^{5,6} instead of pure water and thus gaining differential diffusion coefficients directly, was adopted in the present study. This communication reports the results of such an investigation for AgNO_3 , at 25° in the concentration range from 0.1 to 9.0 M . Diffusion studies for AgNO_3 in nonaqueous media (acetonitrile, benzonitrile) are in progress and will be reported later.

Experimental Section

Conductivity water and certified reagent grade quality AgNO_3 were used for all solutions. The compositions of the latter were determined by gravimetric chloride analysis and by conductometric analysis;^{7a}

the analytical results by these two techniques were in excellent agreement.

The stirred diaphragm diffusion cell and rotating magnet assembly were basically that given by Stokes elsewhere;^{7b} it is sufficient to remark on a few salient experimental features. Each cell reservoir had a capacity of about 50 ml, and the diaphragm, about 0.5 ml. The most suitable diaphragms were those having pores that average 15 μ , with none smaller than 10 μ or larger than 20 μ (Gallenkamp, England). The stirrers consisted of soft iron wire sealed in glass, and of such weight that the lower stirrer would "float" to the underside of the diaphragm while the upper stirrer would sink down to the upper diaphragm side; an external horseshoe magnet (Model A Ford, ignition magnets), coated with a protective paint (Corrosite

(1) A. N. Campbell and E. M. Kartzmark, *Can. J. Chem.*, **28B**, 43 (1950).

(2) G. J. Janz, A. E. Marcinkowsky, and I. Ahmad, *J. Electrochem. Soc.*, **112**, 104 (1965).

(3) H. S. Harned and C. L. Hildreth, *J. Am. Chem. Soc.*, **73**, 3292 (1951).

(4) J. G. Firth and H. J. V. Tyrrell, *J. Chem. Soc.*, 2042 (1962).

(5) R. H. Stokes, *J. Am. Chem. Soc.*, **72**, 2243 (1950).

(6) F. J. Kelly, Ph.D. Dissertation, University of New England, Armidale, New South Wales, 1961. F. J. Kelly and R. H. Stokes, "Electrolyte Solutions," B. Pesce, Ed., Pergamon Press, London, 1962, p 96.

(7) (a) Precise conductance measurements of aqueous AgNO_3 solutions from 0.075 to 1.20 M were made since there was a gap in this region¹ and the results were used for computing the concentrations of solutions from diffusion experiments. The values of concentrations (M) and specific conductance ($\text{ohm}^{-1} \text{cm}^{-1} \times 10^2$), respectively, are: 0.0775, 0.8669; 0.1849, 1.908; 0.3899, 3.620; 0.6092, 5.239; 0.9420, 7.396; and 1.1961, 8.830. The quadratic equation: $K = 0.002074 + 0.088093c - 0.012177c^2$ is found to be an excellent expression for the concentration region, 0.02 to 2 M . (b) R. H. Stokes, *J. Am. Chem. Soc.*, **72**, 763 (1950).

Table I: Diffusion Coefficients of AgNO_3 in Water at 25°

\bar{c}, M	c_2, M	c_3, M	c_4, M	Time, sec $\times 10^{-5}$	A/l	$D \times 10^6,$ cm ² /sec
0.0000						1.7675
0.0944	0.0000	0.1436	0.0469	1.792	6.171	1.591
0.1577	0.0613	0.2116	0.1038	2.172	4.670	1.547
0.2543	0.1538	0.3039	0.2048	1.984	6.244	1.510
0.2681	0.1538	0.3361	0.2021	1.494	6.236	1.508
0.3586	0.2572	0.4055	0.3140	2.053	6.260	1.413
0.5100	0.4077	0.5675	0.4539	1.827	6.172	1.364
1.0266	0.9216	1.0914	0.9627	1.732	6.174	1.194
1.5384	1.4181	1.6128	1.4644	1.879	6.175	1.080
2.0403	1.9777	2.0738	2.0075	2.743	6.177	0.984
3.0028	2.9213	3.0454	2.9611	3.293	6.186	0.846
4.0485	3.9661	4.0914	4.0061	3.698	6.189	0.748
5.1590	5.0213	5.2276	5.0933	4.398	6.195	0.667
7.0210	6.9213	7.0972	6.9453	2.454	6.689	0.632
8.9538	8.9347	8.9671	8.9405	3.241	4.708	0.600

Plastic Paint, N. Y.) to inhibit rusting, at 60 rpm, was used for the stirring action. The half-cell reservoirs were closed with 10/20 Teflon-lined capillary bore plugs, to allow a reproducible filling technique (± 0.001 ml) without disturbing the contents of the diaphragm. Calibration of the diffusion cell was after the procedure of Stokes,⁵ using the \bar{D}_c^0 values for KCl reported elsewhere.⁸⁻¹⁰ The cell constant will change with time due to the "wear" of the diaphragm by the stirring bars. Periodic calibrations, and a graph of the cell constant as a function of time (cell life) was used to gain the exact value ($\pm 0.12\%$) for each diffusion experiment. All measurements were made in a glass-front water bath, thermostated at 25° ($\pm 0.003^\circ$). Care was taken to ensure that the diaphragm was horizontal ($\pm 2^\circ$) throughout all measurements.

It was established through a series of exploratory measurements that differential diffusion coefficient data for aqueous AgNO_3 solutions could be obtained by this technique for initial concentration differences up to 35 g/l; the latter was selected for a maximum analytical accuracy; accordingly, an initial concentration difference of 35 g/l between the half-cells was used in all experiments. The initial and final concentrations for the upper half cell, c_2 and c_4 , respectively, and the final concentration for the lower half cell, c_3 are in Table I for the concentration range investigated. The initial concentration for the lower half-cell, c_1 , was gained by the characteristic equation of the cell

$$c_1 = c_3 + (c_4 - c_2)f \quad (1)$$

where f , the cell factor, is given by $(V'' + \frac{1}{2}V)/(V' + \frac{1}{2}V)$. The volumes V' and V'' are the half-cell volumes corrected for the stirrer volumes, and V

is the diaphragm volume. Typical values for f in the present work were 0.96025 and 0.95810, respectively, for the less concentrated and more concentrated solutions. Due cognizance was taken in the design of the stirred-diaphragm cell technique so that diffusion occurred only through the diaphragm pores (*i.e.*, that the solutions are of uniform concentration in each half-cell up to the diaphragm), that the volumes of the two solutions were constant, and that there was no other material transport mechanism (*e.g.*, streaming through pores). As has been shown elsewhere¹¹ for such conditions, the time average diffusion coefficient, \bar{D} , is given by

$$\bar{D} = \frac{1}{kt} \ln \frac{c_1 - c_2}{c_3 - c_4} \quad (2)$$

where c_1 , c_2 , c_3 , and c_4 are the experimental results as discussed above, t is the time of observation, and k is the cell constant. This diffusion constant is also known as the "diaphragm cell integral diffusion coefficient." The cell constant k , defined by $(A/l)(1/V' - 1/V'')$, where A and l are the total cross-sectional pore area and their effective length, respectively, was gained from the calibration experiments, (calibration was repeated every 500 hr of cell life). The variation of A/l with time (cell life, L , hours) thus found was

$$(A/l) = 2.9694 \times 10^{-5}L + 6.0605$$

(8) R. H. Stokes, *J. Am. Chem. Soc.*, **73**, 3527 (1951).

(9) L. J. Gosting, *ibid.*, **72**, 4418 (1950).

(10) H. S. Harned and R. L. Nuttall, *ibid.*, **71**, 1460 (1949).

(11) R. A. Robinson and R. H. Stokes, "Electrolyte Solutions," Butterworth and Co., Ltd., London, 1959.

This expression was used to gain the exact value of A/l for the correct k value in the calculations (eq 2) for each experiment. Over the period of 51 diffusion measurements, the value for cell constant changed about 3% from that of initial calibration. The values for A/l and the results for \bar{D} are also in Table I, and a graph of the $\bar{D} - c^{1/2}$ dependence thus found is in Figure 1a. The results of Firth and Tyrrell⁴ for AgNO_3 together with the results¹² for NH_4NO_3 and LiNO_3 are also shown. The Nernst limiting value D_0 (1.7675×10^{-5} cm²/sec) was obtained using $D_0 = [RT(\nu_1 + \nu_2)\lambda_1^0\lambda_2^0/F^2\nu_1][Z_1(\lambda_1^0 + \lambda_2^0)]$ with 61.90 and 71.42 as the limiting ionic conductances¹³ of Ag^+ and NO_3^- , respectively.

Discussion

Inspection of the results (Figure 1a) shows that agreement with Firth and Tyrrell⁴ is excellent except for the intermediate region of concentrations (0.35 to 3.5 M) where the deviation reaches a maximum of 4% at about 2 M . This occurs in the concentration region where the diffusion coefficients are changing most rapidly with concentration. Since the quantity \bar{D}^0 is decreasing monotonically, the rate of change, $d\bar{D}^0/dc^{1/2}$ is quite large in this concentration range; any inaccuracy in determining this slope, as required in the calculations of Firth and Tyrrell,⁴ would contribute significantly to the ultimate values for the differential diffusion coefficients. The deviation between the two sets of values may be attributed, in large part, to this factor as a possible source of error.

The variation of diffusion coefficients with concentration is largely due to the change of free energy gradient. At higher concentrations, interionic effects, hydration, viscosity, and association are complicating factors. Comparison of the observed diffusion coefficients with those calculated from the theoretical equations of Onsager-Fuoss^{14,15} and of Gordon^{16,16} for strong electrolytes at moderate concentrations (up to 0.5 M) is instructive insofar as such comparisons serve to indicate the direction in which further progress in the extension of the theory can be expected. With a value of 3.03 Å for the ion-size parameter in the Onsager-Fuoss equation, the calculated values agree with the experimental data to within $\pm 0.3 \times 10^{-5}$ cm² sec⁻¹. The Gordon equation consistently gives lower diffusion values (approximately 0.10×10^{-5} cm² sec⁻¹). The lack of specific corrections for electrophoretic effects and use of bulk viscosity value in Gordon's equation undoubtedly contribute to the lower values in the latter treatment.

From the viewpoint of ionic association, the approach of Wishaw and Stokes¹² warrants attention. The

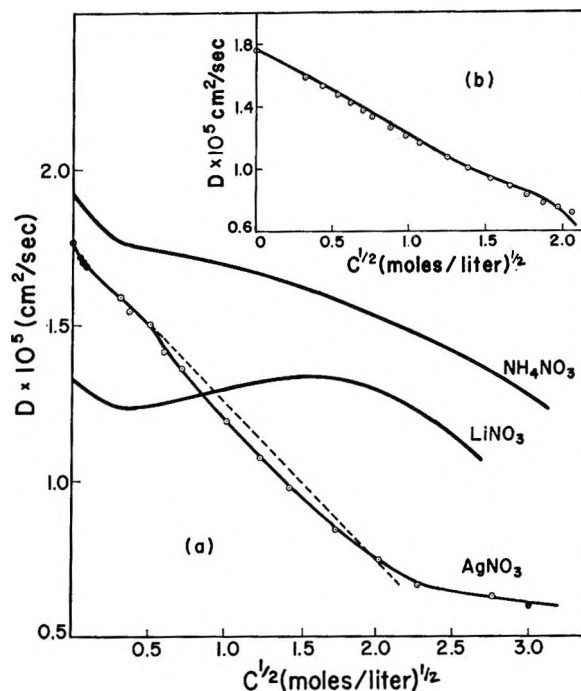


Figure 1. (a) Concentration dependence of diffusion coefficient for AgNO_3 , LiNO_3 , and NH_4NO_3 in water at 25°. Dashed line (—) for AgNO_3 indicates the data of Firth and Tyrrell.⁴ (b) Comparison of the observed and calculated (solid line) diffusion coefficients for AgNO_3 in water.

treatment basically is an extension of Hartley-Crank¹⁷ analysis and leads to the equation

$$D = \left(1 + m \frac{d \ln \gamma_{\pm}}{dm}\right) (1 - 0.018mh) \times \left(1 + 0.018m \left(\frac{2D_{\text{H}_2\text{O}}^*}{D_0} - h\right)\right) \times [\alpha(D_0 + \Delta_1 + \Delta_2) + 2(1 - \alpha)D_{12}] \eta_0/\eta \quad (3)$$

where h is the hydration number; $D_{\text{H}_2\text{O}}^*$ is the self-diffusion coefficient of water; D_{12} is the diffusion coefficient for ion pairs; α is the degree of dissociation; Δ_1 and Δ_2 are the electrophoretic correction terms; and η/η_0 is the relative viscosity. For AgNO_3 , the α values can be gained as a first estimate from the conductance data.¹⁸ To compute the electrophoretic

(12) B. F. Wishaw and R. H. Stokes, *J. Am. Chem. Soc.*, **76**, 2065 (1954).

(13) D. A. MacInnes, T. Shedlovsky, and L. G. Longworth, *ibid.*, **54**, 2758 (1932).

(14) L. Onsager and R. M. Fuoss, *J. Phys. Chem.*, **36**, 2689 (1932).

(15) H. S. Harned and B. B. Owen, "The Physical Chemistry of Electrolytic Solutions," 3rd ed, Reinhold Publishing Corp., New York, N. Y., 1958.

(16) A. R. Gordon, *J. Chem. Phys.*, **5**, 522 (1937).

(17) G. S. Hartley and J. Crank, *Trans. Faraday Soc.*, **45**, 801 (1949).

terms, the value of the ion size parameter, a , was taken as 4.35 Å; *i.e.*, the same as used for the conductance studies in this concentration range.¹⁸ The ion-pair diffusion coefficient, 1.345 was obtained in first approximation by assuming both Ag^+ and NO_3^- ions are spherical and of equal radius. The values for D thus calculated by eq 3, using $h = 0$ and with the viscosity correction taken as unity, are shown in Figure 1b. The agreement with the experimental results is $\pm 2.5\%$ at all concentrations up to 4.0 M . While it is thus possible to give a reasonable account for the experimental diffusion data over a wide concentration range, it is doubtful if much physical significance should be attached to the above values for h and the viscosity correction in view of the known hydration effects and viscosity-diffusive flow correlations.

The existence of ion pairs receives support from conductance data.^{2,18} Additional evidence for ion pairs in aqueous solutions of various nitrates is also found in the recent studies on the vibrational spectroscopy of these solutions.^{19,20} The removal of degeneracy of the asymmetric stretching vibration for the NO_3^- ion in aqueous solutions has been advanced as a spectroscopically based operational criterion for ion-pair formation.^{19,20} This is observed for AgNO_3 solutions for concentrations above 0.75 M .¹⁹

As seen in Figure 1a, the concentration dependence of D for AgNO_3 solutions differs markedly from other nitrates (*e.g.*, LiNO_3 , NH_4NO_3) and the cause is not immediately apparent. While at low concentrations, the trend in D is consistent with the trend of viscosities^{1,21} (*i.e.*, $\eta/\eta_0: \text{LiNO}_3 > \text{AgNO}_3 > \text{NH}_4\text{NO}_3$, all concentrations), beyond 0.72 M the D values for AgNO_3 fall well below those for LiNO_3 . A possible explanation is seen in the thermodynamic nonideality of these electrolytes. Dividing the observed D value by the corresponding activity factor,¹¹ $\partial \ln a_{\pm} / \partial \ln m$, gives a quantity proportional to the actual mobility of the diffusing solute, D_{cor} . The D_{cor} values fall in the order $\text{NH}_4\text{NO}_3 > \text{AgNO}_3 > \text{LiNO}_3$. Apparently, the high hydration of LiNO_3 results in greatly increased activity coefficients and hence in high values for D_{obsd} , whereas for AgNO_3 the smaller activity coefficients undoubtedly contribute to the much lower D_{obsd} values at concentrations above 0.72 M .

The concentration dependence of the empirical mobility ratio, D_{cor}/Λ (ohm sec⁻¹) is illustrated in Figure 2. The variation of this factor with increasing

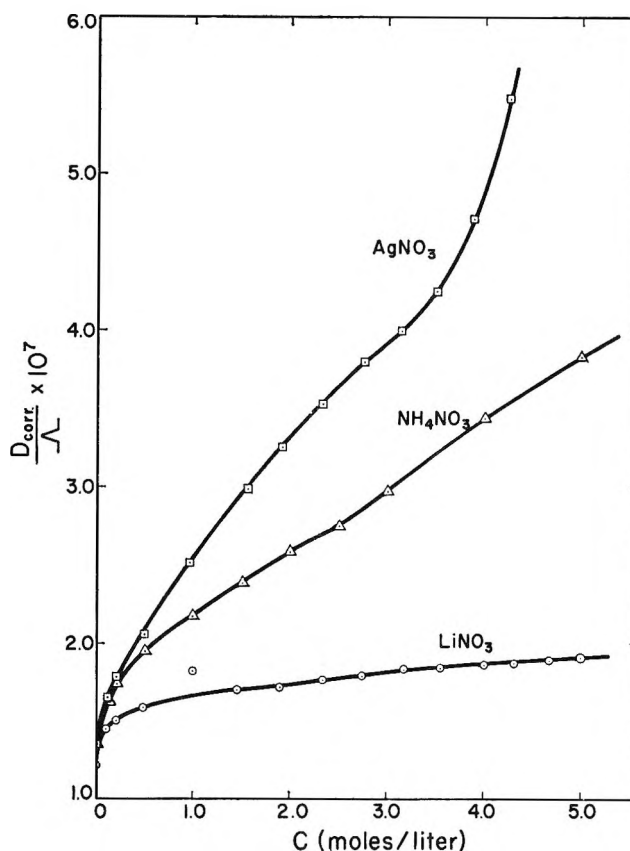


Figure 2. Concentration dependence of mobility ratio, D_{cor}/Λ for AgNO_3 , NH_4NO_3 , and LiNO_3 in water at 25°C.

concentrations is very marked for AgNO_3 and for NH_4NO_3 relative to LiNO_3 . While the possible use of this ratio as a criterion for pronounced ion-ion interactions suggests itself, the applicability of this criterion for diagnosis of ion pairs and possibly higher aggregates must await further studies in concentrated salt solutions.

Acknowledgments. Dr. F. J. Kelly is thanked for the design of the diffusion cells and experimental techniques, and for helpful and constructive discussions in the initial phases of this study. This work was aided by a grant from the Office of Saline Water, U. S. Department of the Interior, Washington, D. C.

- (18) A. N. Campbell and E. M. Kartzmark, *Can. J. Chem.*, **33**, 887 (1955).
- (19) H. Lee and J. K. Wilmshurst, *Australian J. Chem.*, **17**, 943 (1964).
- (20) R. E. Hester and R. A. Plane, *Inorg. Chem.*, **3**, 769 (1964).
- (21) A. N. Campbell, G. H. Debus, and E. M. Kartzmark, *Can. J. Chem.*, **33**, 1508 (1955).

Dissociation of Acetic Acid- d_3 in Aqueous Solution and Related Isotope Effects from 0 to 50°

by Maya Paabo, Roger G. Bates, and R. A. Robinson

National Bureau of Standards, Washington, D. C. (Received September 7, 1965)

The dissociation constant of acetic acid- d_3 (CD_3COOH) in ordinary water (H_2O) has been determined by emf methods at 11 temperatures from 0 to 50°. From the variation of the dissociation constant with temperature the changes of enthalpy, entropy, and heat capacity for the dissociation process have also been derived and compared with similar data for ordinary protoacetic acid in aqueous solution. The pK of the deuterioacetic acid is from 0.012 to 0.016 unit greater than that of the protoacid, and the temperature (22.9°) at which the dissociation constant passes through a maximum is only slightly higher than the corresponding temperature (22.4°) found earlier for the protoacid. Moreover, the changes of enthalpy, entropy, and heat capacity accompanying the dissociation of the two acids at room temperature do not appear to differ by an amount significantly greater than the combined errors of the two determinations.

Introduction

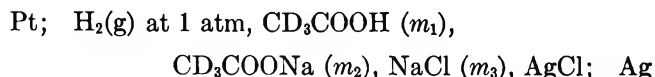
The measurement of the dissociation constant of acetic acid in aqueous solution is an excellent example of concordance between the conductance method¹ and the emf method² for the quantitative study of the ionization of a weak acid. We have recently³ determined the dissociation constant of acetic acid in deuterium oxide. The solution was made by dissolving "ordinary" acetic acid in deuterium oxide, and there should have been complete exchange of the ionizable hydrogen with deuterium from the solvent but, under the conditions of the experiment, no exchange with the hydrogen atoms in the methyl group. Thus it was the dissociation constant of CH_3COOD which was determined.

We have now measured the dissociation constant of acetic acid- d_4 in "ordinary" water as solvent. Again, there should be complete exchange between the ionizable deuterium of the acid and hydrogen in the water molecule but no exchange with deuterium in the deuterated methyl group. Hence, we should obtain the dissociation constant of CD_3COOH from measurements of this sort.

The conductance method has been used recently⁴ to compare the dissociation constants of the two formic acids, $DCOOH$ and $HCOOH$, in aqueous

solution, and it has been found that the pK of the deuterio acid is higher by 0.035 unit. This agrees closely with the difference (0.037) predicted⁵ from a study of the zero-point energies and vibrational frequencies of the two acids in the vapor phase. Streitwieser and Klein⁶ have shown, again by the conductance method, that the effect of deuterium substitution is smaller in acetic, pivalic, and benzoic acids, the difference in pK value being only 0.014 for acetic acid. However, another study,⁷ using potentiometric titration, gave 0.026 as the pK difference for acetic acid.

Our present measurements on CD_3COOH in H_2O , using the cell



- (1) D. A. MacInnes and T. Shedlovsky, *J. Am. Chem. Soc.*, **54**, 1429 (1932).
- (2) H. S. Harned and R. W. Ehlers, *ibid.*, **54**, 1350 (1932); **55**, 652 (1933).
- (3) R. Gary, R. G. Bates, and R. A. Robinson, *J. Phys. Chem.*, **69**, 2750 (1965).
- (4) R. P. Bell and W. B. T. Miller, *Trans. Faraday Soc.*, **59**, 1147 (1963).
- (5) R. P. Bell and J. E. Crooks, *ibid.*, **58**, 1409 (1962).
- (6) A. Streitwieser, Jr., and H. S. Klein, *J. Am. Chem. Soc.*, **85**, 2759 (1963).
- (7) E. A. Halevi, M. Nussim, and A. Ron, *J. Chem. Soc.*, 866 (1963).

complement the conductance studies at 25°. In addition, we have extended the measurements over a temperature range of 0 to 50° so that other thermodynamic quantities for the dissociation process can be obtained.

Experimental Section

A sample of acetic acid- d_4 was obtained through commercial channels. The composition, as determined by gas chromatography, was 96.7 (wt) % acetic acid, 3.0% acetic anhydride, 0.2% malonic acid, and 0.06% of an unknown impurity. The impurity was not a saturated carboxylic or dicarboxylic acid but was probably a compound of low molecular weight containing oxygen. The sample was distilled at atmospheric pressure in a still equivalent to 60–70 theoretical plates, and ten fractions were collected. The first five fractions, which were rejected, contained considerable amounts of impurity. The sixth fraction contained about 0.05% of impurity. The last four fractions contained only acetic acid, acetic anhydride, and a trace of water.

The last five fractions were combined and used to make an approximately 0.2 M solution in "ordinary" water. A portion of this solution was standardized by potentiometric titration with carbonate-free sodium hydroxide which, in turn, had been standardized against a solution of hydrochloric acid; this acid had been assayed by gravimetric silver chloride analysis. The remainder of the acetic acid- d_4 solution was then treated with a weighed amount of sodium carbonate to neutralize about half the acid, and an equivalent amount of sodium chloride was added to give a stock solution approximately 0.1 M in acetic acid, 0.1 M in sodium acetate, and 0.1 M in sodium chloride. The carbonate was a preparation used in an earlier study,³ and the sodium chloride was a portion of that used earlier in isopiestic work.⁸ The stock solution of acetic acid, sodium acetate, and sodium chloride was diluted by weight to give a series of solutions for cell measurements.

The cell used for the emf measurements was that described previously.⁹ Hydrogen gas was used in this cell in place of deuterium gas and "ordinary" water was the solvent instead of deuterium oxide. The emf was measured over a temperature range in the order 25, 10, 5, 0, 15, 20, 25, 30, 35, 40, 45, 50, and 25° for one set of results and in the order 25, 0, 5, 10, 15, 20, 25, 30, 35, 40, 45, 50, and 25° for the other set. The maximum differences among the three measurements at 25° were, for 11 solutions, 0.07, 0.02, 0.04, 0.00, 0.04, 0.06, 0.08, 0.06, 0.09, 0.06, and

0.02 mv. A value of 0.09 mv corresponds to a difference of 0.0015 in pK .

Results and Calculations

The measured values of the emf, corrected to 1 atm of hydrogen, are given in Table I. The emf of the cell is given by the expression

$$(E - E^\circ)/k + \log m_3 = -\log(a_{H^+}\gamma_{Cl^-}) \quad (1)$$

where m is molality and k is written for $(RT \ln 10)/F$. Combining this with the mass action equation for the dissociation constant

$$K = a_{H^+} \frac{m_2 + m_{H^+} \gamma_{Ac^-}}{m_1 - m_{H^+} \gamma_{HAc}} \quad (2)$$

we obtain

$$\begin{aligned} pK' &\equiv pK - \log \frac{\gamma_{Cl^-} \gamma_{HAc}}{\gamma_{Ac^-}} \\ &= \frac{(E - E^\circ)}{k} + \log m_3 + \log \frac{m_1 - m_{H^+}}{m_2 + m_{H^+}} \quad (3) \end{aligned}$$

For all 11 solutions, $m_2 = m_3$ and $m_2 = 1.0012m_1$.

In order to correct the ratio m_1/m_2 to $(m_1 - m_{H^+})/(m_2 + m_{H^+})$, m_{H^+} was estimated by the equation

$$(E - E^\circ)/k + \log m_3 = -\log m_{H^+} - 2 \log \gamma_{HCl} \quad (4)$$

The value of γ_{HCl} was assumed to be equal to the mean activity coefficient of hydrochloric acid in its own solution¹⁰ at the same total ionic strength. This correction was made to all the measurements but its neglect would have affected pK by 0.0064 in the most dilute solution, by 0.0025 in the next most dilute solution, and by only 0.0004 in the most concentrated solution.

As was expected, the term $\log (\gamma_{Cl^-} \gamma_{HAc}/\gamma_{Ac^-})$ proved to be small, and almost horizontal, straight-line plots of pK' vs. ionic strength ($2m_2 + m_{H^+}$) were obtained. Extrapolation to zero ionic strength was made by the method of least squares. Values of the intercepts (pK) obtained in this way are given in Table II. The standard deviations (σ_i) of the intercepts were 0.001 at each temperature.

Discussion

The experimental values of pK have been fitted, by the method of least squares, to the equation¹¹

(8) V. E. Bower and R. A. Robinson, *J. Phys. Chem.*, **67**, 1524 (1963).

(9) R. Gary, R. G. Bates, and R. A. Robinson, *ibid.*, **68**, 1186 (1964).

(10) H. S. Harned and R. W. Ehlers, *J. Am. Chem. Soc.*, **55**, 2179 (1933).

Table I: Electromotive Force of the Cell

H ₂ (g) at 1 atm, CD ₃ COOH(<i>m</i> ₁), CD ₃ COONa(<i>m</i> ₂), NaCl(<i>m</i> ₃), AgCl, Ag (in volts) (<i>m</i> ₂ = <i>m</i> ₃ = 1.0012 <i>m</i> ₁)											
<i>m</i> ₂ = <i>m</i> ₃	0°	5°	10°	15°	20°	25°	30°	35°	40°	45°	50°
0.002539	0.63758	0.64183	0.64604	0.65040	0.65448	0.65865	0.66276	0.66670	0.67095	0.67509	0.67910
0.008033	0.61021	0.61412	0.61776	0.62147	0.62518	0.62879	0.63242	0.63605	0.63960	0.64315	0.64671
0.009879	0.60538	0.60911	0.61272	0.61641	0.61998	0.62348	0.62708	0.63055	0.63406	0.63758	0.64103
0.01511	0.59530	0.59882	0.60231	0.60578	0.60915	0.61248	0.61587	0.61919	0.62247	0.62576	0.62906
0.01992	0.58894	0.59225	0.59563	0.59900	0.60223	0.60543	0.60872	0.61188	0.61509	0.61830	0.62144
0.02487	0.58360	0.58694	0.59014	0.59337	0.59653	0.59965	0.60278	0.60589	0.60896	0.61201	0.61508
0.03021	0.57921	0.58244	0.58558	0.58873	0.59177	0.59481	0.59788	0.60088	0.60387	0.60689	0.60986
0.03497	0.57575	0.57893	0.58200	0.58508	0.58811	0.59105	0.59404	0.59700	0.59992	0.60284	0.60576
0.04062	0.57226	0.57539	0.57839	0.58143	0.58437	0.58721	0.59018	0.59303	0.59591	0.59879	0.60163
0.04526	0.56981	0.57286	0.57582	0.57878	0.58167	0.58448	0.58741	0.59021	0.59303	0.59590	0.59869
0.05059	0.56717	0.57019	0.57306	0.57597	0.57883	0.58160	0.58446	0.58725	0.59000	0.59274	0.59551

Table II: Dissociation Constants of Acetic Acid

Temp, °C	pK of CD ₃ COOH in H ₂ O		pK of CH ₃ COOH in H ₂ O	ΔpK ^b
	Obad	Calcd ^a		
0	4.796	4.795	4.780	0.015
5	4.785	4.784	4.770	0.014
10	4.777	4.778	4.763	0.015
15	4.775	4.774	4.758	0.016
20	4.771	4.772	4.756	0.016
25	4.772	4.771	4.756	0.015
30	4.774	4.773	4.758	0.015
35	4.776	4.777	4.762	0.015
40	4.782	4.783	4.769	0.014
45	4.790	4.790	4.777	0.013
50	4.799	4.799	4.787	0.012

^a Calculated by the equation, $pK = 1079.37/T - 2.5200 + 0.012313T$. ^b $\Delta pK = pK(\text{CD}_3\text{COOH}) - pK(\text{CH}_3\text{COOH})$.

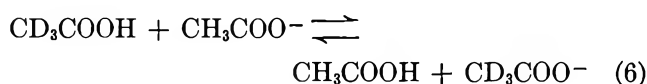
$$pK = A_1/T - A_2 + A_3T \quad (5)$$

where T is the temperature in °K, giving $A_1 = 1079.37$, $A_2 = 2.5200$, and $A_3 = 0.012313$. The pK calculated in this way is given in the third column of Table II. Similar values for "ordinary" acetic acid are given in the next column; these are from the data of Harned and Ehlers,² which give $A_1 = 1170.48$, $A_2 = 3.1649$, and $A_3 = 0.013399$.¹² The last column gives the difference between the pK values of the two acetic acids, that of the deuterated acid being the higher. The difference at 25° is 0.015; this compares well with the value of 0.014 ± 0.002 obtained from conductance data by Streitwieser and Klein.⁶

The numerical values of A_1 , A_2 , and A_3 for acetic acid-*d*₃ permit the calculation of the standard molal enthalpy, entropy, and heat capacity changes on dissociation. These are given in Table III where they are compared with similar quantities for "ordinary" acetic acid both in water and in deuterium oxide as

solvent. A comparison of the pK data in Table II with those for CH₃COOD in D₂O given previously¹³ shows that the pK value for all three dissociation processes has a minimum value near room temperature. Consequently, as is clear from Table III, for each of the processes there is a temperature close to room temperature where $\Delta H^\circ = 0$. The temperature of this minimum pK value or maximum K value in °K is $(A_1/A_3)^{1/2}$, and the value of $pK(-\log K_{\max})$ at this temperature is $A_2 - 2(A_1A_3)^{1/2}$. These values are given in Table III.

It will be seen that there is a marked difference between these quantities for CD₃COOD in D₂O and for CH₃COOH in H₂O, but the difference is comparatively small if the same quantities for CH₃COOH and CD₃COOH in H₂O are compared. Indeed, the latter differences correspond to the exchange reaction



The thermodynamic quantities for this exchange reaction (designated Δ_{ex}) are given in the last column of Table III. The entropy change is seen to be virtually zero. The change in heat capacity is a second differential of the experimental data; consequently, it would be unwise to attribute any significance to the value of 3.0 cal deg⁻¹ mole⁻¹. Likewise, the enthalpy changes at 0 and 25° are probably insignificant; they correspond to changes of 0.001 in ΔpK (see Table II). However, ΔpK has fallen to 0.012 at 50° and, cor-

(11) H. S. Harned and R. A. Robinson, *Trans. Faraday Soc.*, **36**, 973 (1940).

(12) R. A. Robinson and R. H. Stokes, "Electrolyte Solutions," 2nd ed, Butterworth and Co., Ltd., London, 1959, p 517.

(13) See Table II of ref 3.

Table III: Thermodynamic Quantities for the Dissociation of Acetic Acid (ΔH° in cal mole⁻¹; ΔS° and ΔC_p° in cal deg⁻¹ mole⁻¹; 1 cal = 4.1840 joules)

	CD ₃ COOH in H ₂ O	CH ₃ COOH in H ₂ O	CH ₃ COOD in D ₂ O	Δ_{ex}
ΔH° at 0°	735	781	1192	-46 ^a
25°	-69	-98	275	29
50°	-945	-1047	-730	102
ΔS° at 0°	-19.2	-18.8	-20.2	-0.4
25°	-22.1	-22.1	-23.4	0
50°	-24.9	-25.1	-26.6	0.2
ΔC_p° at 25°	-33.6	-36.6	-38.6	3.0
t_{max}	22.9°	22.4°	32.0°	...
-Log K_{max}	4.771	4.756	5.3096	...

^a Quantities in this column are for the exchange reaction: CD₃COOH + CH₃COO⁻ ⇌ CH₃COOH + CD₃COO⁻.

respondingly, the enthalpy change at 50° is 102 cal mole⁻¹. This increase, which may be significant, will be examined further by measuring the pK value of acetic acid-d₄ in deuterium oxide.

Acknowledgments. The authors are indebted to Dr. R. T. Leslie for the fractional distillation of the acetic acid-d₄ and to Mr. E. E. Hughes for the analyses by gas-liquid partition chromatography.

Vibrational Spectra of the Hydrogen Dihalide Ions. III. F⁻HCl, F⁻HBr, and F⁻HI

by J. C. Evans and G. Y-S. Lo

Chemical Physics Research Laboratory, The Dow Chemical Company, Midland, Michigan 48640
(Received September 13, 1965)

Salts of these mixed hydrogen dihalide anions were prepared by treating solid tetraalkylammonium halides with gaseous HF. Infrared absorption spectra demonstrated that the anions are stable in the solid phase and also in solution in acetonitrile and in methylene chloride. The three fundamental vibrational modes of each anion were assigned; approximate force constants were calculated. Qualitatively, it was concluded that the HF bonds in the mixed anions are much weaker than that in HF monomer.

A notable gap exists in the literature concerned with the XHY series of ions, where X and Y are halogen atoms with one being fluorine. Only the very stable, symmetrical FHF⁻ ion has been reported and no reference to the preparation of F⁻HCl, F⁻HBr, and F⁻HI could be found. The molecular orbital description of

the hydrogen bond, which Pimentel has demonstrated to be qualitatively appealing in the case of FHF⁻,¹ suggests that, because the fluorine 2p-orbitals are not

(1) G. C. Pimentel and A. L. McClellan, "The Hydrogen Bond," Freeman and Co., San Francisco, Calif., 1960, p. 236.

Table I: Infrared Absorption Bands of $[\text{F}-\text{H}-\text{X}]^-$ ^a

$[\text{F}-\text{H}-\text{Cl}]^-$		$[\text{F}-\text{H}-\text{Br}]^-$		$[\text{F}-\text{H}-\text{I}]^-$		Assignment
Solid	Solution	Solid	Solution	Solid	Solution	
2710 ± 20 vs	~2850 vs	~2900 vs	~3050 vs	3145 ± 15 vs	~3200	ν_3
1588 ± 3 m	1570 m					$2\nu_2$
863 ± 2 ms	835 ms	740 ± 10 s	220 ± 3 w	635 ± 3 m	625	ν_2
823 ± 2 ms						
275 ± 3 w			~215 w	180 ± 3 w		ν_1

^a Salts examined were $(\text{C}_2\text{H}_5)_4\text{N}^+\cdot\text{Cl}^-\text{HF}$, $(\text{C}_2\text{H}_5)_4\text{N}^+\cdot\text{Br}^-\text{HF}$, and $(\text{C}_4\text{H}_9)_4\text{N}^+\cdot\text{I}^-\text{HF}$. Abbreviations: vs = very strong; m = medium; w = weak. Solvents used were methylene chloride in 3000-cm.⁻¹ region and acetonitrile in 700- and 220-cm.⁻¹ regions. For ν_3 of $\text{F}\bar{\text{H}}\text{Br}$, cation bands interfere seriously.

well matched energetically with the valence p-orbitals of the other halogens, the bonding in the mixed $\text{F}\bar{\text{H}}\text{X}$ ions should not be strong. The purpose of this note is to present infrared spectroscopic data which demonstrate that the $\text{F}\bar{\text{H}}\text{X}$ ions are stable in the solid phase in certain salts and also in solutions of these salts in nonaqueous solvents. The three fundamental vibrational modes of each of the three ions, $\text{F}\bar{\text{H}}\text{Cl}$, $\text{F}\bar{\text{H}}\text{Br}$, and $\text{F}\bar{\text{H}}\text{I}$, are also reported (Table I).

The dihalide salts were prepared by slowly treating crystalline tetraalkylammonium halides with HF gas (99.9% min., The Matheson Co.) at 25° in a polyethylene system²; the halides were Eastman grade materials (Eastman Kodak Co.) further purified by recrystallization and careful drying. Reaction occurred readily and was allowed to proceed until the ratio of salt to HF approached unity; this ratio was determined by titrating aqueous solutions of the product with standard alkali. Infrared absorption spectra of the partly converted salts were also recorded and the growth of the $\text{F}\bar{\text{H}}\text{X}$ concentration was readily apparent. In each case the band positions were independent of the anion concentration. Figure 1 illustrates the anion bands redrawn from spectra of suspensions of the solid salts in Nujol; cation bands, which are readily identified, and Nujol bands are omitted. The anion bands were also observed in solutions of the salts in methylene chloride and in acetonitrile.

The anion bands are readily assigned to the three fundamental modes expected for the linear structure which we shall assume for these ions; the assignments are summarized in Table I. The strong, very broad bands (half-widths approximately 250 cm.⁻¹) observed near 3000 cm.⁻¹ are assigned to ν_3 for each anion; this is the antisymmetric stretching mode which is largely an axial motion of the hydrogen between the two halogens. In the symmetrical anion $\text{F}\bar{\text{H}}\text{F}$, which has a hydrogen-bond energy of about 37 kcal./mole,³

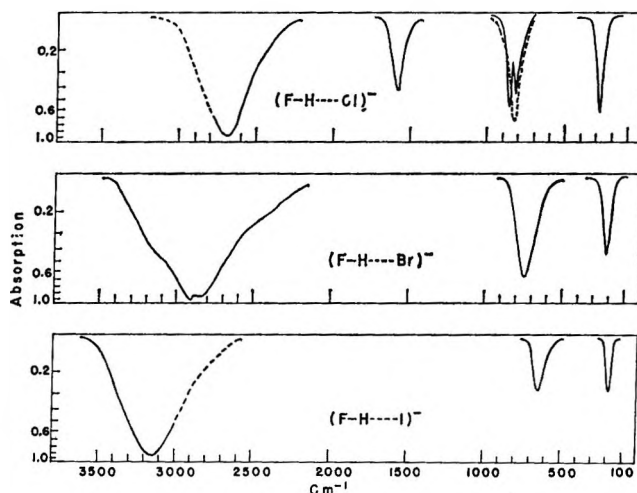


Figure 1. The infrared absorption bands of the mixed $\text{F}\bar{\text{H}}\text{X}$ species redrawn from spectra of salts suspended in hydrocarbon (Nujol) mulls; for $\text{F}\bar{\text{H}}\text{Br}$, a Fluorolube mull was used in the 3000-cm.⁻¹ region. The low-frequency bands (below 300 cm.⁻¹) are not drawn to the same scale; they are weaker, and much thicker mulls were necessary.

this mode appears near 1450 cm.⁻¹,⁴ whereas the corresponding mode for HF polymers with hydrogen-bond energy of about 7 kcal./mole,⁵ appears in the 3400-cm.⁻¹ region.⁶ This comparison suggests that the hydrogen-bond energies of these mixed dihalide anions are of the order of 10 kcal./mole and that the energy increases in the series, $\text{F}\bar{\text{H}}\text{I} < \text{F}\bar{\text{H}}\text{Br} < \text{F}\bar{\text{H}}\text{Cl}$.

(2) When HCl gas reacted with tetramethylammonium fluoride solid, the complex anion produced was identified by its infrared spectrum as the hydrogen difluoride ion.

(3) S. A. Harrell and D. H. McDaniel, *J. Am. Chem. Soc.*, **86**, 4497 (1964).

(4) G. L. Coté and H. W. Thompson, *Proc. Roy. Soc. (London)*, **A210**, 206 (1951).

(5) See ref. 1, p. 212.

(6) R. D. Shelton and A. H. Nielsen, *J. Chem. Phys.*, **39**, 1312 (1951).

The frequencies of the bands assigned to ν_2 , the degenerate bending mode, which is again largely a motion of the hydrogen atom, are in accord with this interpretation. The value of ν_2 increases in frequency in the same order as that of ν_3 decreases, and the frequencies of the two modes are almost linearly related for the three anions. For one salt, the tetraethylammonium protium fluorochloride, the ν_2 band is a well-defined doublet in the solid spectrum, but is a single band at an intermediate position in the solution spectrum; also, in the solid-phase spectrum of the salt of another cation, tetramethylammonium, the band is single and at an intermediate position. Presumably, the degeneracy of ν_2 is split in the solid tetraethylammonium salt.

The third mode, the symmetric stretching mode ν_1 , is essentially an oscillation of the FH against the heavier halogen. For $\overline{\text{FHF}}$, where ν_1 is a slightly different mode and the hydrogen is stationary, ν_1 is at 600 cm.^{-1} . The mixed anions with greater reduced masses and much weaker halogen to halogen bonding should show much lower ν_1 frequencies. A prominent absorption band, which is not assignable to the cation or to lattice modes, appears in the spectrum of each salt examined. The band behaves qualitatively as expected and shifts to lower wave number in the series, chloride, bromide, to iodide; the diatomic, harmonic-oscillator approximation gives values of

0.57, 0.46, and 0.33 mdyne/Å. for the force constants in the same series. These do not, of course, reflect the bonding energies directly. More significant is the triatomic harmonic-oscillator approximation, but the data allow only two force constants of the bond-stretching potential function to be determined; these are k_1 and k_2 , the F-H and the H-X bond stretching constants; k_{12} , the interaction force constant, is very significant for the $\overline{\text{FHF}}$ ion⁷ and should undoubtedly be considered for the mixed anions. However, for qualitative purposes we shall consider the k_1 and k_2 values obtained (in units of mdyne/Å.) when k_{12} is assumed to be zero. These are: for $\overline{\text{FHFCl}}$, $k_1 = 3.50$, $k_2 = 0.67$; for $\overline{\text{FHFBr}}$, $k_1 = 4.23$, $k_2 = 0.50$; for $\overline{\text{FHF I}}$, $k_1 = 5.22$, $k_2 = 0.35$. Qualitative comparisons with monomeric HF, $k_1 = 8.78$, are probably valid. The decrease in k_1 with increasing hydrogen-bond strength is well known; the concurrent increase in k_2 is consistent. The extent of the decrease in k_1 suggests that the H-F bond is modified considerably in the anions and that, in the molecular orbital picture,¹ the heavier halide ion participates to a considerable extent in the bonding orbital with the accompaniment of considerable transfer of charge to the fluorine atom.

(7) W. B. Person, G. R. Anderson, J. N. Fordemwalt, H. Stammreich, and R. Forneris, *J. Chem. Phys.*, 15, 908 (1961).

Kinetics of the Isomerization of Perfluorovinylcyclopropane and the Pyrolysis of Perfluoroallylcyclopropane

by Ronald A. Mitsch and Erwin W. Neuvar

Contribution No. 361 from the Central Research Laboratories, Minnesota Mining and Manufacturing Company, Saint Paul, Minnesota 55119 (Received September 13, 1965)

The synthesis and identification of perfluorovinylcyclopropane and perfluoroallylcyclopropane are described. The kinetics of the thermal isomerization of perfluorovinylcyclopropane to perfluorocyclopentene has been studied in the high-pressure region and appears to be a clean homogeneous unimolecular isomerization with no side reactions. The rate constant was found to be k (sec^{-1}) = $10^{13.9 \pm 0.2} \exp(-34,600 \pm 400/RT)$. The kinetics of the pyrolysis of perfluoroallylcyclopropane, in which difluorocarbene is eliminated and perfluoro-1,4-pentadiene is formed, has also been studied. The reaction appears to be homogeneous and unimolecular in nature, and the rate constant is given by k (sec^{-1}) = $10^{14.8 \pm 0.2} \exp(42,700 \pm 500/RT)$. The decrease in activation energy for the thermal reactions of perfluorocyclopropanes compared to hydrocarbon cyclopropanes is discussed, primarily in terms of increased ring strain in the perfluorocyclopropanes.

Introduction

The thermal isomerization of hydrocarbon cyclopropanes has been investigated quite thoroughly in the past. For example, the rate constant for the unimolecular isomerization of vinylcyclopropane to cyclopentene is given by k (sec^{-1}) = $10^{13.5} \exp(-49,600/RT)$.¹ Recently, however, the effect of fluorine substitution upon molecular properties is an area which has been receiving increased attention. Thus, the thermal isomerization of monofluorocyclopropane, involving hydrogen migration to the four possible monofluoropropenes, has been shown to have a normal preexponential factor and an activation energy of 61.0 kcal mole⁻¹.² In the only study in which direct comparison between hydrocarbon and perfluorocarbon systems can be made, Schlag and Peatman³ have shown that replacement of hydrogen by fluorine reverses the isomerization equilibrium in the 1,3-butadiene-cyclobutene system. To date, quantitative studies on perfluorinated cyclopropane systems have not been reported. The object of this paper is to describe the synthesis of perfluorovinyl- and perfluoroallylcyclopropane and the kinetics of thermal isomerization and pyrolysis, respectively.

Results

Synthesis. The addition of difluorocarbene to perfluoroolefins is not without precedent. The pyrolysis of difluorodiazirine,^{4a} as well as trifluoromethyl derivatives of iron,^{4b} phosphorus,^{4c} tin,^{4d} and germanium,^{4e} in the presence of tetrafluoroethylene, have all resulted in the formation of perfluorocyclopropane.

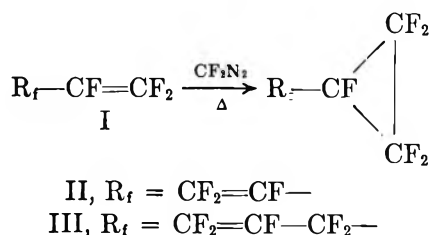
Most of the above techniques would be expected to yield the perfluorocyclopropanes described herein; in the present work, the preparation of II and III was conveniently carried out by pyrolysis of difluorodiazirine at 140° in the presence of a 10 *M* excess of the respective perfluorodiene. No appreciable change in yield or product distribution was observed when either glass ampoules or a stainless steel autoclave was used as the reaction vessel.

(1) H. M. Frey, *Trans. Faraday Soc.*, **58**, 516 (1962).

(2) F. Casas, J. A. Kerr, and A. F. Trotman-Dickenson, *J. Chem. Soc.*, 3655 (1964).

(3) E. W. Schlag and W. B. Peatman, *J. Am. Chem. Soc.*, **86**, 1676 (1964).

(4) (a) R. A. Mitsch, *J. Heterocyclic Chem.*, **1**, 59, 271 (1964); (b) R. B. King, S. L. Stafford, P. M. Treichel, and F. G. A. Stone, *J. Am. Chem. Soc.*, **83**, 3604 (1961); (c) W. Mahler, *Inorg. Chem.*, **2**, 230 (1963); (d) H. C. Clark and C. J. Willis, *J. Am. Chem. Soc.*, **82**, 1888 (1960); (e) H. C. Clark and C. J. Willis, *ibid.*, **84**, 898 (1962).



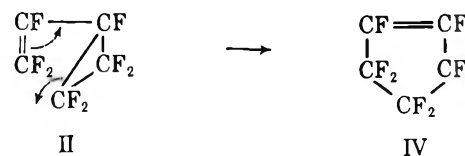
In the addition reaction of difluorocarbene to perfluoro-1,3-butadiene, initial experiments were carried out by heating the reactants for 4 hr at 140°. Under these conditions the C₅F₈ product mixture, obtained in an 85% yield, was a 2:1 mixture of II and perfluorocyclopentene (formed by thermal isomerization of II). Although the yield was decreased slightly by modification of the experimental conditions (140°, 3 hr), the product mixture was upgraded to approximately 95% II. The separation of these C₅F₈ isomers is very difficult. The only column found to be effective for vapor phase chromatography separation was composed of 25% dimethylformamide on Chromosorb P.

In a manner analogous to the reaction with perfluoro-1,3-butadiene, difluorocarbene was generated in the presence of perfluoro-1,4-pentadiene at 140°. The corresponding cyclopropane, perfluoroallylcyclopropane (III), was obtained in a 34% yield (based on CF₂-N₂).

Both II and III were identified by infrared and F¹⁹ nuclear magnetic resonance spectral measurements and elemental analyses. The infrared spectrum of II shows characteristic absorptions at 6.56 and 5.62 μ due to the presence of the perfluorocyclopropyl moiety^{4a} and unsaturation, respectively. The corresponding bands for perfluoroallylcyclopropane appear at 6.55 and 5.55 μ. The F¹⁹ nuclear magnetic resonance spectra are consistent^{4a} with the assigned structures and are recorded in Table IV.

The lack of quantitative data on the pyrolysis of perfluorocyclopropanes as well as the observation that perfluorocyclopentene (IV) is an isolable product from the reaction of difluorocarbene with perfluoro-1,3-butadiene led to a study of the thermal behavior of II and III.

Kinetics (Perfluorovinylcyclopropane Isomerization). The thermal isomerization of perfluorovinylcyclopropane to perfluorocyclopentene was studied in a 90-cc monel cylinder in a temperature range of 131–183° and a pressure region of 1–90 mm. This was confirmed to be in the high-pressure region⁵ for the reaction. Authentic samples of perfluorovinylcyclopropane and perfluorocyclopentene were prepared and identified by infrared and F¹⁹ nmr spectral measurements and elemental analyses. The F¹⁹ nmr spectrum



of perfluorocyclopentene obtained by the pyrolysis of perfluorovinylcyclopropane was identical with that which has been reported.⁶ The sample of perfluorovinylcyclopropane (II) which was used throughout the study initially contained about 5% of IV and 10% of CF₃Cl (used as an internal standard to correct the vpc data for instrument drift and sample depletion).

In all cases, the first-order rate constants were determined from plots of log concentration of II *vs.* time. The reaction was monitored to at least 90% completion at each temperature and did not deviate from linearity. The rate constants were calculated by the least-squares method. Table I contains values for the observed rate constants over the described temperature range. The consistency of *k* at the various temperatures and the fact that rate data showed a first-order dependence over greater than a 100-fold variation in pressure (see Figure 1 for a semi-log plot of concentration *vs.* time for run 9 in Table I) illustrates that the rate equation is satisfactory.

Table I: Isomerization of Perfluorovinylcyclopropane

Run	Temp., °C	<i>k</i> _{obsd.} , sec ⁻¹ × 10 ⁴
1 ^a	131.3	0.17
2	141.9	0.51
3	152.2	1.35
4	160.9	3.05
5	172.7	9.06
6	183.1	22.76
7 ^b	152.2	1.38
8 ^c	152.2	1.44
9 ^d	155.1	1.84
10 ^e	152.2	1.35

^a All runs were at an initial pressure of 90 mm and *S/V* = 1.4 cm⁻¹ unless otherwise indicated. Only runs 1–6 were used in the calculation of the Arrhenius parameters. Uncertainty limits (90% confidence level) of *k*_{obsd.} are estimated from least-squares analysis to be ±5%. ^b *S/V* = 10 cm⁻¹. ^c 10% NO added. ^d Initial pressure was 3 mm; no change in linearity when followed to 97% completion. See Figure 1. ^e Rate constant calculated from the formation of perfluorocyclopentene.

(5) S. W. Benson, "The Foundations of Chemical Kinetics," McGraw-Hill Book Co., Inc., New York, N. Y., 1960, Chapter 11.

(6) Technical Information from the Laboratories of Varian Associates, Palo Alto, Calif., Vol. 1, No. 2, p 3.

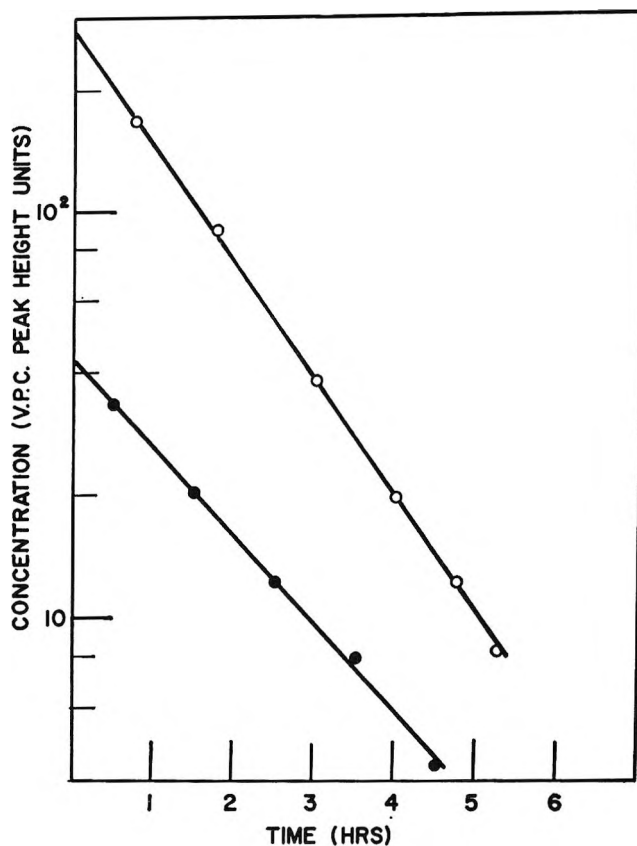


Figure 1. Concentration (vpc peak height units) vs. time: run 9 in Table I, O; run 8 in Table II, ●.

The possibility of polymerization or other side reactions was excluded from consideration since there were no extraneous peaks in the vpc trace and the same rate constants were obtained, within experimental error, by monitoring either the disappearance of II or the rate of formation of perfluorocyclopentene (Table I, run 10).

The homogeneity of the reaction was tested with one run in a vessel with a sevenfold greater surface to volume ratio than the normal vessel. No effect was detected at 152.2°, which is in the middle of the temperature range studied here (Table I, run 7).

Furthermore, in order to exclude the possibility of a radical reaction, a run was carried out in the presence of 10% added nitric oxide (Table I, run 8). The rate constant was not affected by this modification.

Figure 2 shows an Arrhenius plot of the rate constants listed in Table I which fit the equation $k \text{ (sec}^{-1}\text{)} = 10^{13.9 \pm 0.2} \exp(-34,600 \pm 400/RT)$. Thus, it appears that the thermal isomerization of perfluorovinylcyclopropane to perfluorocyclopentene is a homogeneous, unimolecular reaction with no apparent side reactions.

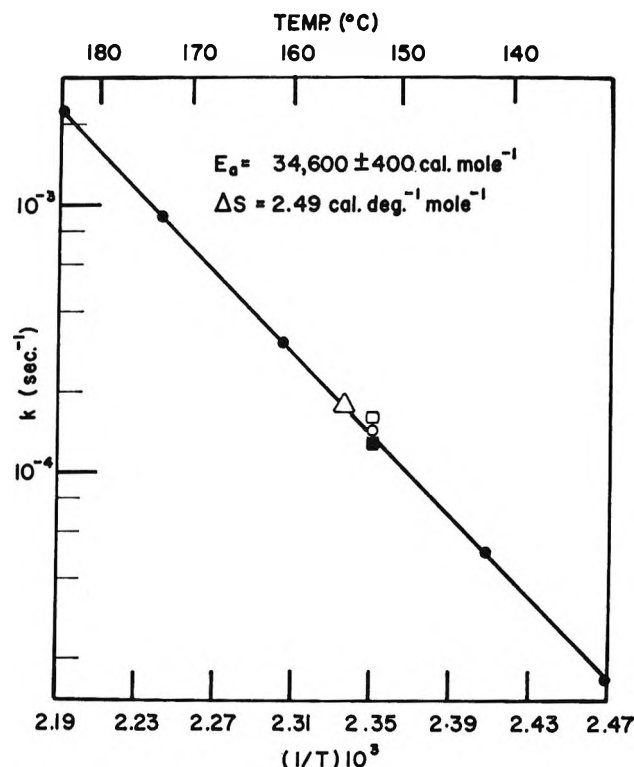
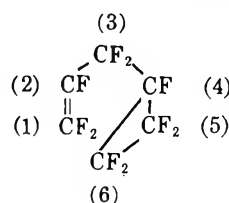
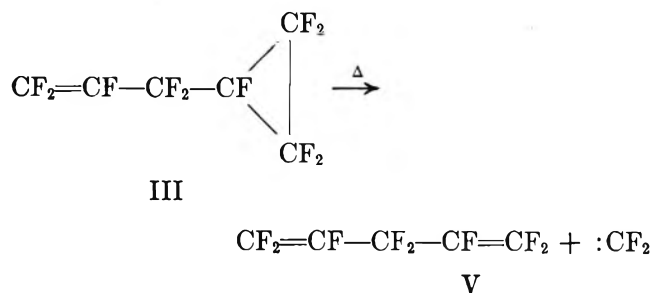


Figure 2. Arrhenius plot of the isomerization of perfluorovinylcyclopropane: ●, runs 1, 2, 4-6; O, run 7; □, run 8; △, run 9; ■, runs 3 and 10.

Kinetics (Perfluoroallylcyclopropane Pyrolysis). Superficially, the pyrolysis of perfluoroallylcyclopropane (III) might be expected, by analogy to the perfluorovinylcyclopropane isomerization, to yield the C_6F_{10} isomers, perfluorocyclohexene or perfluoro-1,5-hexadiene. However, the formation of either of these products requires an energetically unfavorable step, namely, a fluorine migration in addition to a carbon-carbon bond cleavage. The formation of perfluorocyclohexene would require fluorine migration from C_3 to C_4 whereas the formation of perfluoro-1,5-hexadiene requires a corresponding fluorine shift from C_5 to C_4 . On the other hand, a decomposition which does not



involve the breaking of a carbon-fluorine bond is that resulting from elimination of difluorocarbene and regeneration of perfluoro-1,4-pentadiene (the reverse of the reaction by which III was prepared). In agree-



ment with the last mechanism, perfluoro-1,4-pentadiene, tetrafluoroethylene, and perfluorocyclopropane are obtained when pure III is pyrolyzed in a sealed ampoule at 235°.

The kinetics of the pyrolysis of perfluoroallylcyclopropane to perfluoro-1,4-pentadiene and difluorocarbene was studied in detail in the previously described equipment in a temperature range of 196 to 250° and a pressure region of 1–40 mm. Authentic samples of III, perfluoro-1,4-pentadiene, tetrafluoroethylene, and perfluorocyclopropane were available for use as spectral and chromatographic standards.

In the initial pyrolysis experiments in which pure perfluoroallylcyclopropane (containing 10% CF_2Cl_2 as an internal standard) was used, the reaction rate decreased with time, suggesting that as the concentration of perfluoro-1,4-pentadiene product increases in the reactor, the readdition of difluorocarbene to the diene contributes significantly to the system under study. Equilibrium is not realized, however, because of the continuing removal of difluorocarbene from the system by dimerization to C_2F_4 and formation of perfluorocyclopropane. In order to minimize the reverse reaction by trapping the difluorocarbene as it was formed, excess tetrafluoroethylene (4 molar equiv) was added to the mixture. The perfluorocyclopropane formed by the trapping reaction might have led to complications but for the fact that at the temperatures involved perfluorocyclopropane only slowly regenerates difluorocarbene and tetrafluoroethylene. Thus, under these conditions, there was no observed fall-off in pyrolysis reaction rate even when followed to 97–99% completion. All of the reactions carried out in this study were followed to at least 90% completion. Thus, the standard mixture which was used throughout the study contained III (1 molar equiv), tetrafluoroethylene (4 molar equiv), and CF_2Cl_2 (0.5 molar equiv). The first-order rate constants (Table II) were determined from plots of log concentration of perfluoroallylcyclopropane *vs.* time and using a least-squares reduction of the data. A semilog plot of concentration of III *vs.* time for the low-pressure experiment (Table II, run 8) is shown in Figure 1 and illustrates that the rate data show a

first-order dependence for an over-all 50-fold variation in pressure.

Table II: Pyrolysis of Perfluoroallylcyclopropane

Run	Temp, °C	k_{obsd} , $\text{sec}^{-1} \times 10^5$
1 ^a	249.9	89.76
2	240.1	41.80
3	228.9	16.07
4	205.7	2.12
5	196.7	0.84
6 ^b	235.1	28.17
7 ^c	235.0	27.22
8 ^d	226.3	13.97
9 ^e	205.7	2.22

^a All runs were at an initial pressure of 40 mm and $S/V = 1.4 \text{ cm}^{-1}$ unless otherwise stated. Only runs 1–5 were used in the calculation of the Arrhenius parameters. Uncertainty limits (90% confidence level) for k_{obsd} are estimated from least-squares analysis to be $\pm 5\%$. ^b $S/V = 10 \text{ cm}^{-1}$. ^c 10% added NO. ^d Initial pressure = 7 mm, no change in linearity when followed to 90% completion. See Figure 1. ^e Rate constants calculated from growth of perfluoro-1,4-pentadiene.

As in the case of the perfluorovinylcyclopropane isomerization, polymerization or other side reactions were not considered since the same rate constant is obtained by monitoring either the disappearance of III or the formation of V (Table II, run 9). Furthermore, effects due to free-radical reaction or inhomogeneity are considered to be insignificant since 10% added nitric oxide (Table II, run 7) and increasing the surface to volume ratio by a factor of seven (Table II, run 6) did not affect the rate constants.

Figure 3 shows an Arrhenius plot of the observed rate constants listed in Table II which fit the equation $k \text{ (sec}^{-1}\text{)} = 10^{14.8 \pm 0.2} \exp(-42,700 \pm 500/RT)$. Since excellent agreement is obtained from the above first-order rate expression, it follows that the pyrolysis of perfluoroallylcyclopropane, involving difluorocarbene as a leaving group and formation of perfluoro-1,4-pentadiene, is a homogeneous unimolecular reaction.

Discussion

One of the most significant findings of this work is the relatively low activation energy required for either isomerization or pyrolysis of the perfluorinated cyclopropane derivatives. In the case of the hydrocarbon¹ and fluorocarbon vinylcyclopropanes direct comparison can be made. However, quantitative studies on systems analogous to perfluoroallylcyclopropane have not been reported. Nevertheless, it should be pointed out that, in general, nonvinylic, hydrocarbon cyclopropanes

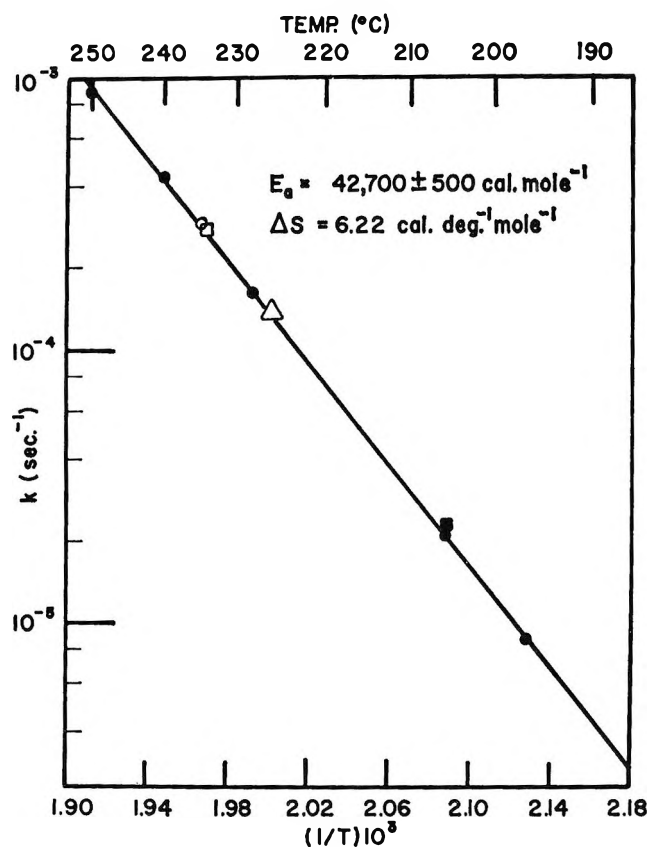


Figure 3. Arrhenius plot of the pyrolysis of perfluoroallylcyclopropane: ●, runs 1-5; ○, run 6; □, run 7; △, run 8; ■, run 9.

have isomerization activation energies in the 60-65-kcal mole⁻¹ range. However, the principal mode of isomerization of "normal" hydrocarbon cyclopropanes involves a hydrogen migration and propene formation. In the completely fluorinated series, on the other hand, the relatively high mass of fluorine as well as the carbon-fluorine bond strength (110 kcal mole⁻¹) suggests that a corresponding fluorine migration would be a highly unlikely process.

Although not strictly analogous in some cases, it is evident that the activation energies for the thermal reactions of the perfluorinated cyclopropanes are 15-20 kcal mole⁻¹ lower than those observed for the hydrocarbon species. This reduction in activation energy can be rationalized as being in large part due to the increased strain energy of the perfluoro derivatives. Bent⁷ has suggested that the replacement of a hydrogen by a more electronegative substituent causes the carbon to rehybridize so that more p-character is transmitted to the electronegative atom-carbon bond and conversely more s-character to the remaining bonds, which in this case are the carbon-carbon bonds in the cyclo-

propyl ring. Such a rehybridization would increase the π -character and the strain of the perfluorocyclopropyl ring.

Although qualitative, support for the postulation of π -electronic character of the perfluorocyclopropyl moiety can be obtained by ultraviolet spectral considerations. Thus, the far-ultraviolet spectra (Table III) of perfluoro-1,3-butadiene, perfluorovinylcyclopropane, and perfluoropropene were obtained for comparison.

Table III: Far-Ultraviolet Spectra

Compound	λ_{\max} , m μ	ϵ , l./mole-cm
CF ₂ =CF-CF=CF ₂	199.0	6550
CF ₂ =CF-CF(CF ₂) ₂	186.6	5660
CF ₂ =CF-CF ₃	177.2	2080

Inspection of Table III indicates that, in agreement with theory, both the position of the ultraviolet absorption maximum as well as the extinction coefficient of perfluorovinylcyclopropane place it intermediate between the perfluorodiene and the terminal olefin. From the above comparison, it is concluded that the perfluorocyclopropyl moiety has π -electronic character which can enter into conjugation with an unsaturated system.

There is, of course, other published evidence bearing on this unique electronic property of hydrocarbon cyclopropanes. Ultraviolet^{8a} and Raman^{8b} spectral studies, as well as nuclear magnetic resonance coupling constants and chemical shifts,^{8c} have been interpreted as indicating some π -electronic character in cyclopropanes.

An estimation of the strain energy of a perfluoroalkylcyclopropane, such as III, can be calculated using the activation energy for the pyrolysis of III to set a lower limit of -42.7 kcal mole⁻¹ for the heat of addition of difluorocarbene to perfluoro-1,4-pentadiene. Assuming the same lower limit is approximately true for the reaction of difluorocarbene with a perfluoroalkene, such as perfluoropropylene, strain energy in a

(7) H. A. Bent, *Chem. Rev.*, **61**, 275 (1961).

(8) (a) E. P. Carr and C. P. Burt, *J. Am. Chem. Soc.*, **40**, 1590 (1918); (b) A. V. Bobrov and Kh. E. Sterin, *Opt. i Spektroskopiya, Akad. Nauk SSSR, Otd. Fiz.-Mat. Nauk, Sb. Statei*, **2**, 315 (1963); *Chem. Abstr.*, **59**, 14766 (1963); (c) K. L. Williamson, C. A. Lanford, and C. R. Nicholson, *J. Am. Chem. Soc.*, **86**, 762 (1964).

perfluorocyclopropane may be arrived at by utilizing the appropriate heats of formation estimated from a bond energy scheme for perhalocarbons.⁹ The perfluorocyclopropane strain energy determined in this manner was found to be 15–25 kcal mole⁻¹ in excess of the "normal" cyclopropane strain energy of 27.6 kcal mole⁻¹.¹⁰

In the case of the isomerization of vinylcyclopropane to cyclopentene, direct comparison of the activation energies for the hydrocarbon and fluorocarbon systems can now be made.

The activation energy for the thermal isomerization of the hydrocarbon compound is 49.6 kcal mole⁻¹, whereas the corresponding value for the perfluorovinylcyclopropane isomerization is 34.6 kcal mole⁻¹. The increased ring strain coupled with the added driving force³ of decreasing the number of sp²-bonded fluorines from three to two can well account for the 15 kcal mole⁻¹ decrease in activation energy.

The unimolecular, thermal transformations of the perfluorocyclopropanes reported herein can perhaps best be understood in terms of concerted mechanisms rather than two-stage processes involving diradicals. This is supported by the normal entropy terms, the relatively low activation energies, and the fact that in neither case did added nitric oxide decrease the reaction rate or alter the products.

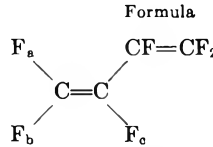
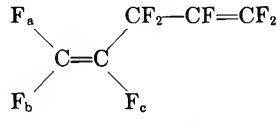
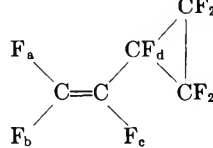
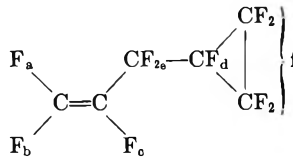
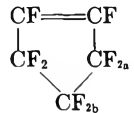
Experimental Section

General. Perfluoro-1,3-butadiene was obtained from Peninsular ChemResearch, Inc., and was shown to be 98–99% pure by vapor phase chromatography. Perfluoro-1,4-pentadiene was prepared by decarboxylation followed by dechlorination of CClF₂CClFCF₂CClFCF₂CO₂Na.¹¹

Infrared spectra were run on a Perkin-Elmer Model 21 double-beam instrument using a 2.5-cm gas cell with NaCl windows. Ultraviolet spectra were obtained on a Beckman DK-2A far-ultraviolet spectrophotometer using 5-cm gas cells. Nuclear magnetic resonance spectra (Table IV) were made with a Varian V-4300-2 instrument operating at 40.0 Mc and utilizing an internal standard of CFCI₃ for the determination of chemical shifts. The values are reported in ϕ^* values¹² at a dilution of about 25%, negative values for low field. Trifluoroacetic acid is 76.5 ϕ^* on this scale.

Perfluorovinylcyclopropane (II). Perfluoro-1,3-butadiene (1.62 g, 10⁻² mole) and difluorodiazirine (0.078 g, 10⁻³ mole) were condensed into a 20-cc heavy-walled glass ampoule which was sealed and heated to 140°. After 4 hr, the total reaction mixture was separated by fractional distillation–condensation using –78, –97, and –196° receivers. The –78 and –97° traps were

Table IV: Nuclear Magnetic Resonance Spectra

Formula	Group ^a	ϕ^*
	CF (a)	109.7
	CF (b)	94.2
	CF (c)	180.1
	CF (a)	107.2
	CF (b)	92.0
	CF (c)	189.2
	CF ₂	106.3
	CF (a)	107.0
	CF (b)	87.1
	CF (c)	184.0
	CF (d)	200.2
	CF ₂	{ 149.4 } { 155.4 } J _{AB} = 194 cps
	CF (a)	107.3
	CF (b)	90.7
	CF (c)	191.5
	CF (d)	212.6
	CF ₂ (e)	109.0
	CF ₂ (f)	153.5 No AB pattern observed
	CF	150.4
	CF ₂ (a)	118.0
	CF ₂ (b)	130.1

^a In general, the spectra recorded in this table represent complex patterns; position indicates the center of absorption.

combined and separated by vapor phase chromatography on a 0.5 in. × 2-m Kel-F tetramer (KF 8126) column. The pure C₅F₈ product (8.5 × 10⁻⁴ mole, 85% yield) was a mixture of II (67%) and IV (33%). Final purification of perfluorovinylcyclopropane was accomplished by vapor phase chromatography on a 0.25 in. × 8-m dimethylformamide (25% on Chromosorb P) column at room temperature.

Anal. Calcd for C₅F₈: C, 28.3; F, 71.7; mol wt, 212. Found: C, 28.2; F, 71.4; mol wt, 210 (gas density method). A 61% yield of C₅F₈ product, consisting of perfluorovinylcyclopropane (95%) and perfluorocyclopentene (5%) was obtained by heating the reactants for 3 hr at 140°.

(9) A. S. Rodgers, private communication, Stanford Research Institute, Menlo Park, Calif. The authors are deeply indebted to Dr. Rodgers for his many helpful suggestions throughout the progress of the experimentation and in the preparation of the manuscript. See Appendix I for the strain energy calculation.

(10) J. D. Dunitz and V. Schomaker, *J. Chem. Phys.*, **20**, 1703 (1952).

(11) W. T. Miller, Jr., W. Frass, and P. R. Resnick, *J. Am. Chem. Soc.*, **83**, 1767 (1961).

(12) G. Filipovich and G. V. D. Tiers, *J. Phys. Chem.*, **63**, 761 (1959).

Isomerization of Perfluorovinylcyclopropane. To a sample of perfluorovinylcyclopropane, containing 5% perfluorocyclopentene, was added about 10% by volume of CF_3Cl (used as an internal standard to correct the vpc data for instrument drift and sample depletion). The sample was degassed and stored as a gas in a glass bulb. All kinetics measurements were made on material removed from this source.

The reaction vessel consisted of a 90-cc high-pressure Hoke monel cylinder with two Hoke M327 valves in series enclosing a sampling volume of 0.68 cc. The reaction vessel was coupled to the gas injection loop of a modified Loenco Model 15A gas chromatograph through a stainless steel vacuum manifold equipped with a Wallace-Tiernan Model 141 differential pressure gauge. Precise thermostating of a stirred Woods metal bath was accomplished with a Thermo Electronic Model 80025 controller which responds to a change of about 0.05° . Temperature was measured with a Fischer E&A mercury-in-glass thermometer readable to 0.1° , which had been calibrated against an NBS platinum resistance thermometer. The temperature was measured with an absolute accuracy of about 0.1° .

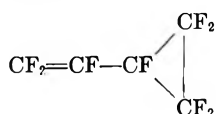
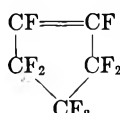
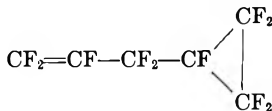
Before kinetic data were taken, the system was conditioned by a 24-hr exposure to gaseous perfluorovinylcyclopropane at an initial pressure of 100 mm and at a temperature of 140° . The reaction vessel was charged with perfluorovinylcyclopropane (containing 5% IV and 10% CF_3Cl) by expansion from a glass bulb to a pressure of 100 mm. Periodic sampling was made by admitting the gas at the total pressure of the cylinder into the evacuated 0.68-cc sampling volume. This small volume of gas was expanded into the evacuated manifold and injection loop with a total volume of 12 cc. Each sampling removed 0.68/90.68 or 0.75% of the total quantity of the material in the cylinder.

Inasmuch as for small samples the height of a gas chromatographic peak was found to be directly proportional to the number of moles of the corresponding compound, and since each sample represents a constant fraction of the volume of the cylinder, it follows that the peak height for small samples is directly proportional to moles per unit volume or concentration (partial pressure) of the corresponding component in the cylinder.

Quantitative analysis of the product mixture was made by gas chromatography (Table V) using a 0.25 in. \times 8-m column of dimethylformamide (25% on Chromosorb P) at room temperature.

Perfluoroallylcyclopropane (III). Perfluoro-1,4-pentadiene (2.12 g, 10^{-2} mole) and difluorodiazirine (0.078 g, 10^{-3} mole) were condensed into a 20-cc

Table V: Vapor Phase Chromatography Data^a

Compound	T_r
C_2F_4 , NO	8.0
$c\text{-C}_3\text{F}_6$	30.0
	129.0
	149.0
$\text{CF}_2=\text{CF}-\text{CF}_2-\text{CF}=\text{CF}_2$	264.0
	364.0

^a Column: 0.25 in. \times 8-m dimethylformamide, 25% on Chromosorb P, 50-60 mesh, 75 cc min^{-1} . ^b T_r = relative retention time = $(T_{\text{cpd}} - T_{\text{air}})/(T_{\text{CF}_2\text{Cl}_2} - T_{\text{air}}) \times 100$.

heavy-walled glass ampoule at -196° . The ampoule was sealed and heated to 140° for 5 hr. After opening the ampoule, the contents were fractionated through -30 , -58 , and -196° traps. The -58 and -196° receivers were combined and separated by vapor phase chromatography on a 0.25 in. \times 2-m Kel-F 8126 column operating at room temperature to afford a 34% yield of pure perfluoroallylcyclopropane (III).

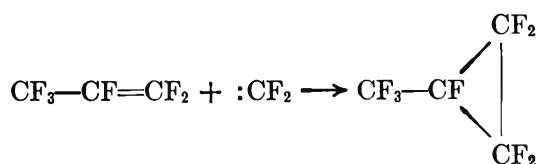
Anal. Calcd for C_6F_{10} : C, 27.5; F, 72.5; mol wt, 262. Found: C, 27.7; F, 72.2; mol wt, 258 (gas-density method).

Pyrolysis of Perfluoroallylcyclopropane (III). To a sample of chromatographically pure perfluoroallylcyclopropane was added 4 molar equiv of tetrafluoroethylene and about 0.5 molar equiv of CF_2Cl_2 (used as an internal standard to correct the vpc data for instrument drift and sample depletion). The mixture was degassed and stored in a glass bulb. All kinetic measurements were made on material removed from this source. The reaction vessel and thermostating were as previously described. The system was conditioned by a 24-hr exposure to the gaseous mixture of perfluoroallylcyclopropane-tetrafluoroethylene at an initial pressure of 200 mm and at a temperature of 225° . The reaction vessel was charged with the 1:4 perfluoroallylcyclopropane-tetrafluoroethylene mixture by expansion from a gas bulb to a pressure of 200 mm. The sampling and vpc analysis techniques were as described above. The relative retention times of the various fluorocarbons are listed in Table V.

Acknowledgment. The authors wish to express their appreciation to Mr. A. H. Stoskopf for his excellent technical assistance, and Dr. J. W. Todd and Mr. M. C. Eagen for vpc assistance. The authors also wish to thank Dr. R. L. Hansen for obtaining the far-ultraviolet spectra and Dr. A. S. Rodgers for his valuable discussions.

Appendix I

Estimation of Strain Energy. We have shown that the lower limit of the heat of addition of difluorocarbene to perfluoro-1,4-pentadiene is -42.7 kcal mole⁻¹. Assuming a similar value for the heat of addition of :CF₂ to CF₃CF=CF₂



we obtain

$$\Delta H_f \left(\text{CF}_3\text{CF} \begin{array}{l} \diagup \text{CF}_2 \\ | \\ \diagdown \text{CF}_2 \end{array} \right) - \Delta H_f(\text{CF}_3\text{CF}=\text{CF}_2) - \Delta H_f(\text{CF}_2) = -42.7 - \epsilon_0 \text{ kcal mole}^{-1}$$

where ϵ_0 is the activation energy of the addition of :CF₂ to CF₃CF=CF₂.

Using estimates⁹ for the heat of formation of the relevant quantities we arrive at

$$-126.6 + Y - \Delta H_f(\text{CF}_2) = -42.7 + \epsilon_0 \text{ kcal mole}^{-1}$$

The heat of formation of CF₃CF $\begin{array}{l} \diagup \text{CF}_2 \\ | \\ \diagdown \text{CF}_2 \end{array}$ was estimated on

the basis of a linear compound with a strain energy correction Y kcal mole⁻¹.

$$Y = 83.9 + \epsilon_0 + \Delta H_f(\text{CF}_2) \text{ kcal mole}^{-1}$$

$\Delta H_f(\text{CF}_2)$ has been assigned a best value of -35 kcal mole⁻¹; however, it may actually be as low as -45 kcal mole⁻¹.¹³

Thus, $Y = (48.9 + \epsilon_0)$ to $>(38.9 + \epsilon_0)$ kcal mole⁻¹. Assuming an activation energy of 3–5 kcal mole⁻¹ for ϵ_0 , we find the strain energy in a perfluorocyclopropane to be 43–53 kcal mole⁻¹. The strain energy of cyclopropane is 27.6 kcal mole⁻¹.¹⁰

(13) I. P. Fisher, J. B. Homer, and F. P. Lossing, *J. Am. Chem. Soc.*, **87**, 957 (1965).

Water ^{17}O Nuclear Magnetic Resonance Shift in Aqueous Solutions of 1:1 Electrolytes

by Zeev Luz and Gad Yagil

The Isotope Department and The Radioisotope Training Center, The Weizmann Institute of Science, Rehovoth, Israel (Received September 13, 1965)

The frequency shift of the water ^{17}O signal in aqueous solutions containing varying amounts of diamagnetic electrolytes at 25° was measured. Both high- and low-field shifts were observed. It is shown that the molal shifts in dilute solutions can be divided into the contributions of the constituting ions. Most univalent cations give rise to about the same ionic shift, while the shifts due to anions differ considerably from each other. ^{17}O shift of dilute solutions of water in several organic solvents and of water at various temperatures is also reported. From these measurements it is estimated that the breaking of a hydrogen bond shifts the ^{17}O resonance 16 ppm toward high field. Analysis of the experimental data shows that the main cause of the shifts in electrolyte solutions is not the modification of the structure of water, but rather direct interaction between the ions and adjacent water molecules.

Introduction

The proton magnetic resonance line of water undergoes considerable shift when electrolytes are dissolved in water.¹ This effect offers a method to study ion-solvent and solvent-solvent interaction on the molecular level. Several investigations have been carried out on the proton shift in aqueous solutions,²⁻⁶ and the dependence of the shift on concentration for a large number of simple diamagnetic 1:1 electrolytes was determined. It has been found that it is possible to express the observed shift as a sum of individual shifts due to the cations and anions. These ionic shifts were interpreted as being caused not only by specific ion-solvent interactions, but also by modifications of solvent-solvent interactions such as changes in the number of hydrogen bonds in bulk water caused by the presence of the salt. These findings are in line with a series of investigations dealing with the structure of aqueous electrolyte solutions which emphasize the role of hydrogen bond breaking in explaining the properties of these solutions.⁷⁻⁹ On the other hand, at least some work on the thermodynamic properties of electrolyte solutions¹⁰ has been done which does not invoke changes in the bulk water to explain the properties of these solutions.

In this paper we report measurements on the ^{17}O shift of water in aqueous electrolyte solutions. The question posed was to what extent do the ^{17}O shifts obey a pattern similar to that of the proton shifts, and whether additional information on ion-solvent interactions can be gained. The ^{17}O shifts were found to be of the same order or magnitude (in ppm) as the proton shifts and could again be broken down into contributions of individual ions. Some notable differences were observed, however. In particular, the ^{17}O ionic shift of the halide and halate ions follows an inverse order with respect to their ionic size to that found with protons, an order which is also inverse to that expected if hydrogen bond breaking between solvent

- (1) J. N. Shoolery and B. J. Alder, *J. Chem. Phys.*, **23**, 805 (1955).
- (2) H. S. Gutowsky and A. Saika, *ibid.*, **21**, 1688 (1953).
- (3) H. G. Hertz and W. Spalthoff, *Z. Elektrochem.*, **63**, 1096 (1959).
- (4) M. S. Bergquist and E. Forslind, *Acta Chem. Scand.*, **16**, 2069 (1962).
- (5) J. C. Hindman, *J. Chem. Phys.*, **36**, 1000 (1962).
- (6) B. P. Fabricand and S. Goldberg, *ibid.*, **34**, 1624 (1961).
- (7) H. S. Frank and W.-Y. Wen, *Discussions Faraday Soc.*, **24**, 133 (1957).
- (8) M. Kaminsky, *ibid.*, **24**, 171 (1957).
- (9) G. R. Choppin and K. Buijs, *J. Chem. Phys.*, **39**, 2042 (1963).
- (10) E. Glueckhauf, *Trans. Faraday Soc.*, **51**, 1235 (1955).

molecules was the dominant cause of the shift. Although we were not able to give a quantitative interpretation of the results, it is shown by comparing the shifts with similar shifts in auxiliary systems that direct ion-solvent interaction is the main cause of the ^{17}O shifts in aqueous solutions.

Experimental Section

Preparation of Solutions. The solutions were prepared by weighing commercial analytical grade electrolytes into a weighed amount of water. Water was obtained from the Institute's plant and contained 0.45 atom % ^{17}O . The water also contained about 20 atom % deuterium. The concentrations of the solutions were determined as follows: potassium fluoride by thorium nitrate titration, salts of the other halides by argentometric titration, and perchlorates and nitrates by gravimetric determination of the cation. The presence of metal ion impurities was checked by spectrographic analysis.¹¹ In a few cases impurities of paramagnetic ions were detected, and indeed appreciable broadening of the ^{17}O line was observed; in purified substances the excess broadening disappeared. For a number of salts the shift was measured both in neutral and in acidified solutions. The amount by which the lines were shifted was not affected by the addition of acid, but very often the lines were broadened in neutral solution due to slow proton exchange.¹² The reported measurements were all performed in 0.01 *M* HCl, except for KF, KNO_2 , and NaNO_2 , which are salts of weak acids.

Nuclear magnetic resonance measurements were performed on a Varian DP-60 spectrometer, operating at 8.13 Mc. Water of the same isotopic content and acidity as those of the samples was used as a reference. The shift was measured as follows: first the reference sample was run and the position of the line was recorded in terms of field dial units; next, the sample was run, and its position was recorded; finally, the reference was rerun. The field dial units were calibrated by the side-band technique, and the shift was calculated as the difference between the sample and the mean of the two reference readings. The accuracy of the shifts determination is estimated at 0.5 ppm which is about 10% of the water line width.

We denote a shift as positive when the observed resonance of the electrolyte was at a higher field than the reference water at fixed radiofrequency. To eliminate contributions to the shift from differences in bulk susceptibilities, spherical sample holders were employed. All of the measurements were conducted at room temperature, which was $25 \pm 2^\circ$. The temperature dependence of the ^{17}O shift was determined

by measuring the position of the water resonance at the desired temperature between two reference water samples at room temperature. The sample holder used in these measurements was a dewar-like test tube, to keep the temperature constant during the measurements.

Results

The shift of the ^{17}O resonance line of water in solutions of 30 1:1 electrolytes as function of concentration is shown in Figures 1-5. The ordinate represents the observed shift of the ^{17}O line as defined in the Experimental part, and the abscissa gives the concentration in moles of electrolyte/1000 g of solvent water. Some of the electrolytes gave straight-line plots, while others deviated from linearity at high concentrations. Within our experimental accuracy all the lines passed smoothly through the origin; it should, however, be noted that the lowest concentrations of electrolyte that gave measurable shifts were around 0.5-1 *m*. A change in the slope of the curve at more

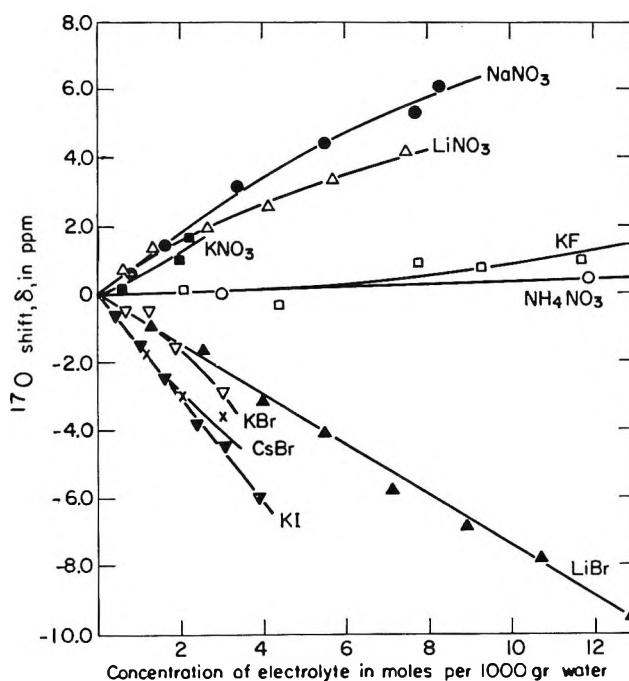


Figure 1. ^{17}O shift, δ , of water in electrolyte solutions, relative to pure water, as a function of the electrolyte concentration, for nitrates and some halides. Shifts are positive when the resonance of the electrolyte solution is at a higher field than that of the reference water.

(11) We are indebted to Mrs. I. Schoenfeld and Mrs. S. Held of the Spectrochemical Laboratory of the IAEA, Soreq, for carrying out these analyses.

(12) S. Meiboom, *J. Chem. Phys.*, **34**, 375 (1961).

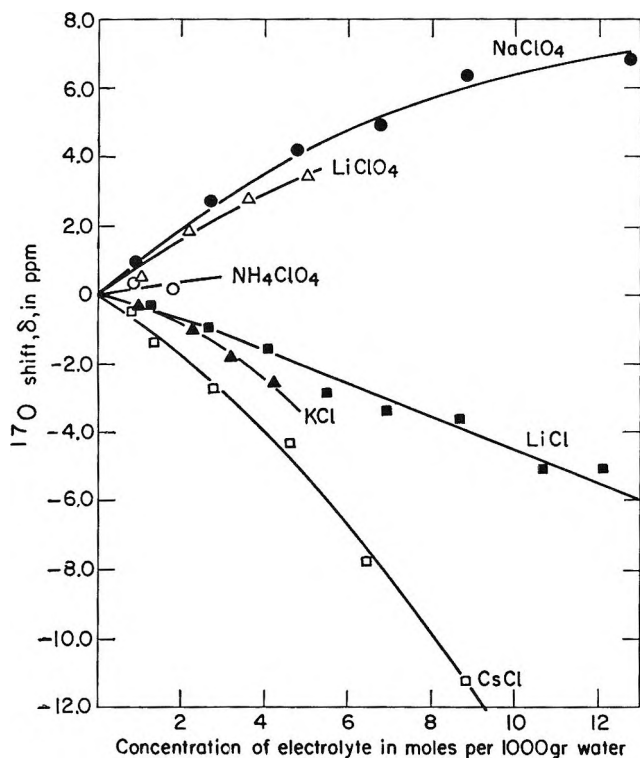


Figure 2. Same as Figure 1 for perchlorates and chlorides.

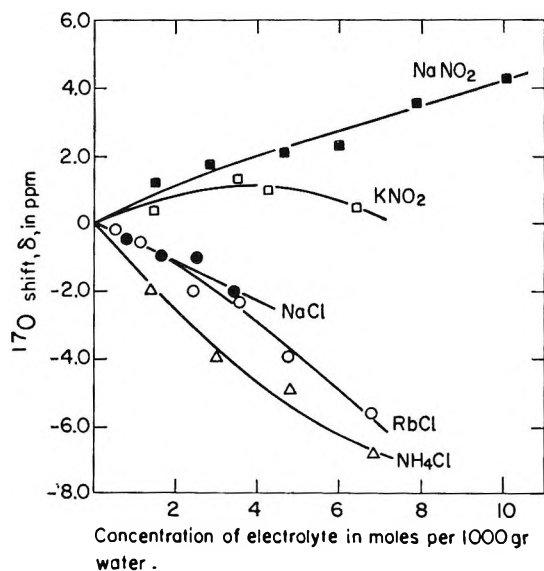


Figure 3. Same as Figure 1 for nitrites and chlorides.

dilute solutions can therefore not be ruled out completely. In line with analogous work,¹⁻⁶ we shall express the results in terms of the molal shift δ^0 which is the initial slope of the experimental curves, $(d\delta/dm)_{m=0}$. Values of δ^0 thus obtained are listed in the third column of Table I. Most of the subsequent

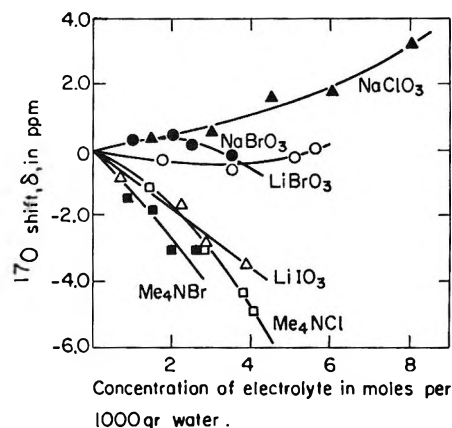


Figure 4. Same as Figure 1 for halates and tetramethylammonium salts.

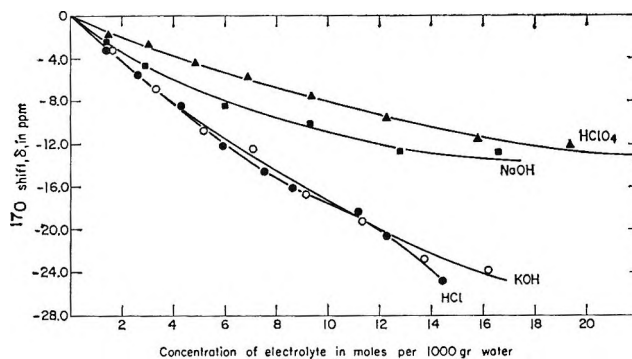


Figure 5. Same as Figure 1 for strong acids and bases.

discussion is centered around these molal shifts. The deviations from linearity at high concentration of some electrolytes, observed also with the proton resonance, are probably due to interionic interactions. The curvatures are sometimes negative and sometimes positive, so that more than one effect is operative, and no quantitative interpretation can be suggested at present.

The proton molal shift was shown¹⁻⁶ to be expressible as the sum of the contributions of the constituting ions; these are called ionic molal shifts or just ionic shifts. ^{17}O molal shifts can be treated similarly. In order to make an assignment, the ionic molal shift of one ion has to be determined arbitrarily. We chose to assign the value of $\delta^0 = 0$ to the ammonium ion. The molal shifts of the ammonium salts yielded then preliminary values for the ionic molal shifts of Cl^- , NO_3^- , and ClO_4^- . From these, the ionic shifts for the other cations, and then anions, were evaluated. The final values for the ionic molal shifts, shown in Table II, were obtained by further adjusting these values to give the best additivity for each electrolyte.

Table I: Molal Shift $\delta^0 = (d\delta/dm)_{m=0}$, of Water ¹⁷O Resonance Line in Aqueous Electrolyte

Salt	Maximum concn, <i>m</i>	$\delta^0_{\text{obsd.}}$, ppm/ <i>m</i>	$\delta^0_{\text{calcd.}}$, ppm/ <i>m</i>	$\delta^0_{\text{calcd.}} - \delta^0_{\text{obsd.}}$, ppm/ <i>m</i>
KF	11.8	0.0	0.0	(0)
LiCl	12.1	-0.27	-0.28	-0.01
NaCl	3.4	-0.31	-0.31	(0)
KCl	4.1	-0.37	-0.39	-0.02
RbCl	6.8	-0.43	-0.43	(0)
CsCl	8.9	-0.74	-0.88	-0.14
NH ₄ Cl	6.8	-1.35	-1.35	0.00
(CH ₃) ₄ NCl	4.1	-0.80	-0.92	-0.12
LiBr	12.9	-0.74	-0.69	0.05
KBr	3.1	-0.62	-0.86	-0.24
CsBr	3.0	-1.40	-1.26	0.14
(CH ₃) ₄ NBr	2.7	-1.41	-1.29	0.12
KI	3.9	-1.48	-1.48	(0)
LiNO ₃	7.5	0.98	0.97	-0.01
NaNO ₃	6.5	0.98	0.95	-0.03
KNO ₃	2.3	0.62	0.80	0.18
NH ₄ NO ₃	20.1	0.0	-0.06	-0.06
NaClO ₃	10.0	0.25	0.25	(0)
LiBrO ₃	5.6	-0.18	0.02	0.20
NaBrO ₃	2.9	0.25	0.0	-0.25
LiIO ₃	3.9	-0.86	-0.86	(0)
LiClO ₄	5.0	0.86	0.97	0.11
NaClO ₄	12.8	0.98	0.95	-0.03
NH ₄ ClO ₄	1.8	0.18	-0.06	-0.24
NaNO ₂	10.0	0.74	0.65	-0.09
KNO ₂	6.4	0.43	0.50	0.07
HCl	14.4	-2.21	-2.28	-0.07
HClO ₄	21.9	-1.05	-0.98	0.07
NaOH	16.6	-1.78	-1.82	-0.04
KOH	16.2	-1.97	-1.94	0.03

Table II: Ionic Molal Shifts of ¹⁷O in Aqueous Electrolyte Solutions

Ion	δ^0 , ppm/ <i>m</i>	Ion	δ^0 , ppm/ <i>m</i>
H ⁺	-0.92	OH ⁻	-2.80
Li ⁺	1.03	F ⁻	-0.92
Na ⁺	1.00	Cl ⁻	-1.35
K ⁺	0.85	Br ⁻	-1.72
Rb ⁺	0.92	I ⁻	-2.35
Cs ⁺	0.47	NO ₂ ⁻	-0.36
NH ₄ ⁺	0.00 ^a	NO ₃ ⁻	-0.06
(CH ₃) ₄ N ⁺	0.43	ClO ₃ ⁻	-0.76
		BrO ₂	-1.00
		IO ₃ ⁻	-1.90
		ClO ₄ ⁻	-0.06

^a Assumption, see text.

The molal shifts δ^0_{calcd} obtained by adding the individual ionic shifts listed in Table II are shown in the fourth column of Table I. The differences between

δ^0_{obsd} and δ^0_{calcd} are shown in the last column of that table. When only one salt of a certain cation or anion is measured, this value has to be zero and is bracketed in the table. The other cases demonstrate that the additivity relation is fairly well obeyed for ¹⁷O. The ionic molal shifts are also represented diagrammatically in Figure 6. The cations and anions are shown on separate lines, because only the differences between the various cations (and anions) are directly determined by the experiment; the relative position of the two lines is determined by the arbitrary value assumed for the ammonium ion. A different assumption would necessitate a shift of both lines by the same amount and in opposite directions, since the sum of the ionic shifts has to give the experimentally determined value for the electrolyte. For example, if one assigns to K⁺ or Na⁺ the value $\delta^0 = 0$, the ionic shift of practically all cations will be negative while half of the anions will give a positive shift. Still the difference in δ^0 between each two cations (or between each two anions) will remain unchanged.

It is interesting to compare these data with the proton molal shifts. Most oxyanion salts shift both the proton and ¹⁷O resonances toward high field, while the strong acids and bases shift to low field. The situation is different for the halides; while the proton resonance shifts in most cases toward high field, the ¹⁷O resonance undergoes a downfield shift. This is also reflected in the ionic shifts. Most notably, the order of the shifts of the four halide anions is inverted; iodide, which has the largest upfield shift in the case of protons, causes the largest downfield shift in H₂¹⁷O. The main difference observed with cations is the relative position of the Li⁺ ionic shift.

The two ions H⁺ and OH⁻ undergo exceptionally

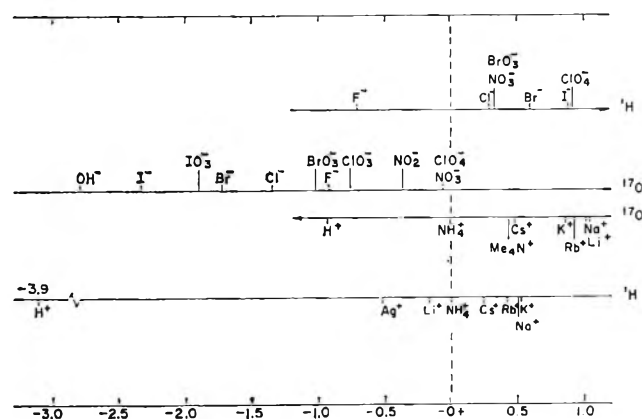


Figure 6. ¹⁷O and ¹H ionic molal shifts in ppm. The ¹⁷O results are from the present work and the ¹H results are averages from ref 3-6 and adjusted to $\delta^0_{\text{NH}_4^+} = 0$.

large negative shifts (*cf.* Figure 5). This is most probably due to the contribution of the oxygen in the two species H_3O^+ and OH^- . If we neglect the shift of solvent ^{17}O , the results of Figure 5 lead to an estimated shift of -40 ppm for H_3O^+ and -70 ppm for OH^- , relative to water.

In order to get more information on the contribution of hydrogen bond breaking to the observed results, the shift of the ^{17}O line of water when diluted in several solvents was determined. The results are shown in Table III and demonstrate that hydrogen bond breaking, which occurs upon diluting water in these solvents, shifts the ^{17}O resonance of water toward high field.

Table III: The ^{17}O Shift of Water Dissolved in Several Solvents

Solvent	Acetone ^a	Acetonitrile	Dioxane ^b	Chloroform ^c	Methanol
Mole fraction of E_2O	0.11	0.006	0.01	Saturated	0.007
Shift of H_2^{17}O , in ppm	10.9	11.3	18.3	10.3	10.1

^a Taken from J. Reuben, A. Tzalmona, and D. Samuel, *Proc. Chem. Soc.*, 353 (1962). ^b The values obtained at 0.04 and 0.10 mole fraction were 18 and 17.3, respectively. It can thus be assumed that the quoted value represents the shift at infinite dilution. ^c Measured in a saturated solution of water in chloroform; the same result was obtained in a solution containing half that amount of water.

The temperature dependence of the ^{17}O chemical shift of pure water was determined by measuring the position of the resonance line at 4, 29, and 72° as explained in the Experimental Section. The results are given in Table IV, where the shift at 4° was as-

Table IV: The ^{17}O Shift of Water as Function of Temperature

t , °C	4	29	72
δ , ppm	0	1.4	2.1

signed the value of zero. The values of these shifts are not much larger than the experimental accuracy, so that not too much significance can be given to the individual numbers. The occurrence of a high-field shift upon heating of water is demonstrated, however.

Discussion

A water molecule in pure water or in an aqueous solution is not a uniquely defined species, but can assume one of several states, depending on the interactions that it undergoes with its neighboring molecules.¹³ In pure water, molecules may form from one up to four hydrogen bonds with neighboring water molecules, or may not be bonded at all. In each state the ^{17}O has its distinct magnetic environment. However, because of the rapid transitions between the various states,¹² only a single ^{17}O line is observed. If these transitions are fast compared with the frequency shifts and with their line width, the observed shifts, δ , will be the weighted average of the shifts of the various states: $\delta = \sum_i \delta_i p_i$ where δ_i is the shift and p_i is the fraction of water molecules in the i 's state.

This relation applies also to solutions of electrolytes in water, only that additional states have to be considered, *e.g.*, water molecules coordinated to a cation, hydrogen bonded to an anion, or water molecules the dipole of which is oriented in the ionic field. Again, as long as such water molecules exchange rapidly with water in the bulk, only the single resonance line is observed. This is the case in 1:1 electrolytes solutions, in which no separate ^{17}O line for solvation shell molecules could be detected.^{14,15}

The shifts observed in electrolyte solutions may come about in two ways: (1) the contribution of water molecules in direct interactions with the ions, *i.e.* ion-solvent interaction; this introduces δ_i terms not present in pure water; (2) changes in the p_i 's in the bulk water over and above the changes required by the passing of some molecules to the neighborhood of ions. This is commonly termed modification of water structure. It would have been desirable to employ values of δ_i and the observed shifts to derive values for the various p_i 's, such as the number of water molecules coordinated to a certain ion. Unfortunately, the pertinent δ_i values are not obtainable from the experiments. What shall be done instead is to obtain a value for the ^{17}O shift due to the breaking of a single hydrogen bond from the shifts caused by varying the temperature of pure water, and by dissolving water in solvents. This value will then be used to estimate the relative contribution of the two ways described above.

Modification of Water Structure. The changes in the

(13) For a recent review of the literature on the structure of water see J. L. Kavanau, "Water and Water-Solute Interactions," Holden-Day, Inc., San Francisco, Calif., 1964.

(14) J. A. Jackson, J. F. Lemons, and H. Taube, *J. Chem. Phys.*, **32**, 553 (1960).

(15) H. Taube in "Progress in Stereochemistry," Vol. III, Butterworth and Co. Ltd., London, 1962, p 104.

degree of hydrogen bonding in the bulk (no. 2 above) has been suggested to be the dominant effect of various electrolytes on the proton resonance shift (δ_{H} of ref 5; cf. Table II of ref 4; δ_{B} of ref 6). This effect on the ¹⁷O shift will be discussed first. The contribution of hydrogen bond breaking to the observed shift can be obtained from the data in Tables III and IV. From infrared and proton magnetic resonance measurements,¹⁶ it is known that at the low concentration employed in Table III practically all hydrogen bonds between water molecules are broken. In some solvents, new hydrogen bonds between water and solvent are formed instead.¹⁷ If we assume that this new association to the water molecule does not influence the ¹⁷O resonance, the observed shift gives directly the effect of hydrogen bond breaking. Table III indicates that the shift is then of the order of 10 to 18 ppm at 25° (or somewhat higher, since H-bond formation is not complete in pure water at 25°). Alternatively, it is plausible that the formation of a solvent-water bond compensates, at least partly, for the rupture of the water-water bond. In hydrogen-donating solvents (*e.g.*, chloroform) the hydrogen end of the water molecule will now be unbonded, and this will be the main cause for the shift. In the hydrogen-accepting solvents (acetone, acetonitrile, dioxane) the main effect is now due to the water oxygen remaining unbonded. A complete rupture of all hydrogen bonds to a water molecule is then the sum of the shifts in the two kinds of solvents, *i.e.*, at least 20 ppm. In any case the breaking of hydrogen bonds shifts the ¹⁷O resonance toward higher field.

A third possibility should really be considered, namely that the contribution of solvent-water interaction is so large as to overcompensate a negative shift upon H-bond breaking in water. If, however, we assume that the shift is related to the degree of interaction between water and solvent, this possibility can be ruled out on the basis of infrared and pmr data.¹⁶ Methanol can, in principle, bind to both the oxygen and hydrogen ends of the water molecules; however, while it has two hydrogen-accepting sites, it can donate only one hydrogen. If this hydrogen is not preferentially donated to water, the ¹⁷O shift in methanol is expected to be half that observed in dioxane. The results of Table III show that this is very nearly the case. Still, it is possible that other kinds of water-solvent interaction besides hydrogen bonding cannot be ignored.

The positive shift observed upon heating water (Table IV) also supports the conclusion that hydrogen bond breaking shifts the ¹⁷O resonance line toward high field. In order to evaluate the contribution of breaking a

single hydrogen bond to the shift, it is necessary to know the number of hydrogen bonds broken in the temperature interval 4–72°. Several recent estimates of this number, based on different approaches, are listed in Table V.

It is evident from Table V that a generally accepted value for the degree of hydrogen bonding in water cannot be quoted. The largest extent of hydrogen bond breaking between 4 and 72° is indicated by the Raman data.¹⁸ However, these figures are very sensitive to the choice of the base line for the determination of absorption intensity of the H-bond bending line at 175 cm⁻¹. Also, the assumption of a simple equilibrium between "bound" and "unbound" water molecules seems to be an oversimplification. We shall not discuss in detail the other four sets of values quoted, but use a mean estimate of 0.13 as the fraction of hydrogen bonds broken between 4 and 72°. This leads to a value of 2.1/0.13 = 16 ppm (see Table IV) upfield shift for the breaking of two hydrogen bonds per water molecule. Taking for the fraction of hydrogen bonds formed at 25° an average of 0.6 bond, the value estimated above from dilution in solvents is at least 10/0.6 = 16 ppm and possibly somewhat higher, in concurrence with the value estimated from the temperature dependence.

To what extent can this value for the shift, due to a hydrogen bond breaking, explain the shifts observed with the various electrolytes and individual ions? If hydrogen-bond breaking is the dominant contribution to the ¹⁷O shift, salts like KI, CsCl, CsBr, and NaClO₄ which are generally regarded as the most effective in structure breaking⁷⁻⁹ would have been expected to show the largest upfield shifts. While this is true for NaClO₄, the opposite is observed for the salts of the larger alkali halide salts. Moreover, the relative molal shifts of the halide and halate ions are in opposite direction to that expected from their structure-breaking capacity, iodide having the most negative shift. Structure breaking thus cannot be the dominant contribution to the ¹⁷O shifts observed in electrolyte solutions.

Direct Ion-Solvent Interaction. We now turn to examine the effect on the ¹⁷O shift due to direct interaction between ions and water molecules. The linear dependence of the ¹⁷O shift on electrolyte concentration up to relatively high concentrations means that the number of molecules affected is propor-

(16) J. R. Holmes, D. Kivelson, and W. C. Drinkard, *J. Am. Chem. Soc.*, **84**, 4677 (1962).

(17) E. Greinacher, W. Luttko, and R. Mecke, *Z. Elektrochem.*, **59**, 23 (1955).

(18) See footnote *g* in Table V.

Table V: Degree of Hydrogen Bonding in Water According to Literature^a

Temp, °C				Method	Reference
4	25	72	4-72 ^b		
0.90	0.89	0.83	0.07	Dielectric constant	Haggis, <i>et al.</i> ^c
0.53	0.47	0.39	0.14	Infrared	Buijs and Choppin ^d
0.51	0.45	0.35	0.16	Model to fit thermo- dynamic data	Némethy and Scheraga ^e
>0.85	>0.80	>0.70	0.15	Infrared up to T_c	Luck ^f
0.86	0.58	0.10	0.76	Raman	Walrafen ^g

^a The numbers give the fraction of hydrogen bonds formed. The fraction is unity when all water molecules participate in four hydrogen bonds, so that there is an average of two bonds per molecule. ^b The fraction of hydrogen bonds broken upon heating from 4 to 72°. ^c G. H. Haggis, J. B. Hasted, and T. J. Buchanan, *J. Chem. Phys.*, **20**, 1452 (1952). ^d K. Buijs and G. R. Choppin, *ibid.*, **39**, 2035 (1963). ^e G. Némethy and H. A. Scheraga, *ibid.*, **36**, 3382 (1962). ^f Figures 50 and 58 in W. Luck, *Fortsch. Chem. Forsch.*, **4**, 43 (1965). ^g G. E. Walrafen, *J. Chem. Phys.*, **40**, 3249 (1964).

tional to the number of ions present. This already indicates that direct ion-water interaction makes an important contribution to the observed shift. Referring to Figure 6, one observes that most cations are grouped together at approximately 0.8 ppm/m. The same, though less pronounced, is observed in the case of the proton shifts. It seems that the effect of the univalent cations on the ¹⁷O shift is small compared to the effect of the anions. This is surprising because oxygen is the part of the water molecule that is expected to be closest to the cation and thus be subjected to the strongest influence of the ion, while the anions are more likely to approach the hydrogen end of the water molecule. It can only be added that a similar lack of effect of cations has been observed before, *e.g.*, on the Raman spectra of electrolytes in water,¹⁹ on the infrared of methanol OH stretching frequency discussed below,²⁰ and on the solubility of some nonelectrolytes in water.²¹ On the other hand, preliminary measurements on salts of the alkaline earth metals indicate a somewhat larger spread of the molal shifts. In addition, the shift of the solvation shell of the Al³⁺ ion, which can be observed separately from the solvent peak, was found²² to be -11 ppm, corresponding to a molal shift of -1.1 ppm/m. (Susceptibility correction will lead to an even larger figure.)

With anions, a different picture is observed. Roughly, in the two series halides and halates, the ionic shift becomes more negative with increasing ionic size. An attempt to correlate the ionic shift with the ionic volume is shown in Figure 7. In this figure the ionic molal shift (based on $\delta_{\text{NH}_4^+} = 0$) is plotted against the cube of the ionic crystal radii. The values for the ionic radii were taken from ref 23; those for the oxyanions were calculated from the covalent radii of the constituting atoms.²³ It is seen that within each

series the correlation is quite linear, but the shift is less negative for the oxyanions. The ionic shift thus cannot be explained solely by the size of the anion. It appears that the oxygen atoms of the oxyanion have a specific effect on the water molecules causing an up-field shift. The points for nitrate, nitrite, and perchlorate in Figure 7 support this idea. Nitrate, having three oxygen atoms, falls on the line of the halates, while perchlorate and nitrate are displaced above and below the halate line in accordance with the number of oxygens they contain. There are at least two possible explanations to the effect of ionic volume (size) on the anionic shifts. The first, suggested, *e.g.*, by Bergquist and Forslind,⁴ is that the larger the anion, the more efficiently it breaks the water structure ("the steric effect"). However, as discussed above, this effect should shift the ¹⁷O resonance line in a direction opposite to the observed one, and can therefore be ruled out. Alternatively, what might be involved is not the ionic volume itself but a related property such as the ionic polarizability (which indeed gives similar patterns to Figure 7). The larger the polarizability of an anion in a series, the more likely are interactions between it and adjacent water molecules which underlie the chemical shift. However, the theory of the ¹⁷O shift is not sufficiently advanced to permit further examination of this possibility.

Recent infrared and ultraviolet measurements by several authors^{24,25} bring evidence for the existence of solute-solvent interaction between halide ions and

(19) G. E. Walrafen, *J. Chem. Phys.*, **36**, 1035 (1963).

(20) A. Allerhand and P. von R. Schleyer, *J. Am. Chem. Soc.*, **85**, 1233 (1963).

(21) P. R. Robinson and W. P. Jencks, *ibid.*, **87**, 2470 (1965).

(22) R. E. Connick and D. N. Fiat, *J. Chem. Phys.*, **39**, 1349 (1963).

(23) M. W. Sidgwick, "The Chemical Elements and Their Compounds," Vol. I, Oxford University Press, London, 1950, Table V.

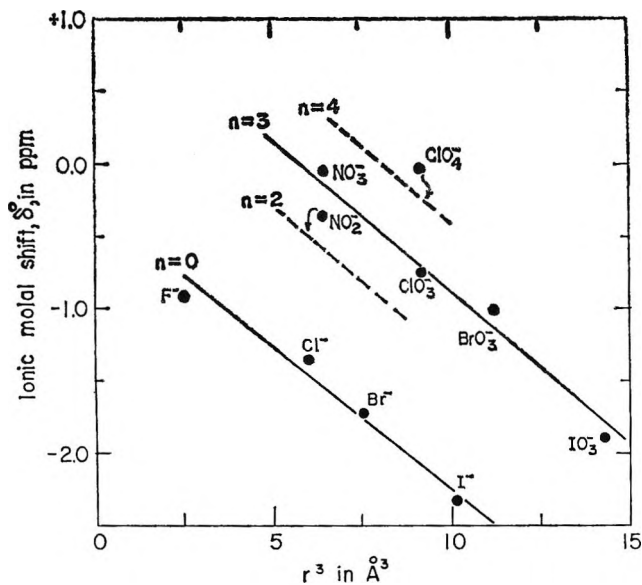


Figure 7. Ionic molal shift of anions as function of the cube of their crystal radii.

methanol. Thus, Allerhand and Schleyer²⁰ measured the shift of the OH stretching frequency, (around 3600 cm⁻¹) of methanol highly diluted in solvents such as methylene chloride. Upon the introduction of various tetraalkylammonium halides, shifts of this line up to 340 cm⁻¹ were observed. The infrared shift was almost independent of the cation, but strongly dependent on the anion, as in the ¹⁷O shift, leading to the conclusion^{20, 25} that anion-methanol interactions are responsible for the shift. Since methanol is very similar to water, this system is a suitable one to examine whether direct interaction of anion with hydroxyl group can lead to shifts similar to those observed in the aqueous electrolyte solutions. For that purpose a series of solutions of methanol (0.2 M) and each of the four tetrabutylammonium halides (0.6 M) was

prepared in methylene chloride. The ¹⁷O resonance of methanol in these solutions was measured relative to a methylene chloride solution containing only methanol at the same concentration.²⁶ The results are: tetrabutylammonium fluoride, -0.9 ppm; tetrabutylammonium chloride, -7.9 ppm; tetrabutylammonium bromide, -5.7 ppm; tetrabutylammonium iodide, -8.0 ppm. These figures clearly demonstrate that anion-OH interaction causes a considerable low-field shift of the ¹⁷O resonance line. Moreover, except for the chloride, the shift increases with ionic size, iodide causing the largest shift. These results cannot be compared quantitatively with the ionic molal shift of the halides because it is not known to what extent association between methanol and the anions is complete and because the solvation number of the halide anions in water is not known; also, the effect of an anion on methanol probably differs somewhat from the effect on water. More recently, it has been shown that similar infrared shifts occur when H₂O interacts with anions in CCl₄.²⁷

The ¹⁷O shifts described above are, however, large enough to support the conclusion that direct anion-water interaction is the dominant cause for the ¹⁷O shift in aqueous solutions. This conclusion suggests that more attention be paid in future examination of electrolyte solutions to the interactions of anions with their neighboring solvent molecules.

(24) (a) H. Lund, *Acta Chem. Scand.*, **12**, 298 (1958); (b) J. Buffalini and K. H. Stern, *J. Am. Chem. Soc.*, **83**, 4362 (1961); (c) J. B. Hyne, *ibid.*, **85**, 304 (1963).
 (25) M. S. Blandamer, T. E. Gough, and M. C. R. Symons, *Trans. Faraday Soc.*, **60**, 423 (1964).
 (26) Tetraalkylammonium salts were recrystallized from benzene or chloroform. Tetrabutylammonium fluoride was prepared as suggested by Allerhand and Schleyer.²⁰
 (27) S. C. Mohr, W. D. Wilk, and G. M. Barrow, *J. Am. Chem. Soc.*, **87**, 3048 (1965).

Procedures for Isothermal Diffusion Studies of Four-Component Systems¹

by Hyoungman Kim

Institute for Enzyme Research, University of Wisconsin, Madison, Wisconsin 53706
(Received September 13, 1965)

The basic differential equations are solved for the case of free diffusion in four-component systems. From the resulting expressions for the solute concentrations, corresponding equations are readily obtained for the solute concentrations in both restricted diffusion and steady-state diffusion. By using these expressions, procedures are developed for computing the nine diffusion coefficients from free, restricted, and steady-state diffusion experiments, respectively. It is found that in each case three different types of quantities, obtained from at least three diffusion experiments at given mean solute concentrations but with different initial relative solute concentration differences, are required to obtain nine relations which can be solved for the nine diffusion coefficients.

Introduction

During the past decade, procedures have been developed for obtaining four diffusion coefficients from free,²⁻⁶ restricted,⁶ and diaphragm cell⁷⁻⁹ diffusion experiments with ternary systems. Some data were obtained for a number of systems by using the Gouy diffusimeter^{3,10-21} and the diaphragm cell method.^{7-9,22-24} These results have shown that the cross-term diffusion coefficients are significant not only in the systems containing strong electrolytes but also in systems composed entirely of nonelectrolytes. The Onsager reciprocal relationship was verified for several of these systems.^{13-15,25,26}

From the earlier of these findings, it was emphasized²⁷ that generalized flow equations should be used for properly describing transport of biological macromolecules in buffer solutions and the transport of small molecules into and within the living cell. Theories for obtaining the molecular weights of macromolecules from sedimentation-diffusion experiments with multi-component systems have been published recently by a number of workers.²⁸⁻³²

The present study extends the Fujita-Gosting procedures^{4,5} for studying free diffusion of three-component systems into a procedure applicable to diffusion experiments on four-component systems. Fujita's procedures⁶ for studying restricted diffusion of ternary systems are also extended to a procedure for four-component systems, and it is found that a similar procedure can also be used in diaphragm cell studies of

four-component systems. It is hoped that these procedures will be of help in making improved diffusion studies of biological systems which can be treated as four-component systems.

(1) Part of this work was presented at the 148th National Meeting of the American Chemical Society, Chicago, Ill., Sept 1964. This investigation was supported in part by Public Health Service Research Grant AM-05177 from the National Institute of Arthritis and Metabolic Diseases.

(2) R. L. Baldwin, P. J. Dunlop, and L. J. Gosting, *J. Am. Chem. Soc.*, **77**, 5235 (1955).

(3) P. J. Dunlop and L. J. Gosting, *ibid.*, **77**, 5238 (1955).

(4) H. Fujita and L. J. Gosting, *ibid.*, **78**, 1099 (1956).

(5) H. Fujita and L. J. Gosting, *J. Phys. Chem.*, **64**, 1256 (1960).

(6) H. Fujita, *ibid.*, **63**, 242 (1959).

(7) E. R. Gilliland, R. F. Baddour, and D. J. Goldstein, *Can. J. Chem. Eng.*, **35**, 10 (1957).

(8) F. J. Kelly, Ph.D. Thesis, University of New England, Armidale, New South Wales, Australia, 1961.

(9) J. K. Burchard and H. L. Toor, *J. Phys. Chem.*, **66**, 2015 (1962).

(10) P. J. Dunlop, *ibid.*, **61**, 994, 1619 (1957).

(11) F. E. Weir and M. Dole, *J. Am. Chem. Soc.*, **80**, 302 (1958).

(12) I. J. O'Donnell and L. J. Gosting in "The Structure of Electrolytic Solutions," W. J. Hamer, Ed., John Wiley and Sons, Inc., New York, N. Y., 1959, p 160.

(13) P. J. Dunlop, *J. Phys. Chem.*, **61**, 63, 2091 (1959).

(14) L. A. Woolf, D. G. Miller, and L. J. Gosting, *J. Am. Chem. Soc.*, **84**, 317 (1962).

(15) R. P. Wendt, *J. Phys. Chem.*, **66**, 1279 (1962).

(16) L. A. Woolf, *ibid.*, **67**, 273 (1963).

(17) J. M. Creeth and L. A. Woolf, *ibid.*, **67**, 2777 (1963).

(18) G. Reinfelds and L. J. Gosting, *ibid.*, **68**, 2464 (1964).

(19) P. J. Dunlop, *ibid.*, **68**, 3062 (1964).

(20) P. J. Dunlop and L. J. Gosting, *ibid.*, **68**, 3874 (1964).

Basic Differential Equations and Their Solutions

In recent years some solutions of the differential equations of diffusion for any number of components have appeared.³³⁻³⁷ Of these, the solutions with matrix methods of Toor and of Stewart and Prober are most general and can be used for a number of boundary conditions. Although Toor's expressions for four-component systems (eq 26-28 of ref 36b) may be used in developing methods of obtaining the nine diffusion coefficients, the solution of the basic differential equations using the procedure adopted by Fujita and Gosting⁴ will be described briefly in order to define symbols and to relate this development to current procedures for studying ternary systems. The same final solutions can be obtained, after some manipulations, from eq 26-28 of ref 36b.

The differential equations for isothermal diffusion of a four-component system in one dimension can be written^{2,38}

$$\frac{\partial C_1}{\partial t} = D_{11} \frac{\partial^2 C_1}{\partial x^2} + D_{12} \frac{\partial^2 C_2}{\partial x^2} + D_{13} \frac{\partial^2 C_3}{\partial x^2} \quad (1a)$$

$$\frac{\partial C_2}{\partial t} = D_{21} \frac{\partial^2 C_1}{\partial x^2} + D_{22} \frac{\partial^2 C_2}{\partial x^2} + D_{23} \frac{\partial^2 C_3}{\partial x^2} \quad (1b)$$

$$\frac{\partial C_3}{\partial t} = D_{31} \frac{\partial^2 C_1}{\partial x^2} + D_{32} \frac{\partial^2 C_2}{\partial x^2} + D_{33} \frac{\partial^2 C_3}{\partial x^2} \quad (1c)$$

where t is time and x is the position coordinate measured downward from the position of the sharp initial boundary. Here it is assumed that the diffusion coefficients, D_{ij} , are independent of solute concentrations, C_1 , C_2 , and C_3 , within the diffusion cell and that no volume change occurs on mixing.³⁹⁻⁴¹

For free diffusion where a sharp boundary is formed at $t = 0$ between the upper and lower initial solutions, the combined initial and boundary conditions are⁴

$$C_i \longrightarrow \bar{C}_i + \Delta C_i/2 \quad (y \longrightarrow \infty) \quad (2a)$$

$$C_i \longrightarrow \bar{C}_i - \Delta C_i/2 \quad (y \longrightarrow -\infty) \quad (2b)$$

where

$$y = x/2\sqrt{t} \quad (3)$$

$$\bar{C}_i = [(C_i)_A + (C_i)_B]/2 \quad (4a)$$

and

$$\Delta C_i = (C_i)_B - (C_i)_A \quad (4b)$$

In eq 4, $(C_i)_A$ is the concentration of solute i in the upper initial solution and $(C_i)_B$ is the concentration of solute i in the lower initial solution.

Equations 1 can be converted into ordinary differential equations by using eq 3, and the resultant second-

order ordinary differential equations are transformed into first-order equations by substituting α for dC_1/dy , β for dC_2/dy , γ for dC_3/dy , and η for y .² The final equations thus obtained are

$$-(d\alpha/d\eta) = E_1\alpha + E_2\beta + E_3\gamma \quad (5a)$$

$$-(d\beta/d\eta) = F_1\alpha + F_2\beta + F_3\gamma \quad (5b)$$

$$-(d\gamma/d\eta) = G_1\alpha + G_2\beta + G_3\gamma \quad (5c)$$

where

$$E_1 = (D_{22}D_{33} - D_{23}D_{32})/|D_{ij}| \quad (6a)$$

$$E_2 = (D_{13}D_{32} - D_{12}D_{33})/|D_{ij}| \quad (6b)$$

$$E_3 = (D_{12}D_{23} - D_{13}D_{22})/|D_{ij}| \quad (6c)$$

$$F_1 = (D_{23}D_{31} - D_{21}D_{33})/|D_{ij}| \quad (6d)$$

$$F_2 = (D_{11}D_{33} - D_{13}D_{31})/|D_{ij}| \quad (6e)$$

$$F_3 = (D_{13}D_{21} - D_{11}D_{23})/|D_{ij}| \quad (6f)$$

(21) R. Fleming and L. J. Gosting, unpublished results.

(22) F. J. Kelly and R. H. Stokes in "Electrolytes," B. Presce, Ed., Pergamon Press, London, 1962.

(23) F. O. Shuck and H. L. Toor, *J. Phys. Chem.*, **67**, 540 (1963).

(24) P. N. Henrion, *Trans. Faraday Soc.*, **60**, 75 (1964).

(25) P. J. Dunlop and L. J. Gosting, *J. Phys. Chem.*, **63**, 86 (1959).

(26) D. G. Miller, *ibid.*, **63**, 570 (1959).

(27) L. J. Gosting in "Advances in Protein Chemistry," Vol. XI, Edsall, et al, Ed., Academic Press Inc., New York, N. Y., 1956.

(28) R. L. Baldwin, *J. Am. Chem. Soc.*, **80**, 496 (1958).

(29) J. W. Williams, K. E. Van Holde, R. L. Baldwin, and H. Fujita, *Chem. Rev.*, **58**, 715 (1958).

(30) L. Peller, *J. Chem. Phys.*, **29**, 415 (1958).

(31) H. Schönert, *J. Phys. Chem.*, **64**, 733 (1960).

(32) R. Haase in "Ultracentrifugal Analysis," J. W. Williams, Ed., Academic Press Inc., New York, N. Y., 1963.

(33) J. S. Kirkaldy, *Can. J. Phys.*, **37**, 30 (1959).

(34) L.-O. Sundelöf and I. Södervi, *Arkiv Kemi*, **21**, 143 (1963).

(35) E. L. Cussler, Jr., and E. N. Lightfoot, Jr., *A.I.Ch.E. J.*, **9**, 702 (1963).

(36) H. L. Toor, *ibid.*, (a) **10**, 448 (1964); (b) **10**, 460 (1964). Professor Toor's articles were brought to our attention when we had obtained the final solutions for free diffusion; we are indebted to him for sending us manuscripts of his papers, which were of help in generalizing those results to other boundary conditions.

(37) W. E. Stewart and R. Prober, *Ind. Eng. Chem. Fundamentals*, **3**, 224 (1964).

(38) G. J. Hooyman, *Physica*, **22**, 751 (1956).

(39) Here the unit of the concentration is left unspecified, except that it should be expressed as amount of solute per unit volume of solution. The numerical values of the cross-term diffusion coefficients vary with the unit of concentration used,¹⁰ e.g., grams or moles. All the diffusion coefficients are those for the volume-fixed frame of reference.

(40) These nine diffusion coefficients are not entirely independent, but are subject to the Onsager reciprocal relations, $L_{ij} = L_{ji}$. The relationship between the fundamental diffusion coefficients, L_{ij} , for the solvent-fixed reference frame and the practical diffusion coefficients of four-component systems for the volume-fixed reference frame are readily obtainable from eq 25 and 30 of ref 41.

(41) J. G. Kirkwood, R. L. Baldwin, P. J. Dunlop, L. J. Gosting, and G. Kegeles, *J. Chem. Phys.*, **33**, 1505 (1960).

$$G_1 = (D_{21}D_{32} - D_{22}D_{31})/|D_{ij}| \quad (6g)$$

$$G_2 = (D_{12}D_{31} - D_{11}D_{32})/|D_{ij}| \quad (6h)$$

$$G_3 = (D_{11}D_{22} - D_{12}D_{21})/|D_{ij}| \quad (6i)$$

and

$$|D_{ij}| = \begin{vmatrix} D_{11} & D_{12} & D_{13} \\ D_{21} & D_{22} & D_{23} \\ D_{31} & D_{32} & D_{33} \end{vmatrix} \quad (7)$$

The general solutions of eq 5 are⁴²

$$\alpha = P_1 e^{-\sigma_1 y} + P_2 e^{-\sigma_2 y} + P_3 e^{-\sigma_3 y} \quad (8a)$$

$$\beta = Q_1 e^{-\sigma_1 y} + Q_2 e^{-\sigma_2 y} + Q_3 e^{-\sigma_3 y} \quad (8b)$$

$$\gamma = S_1 e^{-\sigma_1 y} + S_2 e^{-\sigma_2 y} + S_3 e^{-\sigma_3 y} \quad (8c)$$

where P_i , Q_i , and S_i are the integration constants and the roots, σ_1 , σ_2 , and σ_3 , are obtained from the condition⁴²

$$\begin{vmatrix} E_1 - \sigma & E_2 & E_3 \\ F_1 & F_2 - \sigma & F_3 \\ G_1 & G_2 & G_3 - \sigma \end{vmatrix} = 0$$

which can be expanded to get a cubic equation

$$\begin{aligned} \sigma^3 - (E_1 + F_2 + G_3)\sigma^2 + (E_1F_2 + E_1G_3 + \\ F_2G_3 - E_2F_1 - E_3G_1 - F_3G_2)\sigma - \\ (E_1F_2G_3 + E_2F_3G_1 + E_3F_1G_2 - \\ E_1F_3G_2 - E_2F_1G_3 - E_3F_2G_1) = 0 \end{aligned} \quad (9)$$

From the properties of roots of polynomials it is easy to see that⁴³

$$\begin{aligned} \sigma_1 + \sigma_2 + \sigma_3 = E_1 + F_2 + G_3 = \\ (D_{11}D_{22} + D_{11}D_{33} + D_{22}D_{33} - \\ D_{12}D_{21} - D_{13}D_{31} - D_{23}D_{32})/|D_{ij}| \end{aligned} \quad (10a)$$

$$\begin{aligned} \sigma_1\sigma_2 + \sigma_1\sigma_3 + \sigma_2\sigma_3 = (E_1F_2 + E_1G_3 + \\ F_2G_3 - E_2F_1 - E_3G_1 - F_3G_2) = \\ (D_{11} + D_{22} + D_{33})/|D_{ij}| \end{aligned} \quad (10b)$$

$$\begin{aligned} \sigma_1\sigma_2\sigma_3 = (E_1F_2G_3 + E_2F_3G_1 + E_3F_1G_2 - \\ E_1F_3G_2 - E_2F_1G_3 - E_3F_2G_1) = 1/|D_{ij}| \end{aligned} \quad (10c)$$

The integration constants P_i , Q_i , and S_i are evaluated in the usual way, and the final solutions of the original differential equations are

$$C_1 = \bar{C}_1 + \Psi_{11}\Phi(\sqrt{\sigma_1}y) + \Psi_{12}\Phi(\sqrt{\sigma_2}y) + \Psi_{13}\Phi(\sqrt{\sigma_3}y) \quad (11a)$$

$$C_2 = \bar{C}_2 + \Psi_{21}\Phi(\sqrt{\sigma_1}y) + \Psi_{22}\Phi(\sqrt{\sigma_2}y) + \Psi_{23}\Phi(\sqrt{\sigma_3}y) \quad (11b)$$

$$C_3 = \bar{C}_3 + \Psi_{31}\Phi(\sqrt{\sigma_1}y) + \Psi_{32}\Phi(\sqrt{\sigma_2}y) + \Psi_{33}\Phi(\sqrt{\sigma_3}y) \quad (11c)$$

where

$$\Phi(q) = \frac{2}{\sqrt{\pi}} \int_0^q e^{-q^2} dq$$

$$\begin{aligned} \Psi_{1i} = \frac{(\sigma_k - \sigma_j)}{2g_1(\sigma)} \left\{ \Delta C_1 \left[\frac{D_{11}}{|D_{ij}|} + E_1\sigma_i - \sigma_i(\sigma_j + \sigma_k) \right] + \right. \\ \left. \Delta C_2 \left[\frac{D_{12}}{|D_{ij}|} + E_2\sigma_i \right] + \Delta C_3 \left[\frac{D_{13}}{|D_{ij}|} + E_3\sigma_i \right] \right\} \end{aligned} \quad (12a)$$

$$\begin{aligned} \Psi_{2i} = \frac{(\sigma_k - \sigma_j)}{2g_1(\sigma)} \left\{ \Delta C_1 \left[\frac{D_{21}}{|D_{ij}|} + F_1\sigma_i \right] + \right. \\ \left. \Delta C_2 \left[\frac{D_{22}}{|D_{ij}|} + F_2\sigma_i - \sigma_i(\sigma_j + \sigma_k) \right] + \right. \\ \left. \Delta C_3 \left[\frac{D_{23}}{|D_{ij}|} + F_3\sigma_i \right] \right\} \end{aligned} \quad (12b)$$

$$\begin{aligned} \Psi_{3i} = \frac{(\sigma_k - \sigma_j)}{2g_1(\sigma)} \left\{ \Delta C_1 \left[\frac{D_{31}}{|D_{ij}|} + G_1\sigma_i \right] + \right. \\ \left. \Delta C_2 \left[\frac{D_{32}}{|D_{ij}|} + G_2\sigma_i \right] + \right. \\ \left. \Delta C_3 \left[\frac{D_{33}}{|D_{ij}|} + G_3\sigma_i - \sigma_i(\sigma_j + \sigma_k) \right] \right\} \end{aligned} \quad (12c)$$

and

$$\begin{aligned} g_1(\sigma) = \sigma_1^2(\sigma_3 - \sigma_2) + \\ \sigma_2^2(\sigma_1 - \sigma_3) + \sigma_3^2(\sigma_2 - \sigma_1) \end{aligned} \quad (13)$$

Equations 12 are subject to the following restrictions: if $i = 1$, then $j = 2$ and $k = 3$; if $i = 2$, then $j = 3$ and $k = 1$; if $i = 3$, then $j = 1$ and $k = 2$.

The boundary conditions of restricted diffusion are given by

$$\partial C_i / \partial x = 0 \quad (x = \pm l, t \geq 0) \quad (14)$$

where l is one-half of the cell height and the x coordinate, which is measured downward, originates at the middle of the cell where initial solutions A and B meet at $t = 0$. It should be noted that the boundary condition of free diffusion is a special case of that of restricted diffusion when $l \rightarrow \infty$. It is apparent, therefore, when the initial conditions are the same, *i.e.*

(42) See, for example, W. T. Martin and E. Reissner, "Elementary Differential Equations," Addison-Wesley Publishing Co., Inc., Reading, Mass., 1957, p 146.

(43) See, for example, H. Margenau and G. M. Murphy, "The Mathematics of Physics and Chemistry," 2nd ed, D. Van Nostrand Co., Inc., New York, N. Y., 1956, p 318.

$$C_i = \bar{C}_i + \Delta C_i/2 \quad (0 < x < l, t = 0) \quad (15a)$$

$$C_i = \bar{C}_i - \Delta C_i/2 \quad (-l < x < 0, t = 0) \quad (15b)$$

that the coefficients Ψ_{ij} , which are independent of x and t , in eq 12 should remain the same when the boundary condition is changed from restricted diffusion to free diffusion or *vice versa*. This has been shown for a three-component system⁶ where the expressions for solute concentrations in restricted diffusion were reduced to the expressions for solute concentrations in free diffusion as $l \rightarrow \infty$. In that case⁴⁴

$$\Phi(\sigma_i, x, t) \rightarrow \Phi(\sqrt{\sigma_i}y) \quad (l \rightarrow \infty) \quad (16a)$$

where

$$\Phi(\sigma_i, x, t) = \frac{4}{\pi} \sum_{n=0}^{\infty} \frac{\sin [(2n+1)\pi x/2l]}{2n+1} \times \exp[-(2n+1)^2\pi^2 t/4l^2\sigma_i] \quad (16b)$$

From this it may be inferred that, for systems with any number of components, it is possible to obtain expressions of solute concentrations for one of these two boundary conditions from known solutions for the other boundary condition. This was clearly shown by Toor³⁶ and Stewart and Prober³⁷ in their elegant papers.

The expressions for solute concentrations in the case of restricted diffusion of a four-component system can be, therefore, obtained from eq 11, 12, and 16.⁴⁵

$$C_1 = \bar{C}_1 + \Psi_{11}\Phi(\sigma_1, x, t) + \Psi_{12}\Phi(\sigma_2, x, t) - \Psi_{13}\Phi(\sigma_3, x, t) \quad (17a)$$

$$C_2 = \bar{C}_2 + \Psi_{21}\Phi(\sigma_1, x, t) + \Psi_{22}\Phi(\sigma_2, x, t) + \Psi_{23}\Phi(\sigma_3, x, t) \quad (17b)$$

$$C_3 = \bar{C}_3 + \Psi_{31}\Phi(\sigma_1, x, t) + \Psi_{32}\Phi(\sigma_2, x, t) + \Psi_{33}\Phi(\sigma_3, x, t) \quad (17c)$$

All of the notations in eq 17 were defined previously.

It is interesting to note that the coefficients, Ψ_{ij} , of the probability integrals in the expressions for solute concentrations in ternary free diffusion are identical with the corresponding coefficients in the expressions for the diaphragm cell method.^{7,8} This will now be shown to be true for four-component systems also. The basic differential equations describing four-component steady-state diffusion in the diaphragm cell are^{7-9,46}

$$-\frac{d\Delta C_i(t)}{kdt} = D_{i1}\Delta C_1(t) + D_{i2}\Delta C_2(t) + D_{i3}\Delta C_3(t) \quad (i = 1, 2, 3) \quad (18)$$

where k is the diaphragm cell constant⁴⁷ and $\Delta C_i(t)$

is the concentration difference of solute i between the upper and the lower compartments of the diaphragm cell at any time t . Using a procedure similar to that adopted for solving eq 5, one may obtain the following solutions.⁴⁸

$$\Delta C_1(t) = 2\{\Psi_{11}\Phi(t/\sigma_1) + \Psi_{12}\Phi(t/\sigma_2) + \Psi_{13}\Phi(t/\sigma_3)\} \quad (19a)$$

$$\Delta C_2(t) = 2\{\Psi_{21}\Phi(t/\sigma_1) + \Psi_{22}\Phi(t/\sigma_2) + \Psi_{23}\Phi(t/\sigma_3)\} \quad (19b)$$

$$\Delta C_3(t) = 2\{\Psi_{31}\Phi(t/\sigma_1) + \Psi_{32}\Phi(t/\sigma_2) + \Psi_{33}\Phi(t/\sigma_3)\} \quad (19c)$$

where

$$\Phi(t/\sigma_i) = e^{-(k/\sigma_i)t} \quad (19d)$$

(44) Strictly speaking, the symbol $\Phi(\sigma_i, x, t)$ should be used instead of $\Phi(\sigma_i, x, t)$. For the sake of brevity of equations, l is not included in the symbol; l is constant for a given diffusion cell.

(45) These equations may be also obtained from the general equations of Cussler and Lightfoot.³⁶

(46) Although ref 7-9 did not give equations for four-component systems, the derivations in those articles are readily extended to show that eq 18 describes the diffusion of a four-component system in the diaphragm cell.

(47) k is the characteristic constant of the cell defined as $k = (A'/l')[1/V' + 1/V'']$, and is obtained by calibration; A' is the total effective cross section and l' is average effective diffusional length of the pores of the diaphragm, respectively. V' and V'' are the volumes of upper and lower compartments, respectively.

(48) Solutions of eq 18 actually give

$$\Delta C_i(t) = \sum_{j=1}^3 K_{ij}e^{-\sigma_j'kt} \quad (1')$$

$$K_{1j} = \frac{(\sigma_k' - \sigma_l')}{g_1(\sigma_j')} \{ \Delta C_1 [D_{23}D_{32} - (D_{22} - \sigma_j')(D_{33} - \sigma_j')] + \Delta C_2 [D_{12}(D_{33} - \sigma_j') - D_{13}D_{32}] + \Delta C_3 [D_{13}(D_{22} - \sigma_j') - D_{12}D_{23}] \} \quad (2')$$

$$K_{2j} = \frac{(\sigma_k' - \sigma_l')}{g_2(\sigma_j')} \{ \Delta C_1 [D_{21}(D_{33} - \sigma_j') - D_{23}D_{31}] + \Delta C_2 [D_{13}D_{31} - (D_{11} - \sigma_j')(D_{33} - \sigma_j')] + \Delta C_3 [D_{23}(D_{11} - \sigma_j') - D_{13}D_{21}] \} \quad (3')$$

$$K_{3j} = \frac{(\sigma_k' - \sigma_l')}{g_3(\sigma_j')} \{ \Delta C_1 [D_{31}(D_{22} - \sigma_j') - D_{21}D_{32}] + \Delta C_2 [D_{32}(D_{11} - \sigma_j') - D_{12}D_{31}] + \Delta C_3 [D_{12}D_{21} - (D_{11} - \sigma_j')(D_{22} - \sigma_j')] \} \quad (4')$$

and

$$g_1(\sigma') = \sigma_1'^2(\sigma_3' - \sigma_2') + \sigma_2'^2(\sigma_1' - \sigma_3') + \sigma_3'^2(\sigma_2' - \sigma_1') \quad (5')$$

Equations 1'-4' are subject to the following restrictions: if $j = 1$, $k = 2$ and $l = 3$; if $j = 2$, $k = 3$ and $l = 1$; if $j = 3$, $k = 1$ and $l = 2$. The roots σ' are obtained from the condition

$$|D_{ij} - \sigma'\delta_{ij}| = 0 \quad (6')$$

where δ_{ij} is the Kronecker delta. Using the relation $\sigma_i' = 1/\sigma_i$ and eq 10, eq 1' can be converted into eq 19.

It is, therefore, clear that all the solutions for free, restricted, and steady-state diffusions have the same coefficients Ψ_{ij} . The factor 2 in eq 19 derives from the facts that these expressions are for ΔC_i instead of C_i and that $\exp(-kt/\sigma_i)$ are odd functions. The functions Φ in eq 11 and 17 are also odd functions.

Methods for Determination of the Nine D_{ij}

Free Diffusion Using the Gouy Diffusometer. In the procedures for studying free diffusion of ternary systems using the Gouy diffusometer,²⁻⁵ the measurement of two "experimental quantities" in each of two or more experiments is required for each procedure. The experimental quantities which have been used are: reduced height-area ratio, reduced second and fourth moments, a particular reduced fringe deviation, and the area under the reduced deviation graph. The present study employs three of these experimental quantities, which provide more accuracy than do the other two, to obtain a procedure for studying of four-component systems. The notation of Fujita and Gosting^{4,5} is followed wherever practical.

The refractive index, n , of a solution with three solutes may be represented by

$$n = n(\bar{C}_1, \bar{C}_2, \bar{C}_3) + \sum_{i=1}^3 R_i(C_i - \bar{C}_i) \quad (20)$$

if the values of $(C_i - \bar{C}_i)$ are sufficiently small. In eq 20, $n(\bar{C}_1, \bar{C}_2, \bar{C}_3)$ is the refractive index of a solution in which the solute concentrations are \bar{C}_1 , \bar{C}_2 , and \bar{C}_3 , respectively. Each R_i is the refractive index derivative for the i th solute; these are assumed to be constants for the relatively small concentration differences within the diffusion cell.

Introduction of eq 11 and 12 into eq 20 after identifying \bar{C}_i with \bar{C}_i , and use of eq 10a, gives

$$n = n(\bar{C}_1, \bar{C}_2, \bar{C}_3) + \frac{\Delta n}{2} \sum_{i=1}^3 \Gamma_i(R) \Phi(\sqrt{\sigma_i} y) \quad (21)$$

Here $n(\bar{C}_1, \bar{C}_2, \bar{C}_3)$ is the refractive index of the solution at the initial boundary position, where each $\bar{C}_i = \bar{C}_i$, and

$$\Gamma_1(R) = \frac{(\sigma_3 - \sigma_2)}{g_1(\sigma)} \left\{ \sum_{i=1}^3 \alpha_i(R) [X_i(R) + Y_i(R)\sigma_1 - \sigma_1(\sigma_2 + \sigma_3)] \right\} \quad (22a)$$

$$\Gamma_2(R) = \frac{(\sigma_1 - \sigma_3)}{g_1(\sigma)} \left\{ \sum_{i=1}^3 \alpha_i(R) [X_i(R) + Y_i(R)\sigma_2 - \sigma_2(\sigma_1 + \sigma_3)] \right\} \quad (22b)$$

$$\Gamma_3(R) = \frac{(\sigma_2 - \sigma_1)}{g_1(\sigma)} \left\{ \sum_{i=1}^3 \alpha_i(R) [X_i(R) + Y_i(R)\sigma_3 - \sigma_3(\sigma_1 + \sigma_2)] \right\} \quad (22c)$$

$$\alpha_i(R) = R_i \Delta C_i / \Delta n \quad (23)$$

$$\Delta n = \sum_{i=1}^3 R_i \Delta C_i \quad (24)$$

$$X_i(R) = (R_1 D_{1i} + R_2 D_{2i} + R_3 D_{3i}) / R_i |D_{ij}| \quad (25)$$

$$Y_i(R) = (R_1 E_i + R_2 F_i + R_3 G_i) / R_i \quad (i = 1, 2, 3) \quad (26)$$

From eq 22 it can be shown that

$$\Gamma_1(R) + \Gamma_2(R) + \Gamma_3(R) = 1 \quad (27)$$

since

$$\alpha_1(R) + \alpha_2(R) + \alpha_3(R) = 1 \quad (28)$$

(a) *Reduced Height-Area Ratios.* The reduced height-area ratio is defined by³

$$\mathfrak{D}_A = (\Delta n)^2 / 4\pi t (\partial n / \partial x)_{\max}^2 \quad (29)$$

Introduction of the maximum value of the first derivative of eq 21 with respect to x into eq 29 yields

$$1/\sqrt{\mathfrak{D}_A} = \Gamma_1(R)\sqrt{\sigma_1} + \Gamma_2(R)\sqrt{\sigma_2} + \Gamma_3(R)\sqrt{\sigma_3} \quad (30)$$

By rearranging this equation in terms of the solute refractive fractions, $\alpha_i(R)$, one obtains

$$1/\sqrt{\mathfrak{D}_A} = \mu_1 \alpha_1(R) + \mu_2 \alpha_2(R) + \mu_3 \alpha_3(R) \quad (31)$$

where

$$\mu_i = \frac{1}{g_1(\sigma)} [X_i(R)g_2(\sigma) + Y_i(R)g_3(\sigma) - g_4(\sigma)] \quad (32)$$

$$g_2(\sigma) = (\sigma_3 - \sigma_2)\sqrt{\sigma_1} + (\sigma_1 - \sigma_3)\sqrt{\sigma_2} + (\sigma_2 - \sigma_1)\sqrt{\sigma_3} \quad (33a)$$

$$g_3(\sigma) = (\sigma_3 - \sigma_2)\sigma_1\sqrt{\sigma_1} + (\sigma_1 - \sigma_3)\sigma_2\sqrt{\sigma_2} + (\sigma_2 - \sigma_1)\sigma_3\sqrt{\sigma_3} \quad (33b)$$

and

$$g_4(\sigma) = (\sigma_3^2 - \sigma_2^2)\sigma_1\sqrt{\sigma_1} + (\sigma_1^2 - \sigma_3^2)\sigma_2\sqrt{\sigma_2} + (\sigma_2^2 - \sigma_1^2)\sigma_3\sqrt{\sigma_3} \quad (33c)$$

The μ_i may be calculated from the values of \mathfrak{D}_A for three or more Gouy diffusion experiments at given mean solute concentrations and different values of $\alpha_i(R)$.

(b) *Reduced Second Moment.* The reduced second moment is defined by²

$$\mathfrak{D}_{2m} = m_2/2t \quad (34)$$

where m_2 is the second moment of the refractive index gradient curve at time t , and for four-component systems

$$m_2 = \sum_{i=1}^3 (m_2)_i \tag{35a}$$

in which

$$(m_2)_i = 2t \sum_{j=1}^3 (R_i/R_j) D_{ij} \alpha_j(R) \tag{35b}$$

From eq 34 and 35⁴⁹

$$\mathcal{D}_{2m} = \sum_{i=1}^3 \alpha_i(R) \epsilon_i(R) \tag{36a}$$

where

$$\epsilon_i(R) = (R_1 D_{1i} + R_2 D_{2i} + R_3 D_{3i})/R_i \tag{36b}$$

Here again the values of ϵ_i defined in eq 36b may be calculated from the values of \mathcal{D}_{2m} for the three or more experiments used to obtain \mathcal{D}_A and μ_i .

(c) *Area under the Fringe Deviation Graph.* The area Q of a fringe deviation graph is defined as⁵

$$Q = \int_0^1 \Omega(\zeta) df(\zeta) \tag{37}$$

Here the reduced fringe deviation $\Omega(\zeta)$ is⁵⁰

$$\Omega(\zeta) = e^{-\zeta^2} - Y/C_t \tag{38}$$

where Y is the downward displacement of a Gouy fringe below the undeviated slit image and may be expressed by $Y = ab(\partial n/\partial x)$; C_t is the maximum displacement of light predicted by ray optics and is defined as $C_t = ab(\partial n/\partial x)_{\max}$. The quantities a and b are the thickness of the diffusion cell in the direction of the optical axis and the optical lever arm, respectively. Introduction of the values of $\partial n/\partial x$ and $(\partial n/\partial x)_{\max}$, obtained from eq 21 yields

$$\Omega(\zeta) = e^{-\zeta^2} - \frac{\sum_{i=1}^3 \Gamma_i(R) \sqrt{\sigma_i} e^{-\sigma_i y^2}}{\sum_{i=1}^3 \Gamma_i(R) \sqrt{\sigma_i}} \tag{39}$$

The interference conditions for the zeros of intensity in a Gouy fringe pattern arising from any symmetrical refractive index gradient curve is given by^{5,51,52}

$$f(\zeta)J = \frac{2a}{\lambda} [(n - n_m) - x(\partial n/\partial x)] \simeq Z_j \tag{40}$$

where Z_j is related to zeros of the Airy integral⁵³ and $J = a\Delta n/\lambda$ is the total number of fringes, λ being the wavelength of the light. The symbol n_m denotes the refractive index of the solution at the position of

maximum refractive index gradient; for the symmetrical refractive index gradients considered here this is at $x = 0$ and is equal to $n(\bar{C}_1, \bar{C}_2, \bar{C}_3)$. Introduction of eq 21 and its derivative into eq 40 and use of the definition

$$f(q) = \Phi(q) - \frac{2}{\sqrt{\pi}} q e^{-q^2}$$

yields

$$f(\zeta) = \sum_{i=1}^3 \Gamma_i(R) f(\sqrt{\sigma_i} y) \tag{41}$$

By combining eq 37, 39, and 41 one obtains

$$Q = \int_0^\infty e^{\zeta^2} \frac{df(\zeta)}{d\zeta} d\zeta - \int_0^\infty \frac{\sum_{i=1}^3 \Gamma_i(R) \sqrt{\sigma_i} e^{-\sigma_i y^2}}{\sum_{i=1}^3 \Gamma_i(R) \sqrt{\sigma_i}} \frac{df(\zeta)}{dz} dz \tag{42}$$

where

$$z = \sqrt{\sigma_1} y$$

$$\frac{df(\zeta)}{d\zeta} = \frac{4}{\sqrt{\pi}} \zeta^2 e^{-\zeta^2} \tag{43}$$

and

$$\frac{df(\zeta)}{dz} = \frac{4}{\sqrt{\pi}} \left\{ \Gamma_1(R) z^2 e^{-z^2} + \Gamma_2(R) \left(\frac{\sigma_2}{\sigma_1}\right)^{1/2} z^2 e^{-\frac{\sigma_2}{\sigma_1} z^2} + \Gamma_3(R) \left(\frac{\sigma_3}{\sigma_1}\right)^{1/2} z^2 e^{-\frac{\sigma_3}{\sigma_1} z^2} \right\} \tag{44}$$

The integration of eq 42 is straightforward and the final result, after use of eq 27 becomes

$$Q = [\Gamma_1(R)\Gamma_2(R)g(\sqrt{\sigma_1}, \sqrt{\sigma_2}) + \Gamma_1(R)\Gamma_3(R)g(\sqrt{\sigma_1}, \sqrt{\sigma_3}) + \Gamma_2(R)\Gamma_3(R)g(\sqrt{\sigma_2}, \sqrt{\sigma_3})] / [\Gamma_1(R)\sqrt{\sigma_1} + \Gamma_2(R)\sqrt{\sigma_2} + \Gamma_3(R)\sqrt{\sigma_3}] \tag{45}$$

(49) The same equation may be obtained by introducing eq 21 into the relation

$$m_2 = \frac{1}{\Delta n} \int_{-\infty}^{+\infty} x^2 (\partial n/\partial x) dx$$

which defines the second moment of the refractive index gradient curve.³

(50) D. F. Akeley and L. J. Gosting, *J. Am. Chem. Soc.*, **75**, 5685 (1953).

(51) G. Kegeles and L. J. Gosting, *ibid.*, **69**, 2516 (1947).

(52) L. J. Gosting and L. Onsager, *ibid.*, **74**, 6066 (1952).

(53) L. J. Gosting and M. S. Morris, *ibid.*, **71**, 1998 (1949).

where

$$g(\sqrt{\sigma_i}, \sqrt{\sigma_j}) = \frac{\sqrt{\sigma_i} + \sqrt{\sigma_j}}{2\sqrt{2}} - \frac{\sqrt{\sigma_i\sigma_j}}{\sqrt{\sigma_i} + \sigma_j} \quad (46)$$

The use of eq 30 transforms eq 45 into

$$Q/\sqrt{\mathcal{D}_A} = \Gamma_1(R)\Gamma_2(R)g(\sqrt{\sigma_1}, \sqrt{\sigma_2}) + \Gamma_1(R)\Gamma_3(R)g(\sqrt{\sigma_1}, \sqrt{\sigma_3}) + \Gamma_2(R)\Gamma_3(R)g(\sqrt{\sigma_2}, \sqrt{\sigma_3}) \quad (47)$$

No direct way has been found yet to solve the functions obtained from the reduced height-area ratio, reduced second moment, and the area under the reduced deviation graph, for the nine diffusion coefficients. It is, however, possible to convert functions of D_{ij} and σ_i obtained from Q entirely into functions of σ_i , and using the data from three experiments, values of σ_1 , σ_2 , and σ_3 are obtained in the following way.

(d) *Evaluation of the σ_i Using a Method of Successive Approximation.* From eq 10c, 25, and 36b, one obtains

$$X_i(R) = \sigma_1\sigma_2\sigma_3\epsilon_i(R) \quad (48)$$

And from eq 32 and 48

$$Y_i(R) = [\mu_i g_1(\sigma) - \sigma_1\sigma_2\sigma_3\epsilon_i(R)g_2(\sigma) + g_4(\sigma)]/g_3(\sigma) \quad (49)$$

By substituting eq 22, and then eq 48 and 49, into eq 47, one obtains an expression for $Q/\sqrt{\mathcal{D}_A}$ in which σ_1 , σ_2 , and σ_3 are the only unknowns since the μ_i and $\epsilon_i(R)$ can be obtained from \mathcal{D}_A and \mathcal{D}_{2m} measured in the experiments. From three diffusion experiments with the same mean solute concentrations and different $\alpha_i(R)$ values one may obtain three equations for $Q/\sqrt{\mathcal{D}_A}$. A digital computer may be used to obtain the values of σ_i by successive approximations in the following manner.

First, approximate values are chosen for σ_1 , σ_2 , and σ_3 and these are introduced into the right-hand side of eq 47 obtained from the first experiment (hereafter denoted as eq 47-I). Next the value of σ_1 is adjusted until the value of the right-hand side of eq 47-I becomes identical with the value of $Q/\sqrt{\mathcal{D}_A}$. This σ_1 value and the previously chosen σ_3 value are now introduced into eq 47 obtained from the second experiment (eq 47-II) and the value of σ_2 is adjusted this time until the right-hand side of eq 47-II becomes identical with the value of $Q/\sqrt{\mathcal{D}_A}$. These improved values of σ_1 and σ_2 are introduced into eq 47 obtained from the third diffusion experiment (eq 47-III) and the value of σ_3 is adjusted until σ_3 value satisfies eq 47-III. These three improved σ_i values are now used

as the starting values of the second series of successive approximations and these cycles are repeated until σ_i values from consecutive cycles become identical. In the process of the above operations $Y_i(R)$ are automatically obtained.

(e) *Expressions for the Nine Diffusion Coefficients.* Once the three values of σ_i and three values of $Y_i(R)$ are known, it is possible to derive the following nine equations. From eq 7 and 10

$$(\sigma_1 + \sigma_2 + \sigma_3)/\sigma_1\sigma_2\sigma_3 = D_{11}D_{22} + D_{11}D_{33} + D_{22}D_{33} - D_{12}D_{21} - D_{13}D_{31} - D_{23}D_{32} \quad (50a)$$

$$(\sigma_1\sigma_2 + \sigma_1\sigma_3 + \sigma_2\sigma_3)/\sigma_1\sigma_2\sigma_3 = D_{11} + D_{22} + D_{33} \quad (50b)$$

$$1/\sigma_1\sigma_2\sigma_3 = D_{11}D_{22}D_{33} + D_{12}D_{23}D_{31} + D_{13}D_{21}D_{32} - D_{11}D_{23}D_{32} - D_{12}D_{21}D_{33} - D_{13}D_{22}D_{31} \quad (50c)$$

From eq 6, 10c, and 26

$$Y_1(R)/\sigma_1\sigma_2\sigma_3 = (D_{22}D_{33} - D_{23}D_{32}) + \frac{R_2}{R_1}(D_{23}D_{31} - D_{21}D_{33}) + \frac{R_3}{R_1}(D_{21}D_{32} - D_{22}D_{31}) \quad (51a)$$

$$Y_2(R)/\sigma_1\sigma_2\sigma_3 = \frac{R_1}{R_2}(D_{13}D_{32} - D_{12}D_{33}) + (D_{11}D_{33} - D_{13}D_{31}) + \frac{R_3}{R_2}(D_{12}D_{31} - D_{11}D_{32}) \quad (51b)$$

$$Y_3(R)/\sigma_1\sigma_2\sigma_3 = \frac{R_1}{R_3}(D_{12}D_{23} - D_{13}D_{22}) + \frac{R_2}{R_3}(D_{13}D_{21} - D_{11}D_{23}) + (D_{11}D_{22} - D_{12}D_{21}) \quad (51c)$$

and from eq 36b

$$\epsilon_1(R) = D_{11} + (R_2/R_1)D_{21} + (R_3/R_1)D_{31} \quad (52a)$$

$$\epsilon_2(R) = (R_1/R_2)D_{12} + D_{22} + (R_3/R_2)D_{32} \quad (52b)$$

$$\epsilon_3(R) = (R_1/R_3)D_{13} + (R_2/R_3)D_{23} + D_{33} \quad (52c)$$

Equations 50-52 may be solved for the nine diffusion coefficients, and the following relations are obtained after some manipulations

$$(R_1/R_i)D_{1i} = \{ [Y_3(R) - Y_2(R)]G_i(R) + [\epsilon_2(R) - \epsilon_3(R)] + \epsilon_1(R)[\epsilon_3(R)Y_2(R) - \epsilon_2(R)Y_3(R)] \} / U(R) \quad (53a)$$

$$(R_2/R_i)D_{2i} = \{ [Y_1(R) - Y_3(R)]G_i(R) + [\epsilon_3(R) - \epsilon_1(R)] + \epsilon_i(R)[\epsilon_1(R)Y_3(R) - \epsilon_3(R)Y_1(R)] \} / U(R) \quad (53b)$$

$$(R_3/R_i)D_{3i} = \{ [Y_2(R) - Y_1(R)]G_i(R) + [\epsilon_1(R) - \epsilon_2(R)] + \epsilon_i(R)[\epsilon_2(R)Y_1(R) - \epsilon_1(R)Y_2(R)] \} / U(R) \quad (53c)$$

where

$$G_i(R) = \{ \epsilon_i(R)(\sigma_1\sigma_2 + \sigma_1\sigma_3 + \sigma_2\sigma_3) - (\sigma_1 + \sigma_2 + \sigma_3) + Y_i(R) \} (\sigma_1\sigma_2\sigma_3)^{-1} \quad (54)$$

and

$$U(R) = \epsilon_1(R)\{Y_3(R) - Y_2(R)\} + \epsilon_2(R)\{Y_1(R) - Y_3(R)\} + \epsilon_3(R)\{Y_2(R) - Y_1(R)\} \quad (55)$$

The values of the refractive index derivative R_i may be obtained from the same Gouy diffusion experiments which are performed to obtain other quantities necessary for the computation of the diffusion coefficients. Introduction of the relationship $J = a\Delta n/\lambda$ into eq 24 gives

$$\lambda J/a = R_1\Delta C_1 + R_2\Delta C_2 + R_3\Delta C_3 \quad (56)$$

which will give the values of R_1 , R_2 , and R_3 from three experiments at the same mean solute concentrations and with different combinations of ΔC_i .

Restricted Diffusion Using the Conductance Method. Fujita developed two procedures of studying ternary strong electrolyte systems employing Harned's conductance method.⁵⁴ One uses the zeroth and first moments of curves of specific conductance differences at two levels in the cell *vs.* time for at least two experiments, and the other procedure employs data from at least two experiments for certain specific conductance differences at various times and the zeroth moments of the specific conductance difference *vs.* time curve. Although the same equations are applicable to any restricted diffusion experiments in which an appropriate intensive property (conductance, refractive index, optical rotation, etc.) which is linearly related to the solute concentrations at two suitable levels in the cell is measured, the conductance method has received more attention than others so far. The present study extends these procedures to the study of four-component electrolyte systems; all three quantities mentioned above are needed in studying these systems.⁵⁵⁻⁵⁷

The requirement of linear dependence of the specific conductance of the solution on the solute concentration is inherent in Harned's method, and we assume here that the specific conductance $K(t)$ in a four-component system is represented by

$$K(t) = K(\bar{C}_1, \bar{C}_2, \bar{C}_3) + \sum_{i=1}^3 \kappa_i(C_i - \bar{C}_i) \quad (57)$$

where $K(\bar{C}_1, \bar{C}_2, \bar{C}_3)$ is the specific conductance of the solution in which the solute concentrations are \bar{C}_1 , \bar{C}_2 , and \bar{C}_3 , respectively. Each κ_i is the specific conductance derivative for the i th solute and it is assumed to be constant within the concentration range in the diffusion cell for each experiment.

Introduction of eq 12 and 17 into eq 57, after identifying \bar{C}_i with \bar{C}_i and use of eq 10a, gives

$$K(t) = K(\bar{C}_1, \bar{C}_2, \bar{C}_3) + \frac{\Delta K(0)}{2} \sum_{i=1}^3 \Gamma_i(\kappa) \Phi(\sigma_i, a, t) \quad (58)$$

where $K(\bar{C}_1, \bar{C}_2, \bar{C}_3)$ is the specific conductance of the solution at the initial boundary position. The notations $\Gamma_i(\kappa)$ represent eq 22 when all the R_i are replaced by κ_i in eq 23 through eq 26 and $\alpha_i(\kappa)$ is defined by

$$\alpha_i(\kappa) = \kappa_i \Delta C_i / \Delta K(0) \quad (59)$$

where

$$\Delta K(0) = \sum_{i=1}^3 \kappa_i \Delta C_i \quad (60)$$

Here again it can be shown that

$$\sum_{i=1}^3 \Gamma_i(\kappa) = \sum_{i=1}^3 \alpha_i(\kappa) = 1 \quad (61)$$

In the procedures of Harned, *et al.*,⁵⁴ two pairs of electrodes are placed at the two levels $x = \pm 2l/3$ of the diffusion cell, and the difference in specific conductance of the solution at these two levels is measured as a function of time. From eq 58 this difference is

$$\Delta K(t) = \Delta K(0) \sum_{i=1}^3 \Gamma_i(\kappa) \Phi(\sigma_i, 2l/3, t) \quad (62)$$

The zeroth moment of the $\Delta K(t)$ curve about the axis $t = 0$ may be obtained by integrating eq 62 with the use of eq 35 of ref 6.

$$\int_0^{\infty} \Delta K(t) dt = [4l^2 \Delta K(0) / 9] \sum_{i=1}^3 \alpha_i(\kappa) Y_i(\kappa) \quad (63)$$

(54) H. S. Harned and D. M. French, *Ann. N. Y. Acad. Sci.*, **46**, 267 (1945); H. S. Harned and R. L. Nuttall, *J. Am. Chem. Soc.*, **69**, 736 (1947).

(55) In recent years, Harned's conductance method has been extended to binary systems containing weak 1-1 electrolyte, when the degree of ionization of the weak electrolyte is known.⁵⁶ It may be possible to study multicomponent systems including a simple weak electrolyte when the degree of ionization of the weak electrolyte in the presence of other salts is known *a priori*. The Gouy optical method of restricted diffusion developed by Kegeles and associates,⁵⁷ though applicable to any system including nonelectrolytes, seems too complicated for studying system with three or more components at the moment.

(56) E. L. Holt and P. A. Lycns, *J. Phys. Chem.*, **69**, 2341 (1965); also E. L. Holt, Ph.D. Thesis, Yale University, 1961.

(57) H. Kim, B. S. Patel, and G. Kegeles, *J. Phys. Chem.*, **66**, 1960 (1962).

The first moment of the $\Delta K(t)$ curve about the $t = 0$ axis⁶ can also be obtained in a similar way and the final result is found to be

$$\int_0^{\infty} \Delta K(t) dt = [44l^4 \Delta K(0)/243] \sum_{i=1}^3 \alpha_i(\kappa) \phi_i(\kappa) \quad (64)$$

where

$$\phi_i(\kappa) = [X_i(\kappa)g_1(\sigma) + Y_i(\kappa)g_5(\sigma) - g_6(\sigma)]/g_1(\sigma) \quad (65)$$

$$g_5(\sigma) = \sigma_1^3(\sigma_3 - \sigma_2) + \sigma_2^3(\sigma_1 - \sigma_3) + \sigma_3^3(\sigma_2 - \sigma_1) \quad (66a)$$

$$g_6(\sigma) = \sigma_1^3(\sigma_3^2 - \sigma_2^2) + \sigma_2^3(\sigma_1^2 - \sigma_3^2) + \sigma_3^3(\sigma_2^2 - \sigma_1^2) \quad (66b)$$

From at least three restricted diffusion experiments with given mean solute concentrations and different combinations of $\alpha_i(\kappa)$ it is possible to evaluate $Y_i(\kappa)$ and $\phi_i(\kappa)$ from eq 63 and 64.

When t is large, *i.e.*, during the later stages of the restricted diffusion, only the first term of the Fourier series in Φ is important. Introduction of expressions for $\Gamma_i(\kappa)$ into eq 62 for such cases when t is large and rearrangement of the resulting equation in terms of $\alpha_i(\kappa)$ gives

$$\frac{\pi \Delta K(t)}{2\sqrt{3} \Delta K(0)} = \sum_{i=1}^3 \frac{\alpha_i(\kappa)}{g_1(\sigma)} [X_i(\kappa)f(\sigma, \tau) + Y_i(\kappa)g(\sigma, \tau) - h(\sigma, \tau)] \quad (67)$$

where

$$f(\sigma, \tau) = (\sigma_3 - \sigma_2)e^{-\tau/\sigma_1} + (\sigma_1 - \sigma_3)e^{-\tau/\sigma_2} + (\sigma_2 - \sigma_1)e^{-\tau/\sigma_3} \quad (68a)$$

$$g(\sigma, \tau) = \sigma_1(\sigma_3 - \sigma_2)e^{-\tau/\sigma_1} + \sigma_2(\sigma_1 - \sigma_3)e^{-\tau/\sigma_2} + \sigma_3(\sigma_2 - \sigma_1)e^{-\tau/\sigma_3} \quad (68b)$$

$$h(\sigma, \tau) = \sigma_1(\sigma_3^2 - \sigma_2^2)e^{-\tau/\sigma_1} + \sigma_2(\sigma_1^2 - \sigma_3^2)e^{-\tau/\sigma_2} + \sigma_3(\sigma_2^2 - \sigma_1^2)e^{-\tau/\sigma_3} \quad (68c)$$

and

$$\tau = \pi^2 t / 4l^2 \quad (69)$$

Equation 65 is now rearranged to get

$$X_i(\kappa) = [\phi_i(\kappa)g_1(\sigma) - Y_i(\kappa)g_5(\sigma) + g_6(\sigma)]/g_1(\sigma) \quad (70)$$

Introduction of eq 70 brings eq 67 into an equation with σ_1 , σ_2 , and σ_3 as unknowns if t is known. If one has three values of $\Delta K(t)/\Delta K(0)$ obtained from the same experiments from which $Y_i(\kappa)$ and $\phi_i(\kappa)$ are obtained,⁵⁸ the successive approximation method may

be used to evaluate three values of σ_i and then the three values of $X_i(\kappa)$.

Once we have all the values of σ_i , $X_i(\kappa)$, and $Y_i(\kappa)$, it is possible to obtain the nine relations designated previously as eq 50–52, when all the R_i are replaced by κ_i . From these it is possible to obtain expressions for individual diffusion coefficients which are identical with eq 53 when R_i are replaced by κ_i . The values of κ_i may be obtained using eq 60.

Diaphragm Cell Method. In the diaphragm cell method it is frequently possible to determine experimentally the concentration differences of all the solutes during the diffusion experiments. For this case eq 19 (after substituting eq 12) may be rearranged in terms of ΔC_i and use of eq 10 gives

$$\Delta C_1(t) = \Delta C_1 [D_{11}\sigma_1\sigma_2\sigma_3 f(\sigma, kt) + E_1 g(\sigma, kt) - h(\sigma, kt)]/g_1(\sigma) + \Delta C_2 [D_{12}\sigma_1\sigma_2\sigma_3 f(\sigma, kt) + E_2 g(\sigma, kt)]/g_1(\sigma) + \Delta C_3 [D_{13}\sigma_1\sigma_2\sigma_3 f(\sigma, kt) + E_3 g(\sigma, kt)]/g_1(\sigma) \quad (71a)$$

$$\Delta C_2(t) = \Delta C_1 [D_{21}\sigma_1\sigma_2\sigma_3 f(\sigma, kt) + F_1 g(\sigma, kt)]/g_1(\sigma) + \Delta C_2 [D_{22}\sigma_1\sigma_2\sigma_3 f(\sigma, kt) + F_2 g(\sigma, kt) - h(\sigma, kt)]/g_1(\sigma) + \Delta C_3 [D_{23}\sigma_1\sigma_2\sigma_3 f(\sigma, kt) + F_3 g(\sigma, kt)]/g_1(\sigma) \quad (71b)$$

$$\Delta C_3(t) = \Delta C_1 [D_{31}\sigma_1\sigma_2\sigma_3 f(\sigma, kt) + G_1 g(\sigma, kt)]/g_1(\sigma) + \Delta C_2 [D_{32}\sigma_1\sigma_2\sigma_3 f(\sigma, kt) + G_2 g(\sigma, kt)]/g_1(\sigma) + \Delta C_3 [D_{33}\sigma_1\sigma_2\sigma_3 f(\sigma, kt) + G_3 g(\sigma, kt) - h(\sigma, kt)]/g_1(\sigma) \quad (71c)$$

where

$$f(\sigma, kt) = (\sigma_3 - \sigma_2)e^{-kt/\sigma_1} + (\sigma_1 - \sigma_3)e^{-kt/\sigma_2} + (\sigma_2 - \sigma_1)e^{-kt/\sigma_3} \quad (72a)$$

$$g(\sigma, kt) = \sigma_1(\sigma_3 - \sigma_2)e^{-kt/\sigma_1} + \sigma_2(\sigma_1 - \sigma_3)e^{-kt/\sigma_2} + \sigma_3(\sigma_2 - \sigma_1)e^{-kt/\sigma_3} \quad (72b)$$

$$h(\sigma, kt) = \sigma_1(\sigma_3^2 - \sigma_2^2)e^{-kt/\sigma_1} + \sigma_2(\sigma_1^2 - \sigma_3^2)e^{-kt/\sigma_2} + \sigma_3(\sigma_2^2 - \sigma_1^2)e^{-kt/\sigma_3} \quad (73)$$

From at least three experiments with given mean solute concentrations and different combinations of ΔC_i , it should, in principle, be possible to obtain nine rela-

(58) Measurements of $\Delta K(t)/\Delta K(0)$ at the same t helps to facilitate the computation which follows, although this is not absolutely necessary. In the later stages of restricted diffusion the zero time correction may not be necessary.

tionships to solve for the nine diffusion coefficients using a method of successive approximation. As it appears that this general approach is hardly a practical method at present, some additional experimental quantities are considered.

As was the case for restricted diffusion,⁶ the choice of moments of the $\Delta C_i(t)$ vs. time curves as additional quantities is a mathematically convenient one because the exponential functions in eq 73 can then be converted into simple constants. The zeroth and first moments obtained from eq 71 through 73 are

$$\int_0^\infty \Delta C_1(t) dt = \frac{\Delta C_1}{k} E_1 + \frac{\Delta C_2}{k} E_2 + \frac{\Delta C_3}{k} E_3 \quad (74a)$$

$$\int_0^\infty \Delta C_2(t) dt = \frac{\Delta C_1}{k} F_1 + \frac{\Delta C_2}{k} F_2 + \frac{\Delta C_3}{k} F_3 \quad (74b)$$

$$\int_0^\infty \Delta C_3(t) dt = \frac{\Delta C_1}{k} G_1 + \frac{\Delta C_2}{k} G_2 + \frac{\Delta C_3}{k} G_3 \quad (74c)$$

$$\int_0^\infty \Delta C_1(t) t dt = (\Delta C_1/k^2) \{ D_{11} \sigma_1 \sigma_2 \sigma_3 + E_1 g_5(\sigma)/g_1(\sigma) - g_6(\sigma)/g_1(\sigma) \} + (\Delta C_2/k^2) \{ D_{12} \sigma_1 \sigma_2 \sigma_3 + E_2 g_5(\sigma)/g_1(\sigma) \} + (\Delta C_3/k^2) \{ D_{13} \sigma_1 \sigma_2 \sigma_3 + E_3 g_5(\sigma)/g_1(\sigma) \} \quad (75a)$$

$$\int_0^\infty \Delta C_2(t) t dt = (\Delta C_1/k^2) \{ D_{21} \sigma_1 \sigma_2 \sigma_3 + F_1 g_5(\sigma)/g_1(\sigma) \} + (\Delta C_2/k^2) \{ D_{22} \sigma_1 \sigma_2 \sigma_3 + F_2 g_5(\sigma)/g_1(\sigma) - g_6(\sigma)/g_1(\sigma) \} + (\Delta C_3/k^2) \{ D_{23} \sigma_1 \sigma_2 \sigma_3 + F_3 g_5(\sigma)/g_1(\sigma) \} \quad (75b)$$

$$\int_0^\infty \Delta C_3(t) t dt = (\Delta C_1/k^2) \{ D_{31} \sigma_1 \sigma_2 \sigma_3 + G_1 g_5(\sigma)/g_1(\sigma) \} + (\Delta C_2/k^2) \{ D_{32} \sigma_1 \sigma_2 \sigma_3 + G_2 g_5(\sigma)/g_1(\sigma) \} + (\Delta C_3/k^2) \{ D_{33} \sigma_1 \sigma_2 \sigma_3 + G_3 g_5(\sigma)/g_1(\sigma) - g_6(\sigma)/g_1(\sigma) \} \quad (75c)$$

It will be shown that measurements of only one of the three $\Delta C_i(t)$ in the course of the three or more diffusion experiments will give the nine diffusion coefficients, if the initial concentration differences of all of the solutes are known. For example, if $\Delta C_1(t)$ can be measured more accurately than $\Delta C_2(t)$ and $\Delta C_3(t)$, the following quantities may be obtained from at least three diffusion experiments at given mean solute concentrations and different values of ΔC_i : from the zeroth moment

$$E_1; E_2; E_3$$

and from the first moment

$$\begin{aligned} & \{ D_{11} \sigma_1 \sigma_2 \sigma_3 + E_1 g_5(\sigma)/g_1(\sigma) - g_6(\sigma)/g_1(\sigma) \}; \\ & \{ D_{12} \sigma_1 \sigma_2 \sigma_3 + E_2 g_5(\sigma)/g_1(\sigma) \}; \\ & \{ D_{13} \sigma_1 \sigma_2 \sigma_3 + E_3 g_5(\sigma)/g_1(\sigma) \} \end{aligned}$$

Introduction of these quantities into eq 71a brings it into function of σ_i only, and these three σ_i may be evaluated using the successive approximation method which was described before. Three values of $\Delta C_1(t)$ have to be obtained at a given t from the same experiments which are performed to obtain the values of moments. It should be noticed that D_{11} , D_{12} , and D_{13} are also evaluated in the course of the successive approximation. One now obtains the following equations with the help of eq 6 and the relation $1/|D_{ij}| = \sigma_1 \sigma_2 \sigma_3$ (eq 10c).

$$E_1/\sigma_1 \sigma_2 \sigma_3 = D_{22} D_{33} - D_{23} D_{32} \quad (76a)$$

$$E_2/\sigma_1 \sigma_2 \sigma_3 = D_{13} D_{32} - D_{12} D_{33} \quad (76b)$$

$$E_3/\sigma_1 \sigma_2 \sigma_3 = D_{12} D_{23} - D_{13} D_{22} \quad (76c)$$

These equations, together with eq 50, make a total of six equations which may be solved readily for the rest of the six diffusion coefficients, *i.e.*, D_{21} , D_{22} , D_{23} , D_{31} , D_{32} , and D_{33} . Similarly, the nine diffusion coefficients may be obtained from corresponding experimental measurements of either $\Delta C_2(t)$ or $\Delta C_3(t)$.⁵⁹

When it is difficult to determine the concentration difference or some related property of any of the solutes individually throughout the duration of an experiment, a suitable intensive property which is a linear function of all the solute concentrations (*e.g.*, eq 20 or 57) may be employed.⁶⁰ Here, a procedure will be developed for the case when the specific conductance is measured as that property. The same equations can be used for methods employing other types of measurements if each κ_i is replaced by other appropriate coefficients.

From eq 57 and 71 and relations defining $\Delta K(0)$, $\alpha_i(\kappa)$, $X_i(\kappa)$, $Y_i(\kappa)$, and $g_1(\sigma)$, the expression for the difference in total specific conductance between two compartments becomes

(59) Any intensive property which has some simple relation to the concentration of one of the solutes (such as optical rotation or light absorption) can be employed here if the contributions to the intensive property by the other solutes are negligible.

(60) Systems containing strong electrolyte solutes where either an anion or a cation is common for all the solutes may be put into this general category if the concentration of this common ion can be determined more accurately than the other ionic concentrations. One example is the system $H_2O-LiCl-NaCl-KCl$ where the concentration of the ion Cl^- is the easiest to determine.

$$\frac{\Delta K(t)}{\Delta K(0)} = \sum_{i=1}^3 \frac{\alpha_i(\kappa)}{g_i(\sigma)} \times [X_i(\kappa)f(\sigma, kt) + Y_i(\kappa)g(\sigma, kt) - h(\sigma, kt)] \quad (77)$$

where $\Delta K(t)$ is the specific conductance difference between the two compartments at time t , and $\Delta K(0)$ is the initial specific conductance difference. The zeroth and first moments of the $\Delta K(t)$ vs. t curve become

$$[1/k\Delta K(0)] \int_0^{\infty} \Delta K(t) dt = \sum_{i=1}^3 \alpha_i(\kappa) Y_i(\kappa) \quad (78)$$

and

$$[1/k^2\Delta K(0)] \int_0^{\infty} \Delta K(t) t dt = \sum_{i=1}^3 \alpha_i(\kappa) \phi_i(\kappa) \quad (79)$$

where $\phi_i(\kappa)$ has been already defined in eq 65. It should be noted that eq 77-79 are similar to eq 63, 64, and 67 and therefore the procedure described in the previous section for analyzing data from restricted diffusion can be also used to evaluate σ_i , $X_i(\kappa)$, and $Y_i(\kappa)$. These values are then introduced into eq 53, after all the R_i are replaced by corresponding κ_i , in order to evaluate the diffusion coefficients.

Discussion

Perhaps the most significant feature in the preceding developments is that the final expressions for individual diffusion coefficients (eq 53) are essentially the same for all three boundary conditions. This may be ascribed to the following facts.

(1) The expressions describing solute concentrations for these three boundary conditions (eq 11, 17, and 19) have basically the same mathematical form, *i.e.*, a linear combination of three exponential functions, Φ_j , with coefficients, Ψ_{ij} , which are identical for all the boundary conditions, plus constants, \bar{C}_i .⁶¹ The coefficients Ψ_{ij} are *linear* functions of the three ΔC_i with functions of the D_{ij} and σ_i as coefficients; the Φ_j are functions of x , t , and σ_i , or just t and σ_i , and *do not* contain either D_{ij} (apart from σ_i) or ΔC_i .

(2) When equations for solute concentrations are introduced into the expression for some intensive property such as eq 20 or 57, the resulting equations (such as eq 21 and 58) have the same coefficients, Γ_j , for corresponding Φ_j for all the boundary conditions.⁶²

(3) The choice of two of three quantities (referred to as "experimental quantities" in the text) to be obtained as experimental data in each boundary condition is such that the mathematical operations transform functions Φ_j into simple constants; the coefficients Ψ_{ij} and hence Γ_i remain intact during these operations.

Because of the absence of ΔC_i from Φ_j , the resulting equations for these two experimental quantities can be rearranged to obtain expressions linear in α_i . The absence of individual D_{ij} (other than σ_i) from Φ_j also allows the coefficients of α_i to contain X_i and Y_i which are originally present in Γ_i and common in all the boundary conditions. It is obvious that a minimum of three diffusion experiments at given \bar{C}_i , but different combinations of α_i , are required in order to evaluate these six coefficients of α_i . Once the coefficients are obtained it is possible to relate X_i and Y_i to functions of σ_i .

(4) It is immaterial whether the third experimental quantity is a linear function of α_i (as the values of $\Delta K(t)$ at given t in both restricted and diaphragm cell experiments) or not (as the Q in free diffusion), as long as the expressions contain intact X_i and Y_i . The expressions for these third quantity can be converted into functions of σ_i only by using the relations between X_i and Y_i and functions of σ_i obtained from the coefficients of α_i in the previous two quantities. Here again at least three experiments are required for evaluating three σ_i using the successive approximation method.

(5) In all three boundary conditions, the quantities computed from the experimental quantities are three σ_i , three X_i , and three Y_i , and it is obvious that the final expressions for each diffusion coefficient will become identical for all the boundary conditions.

It is interesting to note that three different types of experimental quantities are necessary for a four-component system while two are required for a three-component system. This is because, for a four-component system, three relations between experimentally derivable quantities (*e.g.*, X_i and Y_i) and D_{ij} are obtained from one type of experimental quantity with three (or more) experiments, and it is necessary to have two additional types of experimental quantities in order to have a total of nine relations which may in turn be solved for nine diffusion coefficients. A similar argument explains the requirement of two experimental quantities for a three-component system.

For the general case of a system with $n + 1$ components, it has been shown³⁶⁻³⁷ that the expressions for solute concentration distributions are similar to

(61) In the case of the diaphragm cell method, \bar{C}_i is the mean concentration of solute i for the two initial solutions in the upper and lower compartments of the cell. The position in the cell corresponding to each average concentration \bar{C}_i will be close to the midpoint of the diaphragm, but the location of this position is not required.

(62) In order to simplify the arguments, it is assumed that the same intensive property is used for all the boundary conditions. It is, of course, possible to obtain an equation for the diaphragm cell method which corresponds to either eq 21 or 58, although this is not necessary.

the equations for a system with three or four components. For this general case each Ψ_{ij} is a linear function of the n -concentration differences ΔC_i , and σ_i are roots of a polynomial of n th degree. The mathematical operations for relating experimental quantities to the n^2 diffusion coefficients are expected to be more or less the same as for systems with three or four-components, because the starting equations have the same mathematical forms. From the preceding arguments, it may be predicted that n different experimental quantities have to be obtained from at least n different experiments at given mean solute concentrations, and with different combinations of α_i , in order to evaluate the n^2 diffusion coefficients.

One encounters, however, at least two main difficulties when the number of components is increased. First, the number of accurately measurable experimental quantities is limited with a given instrument, and even with additional quantities from other boundary conditions only a limited number of experimental quantities may be obtained. Second, the successive approximation method with a large number of parameters to be adjusted may not be practical even with the high-speed computers available.

One advantage of restricted diffusion over other boundary condition is that it is possible with this method to study systems with highly concentration-dependent diffusion coefficients if the measurements can be made during the later stages of the diffusion. Unfortunately, the procedure for four-component system described here as well as Fujita's procedure⁶ for ternary systems is not particularly useful for studying such nonideal systems because the measurements have to be made from the time of boundary formation in order to obtain the moments. In the diaphragm cell method it is hoped that the experiments can be continued until the concentration differences come close to zero and that the concentration differences (or any related quantities) at this late stage can be measured accurately enough to give meaningful values for the final diffusion coefficients.

Appendix

Although the procedures for studying four-component systems described in the main text of this communication are related to some previous ones studying ternary diffusion,⁴⁻⁶ those procedures for ternary systems are different from each other and from the procedures for four-component systems in some details. Current ways of using the diaphragm cell method for ternary systems^{8,9} require a certain approximation. It will be shown in this section that for ternary systems the same final expressions for individual dif-

fusion coefficients can be obtained for the cases of free, restricted, and diaphragm cell diffusion.

In the procedure of restricted diffusion of ternary systems which employs the values of specific conductance at given times and the zeroth moment of that curve,⁶ Fujita obtains the values of σ_+ and σ_- after the equation for the specific conductance is transformed into a function in which only σ_+ and σ_- are unknown (eq F-59),⁶³ that is similar to the procedures for four-component systems described in this communication. Equations F-48 through F-51 may now be reexpressed by using eq F-68 and F-69 to obtain⁶⁴

$$D_{11} = \{1 - \epsilon_+(\kappa)[(\sigma_+ + \sigma_-) - \epsilon_-(\kappa)\sigma_+\sigma_-]\}/\psi(\kappa) \quad (80a)$$

$$(\kappa_1/\kappa_2)D_{12} = \{1 - \epsilon_+(\kappa)[(\sigma_+ + \sigma_-) - \epsilon_+(\kappa)\sigma_+\sigma_-]\}/\psi(\kappa) \quad (80b)$$

$$(\kappa_2/\kappa_1)D_{21} = \{\epsilon_-(\kappa)[(\sigma_+ + \sigma_-) - \epsilon_-(\kappa)\sigma_+\sigma_-] - 1\}/\psi(\kappa) \quad (80c)$$

$$D_{22} = \{\epsilon_-(\kappa)[(\sigma_+ + \sigma_-) - \epsilon_+(\kappa)\sigma_+\sigma_-] - 1\}/\psi(\kappa) \quad (80d)$$

where

$$\psi(\kappa) = \{\epsilon_-(\kappa) - \epsilon_+(\kappa)\}\sigma_+\sigma_- \quad (81)$$

$$\epsilon_+(\kappa) = [E - F(\kappa_1/\kappa_2)]/\sigma_+\sigma_- = D_{11} - (\kappa_1/\kappa_2)D_{12} \quad (82a)$$

and

$$\epsilon_-(\kappa) = [H - G(\kappa_2/\kappa_1)]/\sigma_+\sigma_- = D_{22} - (\kappa_2/\kappa_1)D_{21} \quad (82b)$$

For free diffusion eq F,GII-13 may be rewritten to obtain

$$Q/\sqrt{\mathcal{D}_A} = \Gamma_+\Gamma_-g(\sqrt{\sigma_+}, \sqrt{\sigma_-}) \quad (83)$$

where $g(\sqrt{\sigma_+}, \sqrt{\sigma_-})$ is defined by eq 46. From eq F,GI-30, F,GI-31, F,GI-50, F,GI-51, and F-39, and retaining the notations of ref 4, one gets

(63) In this Appendix, F refers to equations in ref 6, F,GI to those in ref 4, and F,GII to those in ref 5.

(64) Instead of using Fujita's linear relations (F-66 and F-67) to evaluate σ_+ and σ_- , these quantities may also be evaluated directly from eq F-59 by using a successive approximation method when the values of $\Delta K(t)/\Delta K(0)$ are obtained from two experiments at given mean solute concentrations and different combinations of $\alpha_i(\kappa)$. Equation 80 may be obtained more directly by solving eq F-41, F-42, F-39, and F-44. It should be noted that the following changes in notations are necessary in order to convert symbols from ref 6 to those in the present article.

$$\beta_i \longrightarrow \alpha_i(\kappa)$$

$$S_i \longrightarrow \kappa_i$$

$$L(t) \longrightarrow K(t)$$

$$\Gamma_+ = \{(\sqrt{\sigma_+} + \sqrt{\sigma_-})(S_A\alpha_1 + I_A) - (\sigma_+ + \sqrt{\sigma_+\sigma_-})\}/(\sigma_+ - \sigma_-) \quad (84a)$$

$$\Gamma_- = \{(\sqrt{\sigma_+} + \sqrt{\sigma_-})(S_A\alpha_1 + I_A) - (\sigma_+ + \sqrt{\sigma_+\sigma_-})\}/(\sigma_+ - \sigma_-) \quad (84b)$$

Introduction of these equations makes eq 83 a function of σ_+ and σ_- as the only unknowns. Hence, σ_+ and σ_- may be evaluated using a successive approximation method and values of

$$\epsilon_+(R) = D_{11} - (R_1/R_2)D_{12} \quad (85a)$$

$$\epsilon_-(R) = D_{22} - (R_2/R_1)D_{21} \quad (85b)$$

may be obtained using eq F,GI-58 and F,GI-59 once the values of σ_+ and σ_- are determined. Solution of these equations and eq 86 which are obtained from eq F-39 and F-44 (or F,GI-64) gives eq 80 if κ_t is replaced by R_t .

$$(\sigma_+ + \sigma_-)/\sigma_+\sigma_- = D_{11} + D_{22} \quad (86a)$$

$$1/\sigma_+\sigma_- = D_{11}D_{22} - D_{12}D_{21} \quad (86b)$$

Using the notations of Fujita and Gosting,⁴ the equations for the concentration differences in the diaphragm cell for a three-component system are⁷⁻⁹

$$\Delta C_i(t) = 2[K_i^+ e^{-(k/\sigma_+)t} + K_i^- e^{-(k/\sigma_-)t}] \quad (87)$$

Substitution of eq F,GI-41 through F,GI-44 into eq 87 and use of the notation $\alpha_i(C) = \Delta C_i/(\Delta C_1 + \Delta C_2) = \Delta C_i/\Delta C(0)$ as the solute fraction gives

$$\frac{\Delta C_1(t)}{\Delta C(0)} = \frac{\alpha_1(C)}{(\sigma_+ - \sigma_-)} \{(\sigma_+ - E)e^{-(k/\sigma_+)t} - (\sigma_- - E)e^{-(k/\sigma_-)t} + F[e^{-(k/\sigma_+)t} - e^{-(k/\sigma_-)t}]\} - \frac{F}{(\sigma_+ - \sigma_-)} \{e^{-(k/\sigma_+)t} - e^{-(k/\sigma_-)t}\} \quad (88a)$$

$$\frac{\Delta C_2(t)}{\Delta C(0)} = \frac{\alpha_2(C)}{(\sigma_+ - \sigma_-)} \{(\sigma_+ - H)e^{-(k/\sigma_+)t} - (\sigma_- - H)e^{-(k/\sigma_-)t} + G[e^{-(k/\sigma_+)t} - e^{-(k/\sigma_-)t}]\} - \frac{G}{(\sigma_+ - \sigma_-)} \{e^{-(k/\sigma_+)t} - e^{-(k/\sigma_-)t}\} \quad (88b)$$

As in the case of diaphragm cell studies of four-component systems, procedures for obtaining the four diffusion coefficients will be discussed for three different cases: (1) when the concentration differences of both solutes can be determined, (2) when the concentration difference of only one solute can be determined, and (3) when only some over-all property such as refractive index or specific conductance can be determined.

For the first case the following four quantities may be obtained by plotting $\Delta C_1(t)/\Delta C(0)$ at given t against $\alpha_1(C)$ and $\Delta C_2(t)/\Delta C(0)$ at the same t against $\alpha_2(C)$.

$$\{(\sigma_+ - E)e^{-(k/\sigma_+)t} - (\sigma_- - E)e^{-(k/\sigma_-)t}\}/(\sigma_+ - \sigma_-) \quad (89a)$$

$$\{(\sigma_+ - H)e^{-(k/\sigma_+)t} - (\sigma_- - H)e^{-(k/\sigma_-)t}\}/(\sigma_+ - \sigma_-) \quad (89b)$$

$$F\{e^{-(k/\sigma_+)t} - e^{-(k/\sigma_-)t}\}/(\sigma_+ - \sigma_-) \quad (89c)$$

and

$$G\{e^{-(k/\sigma_+)t} - e^{-(k/\sigma_-)t}\}/(\sigma_+ - \sigma_-) \quad (89d)$$

By dividing eq 89c with eq 89d and using eq F,GI-21 and F,GI-22, one obtains the value of D_{12}/D_{21} . There are three unknowns now; D_{11} , D_{22} , and either D_{12} or D_{21} and any three of eq 89 may be used to determine these unknowns by a method of successive approximations.

For the second case, it is assumed that solute 1 can be determined. In this case one additional quantity is required and the zeroth moment of the curve of $\Delta C(t)/\Delta C(0)$ vs. t is adopted as the additional quantity.^{5,9} From eq. 88a

$$\int_0^\infty \frac{\Delta C_1(t)}{\Delta C(0)} dt = \frac{\alpha_1(C)}{k} \{\sigma_+ + \sigma_- + F - E\} - \frac{F}{k} \quad (90)$$

By plotting the value of this reduced zeroth moment against $\alpha_1(C)$ one can evaluate $\{\sigma_+ + \sigma_- + F - E\}$ and F . Introduction of these quantities into eq 89a and 89c reduces them to expressions containing only known quantities and σ_+ and σ_- . Using the successive approximation method, σ_+ , σ_- , and E may be evaluated, and the four diffusion coefficients are obtained using the relations

$$D_{11} = E/\sigma_+\sigma_- \quad (91a)$$

$$D_{12} = F/\sigma_+\sigma_- \quad (91b)$$

$$D_{22} = (\sigma_+ + \sigma_-)/\sigma_+\sigma_- - D_{11} \quad (91c)$$

$$D_{21} = (D_{11}D_{22} - 1/\sigma_+\sigma_-)/D_{12} \quad (91d)$$

To illustrate the third case, it is assumed that the specific conductance difference between the upper and lower solutions is measured in the course of the diffusion experiments. When other intensive properties which are linear in the solute concentrations are used, the mathematical treatment and the final expressions

should still be the same if the κ_i are replaced by appropriate corresponding coefficients. The expression for the specific conductance difference for a three-component system can be expressed by

$$\Delta K(t) = \kappa_1 \Delta C_1(t) + \kappa_2 \Delta C_2(t) \quad (92)$$

Equation 87 is now introduced into eq 92, and the use of eq F-39 gives

$$\begin{aligned} \frac{\Delta K(t)}{\Delta K(0)} = & \frac{\alpha_1(\kappa)}{(\sigma_+ - \sigma_-)} \left\{ \left(H - \frac{\kappa_2}{\kappa_1} G \right) \times \right. \\ & \left. [e^{-(k/\sigma_+)t} - e^{-(k/\sigma_-)t}] + \sigma_+ e^{-(k/\sigma_-)t} - \sigma_- e^{-(k/\sigma_+)t} \right\} + \\ & \frac{\alpha_2(\kappa)}{(\sigma_+ - \sigma_-)} \left\{ \left(E - \frac{\kappa_1}{\kappa_2} F \right) [e^{-(k/\sigma_+)t} - e^{-(k/\sigma_-)t}] + \right. \\ & \left. \sigma_+ e^{-(k/\sigma_-)t} - \sigma_- e^{-(k/\sigma_+)t} \right\} \quad (93) \end{aligned}$$

where the $\alpha_i(\kappa)$ are already defined in the main text

of this article. From this equation the zeroth moment can be easily shown to be

$$\int_0^\infty \frac{\Delta K(t)}{\Delta K(0)} dt = \frac{\alpha_1(\kappa)}{k} \left(H - \frac{\kappa_2}{\kappa_1} G \right) + \frac{\alpha_2(\kappa)}{k} \left(E - \frac{\kappa_1}{\kappa_2} F \right) \quad (94)$$

The values of $(H - (\kappa_2/\kappa_1)G)$ and $(E - (\kappa_1/\kappa_2)F)$ obtained using eq 94 may be introduced into eq 93. At some given values of t eq 93 is now a function of only σ_+ and σ_- , and these values may be obtained by using a method of successive approximation. Now we have eq 82 and 86 and again the final expressions for the individual diffusion coefficients are given by eq 80.

Acknowledgment. The author wishes to thank Professor Louis J. Gosting for his continuous assistance and encouragement during the course of this work and for his criticism of the manuscript.

The Standard Oxidation Potential of the Ferrocyanide–Ferricyanide Electrode at 25° and the Entropy of Ferrocyanide Ion

by Peter A. Rock

Department of Chemistry, University of California, Davis, California (Received September 22, 1965)

The standard oxidation potential of the ferrocyanide–ferricyanide electrode has been redetermined in a cell free from salt bridges, in which the liquid junction potential has been minimized by an appropriate choice of reference electrode. The need for an extrapolation to infinite dilution has been avoided by treating the potassium ferrocyanide–ferricyanide solution as a mixed electrolyte system using the available activity coefficient data for the pure salts. The value obtained at 25° is $E^\circ = -0.3704 \pm 0.0005$ v. Using this potential and the available thermodynamic data, the standard partial molal entropy of aqueous ferrocyanide ion has been calculated as $S^\circ = 22.8$ cal/deg mole at 25°. The entropy of ferrocyanide ion has in turn been combined with existing thermodynamic data to calculate $S^\circ = 147.8$ cal/deg mole for $K_4Fe(CN)_6 \cdot 3H_2O(s)$ and $S^\circ = 105$ cal/deg mole for $K_4Fe(CN)_6(s)$ both at 25°.

Introduction

The study of electrochemical cells in which the electrode of interest involves soluble oxidized and reduced species yielding a mixed electrolyte system presents special problems in the interpretation of the cell data. It has not been possible to devise a cell involving such an electrode that is entirely free of liquid junctions. This fact of itself is not necessarily a serious problem, for, as Guggenheim has pointed out,¹ liquid junction potentials exist in every electrochemical cell. This problem can be overcome in many cases by the appropriate choice of reference electrode. In the type of cell under discussion the liquid junction potential is predicted² to approach zero as the electrolyte compositions of the two solutions forming the junction approach identity in the transport properties and ionic activities of their cations and anions. It is also to be noted that the use of salt bridges in such cells is to be avoided, first, because they are unnecessary and, second, because they can introduce significant uncertainties in the cell data.² The problem of liquid junction potentials has been overcome in the present investigation by employing the $Pb(Hg)(\text{two-phase, 5 wt } \% \text{ Pb})|Pb_2Fe(CN)_6(s)|Fe(CN)_6^{4-}(aq)$ electrode as a reference in the determination of the $Fe(CN)_6^{4-}(aq)-Fe(CN)_6^{3-}(aq)$ standard oxidation potential.

The difficulties associated with the extrapolation to infinite dilution of the data for a cell involving a mixture of highly charged electrolytes in which ionic association effects are important has been circumvented by employing the available activity coefficient data for potassium ferrocyanide and potassium ferricyanide to treat the mixed electrolyte solution as a multicomponent system. The results obtained in this way are compared with the previously reported value for the ferrocyanide–ferricyanide oxidation potential. The standard potential obtained has been used in combination with existing data to calculate several thermodynamic properties of interest for ferrocyanides.

Experimental Section

Reagents. J. T. Baker reagent grade $K_3Fe(CN)_6$ (assay: 99.9%) was used without further purification. J. T. Baker reagent grade $K_4Fe(CN)_6 \cdot 3H_2O$ was recrystallized from a hot (55°) aqueous solution under nitrogen, air dried, and stored over a saturated aqueous solution of $NaBr \cdot 2H_2O$ in the dark.³ Cell

(1) E. A. Guggenheim, "Thermodynamics," North-Holland Publishing Co., Amsterdam, 1949, pp 342–347.

(2) D. A. MacInnes, "The Principles of Electrochemistry," Dover Publications, Inc., New York, N. Y., 1939, Chapters 13, 14, and 16.

(3) I. M. Kolthoff and W. J. Tomsicek, *J. Phys. Chem.*, **39**, 945 (1935).

Table I: Results of Measurements on the Cell

Pb(2-phase Hg) Pb ₂ Fe(CN) ₆ (s) K ₄ Fe(CN) ₆ (m ₁) K ₄ Fe(CN) ₆ (m ₂),K ₃ Fe(CN) ₆ (m ₃) Au				
m ₁ (γ _±) ^a	m ₂ (γ _±) ^a	m ₃ (γ _±) ^a	E _{cell}	E ^o _b
0.1750 (0.106)	0.1030 (0.114)	0.1000 (0.186)	0.7803	-0.3705
0.1100 (0.133)	0.0830 (0.141)	0.0400 (0.216)	0.7553	-0.3709
0.0875 (0.148)	0.0530 (0.157)	0.0500 (0.236)	0.7703	-0.3709
0.1030 (0.137)	0.1030 (0.142)	0.00400 (0.216)	0.6887	-0.3696
0.1375 (0.118)	0.1000 (0.126)	0.0500 (0.199)	0.7575	-0.3695

^a Mean molal activity coefficients calculated as described under Activity Coefficients in this section. ^b Standard oxidation potential of the ferrocyanide-ferricyanide electrode; see calculation of the standard oxidation potential.

solutions were prepared on a molal basis using nitrogen-saturated distilled water. These solutions were stored in brown polyethylene bottles and always used on the same day as prepared.

Electrical Cell Measurements. Voltages were measured with a Leeds and Northrup Type K-3 certified potentiometer and a Leeds and Northrup galvanometer. External guarding was employed in the galvanometer and working battery circuits. Electrode compartments were similar to those described by Hills and Ives, and the interiors of the electrode compartments were silicone coated.⁴ The lead amalgam-lead ferrocyanide reference electrode was prepared as has been described.⁵ The liquid junction connector used was similar to that employed by Gordon and co-workers.⁶ In the ferrocyanide-ferricyanide electrode a gold wire⁷ was brought in through a capillary to the base of the electrode compartment and wound in a coil of several turns. The end of the wire was then submerged in paraffin wax (used to seal the capillary opening) to avoid any sharp points that might give rise to spurious emf values. Air was excluded from both electrodes by a stream of purified nitrogen from a presaturator filled with electrode electrolyte solution. Light was excluded from the ferrocyanide-ferricyanide electrode⁸ by wrapping the electrode compartment in aluminum foil. The cell was maintained at 25.0 ± 0.005° in a grounded water bath.

Results

Cell Data. The cell employed was as follows: Pb(5 wt % in Hg)|Pb₂Fe(CN)₆(s)|K₄Fe(CN)₆(m₁)|K₄Fe(CN)₆(m₂),K₃Fe(CN)₆(m₃)|Au, in which the two cell electrolytes were brought into contact in the liquid junction connector. Unfortunately, the cell electrolyte cannot be made uniform throughout the cell, even though lead ferricyanide is soluble, because the lead amalgam spontaneously reduces ferricyanide to ferrocyanide. The cells set up as indicated attained a steady voltage in less than 10 min, and, in three of

the five cells set up, the observed voltage was remarkably stable to within a few hundredths of a millivolt for several hours. Voltage fluctuations in all cells were within ±0.1 mv for at least 3-5 hr, and three of the cells were stable for over 24 hr. In all cases the observed cell voltages were insensitive to the renewal of the liquid junction. The results of experiments on this cell at various values of m₁, m₂, and m₃ are presented in Table I.

Activity Coefficients. The mean molal activity coefficients of K₄Fe(CN)₆(aq) and K₃Fe(CN)₆(aq) at 25° have been reported.⁸ These activity coefficients were determined isopiesticly, and the data were not extrapolated to the conventional solute standard state [*i.e.*, a (of K₄Fe(CN)₆) = $a_{K^+} a_{Fe(CN)_6^{4-}}$ and a (of K₃Fe(CN)₆) = $a_{K^+} a_{Fe(CN)_6^{3-}}$], but rather it was assumed for both salts that $\gamma_{\pm}(0.05 m, 0^\circ) = \gamma_{\pm}(0.05 m, 25^\circ)$, where the value of $\gamma_{\pm}(0.05 m, 0^\circ)$ was obtained from the Landolt-Börnstein Tables.⁹ These γ_{\pm} values in turn were obtained from freezing point data by assuming the validity of the Debye-Hückel limiting law at 0.001 *m*, and then γ_{\pm} values at higher concentrations were calculated from the freezing point data. Since there is no real assurance that the limiting law holds at these concentrations for such highly charged electrolytes and the temperature variation of the γ_{\pm} values cannot be safely neglected, the γ_{\pm} values reported for these salts⁸ are, as the authors point out, based on an arbitrary standard state. It is desirable, therefore, to find a better method to establish the conventional solute standard state. Using the available

(4) G. J. Hills and D. J. G. Ives, *J. Chem. Soc.*, 311 (1951).

(5) P. A. Rock and R. E. Powell, *Inorg. Chem.*, 3, 1593 (1964).

(6) W. J. Hornibrook, G. J. Janz, and A. R. Gordon, *J. Am. Chem. Soc.*, 64, 513 (1942).

(7) G. N. Lewis and L. W. Sargent, *ibid.*, 31, 355 (1909).

(8) R. A. Robinson and R. H. Stokes, "Electrolyte Solutions," 2nd ed, Butterworth and Co. Ltd, London, 1959.

(9) Landolt-Börnstein Tabellen, 5th ed, 2nd supplementary volume, p 1121.

freezing point data¹⁰ and extrapolating to infinite dilution¹¹ yield $B = 0.924$ (0°) for $\text{K}_4\text{Fe}(\text{CN})_6(\text{aq})$. A similar treatment of the freezing point data for $\text{K}_3\text{Fe}(\text{CN})_6$ yields an extrapolation plot with considerable scatter, and a reliable B value cannot be obtained from the data. To correct γ_{\pm} values at 0 to 25° , the heat of dilution, and its temperature dependence are needed for both $\text{K}_4\text{Fe}(\text{CN})_6(\text{aq})$ and $\text{K}_3\text{Fe}(\text{CN})_6(\text{aq})$. Although heat of dilution data are available,¹² heat capacity data for these solutions are nonexistent. Since the $\bar{J}(T_2 - T_1)$ term cannot be safely neglected in correcting $\gamma_{\pm}(0^\circ)$ to $\gamma_{\pm}(25^\circ)$ and B is not known for $\text{K}_3\text{Fe}(\text{CN})_6(\text{aq})$, an approximate procedure for the establishment of the conventional solute standard state has been employed. Brubaker and co-workers have reported the mean molal activity coefficients of $\text{K}_3\text{Co}(\text{CN})_6$ ¹³ and $\text{K}_4\text{Mo}(\text{CN})_6$ ¹⁴ obtained from isopiestic data which they successfully extrapolated to infinite dilution. It has been assumed that γ_{\pm} for $\text{K}_3\text{Fe}(\text{CN})_6$ is equal to γ_{\pm} of $\text{K}_3\text{Co}(\text{CN})_6$ at 0.1 m and from the value of γ_{\pm} for $\text{K}_3\text{Co}(\text{CN})_6$ at 0.1 m and that reported⁸ for $\text{K}_3\text{Fe}(\text{CN})_6$ it was computed that by adding 0.0131 to the $-\log \gamma_{\pm}$ values, the existing data could be converted to the conventional solute standard state; *e.g.*, we compute at 0.20 m for $\text{K}_3\text{Fe}(\text{CN})_6$ that $\gamma_{\pm} = 0.206$ whereas the reported value is $\gamma_{\pm} = 0.210$. Similarly, in treating the $\text{K}_4\text{Fe}(\text{CN})_6$ data it was assumed that $\gamma_{\pm} = 0.194$ for this salt at 0.05 m (the value obtained for $\text{K}_4\text{Mo}(\text{CN})_6$ at this concentration) and by subtracting 0.0113 from the $-\log \gamma_{\pm}$ values for $\text{K}_4\text{Fe}(\text{CN})_6$ the activity coefficients for this salt have been corrected to the conventional solute standard state; *e.g.*, we compute for $\text{K}_4\text{Fe}(\text{CN})_6$ at 0.1 m that $\gamma_{\pm} = 0.143$ whereas the reported value⁸ is $\gamma_{\pm} = 0.139$.

The electrolyte solution in the ferrocyanide-ferri-cyanide electrode is a multicomponent system. From the Brønsted-Guggenheim equation¹⁵ one obtains for $\text{K}_4\text{Fe}(\text{CN})_6$ of molality m_2 in a solution containing $\text{K}_3\text{Fe}(\text{CN})_6$ of molality m_3 : $\log \gamma_{\pm}(\text{mixture}) - \log \gamma_{\pm}(\text{pure}) = m_3(4/5B_3 - 3/25B_2)$, wherein $\gamma_{\pm}(\text{mixture})$ refers to the mean molal activity coefficient of $\text{K}_4\text{Fe}(\text{CN})_6$ in the mixed electrolyte solution having the same total ionic strength as that to which $\gamma_{\pm}(\text{pure})$ (the mean molal γ_{\pm} for $\text{K}_4\text{Fe}(\text{CN})_6(\text{aq})$) refers, and B_2 and B_3 refer to $\text{K}_4\text{Fe}(\text{CN})_6(\text{aq})$ and $\text{K}_3\text{Fe}(\text{CN})_6(\text{aq})$, respectively. For $\text{K}_3\text{Fe}(\text{CN})_6$ of molality m_3 in a solution containing $\text{K}_4\text{Fe}(\text{CN})_6$ of molality m_2 one obtains: $\log \gamma_{\pm}(\text{mixture}) - \log \gamma_{\pm}(\text{pure}) = m_2(3/4B_2 - 3/2B_3)$, where here again $\gamma_{\pm}(\text{mixture})$ refers to the mean molal activity coefficient of $\text{K}_3\text{Fe}(\text{CN})_6$ in the mixed electrolyte solution having the same

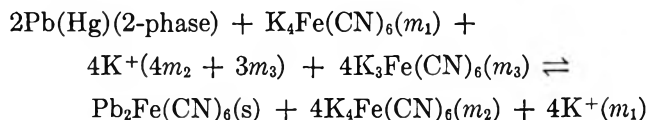
total ionic strength as that concentration to which $\gamma_{\pm}(\text{pure})$ refers.

If we now assume that Harned's rule¹⁶ applies to the mixture we obtain from the relationship $4/5B_3 - 3/25B_2 = 3/4B_2 - 3/2B_3 = \alpha$, the result that $B_3 = 0.4826 \cdot B_2$, which permits the calculation of B_3 from B_2 , and hence the estimation of α . We compute $\alpha = 0.0241$ (at 0°). If we now assume $\alpha(0^\circ) \approx \alpha(25^\circ)$, an estimation of the contribution of the interaction terms αm_3 and αm_2 to E° can be made. The magnitude of this contribution (see the following section) is $0.05916\alpha(5m_3 - 4m_2)$ and the largest contribution that this term makes to any of the five cells (see Table I) is of the order of 0.0003 v. Since α is not accurately known and the experimental uncertainty in E° is ± 0.0005 v, this term has been neglected in the calculation of the standard potential. That is to say, for a solution containing $\text{K}_4\text{Fe}(\text{CN})_6$ and $\text{K}_3\text{Fe}(\text{CN})_6$ of molalities m_2 and m_3 , respectively, having a total ionic strength of $10m_2 + 6m_3$, the mean molal activity coefficients of the two salts are taken as the values of γ_{\pm} for the pure electrolytes at the same ionic strength as that of the mixture. In this way the γ_{\pm} values for the mixed electrolyte solutions given in Table I (interpolated at intermediate concentrations from linear plots⁵ of $\log \gamma_{\pm}$ vs. $\log m$) have been obtained.

The standard oxidation potential of the lead amalgam-lead ferrocyanide electrode⁵ was calculated using the reported⁸ values of γ_{\pm} for $\text{K}_4\text{Fe}(\text{CN})_6(\text{aq})$ and therefore these values must be used for the pure $\text{K}_4\text{Fe}(\text{CN})_6(\text{aq})$ (at molality m_1 , see cell diagram) solutions. Alternatively, of course, E° for this electrode could be recalculated with the new γ_{\pm} values; however, this is unnecessary for the present purposes.

Calculation of the Standard Oxidation Potential.

From the cell diagram one obtains the cell reaction



and hence at 25°

(10) For $\text{K}_4\text{Fe}(\text{CN})_6(\text{aq})$: A. A. Noyes and J. Johnston, *J. Am. Chem. Soc.*, **31**, 987 (1909). For $\text{K}_3\text{Fe}(\text{CN})_6$: "International Critical Tables," Vol. 4, p 260, and C. Robertson and V. K. La Mer, *J. Phys. Chem.*, **35**, 1953 (1931).

(11) G. N. Lewis and M. Randall, "Thermodynamics," 2nd ed, revised by K. S. Pitzer and L. Brewer, McGraw-Hill Book Co., Inc., New York, N. Y., 1961, p 410.

(12) E. Lange and W. Miederer, *Z. Elektrochem.*, **60**, 34 (1958).

(13) R. A. Wynveen, J. L. Dye, and C. H. Brubaker, Jr., *J. Am. Chem. Soc.*, **82**, 4441 (1960).

(14) C. H. Brubaker, Jr., *ibid.*, **87**, 5762 (1965).

(15) See ref 11, p 346, eq 23-38.

(16) See ref 11, p 568.

$$E = E^\circ - \frac{0.05916}{4} \log \frac{a_2^4 a_{K^+}^4 \text{ (at } 4m_1)}{a_1 a_3^4 a_{K^+}^4 \text{ (at } 4m_2 + 3m_3)}$$

Since $a_{K^+} = m_{K^+} \gamma_{K^+}$ and single-ion activity coefficients are not measurable properties of electrolytes, it is desirable, in order to bring about cancellation of the a_{K^+} terms in the numerator and denominator, that $4m_1 = 4m_2 + 3m_3$ and that the ionic strengths of both solutions be at least approximately equal, *i.e.*, $10m_1 = 10m_2 + 6m_3$. These two requirements are not entirely compatible but are simultaneously satisfied, at least approximately, when $m_1 \simeq m_2 \geq m_3$. The liquid junction in this cell is also negligible when $m_1 \simeq m_2$. In choosing the cell concentrations the condition $4m_1 = 4m_2 + 3m_3$ was always satisfied, and in addition $m_3 \leq m_2$ was maintained. The ultimate criterion for the validity of these assumptions was taken as the constancy of the calculated E° values.

Applying the thermodynamic definition of activity and assuming $a_{K^+} \text{ (at } 4m_1) = a_{K^+} \text{ (at } 4m_2 + 3m_3)$ we have

$$E = E^\circ + 0.07395 \log 256^{1/6} m_1 \gamma_{\pm} - 0.05916 \log \frac{\gamma_{K^+}^4 (4m_2 + 3m_3)^4 \gamma_{\text{Fe(CN)}_6^{4-}}^{m_2}}{\gamma_{K^+}^3 (4m_2 + 3m_3)^3 \gamma_{\text{Fe(CN)}_6^{3-}}^{m_3}}$$

$$E = E^\circ + 0.07395 \log 256^{1/6} m_1 \gamma_{\pm} - 0.05916 \left[5 \log \gamma_{\pm}(o) - 4 \log \gamma_{\pm}(i) + \log \frac{m_2(4m_2 + 3m_3)}{m_3} \right]$$

in which (o) and (i) refer to potassium ferrocyanide and ferricyanide, respectively. Inserting the data in Table I into this equation and taking the standard oxidation potential of the $\text{Pb(5 wt \% in Hg, 2-phase)|Pb}_2\text{Fe(CN)}_6\text{(s)|Fe(CN)}_6^{4-}\text{(aq)}$ electrode⁵ as +0.3870 v, the values of the standard oxidation potential of the ferrocyanide-ferricyanide electrode given in Table I were computed. The average of these values is $E^\circ = -0.3704 \pm 0.0005$ v at 25°. The constancy of the calculated E° values lends support to the assumption that the liquid junction potential is negligible. As a further check on this point a saturated KCl salt solution was inserted in the second cell in Table I and had no effect (within ± 0.01 mv) on the observed cell voltage as would be expected if the liquid junction potential is indeed small.

Discussion

The work of Lewis and Sargent⁷ on the ferrocyanide-ferricyanide electrode was exploratory in nature and these workers did not obtain a standard potential.

Kolthoff and Tomsicek³ obtained $E^\circ = -0.356$ v in their investigation of this electrode. We feel that the difference between the value of E° obtained in this study and that obtained by Kolthoff and Tomsicek is due to the difficulties in extrapolating their data to infinite dilution, especially since the limiting law was used in solutions of rather high ionic strength. The possible existence of nonnegligible junction potentials may also be a contributing factor to this difference since these workers employed a KCl (saturated) in agar salt bridge in their cell. Lin and Breck¹⁷ report $E^\circ = -0.3644$ v for the standard oxidation potential. This value was obtained from the cell: $\text{Hg(l)|Hg}_2\text{-Cl}_2\text{(s)|KCl(satd)|K}_4\text{Fe(CN)}_6\text{, K}_3\text{Fe(CN)}_6\text{Pt}$, for which cell data at equal molalities of $\text{K}_4\text{Fe(CN)}_6$ and $\text{K}_3\text{Fe(CN)}_6$ were extrapolated to infinite dilution against $\mu^{1/2}/(1 + \mu^{1/2})$, μ = ionic strength. Although the agreement between the two potentials is good, the difference of 6.0 mv cannot be considered negligible. Since these workers did not attempt to assess the importance of the liquid junction potential in their cell and in particular did not vary the ferrocyanide to ferricyanide ratio at constant ionic strength to test experimentally their assumption of zero liquid junction potential, it remains a strong possibility that their E° has incorporated in it a nonnegligible liquid junction potential. Lin and Breck also investigated the temperature dependence of the emf of their cell and obtained 49.0 cal/deg mole for the entropy difference between $\text{Fe(CN)}_6^{3-}\text{(aq)}$ and $\text{Fe(CN)}_6^{4-}\text{(aq)}$, whereas the value obtained in this study (*vide infra*) is 40.6 cal/deg mole.

From the enthalpies of formation of $\text{Fe(CN)}_6^{4-}\text{(aq)}$ and $\text{Fe(CN)}_6^{3-}\text{(aq)}$ from their respective ions¹⁸ and Latimer's values¹⁹ for the standard enthalpies of formation from the elements of $\text{CN}^-\text{(aq)}$, $\text{Fe}^{3+}\text{(aq)}$, and $\text{Fe}^{2+}\text{(aq)}$, we compute for $\text{Fe(CN)}_6^{4-}\text{(aq)}$, $\Delta H_f^\circ = 109.8$ kcal and for $\text{Fe(CN)}_6^{3-}\text{(aq)}$, $\Delta H_f^\circ = 135.1$ kcal. From E° determined in this investigation we compute for $\text{Fe(CN)}_6^{4-}\text{(aq)} = \text{Fe(CN)}_6^{3-}\text{(aq)} + e^-$, $\Delta G^\circ = 8.54$ kcal; combining this ΔG° with $\Delta H^\circ = 25.3$ kcal yields $\Delta S^\circ = 56.2$ cal/deg mole.

Hepler and co-workers report²⁰ $S^\circ = 63.4$ cal/deg mole for the standard partial molal entropy of $\text{Fe(CN)}_6^{3-}\text{(aq)}$. This yields $S^\circ = 22.8$ cal/deg mole at 25° for $\text{Fe(CN)}_6^{4-}\text{(aq)}$ to be compared with $\bar{S}^\circ =$

(17) J. Lin and W. G. Breck *Can. J. Chem.*, **43**, 766 (1965).

(18) G. D. Watt, J. J. Christensen, and R. M. Izatt, *Inorg. Chem.*, **4**, 220 (1965).

(19) W. M. Latimer, "Oxidation Potential," 2nd ed, Prentice-Hall, Inc., New York, N. Y., 1952

(20) L. G. Hepler, J. R. Sweet, and R. A. Jessor, *J. Am. Chem. Soc.*, **82**, 304 (1960).

17 (± 5 –15) cal/deg mole, obtained by Hepler and co-workers,²⁰ from their thermal data and Kolthoff and Tomsicek's standard oxidation potential. Since the values of γ_{\pm} used in this study are probably uncertain to about ± 0.005 , a recalculation of the entropy of ferricyanide ion is not warranted at this time. Hepler and co-workers used $\gamma_{\pm} = 0.122$ for a saturated solution of $\text{K}_3\text{Fe}(\text{CN})_6$,⁸ whereas the value obtained by the approximate methods discussed in this investigation is $\gamma_{\pm} = 0.118$. This difference leads to a difference in ΔG° of solution for potassium ferricyanide of 0.06 kcal/mole and a difference of 0.2 in the entropy of ferricyanide ion. Accordingly, we take $S^{\circ} = 22.8 \pm 0.3$ cal/deg mole as the entropy of ferrocyanide ion. The entropy of ferrocyanide ion can be combined with the heat of solution²⁰ of $\text{K}_4\text{Fe}(\text{CN})_6 \cdot 3\text{H}_2\text{O}(\text{s})$ and the free energy of solution of this salt (calculated using m (satd) = 0.8559,²¹ $\gamma_{\pm}(\text{satd}) = 0.0478$ (based on the solute standard state established in this work), $a_{\text{H}_2\text{O}}(\text{satd soln}) = 0.9623$ (calculated from $\phi = 0.498$ given in ref 8) to yield $\Delta G^{\circ}_{\text{soln}} = -RT \ln (4m)^4 m \cdot \gamma_{\pm}^5 a_{\text{H}_2\text{O}}^3 = 6.243$ kcal) to give $\Delta S^{\circ}_{\text{soln}} = 23.16$ cal/deg mole, from which we compute¹⁹ $S^{\circ} = 147.8$ cal/deg mole for $\text{K}_4\text{Fe}(\text{CN})_6 \cdot 3\text{H}_2\text{O}(\text{s})$ at 25°.

From the heats of solution²⁰ of $\text{K}_4\text{Fe}(\text{CN})_6 \cdot 3\text{H}_2\text{O}(\text{s})$ and $\text{K}_4\text{Fe}(\text{CN})_6(\text{s})$ and ΔH° at 25° for the process¹⁹ $\text{H}_2\text{O}(\text{l}) = \text{H}_2\text{O}(\text{g})$, we compute for the reaction: $\text{K}_4\text{Fe}(\text{CN})_6 \cdot 3\text{H}_2\text{O}(\text{s}) = \text{K}_4\text{Fe}(\text{CN})_6(\text{s}) + 3\text{H}_2\text{O}(\text{g})$, $\Delta H^{\circ} = 35.10$ kcal. Schottky²² reports 7.35 mm at 20° for the dissociation pressure of the trihydrate. From the above ΔH° for the reaction we calculate 10.30 mm for the dissociation pressure at 25°. From this dissociation pressure we compute $\Delta G^{\circ}_{298} = 7.65$

kcal for the above reaction, and hence $\Delta S^{\circ} = 92.08$ cal/deg. This yields $S^{\circ} = 105$ cal/deg mole for the entropy of $\text{K}_4\text{Fe}(\text{CN})_6(\text{s})$ at 25°. Although this is not an unreasonable value for the entropy of this salt considering that Stephenson and Morrow report²³ $S^{\circ} = 100.4$ cal/deg mole for $\text{K}_3\text{Fe}(\text{CN})_6(\text{s})$ at 25°, it may be too low a value since, if one considers that the average entropy per mole of hydrated water is 9.4 cal/deg mole,²⁴ the entropy of $\text{K}_4\text{Fe}(\text{CN})_6(\text{s})$ may be estimated from the entropy of $\text{K}_4\text{Fe}(\text{CN})_6 \cdot 3\text{H}_2\text{O}(\text{s})$ as 119.6 cal/deg mole. The most likely source of error in the calculation of the entropy of $\text{K}_4\text{Fe}(\text{CN})_6(\text{s})$ is the dissociation pressure of $\text{K}_4\text{Fe}(\text{CN})_6 \cdot 3\text{H}_2\text{O}$, since the author²² emphasized the difficulty in obtaining reliable dissociation pressures in his measurements.

From the available thermal data¹⁸ and the entropies of the ions,^{19,20} together with the entropy of ferrocyanide ion determined in this investigation, we compute the standard free energies of formation from the elements of ferrocyanide and ferricyanide ions at 25° as 167.1 and 175.6 kcal/mole, respectively.²⁵

(21) R. H. Vallance, *J. Chem. Soc.*, 1328 (1927).

(22) H. Schottky, *Z. Physik. Chem.*, **64**, 415 (1909).

(23) C. C. Stephenson and J. C. Morrow, *J. Am. Chem. Soc.*, **78**, 275 (1956).

(24) See ref 19, p 364.

(25) NOTE ADDED IN PROOF. R. H. Busey, *J. Phys. Chem.*, **69**, 3179 (1965), has recalculated the entropy of $\text{K}_3\text{Fe}(\text{CN})_6(\text{s})$ and obtained $S^{\circ} = 101.8$ cal/deg mole at 25°. This entropy is 1.4 units larger than the previously reported value and leads to an increase of 1.4 cal/deg mole in the entropies of $\text{Fe}(\text{CN})_6^{4-}(\text{aq})$, $\text{K}_4\text{Fe}(\text{CN})_6 \cdot 3\text{H}_2\text{O}(\text{s})$, and $\text{K}_4\text{Fe}(\text{CN})_6(\text{s})$ reported in this paper. The revised values for the entropies are 24.2, 149.2, and 106 cal/deg mole, respectively. ΔG° and ΔH° values reported here are unaffected by this change.

NOTES

Temperature Dependence of Absorption of Liquid Water in the Far-Ultraviolet Region

by M. Halmann and I. Platzner

Isotope Department, The Weizmann Institute of Science, Rehovoth, Israel (Received September 16, 1965)

For the absorption spectrum of liquid water in the 200- to 180- μ region at room temperature, several

conflicting results have been reported.¹⁻³ Only a few data are available in these reports on the absorption at other temperatures. For photochemical studies in dilute aqueous solutions in the far-ultraviolet region,⁴

(1) J. Barrett and J. H. Baxendale, *Trans. Faraday Soc.*, **56**, 37 (1960).

(2) J. Barrett and A. L. Mansell, *Nature*, **187**, 138 (1960).

(3) J. L. Weeks, G. M. A. C. Meaburn, and S. Gordon, *Radiation Res.*, **19**, 559 (1963).

(4) M. Halmann and I. Platzner, *J. Chem. Soc.*, 1440 (1965).

Table I

	Temp., °C.							
	21.5	24.0	25.0	30.7	36.5	45.5	62.5	80.0
k (cm. ⁻¹), ref. 1			1.2					
k (cm. ⁻¹), ref. 2			1.46					
k (cm. ⁻¹), ref. 3	1.67		1.80	2.09	2.50			
k (cm. ⁻¹), this work		1.47				2.63	4.55	7.05

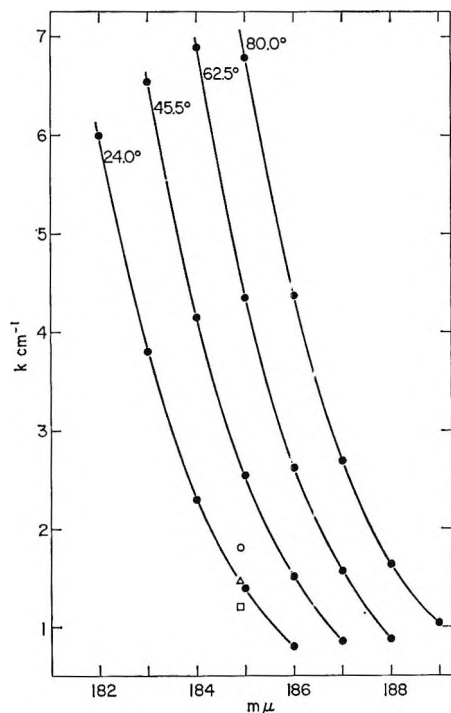


Figure 1. Absorption of liquid water (in k , cm.⁻¹) at several temperatures: □, ref. 1; △, ref. 2; ○, ref. 3; ●, present work.

it was necessary to obtain reliable values for the absorption over a wider range of temperature.

Experimental Section

Absorption spectra were measured with a Zeiss PMQII far-ultraviolet spectrophotometer, in which the whole optical path was flushed with nitrogen (99.9% pure; 2 l. min.⁻¹ flow rate). Absorption spectra of triply distilled water (redistilled from alkaline permanganate and then from phosphoric acid in an all-glass still) in Suprasil quartz cells (1.00-mm. path length) were measured against empty cells in a temperature-controlled cell holder ($\pm 0.5^\circ$).

Results

The absorption spectrum of water at different temperatures is presented in Figure 1, which includes available literature data. For 184.9 mμ, which is particularly important in photochemistry because of

the emission at this wave length from low-pressure mercury lamps, the absorption data listed in Table I were obtained.

Our results agree with that at 25.0° by Barrett and Mansell² and are considerably lower than those reported by Weeks, *et al.*³

Phosphorus-31 Chemical Shifts of Quaternary Phosphonium Salts

by Samuel O. Grim, William McFarlane, Edward F. Davidoff, and Tobin J. Marks¹

Department of Chemistry, University of Maryland, College Park, Maryland (Received July 12, 1965)

It has been shown that the phosphorus chemical shifts of tertiary and secondary phosphines can be predicted very accurately from empirically determined additive group contributions (σ^P), which have been assigned for phenyl and various alkyl groups.² This type of behavior had been suggested previously for trivalent phosphorus compounds but the predictions were only moderately successful,³ and similar attempts to predict the phosphorus chemical shift in "quadruply connected" phosphorus compounds, such as phosphine oxides, were unsuccessful.³ Groenweghe, Maier, and Moedritzer⁴ observed a regular variation in the P³¹ chemical shift of a tertiary, secondary, or halophosphine, or a "quadruply connected" organophosphorus compound upon stepwise substitution of the organic groups by other organic groups.

In addition, two very recent theoretical treatises^{5,6}

(1) National Science Foundation Undergraduate Research Participant, 1963-1965.

(2) S. O. Grim and W. McFarlane, *Nature*, in press.

(3) J. R. Van Wazer, C. F. Callis, J. N. Shoolery, and R. C. Jones, *J. Am. Chem. Soc.*, **78**, 5715 (1956).

(4) L. C. D. Groenweghe, L. Maier, and K. Moedritzer, *J. Phys. Chem.*, **66**, 901 (1962).

have dealt with the problem of calculation of P^{31} chemical shifts.

Since the number of reported phosphorus chemical shifts in quaternary phosphonium salts is very small,⁷⁻⁹ we undertook a study of phosphonium halides to determine the effect of slight differences in a homologous series of phosphonium salts on the chemical shift and also to attempt predictions similar to those for phosphines.²

The phosphorus chemical shifts of 49 phosphonium salts are reported in Tables I and II. All chemical shifts are given for solutions in dimethyl sulfoxide unless otherwise indicated. The measurements were made using a Varian DP 60 nmr spectrometer at 24.3 Mc/sec in 15 × 120 mm tubes with 85% phosphoric

Table I: P^{31} Chemical Shifts of Some Quaternary Triphenylphosphonium Salts

Compound ^c	Obsd Δ, ppm
[Ph ₃ PMe]Br	-22.7 ^a
[Ph ₃ PEt]Br	-26.2 ^b
[Ph ₃ PPr]Br	-24.1
[Ph ₃ PBu]Br	-24.0
[Ph ₃ PHx]Br	-24.4
[Ph ₃ P(<i>i</i> -Pr)]Br	-30.9
[Ph ₃ P(<i>sec</i> -Bu)]Br	-30.2
[Ph ₃ P(<i>c</i> -Hx)]Br	-26.6
[Ph ₃ P(<i>c</i> -Pe)]Br	-30.7
[Ph ₃ PCH(CH ₂ CH ₃) ₂]Br	-30.1
[Ph ₃ PCH(CH ₂ CH ₃)(CH ₂ CH ₂ CH ₃)]Br	-30.3
[Ph ₂ P(<i>t</i> -Bu)]I	-34.7
[Ph ₃ PC(CH ₃) ₂ CH ₂ CH ₃]I	-36.7
[Ph ₃ PC(CH ₃) ₃]I	-35.1
[Ph ₃ PCH ₂ Cl]Cl	-23.8
[Ph ₃ PC ₇ H ₇]Br	-22.6
[Ph ₃ PCH ₂ CH=CH ₂]Br	-21.4
[Ph ₃ PCH ₂ C(CH ₃)=CH ₂]Cl	-21.0
[Ph ₃ PCH ₂ CH=CHPh]Br	-22.2
[Ph ₃ PCH ₂ CO ₂ CH ₃]Br	-20.3
[Ph ₃ PCH ₂ COCH ₃]Br	-19.4
[Ph ₃ PCH ₂ OH]Cl	-17.7
[Ph ₃ PCH ₂ Br]Br	-22.6 ^c
[Ph ₃ P(CH ₂) ₃]Br	-24.0
[Ph ₃ P(CH ₂) ₄]Br	-24.2
[Ph ₃ PCH ₂ Ph]Br	-23.5
[Ph ₃ PCHPh ₂]Br	-21.4
[Ph ₃ PCH ₂ (<i>m</i> -NO ₂ C ₆ H ₄)]Br	-24.0
[Ph ₃ PCH ₂ (<i>p</i> -NO ₂ C ₆ H ₄)]Br	-23.8
[Ph ₃ P(CH ₂) ₃ PPh ₃]Br ₂	-23.2 ^d
[Ph ₃ PCH ₂ C ₆ H ₄ CH ₂ PPh ₃]Br ₂	-22.8 ^d

^a Lit.⁷ [Ph₃PMe]I, -20 in MeOH. ^b Lit.⁷ [Ph₃PEt]I, -26 in MeOH. ^c Lit.⁸ -24.0 in CHCl₃. ^d In MeOH. ^e Ph = phenyl, Me = methyl, Et = ethyl, Pr = propyl, *i*-Pr = isopropyl, Hx = hexyl, *c*-Hx = cyclohexyl, *c*-Pe = cyclopentyl.

Table II: Calculated and Observed P^{31} Chemical Shifts of Quaternary Phosphonium Salts

Compound	Calcd Δ, ppm	Obsd Δ, ppm
[Ph ₄ P]I	-22.0	-23.2 ^a
[Ph ₃ MeP]Br	-22.8	-22.7
[Ph ₃ EtP]Br	-26.4	-26.2
[Ph ₃ PrP]Br	-25.4	-24.1
[Ph ₃ BuP]Br	-25.4	-24.0
[Ph ₃ (<i>i</i> -Pr)P]Br	-29.8	-30.9
[Ph ₃ (<i>c</i> -Pe)P]Br	-28.3	-30.7
[Ph ₂ Me ₂ P]Br	-23.6	-22.1
[Ph ₂ Me(<i>i</i> -Pr)P]Br	-30.6	-30.9
[Ph ₂ Me(<i>c</i> -Pe)P]Br	-29.1	-29.8
[Ph ₂ Et(<i>i</i> -Pr)P]Br	-34.3	-36.2
[Ph ₂ Et(<i>c</i> -Pe)P]Br	-32.7	-34.8
[Ph ₂ Pr(<i>c</i> -Pe)P]Br	-31.7	-32.5
[PhEt(<i>i</i> -Pr) ₂ P]Br	-42.2	-42.2
[PhPr(<i>i</i> -Pr) ₂ P]Br	-41.0	-39.9
[PhMe(<i>c</i> -Pe) ₂ P]Br	-35.4	-36.4
[PhEt(<i>c</i> -Pe) ₂ P]Br	-39.1	-37.3
[PhPr(<i>c</i> -Pe) ₂ P]Br	-37.9	-35.6
[Me ₄ P]Br	-25.2	-25.1
[Me ₃ EtP]Br	-28.8	-28.0
[Me(<i>c</i> -Pe) ₃ P]Br	-41.6	-40.0
[Me(<i>i</i> -Pr) ₃ P]Br	-46.2	-45.1
[Bu ₃ EtP]Br	-36.6	-35.5
[Bu ₄ P]Br	-35.6	-33.9

^a In CH₂Cl₂.

acid as an external reference in a 5-mm o.d., thin-wall tube inserted concentrically into the sample tube through a serum cap. Within the moderately high concentration range (1.0 to 0.13 *M*) needed for detection of the signal, there was no change of the chemical shift of methyltriphenylphosphonium bromide in dimethyl sulfoxide upon concentration changes. Substitution of bromide by chloride and iodide likewise had no effect on the chemical shift of the methyltriphenylphosphonium cation. However, solvent effects were noted in a brief study (see Table III) with methyltriphenylphosphonium bromide and more extensive solvent studies are in progress.

Table I includes the P^{31} chemical shifts of 31 triphenylphosphonium salts. From inductive effect con-

(5) H. S. Gutowsky and J. Larmann, *J. Am. Chem. Soc.*, **87**, 3815 (1965).

(6) J. H. Letcher and J. R. Van Wazer, *J. Phys. Chem.*, in press. We are grateful to Dr. Van Wazer for sending us his manuscript prior to its publication.

(7) D. B. Denney and L. C. Smith, *J. Org. Chem.*, **27**, 3404 (1962), footnote 5.

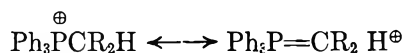
(8) J. S. Driscoll, D. W. Grisley, Jr., J. V. Pustinger, J. E. Harris, and C. N. Matthews, *ibid.*, **29**, 2427 (1964).

(9) K. Moedritzer, L. Maier, and L. C. D. Groenweghe, *J. Chem. Eng. Data*, **7**, 307 (1962).

Table III: P³¹ Chemical Shifts of [MePh₃P]Br in Various Solvents

Solvent	Chemical shift, ppm, vs. 85% H ₃ PO ₄
DMSO	-22.7
CH ₂ Cl ₂	-22.0
MeOH	-21.5
<i>i</i> -PrOH	-21.3
H ₂ O	-20.5

siderations, one would expect that in the series [Me-Ph₃P]Br, [EtPh₃P]Br, [(*i*-Pr)Ph₃P]Br, and [(*t*-Bu)-Ph₃P]Br, the shielding of the phosphorus would increase and the chemical shift would likewise move upfield. However, the opposite order is observed. One explanation for this behavior which is consistent with the experimental data is hyperconjugation of the α -hydrogens and use of the 3d orbitals of phosphorus



The greater the number of α -hydrogens (three for methyl, two for normal alkyl, one for secondary alkyl, and zero for tertiary alkyl), the more extensive would be the involvement in hyperconjugation and the larger the shielding of the phosphorus nucleus.

The chemical shifts of the simple alkyltriphenylphosphonium salts in Table I can be rationalized rather well by this explanation. More mathematically based arguments have been presented by others⁶ to explain this phenomenon.

Table II lists the phosphorus chemical shifts of 24 (including six repeated from Table I) phosphonium salts which contain only those groups for which the σ^{P} values are known.¹⁰ Of these 24 salts, the following numbers contain at least one of the indicated groups: methyl, 9; ethyl, 7; propyl, 4; butyl, 3; isopropyl, 6; cyclopentyl, 8; and phenyl, 18.

The P³¹ chemical shift of these phosphonium salts can be predicted by adding the group contribution listed in Table IV for each group in the quaternary compound. For example, the predicted chemical shift of diphenylmethylisopropylphosphonium bromide is $2(-5.5) - 6.3 - 13.4 = -30.7$, whereas the observed chemical shift is -30.9 ppm.

If the group contributions from Table IV (with the exception of phenyl) are plotted vs. the corresponding σ^{P} values, a straight line is obtained. See Figure 1. Thus, the values of Table IV can be replaced (except for phenyl) by σ^{P} values multiplied by the slope of the line in Figure 1 and the P³¹ chemical shift in quaternary

Table IV: Group Contributions to P³¹ Chemical Shift of a Quaternary Phosphonium Compound

Group	Contribution
Ph	-5.5
Me	-6.3
Et	-10.1
Pr	-8.5
Bu	-8.5
<i>i</i> -Pr	-13.4
<i>c</i> -Pe	-11.8

phosphonium salts can be predicted by eq 1.

$$\Delta \text{ (ppm)} = -6.3n - 5.5(4 - n) - 0.26 \sum_{r=1}^n \sigma^{\text{P}}$$

$$\Delta \text{ (ppm)} = -22.0 - 0.8n - 0.26 \sum_{r=1}^n \sigma^{\text{P}} \quad (1)$$

where n is the number of alkyl groups. The values calculated from eq 1 are listed in Table II.

The position of phenyl in Figure 1 suggests that its ability to shield the phosphorus atom is much greater in the quaternary phosphonium salts than in the tertiary phosphines. This is consistent with the fact that phenyl can act as a π -electron donor to the empty 3d orbitals of phosphorus in the phosphonium compounds and as a π^* -electron acceptor of the free electron pair of phosphorus in the phosphines.

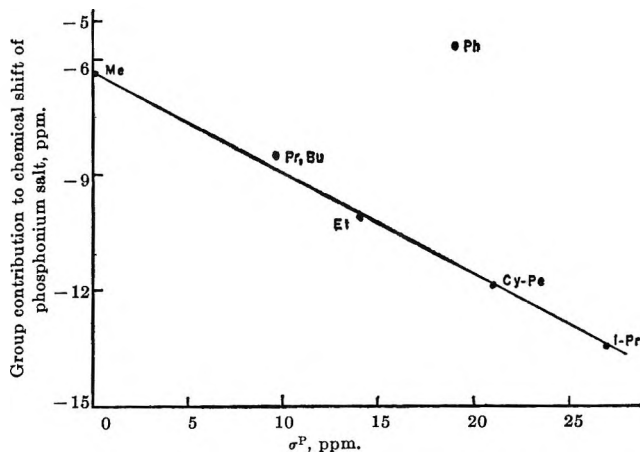


Figure 1. Group contribution to chemical shift of phosphonium salt vs. σ^{P} .

Work is in progress to expand the list of σ^{P} values since only nine groups have been assigned to date. It should be pointed out, however, that the P³¹ chemical shift of 1209 tertiary and secondary phosphines

(10) σ^{P} for cyclopentyl is 21 (determined since publication of ref 2).

and quaternary phosphonium salts can be predicted from the values for the nine groups.

Acknowledgment. We thank the National Science Foundation (G-24443) for support of this work, the Advanced Research Projects Agency, Department of Defense, for purchase of nmr equipment, and M. and T. Chemicals, Inc., for gifts of phosphorus chemicals.

Charge-Transfer Complexes of N-Isopropylcarbazole

by James H. Sharp

Xerox Corporation, Rochester, New York (Received July 22, 1965)

Intermolecular charge-transfer complexes between aromatic molecules which can act as electron donors and electron-acceptor molecules such as quinones, halogens, cyano and nitro compounds are well known and have been studied extensively.¹ These complexes are generally characterized by an electronic absorption in the visible or near ultraviolet which is a unique property of the complex.

Mulliken² has considered these complexes to be the result of an acid-base reaction between the aromatic molecule (Lewis base) and the electron acceptor (Lewis acid). The ground- and excited-state wave functions of the complex are treated as a resonance hybrid between a nonbonded state, $\psi_0(D,A)$ and a dative state $\psi_D(D^+A^-)$. Thus the ground-state wave function is given by $\psi_G = a\psi_0(D,A) + b\psi_D(D^+A^-)$, whereas the excited state is represented by $\psi_E = a^*\psi_D(D^+A^-) - b^*\psi_0(D,A)$. This interpretation has been successful in explaining the energetics of the spectroscopically observed charge-transfer bands of such complexes.

In recent work, Taniguchi, *et al.*,³ have described the electrical and optical properties of the charge-transfer complex between poly-N-vinylcarbazole (PVK) and tetracyanoquinodimethane (TCNQ). In a later publication, Hoegl⁴ applied electrostatic imaging techniques to the study of the photoresponse of PVK and other organic polymers. He has shown that the photoresponse may be strongly improved by doping with a variety of electron acceptors.

In order to determine the effect of charge-transfer interactions on the photoconductive properties of organic crystals, N-isopropylcarbazole (NIPC) has been

chosen as a model compound. This note describes the intermolecular charge-transfer complexes formed in dichloromethane between NIPC and four electron acceptors, 1,3,5-trinitrobenzene (TNB), picryl chloride (PC), 2,4,7-trinitro-9-fluorenone (TNF), and tetracyanoethylene (TCNE).

Experimental Section

Materials. NIPC, PC, TNB, TNF, and dichloromethane were obtained from Eastman Organic Chemicals. TCNE was obtained from K & K Laboratories, Inc. The solid compounds were recrystallized once from ethanol or chlorobenzene before use.

Optical Measurements. Absorption spectra in the visible and infrared were measured with an automatic, recording Cary 14 spectrophotometer. The 1-cm sample cell was housed in a thermostatable cell compartment through which thermostated water was circulated. The temperature of the sample could be maintained to within $\pm 0.5^\circ$ throughout the temperature range from 5 to 60° .

For the particular complex under study, a series of solutions was prepared in which the acceptor concentration was invariant ($\sim 2 \times 10^{-3} M$) and small compared to the NIPC concentration which was usually varied from 0.6 to 0.12 M . In the case of the NIPC·TCNE complex, the NIPC concentration was varied from 0.2 to 0.05 M . In each series, blanks consisting of the acceptor alone and NIPC alone were run. Any slight absorption due to NIPC or the acceptor in the region of the complex was subsequently subtracted from the charge-transfer absorption. All samples were run against a 1-cm cell containing dichloromethane in the reference beam.

Analysis of the Charge-Transfer Absorption Spectra. An analysis, similar to that by Benesi and Hildebrand⁵ and Keefer and Andrews,⁶ was used to interpret the spectra. The formation of a 1:1 molecular complex may be represented by the following equilibrium between the donor-acceptor pair



(1) For recent reviews see: (a) R. S. Mulliken and W. B. Person, *Ann. Rev. Phys. Chem.*, **13**, 107 (1962); (b) G. Briegleb, "Elektronen-Donator-Acceptor-Komplexe," Springer-Verlag, Berlin-Göttingen-Heidelberg, 1961; (c) R. S. Mulliken, *J. Chim. Phys.*, **61**, 20 (1964); (d) V. P. Parini, *Russ. Chem. Rev.*, **31**, 408 (1962).

(2) (a) R. S. Mulliken, *J. Am. Chem. Soc.*, **74**, 811 (1952); (b) R. S. Mulliken, *J. Phys. Chem.*, **56**, 801 (1952).

(3) A. Taniguchi, S. Kanda, T. Nogaito, S. Kusabayashi, H. Mikawa, and K. Ito, *Bull. Chem. Soc. Japan*, **37**, 1386 (1964).

(4) H. Hoegl, *J. Phys. Chem.*, **69**, 755 (1965).

(5) H. A. Benesi and J. H. Hildebrand, *J. Am. Chem. Soc.*, **71**, 2703 (1949).

(6) (a) R. M. Keefer and L. J. Andrews, *ibid.*, **72**, 4677 (1950); (b) L. J. Andrews and R. M. Keefer, *ibid.*, **73**, 462 (1951).

Table I: A Summary of the Heats of Formation, Entropy Changes, and Equilibrium Constants of the 1:1 Complexes of NIPC at 24° (ϵ^{\max} and λ^{\max} of the Respective Charge-Transfer Bands Are Also Included)

Complex	$-\Delta H^\circ$, kcal/mole	$-\Delta S^\circ$, eu	K , l/mole.	λ^{\max} , Å	ϵ^{\max} , l./mole-cm
NIPC·TCNE	2.60 ± 0.20	6.3 ± 0.3	3.40 ± 0.05	6000	980
NIPC·TNF	2.20 ± 0.33	6.6 ± 0.5	1.52 ± 0.16	4400	2420
NIPC·TNB	2.35 ± 0.24	8.1 ± 0.3	0.90 ± 0.05	4050	1840
NIPC·PC	1.41 ± 0.17	5.3 ± 0.2	0.70 ± 0.04	4150	1590

Under conditions where $[D] \gg [A]$, where the molar extinction coefficients of D and A are negligible in the wavelength region of the charge-transfer absorption band and where Beer's law is valid, the molar extinction coefficient of the complex, ϵ_{DA} , and the equilibrium constant, K , are related by

$$\frac{[A]l}{\alpha} = \frac{1}{\epsilon_{DA}} + \frac{1}{\epsilon_{DA}K[D]} \quad (2)$$

where α is the absorbance and l is the path length of the light through the sample cell. If a 1:1 complex is formed, then a plot of $[A]l/\alpha$ against $1/[D]$ will yield a straight line with a slope equal to $1/\epsilon_{DA}K$. Furthermore, if ϵ_{DA} is temperature independent, then the equilibrium constant K can be evaluated at various temperatures.

Results and Discussion

The absorption spectra of the four molecular complexes are shown in Figure 1. The molar extinction coefficients were determined by plotting eq 2 at various wavelengths throughout the charge-transfer band. All the complexes proved to have 1:1 stoichiometry. In the case of the PC, TNB, and TNF molecular complexes, the charge-transfer band overlaps quite strongly with the long wavelength absorption of the respective acceptor. The absorption edge of the NIPC is located at 3500 Å.

The NIPC·TCNE absorption band is not symmetrical and suggests that it may be double. These two bands are probably associated with an electron transfer from the highest occupied and the second highest occupied orbitals of NIPC to the lowest vacant orbitals of TCNE. Similar "multiple" charge-transfer bands have been observed for TCNE complexes by Kuroda, *et al.*,⁷ and by Voigt.⁸

From an analysis of the charge-transfer bands observed between TNB and donor molecules, Briegleb⁹ has obtained the empirical formula

$$h\nu_{CT} = I - 5.00 + \frac{0.7}{I - 5.00} \quad (3)$$

where I is the ionization potential of the donor molecule

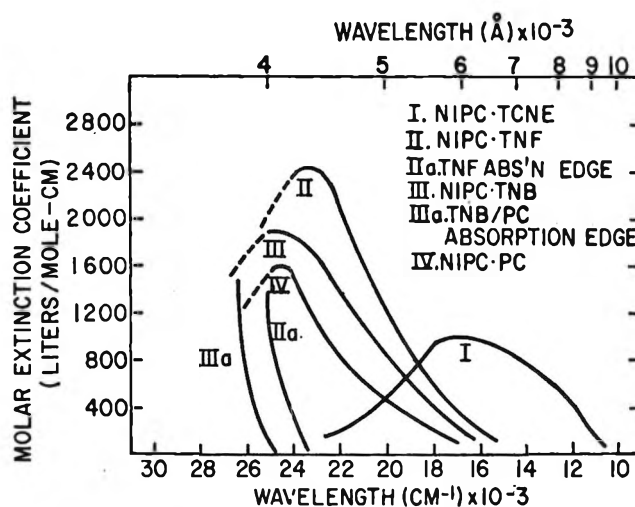


Figure 1. Absorption spectra of four charge-transfer complexes of N-isopropylcarbazole.

and ν_{CT} is the frequency at the maximum of the charge-transfer absorption band. Employing this relation, the ionization potential of NIPC is found to be 7.81 eV. Kuroda, *et al.*,⁷ have reported a similar relation for the complexes of polycyclic aromatic hydrocarbons and TCNE which has the form

$$h\nu_{CT} = 0.92I - 5.10 \quad (4)$$

Using this expression for the NIPC·TCNE complex, the ionization potential of NIPC is found to be 7.79 eV, which is in excellent agreement with that calculated above.

The equilibrium constants of the complexes were determined as a function of temperature from approximately 8 to 58°. (The extinction coefficients of the charge-transfer complexes, ϵ_{DA} , proved to be temperature independent throughout this temperature range.) Equilibrium constants were also determined at various wavelengths for a given complex and good agreement

(7) H. Kuroda, M. Kobayashi, M. Kinoshita, and S. Takimoto, *J. Chem. Phys.*, **36**, 457 (1962).

(8) E. M. Voigt, *J. Am. Chem. Soc.*, **86**, 3611, 3930 (1964).

(9) Chapter VI of ref 1b.

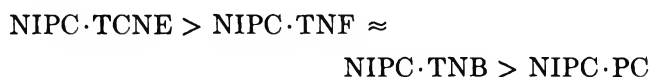
was realized. For example, in the case of the NIPC·TCNE complex, the equilibrium constants at 24° determined by plotting eq 2 at 5500, 6000, 6500, and 7000 Å were 3.40, 3.45, 3.35, and 3.41 l./mole, respectively.

Heats of formation, ΔH° , for the molecular complexes were obtained from the Gibbs-Helmholtz expression for the temperature dependence of the equilibrium constant

$$\frac{d \ln K}{d(1/T)} = \frac{-\Delta H^\circ}{R} \quad (5)$$

Table I summarizes the heats of formation, the entropy change, and the equilibrium constants at 24° along with ϵ^{\max} and λ^{\max} of the respective charge-transfer band.

The heats of formation and equilibrium constants indicate that the complexes may be qualitatively arranged according to complex strength. Such an evaluation gives the series



which also reflects the relative electron affinities of the acceptor molecules, *i.e.*, $E_A^{\text{TCNE}} = 1.6$ eV and $E_A^{\text{TNB}} = 0.6$ eV.¹⁰

A sandwich configuration which would allow maximum overlap between the π -molecular orbitals of the respective donor-acceptor pair predicts the above order. TCNE has a large planar conjugated π -electronic system which will allow a maximum of overlap with the NIPC π -electronic system. Both TNF and TNB, although containing the powerful electron-attracting nitro groups, will be slightly less planar. PC is expected to be less planar and a weaker electron acceptor than TNB. A less planar structure would be predicted on the basis of steric interaction between the adjacent chloro and nitro groups and the electron-attracting power of the nitro groups is partially nullified by the electron-donating effect of the chloro group.

NIPC might also be expected to interact with electron acceptors through the pair of nonbonding electrons of the nitrogen atom. However, if this were the case, one would expect much greater differences due to steric factors.

Acknowledgment. The Xerox Corp. and the author are indebted to Battelle Memorial Institute, Geneva, and in particular to Dr. H. Hoegl and his co-workers,

for the initiation of this work. It is a pleasure to acknowledge the interest and helpful contributions of Dr. P. K. Watson and Mr. Paul Regensberger.

The Critical Solution Temperatures of Some Phenols in Water and Deuterium Oxide

by Eugene E. Schrier, Robert J. Loewinger, and Arthur H. Diamond

Harpur College, State University of New York at Binghamton, Binghamton, New York 13901 (Received July 29, 1965)

Interest has been shown recently in comparing the structural features of liquid water and liquid deuterium oxide.^{1,2} The thermodynamic properties of nonelectrolyte solutions³ prepared with either H₂O or D₂O as one of the components have also been studied, as well as the effects of isotopic substitution on phase relationships in binary solutions. The substitution of D₂O for H₂O produces, in all cases studied, a sizable increase⁴ in the upper critical solution temperature (ucst) of a binary aqueous solution. The ucst for the phenol-water system is reported^{5,6} to be increased by 13° when D₂O is substituted for H₂O and the acidic hydrogen of phenol is exchanged.

In this study, we have measured the ucst values for phenol, *m*-hydroxybenzaldehyde, and *p*-hydroxybenzaldehyde in H₂O and the same quantity for these compounds, in which the phenolic hydrogen has been exchanged for deuterium, in D₂O. The results and their interpretation provide information regarding the relative strengths of hydrogen and deuterium bonds in these systems.

Experimental Section

Baker and Adamson reagent grade phenol was used without further purification. Eastman *p*-hydroxybenzaldehyde and Aldrich *m*-hydroxybenzaldehyde were purified by vacuum distillation followed by recrystallization from water using decolorizing charcoal. The resulting white crystals gave melting ranges of

- (1) G. Nemethy and H. A. Scheraga, *J. Chem. Phys.*, **41**, 680 (1964).
- (2) M. R. Thomas, H. A. Scheraga, and E. E. Schrier, *J. Phys. Chem.*, **69**, 3722 (1965).
- (3) L. Benjamin and G. C. Benson, *ibid.*, **67**, 858 (1963).
- (4) J. D. Cox, *J. Chem. Soc.*, 4606 (1952).
- (5) I. B. Rabinovitch, V. D. Fedorov, N. P. Pashkin, M. A. Avdesnyak, and N. Y. Piminov, *Dokl. Akad. Nauk SSSR*, **105**, 108 (1955).
- (6) M. R. Cardinaud, *Compt. Rend.*, **246**, 415 (1958).

(10) Chapter XI of ref 1b.

117–118 and 103.5–104.5° for *para*- and *meta*-substituted compounds, respectively. The values reported previously⁷ for these compounds were 116 and 106°. Deuterium oxide, having an isotopic purity of 99.77%, was obtained from Bio-Rad Laboratories, Richmond, Calif.

The phenolic hydrogen of the compounds was exchanged by dissolving the material with D₂O and evacuating to dryness in a vacuum desiccator. This procedure was repeated for each compound.

Critical solution temperatures were measured in an open test tube using an accurate thermometer which could be read to 0.03°. Duplicate readings at the same composition were usually within 0.1°.

Results

The results of these measurements are given in Table I.

Table I: Upper Critical Solution Temperatures for Phenols in H₂O and D₂O

Compound	H ₂ O	D ₂ O	$\frac{(\text{ucst})_{\text{D}_2\text{O}}}{(\text{ucst})_{\text{H}_2\text{O}}}$
Phenol	66.4	80.1	13.7
<i>p</i> -Hydroxybenzaldehyde	64.9	74.8	9.9
<i>m</i> -Hydroxybenzaldehyde	67.0	76.6	9.6

The value obtained for phenol in H₂O compares well with the many results⁸ previously reported. Sidgwick and Allot⁷ obtained 64.4 and 66.1° for the *para*- and *meta*-substituted benzaldehydes, respectively. Values of 79.2 and 79.0° have been reported previously^{5,6} for phenol-*d* in D₂O. In all cases, the ucst values appeared at approximately 10 mole % phenol or aldehyde.

Discussion

We will be concerned here with the last column of Table I. The difference $\delta T_c = (\text{ucst})_{\text{D}_2\text{O}} - (\text{ucst})_{\text{H}_2\text{O}}$ is seen to be about the same for the substituted phenols, *i.e.*, 9.6 to 9.9°, but δT_c for phenol is greater than this value by about 4°. While the ucst values of all of the compounds are nearly the same in water, those of the substituted phenols are lowered relative to that of phenol-*d* in D₂O.

We infer that this difference is due to the presence of the additional H-bond accepting group in the substituted phenols. The influence on the ucst values of H-bonding interaction of water with the —C(=O)H group is clearly seen in the fact that the *p*- and

m-cresols (methyl-substituted phenols) give ucst values of 143.5 and 147.0°, respectively, in H₂O.⁹ The replacement of an unfavorably interacting methyl group in a cresol by a hydrogen-bond acceptor, the aldehyde group, succeeds in reducing the ucst back to approximately the value for phenol. If the hydroxybenzaldehyde is transferred to a solvent in which slightly stronger acceptor-solvent hydrogen bonds are possible, the stronger interaction should permit complete miscibility at a lower temperature than that observed for the unsubstituted phenol. This is the explanation of the observed difference between the ucst values in D₂O and is based on the premise that C=O--D₂O bonds are stronger than C=O--H₂O interactions. While some other variations in interactions are canceled out by taking differences, the difference between the phenolic —OH interactions with the carbonyl group or with other phenolic —OH's of hydroxybenzaldehyde molecules in the aldehyde-rich layer and the corresponding —OD interactions with the carbonyl group or other —OD's is not completely accounted for in this interpretation. We may say, however, that phenolic —OH interactions with each other, which account for a number of the hydrogen bonds in the organic-rich phases of the aldehydes, occur with the unsubstituted phenol as well. Since the number of phenolic —OH's is approximately the same in the organic-rich layers of all the systems studied, the —C=O--HO— bonds of the substituted phenols form at the expense of —OH--OH interactions which would be possible with phenol. We infer from this that, while the values of $\delta T_c(\text{hydroxybenzaldehyde})$ and $\delta T_c(\text{phenol})$ show the full effect of isotopic substitution in the organic-rich phase, the difference $\delta T_c(\text{hydroxybenzaldehyde}) - \delta T_c(\text{phenol})$, although affected, is less dependent on this substitution than the individual δT_c values. In any case, the possible effects of competing influences in these systems on the interpretation of the data cannot be overlooked although orientation effects appear to be of lesser significance because of the similarity in the structures of the compounds and the fact that the temperatures are approximately the same throughout the comparison. The desire to make these comparisons at approximately the same temperatures precluded measurements with *o*-hydroxybenzaldehyde since the ucst of this compound in water has been reported⁷ to be over 200°.

(7) N. V. Sidgwick and E. N. Allot, *J. Chem. Soc.*, **123**, 2819 (1923).

(8) J. Timmermans, "The Physico-Chemical Constants of Binary Systems," Vol. 4, Interscience Publishers, Inc., New York, N. Y., 1960, pp 326–327.

(9) See ref 8, pp 336–337.

A quantitative development of the above explanation of the difference between the ucst values of the hydroxybenzaldehydes and phenol in D₂O may be given. Copp and Everett¹⁰ have deduced an approximate relationship between the excess free energy of mixing and the critical solution temperature

$$F^E(x_2 = 0.5) = 0.5RT_c \quad (1)$$

where $F^E(x_2 = 0.5)$ is the excess free energy per mole of solution at solute mole fraction, $x_2 = 0.5$, and T_c is the critical solution temperature. While this equation is strictly true only for regular solutions, these authors^{11,12} have shown that only slight variations are produced in the value of 0.5 on the right side of eq 1 by considerable asymmetry in plots of F^E vs. x_2 . At $x_2 = 0.5$, therefore, F^E is approximately T_c calories/mole. We define

$$\delta F^E = \delta T_c = (\text{ucst})_{\text{D}_2\text{O}} - (\text{ucst})_{\text{H}_2\text{O}} \quad (2)$$

The difference, discussed above, between δT_c for the substituted phenols and δT_c for phenol is given as $\delta T_c(\text{hydroxybenzaldehyde}) - \delta T_c(\text{phenol})$ and is, by eq 1 and 2, equal to -4 cal/mole of solution. We assume, as we did above, that entropic factors do not contribute significantly to this value on account of similarities in both the structures of the compounds and in the number of possible hydrogen bonds formed. Therefore, the change in the excess free energy per mole of solution in going from H₂O to D₂O solutions is attributed to variations in the excess enthalpy, which is 4 cal more negative for the substituted phenols than for phenol. This difference is caused by the ability of the additional acceptor group on the substituted phenols to form a slightly stronger hydrogen bond with D₂O than with H₂O.

Support for this contention comes from a comparison of this value of the enthalpy difference with data given by Benjamin and Benson³ for the excess enthalpies of mixing in the CH₃OH + H₂O and CH₃OD + D₂O systems. In the concentration range $x_{\text{CH}_3\text{OH}}$ (or D) between 0.05 and 0.5, $\delta H^E = H^E(\text{CH}_3\text{OD} + \text{D}_2\text{O}) - H^E(\text{CH}_3\text{OH} + \text{H}_2\text{O})$ is negative with a value of -2 cal/mole at $x_{\text{CH}_3\text{OH}}$ (or D) = 0.5 and a value at the minimum of the H^E vs. x curve, *i.e.*, where $x_{\text{CH}_3\text{OH}}$ (or D) = 0.3, of -4 cal/mole. The order of magnitude of this isotope effect on the excess enthalpy is in good agreement with the value derived from the interpreta-

tion of the critical solution temperature data given above.

Acknowledgment. We are grateful for the assistance of Mr. John Welsh in purifying the phenols.

Dipole Moments of Some Hydrogen-Bonded Complexes

by Charles F. Jumper¹ and Bentz B. Howard²

Department of Chemistry, Florida State University, Tallahassee, Florida (Received July 6, 1965)

As part of a study of hydrogen-bond formation between chloroform and various organic bases, we have measured the dipole moments of the complexes formed. One of our objects was to determine if dielectric measurements can give dipole moments of the complexes of sufficient accuracy to allow the geometry of the complex (the angle between the dipole moments of the donor and acceptor molecule) to be deduced by applying the law of cosines. Our results indicate that this cannot be done.

The main stumbling block seems to be the changes in the dipole moments of the donor and acceptor molecules when they interact to form the complex. This interaction causes a polarization which changes both dipole moments by an unknown amount; thus we do not know the dipole moments of the donor and acceptor molecules *as they occur in the complex*. At the present time there seems to be no way of calculating the amount of this "enhancement" of the dipole moments. Nevertheless, our results for the dipole moments of the complexes allow us to get some idea of the magnitude of this enhancement, and it appears to be several tenths of one Debye unit.

We need to determine the dipole moment of a complex from measured values of the dielectric constant of solutions of chloroform and a base in a nonpolar solvent. It is desirable that the dipole moment so obtained be independent of the surrounding medium. Onsager³ has given an equation that should give just this dipole moment. His theory takes into account both the "reaction field" of the dipole and the "cavity field" which tends to orient the dipole in the electric field. He assumes the dipole is in a spherical cavity.

(10) J. L. Copp and D. H. Everett, *Discussions Faraday Soc.*, **15**, 174 (1953).

(11) J. L. Copp and D. H. Everett, *ibid.*, **15**, 267 (1953).

(12) J. L. Copp and D. H. Everett, *Trans. Faraday Soc.*, **53**, 9 (1957).

(1) National Science Foundation Fellow, 1959-1960. Department of Chemistry, The Citadel, Charleston, S. C.

(2) Deceased.

(3) L. Onsager, *J. Am. Chem. Soc.*, **58**, 1486 (1936).

Onsager's equation has been refined slightly by Böttcher⁴ and by Scholte⁵ so as to apply to dipoles in ellipsoidal cavities. The resulting equation⁶ for a solution of i components is

$$\frac{\epsilon - 1}{4\pi} = \sum_i \left[\frac{3\epsilon N_i}{2\epsilon + 1} \frac{\alpha_i}{1 - f_i \alpha_i} + \frac{\epsilon N_i}{\epsilon + (1 - \epsilon)A_i} \frac{1}{[1 - (f_m)_i(\alpha_m)_i]^2} \frac{\mu_i^2}{3kT} \right] \quad (1)$$

where ϵ is the dielectric constant of the solution, N is the volume concentration, α is the polarizability, α_m is the polarizability in the direction of the dipole moment, μ is the dipole moment, k is Boltzmann's constant, and T is the absolute temperature. The quantities f_i and $(f_m)_i$ are given by

$$f_i = \frac{1}{a_i^3} \frac{(2\epsilon - 2)}{(2\epsilon + 1)}$$

where a is obtained from the molar volume, $V = (4\pi/3)a^3 N_{\text{avogadro}}$ and

$$(f_m)_i = \frac{3}{xyz} \frac{A(1 - A)(\epsilon - 1)}{\epsilon + (1 - \epsilon)A}$$

The shape factor (or "depolarization factor"), A , is defined by

$$A = \frac{xyz}{2} \int_0^\infty \frac{ds}{(s + x^2)^{1/2}(s + y^2)^{1/2}(s + z^2)^{1/2}}$$

where x , y , and z are the semi-axes of the ellipsoidal cavity, with the dimension x chosen in the direction of the dipole moment. This integral cannot be evaluated in closed analytical form, so we have obtained empirical values of A for chloroform and each base molecule from measurements of the dielectric constants of binary solutions of each of these substances individually in the nonpolar solvent. In obtaining A we treated our data according to eq 2 (see below) and found A from the coefficient of N_t , using the gas phase dipole moments given in Table II as parameters. The value of A for the hydrogen-bonded complex is obtained from the graphs of the "demagnetization factors" given by Osborn,⁷ using dimensions estimated from Stuart models of the complexes.

In order to simplify the calculations, we have carried out all our experiments using a nonpolar solvent, and with the stoichiometric concentrations of chloroform and base kept equal.

Equation 1 is expanded in ϵ Taylor series in the concentration, which is truncated after the quadratic term, so that we obtain an equation in the form⁸

$$\epsilon = \epsilon_0 + WN_t + ZN_t^2 \quad (2)$$

where ϵ_0 is the dielectric constant of pure solvent and N_t is the stoichiometric concentration of chloroform (or base). The function W is the sum of three parts: a solvent term, a chloroform term, and a base term. Each of these terms depends on the respective polarizabilities, shape factors, and dipole moments. The function Z consists of four parts, and has the form

$$Z = Q_1 - Q_2 - Q_3 + Q_4$$

where Q_1 depends only upon solvent parameters; Q_2 depends upon chloroform parameters and the association constant, K ; Q_3 depends upon base parameters and K ; and Q_4 depends upon parameters of the complex and K . The association constants K were obtained from the paper by Howard, *et al.*⁹

The experimental values of ϵ are fitted by least squares to a quadratic function in the concentration, and the value of Z so obtained is used to find the dipole moments of the complex.¹⁰ We have satisfied ourselves that eq 2 fits our data well within experimental error. In Table I we tabulate the range of molarities used and the equations obtained from the least-squares fit.

Experimental Section

Eastman Kodak Spectrograde chloroform was extracted with concentrated H_2SO_4 , washed, and distilled from P_2O_5 . Dielectric constants of solutions were measured within 3 days after preparation so as to minimize errors caused by the slow decomposition of chloroform.

Carbon tetrachloride and cyclohexane solvents were Eastman Kodak Spectrograde and were used without further purification.

Diethyl ether, isopropyl ether, pyridine, acetone, triethylamine, and acetonitrile were purified by standard methods, especial care being taken to remove traces of water. Solutions were prepared by weight using the utmost care. All glassware was calibrated.

(4) C. J. F. Böttcher, "The Theory of Electric Polarization," Elsevier Publishing Co., New York, N. Y., 1952.

(5) T. G. Scholte, *Physica*, **15**, 437 (1949).

(6) See ref 4, p 321.

(7) J. A. Osborn, *Phys. Rev.*, **67**, 351 (1945).

(8) In the interest of conserving space, the derivation of eq 2, as well as the exact forms of W and Z , is omitted. Details can be obtained from C. F. Jumper, "A Study of Hydrogen Bonding by Dielectric Methods and by Nuclear Magnetic Resonance," University Microfilms, Ann Arbor, Mich., L. C. Card No. Mic. 61-1285, \$2.75.

(9) B. B. Howard, C. F. Jumper, and M. T. Emerson, *J. Mol. Spectry*, **10**, 117 (1963).

(10) Details of the very involved calculations, as well as the values of all the constants used, are found in the reference given in footnote 8.

Table I: Fit of Experimental Data to Eq 2 ($t = 25.0^\circ$)

Base	Range of N_t^a	Eq 2
Acetonitrile (CCl_4)	0 to 0.71	$\epsilon = 2.2319 + 1.5265N_t + 0.04291N_t^2$
Triethylamine (C_6H_{12})	0 to 0.46	$\epsilon = 2.0147 + 0.21466N_t + 0.15433N_t^2$
Pyridine (CCl_4)	0 to 0.25	$\epsilon = 2.2275 + 0.83326N_t + 0.19112N_t^2$
Acetone (CCl_4)	0 to 0.26	$\epsilon = 2.2282 + 1.1300N_t + 0.15865N_t^2$
Isopropyl ether (CCl_4)	0 to 0.46	$\epsilon = 2.2284 + 0.35799N_t + 0.11430N_t^2$
Diethyl ether (CCl_4)	0 to 0.55	$\epsilon = 2.2277 + 0.34144N_t + 0.07791N_t^2$
Diethyl ether (C_6H_{12})	0 to 0.82	$\epsilon = 2.0140 + 0.32695N_t + 0.10430N_t^2$

^a Molarity of base or of chloroform, since the two are made equal.

Table II: Dipole Moments of Chloroform-Base Complexes

Base	μ_{base} , D.	Solvent	μ_{complex} , D.	Possible angle	Vector sum ^a	Apparent enhance- ment, D.
Acetonitrile	3.96 ^b	CCl_4	5.12	0°	4.97	0.15
Triethylamine	0.66 ^b	C_6H_{12}	2.07	0°	1.67	0.4
Pyridine	2.23 ^c	CCl_4	3.88	0°	3.24	0.6
Acetone	2.87 ^b	CCl_4	3.97	0°	3.88	0.1
Acetone	2.87 ^b	CCl_4	3.90	60°	3.49	0.4
Isopropyl ether	1.15 ^d	CCl_4	2.54	0°	2.16	0.4
Isopropyl ether	1.15 ^d	CCl_4	2.62	55°	1.92	0.7
Diethyl ether	1.15 ^b	C_6H_{12}	2.16	0°	2.16	0.0
Diethyl ether	1.15 ^b	C_6H_{12}	2.13	55°	1.92	0.2
Diethyl ether	1.15 ^b	CCl_4	2.59	0°	2.16	0.4
Diethyl ether	1.15 ^b	CCl_4	2.66	55°	1.92	0.7

^a Calculated using the law of cosines. Dipole moment of chloroform is 1.013 D.; see footnote b. ^b A. A. Maryott and F. Buckley, "Table of Dielectric Constants and Electric Dipole Moments of Substances in the Gaseous State," National Bureau of Standards Circular 537, U. S. Government Printing Office, Washington, D. C., 1953. ^c A. D. Buckingham, *et al.*, *J. Chem. Soc.*, 1405 (1956). ^d Estimated by comparison with other aliphatic ethers.

Dielectric constants were measured by standard methods using a General Radio Type 1302-A oscillator, a GR Type 716-C capacitance bridge, and a GR Type 1231-B amplifier and null detector with Type 1231-P5 filter and a GR Type 722-N precision condenser. The dielectric cell was Type 2TN50, purchased from J. C. Balsbaugh, Marshfield Hills, Mass. The cell was thermostated in a cottonseed oil bath at 25.0° . The reproducibility of the capacitances was $0.0007 \mu\mu\text{f}$ or less on duplicate series of solutions.

Results and Conclusions

The results are summarized in Table II. The experimentally determined dipole moments of the complexes are given in column four. The small variation in the μ_{complex} with different assumed geometries (column five) comes about because the shape factor, A , depends slightly on the geometry of the complex. For the ether molecules and for acetone, we have assumed geometries that probably represent the extreme possibilities.

The reliability of the dipole moments of the complexes depends largely on how strongly μ depends on the three parameters A , a , and K . Calculations have shown that the final value for μ is quite insensitive to all the radii, a , and to the shape factors, A , for chloroform and base. Reference 9 indicates that the probable error in K is about 3%. Such an error causes about a 1–2% error in μ . The necessity of estimating A for the complex from Stuart models might introduce a considerable error in this parameter. Here again, though, μ is not seriously dependent on the value chosen. For example, changing A by 20% only causes μ to change by 3%. Taking all these factors into consideration, we feel that the maximum error in μ_{complex} is about 0.2 D.

In the cases of acetonitrile, triethylamine, and pyridine it seems likely that the complex will form with the hydrogen atom of the chloroform molecule near the nitrogen atom of the base and with the dipole moments of chloroform and base aligned. With acetonitrile, for example, we might expect a complex: $\text{H}_3\text{CCN}\cdots$

HCCl_3 . If this be so, then with no enhancement the dipole moment of the complex would be $\mu_{\text{HCCl}_3} + \mu_{\text{CH}_3\text{CN}} = 1.013 + 3.96 = 4.97$ D. The experimentally determined value for this complex is 5.12 D. Therefore, it appears that there is an enhancement of 0.15 D. In view of the probable error in μ_{complex} , this small an enhancement could be a fiction.

On the basis of the first three entries in Table II, it appears that there is a relationship between the enhancement and α_m , the polarizability in the direction of the dipole moment of the base molecule. For acetonitrile, triethylamine, and pyridine, α_m is,¹⁰ respectively, 0.56, 1.02, and 1.24×10^{-23} cm³. The enhancements are 0.15, 0.4, and 0.6 D. This apparent correlation might well be fortuitous, for the enhancement probably depends on other factors in addition to α_m . It is difficult to include acetone and the two ethers in the comparison because of the uncertainty of the geometry of the complexes.

The results for diethyl ether present one very curious feature. Taken at face value, our data indicate the dipole moment of the diethyl ether-chloroform complex is different, depending on whether the solvent is cyclohexane or carbon tetrachloride. The ether-chloroform association constant is apparently different in these solvents as well.⁹ A number of possible explanations for this come to mind, but our ideas on this are so speculative that we do not care to present them at this time.

The foregoing results indicate that there is considerable mutual polarization when chloroform forms hydrogen bonds with various bases and that any attempt to deduce the geometry of a complex from a measurement of the dipole moment must wait until a satisfactory way is found to correct for this polarization.

Acknowledgment. It is a pleasure to acknowledge the support of this work by the Research Corporation.

Alicyclic Ketyls. III. Conformational Mobility of Cyclononane Ketyl Examined by Electron Paramagnetic Resonance

by J. W. Lown

Department of Chemistry, University of Alberta, Edmonton, Alberta, Canada (Received September 10, 1965)

Very few studies have been reported of the conformation of nine-membered ring compounds in general¹⁻⁴

and cyclononane in particular.² It had been concluded from an examination of the scissoring mode $\delta(\text{CH}_2)$ in the infrared and by studies of the association between cyclononane and phenols that the ketone existed largely in one conformation possessing C_s symmetry in solution. On the other hand, deviations from the anticipated linear relationship between ultraviolet absorption maxima for $n \rightarrow \pi^*$ transitions and solvent Z values indicated appreciable conformational freedom in cyclononane at room temperature in various solvents.⁵ The possibility arose of applying electron paramagnetic resonance (epr) spectroscopy to study the conformation of the corresponding ketyl in solution.

We have recently demonstrated⁶ how an examination of the epr spectra of ketyls generated from alicyclic ketones by the action of alkali metals in 1,2-dimethoxyethane can give valuable information concerning the type and symmetry of the conformation adopted in solution by these radical anions. Hyperfine coupling from only the α protons is observed and the predicted⁷ dihedral angular dependence of this hyperfine coupling was confirmed and could be used to deduce the dihedral angles with the $C_1-2p\pi$ orbital.

Treatment of cyclononane in 1,2-dimethoxyethane with potassium metal at room temperature afforded a yellow solution which gave the epr spectrum shown in Figure 1A, consisting of seven equally spaced lines (1:2:3:4:3:2:1), $a_H = 2.46$ oersteds. The hyperfine splitting may be interpreted in terms of coupling of 4.92 oersteds to two equivalent protons at the C_2 and C_9 positions and of 2.46 oersteds to a second pair of equivalent protons. The epr spectrum was unchanged in appearance on cooling the solution down to -39° , but raising the temperature moderately to 58° (Figure 1B) resulted in five equally spaced lines (1:4:6:4:1), $a_H = 3.68$ oersteds, clearly arising from coupling of the unpaired electron with four equivalent protons at the C_2 and C_9 positions. The change in the appearance of the spectrum with temperature was completely reversible. The spectrum was unchanged in appearance on raising the temperature to 89° . Since the coupling constant at 58° is equal

(1) G. Chiurdoghu, T. Doehard, and B. Tursch, *Chem. Ind.* (London), 1453 (1959).

(2) G. Chiurdoghu, T. Doehard, and B. Tursch, *Bull. Soc. Chim. France*, 1322 (1960).

(3) J. D. Dunitz and V. Prelog, *Angew. Chem.*, 72, 896 (1960).

(4) R. F. Bryan and J. D. Dunitz, *Helv. Chim. Acta*, 43, 1 (1960).

(5) E. M. Kosower and G. S. Wu, *J. Am. Chem. Soc.*, 83, 3142 (1961).

(6) J. W. Lown, *Can. J. Chem.*, in press.

(7) C. Heller and H. M. McConnell, *J. Chem. Phys.*, 32, 1535 (1960).

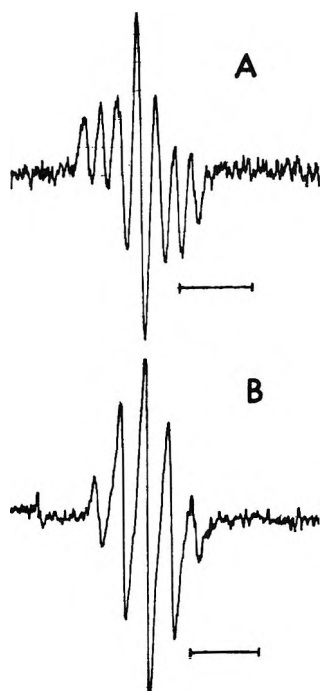


Figure 1. First-derivative epr spectra in 1,2-dimethoxyethane of cyclononanone ketyl: A, at 25°; B, at 60°. The bar in each case represents 10 oersteds.

to the average of the two coupling constants observed at 25° we interpret the change in the epr spectrum with increasing temperature to a conformational averaging of two forms which possess a plane of symmetry through the C-O bond axis. At room temperature, therefore, the ketyl is equilibrating between the two conformers at a rate slow with respect to that corresponding to the frequency difference of the two couplings (of the order of $3 \times 10^7 \text{ sec}^{-1}$).

In the case of medium-sized cyclic ketones (8 to 11 carbon atoms) it had been proposed⁸ that the "O-inside" conformations are stabilized by transannular hydrogen bonding (this would also apply to the corresponding ketyls).

However, such interactions have been shown to be unimportant,⁹ leading to only small energy changes and we may therefore restrict ourselves to the consideration of "open" conformations.

The most elaborate calculations of the conformation of cyclononane yet reported¹⁰ predict that the hydrocarbon has two conformations, very close in energy, which are much more stable than other possibilities. The most stable form has D_3 symmetry, with identical axes of symmetry passing through the equivalent C_1 , C_4 , and C_7 positions. The most

comfortable position for the carbonyl group in cyclononanone would be in any of these equivalent positions. The corresponding ketyl would have two pairs of equivalent protons at the C_2 and C_9 positions which is consistent with our experimental observations.

Possible values for the dihedral angles and ketyl carbon spin density may be calculated by a literature method.¹¹ $\theta_{ax} = -54$ or -13° , $\theta_{eq} = (\theta_{ax} + 120^\circ) = 66$ or 107° , spin density $\rho = 0.25$ or 0.09 , respectively, where θ_{ax} and θ_{eq} are the dihedral angles subtended by α protons in positions analogous to axial and equatorial positions, respectively.

Experimental Section

First-derivative epr spectra were measured on a Varian V-2503 spectrometer fitted with a V-4532 dual cavity, operating at a nominal frequency of 9.5 cps. Hyperfine couplings were measured by comparison with a peroxyamine disulfonate solution ($a_N = 13.0$ oersteds). As was observed previously⁶ coupling due to the attendant potassium cation could not be resolved under these conditions.

Freshly cut potassium was added to a degassed 5% solution of cyclononanone (pure commercial sample) in 1,2-dimethoxyethane, cooled, and transferred to an epr sample tube. The temperature in the cavity was controlled by passing cold, dry nitrogen gas through the temperature-variable unit. The temperature of the sample was measured with a copper-constantan thermocouple.^{12,13}

(8) V. Prelog, *J. Chem. Soc.*, 420 (1950).

(9) N. L. Allinger, *J. Am. Chem. Soc.*, **81**, 5727 (1959).

(10) J. B. Hendrickson, *ibid.*, **86**, 4854 (1964).

(11) G. A. Russell and E. T. Strom, *ibid.*, **86**, 744 (1964).

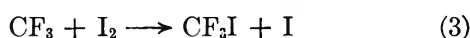
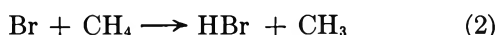
(12) This research was supported by a grant-in-aid of research of the National Research Council of Canada.

(13) NOTE ADDED IN PROOF. E. R. Talaty and G. A. Russell (*J. Am. Chem. Soc.*, **87**, 4867 (1965)) have recently suggested that the reaction of potassium with alicyclic ketones in 1,2-dimethoxyethane actually gives the semidione under conditions of incomplete deoxygenation and not the ketyl as is claimed here. Although precautions were taken to exclude oxygen from the system, it was found that deliberate addition of air enhances the epr signals obtained. Therefore this objection is valid. Since comparable spin densities and hfsc are to be anticipated for ketyl and corresponding semidione, any attempt at distinction must depend on the symmetry of the species. The proof offered by the author of the ketyl structure (*Can. J. Chem.*, in press) by deuteration of cyclohexanone is rendered suspect by the observation that deuterium exchange occurs α to the oxygens in cyclohexane semidione, at least in deuterated dimethyl sulfoxide (G. A. Russell, personal communication). 3,5-Dimethylcyclohexanone, a suitable model, has not yet provided a spectrum well enough resolved to provide an answer. If subsequent work proves that the ketyl is rapidly oxidized to the semidione, it would follow that the temperature studies and symmetry arguments on the radical anions reported in part II actually apply to the semidiones. This method of generation does, however, have the advantage that the radical anions are stable over a remarkably large temperature range.

COMMUNICATIONS TO THE EDITOR

The C-H Bond Dissociation Energy in Fluoroform

Sir: Current estimates of the bond dissociation energy $D(\text{CF}_3\text{-H})$ do not agree. Whittle and co-workers^{1,2} studied reactions 1, -1, 2, and 3 using competitive methods.



They obtained an activation energy difference of $E_1 - E_2 = 3.76 \pm 0.14$ kcal mole⁻¹ using $\text{C}_2\text{F}_5\text{H}$ to bridge the gap between CF_3H and CH_4 which differ too greatly in reactivity to compete directly for bromine atoms. They also obtained $E_{-1} - E_3 = 2.98 \pm 0.12$ kcal mole⁻¹ which equals E_{-1} if we assume that $E_3 = 0$. These results lead to

$$D(\text{CF}_3\text{-H}) - D(\text{CH}_3\text{-H}) = 2.2 \pm 0.5 \text{ kcal mole}^{-1} \text{ at } 298^\circ\text{K}$$

Trotman-Dickenson and co-workers³ have recommended that $D(\text{CH}_3\text{-H}) = 103.8$ kcal mole⁻¹. This is a weighted mean of determinations which include $D(\text{CH}_3\text{-H}) = 103.9$ kcal mole⁻¹ from bromination studies. However, the latter value should be corrected⁴ to 102.9 kcal mole⁻¹. Also, since Trotman-Dickenson's recommendation, Benson and co-workers⁵ have obtained $D(\text{CH}_3\text{-H}) = 104.1$ kcal mole⁻¹ from a study of the equilibrium $\text{I}_2 + \text{CH}_4 \rightleftharpoons \text{HI} + \text{CH}_3\text{I}$. Their equilibrium data are confirmed by Goy and Pritchard.⁶ The combined result of these two amendments (giving the iodination work slightly more weight) endorses Trotman-Dickenson's recommendation of $D(\text{CH}_3\text{-H}) = 103.8$ kcal mole⁻¹ at 298°K; this is probably accurate to ± 0.5 kcal mole⁻¹. If this value is combined with the difference $D(\text{CF}_3\text{-H}) - D(\text{CH}_3\text{-H})$ given above, we obtain

$$D(\text{CF}_3\text{-H}) = 106.0 \pm 0.7 \text{ kcal mole}^{-1} \text{ at } 298^\circ\text{K}$$

However, reaction 4



was studied by Pritchard, *et al.*,⁷ and more recently by Pritchard and Thommarson.⁸ Their value of E_4 together with independent data on E_{-4} leads to $D(\text{CF}_3\text{-H}) - D(\text{CH}_3\text{-H}) = -0.6 \pm 1.9$ kcal mole⁻¹ so that $D(\text{CF}_3\text{-H}) = 103.2$ kcal mole⁻¹. Since this dis-

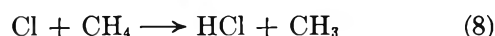
agrees with our value, we have checked our results as follows.

First, the difference $E_1 - E_2$ was redetermined using another bridge compound, $n\text{-C}_3\text{F}_7\text{H}$, the result being $E_1 - E_2 = 3.71 \pm 0.11$ kcal mole⁻¹. Secondly, an absolute value of E_{-1} has been measured by studying the reactions



By photolyzing hexafluoroacetone, HFA, with HCl in the vapor phase, it was found that $E_5 - \frac{1}{2}E_6 = 5.1 \pm 0.1$ kcal mole⁻¹ so that, if $E_6 = 0$,⁹ E_5 is known. Next, HFA was photolyzed with a mixture of HCl + Br₂ from which $E_5 - E_7 = 4.43 \pm 0.08$ kcal mole⁻¹. Tucker and Whittle² found that $E_{-1} - E_7 = 2.17 \pm 0.16$ kcal mole⁻¹, so that combining all these results, we have $E_{-1} = 2.84 \pm 0.30$ kcal mole⁻¹. The new determinations of $E_1 - E_2$ and E_{-1} agree well with our previous ones and the need to assume that $E_3 = 0$ has been eliminated.

A further determination of $D(\text{CF}_3\text{-H})$ has been made by studying the reactions



From a study of the competitive chlorination of mixtures of $\text{CF}_3\text{H} + \text{C}_2\text{F}_5\text{H}$ and $\text{CH}_4 + \text{C}_2\text{F}_5\text{H}$, we find that $E_{-5} - E_8 = 4.53 \pm 0.08$ kcal mole⁻¹. Knox¹⁰ gives $E_8 = 3.85$ kcal mole⁻¹ so that $E_{-5} = 8.4$ kcal mole⁻¹. Thus $\Delta H_{-5} = E_{-5} - E_5 = 3.3$ kcal mole⁻¹ at an average temperature of 360°K. At this temperature, $D(\text{H-Cl}) = 103.3$ kcal mole⁻¹ and, since

(1) A. M. Tarr, J. W. Coomber, and E. Whittle, *Trans. Faraday Soc.*, **61**, 1182 (1965).

(2) B. G. Tucker and E. Whittle, *ibid.*, **61**, 866 (1965).

(3) J. Grzechowiak, J. A. Kerr, and A. F. Trotman-Dickenson, *Chem. Commun.*, 109 (1965).

(4) P. Corbett, A. M. Tarr, and E. Whittle, *Trans. Faraday Soc.*, **59**, 1609 (1963).

(5) D. M. Golden, R. Walsh, and S. W. Benson, *J. Am. Chem. Soc.*, **87**, 4053 (1965).

(6) C. A. Goy and H. O. Pritchard, *J. Phys. Chem.*, **69**, 3040 (1965).

(7) G. O. Pritchard, H. O. Pritchard, H. I. Schiff, and A. F. Trotman-Dickenson, *Trans. Faraday Soc.*, **52**, 849 (1956).

(8) G. O. Pritchard and R. L. Thommarson, *J. Phys. Chem.*, **68**, 568 (1964).

(9) R. D. Giles and E. Whittle, *Trans. Faraday Soc.*, **61**, 1425 (1965).

(10) J. H. Knox, *ibid.*, **58**, 275 (1962).

$\Delta H_{-5} = D(\text{CF}_3\text{-H}) - D(\text{H-Cl})$, we have $D(\text{CF}_3\text{-H}) = 106.3$ kcal mole⁻¹ after correction to 298°K.

This agrees well with $D(\text{CF}_3\text{-H}) = 106.0$ kcal mole⁻¹ from our bromination work and we believe that the average value of $D(\text{CF}_3\text{-H}) = 106.2$ kcal mole⁻¹ is accurate to ± 0.5 kcal mole⁻¹.

CHEMISTRY DEPARTMENT
UNIVERSITY COLLEGE
CATHAYS PARK
CARDIFF, GREAT BRITAIN

J. C. AMPHLETT
J. W. COOMBER
E. WHITTLE

RECEIVED OCTOBER 29, 1965

Infrared Studies of Carbon Monoxide Chemisorbed on Metallic Surfaces

Sir: Relatively recent papers by Garland, Lord, and Troiano¹ presented a new method of forming metal films evaporated in carbon monoxide onto the windows of the infrared cell. They report a new band at 1620 cm⁻¹ which was not reported previously for supported nickel surfaces and was not reported by Pickering and Eckstrom² for bulk evaporated nickel films. Our work on infrared studies of carbon monoxide chemisorbed on nickel and on rhodium evaporated films using the multiple-reflection technique² reveals the possibility of a very weak band at approximately 1620 cm⁻¹ for carbon monoxide on nickel and several very weak absorption bands in the region from 1350 to 750 cm⁻¹; many of these bands are coincident for both nickel and rhodium. The experimental method used by Pickering and Eckstrom makes the unequivocal assignment of absorption bands in the water region difficult³ and, in addition, the band at 1620 cm⁻¹ is very weak, appearing as a shoulder on a water line; in the region from 1350 to 750 cm⁻¹ several bands may be assigned, and even though they are very weak they are nevertheless "real."

The assignment of many bands to carbon monoxide chemisorbed on nickel and on rhodium confirms the complicated nature of "surface complexes" and complicates the theoretical interpretation. The number of assignments for hydrogen chemisorbed on evaporated rhodium films² was large and our later studies have indicated there are more bands. Also, our studies of deuterium chemisorbed on rhodium films are showing approximately as many bands as for hydrogen.

The "strongest" of the bands we have observed in this region for carbon monoxide are as follows: on nickel (cm⁻¹): 1195, 1069, 1056, 1036, 1028, 1017, 1011, 1004, 999, 981, 964, 948, 933, 927, 920, 906, 896, 891, 883, 875, 864, 856, 775; on rhodium (cm⁻¹):

1070, 1030, 1025, 1008, 988, 969, 958, 933, 923, 912, 900, 891, 882, 877, 871, 867, 861. It should also be noted that evidence of the 2060-cm⁻¹ band observed and reported early² was found in the studies of the nickel films reported above, and the background data in this region were also free of structure. Further studies of carbon monoxide on evaporated metal films are in progress.

Acknowledgment. The infrared studies of chemisorbed molecules at the University of Kentucky are supported in part by the United States Atomic Energy Commission Contract No. AT-(40-1)-2948.

(1) C. W. Garland, R. C. Lord, and P. F. Troiano, *J. Phys. Chem.*, **69**, 1188, 1195 (1965). Also, for the purposes of this Communication these papers should be referred to for literature references and review of studies in this field.

(2) H. L. Pickering and H. C. Eckstrom, *ibid.*, **63**, 512 (1959).

(3) Water spectra appears in their calculations because of very small changes in water vapor content in the "comparison cell" after the taking of the "background data," upon which all calculations are based. It should be emphasized that no water vapor is present in the cell used for the chemisorption studies and any contamination is very unlikely because of outgassing procedures and vacuums maintained during film preparation.

DEPARTMENT OF CHEMISTRY
UNIVERSITY OF KENTUCKY
LEXINGTON, KENTUCKY

HARTLEY C. ECKSTROM

RECEIVED NOVEMBER 5, 1965

The Change of the Rate-Determining Step of the Ammonia Decomposition over an Ammonia Synthetic Iron Catalyst

Sir: Two mechanisms have been proposed on the ammonia decomposition over the doubly promoted iron catalysts. Thus, on the one hand, Temkin and Pyzhev¹ proposed the rate equation on the basis of the desorption of adsorbed nitrogen as the rate-determining step which could explain many of the experimental results.² On the other hand, the dehydrogenation of NH₃(a), NH₂(a), or NH(a) was proposed as the rate-determining step.³ Here the (a)'s signify the adsorbed state. This disagreement has frequently been considered as due to differences in the catalysts used.

(1) M. I. Temkin and V. Pyzhev, *Acta Physicochim. U.R.S.S.*, **12**, 327 (1940).

(2) W. G. Frankenburg, "Catalysis," Vol. III, P. H. Emmett, Ed., Reinhold Publishing Corp., New York, N. Y., 1955, p 171; C. Bokhoven, C. van Heerden, R. Westrik, and P. Zwietering, *ibid.*, p 265; A. Nielsen, *Advan. Catalysis*, **5**, 1 (1953).

(3) S. Enomoto and J. Horiuti, *Proc. Japan Acad.*, **28**, 493, 499 (1952); *J. Res. Inst. Catalysis, Hokkaido Univ.*, **2**, 87 (1952); J. Horiuti and I. Toyoshima, *ibid.*, **5**, 120 (1957); **6**, 68 (1958); J. Horiuti and N. Takezawa, *ibid.*, **8**, 170 (1961).

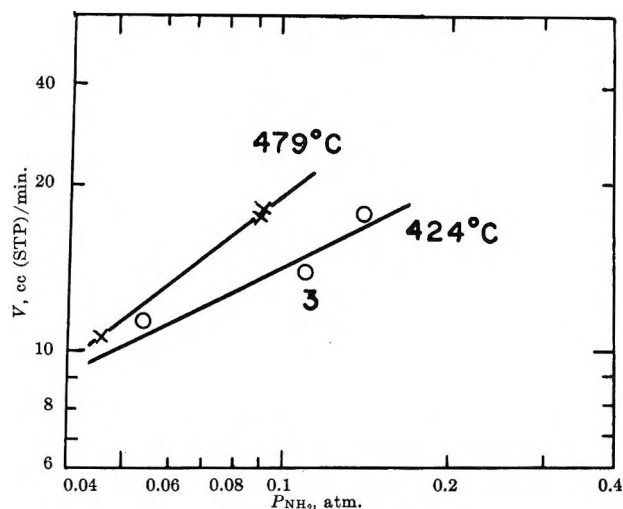


Figure 1. Rate of ammonia decomposition vs. partial pressure of ammonia: 424° (10 g of catalyst); total flow, 890 cc (STP)/min; hydrogen flow, 398 cc (STP)/min; 479° (2 g of catalyst); total flow, 1090 cc (STP)/min; hydrogen flow, 668 cc (STP)/min; helium as diluent. Number in the figure indicates the number of the experimental points observed in different runs.

In this Communication, it is suggested from recent studies on the dependence of the rate of ammonia decomposition on the ammonia, hydrogen, and nitrogen pressures that the mechanism depends on the experimental conditions even on a given catalyst.

The decomposition of ammonia over an ammonia synthetic catalyst (4.72% alumina, 0.31% potassium oxide, 0.05% silica) was performed in a flow system at 1 atm by a differential reactor. The catalyst was reduced at 600° for 50 hr in a stream of well-purified hydrogen at a flow rate of 500 cc (STP)/min. A mixture of purified hydrogen, ammonia, and helium or nitrogen was led over the catalyst. The undecomposed ammonia was determined by absorbing it in a sulfuric acid solution. Helium was used as diluent. The rate of decomposition was estimated from the difference between the inflow and outflow rates of ammonia. In order to determine the dependence of the decomposition rate on the ammonia pressure, the temperature of the catalyst, the hydrogen inflow, and the total inflow rate were held constant and the ammonia inflow was varied. The dependence of the rate on the hydrogen or nitrogen pressures was obtained in a similar manner. These results are plotted in Figures 1 and 2. From these figures, the reaction order with respect to the ammonia or hydrogen pressure could be obtained as long as the per cent decomposition of ammonia was small. A slight inhibitive effect of nitrogen on the rate was observed above 479° with a reaction order of

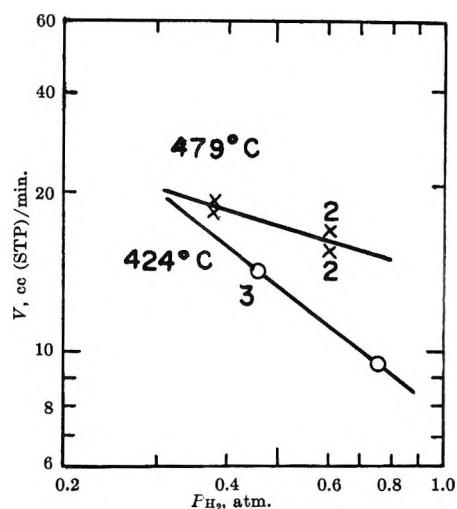


Figure 2. Rate of ammonia decomposition vs. partial pressure of hydrogen: 424° (10 g of catalyst); total flow, 890 cc (STP)/min; ammonia flow, 99.2 cc (STP)/min; 479° (2 g of catalyst); total flow, 1090 cc (STP)/min; ammonia flow, 99 cc (STP)/min; helium as diluent. Numbers in the figure indicate the number of the experimental points observed in different runs.

less than 0.1. This was not observed below 479°. From those results, the rate can be expressed approximately as

$$V = k_1(P_{\text{NH}_3}/P_{\text{H}_2}^{1.5})^{0.48} \text{ (at } 420^\circ\text{);}$$

$$V = k_2(P_{\text{NH}_3}/P_{\text{H}_2}^{0.5})^{0.76} \text{ (at } 479^\circ\text{)}$$

where P_{NH_3} etc. represent ammonia pressure etc., and k_1 and k_2 are the rate constants. The rate expression at lower temperatures is clearly explained by the theory proposed by Temkin and Pyzhev, while the different expression valid at higher temperatures suggests that the rate-determining step is then the dehydrogenation of adsorbed amino radical $\text{NH}_2(\text{a})$.

These results and the kinetic expressions indicate that the rate-determining step of ammonia decomposition changes from the desorption of adsorbed nitrogen to the dehydrogenation of the adsorbed amino radical $\text{NH}_2(\text{a})$ with the reaction temperature. Details will be published elsewhere.

Acknowledgment. The authors are grateful to Professor Emeritus J. Horiuti for his encouragement in this work and also the Ministry of Education for the grant for the scientific research.

RESEARCH INSTITUTE FOR CATALYSIS
HOKKAIDO UNIVERSITY
SAPPORO, JAPAN

N. TAKEZAWA
I. TOYOSHIMA

RECEIVED NOVEMBER 8, 1965

On the Validity of Raoult's and Henry's Laws as Limiting Laws for Dilute Solutions

Sir: There has recently been some discussion¹⁻⁴ in this journal of the validity of Raoult's law as a limiting law for a dilute solution. Elliot, Lemons, and Swofford¹ presented very precise data on dilute solutions of gallium in cadmium which could not be fitted to Raoult's law as the gallium concentration went to zero.

This result has been criticized on thermodynamic grounds,^{2,4} but in view of the apparent excellence of the data, it does not seem to be a very satisfactory course merely to reject the measurements. The difficulty arises because Elliot, *et al.*, attempted to explain their results while retaining Henry's law. However, as Gokcen⁴ has discussed, Henry's law is incompatible with the observation that Raoult's law is not obeyed by virtue of the Gibbs-Duhem equation.

It appears to the present author that in the discussion to date the essential point has been missed. Raoult's law has no basis in thermodynamics apart from derivation from Henry's law and the Gibbs-Duhem equation.⁵ Thus if we are to accept the validity of the Gibbs-Duhem equation (and the alternative is tantamount to rejecting thermodynamics) we must inquire into the general validity of Henry's law.

Henry's law may readily be derived for an infinitely dilute solution; however, for a solution in a conductor in which some sort of electron transfer may occur, there is a sense in which it is impossible to have a dilute solution. Consider, for example, solution of B in conductor A in which there is charge transfer (*e.g.*, $B \rightarrow B^+ + e^-$). Successive electrons will have to go into different energy states which are collective states of the system as a whole. The chemical potential of the electrons is simply the Fermi energy, E_F .⁶ On dissolving B in A, there is a change in the chemical potential of the electrons which we may write as

$$\mu_e = \mu_e^0 + \Delta\mu_e = E_F^0 + \Delta E_F \quad (1)$$

where the superscript zero refers to pure A.

Retaining, on the other hand, the conventional form of the chemical potential for B^+ in a dilute solution

$$\mu_{B^+} = \mu_{B^+}^0 + RT \ln N_B \quad (2)$$

we obtain for equilibrium in the process of B dissolving to give a dilute solution of B^+ together with electrons

$$N_B \exp(\Delta E_F/RT) = \exp(-\Delta\mu^0/RT)a_B \quad (3)$$

In the case of metals, Friedel⁷ has shown that to a good approximation, the Fermi energy is unchanged in

going from the pure metal to a dilute alloy so that (3) reduces to Henry's law. It is not clear, however, that this is rigorously correct.⁸

In the case that A is a poor conductor with no electron states at the Fermi level (*i.e.*, a semiconductor with a band gap), the electrons from B must go to a higher energy level (the conduction band). In the limit of a large band gap, the electrons obey Boltzmann statistics and one obtains the well-known result⁶

$$\exp(\Delta E_F/RT) = \text{constant} \times N_B \quad (4)$$

Equation 3 is now the corresponding form of Henry's law for dissolution with dissociation.

A more interesting situation arises when the solvent A already has available electron states with energy not much greater than the Fermi energy (as in a semiconductor with a small band gap or at high temperature). In this intermediate case it seems logical to suppose that the value of $\partial \ln a_B / \partial \ln N_B$ will be intermediate between the two extremes (*i.e.*, between 1 and 2) and we conclude then that in this situation Henry's law and hence Raoult's law is not obeyed. Departures from these limiting laws are most likely to be encountered in metal systems with a low density of states at the Fermi energy. It is possibly significant that Elliot, *et al.*, obtained anomalous results with cadmium which has indeed a low density of states.

Finally, it is of interest to return to eq 3. One can consider any composition of alloy to be the solvent and suppose the solute to be the extra added material.⁹ In a metal the density of states may fluctuate rapidly with composition (or indeed even have singularities¹⁰) so that it is quite possible that ΔE_F is not a smooth function of composition. If this is the case it is in turn possible that the concentration of B will not be a smooth function of the activity of B. It is interesting in this connection that Elliot and Lemons¹¹ observed

(1) G. R. B. Elliot, J. F. Lemons, and H. S. Swofford, *J. Phys. Chem.*, **69**, 933 (1965).

(2) S. D. Christian and N. Fogel, *ibid.*, **69**, 2135 (1965).

(3) G. R. B. Elliot and J. F. Lemons, *ibid.*, **69**, 2135 (1965).

(4) N. A. Gokcen, *ibid.*, **69**, 3222 (1965).

(5) See, for example, K. S. Pitzer and L. Brewer, "Thermodynamics," G. N. Lewis and M. Randall, Ed., rev ed, McGraw-Hill Book Co., Inc., New York, N. Y., 1961, p 231, and A. H. Wilson "Thermodynamics and Statistical Mechanics," Cambridge University Press, New York, N. Y., 1957, p 399.

(6) N. B. Hannay, "Semiconductors," Reinhold Publishing Corp., New York, N. Y., 1959, Chapter 1.

(7) J. Friedel, *Advan. Phys.*, **3**, 446 (1954).

(8) Friedel (ref 7) suggests that for dilute alloys $\Delta E_F \sim N_B^{5/3}$.

(9) See K. S. Pitzer and L. Brewer, ref 5, p 232.

(10) J. C. Phillips, *Phys. Rev.*, **104**, 1263 (1956).

(11) G. R. B. Elliot and J. F. Lemons in "Nonstoichiometric Compounds," Advances in Chemistry Series, No. 39, American Chemical Society, Washington, D. C., 1963, p 153.

just this type of behavior in the Ce-Cd system (although it should be remarked that their interpretation of their results is quite different).

DEPARTMENT OF CHEMISTRY
ARIZONA STATE UNIVERSITY
TEMPE, ARIZONA

M. O'KEEFE

RECEIVED NOVEMBER 23, 1965

The States of Nitrogen Adsorbed on an Ammonia Synthetic Iron Catalyst and the Reactivity

Sir: For understanding heterogeneous catalysis, the information of the activity of chemical species in various adsorbed states is valuable since such an adsorbed species is expected to take part in the reaction as an intermediate.

Recently, Emmett and the present author¹ found that the state of the chemisorbed nitrogen on an ammonia synthetic catalyst changes with the temperature at which chemisorption took place. It is widely accepted that the ammonia synthesis on this catalyst proceeds through the steps of the nitrogen chemisorption and hydrogenation of the chemisorbed nitrogen.^{2,3} If the nitrogen chemisorbed in different states is brought in contact with hydrogen, the rate of ammonia formation by the latter step is expected to be different at a given experimental condition.

An iron synthetic ammonia catalyst (2.6 g, 2.03% alumina, 0.81% potassium oxide, 0.16% silica as promoters) was reduced in a stream of hydrogen at a flow rate of 500 cc (STP)/min at 450 and 600° for 45 and 40 hr, respectively. Between the runs, the catalyst was reduced at 450 and 600° for 2 and 16 hr, respectively. At the end of the reduction, the catalyst was evacuated at 600° for 3 hr to 2×10^{-6} mm. Purified nitrogen was adsorbed at temperatures ranging from 208 to 445° and at pressures of 20 to 120 mm. After the nitrogen adsorption, the temperature of the catalyst was decreased to a reaction temperature and nitrogen in the gaseous phase was removed by a Toepler pump. The amount of nitrogen adsorbed during the process of decreasing the temperature was less than 0.15 cc (STP). Thereafter, purified hydrogen at a flow rate of 450 cc (STP)/min was passed over the catalyst on which nitrogen had been chemisorbed. The amount of ammonia thus formed was successively followed by absorption in a sulfuric acid solution. The rate of ammonia formation gradually decreases with time due to a decrease in the amount of adsorbed

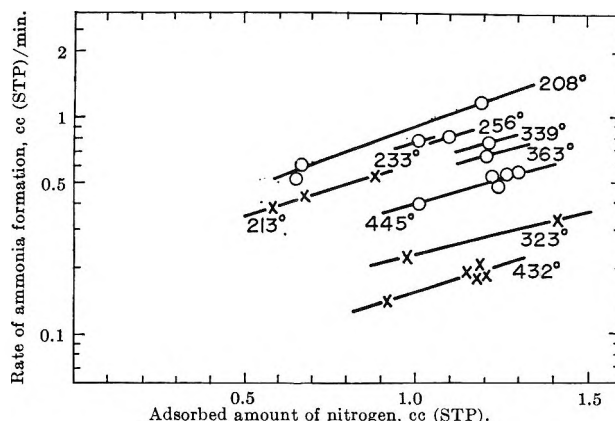


Figure 1. Plots of the rate of ammonia formation vs. the amount of nitrogen adsorbed: reaction temperature, 162° (×) and 208° (○); adsorption temperature is shown in the figure.

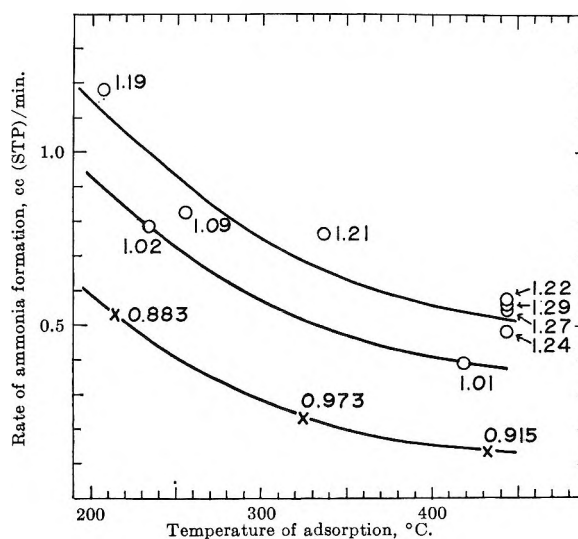


Figure 2. Plots of the rate of ammonia formation at a given amount of nitrogen adsorbed vs. temperature of adsorption: reaction temperature, 162° (×) and 208° (○). Numbers designate the amount of nitrogen adsorbed.

nitrogen. The initial rates at several temperatures for the nitrogen adsorbed at different temperatures are shown in Figure 1 as a function of the amount of adsorbed nitrogen. The plots of the rate at the given temperatures and given amount of nitrogen adsorbed against the temperature of nitrogen adsorption are shown in Figure 2. As seen from Figure 2, it is clear that the nitrogen adsorbed at lower temperature has

(1) P. H. Emmett and N. Takezawa, to be published.

(2) W. G. Frankenburg, "Catalysis," Vol. III, P. H. Emmett, Ed., Reinhold Publishing Corp., New York, N. Y., 1955, p 171.

(3) C. Bokhoven, C. van Heerden, R. Westrik, and P. Zwietering, ref 2, p 265.

higher activity for ammonia formation than that at higher temperature. This suggests that the state of adsorbed nitrogen is varied by the temperature at which the adsorption was made.

Acknowledgment. The author wishes to express his sincere thanks to Professor P. H. Emmett of Johns Hopkins University and Dr. I. Toyoshima of Hokkaido University for their profound interest and valuable discussions on the present work.

RESEARCH INSTITUTE FOR CATALYSIS NOBUTSUNE TAKEZAWA
HOKKAIDO UNIVERSITY
SAPPORO, JAPAN

RECEIVED NOVEMBER 23, 1965

Charge-Transfer Spectra in Nonpolar Solvents

Sir: The problem of the effects of solvent interactions on charge transfer (ct) spectra is an extremely complex one and various aspects of it have been studied in the past.¹ From these it appears that existing theories which are based on the Onsager model² of the solute point dipole embedded in the dielectric continuum of the solvent do not account for the observed facts. Even for pure compounds the electronic spectra were found to deviate from the predicted linear relation between solvent refractive index function and band shift in the region of low refractive index.³

One reason for the confused situation of the effects of solvent on ct spectra has been the total lack of gas phase ct data. Recently, a few such measurements were published.^{4,5} They allow us now to test existing solvent theories as to their applicability to ct spectra.

We wish to report here preliminary results of a comprehensive study on solvent interactions in ct complexes which will be published in full somewhat later.⁶ We have measured the ct energies of complexes of five nonpolar aromatic donors with tetracyanoethylene (TCNE) as acceptor in a set of six selected nonpolar solvents (three perfluoro and three hydrocarbon solvents with a refractive index range between 1.26 and 1.47 and which are not expected to show specific interactions). The results are shown in Table I. The data were plotted in terms of a refractive index function, $(n^2 - 1)/(2n^2 + 1)$, as derived in McRae's solvent perturbation theory.⁷ Examples of such plots are shown in Figure 1 for two of the complexes measured.

The measurements were made on a Cary-14 recording spectrophotometer. Matched, stoppered absorption cells of varying path lengths were used to obtain spectra

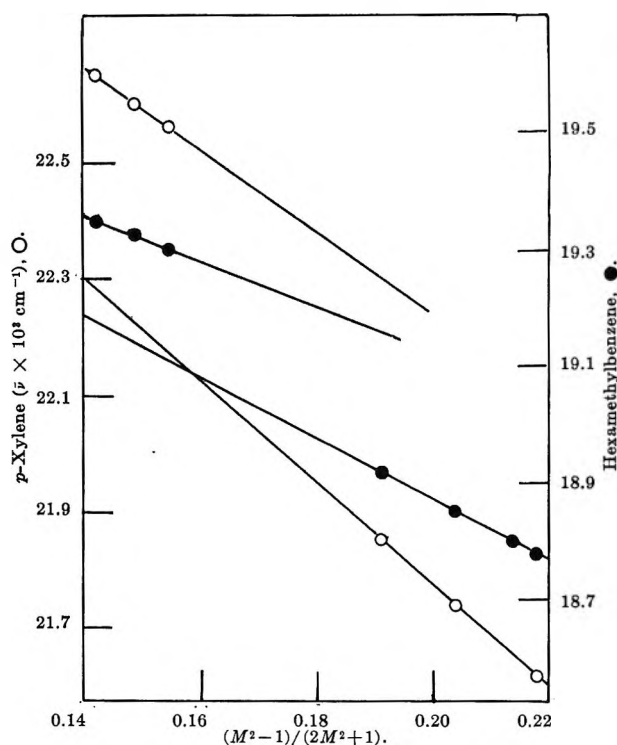


Figure 1. Charge-transfer energies of tetracyanoethylene (TCNE) complexes with aromatic donors vs. refractive index function of the nonpolar solvents.

of optical densities between 0.5 and 0.9 (and relative donor-acceptor concentrations from approximately 50:1 to 100:1). The cells were thermostated at 22°. The solvents and materials used were spectrograde where available; where not, they were purified appropriately. Details of this and further experimental information will be given in the forthcoming paper.⁶

The results are striking. For each ct complex the data could best be analyzed in terms of two straight solvent lines of different slope: one of greater slope deriving from the saturated hydrocarbons and one of lower slope from the perfluoro solvents (Figure 1). These pairs of lines extrapolate in each case to the same intercept with the ordinate, $(n^2 - 1)/(2n^2 + 1) = 0$

(1) (a) G. Briegleb, "Elektronen Donator Acceptor Komplexe," Springer-Verlag, Berlin, 1961, p 38; (b) C. C. Thompson, Jr., and P. A. D. deMaine, *J. Am. Chem. Soc.*, **85**, 3096 (1963); (c) K. M. C. Davis and M. C. R. Symons, *J. Chem. Soc.*, 2079 (1965); (d) H. M. Rosenberg and D. Hale, *J. Phys. Chem.*, **69**, 2490 (1965).

(2) L. Onsager, *J. Am. Chem. Soc.*, **58**, 1486 (1936).

(3) E. A. Bovey and S. S. Yanari, *Nature*, **186**, 1042 (1960).

(4) (a) F. T. Lang and R. L. Strong, *J. Am. Chem. Soc.*, **87**, 2345 (1965); (b) J. M. Goodenow and M. Tamres, *J. Chem. Phys.*, **43**, 3393 (1965); (c) J. Prochorow, *ibid.*, **43**, 3394 (1965).

(5) M. Kroll and M. L. Ginter, *J. Phys. Chem.*, **69**, 3672 (1965).

(6) C. Reid and E. M. Voigt, to be published.

(7) E. G. McRae, *J. Phys. Chem.*, **61**, 562 (1957).

Table I

Solvent ^a	n^{20D}	Benzene		<i>p</i> -Xylene		Mesitylene		Durene	Hexamethylbenzene	
		$\bar{\nu}_{\max}$	$\Delta\bar{\nu}_{1/2}$	$\bar{\nu}_{\max}(I)$	$\bar{\nu}_{1/2}(I)$	$\bar{\nu}_{\max}$	$\Delta\bar{\nu}_{1/2}$	$\bar{\nu}_{1/2}(I)$	$\bar{\nu}_{\max}$	$\Delta\bar{\nu}_{1/2}$
<i>n</i> -Perfluoroheptane	1.26	27.35	5.3	22.65	20.45	22.80	5.3	18.17	19.35	5.2
Perfluoroether (C ₈ H ₁₆ O)	1.278	27.29	5.3	22.60	20.41	22.75	5.3	18.13	19.33	5.2
Perfluorobutylamine (C ₄ F ₉) ₃ N	1.291	27.25	5.3	22.57	20.37	22.73	5.3	18.10	19.30	5.2
<i>n</i> -Heptane	1.388	26.32	5.3	21.86	19.66	22.05	5.3	16.63	18.92	5.2
<i>c</i> -Hexane	1.426	26.18	5.3	21.74	19.53	21.94	5.3	16.53	18.85	5.2
<i>c</i> -Octane	1.457	26.04	5.3	18.80	5.2
<i>trans</i> -Decalin	1.467	21.62	19.42	21.83	5.3	16.43	18.78	5.2
Slope $\begin{cases} \text{C-H} \\ \text{C-F} \end{cases}$		1.11	...	0.87	0.86	0.80	...	0.74	0.52	...
	Ratio of slopes	0.76	...	0.64	0.64	0.58	...	0.57	0.40	...
Gas phase Ct transition $\begin{cases} \text{CH} \\ \text{CF} \\ \text{expt}^b \end{cases}$		1.46	...	1.40	...	1.38	...	1.30	1.33	...
		28.44	...	23.51	21.30	23.60	...	18.04	19.92	...
		28.42	...	23.53	21.31	23.62	...	17.98	19.91	...
$\Delta\bar{\nu}$ (gas \rightarrow <i>n</i> -heptane)		23.50	21.3
		2.12	...	1.65	1.65	1.55	...	1.41	0.99	...

^a n^{20D} is the refractive index for sodium D-line at 20°; $\bar{\nu}_{\max}$ is the frequency at maximum intensity; $\bar{\nu}_{1/2}$ is the frequency at half maximum intensity on low energy side of band; $\Delta\bar{\nu}_{1/2}$ is the width of ct band at half maximum intensity; (I) refers to lowest energy ct band in complexes showing double transitions.

for $n = 1$, the gas phase refractive index, and so, for a given complex, a single gas phase transition value is obtained. The vapor phase ct energy for the *p*-xylene-TCNE complex obtained in this manner was found to be identical with the value reported in the literature from direct gas phase measurements⁵ (Table I). This suggests that simple, accurate measurements in several nonpolar solvents may give good estimates of gas phase transition energies, at least for ct complexes of the type investigated here. If the positions of band maxima ($\bar{\nu}_{\max}$) cannot be obtained accurately, one can measure instead the corresponding frequencies at half maximum intensity ($\bar{\nu}_{1/2\max}$) on the low-energy side of the band since, as our data show, for a given complex the band half-width ($\Delta\bar{\nu}_{1/2}$) appears to be independent of solvent (Table I).

A comparison between results and theory reveals large discrepancies, despite the linear relation found between solvent shift and the refractive index function. First, there are two different refractive index dependencies for a given electronic transition. Second, the gas-to-solution shifts of the various TCNE complexes are seen to decrease in the order: benzene (B) > *p*-xylene > mesitylene > durene > hexamethylbenzene (HMB). This order is the reverse of the strength of

these complexes and opposite to the shift order predicted by theory, assuming relatively small differences in ground-state polarity of these complexes, which is reasonable according to Briegleb's calculations.^{1a} Further, from Table I the ratio of gas-to-solution shifts $\Delta\nu(\text{B-TCNE})/\Delta\nu(\text{HMB-TCNE}) = 2.14$ matches closely the ratio of the measured heats of formation of these complexes in CCl₄ (at 20°):⁸ $\Delta H_f^\circ(\text{benz-TCNE})/\Delta H_f^\circ(\text{HMB-TCNE}) = 2.3$. The corresponding figures for the benzene-TCNE and durene-TCNE complexes are $\Delta\nu$ ratio = 1.42 (Table I), which compares to a ΔH_f° ratio of 1.41.⁸ Finally, there is the considerable difference in the behavior of ct transitions in perfluoro- and hydrocarbon solvents, corresponding to the now well-known fact that the attractive London interactions in perfluorocarbons are considerably less than those in the hydrocarbon liquids.

The results summarized above seem to be in agreement with the suggestion put forward very recently by Murrell, *et al.*,⁹ that ct processes in solution are in

(8) G. Briegleb, J. Czekalla, and G. Reuss, *Z. Physik. Chem. (Frankfurt)*, **30**, 316 (1961).

(9) S. Carter, J. N. Murrell, and E. J. Rosch, *J. Chem. Soc.*, 2048 (1965).

competitive equilibrium with fairly tightly bound solvation shells surrounding the various solute components.

Acknowledgment. This work was carried out in the laboratory of Prof. J. H. Hildebrand and supported by the National Science Foundation; this support is gratefully acknowledged.

DEPARTMENT OF CHEMISTRY
UNIVERSITY OF CALIFORNIA
BERKELEY, CALIFORNIA 94720

EVA M. VOIGT

RECEIVED NOVEMBER 29, 1965

Absorption Spectra of Mercury in Perfluoropropane at Various Densities

Sir: The broad, double maximum absorption band near 2537 Å which appears in the spectrum of Hg dissolved in hydrocarbons, alcohols, water, and in highly compressed rare gases has not yet been fully explained. Vinogradov and Gunning¹ have listed several hypotheses which have been advanced. They have suggested, on the basis of a large number of observations of the spectrum of Hg in different solvents, that the double environment and cage quantization hypotheses of Robinson² and Robin,³ respectively, are more consistent with their observations than the Stark splitting hypothesis of Reichardt and Bonhoeffer.⁴ Hg₂ molecules and Hg solvent-bound states were considered unlikely to be important on the basis of some Beer's law and nmr studies. In the course of investigating the absorption spectrum of Hg in solvents at elevated temperatures, we found what seems to be a simple refutation of both Robinson's and Robin's hypotheses.

In Figure 1 are shown two spectra of Hg in propane at temperatures above and below the critical temperature (T_c) and at the densities indicated. The difference in these spectra is typical for mercury-hydrocarbon systems. As the temperature increases and the density decreases, the double-band structure disappears. These observations alone do not permit distinction among the several hypotheses mentioned above.

Spectra of Hg in perfluoropropane are shown in Figure 2.⁵ In contrast to the spectra in propane, the double band structure persists above T_c and at densities well below the liquid density. Furthermore, the separation of the band components appears to be little affected by changes in the density while the relative intensities change considerably.

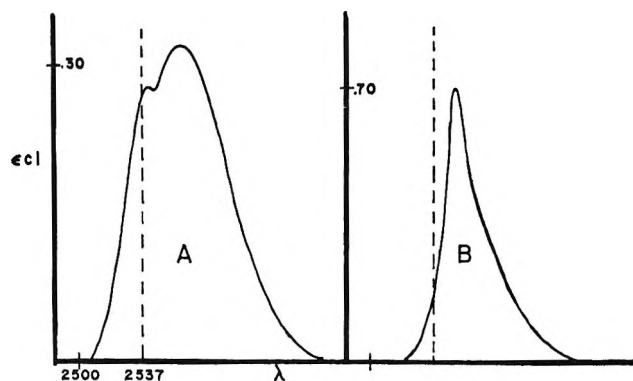


Figure 1. Absorption spectra of mercury in propane ($T_c = 96.8^\circ$): A, density, 10.7 mmoles/cc; temp, 42° ; B, density, 3.7 mmoles/cc; temp, 115° .

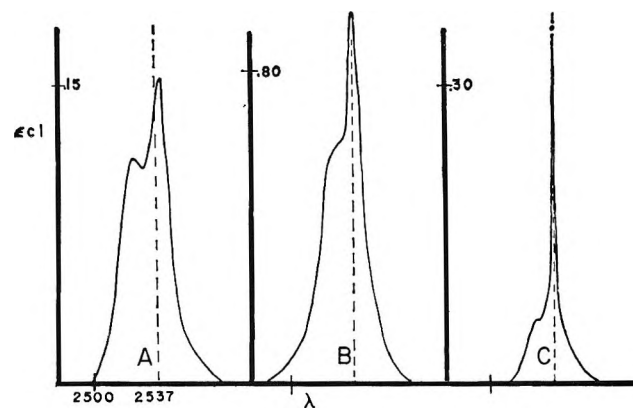


Figure 2. Absorption spectra of mercury in perfluoropropane ($T_c = 71.9^\circ$): A, density, 6 mmoles/cc; temp, 58° ; B, density, 2.68 mmoles/cc; temp, 100° ; C, density, 1.40 mmoles/cc; temp, 100° .

If the spectra in the two systems are analogous, these observations are evidence against interpretations of the double band in terms of a liquid phase double environment, cage effects, or Stark splitting. The first two interpretations imply a strong dependence of the phenomenon on the state of aggregation of the solvent, which, while observed in propane, is not observed in the perfluorinated solvent. The Stark splitting interpretation is basically questionable in

(1) S. N. Vinogradov and H. E. Gunning, *J. Phys. Chem.*, **68**, 1962 (1964).

(2) G. W. Robinson, *Mol. Phys.*, **3**, 301 (1960).

(3) J. Robin, *et al.*, *Discussions Faraday Soc.*, **22**, 30 (1956).

(4) H. Reichardt and K. F. Bonhoeffer, *Z. Physik*, **67**, 780 (1931).

(5) The spectra shown in Figures 1 and 2 were recorded using an automatic-scanning single-beam spectrophotometer built around a Bausch and Lomb 16-A/mm dispersion grating monochromator operated at 0.3-mm slits. The %T read-out was converted to optical density and the spectra were replotted on an expanded wavelength scale.

light of Holtzmark's theory of line broadening which does not predict splitting at all.⁶ Even if one discounts this early theory as inapplicable at high densities, it is difficult to maintain the Stark splitting hypothesis when the double band is observed at densities as low as those employed in the Hg-C₃F₈ system.

At present, we feel that the short wavelength component of the band observed in C₃F₈ and, by analogy, that in C₃H₈, is related to the "violet bands" observed in the spectrum of Hg and alkali metals perturbed by a wide variety of gases at low pressures.⁷ For Hg perturbed by argon, de Klavier⁸ and Robin⁹ have shown that these bands, initially quite weak, approach and eventually exceed the intensity of the principal line as the density increases. At densities near the critical density of argon, two peaks of approximately equal intensity are observed. At higher densities, near that of the solid, the principal line is replaced by the appearance of a second satellite, and at 6 kbars pressure where the argon density is near that of a close-packed solid, a double peak is again observed and is due wholly to the satellites. It is this latter spectrum that Robinson² compared to the spectrum of Hg in neopentane. On the other hand, Gunning assigns the bands in hydrocarbons as R and S which are Robin's terms for the principal line and the S, satellite, respectively. Our results are in accord with Gunning's assignment; we find no evidence for more than two bands in the density ranges employed.

We see, then, no compelling reason to invoke exclusively high density properties of the solvent to explain the observation of a double band in solutions of Hg. Our results in C₃F₈ supplement Robin's results in argon in indicating the connection between the high and low density satellite bands. Only if there appear additional satellites at higher C₃F₈ densities will there be a possibility for explanations such as those listed by Gunning. Even if this is observed, as it is in argon, we feel that the known increase in satellite band intensity with density and the fact that more than one satellite is observed at low densities are strong indications that the exclusively high density interpretations are superfluous.

We are currently investigating further the analogy between the Hg spectra in hydro- and fluorocarbon solvents over a wider density range. A more complete and detailed discussion of the subjects presented here,

along with the results of experiments now in progress, will be submitted for publication in the near future.

Acknowledgment. Acknowledgment is made to the Union Carbide Corporation and to the Atomic Energy Commission for support of this research.

DEPARTMENT OF CHEMISTRY
LEHIGH UNIVERSITY
BETHLEHEM, PENNSYLVANIA

JAMES D. LEAR
JAMES E. STURM

RECEIVED DECEMBER 6, 1965

Self-Diffusion in Cyclohexane-Benzene Solutions

Sir: Solutions of cyclohexane and benzene have been the subject of a recent diffusion study by Rodwin, Harpst, and Lyons.¹ This system is of considerable interest because it is well characterized with regard to thermodynamic variables. Rodwin, Harpst, and Lyons¹ chose to phrase their discussion in terms of an equation^{2,3} which can be written as

$$D = Q(x_c D_b + x_b D_c) \quad (1)$$

where D is the mutual diffusion coefficient, x is the mole fraction, D_b and D_c are the self-diffusion coefficients, and

$$Q = (\partial \ln x_c f_c / \partial \ln x_c) \quad (2)$$

The subscripts c and b refer to cyclohexane and benzene. Rodwin, Harpst, and Lyons obtained D_c and D_b by means of an extrapolation procedure and compared measured D values with D values calculated by means of eq 1.

In this note we wish to report the results of self-diffusion studies in C₆H₅-C₆D₁₂ solutions and C₆D₆-C₆H₁₂ solutions by proton magnetic resonance spin-echo methods. These results provide a test of eq 1 that does not depend upon the extrapolations previously¹ employed.

Solutions were prepared from benzene and cyclohexane of about 99% isotopic purity. The solutions were examined by high resolution nmr and it was found that exchange did not occur. The spin-echo self-diffusion technique has been described previously.^{4,5} All measurements were made at 25°. We expect an

(6) R. G. Breene, "The Shift and Shape of Spectral Lines," Pergamon Press Inc., New York, N. Y., 1961, Chapter 4.

(7) S. Ch'en and M. Takeo, *Rev. Mod. Phys.*, **29**, 64 (1957).

(8) H. de Klavier, *Discussions Faraday Soc.*, **22**, 80 (1956).

(9) J. Robin and S. Robin, *Compt. Rend.*, **233**, 928 (1951).

(1) L. Rodwin, J. A. Harpst, and P. A. Lyons, *J. Phys. Chem.*, **69**, 2783 (1965).

(2) G. S. Hartley and J. Crank, *Trans. Faraday Soc.*, **45**, 801 (1949).

(3) R. M. Barrer, *J. Phys. Chem.*, **61**, 178 (1957).

(4) H. Y. Carr and E. M. Purcell, *Phys. Rev.*, **94**, 630 (1954).

(5) D. C. Douglass and D. W. McCall, *J. Phys. Chem.*, **62**, 1102 (1958).

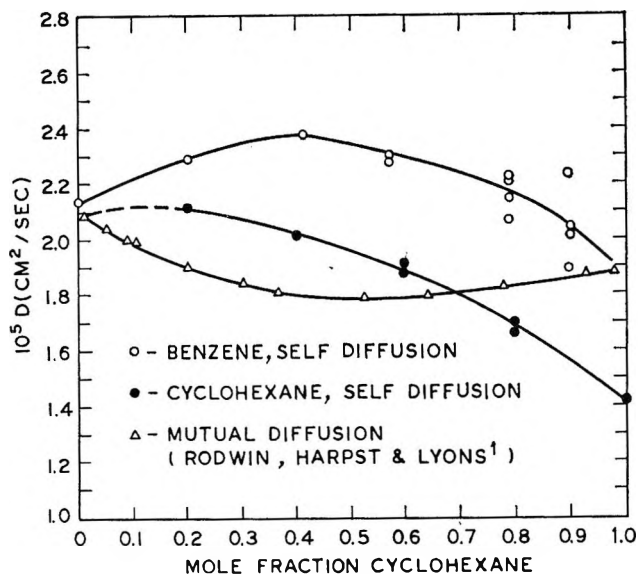


Figure 1. The concentration dependence of self-diffusion coefficients in benzene-cyclohexane solutions, 25°.

absolute accuracy of better than 5% with the pure liquids but the errors can be expected to be greater in solutions dilute in protons. This is particularly true in dilute solutions of C_6H_6 in C_6D_{12} .

The results are shown in Figure 1 together with the mutual diffusion results of Rodwin, Harpst, and Lyons.¹ It is clear that the spin-echo results (which are absolute and have not been adjusted to fit the tracer data) exhibit the correct limiting behavior, *i.e.*

$$\lim_{x_c \rightarrow 0} D = D_c$$

and

$$\lim_{x_b \rightarrow 0} D = D_b \quad (3)$$

Table I shows a comparison of experimental D values with D values calculated from eq 1. It is clear that the agreement is poor. Bearman⁶ has discussed eq 1 from a theoretical viewpoint and casts some doubt upon the general validity of the relation. Thus, the discrepancies observed are not too surprising.

A simple equation that describes the data well is

$$D = (x_c D_b + x_b D_c) \eta / (x_b \eta_b + x_c \eta_c) \quad (4)$$

where η is the solution viscosity. Table I also contains D values computed from eq 4. The agreement is well within experimental error. We have not corrected the viscosities for the isotope effect.^{7,8}

Equation 4 can be regarded as the simplest mixture formula corrected for the "viscosity defect," $[1 - \eta / (x_c \eta_c + x_b \eta_b)]$. The discussion could also be phrased

Table I

$10^5 D$	$10^5 D$, eq 1	$10^5 D$, eq 4	x_B
1.88	1.88	1.88	0.0
1.86	1.85	1.86	0.1
1.83	1.79	1.83	0.2
1.81	1.72	1.79	0.3
1.79	1.66	1.77	0.4
1.79	1.63	1.78	0.5
1.80	1.64	1.80	0.6
1.84	1.68	1.83	0.7
1.90	1.78	1.90	0.8
1.99	1.90	1.98	0.9
2.10	2.09	2.09	1.0

in terms of the "density defect." These quantities are roughly proportional to one another although the "density defect" is about an order of magnitude smaller than the "viscosity defect."⁹

Acknowledgment. We are indebted to D. C. Douglass and B. Ottar for stimulating discussions of this work.

(6) R. J. Bearman, *J. Phys. Chem.*, **65**, 1961 (1961).

(7) J. D. Birkett and P. A. Lyons, *ibid.*, **69**, 2782 (1965).

(8) J. A. Dixon and W. Schiessler, *ibid.*, **58**, 430 (1954).

(9) NOTE ADDED IN PROOF. Rodwin, Harpst, and Lyons¹ do not suggest that the parameters they have deduced (*i.e.*, those corresponding to our D_b and D_c) are self-diffusion coefficients. This interpretation has been made by Bearman.⁶ Dr. Bearman has called our attention to a recent tracer diffusion study of this system by D. A. Collins and H. Watts, *Australian J. Chem.*, **17**, 516 (1964). We have benefited greatly from comments contributed by Professor P. A. Lyons and Professor R. J. Bearman.

BELL TELEPHONE LABORATORIES
MURRAY HILL, NEW JERSEY

DAVID W. McCALL
ERNEST W. ANDERSON

RECEIVED DECEMBER 14, 1965

Heats of Mixing of Benzene with Hexafluorobenzene, Pentafluorobenzene, and 1,2,4,5-Tetrafluorobenzene¹

Sir: As part of our research program on fluorocarbon solutions, we have measured the molar heat of mixing (*i.e.*, the molar excess enthalpy \bar{H}^E) for each of the systems $C_6H_6 + C_6F_6$, $C_6H_6 + C_6F_5H$, and $C_6H_6 + 1,2,4,5$ -tetrafluorobenzene over a wide mole fraction

(1) Contribution No. 1905 from the Department of Chemistry, University of California, Los Angeles, Calif. This work was supported in part by the U. S. Atomic Energy Commission and in part by the University Grants Committee, New Zealand (Postgraduate Scholarship in Science to D. V. F.).

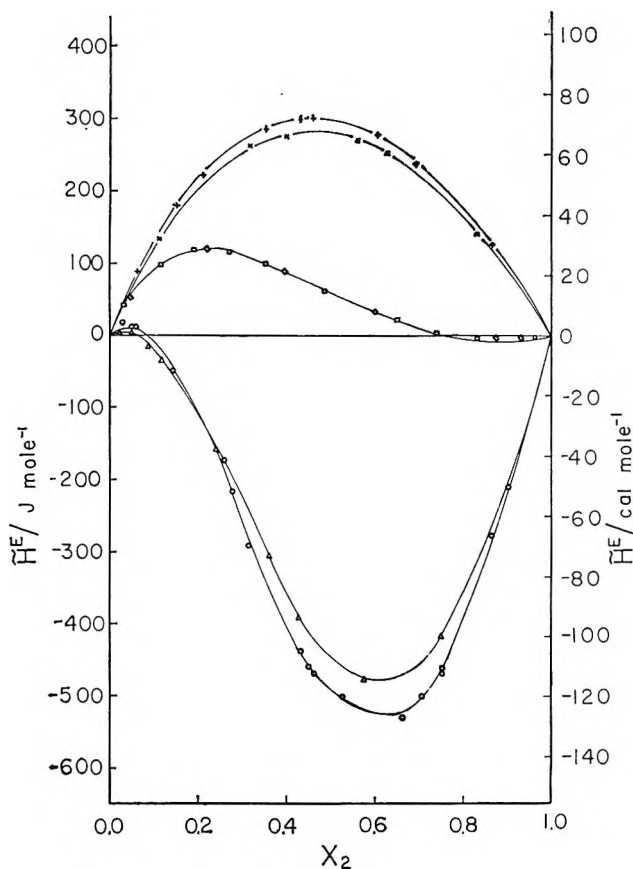


Figure 1. The excess enthalpies of C_6H_6 at 25° (O) and 45° (Δ), $C_6H_6 + C_6H_5H$ at 25° (\square) and 42° (\diamond), and $C_6H_6 + 1,2,4,5$ -tetrafluorobenzene at 25° (+) and 39 (x); x_2 is the mole fraction of the fluorochemical in each case.

range and at two temperatures (Figure 1). The calorimeter used is similar to that described by Larkin and McGlashan² and is described elsewhere.³ The $C_6H_6 + C_6F_6$ results near $x_2 = 0$ and those for $C_6H_6 + C_6F_5H$ near $x_2 = 1$ have been carefully checked and the sign change in the heat of mixing has been definitely established in each case. Since runs at these compositions involve no electrical compensation, the sign of the temperature change unequivocally determines the sign of \bar{H}^E .

The S-shaped curves found in the system 1-hydro-*n*-perfluoroheptane + acetone⁴ were interpreted in terms of the combination of a symmetric exothermic "chemical" interaction arising from the formation of a 1:1 hydrogen-bonded complex and a skewed endothermic "physical" interaction arising from the mixing of hydrocarbon and fluorocarbon groups. The former contribution was obtained independently from nmr data and the latter inferred from the system $C_7F_{16} +$ acetone. We believe the S-shaped curves for $C_6H_6 + C_6F_6$ and $C_6H_6 + C_6F_5H$ may be similarly explained.

There is strong evidence suggesting charge-transfer complex formation between C_6H_6 , acting as donor, and C_6F_6 , acting as acceptor. The freezing point diagram⁵ shows the formation of a 1:1 solid complex. The predominantly exothermic results that we obtain for this system can be understood in terms of such a complex; the positive temperature dependence of \bar{H}^E must be due to a decrease in complex formation with increasing temperature. The more endothermic results for $C_6H_6 + C_6F_5H$ presumably arise from a smaller exothermic contribution; *i.e.*, C_6F_5H is a poorer acceptor than C_6F_6 and forms a weaker complex. Any temperature dependence in this case is small, less than the experimental error. With $C_6H_6 + 1,2,4,5$ -tetrafluorobenzene, the further increase in \bar{H}^E again reflects further decrease in complex formation. The negative temperature dependence for this system corresponds to the normal behavior⁶ of systems with positive \bar{H}^E ; indeed, there is no clear evidence for any complex formation in this case.

Additional measurements with other fluorine substituted benzenes (*e.g.*, $C_6H_3F_3$, $C_6H_4F_2$, C_6H_5F) are underway.

- (2) J. A. Larkin and M. L. McGlashan, *J. Chem. Soc.*, 3425 (1961).
- (3) J. A. Larkin, D. V. Fenby, T. S. Gilman, and R. L. Scott, to be published.
- (4) D. L. Anderson, R. A. Smith, D. B. Myers, S. K. Alley, A. G. Williamson, and R. L. Scott, *J. Phys. Chem.*, **66**, 621 (1962).
- (5) F. L. Swinton, private communication.
- (6) M. L. McGlashan, *Pure Appl. Chem.*, **8**, 157 (1964).

DEPARTMENT OF CHEMISTRY
UNIVERSITY OF CALIFORNIA
LOS ANGELES, CALIFORNIA 90024

DAVID V. FENBY
IAN A. MCLURE
ROBERT L. SCOTT

RECEIVED DECEMBER 27, 1965

Bond Lengths in Iron Pentacarbonyl

Sir: On the basis of an electron diffraction study of gaseous iron pentacarbonyl, Davis and H. P. Hanson recently reported¹ that the axial Fe-C bonds were shorter than the trigonal by 0.045 Å, the values being 1.797 and 1.842 Å, respectively. They stated that the existence of the shorter axial bonds was corroborated by X-ray crystallographic studies of A. W. Hanson,² whose results gave axial bonds of 1.785 and 1.807 Å and trigonal bonds of 1.827, 1.827, and 1.837 Å. Davis and H. P. Hanson were apparently unaware that the crystal structure refinement by A. W. Hanson

- (1) M. I. Davis and H. P. Hanson, *J. Phys. Chem.*, **69**, 3405 (1965).
- (2) A. W. Hanson, *Acta Cryst.*, **15**, 930 (1962).

was carried out using an incorrect space group: when the correct space group is used,³ the molecule has crystal symmetry C_2 -2, with two equivalent axial bonds having length 1.810 ± 0.020 Å and trigonal bonds of length 1.797 ± 0.017 Å (two equivalent) and 1.763 ± 0.034 Å (one),⁴ where the uncertainties given are the standard derivations. The X-ray results thus do not provide support for the axial bonds being shorter, but, if anything, suggest that they are *longer* (as might be expected), although, on the basis of the usual significance test,⁵ neither of the differences between the axial bond length and the two trigonal bond lengths is in the "significant" class.

Furthermore, we doubt whether the electron diffraction data are capable of detecting a difference of only 0.045 Å between the two kinds of Fe-C bonds because of the high correlation between that difference and the vibrational amplitudes. In the refinement¹ by the matrix least-squares method described by Hedberg and Iwasaki,⁶ Davis and Hanson used assumed values for the vibrational amplitudes, a procedure which virtually fixed the bond length difference before the refinement began. It is interesting that in the investigation, by electron diffraction, of the structure of 2,3-dimethylbuta-1,3-diene,⁷ Hedberg and Hedberg were unable to distinguish between models with the bond lengths $C_{\text{methyl}}-C$ equal to C_2-C_3 with vibration amplitudes 0.046 Å and models having a difference of 0.05 Å between the two bond lengths with vibration

amplitudes 0.039 Å. In the present case a satisfactory fit was obtained with a bond length separation of 0.045 Å and assumed vibration amplitudes of 0.041 and 0.059 Å. An equally good fit could probably have been obtained with no bond length separation and somewhat larger vibration amplitudes or even a reversal in the bond length split and different vibration amplitudes. The correlation among these quantities is certainly so great as to preclude their independent determination by the electron diffraction method.

Acknowledgment. This work was supported by a grant from the National Science Foundation. We wish to thank Professor Kenneth Hedberg for helpful discussion.

(3) J. Donohue and A. Caron, *Acta Cryst.*, **17**, 663 (1964).

(4) These three nonequivalent Fe-C bond lengths and their standard derivations were recalculated from the data of ref 3, and are given here to one more significant figure than were given therein.

(5) D. W. J. Cruickshank, *Acta Cryst.*, **2**, 65 (1949).

(6) K. Hedberg and M. Iwasaki, *ibid.*, **17**, 529 (1964).

(7) L. Hedberg and K. Hedberg, American Crystallographic Association Meeting, Gatlinburg, Tenn., July 2, 1965.

DEPARTMENT OF CHEMISTRY
UNIVERSITY OF SOUTHERN CALIFORNIA
LOS ANGELES, CALIFORNIA 90007

JERRY DONOHUE

DEPARTMENT OF CHEMISTRY
UNIVERSITY OF MASSACHUSETTS
AMHERST, MASSACHUSETTS

AIMERY CARON

RECEIVED DECEMBER 14, 1965